

Syracuse University

SURFACE

Biomedical and Chemical Engineering -
Dissertations

College of Engineering and Computer Science

2011

Issues on Clean Diesel Combustion Technology Using Supercritical Fluids: Thermophysical Properties and Thermal Stability of Diesel Fuel

Ronghong Lin
Syracuse University

Follow this and additional works at: https://surface.syr.edu/bce_etd



Part of the [Biomedical Engineering and Bioengineering Commons](#)

Recommended Citation

Lin, Ronghong, "Issues on Clean Diesel Combustion Technology Using Supercritical Fluids: Thermophysical Properties and Thermal Stability of Diesel Fuel" (2011). *Biomedical and Chemical Engineering - Dissertations*. 60.
https://surface.syr.edu/bce_etd/60

This Dissertation is brought to you for free and open access by the College of Engineering and Computer Science at SURFACE. It has been accepted for inclusion in Biomedical and Chemical Engineering - Dissertations by an authorized administrator of SURFACE. For more information, please contact surface@syr.edu.

ABSTRACT

The clean diesel combustion technology using supercritical fluids is aimed to both improve fuel economy and reduce harmful emissions. This novel process involves preparation, injection and combustion of supercritical fuel/diluents mixtures. Design and development of this new process require a deep understanding of fuel properties. The current study has attempted to address three fuel property related issues: fuel surrogates, diffusivity and thermal stability.

Fuel surrogates are often used in engine research to mimic real fuel properties. In this work, ten diesel fuel surrogates were investigated, and the ability of these surrogates to predict diesel fuel properties was evaluated. It was found that none of them were able to predict all properties of interest including volatility, critical points, density, viscosity, heat capacity, and thermal conductivity. Different surrogates are suggested for predictions of different properties.

Diffusion coefficients of diesel fuel and surrogate compounds in SCCO_2 were determined using the Taylor dispersion method at temperatures and pressures up to 373.15 K and 30 MPa, respectively. Results were correlated by Wilke-Chang, Scheibel, He-Yu, $D_{12}/T - \mu$ and $D_{12}/\sqrt{T} - \rho$ correlations. It was found that the He-Yu correlation had the best prediction capability, while the $D_{12}/T - \mu$ correlation gave overall best fit for experimental data with $\text{AAD}\% < 8\%$. Experimental uncertainties caused by sample injection, detector linearity, mobile phase mean velocity, and column orientation were extensively discussed. A dimensionless parameter ϕ was proposed to characterize the effect of the injection volume, and a new $D_{12}-U$ pattern diagram was

generalized based on current results to describe the impact of mobile phase mean velocity on diffusivity measurements.

The effects of temperature, residence time and CO₂ on thermal stability of diesel fuel at high temperatures were investigated by both batch and continuous thermal stressing experiments. Results showed that thermal stability of diesel fuel decreased as temperature and residence time increased. 400-420 °C was found to be the optimal temperature range where supercritical fuel delivery and combustion could work. The presence of 10 wt% CO₂ reduced accumulation of solid deposits due to enhanced solvent capacity. However, CO₂ was not likely to have the ability to chemically prevent fuel coking. Solid deposits of different sizes, morphologies and structures were observed at 300 - 440 °C, which implies different deposit formation mechanisms.

ISSUES ON CLEAN DIESEL COMBUSTION TECHNOLOGY
USING SUPERCRITICAL FLUIDS: THERMOPHYSICAL
PROPERTIES AND THERMAL STABILITY OF DIESEL FUEL

By

RONGHONG LIN

M.Sc., Chemical Engineering, Syracuse University, 2008

B.Eng., Chemical Engineering, Beijing University of Chemical Technology, 2001

DISSERTATION

Submitted in partial fulfillment of the requirements for the
degree of Doctor of Philosophy in Chemical Engineering
in the Graduate School of Syracuse University

May 2011

Copyright 2011 Ronghong Lin

All rights Reserved

TABLE OF CONTENTS

| | |
|---|--------------|
| LIST OF FIGURES | X |
| LIST OF TABLES | XXI |
| NOMENCLATURE..... | XXIV |
| ACKNOWLEDGEMENTS | XXXII |
| CHAPTER I INTRODUCTION | 1 |
| 1.1 BACKGROUND | 1 |
| 1.2 SUPERCRITICAL FLUIDS | 2 |
| 1.3 CONCEPTUAL DESIGN OF THE SUPERCRITICAL FUEL DELIVERY SYSTEM..... | 3 |
| 1.4 RESEARCH NEEDS, PROPOSED WORK AND SIGNIFICANCE..... | 8 |
| CHAPTER II LITERATURE REVIEW..... | 11 |
| 2.1 INTRODUCTION | 11 |
| 2.2 STRATEGIES FOR CLEAN DIESEL COMBUSTION..... | 11 |
| 2.2.1 <i>Early studies on the effect of fuel temperature</i> | <i>12</i> |
| 2.2.2 <i>Hypergolic combustion.....</i> | <i>14</i> |
| 2.2.3 <i>Dissolved gas enhanced spray atomization and fuel combustion</i> | <i>17</i> |
| 2.2.3.1 Studies by Huang and coworkers..... | 17 |
| 2.2.3.2 Studies by Senda and coworkers..... | 19 |
| 2.2.3.3 Studies by others | 21 |
| 2.2.4 <i>Supercritical fuel combustion.....</i> | <i>22</i> |
| 2.3 DEVELOPMENT OF DIESEL FUEL SURROGATES | 26 |
| 2.4 THERMAL STABILITY OF FUELS..... | 31 |

| | |
|---|-----------|
| 2.5 SUMMARY | 38 |
| CHAPTER III DIESEL FUEL SURROGATES | 40 |
| 3.1 INTRODUCTION | 40 |
| 3.2 DEVELOPMENT OF DIESEL FUEL SURROGATES | 41 |
| 3.3 EVALUATION OF DIESEL FUEL SURROGATES | 43 |
| 3.3.1 <i>Determination of volatilities</i> | 43 |
| 3.3.2 <i>Estimation of critical properties</i> | 46 |
| 3.3.2.1 Critical properties of diesel fuel surrogates | 46 |
| 3.3.2.2 Critical properties of diesel fuel..... | 50 |
| 3.3.3 <i>Calculation of thermophysical properties</i> | 55 |
| 3.3.3.1 Thermophysical properties of diesel fuel surrogates | 55 |
| 3.3.3.2 Thermophysical properties of diesel fuel..... | 57 |
| 3.4 RESULTS AND DISCUSSIONS | 59 |
| 3.4.1 <i>Comparison of volatilities</i> | 59 |
| 3.4.2 <i>Comparison of critical properties</i> | 59 |
| 3.4.3 <i>Comparison of thermophysical properties</i> | 70 |
| 3.5 CONCLUSIONS | 79 |
| CHAPTER IV DIFFUSIVITY MEASUREMENTS | 81 |
| 4.1 INTRODUCTION | 81 |
| 4.2 THEORETICAL BACKGROUND | 82 |
| 4.2.1 <i>Taylor dispersion analysis</i> | 82 |
| 4.2.2 <i>Analysis of experimental data</i> | 86 |
| 4.3 EXPERIMENTAL..... | 88 |

| | | |
|---------|---|-----|
| 4.3.1 | <i>Materials</i> | 88 |
| 4.3.2 | <i>Experimental setup</i> | 88 |
| 4.3.3 | <i>Experimental conditions and procedure</i> | 90 |
| 4.4 | EXPERIMENTAL UNCERTAINTIES | 91 |
| 4.4.1 | <i>Sources of experimental uncertainties</i> | 91 |
| 4.4.2 | <i>Peak tailing</i> | 92 |
| 4.4.3 | <i>Effect of sample injection</i> | 94 |
| 4.4.4 | <i>Effect of concentration measurement</i> | 95 |
| 4.4.5 | <i>Effect of column geometry and orientation</i> | 97 |
| 4.4.6 | <i>Effect of mean velocity</i> | 100 |
| 4.5 | MODELING OF EXPERIMENTAL DATA USING PREDICTIVE CORRELATIONS | 102 |
| 4.6 | RESULTS AND DISCUSSIONS | 104 |
| 4.6.1 | <i>Physical properties</i> | 104 |
| 4.6.2 | <i>Validation of the apparatus</i> | 104 |
| 4.6.3 | <i>Diffusion coefficients of diesel fuel and surrogate compounds in SCCO₂</i> | 104 |
| 4.6.4 | <i>Modeling of experimental data using predictive correlations</i> | 112 |
| 4.6.5 | <i>Experimental uncertainties</i> | 117 |
| 4.6.5.1 | <i>Peak tailing</i> | 117 |
| 4.6.5.2 | <i>Effect of wavelength</i> | 121 |
| 4.6.5.3 | <i>Effect of sample injection</i> | 125 |
| 4.6.5.4 | <i>Effect of the mean velocity</i> | 131 |
| 4.6.5.5 | <i>Effect of column orientation</i> | 135 |
| 4.6.5.6 | <i>A new generalized D₁₂-U pattern diagram</i> | 149 |

| | |
|---|------------|
| 4.7 CONCLUSIONS | 152 |
| CHAPTER V THERMAL STABILITY OF DIESEL FUEL..... | 155 |
| 5.1 INTRODUCTION | 155 |
| 5.2 EXPERIMENTAL..... | 156 |
| 5.2.1 <i>Batch thermal stressing of DF</i> | 156 |
| 5.2.2 <i>Batch thermal stressing of DF/CO₂ mixtures</i> | 159 |
| 5.2.3 <i>Continuous thermal stressing of DF and DF/CO₂ mixtures</i> | 166 |
| 5.2.4 <i>Fuel characterization</i> | 168 |
| 5.3 RESULTS AND DISCUSSION..... | 174 |
| 5.3.1 <i>Validation of the $\Delta(PPA)$ analysis</i> | 174 |
| 5.3.2 <i>Batch thermal stressing of DF</i> | 176 |
| 5.3.2.1 <i>Color change</i> | 176 |
| 5.3.2.2 <i>Effect of O₂</i> | 176 |
| 5.3.2.3 <i>Effect of temperature</i> | 184 |
| 5.3.2.4 <i>Effect of residence time</i> | 188 |
| 5.3.2.5 <i>Formation of solid deposits</i> | 192 |
| 5.3.3 <i>Batch thermal stressing of DF/CO₂ mixtures</i> | 193 |
| 5.3.4 <i>Continuous thermal stressing of DF and the DF/CO₂ mixture</i> | 205 |
| 5.4 CONCLUSIONS | 217 |
| CHAPTER VI CONCLUSIONS | 220 |
| CHAPTER VII FUTURE WORK | 224 |
| APPENDIX A DENSITIES, HEAT CAPACITIES, VISCOSITIES, AND | |
| THERMAL CONDUCTIVITIES OF DF AND DFS_s..... | 227 |

| | |
|---|------------|
| APPENDIX B TAYLOR DISPERSION ANALYSIS | 242 |
| APPENDIX C LITERATURE DATA | 253 |
| APPENDIX D EXPERIMENTAL DATA | 262 |
| D-1 MEASURED DIFFUSION COEFFICIENTS OF BENZENE IN CO ₂ | 263 |
| D-2 TEMPERATURE & PRESSURE HISTORIES FOR BATCH THERMAL STRESSING OF DF/CO ₂ MIXTURES..... | 271 |
| D-3 GC-MS REPORTS FOR FRESH DF | 284 |
| D-4 Δ(PPA) ANALYSES FOR THERMALLY STRESSED DF..... | 293 |
| APPENDIX E PERMISSIONS TO QUOTE/REPRODUCE COPYRIGHT MATERIAL..... | 353 |
| BIBLIOGRAPHY | 358 |
| BIOGRAPHICAL DATA | 386 |

LIST OF FIGURES

| | | |
|------------------|---|----|
| FIG. 1-1 | A TYPICAL P-T PHASE DIAGRAM OF A PURE SUBSTANCE. | 4 |
| FIG. 1-2 | SIMULATED STRUCTURE OF THE DIFFUSION FLAME (DEC, 1997). | 5 |
| FIG. 1-3 | SCHEMATIC DIAGRAMS OF CONVENTIONAL (TOP) AND SUPERCRITICAL (BOTTOM) DF DELIVERY SYSTEMS IN DIESEL ENGINES. ECU: ENGINE CONTROL UNIT. | 7 |
| FIG. 2-1 | RELATIVE AMOUNTS OF VARIOUS CHEMICAL CLASSES IN DIESEL FUEL AND POSSIBLE COMPOUNDS TO REPRESENT THESE CHEMICAL CLASSES IN A DIESEL SURROGATE FUEL (PITZ AND MUELLER, 2010). REPRODUCED WITH ELSEVIER'S PERMISSION (ATTACHED IN APPENDIX E). | 30 |
| FIG. 3-1 | ORIGINAL TGA CURVES FOR DF AND DFSS. | 60 |
| FIG. 3-2 | NORMALIZED TGA CURVES FOR DF AND DFSS. | 61 |
| FIG. 3-3 | CRITICAL TEMPERATURES AND PRESSURES OF DFSS AND DF. | 69 |
| FIG. 3-4 | DENSITIES OF DFSS AND DF AT 30 MPa. | 71 |
| FIG. 3-5 | HEAT CAPACITIES OF DFSS AND DF AT 30 MPa. | 72 |
| FIG. 3-6 | VISCOSITIES OF DFSS AND DF AT 30 MPa. | 73 |
| FIG. 3-7 | THERMAL CONDUCTIVITIES OF DFSS AND DF AT 30 MPa. | 74 |
| FIG. 3-8 | COMPARISON OF DFS'S CAPABILITY IN PREDICTING DF DENSITY. | 75 |
| FIG. 3-9 | COMPARISON OF DFS'S CAPABILITY IN PREDICTING DF HEAT CAPACITY. | 76 |
| FIG. 3-10 | COMPARISON OF DFS'S CAPABILITY IN PREDICTING DF VISCOSITY. | 77 |
| FIG. 3-11 | COMPARISON OF DFS'S CAPABILITY IN PREDICTING DF THERMAL CONDUCTIVITY. | 78 |
| FIG. 4-1 | THE IDEALIZED TAYLOR DISPERSION EXPERIMENT. U IS THE MEAN VELOCITY, R IS THE RADIUS OF THE DISPERSION COLUMN, L IS THE LENGTH OF THE DISPERSION COLUMN, AND X IS THE WIDTH OF THE SOLUTE PULSE. | 84 |
| FIG. 4-2 | SCHEMATIC DIAGRAMS OF EXPERIMENTAL SETUPS FOR MEASUREMENT OF DIFFUSION COEFFICIENTS USING THE TAYLOR DISPERSION METHOD. (A) A SIX-PORT INJECTION VALVE WAS USED AND A COLUMN WAS VERTICALLY INSTALLED IN A GC OVEN; (B) A MANUAL INJECTION VALVE WAS USED AND A | |

COLUMN WAS VERTICALLY INSTALLED IN A GC OVEN; (C) A MANUAL INJECTION VALVE WAS USED AND A COLUMN WAS HORIZONTALLY INSTALLED IN A WATER BATH.89

FIG. 4-3 COMPARISON OF IDEAL AND REAL TAYLOR DISPERSION EXPERIMENTS FOR DIFFUSION COEFFICIENT MEASUREMENTS. (A): A STRAIGHT CYLINDRICAL TUBE IS USED A DIFFUSION COLUMN; (B): A COILED CYLINDRICAL TUBE IS USED AS A DIFFUSION COLUMN. D: DIAMETER OF DIFFUSION COLUMNS; V_{INJ} : INJECTION VOLUME; V_{DET} : DETECTION VOLUME.93

FIG. 4-4 DEMONSTRATION OF THE EFFECT OF DETECTOR LINEARITY ON THE ACCURACY OF DIFFUSION COEFFICIENT MEASUREMENTS. OPEN SQUARES (\square): DATA MEASURED IN THIS WORK FOR 1-METHYLNAPHTHALENE AT 353.15 K AND 15 MPa; FILLED DIAMONDS (\blacklozenge): DATA MANIPULATED FOR DEMONSTRATION ONLY.96

FIG. 4-5 TYPICAL RELATIONSHIP BETWEEN MEASURED DIFFUSION COEFFICIENT AND U. 101

FIG. 4-6 DENSITY OF BENZENE AND CO₂ AS A FUNCTION OF PRESSURE.106

FIG. 4-7 DIFFUSION COEFFICIENTS OF BENZENE IN SCCO₂ AS A FUNCTION OF THE DENSITY OF CO₂: A COMPARISON WITH LITERATURE DATA. REFERENCES: [1] (LEVELT SENGERS ET AL., 1993), [2] (AGO AND NISHIUMI, 1999), [3] (NISHIUMI AND KUBOTA, 2007), [4] (FUNAZUKURI ET AL., 2001), [5] (FUNAZUKURI AND NISHIMOTO, 1996), [6] (SASSIAT ET AL., 1987), [7] (SWAID AND SCHNEIDER, 1979), [8] (SUÁREZ ET AL., 1993), AND [9] (BUENO ET AL., 1993). TW: THIS WORK.107

FIG. 4-8 DIFFUSION COEFFICIENTS OF BENZENE, TOLUENE, M-XYLENE, 1-HEXADECENE, 1-METHYLNAPHTHALENE AND DIESEL FUEL IN SCCO₂ (TOP) AND CORRESPONDING CURVE-FITTING ERRORS (BOTTOM) AS A FUNCTION OF THE DENSITY CO₂. ERRORS BARS INDICATE STANDARD DEVIATION.111

FIG. 4-9 D₁₂-T/H CORRELATION FOR DIFFUSION COEFFICIENTS OF BENZENE, TOLUENE, M-XYLENE, 1-HEXADECENE, 1-METHYLNAPHTHALENE AND DIESEL FUEL IN SCCO₂.114

FIG. 4-10 A COMPARISON OF PREDICTED AND MEASURED D₁₂ OF BENZENE IN CO₂.116

FIG. 4-11 TYPICAL PEAK TAILING OF 1-HEXADECENE (TOP), 1-METHYLNAPHTHALENE (MIDDLE) AND DIESEL FUEL (BOTTOM) OBSERVED AT 333.15 K AND 10 MPa USING THE 0.508 MM COLUMN IN THE VERTICAL ORIENTATION.118

FIG. 4-12 THE EFFECT OF PRESSURE ON THE SHAPE OF BENZENE DISPERSION PEAKS. OPEN BLUE DIAMONDS: EXPERIMENTAL DATA; SOLID RED LINES: PREDICTIONS BY EQ. (4-6). BENZENE DISPERSION PEAKS WERE OBTAINED AT 313.15 K AND 7.5 (TOP), 8.5 (MIDDLE), AND 10 (BOTTOM) MPa USING THE 0.508 MM COLUMN IN THE VERTICAL ORIENTATION.119

| | |
|---|-----|
| FIG. 4-13 THE EFFECT OF TEMPERATURE GRADIENTS IN THE INJECTION AND THE DETECTION REGIONS ON THE SHAPE OF BENZENE DISPERSION PEAKS. PEAKS WERE OBTAINED AT 313.15 K AND 10 MPa USING THE 0.508 mm I.D. COLUMN IN THE VERTICAL ORIENTATION. TOP: CONNECTIONS WERE NOT INSULATED; BOTTOM: CONNECTIONS WERE INSULATED. | 120 |
| FIG. 4-14 TYPICAL UV ABSORBANCE SPECTRA OF BENZENE (2), TOLUENE (3), M-XYLENE (4), 1-HEXADECENE (1), 1-METHYLNAPHTHALENE (5) AND DIESEL FUEL (6). | 122 |
| FIG. 4-15 EFFECT OF WAVELENGTH ON DIFFUSION COEFFICIENTS OF BENZENE (TOP), TOLUENE (MIDDLE) AND M-XYLENE (BOTTOM). EXPERIMENTS WERE CONDUCTED AT 313.15 K AND 10 MPa. SOLID LINES: SPECTRA; TRIANGLES: DIFFUSION COEFFICIENTS. | 123 |
| FIG. 4-16 EFFECT OF WAVELENGTH ON DIFFUSION COEFFICIENTS OF 1-HEXADECENE (TOP) AND 1-METHYLNAPHTHALENE (BOTTOM). EXPERIMENTS WERE CONDUCTED AT 313.15 K AND 10 MPa. SOLID LINES: SPECTRA; TRIANGLES: DIFFUSION COEFFICIENTS. | 124 |
| FIG. 4-17 DETECTOR LINEARITY FOR BENZENE AT VARIOUS WAVELENGTHS. | 126 |
| FIG. 4-18 EFFECT OF ϕ ON DIFFUSION COEFFICIENTS (TOP) AND CURVE-FITTING ERRORS (BOTTOM). ERROR BARS REPRESENT STANDARD DEVIATION. EXPERIMENTAL DATA ARE FOR BENZENE AND WERE OBTAINED AT 313.15 K AND 10 MPa USING VERTICALLY INSTALLED COLUMNS. | 130 |
| FIG. 4-19 MEASURED DIFFUSION COEFFICIENTS (TOP) OF BENZENE IN SCCO_2 AND CORRESPONDING CURVE-FITTING ERRORS (BOTTOM) AS A FUNCTION OF THE MEAN VELOCITY AT 313.15 K FOR THE VERTICAL ORIENTATION. THE SOLID LINES IN THE TOP FIGURE CONNECT THE DATA POINTS. THE SOLID LINES IN THE BOTTOM FIGURE ARE TREND LINES. | 132 |
| FIG. 4-20 MEASURED DIFFUSION COEFFICIENTS (TOP) OF BENZENE IN SCCO_2 AND CORRESPONDING CURVE-FITTING ERRORS (BOTTOM) AS A FUNCTION OF THE MEAN VELOCITY AT 333.15 K FOR THE VERTICAL ORIENTATION. THE SOLID LINES IN THE TOP FIGURE CONNECT THE DATA POINTS. THE SOLID LINES IN THE BOTTOM FIGURE ARE TREND LINES. | 133 |
| FIG. 4-21 MEASURED DIFFUSION COEFFICIENTS (TOP) OF BENZENE IN SCCO_2 AND CORRESPONDING CURVE-FITTING ERRORS (BOTTOM) AS A FUNCTION OF THE MEAN VELOCITY AT 313.15 K FOR THE HORIZONTAL ORIENTATION. THE SOLID LINES IN THE TOP FIGURE CONNECT THE DATA POINTS. THE SOLID LINES IN THE BOTTOM FIGURE ARE TREND LINES. | 136 |
| FIG. 4-22 MEASURED DIFFUSION COEFFICIENTS (TOP) OF BENZENE IN SCCO_2 AND CORRESPONDING CURVE-FITTING ERRORS (BOTTOM) AS A FUNCTION OF THE MEAN VELOCITY AT 333.15 K FOR THE HORIZONTAL ORIENTATION. THE | |

SOLID LINES IN THE TOP FIGURE CONNECT THE DATA POINTS. THE SOLID LINES IN THE BOTTOM FIGURE ARE TREND LINES. 137

FIG. 4-23 MEASURED DIFFUSION COEFFICIENTS OF BENZENE IN SCCO₂ (TOP) AND CORRESPONDING CURVE-FITTING ERRORS (BOTTOM) AT 313.15 K AND 9 MPa FOR BOTH VERTICAL AND HORIZONTAL COLUMN ORIENTATIONS. THE SOLID LINES IN THE TOP FIGURE CONNECT THE DATA POINTS. THE SOLID LINES IN THE BOTTOM FIGURE ARE TREND LINES. 138

FIG. 4-24 MEASURED DIFFUSION COEFFICIENTS OF BENZENE IN SCCO₂ (TOP) AND CORRESPONDING CURVE-FITTING ERRORS (BOTTOM) AT 313.15 K AND 9.5 MPa FOR BOTH VERTICAL AND HORIZONTAL COLUMN ORIENTATIONS. 139

FIG. 4-25 MEASURED DIFFUSION COEFFICIENTS OF BENZENE IN SCCO₂ (TOP) AND CORRESPONDING CURVE-FITTING ERRORS (BOTTOM) AT 313.15 K AND 10 MPa FOR BOTH VERTICAL AND HORIZONTAL COLUMN ORIENTATIONS. 140

FIG. 4-26 MEASURED DIFFUSION COEFFICIENTS OF BENZENE IN SCCO₂ (TOP) AND CORRESPONDING CURVE-FITTING ERRORS (BOTTOM) AT 313.15 K AND 12 MPa FOR BOTH VERTICAL AND HORIZONTAL COLUMN ORIENTATIONS. 141

FIG. 4-27 MEASURED DIFFUSION COEFFICIENTS OF BENZENE IN SCCO₂ (TOP) AND CORRESPONDING CURVE-FITTING ERRORS (BOTTOM) AT 313.15 K AND 15 MPa FOR BOTH VERTICAL AND HORIZONTAL COLUMN ORIENTATIONS. 142

FIG. 4-28 MEASURED DIFFUSION COEFFICIENTS OF BENZENE IN SCCO₂ (TOP) AND CORRESPONDING CURVE-FITTING ERRORS (BOTTOM) AT 333.15 K AND 9 MPa FOR BOTH VERTICAL AND HORIZONTAL COLUMN ORIENTATIONS. 143

FIG. 4-29 MEASURED DIFFUSION COEFFICIENTS OF BENZENE IN SCCO₂ (TOP) AND CORRESPONDING CURVE-FITTING ERRORS (BOTTOM) AT 333.15 K AND 10 MPa FOR BOTH VERTICAL AND HORIZONTAL COLUMN ORIENTATIONS. 144

FIG. 4-30 MEASURED DIFFUSION COEFFICIENTS OF BENZENE IN SCCO₂ (TOP) AND CORRESPONDING CURVE-FITTING ERRORS (BOTTOM) AT 333.15 K AND 12 MPa FOR BOTH VERTICAL AND HORIZONTAL COLUMN ORIENTATIONS. 145

FIG. 4-31 MEASURED DIFFUSION COEFFICIENTS OF BENZENE IN SCCO₂ (TOP) AND CORRESPONDING CURVE-FITTING ERRORS (BOTTOM) AT 333.15 K AND 14 MPa FOR BOTH VERTICAL AND HORIZONTAL COLUMN ORIENTATIONS. 146

FIG. 4-32 MEASURED DIFFUSION COEFFICIENTS OF BENZENE IN SCCO₂ (TOP) AND CORRESPONDING CURVE-FITTING ERRORS (BOTTOM) AT 333.15 K AND 15 MPa FOR BOTH VERTICAL AND HORIZONTAL COLUMN ORIENTATIONS. 147

FIG. 4-33 COMPARISON OF DIFFUSION COEFFICIENTS OBTAINED IN VERTICALLY- AND HORIZONTALLY-INSTALLED COLUMNS. V: VERTICAL; H: HORIZONTAL. THE SOLID LINES CONNECT THE DATA POINTS. 149

| | |
|---|-----|
| FIG. 4-34 GENERALIZED RELATIONSHIP BETWEEN MEASURED DIFFUSION COEFFICIENTS AND THE MEAN VELOCITY. THE SOLID LINES INDICATE D_{12} - U CURVES AT DIFFERENT DENSITIES ($P_1 < P_2 < P_3$); THE DASH LINE INDICATES THE BOUNDARY AMONG REGIONS I, II, AND III. | 151 |
| FIG. 5-1 EXPERIMENTAL SETUP FOR BATCH THERMAL STRESSING OF DF. TOP LEFT: STAINLESS STEEL SHEETS USED TO CAPTURE SOLID DEPOSITS; TOP RIGHT: A PHOTO OF THE THERMAL STRESSING CELL; T1 AND T2: OUTSIDE AND INSIDE TEMPERATURES OF THE CELL. | 157 |
| FIG. 5-2 A PRESSURE-TEMPERATURE-DENSITY DIAGRAM FOR DFS-7. | 158 |
| FIG. 5-3 AN EXAMPLE OF TEMPERATURE HISTORY FOR BATCH THERMAL STRESSING OF DF. T1: TEMPERATURE OF THE GC OVEN; T2: TEMPERATURE OF DF INSIDE THE CELL. | 161 |
| FIG. 5-4 A SCHEMATIC DIAGRAM FOR THE EXPERIMENTAL SETUP FOR BATCH THERMAL STRESSING OF DF/CO ₂ MIXTURES. T1 AND T2: THERMOCOUPLES; P: PRESSURE TRANSDUCER; RED SQUARE: HEATING TAPE. | 163 |
| FIG. 5-5 AN EXAMPLE OF TEMPERATURE/PRESSURE HISTORY FOR BATCH THERMAL STRESSING OF DF/CO ₂ MIXTURES (RUN 1-B). T1: OUTSIDE WALL TEMPERATURE OF THE VESSEL; T2: TEMPERATURE OF DF INSIDE THE VESSEL. | 164 |
| FIG. 5-6 A SCHEMATIC DIAGRAM OF THE EXPERIMENTAL SETUP FOR CONTINUOUS THERMAL STRESSING OF DF AND DF/CO ₂ MIXTURES. RED DASH SQUARE INDICATES THE HEATING TAPE. | 167 |
| FIG. 5-7 CHROMATOGRAPHS OF FRESH DF (TOP) AND DF STRESSED AT 440 °C FOR 2 HOURS (BOTTOM). C9 THROUGH C25 INDICATE NORMAL ALKANES. | 172 |
| FIG. 5-8 PART OF INTEGRATED CHROMATOGRAPH OF FRESH DF. NUMBERS ABOVE PEAKS INDICATE ACTUAL RETENTION TIME. HORIZONTAL AND INCLINED RED LINES INDICATE BASE LINES, WHILE VERTICAL RED LINES INDICATE INTEGRATION BOUNDARIES BETWEEN TWO PEAKS. | 173 |
| FIG. 5-9 $\Delta(PPA)$ ANALYSIS OF CHROMATOGRAPHS OF FRESH DF (TOP) AND DF STRESSED AT 400 °C (MIDDLE) AND 440 °C (BOTTOM). THE RESIDENCE TIME WAS 10 MIN FOR BOTH TEMPERATURES. 1K AND 3K INDICATE DF CONCENTRATIONS OF 1000 AND 3000 PPM, RESPECTIVELY. | 175 |
| FIG. 5-10 THERMAL STRESSING OF N-HEXADECANE (TOP), 1-METHYLNAPHTHALENE (MIDDLE), AND BUTYLBENZENE (BOTTOM) AT 400 AND 440 °C FOR 30 MIN. .. | 177 |
| FIG. 5-11 CHROMATOGRAPHS OF N-HEXADECANE. TOP: FRESH; MIDDLE: 400 °C, 30 MIN; BOTTOM: 440 °C, 30 MIN. | 178 |

| | |
|--|-----|
| FIG. 5-12 CHROMATOGRAPHS OF 1-METHYLNAPHTHALENE. TOP: FRESH; MIDDLE: 400 °C, 30 MIN; BOTTOM: 440 °C, 30 MIN. | 179 |
| FIG. 5-13 CHROMATOGRAPHS OF BUTYLBENZENE. TOP: FRESH; MIDDLE: 400 °C, 30 MIN; BOTTOM: 440 °C, 30 MIN. | 180 |
| FIG. 5-14 EFFECT OF TRACE AMOUNTS OF O ₂ ON THERMAL STABILITY OF DF. LEFT COLUMN: FRESH DF; MIDDLE COLUMN: SAMPLES PREPARED IN CO ₂ ENVIRONMENT, NO AIR TRAPPED; RIGHT COLUMN: SAMPLES PREPARED IN AIR ENVIRONMENT. TOP: 300 °C; MIDDLE: 400 °C; BOTTOM: 440 °C. | 182 |
| FIG. 5-15 Δ(PPA) ANALYSIS FOR STRESSED DF. TOP: 400 °C; BOTTOM: 440 °C. “AIR” AND “CO ₂ ” REPRESENT DF SAMPLES PREPARED IN AIR AND CO ₂ ENVIRONMENTS, RESPECTIVELY. | 183 |
| FIG. 5-16 CHANGES IN DF COLOR AT DIFFERENT STRESSING TEMPERATURES FROM 200-440 °C. THE FIRST AND THE SECOND NUMBERS INDICATE STRESSING TEMPERATURE AND RESIDENCE TIME, RESPECTIVELY. | 185 |
| FIG. 5-17 Δ(PPA) ANALYSIS FOR DF THERMALLY STRESSED AT 400-440 °C FOR 30 MIN. | 186 |
| FIG. 5-18 TGA CURVES (TOP) AND THE CORRESPONDING SLOPE CURVES (BOTTOM) FOR DF THERMALLY STRESSED AT 400-440 °C. | 187 |
| FIG. 5-19 CHANGES IN DF COLOR AT 400, 420 AND 440 °C FOR VARYING RESIDENCE TIME. THE FIRST AND THE SECOND NUMBERS INDICATE STRESSING TEMPERATURE AND RESIDENCE TIME, RESPECTIVELY. | 189 |
| FIG. 5-20 Δ(PPA) ANALYSIS OF STRESSED CHANGES IN DF COLOR AT 300, 400, 420 AND 440 °C FOR VARYING RESIDENCE TIME. THE FIRST AND THE SECOND NUMBERS IN LEGEND INDICATE STRESSING TEMPERATURE AND RESIDENCE TIME, RESPECTIVELY. | 190 |
| FIG. 5-21 SLOPE OF Δ(PPA) TREND LINES AS A FUNCTION RESIDENCE TIME AT 300, 400, 420, AND 440 °C. | 191 |
| FIG. 5-22 SEM ANALYSIS OF DF SOLID DEPOSITS. THE FIRST AND THE SECOND NUMBERS INDICATE STRESSING TEMPERATURE AND RESIDENCE TIME, RESPECTIVELY. | 193 |
| FIG. 5-23 PHOTOS OF DF SAMPLES COLLECTED IN BATCH THERMAL STRESSING OF DF/CO ₂ MIXTURES. CONDITIONS FOR RUNS 1-5 ARE INDICATED ON THE BOTTLES AND ALSO GIVEN IN TABLE 5-2 | 195 |
| FIG. 5-24 Δ(PPA) ANALYSIS FOR RUNS 1-5 OF BATCH THERMAL STRESSING OF DF/CO ₂ MIXTURES. | 196 |

| | | |
|------------------|--|-----|
| FIG. 5-25 | CHANGES IN CONCENTRATION OF PAH PRECURSORS IN RUNS 1-5. A1: NAPHTHALENE; A2: 2-METHYLNAPHTHALENE; A3: 1-METHYLNAPHTHALENE; A3: 1, 4, 5-TRIMETHYLNAPHTHALENE. | 198 |
| FIG. 5-26 | TGA CURVES FOR FRESH DF AND THERMALLY STRESSED DF FROM RUNS 1-5. TOP: ORIGINAL TGA CURVES; BOTTOM: SLOPE CURVES. | 199 |
| FIG. 5-27 | P-T DIAGRAMS FOR BATCH THERMAL STRESSING OF DF/CO ₂ MIXTURES: RUNS 1-5. | 201 |
| FIG. 5-28 | P-T DIAGRAMS FOR BATCH THERMAL STRESSING OF DF AND DF/CO ₂ MIXTURES: RUNS 1-A – 3-B. | 202 |
| FIG. 5-29 | Δ (PPA) ANALYSIS FOR SAMPLES FROM RUNS 1-A – 3-B OF BATCH THERMAL STRESSING OF DF/CO ₂ MIXTURES. | 203 |
| FIG. 5-30 | CHANGES IN CONCENTRATION OF PAH PRECURSORS IN RUNS 1-A - 3-B. | 204 |
| FIG. 5-31 | TEMPERATURE AND PRESSURE HISTORY FOR RUN 4-B. TOP: FIRST RUN; BOTTOM: REPEATED RUN. | 206 |
| FIG. 5-32 | A P-T DIAGRAM FOR RUN 4-B. DASH LINE CIRCLES HIGHLIGHT REGIONS WHERE SLOPE CHANGES OCCUR. | 207 |
| FIG. 5-33 | TEMPERATURE AND PRESSURE HISTORY FOR CONTINUOUS THERMAL STRESSING OF DF (TOP) AND THE DF/CO ₂ MIXTURE (BOTTOM). DF:CO ₂ = 9:1 BY MASS. | 208 |
| FIG. 5-34 | PHOTOS OF DF SAMPLES COLLECTED IN THERMAL STRESSING OF DF (TOP) AND THE DF/CO ₂ MIXTURE (BOTTOM). LEFT TO RIGHT: 0 THROUGH 12 HOURS. | 210 |
| FIG. 5-35 | CHANGES IN PRESSURE DROP ACROSS THE MICRO-FILTER DURING CONTINUOUS THERMAL STRESSING OF DF (TOP) AND THE DF/CO ₂ MIXTURE (BOTTOM). RED LINES ARE LINEAR TREND LINES. | 211 |
| FIG. 5-36 | Δ (PPA) ANALYSIS FOR DF SAMPLES COLLECTED DURING THERMAL STRESSING OF DF. | 213 |
| FIG. 5-37 | Δ (PPA) ANALYSIS FOR DF SAMPLES COLLECTED DURING THERMAL STRESSING OF THE DF/CO ₂ MIXTURE. | 214 |
| FIG. 5-38 | SLOPES OF Δ (PPA) TREND LINES. | 215 |
| FIG. 5-39 | VARIATIONS OF CONCENTRATIONS OF PAH PRECURSORS IN THERMAL STRESSING OF DF AND THE DF/CO ₂ MIXTURE. | 216 |
| FIG. A-1 | DENSITIES OF DFSS AND DF AT 10 MPA. | 228 |

| | |
|---|-----|
| FIG. A-2 DENSITIES OF DFSS AND DF AT 50 MPa. | 229 |
| FIG. A-3 DENSITIES OF DFSS AND DF AT 100 MPa. | 230 |
| FIG. A-4 HEAT CAPACITIES OF DFSS AND DF AT 10 MPa. | 231 |
| FIG. A-5 HEAT CAPACITIES OF DFSS AND DF AT 50 MPa. | 232 |
| FIG. A-6 HEAT CAPACITIES OF DFSS AND DF AT 100 MPa. | 233 |
| FIG. A-7 VISCOSITIES OF DFSS AND DF AT 10 MPa. | 234 |
| FIG. A-8 VISCOSITIES OF DFSS AND DF AT 50 MPa. | 235 |
| FIG. A-9 VISCOSITIES OF DFSS AND DF AT 100 MPa. | 236 |
| FIG. A-10 THERMAL CONDUCTIVITIES OF DFSS AND DF AT 10 MPa. | 237 |
| FIG. A-11 THERMAL CONDUCTIVITIES OF DFSS AND DF AT 50 MPa. | 238 |
| FIG. A-12 THERMAL CONDUCTIVITIES OF DFSS AND DF AT 100 MPa. | 239 |
| FIG. D-1 T-P HISTORY FOR BATCH THERMAL STRESSING OF DF/CO ₂ MIXTURES: RUN 1. | 272 |
| FIG. D-2 T-P HISTORY FOR BATCH THERMAL STRESSING OF DF/CO ₂ MIXTURES: RUN 2. | 273 |
| FIG. D-3 T-P HISTORY FOR BATCH THERMAL STRESSING OF DF/CO ₂ MIXTURES: RUN 3. | 274 |
| FIG. D-4 T-P HISTORY FOR BATCH THERMAL STRESSING OF DF/CO ₂ MIXTURES: RUN 4. | 275 |
| FIG. D-5 T-P HISTORY FOR BATCH THERMAL STRESSING OF DF/CO ₂ MIXTURES: RUN 5. | 276 |
| FIG. D-6 T-P HISTORY FOR BATCH THERMAL STRESSING OF DF/CO ₂ MIXTURES: RUN 1-A. | 277 |
| FIG. D-7 T-P HISTORY FOR BATCH THERMAL STRESSING OF DF/CO ₂ MIXTURES: RUN 1-B. | 278 |
| FIG. D-8 T-P HISTORY FOR BATCH THERMAL STRESSING OF DF/CO ₂ MIXTURES: RUN 2-A. | 279 |
| FIG. D-9 T-P HISTORY FOR BATCH THERMAL STRESSING OF DF/CO ₂ MIXTURES: RUN 2-B. | 280 |
| FIG. D-10 T-P HISTORY FOR BATCH THERMAL STRESSING OF DF/CO ₂ MIXTURES: RUN 3-A. | 281 |
| FIG. D-11 T-P HISTORY FOR BATCH THERMAL STRESSING OF DF/CO ₂ MIXTURES: RUN 3-B. | 282 |

| | |
|---|-----|
| FIG. D-12 T-P HISTORY FOR BATCH THERMAL STRESSING OF DF/CO ₂ MIXTURES: RUN 4-B. | 283 |
| FIG. D-13 Δ(PPA) FOR FRESH DF (1000PPM, S1). | 294 |
| FIG. D-14 Δ(PPA) FOR FRESH DF (3000PPM, S1). | 295 |
| FIG. D-15 Δ(PPA) FOR THERMALLY STRESSED DF (200 °C, 15 MIN, DF, S1). | 296 |
| FIG. D-16 Δ(PPA) FOR THERMALLY STRESSED DF (300 °C, 10 MIN, DF, S1). | 297 |
| FIG. D-17 Δ(PPA) FOR THERMALLY STRESSED DF (300 °C, 30 MIN, DF, W/AIR, S1). ... | 298 |
| FIG. D-18 Δ(PPA) FOR THERMALLY STRESSED DF (300 °C, 600 MIN, DF, S1). | 299 |
| FIG. D-19 Δ(PPA) FOR THERMALLY STRESSED DF (400 °C, 10 MIN, DF, S1). | 300 |
| FIG. D-20 Δ(PPA) FOR THERMALLY STRESSED DF (400 °C, 30 MIN, DF, S1). | 301 |
| FIG. D-21 Δ(PPA) FOR THERMALLY STRESSED DF (400 °C, 30 MIN, DF, W/O AIR, S1). . | 302 |
| FIG. D-22 Δ(PPA) FOR THERMALLY STRESSED DF (400 °C, 30 MIN, DF, W/ AIR, S1). .. | 303 |
| FIG. D-23 Δ(PPA) FOR THERMALLY STRESSED DF (400 °C, 60 MIN, DF, S1). | 304 |
| FIG. D-24 Δ(PPA) FOR THERMALLY STRESSED DF (400 °C, 180 MIN, DF, S1). | 305 |
| FIG. D-25 Δ(PPA) FOR THERMALLY STRESSED DF (400 °C, 300 MIN, DF, S1). | 306 |
| FIG. D-26 Δ(PPA) FOR THERMALLY STRESSED DF (400 °C, 600 MIN, DF, S1). | 307 |
| FIG. D-27 Δ(PPA) FOR THERMALLY STRESSED DF (410 °C, 30 MIN, DF, S1). | 308 |
| FIG. D-28 Δ(PPA) FOR THERMALLY STRESSED DF (420 °C, 30 MIN, DF, S1). | 309 |
| FIG. D-29 Δ(PPA) FOR THERMALLY STRESSED DF (420 °C, 60 MIN, DF, S1). | 310 |
| FIG. D-30 Δ(PPA) FOR THERMALLY STRESSED DF (420 °C, 120 MIN, DF, S1). | 311 |
| FIG. D-31 Δ(PPA) FOR THERMALLY STRESSED DF (430 °C, 30 MIN, DF, S1). | 312 |
| FIG. D-32 Δ(PPA) FOR THERMALLY STRESSED DF (440 °C, 10 MIN, DF, S1). | 313 |
| FIG. D-33 Δ(PPA) FOR THERMALLY STRESSED DF (440 °C, 30 MIN, DF, S1). | 314 |
| FIG. D-34 Δ(PPA) FOR THERMALLY STRESSED DF (440 °C, 30 MIN, DF, W/O AIR, S1). . | 315 |
| FIG. D-35 Δ(PPA) FOR THERMALLY STRESSED DF (440 °C, 30 MIN, DF, W/ AIR, S1). .. | 316 |
| FIG. D-36 Δ(PPA) FOR THERMALLY STRESSED DF (440 °C, 120 MIN, DF, S1). | 317 |

| | |
|---|-----|
| FIG. D-37 $\Delta(\text{PPA})$ FOR THERMALLY STRESSED DF (DF/CO ₂ RUN 1, S3). | 318 |
| FIG. D-38 $\Delta(\text{PPA})$ FOR THERMALLY STRESSED DF (DF/CO ₂ RUN 2, S3). | 319 |
| FIG. D-39 $\Delta(\text{PPA})$ FOR THERMALLY STRESSED DF (DF/CO ₂ RUN 3, S3). | 320 |
| FIG. D-40 $\Delta(\text{PPA})$ FOR THERMALLY STRESSED DF (DF/CO ₂ RUN 4, S3). | 321 |
| FIG. D-41 $\Delta(\text{PPA})$ FOR THERMALLY STRESSED DF (DF/CO ₂ RUN 5, S3). | 322 |
| FIG. D-42 $\Delta(\text{PPA})$ FOR THERMALLY STRESSED DF (DF/CO ₂ RUN 1-A, S2). | 323 |
| FIG. D-43 $\Delta(\text{PPA})$ FOR THERMALLY STRESSED DF (DF/CO ₂ RUN 1-B, S2). | 324 |
| FIG. D-44 $\Delta(\text{PPA})$ FOR THERMALLY STRESSED DF (DF/CO ₂ RUN 2-A, S2). | 325 |
| FIG. D-45 $\Delta(\text{PPA})$ FOR THERMALLY STRESSED DF (DF/CO ₂ RUN 2-B, S2). | 326 |
| FIG. D-46 $\Delta(\text{PPA})$ FOR THERMALLY STRESSED DF (DF/CO ₂ RUN 3-A, S2). | 327 |
| FIG. D-47 $\Delta(\text{PPA})$ FOR THERMALLY STRESSED DF (DF/CO ₂ RUN 3-B, S2). | 328 |
| FIG. D-48 $\Delta(\text{PPA})$ FOR THERMALLY STRESSED DF (CONTINUOUS, DF, #1, S4). | 329 |
| FIG. D-49 $\Delta(\text{PPA})$ FOR THERMALLY STRESSED DF (CONTINUOUS, DF, #2, S4). | 330 |
| FIG. D-50 $\Delta(\text{PPA})$ FOR THERMALLY STRESSED DF (CONTINUOUS, DF, #3, S4). | 331 |
| FIG. D-51 $\Delta(\text{PPA})$ FOR THERMALLY STRESSED DF (CONTINUOUS, DF, #4, S4). | 332 |
| FIG. D-52 $\Delta(\text{PPA})$ FOR THERMALLY STRESSED DF (CONTINUOUS, DF, #5, S4). | 333 |
| FIG. D-53 $\Delta(\text{PPA})$ FOR THERMALLY STRESSED DF (CONTINUOUS, DF, #6, S4). | 334 |
| FIG. D-54 $\Delta(\text{PPA})$ FOR THERMALLY STRESSED DF (CONTINUOUS, DF, #7, S4). | 335 |
| FIG. D-55 $\Delta(\text{PPA})$ FOR THERMALLY STRESSED DF (CONTINUOUS, DF, #8, S4). | 336 |
| FIG. D-56 $\Delta(\text{PPA})$ FOR THERMALLY STRESSED DF (CONTINUOUS, DF, #9, S4). | 337 |
| FIG. D-57 $\Delta(\text{PPA})$ FOR THERMALLY STRESSED DF (CONTINUOUS, DF, #10, S4). | 338 |
| FIG. D-58 $\Delta(\text{PPA})$ FOR THERMALLY STRESSED DF (CONTINUOUS, DF, #11, S4). | 339 |
| FIG. D-59 $\Delta(\text{PPA})$ FOR THERMALLY STRESSED DF (CONTINUOUS, DF, #12, S4). | 340 |
| FIG. D-60 $\Delta(\text{PPA})$ FOR THERMALLY STRESSED DF (CONTINUOUS, DF/CO ₂ , #1, S4). .. | 341 |
| FIG. D-61 $\Delta(\text{PPA})$ FOR THERMALLY STRESSED DF (CONTINUOUS, DF/CO ₂ , #2, S4). .. | 342 |

| | | |
|------------------|--|--------|
| FIG. D-62 | $\Delta(\text{PPA})$ FOR THERMALLY STRESSED DF (CONTINUOUS, DF/CO ₂ , #3, S4). | ...343 |
| FIG. D-63 | $\Delta(\text{PPA})$ FOR THERMALLY STRESSED DF (CONTINUOUS, DF/CO ₂ , #4, S4). | ...344 |
| FIG. D-64 | $\Delta(\text{PPA})$ FOR THERMALLY STRESSED DF (CONTINUOUS, DF/CO ₂ , #5, S4). | ...345 |
| FIG. D-65 | $\Delta(\text{PPA})$ FOR THERMALLY STRESSED DF (CONTINUOUS, DF/CO ₂ , #6, S4). | ...346 |
| FIG. D-66 | $\Delta(\text{PPA})$ FOR THERMALLY STRESSED DF (CONTINUOUS, DF/CO ₂ , #7, S4). | ...347 |
| FIG. D-67 | $\Delta(\text{PPA})$ FOR THERMALLY STRESSED DF (CONTINUOUS, DF/CO ₂ , #8, S4). | ...348 |
| FIG. D-68 | $\Delta(\text{PPA})$ FOR THERMALLY STRESSED DF (CONTINUOUS, DF/CO ₂ , #9, S4). | ...349 |
| FIG. D-69 | $\Delta(\text{PPA})$ FOR THERMALLY STRESSED DF (CONTINUOUS, DF/CO ₂ , #10, S4). | ...350 |
| FIG. D-70 | $\Delta(\text{PPA})$ FOR THERMALLY STRESSED DF (CONTINUOUS, DF/CO ₂ , #11, S4). | ...351 |
| FIG. D-71 | $\Delta(\text{PPA})$ FOR THERMALLY STRESSED DF (CONTINUOUS, DF/CO ₂ , #12, S4). | ...352 |

LIST OF TABLES

| | |
|--|-----|
| TABLE 2-1 SIX CLASSES OF HYDROCARBONS AND THEIR MODEL COMPOUNDS NECESSARY TO SIMULATE REAL TRANSPORTATION FUELS (NIST, 2003)..... | 28 |
| TABLE 2-2 CHEMICAL KINETIC MODELS OF DFSS. | 32 |
| TABLE 3-1 COMPONENTS AND COMPOSITIONS OF DIESEL FUEL SURROGATES..... | 42 |
| TABLE 3-2 DENSITIES OF CHEMICALS PROVIDED BY THE MANUFACTURERS. | 45 |
| TABLE 3-3 CONSTANTS FOR DFS COMPOUNDS ^A | 63 |
| TABLE 3-4 GROUP CONTRIBUTIONS FOR CRITICAL PROPERTIES..... | 64 |
| TABLE 3-5 DISTILLATION CURVE DATA FOR DF ^A | 65 |
| TABLE 3-6 DENSITY OF DF AT 0.1 MPa ^A | 66 |
| TABLE 3-7 CRITICAL TEMPERATURES AND CRITICAL PRESSURES OF DFSS..... | 67 |
| TABLE 3-8 CRITICAL TEMPERATURE AND CRITICAL PRESSURE OF DF. | 68 |
| TABLE 4-1 PHYSICAL PROPERTIES OF CO ₂ AS A FUNCTION OF TEMPERATURE AND PRESSURE. | 105 |
| TABLE 4-2 DIFFUSION COEFFICIENTS OF BENZENE, TOLUENE, M-XYLENE, 1-HEXADECENE, 1-METHYLNAPHTHALENE AND DIESEL FUEL IN SCCO ₂ AT 313.15 AND 333.15 K AND 10-30 MPa. | 109 |
| TABLE 4-3 DIFFUSION COEFFICIENTS OF BENZENE, TOLUENE, M-XYLENE, 1-HEXADECENE, 1-METHYLNAPHTHALENE AND DIESEL FUEL IN SCCO ₂ AT 353.15 AND 373.15 K AND 10-30 MPa. | 110 |
| TABLE 4-4 PROPERTIES FOR PURE COMPOUNDS..... | 113 |
| TABLE 4-5 RESULTS OF MODELING OF DIFFUSION COEFFICIENTS BY PREDICTIVE CORRELATIONS. | 115 |
| TABLE 4-6 OPTIMAL RANGES OF WAVELENGTH DETERMINED AND WAVELENGTHS USED IN THE EXPERIMENTS. | 127 |
| TABLE 4-7 DIFFERENT COMBINATIONS OF V_{inj} AND D EXAMINED IN THIS STUDY. | 129 |
| TABLE 5-1 CONDITIONS FOR BATCH THERMAL STRESSING OF DF..... | 160 |

| | |
|--|-----|
| TABLE 5-2 CONDITIONS FOR BATCH THERMAL STRESSING OF DF/CO ₂ MIXTURES..... | 165 |
| TABLE 5-3 DETERMINATION OF PUMP FLOW RATES FOR A GIVEN RESIDENCE TIME OF 30 MINUTES. | 169 |
| TABLE 5-4 EQUIPMENT, CHEMICALS AND KEY PARAMETERS FOR THE GC-MS METHOD. | 170 |
| TABLE 5-5 EXAMPLES OF PRECURSORS OF PAHS IDENTIFIED BY GC-MS..... | 197 |
| TABLE 5-6 PSEUDOCRITICAL POINTS OF DF/CO ₂ MIXTURES..... | 218 |
| TABLE A-1 AAD% IN PREDICTION OF DENSITY AND HEAT CAPACITY OF DF. | 240 |
| TABLE A-2 AAD% IN PREDICTION OF THERMAL CONDUCTIVITY AND VISCOSITY OF DF. | 241 |
| TABLE B-1 VARIABLES AND DIMENSIONS..... | 247 |
| TABLE C-1 DIFFUSION COEFFICIENTS OF BENZENE IN CO ₂ | 254 |
| TABLE D-1 MEASURED DIFFUSION COEFFICIENTS OF BENZENE IN CO ₂ AND CURVE-FITTING ERRORS AS A FUNCTION OF MOBILE PHASE MEAN VELOCITY: 40 °C, 9-9.5 MPa, VERTICAL COIL. | 264 |
| TABLE D-2 MEASURED DIFFUSION COEFFICIENTS OF BENZENE IN CO ₂ AND CURVE-FITTING ERRORS AS A FUNCTION OF MOBILE PHASE MEAN VELOCITY: 40 °C, 10-15 MPa, VERTICAL COIL. | 265 |
| TABLE D-3 MEASURED DIFFUSION COEFFICIENTS OF BENZENE IN CO ₂ AND CURVE-FITTING ERRORS AS A FUNCTION OF MOBILE PHASE MEAN VELOCITY: 40 °C, 9-10 MPa, HORIZONTAL COIL. | 266 |
| TABLE D-4 MEASURED DIFFUSION COEFFICIENTS OF BENZENE IN CO ₂ AND CURVE-FITTING ERRORS AS A FUNCTION OF MOBILE PHASE MEAN VELOCITY: 40 °C, 12 AND 15 MPa, HORIZONTAL COIL. | 267 |
| TABLE D-5 MEASURED DIFFUSION COEFFICIENTS OF BENZENE IN CO ₂ AND CURVE-FITTING ERRORS AS A FUNCTION OF MOBILE PHASE MEAN VELOCITY: 60 °C, 9-15 MPa, VERTICAL COIL. | 268 |
| TABLE D-6 MEASURED DIFFUSION COEFFICIENTS OF BENZENE IN CO ₂ AND CURVE-FITTING ERRORS AS A FUNCTION OF MOBILE PHASE MEAN VELOCITY: 60 °C, 9-12 MPa, HORIZONTAL COIL. | 269 |
| TABLE D-7 MEASURED DIFFUSION COEFFICIENTS OF BENZENE IN CO ₂ AND CURVE-FITTING ERRORS AS A FUNCTION OF MOBILE PHASE MEAN VELOCITY: 60 °C, 14 AND 15 MPa, HORIZONTAL COIL. | 270 |
| TABLE D-8 GC-MS REPORT FOR FRESH DF – SAMPLE 1 (S1)..... | 285 |

| | |
|---|-----|
| TABLE D-9 GC-MS REPORT FOR FRESH DF – SAMPLE 2 (S2) | 286 |
| TABLE D-10 GC-MS REPORT FOR FRESH DF – SAMPLE 3 (S3) | 288 |
| TABLE D-11 GC-MS REPORT FOR FRESH DF – SAMPLE 4 (S4) | 290 |

NOMENCLATURE

| | |
|--|--|
| A | The cross-sectional area of the diffusion column |
| $A, B, C, D, a_{ij}, b_{ij}, c_{ij}, d_{ij}$ | Coefficients used in empirical correlations for thermophysical properties of diesel fuel |
| a, b, c, d, e | Coefficients used in the Taylor dispersion analysis |
| A1 | Naphthalene |
| A2 | 2-methylnaphthalene |
| A3 | 1-methylnaphthalen |
| A4 | 1, 4, 5-trimethylnaphthalene |
| ADD | Average absolute deviation |
| A_i | Area of peak i |
| API | American Petroleum Institute |
| API | The API gravity |
| ASTM | American Society for Testing and Materials |
| AU | Absorbance unit |
| Avg. | Average |
| Ben | Benzene |
| C | Concentration |
| C' | Initial concentration at the center of the dispersion column |
| CFD | Computational fluid dynamics |
| C_m | Mean concentration |
| C_p | Heat capacity |
| D | Diameter of injector nozzle hole Inner diameter of the dispersion column |

| | |
|-----------------|---|
| D_{12} | Diffusion coefficient of solute 1 in solvent 2 |
| De | The Dean number |
| DF | Diesel fuel |
| DFS | Diesel fuel surrogate |
| ECS | Extended corresponding state |
| ECU | Engine control unit |
| EG | Exhaust gas |
| EGR | Recycled exhaust gas, Exhaust gas recirculation |
| EOS | Equation of state |
| f_T, f_P, f_v | Parameters for the Twu correlation |
| GC | Gas chromatography |
| HCCI | Homogeneous charge compression ignition |
| HDe | 1-hexadecene |
| HPLC | High performance liquid chromatography |
| I.D. | Inner diameter |
| k | Thermal conductivity |
| K | Apparent diffusion coefficient or dispersion coefficient |
| L | Length of the injector nozzle hole Length of the dispersion column |
| $L_{e,det}$ | The equivalent length of the volume of the detection cell |
| $L_{e,inj}$ | The equivalent length of the sample injected |
| m | Total number of functional groups in a compound |
| M | Total amount of solute injected into the dispersion column |
| M, L, T | Dimension characteristics of mass, length, and time used in the Taylor dispersion analysis. |

| | |
|------------------------|---|
| Max. | Maximum |
| Min. | Minimum |
| MN | 1-methylnaphthalene |
| Mol. Frac. | Molar fraction |
| MS | Mass spectroscopy |
| <i>MW</i> | molecular weight |
| <i>n</i> | Total data points (Eq. 3-59) |
| NIST | National Institute of Standards and Technology |
| n_j | Number of the type j function group |
| OVR | Optimal velocity range |
| <i>P</i> | Pressure |
| <i>P1</i> | Inlet pressure of the micro-filter |
| <i>P2</i> | Outlet pressure of the micro-filter |
| PAH | Polyaromatic hydrocarbon |
| P_c | Critical pressure |
| $P_{c,AB}$ | Pseudo critical pressure of a binary mixture of A and B |
| P_{cm} | Mean critical pressure |
| P_c^o , | A parameter for the Twu correlation |
| <i>Pk</i> | Peak |
| PM | Particulate matter |
| <i>PPA</i> | Percentage of individual peak area in total peak area |
| $(PPA)_{Fresh\ DF}$ | PPA for fresh DF |
| $(PPA)_{Stressed\ DF}$ | PPA for thermally stressed DF |
| P_{pc} | Pseudocritical pressure |
| PR | Peng-Robinson |

| | |
|-------------------|--|
| q | Total group contribution |
| $q_{i,ss}$ | Harmonic mean of $q_{i,A}$ and $q_{i,B}$ |
| $q_{i,vv}$ | Arithmetic mean of $q_{i,A}$ and $q_{i,B}$ |
| R | Radius of the dispersion column |
| r | r-coordinate in the cylindrical coordinate system |
| R.T. | Residence time |
| R^2 | Standard deviation |
| R_c | Radius of the dispersion coil |
| Re | The Reynolds number |
| s | Critical surface increment fraction |
| S | The sum function of a dispersion peak profile |
| Sc | The Schmidt number |
| SCCO ₂ | Supercritical CO ₂ |
| SCF | Supercritical fluid |
| SEM | Scanning Electron Microscope |
| SG | Specific gravity |
| $(SG)^{\circ}$ | A parameter for the Twu correlation |
| SL | The ASTM slope |
| SMD | Sauter mean diameter |
| $Std.$ | Standard deviation |
| T | Temperature |
| t | Time |
| \bar{t} | The gravity of a dispersion peak profile |
| Tl | Outside temperature of the thermal stressing cells |

| | |
|--|--|
| | Outside temperature of the preheating pipe |
| t_1, t_2 | Times at 1% peak height of an elution profile |
| $T_{10}, T_{30}, T_{50}, T_{70}, T_{90}$ | Distillation temperatures at 10, 30, 50, 70, and 90 vol% distillate point |
| T_2 | Inside temperature of the thermal stressing cells Fuel temperature at the inlet of the thermal stressing coil |
| T_3 | GC oven temperature. |
| T_4 | Fuel temperature at the outlet of the thermal stressing coil |
| T_b | Mean average boiling point |
| $T_{b,AB}$ | Pseudo boiling point of a binary mixture of A and B |
| T_c | Critical temperature |
| $T_{c,AB}$ | Pseudo critical temperature of a binary mixture of A and B |
| T_{cm} | Mean critical temperature |
| T_c^o | A parameter for the Twu correlation |
| TGA | Thermal Gravimetric Analysis |
| THC | Total hydrocarbon |
| Tol | Toluene |
| T_{pc} | Pseudocritical temperature |
| T_v | Volumetric average boiling point |
| U | Mobile phase mean velocity |
| u' | Velocity variable |
| $u(r)$ | Flow velocity at position r |
| UV-vis | Ultraviolet–visible |
| v | Critical volume increment fraction |
| V | Molar volume |

| | |
|------------|--|
| V_b | Molar volume at the normal boiling temperature |
| V_c | Critical volume |
| V_c^o | A parameter for the Twu correlation |
| V_{det} | Volume of the detection cell |
| V_{inj} | Injection volume |
| Vol | Volume |
| Wt | Weight |
| x_i | Molar fraction of component i |
| X | Width of a solute pulse |
| x | Length coordinate used in the Taylor dispersion analysis |
| Xyl | M-xylene |
| y_i, z_i | Properties of DFS for data point i (Eq. 4-59) |
| z | z-coordinate in the cylindrical coordinate system |
| Z_c | Critical compressibility factor |

Greek Letters

| | |
|--|---|
| α | A parameter for the Twu correlation |
| β, γ | Parameters for the $D_{12}/T - \mu$ correlation |
| Γ | A parameter used in Eqs 4-26 and 4-27 |
| $\Delta(PPA)$ | Change in PPA, $\Delta(PPA) = (PPA)_{Stressed\ DF} - (PPA)_{Fresh\ DF}$ |
| $\Delta(SG)_T, \Delta(SG)_P, \Delta(SG)_v$ | Parameters for the Twu correlation |
| $\delta(x)$ | The δ function |
| Δ_j | The critical property increment for the type j group |

| | |
|------------------------|---|
| ε | Curve-fitting error |
| ζ, ξ | Parameters for the $D_{12}/\sqrt{T} - \rho$ correlation |
| η | A variable used in Taylor dispersion analysis |
| Θ | A parameter used in Eqs 4-19 and 4-20 |
| θ_i | Volumetric fraction of component i |
| λ_1, λ_2 | Dual wavelengths for the UV detector |
| μ | Dynamic viscosity |
| ρ | Density |
| ρ_c | Critical density |
| σ^2 | The variance of a dispersion peak profile |
| τ | Residence time |
| ν | Kinematic viscosity |
| φ | A non-dimensional parameter used to characterize the effect of the injection volume |
| χ | A parameter used in Eq. (4-12) |
| ψ | A dimensionless association factor of the solvent used in the Wilke-Chang correlation |
| ω | Acentric factor |

Subscripts

| | |
|------|---------------------------|
| 1 | Solute 1 |
| 2 | Solvent 2 |
| A | Compound A |
| AB | Binary mixture of A and B |
| B | Compound B |

| | |
|------------|--|
| <i>b</i> | Boiling point |
| <i>c</i> | Critical point |
| <i>cal</i> | Calculated value |
| <i>exp</i> | Experimental value |
| <i>i</i> | Either T or P in group contribution equations |
| <i>i</i> | Component i in Eq. (3-13), (3-14), and (3-16)-(3-18) |
| <i>m</i> | Mean value |
| <i>P</i> | Group contributions for critical pressure |
| <i>T</i> | Group contributions for critical temperature |
| <i>v</i> | Group contributions for critical volume |

ACKNOWLEDGEMENTS

I am deeply indebted to my dissertation advisor, Prof. Lawrence L. Tavlarides, for his many years of respectable guidance, support and encouragement. This dissertation would not have been accomplished without his valuable advices and thoughts.

I am grateful for the financial support of this project provided by the New York State Energy Research and Development Authority (NYSERDA) under the agreement number 8915-1-2. I am also grateful for the financial support from Syracuse University through the Graduate Fellowship.

I am also grateful to Professors Rebecca Bader, Mark N. Glauser, James Henderson, Patrick T. Mather and Radhakrishna Sureshkumar for serving on my committee and for valuable comments and suggestions.

I wish to thank Prof. Patrick T. Mather for allowing me to use the TGA instrument in his lab. I would also like to thank Dr. George Anitescu for sharing his valuable experiences with high pressure, high temperature systems and GC-MS analysis, thank Mr. Richard Chave for his assistance in modification of the thermal stressing cell, and thank Mr. John Banas for providing technical support for the data acquisition system.

My special thanks and love go to my parents, my brother and his family for their endless love, support, and encouragement.

Finally, my deepest appreciation and dearest love go to my wife Xinzhu not only for the assistance she provided in the TGA and SEM experiments, but also for her tremendous love and support, without which this work could not have been possible.

CHAPTER I

INTRODUCTION

1.1 BACKGROUND

As world population growth continues and standard of living increases, global demand for energy rapidly expands, which has put energy issues in the global spotlight. Limited supplies of traditional fossil fuels will not be able to meet the requirements for world development in a sustainable way. On the other hand, utilization of traditional fossil fuel has become one of the major causes of many negative environmental and health impacts. Therefore, transforming the way of generating, supplying, storing, and using energy will be one of the critical challenges in the 21st century (Office of Science, US DOE, 2008). This demands not only the discovery of new energy sources but also technological innovations in clean fuel utilization.

Transportation is the second largest consumer of energy in the United States, consuming 28% of total energy as of 2005. 97% of transportation energy derives from petroleum in the form of gasoline (65%), diesel (20%) and aviation fuel (12%) (Office of Science, US DOE, 2007). The dominant role of transportation in energy consumption indicates that efficiency improvement and emission reduction in this sector would significantly influence energy use and hence reduce environmental burdens.

Compared to gasoline engines, diesel engines offer big advantages in terms of energy saving. The high efficiency of diesel engines implies lower CO₂ emission per unit mass of fuels. Therefore, diesel engines have been given significant importance in the

automotive industry and in academia as well, especially in Europe. To improve engine efficiency and simultaneously reduce harmful emissions, mainly nitrogen oxides (NO_x) and particulate matter (PM), a variety of new diesel engine concepts and strategies have been proposed and are under investigation. Among them are homogeneous charge compression ignition (HCCI) combustion (Majt and Foster, 1983; Thring, 1989), premixed charge compression ignition combustion (Lee, 2006), low temperature combustion (Alriksson and Denbratt, 2006), and supercritical fuel combustion (O'Brien et al., 2001; Tavlarides and Anitescu, 2009). HCCI is considered to be the most promising technology and is of great interest to the engine community. However, HCCI is controlled by fuel oxidation kinetics, which limits HCCI engines to low power densities.

Recently, Tavlarides and Anitescu (Tavlarides and Anitescu, 2009) at Syracuse University, Syracuse, New York, proposed a new concept of clean diesel combustion. The core of this concept is preparation, injection, and combustion of mixtures of diesel fuel (DF) and recycled exhaust gas (EGR) in the supercritical state. Injection and combustion of supercritical fuel mixtures are expected to increase engine efficiency and to reduce harmful emissions, simultaneously, due to significant enhancements in fuel air mixing in the supercritical state in engine chambers. Therefore, successful implementation of this new concept and development of technology would significantly improve diesel engine performance. This dissertation was aimed to address some issues encountered in the development of this technology, mainly thermophysical properties and thermal stability of diesel fuel.

1.2 SUPERCRITICAL FLUIDS

In a typical P-T phase diagram of a pure compound as shown in **Fig. 1-1**, solid lines indicate phase boundaries, dividing the P-T plane into solid, liquid and gas regions. The liquid-gas boundary terminates at a certain point, (T_c, P_c) , which is called the critical point. A supercritical fluid (SCF) is any fluid at temperatures and pressures above the critical point. When the temperature is below the critical temperature T_c , the fluid undergoes phase transition from gas to liquid or vice versa by tuning the pressure. As the fluid reaches the critical point, however, the gas-liquid interface disappears and the fluid exhibits unique thermodynamic and transport properties. These properties include liquid-like densities which can significantly increase solubility, and gas-like diffusivities and viscosities and zero surface tensions which benefit mass transfer and fluid mixing. SCFs bring new opportunities to diesel engine combustion research due to these unique properties.

1.3 CONCEPTUAL DESIGN OF THE SUPERCRITICAL FUEL DELIVERY SYSTEM

In a conventional diesel engine, DF is injected in the liquid state into the engine chamber. Upon injection, DF undergoes atomization, vaporization and mixing with air before ignition occurs. Since combustion reactions occurs much faster than fuel mixing with air, diffusion flame forms. **Fig. 1-2** shows a simulated structure of diffusion flame in conventional diesel engines (Dec, 1997). The flame structure is characterized by fuel-rich and fuel-lean reactions inside and outside of the flame, respectively. This results in significant soot formation in the fuel-rich zone and NO_x formation in the fuel-lean zone. Therefore, incomplete fuel air mixing due to slow droplet vaporization is the major obstacle to complete, clean combustion of DF in conventional diesel engines. This has

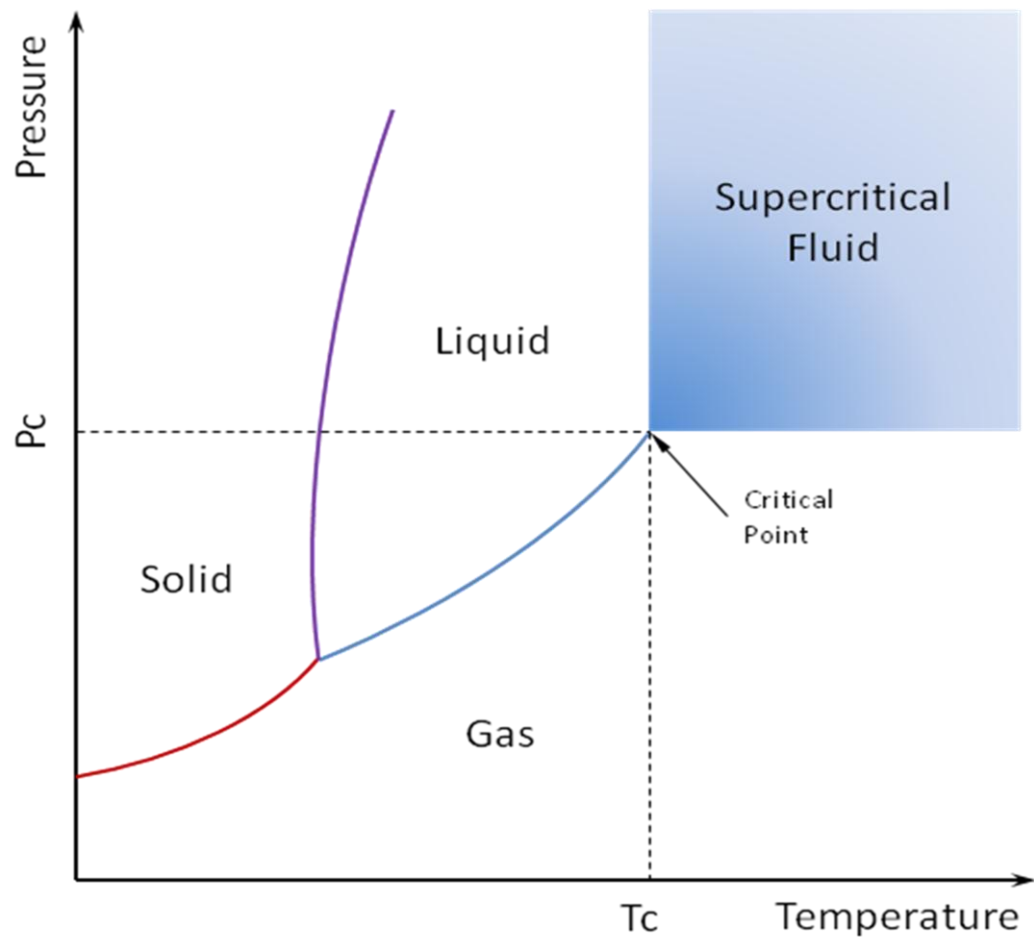


Fig. 1-1 A typical P-T phase diagram of a pure substance.

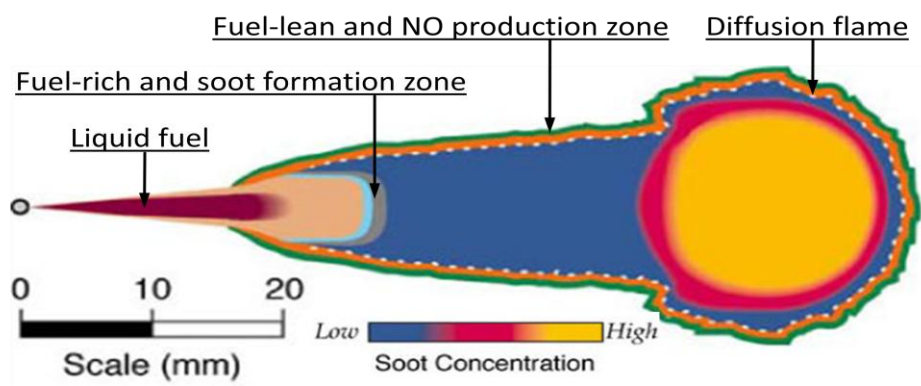


Fig. 1-2 Simulated structure of the diffusion flame (Dec, 1997).

been a long-standing problem that the engine community is still facing.

To improve fuel-air mixing, a variety of strategies have been proposed, including increasing injection pressure, increasing initial fuel temperature, dissolving gases into fuel, and so on. Among them, increasing fuel temperature has been less studied because it is commonly recognized that DF becomes unstable at relatively high temperature. In early 1980s, Hoppie et al. (Hoppie, 1982; Scharnweber, 1984; Scharnweber and Hoppie, 1985) proposed a new concept, called hypergolic combustion, to improve diesel engine combustion. In the hypergolic combustion, DF was heated to high temperatures and pre-vaporized and then injected into the engine chamber. Significant reduction of ignition delay was observed. Their experiments also showed very promising results in terms of emission reduction. However, the engine failed in about half hour due to severe fuel coking in the fuel delivery system.

The new concept proposed by Tavlarides and Anitescu (Tavlarides and Anitescu, 2009) is trying to solve the problem by introducing EGR into DF as diluents to prevent fuel coking. This technology is aimed to both significantly reduce emissions and increase fuel efficiency by innovatively changing the combustion process. A conceptual design of the supercritical fuel delivery system is illustrated schematically in **Fig. 1-3 (bottom)**. For comparison, a schematic diagram of the conventional DF delivery system is shown in **Fig. 1-3 (top)**. In either system, liquid DF is delivered by a transfer pump from the fuel tank through a fuel filter to a fuel pump. The fuel pump increases fuel pressure to a desired value and transports DF to a common rail which is connected to injectors. The common rail is applied to achieve higher injection pressure and a better control. The entire system is controlled by an engine control unit. Different to the conventional design, the new

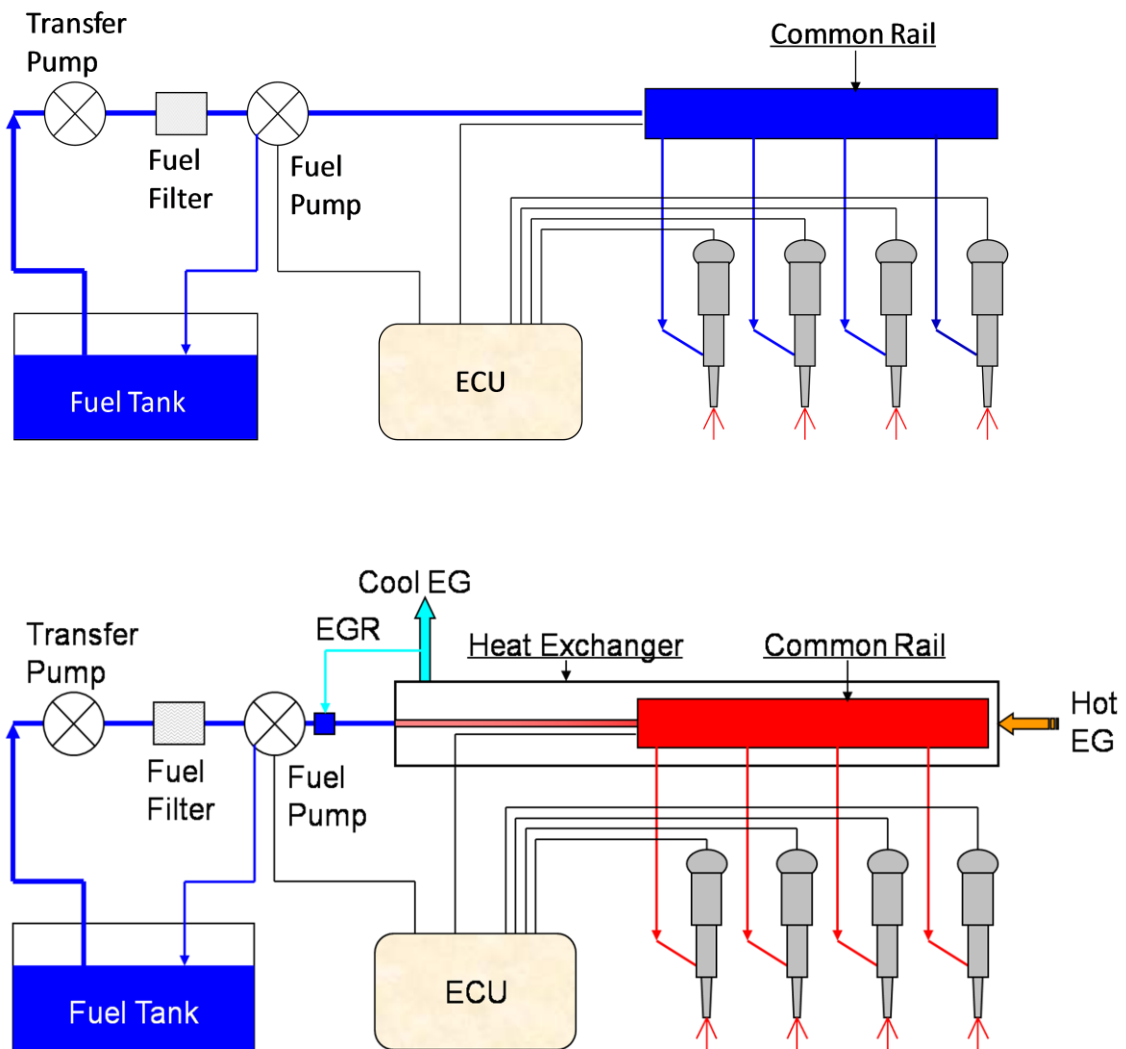


Fig. 1-3 Schematic diagrams of conventional (top) and supercritical (bottom) DF delivery systems in diesel engines. ECU: engine control unit.

concept is characterized by two additional steps, a mixing step where EGR is mixed with DF and a heating step where exhaust gas (EG) is used to heat DF/EGR mixtures to the supercritical state. A heat exchanger is added to the new system to achieve heat transfer from hot EG to the DF/EGR mixture and bring the mixture to the supercritical state. Part of the cool EG out of the heat exchanger is recycled and mixed with liquid DF to dilute the fuel, which is believed to be a practical way of preventing DF coking at high temperature. Compared with conventional liquid DF injection, injection of supercritical fuel mixtures will significantly improve fuel-air mixing due to unique properties of SCFs and hence improve diesel engine efficiency and reduce harmful emissions, simultaneously.

1.4 RESEARCH NEEDS, PROPOSED WORK AND SIGNIFICANCE

Implementation of this new concept and successful development of the technology are associated with critical challenges which could not be tackled without new innovations. These challenges are (1) effective and fast DF/EGR mixture preparation, (2) high-efficiency heat exchanger design, (3) creative injector design to withstand high temperature and high pressure, and (4) measurements and modeling of fuel properties over a wide range of P-T conditions. This dissertation will focus on addressing some issues related to the last challenge.

Fuel properties are needed to enable simulation of DF combustion in diesel engines. These properties include both chemical and physical ones. However, DF is a mixture of hundreds of hydrocarbons and current models are not able to represent all these components. Consequently, simple surrogate fuels of a few components become a

practical choice and have been widely used in engine research and development. A good DF surrogate (DFS) should be able to represent both chemical and physical characteristics. A variety of studies have been conducted to develop detailed kinetic models (Pitz and Mueller, 2010), while relatively less effort has been put on understanding physical properties. These physical properties include density, viscosity, diffusivity, heat capacity, thermal conductivity, surface tension and some others. On the other hand, design and simulation of the supercritical DF combustion system create a special demand for physical properties in the supercritical region, which are usually of less interest in conventional diesel engine designs. Physical properties of DF, DF surrogates and surrogate compounds up to the severe supercritical region are either very limited or have not been reported. Therefore, it is meaningful and necessary to extend the understanding of physical properties.

DF coking is one of the major issues of concern in the development of the supercritical DF combustion technology. It is generally understood that DF becomes unstable when fuel temperature is above ca. 523 K. Higher temperatures will lead to fuel degradation and coking. Fuel degradation has a significant impact on combustion, while fuel coking will plug the delivery system. Since coking is not a major issue in conventional DF delivery systems, the understanding of thermal stability of DF is very limited. Therefore, further studies are required to demonstrate thermal stability and coking behavior of DF in the temperature range of current interest.

Based on the research needs discussed above, the following work is proposed in this dissertation research, as part of the Clean Diesel Combustion Project:

(1) *Development and evaluation of diesel fuel surrogates.* DFSs used in diesel

engine research and development will be analyzed and a new DFS will be proposed. The performance of these DFSs in representing DF will be evaluated by comparing their physical properties. These physical properties include critical properties, volatility, density, viscosity, heat capacity and thermal conductivity. A variety of modeling techniques will be applied to estimate these properties.

(2) ***Diffusivity measurements.*** Diffusivities of DF and surrogate compounds in supercritical CO₂ (SCCO₂) will be measured by using the Taylor dispersion method. Experimental data will be correlated using predictive correlations. Experimental uncertainties will be explored.

(3) ***Thermal stability studies.*** Thermal stability of DF will be investigated in both batch and continuous thermal stressing experiments to demonstrate the effects of temperature, residence time and CO₂ concentration on fuel stability. The temperature and residence time conditions where supercritical fuel delivery can work will be determined. The role of CO₂ in preventing DF coking will be examined and discussed.

Successful execution of the proposed work will greatly expand the knowledge and understanding of DF properties. These results will not only support the development of the novel supercritical DF combustion technology but benefit the entire engine community by providing more comprehensive information for research and development of conventional diesel engines. Also, a better understanding of experimental uncertainties in diffusivity measurements will make a contribution to the improvement of experimental designs.

CHAPTER II

LITERATURE REVIEW

2.1 INTRODUCTION

In this chapter, three topics which are closely related to the proposed work are reviewed. They are strategies for clean diesel combustion, development of diesel fuel surrogates, and thermal stability of fuels. First, previous studies on clean diesel combustion are reviewed with special focuses on the effects of fuel temperature and dissolved gases, hypergolic combustion, and supercritical combustion. Then, latest development on diesel fuel surrogates is outlined and research needs are identified. Finally, thermal stability of fuels is explored. Since studies on DF are limited, some research on jet fuels is also covered in the review. This literature review sets the stage for the proposed work to follow.

2.2 STRATEGIES FOR CLEAN DIESEL COMBUSTION

Since the debut of a prototype diesel engine built by Dr. Rudolph Diesel in 1897, a substantial number of strategies have been proposed over the years to improve engine performance. These strategies may be categorized into several groups: (1) increase in injection pressure, (2) increase in fuel temperature, (3) implementation of aftertreatment units, (4) optimization of engine control systems, (5) exhaust gas recirculation (EGR), (6) dissolved gas enhanced fuel combustion, and some others. Among them, (2) and (6) are closely related to the new concept of supercritical DF combustion. Therefore, previous

studies on the effect of fuel temperature, the effect of dissolved gases, and supercritical fuel combustion are reviewed in this section.

2.2.1 Early studies on the effect of fuel temperature

Investigations on the effect of initial fuel temperature on diesel fuel combustion can be traced back to the 1930s when Gerrish and Ayer (Gerrish and Ayer, 1936) investigated the influence of fuel oil temperature on combustion. Experiments were carried out on a single-cylinder, 4-stroke-cycle, water-cooled, compression-ignition engine operating at 1,500 rpm and at a compression ratio of 13.5. The injection characteristics and spray formation were studied by injecting the fuel oil into the atmosphere. An electric heater was used to heat the fuel oil. Effects of the fuel oil temperature on injection characteristics, the effective ignition delay, combustion, and engine performance were discussed. It was found that with the increasing fuel oil temperature, (a) the injection period and the mean effective pressure were increased, (b) the average rate of injection, the ignition delay time, the rate of pressure rise, and the maximum cylinder pressure were decreased, (c) the power and the thermal efficiency were slightly improved, and (d) the EG was cleaner and the PM was reduced. It was also found that heating the fuel oil improved the engine operation by reducing knock, which was considered to be caused by the change in injection period and rate. The authors also discussed the effect of fuel oil temperature on the fuel compressibility which influenced the start of injection and the fuel spray angle. The effect of fuel oil temperature on fuel composition was not experimentally studied. However, no change in the fuel composition prior to the injection was considered to occur due to small residence time, approximately

12 seconds.

Holmes et al. (Holmes et al., 1953) investigated the effect of vaporization on DF combustion in a turbojet combustion chamber. At air-fuel ratio of 150:1 and fuel pressure of 1.21 and 1.38 MPa (175 and 200 psi), it was found that the combustion efficiency of DF was almost independent of fuel pressure, but improved by preheating the fuel, reaching the maximum value of 90% at around 628 K (670 °F). Experimental data also indicated that the effects of air-fuel ratio and fuel pressure on combustion efficiency were reduced with the increasing DF initial temperature. The increase in combustion efficiency with the increase in fuel temperature was thought to be attributed to the increased and more rapid vaporization of the fuel and increased sensitization of the fuel to oxidation and cracking processes. It was also found that the amount of smoke decreased by preheating the fuel. The investigation confirmed the hypothesis that heating the fuel increases fuel vaporization and fuel-air mixing, reduces soot formation, and improves combustion efficiency.

Reimuller (Reimuller, 1976) patented a fuel pre-vaporization and injection system for internal combustion engines and claimed that the system was able to achieve combustion between the Otto cycle and the Diesel cycle. The liquid hydrocarbon fuel was completely vaporized and superheated in an external fuel boiler partially heated by EG. At the cold start stage, the engine was operated as a conventional gasoline engine by using a carburetor associated with spark ignition.

Spadaccini (Spadaccini, 1976) measured the autoignition characteristics of JP-4, No.2 fuel oil, and No.6 fuel oil at 673-866 K and 0.69-1.65 MPa (6.8-16.3 atm). The results showed that ignition delay decreased with increases in air temperature, air

pressure and fuel temperature. The author also reported that ignition delay was affected by the initial spray characteristics and increased with the nozzle pressure drop, which was explained by the fact that the increased fuel injection pressure forced the fuel spray to collapse and fuel drops to grow and, therefore, ignition delay increased.

2.2.2 Hypergolic combustion

In early 1980s, a new concept called hypergolic combustion was proposed and patented by Hoppie (Hoppie, 1982; Hoppie, 1984). Hypergolic combustion is such an ignition and combustion process that both the ignition delay and the combustion duration are negligible (Scharnweber and Hoppie, 1985). A variety of studies were carried out in the 1980s and early 1990s to understand and develop the new combustion process and a few methods to achieve hypergolic combustion were patented (Hoppie et al., 1987a; Hoppie et al., 1987b; Hoppie et al., 1987c; Hoppie, 1987; Scharnweber et al., 1989).

A mathematical model for predicting ignition delay as a function of initial fuel and air temperatures was developed (Hoppie, 1982). The model was based on the assumption that only fuel molecules in the excited states could react with oxygen and the reaction rate was dependent on concentrations of both oxygen and chemically excited fuel molecules. The concentrations of chemically excited fuel molecules could be increased by means of preheating the fuel. It was shown that the ignition delay could be dramatically reduced if the fuel was sufficiently preheated up to 723 - 873 K.

Scharnweber and Hoppie (Scharnweber, 1984; Scharnweber and Hoppie, 1985) experimentally studied the hypergolic combustion in a reciprocating internal combustion engine by preheating a JP-7 fuel up to about 823 K. The performance of the hypergolic

combustion engine was compared with that of a conventional fuel system with the initial fuel temperature of 302.15 K. It was demonstrated that as the initial fuel temperature approached to the hypergolic combustion temperature, the ignition delay was dramatically reduced, the injection duration and the combustion duration were increased, and the peak cylinder pressure and the rate of pressure rise were decreased. The exhaust smoke emission was also reduced significantly with the increasing initial fuel temperature. The NO_x emission was thought to be reduced under hypergolic combustion since the peak cylinder pressure (and hence peak cylinder temperature) was reduced. However, the engine efficiency was reduced because of long injection duration and resultant later heat release. Another major problem identified by the authors was fuel deposits in the fuel heater, which put a severe restriction to the application of the hypergolic combustion concept.

Min (Min, 1986) developed a mathematical model to optimize the efficiency of the hypergolic combustion engine. The model neglected the mixing delay time and the chemical kinetic delay time. The friction loss was characterized, while the heat loss through the cylinder wall was neglected. The working fluid was assumed to be air and the ideal gas law was applied. The results showed that the optimal efficiency of hypergolic combustion occurred when fuel injection started at approximately 5° crank angle after the top dead center regardless of the amount of fuel injection per cycle. It was also found that the ending of injection varied from approximately 8° to 20° crank angle with the increasing fuel injection amount per cycle. The prediction showed that compared with the OTTO cycle, the hypergolic combustion process would have increase in engine efficiency by up to 10%.

Blank and Shih (Blank and Shih, 1990) extended the hypergolic combustion research work by developing a computational model to characterize fuel injection and combustion in the hypergolic region. Since the reaction rate in hypergolic combustion was thought to be controlled by turbulent mixing rather than chemical kinetics, both turbulent mixing and chemical kinetics were taken into account in the model construction. The k- ϵ model along with continuity, momentum, and energy equations was applied to characterize the engine flow field. Due to the high initial fuel temperature, the fuel-oxygen reactions were assumed to be irreversible and stoichiometric, and only the overall exothermic reactions were considered in the model and characterized by an eddy dissipation combustion model (Magnussen and Hjertager, 1976). The simulations of the compression and combustion strokes were reported. The results showed that the fuel stream significantly affected the flow field and created two recirculation zones above and below the path of the fuel spray. Also, two high temperature regions were observed, which coincided exactly with those two recirculation zones.

In short, both experimental and modeling studies showed that ignition delay decreased significantly with the increasing fuel temperature up to the hypergolic region, which would improve diesel engine performance. Soot formation was found restrained as fuel temperature increased, which is well explained by more homogeneous fuel-lean combustion due to enhanced fuel-air mixing. Since engine maximum pressure was found to decrease with increasing fuel temperature, it is reasonable to conclude that NO_x would reduce with increasing fuel temperature. Engine efficiency, however, was slightly reduced due to the increasing injection and combustion durations. The main challenge that hinders the implementation of the hypergolic combustion is DF coking. Further

investigations, both experimental and modeling, are needed to address this issue.

2.2.3 Dissolved gas enhanced spray atomization and fuel combustion

2.2.3.1 Studies by Huang and coworkers

Huang and coworkers from Shanghai Jiaotong University, China and Gunma University, Japan have done extensive work to understand the effects of dissolved gases on fuel spray atomization and combustion. Some of their work are summarized below.

Huang et al. (Huang et al., 1994a) investigated the effect of dissolved CO₂ on atomization of DF sprays at a constant injection pressure of 5 MPa. Two CO₂ concentrations, 2.23 and 13.3 wt%, were investigated and the pressure characteristics inside injector nozzles were analyzed. It was concluded that the combined effects of pressure characteristics and dissolved CO₂ enhanced DF spray atomization.

Huang et al. (Huang et al., 1994b) further studied the effects of gas concentration, injection pressure, and nozzle geometry (L/D ratio, where L and D are the length and the diameter of the orifice, respectively.) on fuel spray atomization. An optimal gas concentration was observed for certain nozzle geometry. When the gas concentration was below the optimal value, the spray angle increased gradually, while the Sauter mean diameter (SMD) decreased dramatically. When the gas concentration was above that value, the large spray angle remained almost constant and the SMD tended to be constant as well. At low L/D ratio (L/D = 4), the dissolved gas demonstrated a negative effect on spray atomization characterized by a small spray angle and a slightly increased SMD. The beneficial effect of the dissolved gas was realized at high L/D ratio (L/D ≥ 10). Thus, it was concluded that the dissolved gas could improve spray atomization only when the

dissolved gas concentration was above the transition point and the L/D ratio was relatively high (Huang et al., 1994). Xiao et al. (Xiao et al., 2004) confirmed the finding by demonstrating a transitional CO₂ concentration between 2.72% and 10.59%.

Shiga et al. (Shiga et al., 1994) investigated the effects of gas type, L/D ratio, and nozzle configuration on fuel atomization behavior. It was found that N₂ had a more significant effect than CO₂ on the SMD. The sensitivity of dissolved-gas effect was strongly dependent on the L/D ratio, which was related to the residence time. Nozzle configurations were also shown to have influence on spray atomization. Significant effects of L/D ratio on SMD were also reported elsewhere (Shiga et al., 1997).

Huang et al. (Huang et al., 1996) investigated the effect of dissolved gases (air or CO₂) on diesel engine combustion and emissions. Engine experiments showed that with the addition of dissolved gases, the ignition delay was longer, the peak pressure was reduced, and the peak heat release rate was lowered. These phenomena were suggested to be the consequence of reduction in local gas temperature and local oxygen concentration due to CO₂ release upon injection. It was also shown that injection of DF containing dissolved CO₂ significantly reduced NO_x emission and slightly reduced CO and PM levels, while injection of fuel containing air halved PM and CO emissions. It was therefore concluded that injection of DF with dissolved gases would have a potential to reduce NO_x and PM simultaneously.

Xiao et al. (Xiao et al., 2008) investigated flame characteristics of DF jets containing dissolved CO₂. Experiments were carried out under atmospheric conditions with injection pressures of 4 and 6 MPa and CO₂ mass fractions from 0 ~ 17.82 wt%. It was shown that as the CO₂ mass fraction increased, the flame penetration decreased, the

low temperature flame length increased, and the mean flame temperature increased initially and then decreased. The authors argued that the effect of dissolved CO₂ on flame characteristics and emission reduction could be a combination of atomization improvement, the dilution effect, the thermal effect, and the chemical effect.

2.2.3.2 Studies by Senda and coworkers

Senda and co-workers from Doshisha University also made great contribution in advancing the understanding of the mechanisms of dissolved gas enhanced fuel spray atomization and combustion (Senda et al., 1999; Senda et al., 2008). Their studies were based on the understanding of flash boiling phenomena (Senda et al., 1994). By adding CO₂, they argued, reduction of emissions could be achieved through the internal EGR effect of CO₂ and through flash boiling of CO₂ upon injection. Some of their work are summarized below.

Fujimoto et al. (Fujimoto et al., 1995) injected n-tridecane with dissolved CO₂ into quiescent atmosphere of different pressures and found that the spray break-up length decreased with increasing CO₂ mole fraction. They also found that ambient pressure had a significant effect on spray core angles when fuel temperature and CO₂ mole fraction were high. The experimental findings were confirmed by the thermodynamic analysis. The authors finally proposed two models of evaporation of fuel spray containing dissolved gases, the separation and diffusion model and the flash boiling model.

Senda et al. (Senda et al., 1997) conducted combustion experiments in a rapid compression and expansion machine to investigate the effect of dissolved CO₂ in fuel oil (n-tridecane) on NO and soot emissions. It was found that when CO₂ was dissolved in the

fuel, the ignition delay, the combustion period, and the flame temperature decreased. NO and soot emissions could be reduced by 30% at CO₂ mole fraction of 0.6. Similar results were reported elsewhere (Senda et al., 2000). Those results implied that gas separation or flash boiling of CO₂ could simultaneously reduce NO (low flame temperature by improving spray atomization and vaporization) and soot (from relative lean and homogeneous mixture) emissions and increase engine efficiency (reduce combustion period).

Senda et al. (Senda et al., 1997) further studied spray characteristics by dissolving N₂ into n-tridecane. It was found that dissolved N₂ in fuel brought a negative effect on spray atomization, which was believed to be the result of the increase in viscosity due to the formation of bubbling flow inside the spray.

Senda et al. (Senda et al., 2000) extended the fuel design concept by mixing a DF component (n-tridecane) with a gasoline component (n-hexane and n-pentane). It was found that by mixing with n-pentane, total hydrocarbon (THC) and CO emissions increased, while NO_x emission reduced, and that by mixing with n-hexane, n-hexane evaporated first at low temperature and n-tridecane evaporated later. Flash atomization of binary hydrocarbon fuels was also reported by other investigators (Gemci et al., 2004; Zhang et al., 2005).

Senda et al. (Senda et al., 2000) modified the flashing spray model (Senda et al., 1994) to estimate the vaporization process of fuel containing dissolved CO₂. The model estimation showed that flash boiling could be realized for CO₂ mole fraction of 0.6-0.8 at fuel temperature of 383 K and ambient temperature from 1.1-2.0 MPa. The flash boiling model was further modified and implemented into KIVA-3V for numerical simulation

(Kawano et al., 2004; Kawano et al., 2006). More information on atomization models for flash boiling sprays can be found elsewhere (Zeng and Lee, 2001).

2.2.3.3 Studies by others

Solomon et al. (Solomon et al., 1982) investigated injection and combustion properties of Jet A fuels containing dissolved air. Rashkovan et al. (Rashkovan et al., 2004a; Rashkovan et al., 2004b) and Rashkovan and Sher (Rashkovan and Sher, 2006) experimentally investigated atomization behavior of gasoline containing dissolved CO₂. It was observed that the dissolved CO₂ not only affected the spray core angle and the SMD but also improved the droplet volume fraction distribution and reduced the amount of large diameter droplets.

Merkisz et al. (Merkisz et al., 2007) recently proposed a new concept of improving fuel spray in diesel engines by dissolving EGR or air in fuel oil. The mechanism is based on the different solubility of gases in fuel oil under different pressures. Due to a strong pressure gradient upon the injection, the dissolved gas releases spontaneously from the fuel, causing fuel droplets bursting from the outside. Fuel injection and combustion were visualized using a digital video system by injecting fuel oil with dissolved gas into an open chamber at atmospheric pressure. The fuel solution was prepared in a high pressure cylinder pump and then pumped to a high pressure accumulator. The volumetric fraction of CO₂ in EG was 4%, 8%, and 10% and the injection pressure was from 30-70 MPa. It was found that fuel atomization was significantly affected by dissolved gases.

In addition to experimental and modeling studies, several methods using dissolved gases to improve fuel atomization and combustion were patented (Gurin et al.,

2006; Nielsen, 1992; Schefer and Keller, 2007).

In summary, studies on injection and combustion of fuel containing dissolved gases (CO₂, N₂, and air) were reviewed and the following conclusions can be made:

- [1] Under optimal conditions, the presence of dissolved gases significantly influenced spray behavior by increasing spray core angles and reducing spray penetrations and the SMD;
- [2] Nozzle configuration, mainly L/D ratio, affected spray behavior due to the relatively slow bubble growth rate.
- [3] There existed a critical concentration of dissolved gases, below which the negative effect dominates.
- [4] Injection and combustion of fuel containing dissolved gases had the potential to reduce NO_x and PM, simultaneously. However, CO and THC emissions have been seldom examined and reported.
- [5] Although there were discussions on the mechanism of emission reduction by the addition of dissolved gas, more experimental work needs to be done to verify it.
- [6] Few engine experiments were carried out to verify the concept of injecting and combusting fuel containing dissolved gases and the conditions of those experiments were usually away from real diesel engine conditions.

2.2.4 Supercritical fuel combustion

More recently, new concepts were proposed and examined to achieve cleaner, more efficient fuel combustion by injecting and combusting fuels in the supercritical state. Haldeman et al. (Haldeman et al., 1999) invented a supercritical fuel system potentially

used for internal combustion engines, turbine engines or other burners. The supercritical fuel was a mixture of 5-50 % water and a hydrocarbon fuel. The inventors further described the suitable condition where the mixture reached near the critical point and achieved a homogeneous single phase. A suitable temperature was 673 K and a suitable pressure was 27.58 MPa (4000 psi). Haldeman (Haldeman, 2002) filed another patent application which detailed the process to form water-fuel mixtures. The temperature and pressure ranges for water-fuel mixtures were 477 – 699 K and 1.38 – 34.47 MPa (200-5000 psig), respectively. The hydrocarbon fuels could be No. 2 diesel, No. 1 kerosene, No. 6 fuel oil, and gasoline. The inventor also claimed that the energy for heating water, fuel, and the water-fuel mixtures was recovered from hot exhaust gases. Except for the verbal description of the system, however, the benefits of injecting and combusting fuels in the supercritical state were not detailed.

Ahern et al. (Ahern et al., 2001) experimentally confirmed a single phase, homogeneous water-DF mixture near the critical point of water. Combustion of the mixture under atmosphere spray conditions resulted in very low NO_x, smoke, CO and unburned hydrocarbon emissions. Tests were further conducted in a single cylinder direct injection diesel engine equipped with an electronically controlled common rail injection system and a modified injector to operate at temperature above 623 K. Preliminary results demonstrated an 85% decrease in NO_x emission and a virtual elimination of smoke.

Tavlarides and Anitescu (Tavlarides and Anitescu, 2009) invented a supercritical fuel system using EGR or CO₂ as diluents. Suitable temperatures and pressures were greater than about 573 K and 10 MPa, respectively, and the molar fraction of diluents in DF is from 0-0.9. The inventors claimed that delivery of the DF-diluents mixture in the

homogeneous single-phase supercritical state provided a significant increase in engine efficiency and a reduction of harmful emissions including PM, aldehydes, polyaromatic hydrocarbons (PAHs), CO, NO_x, and SO_x.

Cheiky and Grottenthaler (Cheiky and Grottenthaler, 2010) invented a fuel injector which could provide more efficient fuel combustion within internal combustion engines. The fuel injector achieved efficient fuel combustion by (i) fast and responsive actuation, (ii) heating the fuel to a supercritical temperature, (iii) maintaining the fuel at a supercritical pressure, and (iv) using a catalyst in the oxidization of the fuel. A heating element was used to heat the fuel to a supercritical temperature. This technology is currently under commercialization for gasoline engines.

These new concepts involve preheating fuels to the homogeneous supercritical state and injecting and combusting the supercritical fuel in a supercritical environment. Besides, Haldeman et al. (Haldeman et al., 1999) and Tavlarides and Anitescu (Tavlarides and Anitescu, 2009) proposed to use diluents to either prevent coking or reduce harmful emissions, while Cheiky and Grottenthaler (Cheiky and Grottenthaler, 2010) proposed to use a catalyst to pre-oxidize the fuel. Realization of these new concepts relies on not only innovations in engine R&D but also a better understanding of fundamental physical and chemical processes occurring under supercritical conditions.

Krishnan (Krishnan, 1992) studied the heat transfer characteristics in supercritical jet fuel flows using modeling techniques. Numerical simulations captured considerable augmentation of heat transfer near the critical point. Results also showed that large density variation across the critical point had a significant impact on the velocity and temperature profiles near the wall. Others also reported deterioration of heat transfer at

supercritical pressures (Giarratano and Jones, 1975; Kao et al., 2010; Kelbaliev, 2001; Koshizuka et al., 1995; Mokry et al., 2010; Pioro et al., 2004; Shiralkar and Griffith, 1969).

Chen (Chen, 1994) investigated the transport phenomena during the injection of supercritical jet fuels into a subcritical environment and found that the supercritical sprays exhibited flashing-like atomization. Ervin et al. (Ervin et al., 2000) studied jet fuel flow characteristics within a nozzle under supercritical conditions. The authors observed a gas-like fluid rather than a multitude of droplets exiting the nozzle under supercritical conditions and concluded that the injection and mixing mechanisms occurring under supercritical conditions were very different from those occurring under subcritical conditions. Dounghip et al. (Dounghip et al., 2002) examined spray behavior of supercritical jet fuels injected into a supercritical environment using both the Schlieren imaging technique and CFD simulations. It was concluded that the fuel exit temperature and mass flow rate influenced jet penetration and spreading angle. It was also found that under the same fuel mass flow rate and pressure conditions, the penetration depth of a supercritical jet was less than that of a subcritical jet. Jensen et al (Jensen et al., 2004) studied injection of subcritical and supercritical jet fuels into subsonic cross flow and concluded that at the same mass flow rates, the penetration depth was greater for the supercritical fuel injection compared to the subcritical one, which contradicts Dounghip et al.'s findings (Dounghip et al., 2002). Further investigations are necessary to resolve the contradictory. Studies on injection of cryogenic liquids at subcritical and supercritical pressures also showed that jets injected at supercritical pressures behave like turbulent gas jets rather than subcritical liquid jets (Oschwald et al., 2006).

Fan and Yu (Fan and Yu, 2006) studied supersonic combustion of supercritical

kerosene and demonstrated that under the similar stagnation conditions and kerosene equivalence ratios, the combustion efficiency using supercritical kerosene injection conditions increased ca. 10-20% compared to that using liquid kerosene injection.

Others have studied injection of liquid fuels into supercritical environments and discussed unusual spray atomization and droplet vaporization behavior (Bellan, 2004; Edwards, 2008; Kulkarni and Neches, 1994; Yang et al., 1996; Yang, 2000).

In a summary, previous studies on fuel injection under supercritical conditions were mostly focusing on injection of liquid fuels into supercritical conditions, injection of supercritical fuels into subcritical conditions, and understanding of droplet atomization and vaporization under supercritical conditions. Fundamental studies on injection of supercritical fuels into supercritical conditions are very rare and benefits of supercritical fuel combustion have not been well documented. Thus, more investigations on these topics are needed.

2.3 DEVELOPMENT OF DIESEL FUEL SURROGATES

Development of modern diesel engines relies largely on numerical simulations to minimize the number of very expensive, hardworking experimental tests. Simulating DF combustion in diesel engines requires a thorough understanding of both chemical kinetic models and physical properties of DF. DF is a complex mixture of hydrocarbons with carbon numbers spanning mainly from 10 to 20. DF composition is usually determined by performance needs (e.g., cetane number) and varies considerably by refining processes and feedstock. A typical composition of DF given by volume is roughly 41% paraffins, 30% cycloparaffins, and 29% aromatics, or by weight 39% paraffins, 44% cycloparaffins,

and 17% aromatics (Seshadri, 2003). Current modeling and simulation technologies are not able to identify all chemical species and to describe the detailed reaction mechanisms. Thus, it is necessary and important to find a practical way to model DF. This ends up with DFSs or reference fuels. Nowadays, DFSs are always needed at some stages in the engine design and testing processes. Although current DFSs are unable to address all needs for diesel engine combustion simulations, investigations based on DFSs facilitate deeper insights into diesel combustion processes and are crucial to modern engine research and development. A comprehensive review on recent progress in the development of DFSs can be found elsewhere (Pitz and Mueller, 2010).

A DFS is defined as a surrogate composed of a small number of pure compounds whose behavior matches certain characteristics of DF (Pitz and Mueller, 2010). A properly composed DFS should share nearly the same chemical kinetics and thermophysical properties as the real DF (NIST, 2003). Extensive work has been accomplished on the development of chemical kinetic models of DFSs, while investigations on fuel properties for engine applications have attached relatively less importance. A number of reviews on the development of chemical kinetic models of DFSs are available in the literature (Cathonnet, 1994; Miller et al., 1990; Simmie, 2003; Westbrook and Dryer, 1984; Westbrook, 2000).

In response to the increasing needs for combustion process optimization and other key issues, the National Institute of Standards and Technology (NIST) organized in 2003 a workshop entitled “Workshop on Combustion Simulation Databases for Real Transportation Fuels” (NIST, 2003). From that workshop, six chemical classes with specific model compounds as shown in **Table 2-1** were identified to be necessary to

Table 2-1 Six classes of hydrocarbons and their model compounds necessary to simulate real transportation fuels (NIST, 2003).

| Chemical Classes | Specific Model Compounds |
|-------------------------|---------------------------------|
| Iso-paraffins | Iso-octane |
| Normal paraffins | Heptane, Hexadecane, Decane |
| Single-ring aromatics | Toluene, Xylenes |
| Cyclo-paraffins | Methylcyclohexane |
| Olefinic species | 1-pentene |
| Multi-ring aromatics | 1-methylnaphthalene |

describe the complex hydrocarbon chemistry of real transportation fuels and suggested to be implemented in combustion simulations of real fuels. These chemicals include normal-, iso- and cyclo-paraffins, single- and multi-ring aromatics, and olefinic species. For petroleum-based DF, the primary chemical classes are n-alkanes, iso-alkanes, cyclo-alkanes and aromatics (Pitz and Mueller, 2010), as shown in **Fig. 2-1**.

Due to a similar cetane number as DF which is approximately 56, n-heptane is the compound that has been mostly used as a DFS in the testing and modeling of DF combustion in conventional diesel engines. A detailed chemical kinetic model of n-heptane oxidation was reported by Curran et al. (Curran et al., 1998). The model includes 550 chemical species and 2450 reactions. Because of computational and simulation difficulties, reduced kinetic mechanisms of n-heptane are more practical and have mostly been used (Belardini et al., 1996; Curran et al., 2001; Huang and Su, 2005; Kim et al., 2002; Noel et al., 2004; Xi and Zhong, 2006).

Another surrogate of great interest is n-hexadecane which is a key component of diesel fuel and has similar molecular weight to DF. Ristori et al. (Ristori et al., 2001) reported a detailed chemical kinetic model of n-hexadecane, consisting of 242 species and 1801 reactions. Simulation results using this model agreed well with experimental data obtained from a jet-stirred reactor at 1000-1250 K and 0.1 MPa. Fournet et al. (Fournet et al., 2001) generated a detailed mechanism for n-hexadecane by using a computer package called EXGAS. Although n-hexadecane is thought to be a good surrogate of diesel fuel, however, very few studies of diesel fuel combustion have done by using n-hexadecane as a surrogate due to the lack of experimental data for n-hexadecane oxidation.

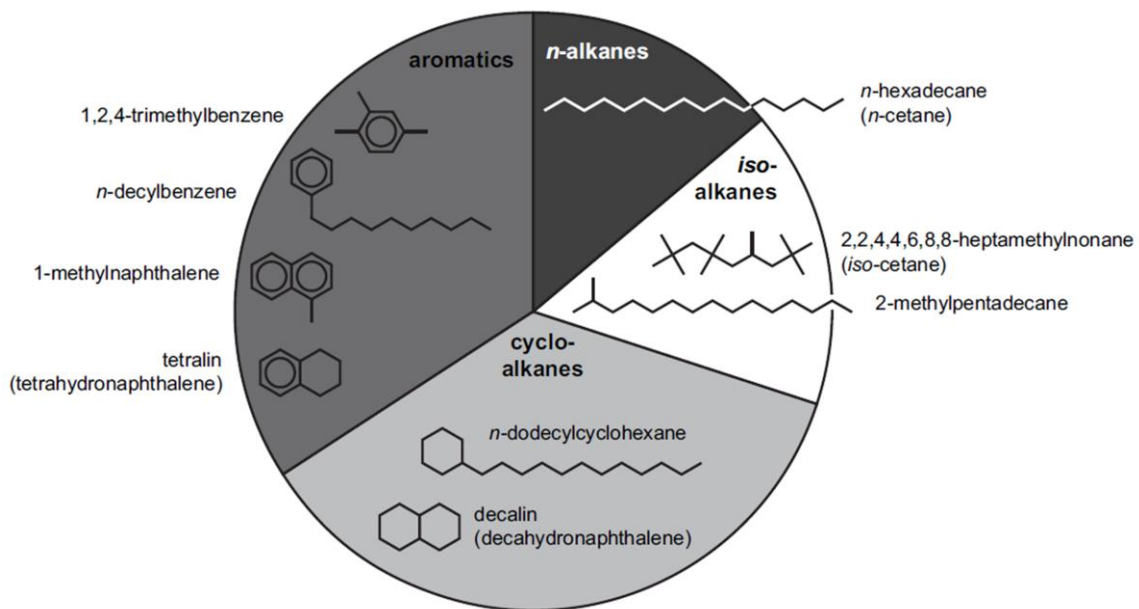


Fig. 2-1 Relative amounts of various chemical classes in diesel fuel and possible compounds to represent these chemical classes in a diesel surrogate fuel (Pitz and Mueller, 2010). Reproduced with Elsevier's permission (attached in Appendix E).

DF contains two-ring cycloalkanes and aromatics and some three-ring aromatics. Although the percentages of these multi-ring compounds are pretty low, they have an important impact on soot formation. Thus, aromatic surrogates have been included in modeling diesel fuel combustion kinetics. Toluene, a product of benzene alkylation, has been mostly added to the reaction mechanisms of n-heptane to simulate diesel fuel behavior (Gustavsson and Golovitchev, 2003; Hernandez et al., 2008). Other aromatics used by some investigators include α -methyl-naphthalene (Barths et al., 2000) and n-propylbenzene (Dagaut, 2002). A summary of DFS chemical kinetic models is given in **Table 2-2**.

Physical properties of these DFSs were less discussed in the literature. These properties include density, viscosity, heat capacity, surface tension, diffusivity, ignition delay, cetane number, and others. Although investigations show that surrogates could reasonably reproduce combustion behavior of diesel fuel in diesel engines, effects of these properties on fuel combustion are less understood.

2.4 THERMAL STABILITY OF FUELS

Thermal stability of a fuel is defined as the capability of the fuel to withstand high temperature stress in a reasonable time period without noticeable deterioration (Batts and Fathoni, 1991). Such deterioration may include color change, formation of coke and solid deposits, change in physical properties, change in chemical properties, change in combustion properties, etc. Previous studies on thermal stability of fuels including diesel fuel and jet fuels and other oils have been mostly focused on formation of solid deposits and on understanding of the mechanisms. Several reviews on this topic can be found

Table 2-2 Chemical kinetic models of DFSs.

| DFSs | # of Species | Reactions | References |
|--|---------------------|------------------|------------------------------------|
| Dodecane | 32 | N/A | (Sahetchian et al., 1995) |
| N-heptane | 550 | 2450 | (Curran et al., 1998) |
| N-hexadecane | 242 | 1801 | (Ristori et al., 2001) |
| N-hexadecane Iso-octane N-propylcyclohexane N-propylbenzene | 298 | 2352 | (Dagaut, 2002) |
| Iso-octane | 860 | 360 | (Curran et al., 2002) |
| Tetradecane | N/A | N/A | (Hamosfakidis and Reitz, 2003) |
| N-heptane, toluene | 68 | 278 | (Gustavsson and Golovitchev, 2003) |

elsewhere (Batts and Fathoni, 1991; Edwards, 2006; Edwards and Zabarnick, 1993; Maurice et al., 2001; Strauss, 1992).

Solid deposit accumulation inside the DF delivery systems due to fuel coking is one major barrier to the development of high temperature fuel delivery systems. Delivery of DF under supercritical conditions requires the fuel to be heated up to more than 673 K which is much higher than the fuel temperature encountered in conventional diesel engines. Previous studies have demonstrated the serious issue caused by fuel coking that led to the failure of the hypergolic combustion system (Scharnweber, 1984). Therefore, a better understanding of fuel thermal stability is required to facilitate the development of the supercritical fuel combustion technology.

A literature survey shows that thermal stability of DF, especially at relatively high temperature, has not been well explored, because fuel stability is not a big issue in design and development of conventional diesel engines. Studies on solid deposit formation in engine chambers are not reviewed because they involve high temperature reactions in air environment. Except a few papers discussing thermal stability of DF below 423 K which is not of interest to this study (Bacha and Lesnini, 1997; Banavali and Chheda, 2000; Kalitchin et al., 1997; Schwab et al., 2000; Stavinoha et al., 1986), only three papers were found discussing thermal stability of DF at relative high temperatures (Anitescu et al., 2009; Beal and Hardy, 1994; Nickolaus and Lefebvre, 1987). Nickolaus and Lefebvre (Nickolaus and Lefebvre, 1987) studied thermal stability of DF and the effect on spray characteristics. Experiments were conducted in a flow system equipped with an injector at 590 K and 2.07 MPa. It was found that the nozzle pressure drop decreased initially and then increased. Black deposits were observed. Beal and Hardy (Beal and Hardy, 1994) applied

the quantitative gravimetric Jet Fuel Thermal Oxidation Tester to the thermal stability study of DF. They found that thermal stressing of DF at 533 K and 3.4 MPa for 6 seconds for duration of 2.5 hours resulted in significant solid deposit formation. Anitescu et al. (Anitescu et al., 2009) studied phase transition and thermal behavior of DF-diluents mixtures at temperatures and pressures up to 750 K and 60 MPa, respectively. It was found that for both n-hexadecane and No.2 DF, thermal decompositions lowered when diluents were added.

Studies on thermal stability of other petroleum fuels such as jet/aviation fuels are beneficial to the understanding of thermal stability of DF. Some researchers (Beaver et al., 2005) proposed that the mechanisms of deposit formation due to thermal oxidative reactions for both DF and Jet fuels are mechanistically similar and that the chemistry involved in deposit formation from both storage and thermal oxidative reactions in middle distillates is generally similar.

Thermal stability of jet fuels has been extensively investigated since the 1960's with the interest in developing high thermally stable jet fuels to be used in high-speed aircraft. Experimental methods applied in those studies can be grouped into three general categories: static tests, dynamic tests, and full-scale fuel system simulators (Batts and Fathoni, 1991); the former two methods have been mostly used. Experiments have been conducted over a broad temperature range covering the supercritical region to identify and understand variables that affect and control fuel degradation and solid deposit formation. Such variables can be classified into two groups: (1) fuel-related variables (or chemical variables) including fuel type (Edwards and Atria, 1995; Taylor, 1974), fuel processing/treatment (Gül et al., 2005), fuel composition (Balster et al., 1996; Eser et al., 2006;

Gül et al., 2006), oxygen/sulfur/nitrogen contents (Edwards and Liberio, 1994; Edwards and Atria, 1995; Ervin et al., 1998; Stewart, 1999; Taylor, 1974; Venkataraman and Eser, 2008; Yu and Eser, 1997a; Yu and Eser, 1997b), and fuel additives (Edwards and Atria, 1995) and (2) operating variables (or physical variables) including temperature (Pande et al., 2001; Taylor, 1974; Yu and Eser, 1997a; Yu and Eser, 1997b), pressure (Gül et al., 2005; Taylor, 1974; Yu and Eser, 1997a; Yu and Eser, 1997b), heat flux (Linne et al., 1997), flow regime (Hazlett, 1992), test duration (Hazlett, 1991), and heated wall characteristics (Edwards and Atria, 1995; Eser et al., 2006; Stiegemeier et al., 2002). The mechanisms of solid deposit formation in jet fuel systems have been explored and extensively discussed in the literature (Altin and Eser, 2004; Beaver et al., 2005; Chin and Lefebvre, 1992; Edwards and Zabarnick, 1993; Hazlett, 1991; Hazlett, 1992; Song et al., 1993; Venkataraman and Eser, 2008). Major findings from previous studies on thermal stability of Jet fuels are summarized below.

Thermal decomposition leading to solid deposition is governed by free-radical chemistry including autoxidation by dissolved oxygen and pyrolysis if oxygen is absent or is depleted by reaction at lower temperature (Hazlett, 1991). Thermal decomposition of jet fuels as well as other hydrocarbon fuels falls into three different regimes (Chin and Lefebvre, 1992):

- a. Thermal oxidation or autoxidation reaction regime: At $T < 573$ K, decomposition occurs by autoxidation reactions and increases with increasing fuel temperature. The temperature range of this regime largely depends on fuel properties. It was also reported that deposition began at 533 K and became worse up to 598-673 K (Hazlett, 1992).
- b. Transition regime: At $T = 573-773$ K, both autoxidation and pyrolysis reactions

contribute to decomposition and the rate of decomposition decreases with increase in fuel temperature. The decrease in the rate of decomposition might be due to the transition between the liquid phase and the supercritical phase which enhanced solvent capability (Taylor, 1974) or due to depletion of hydroperoxides (Hazlett, 1992).

- c. Pyrolysis reaction regime: At $T > 773$ K, direct pyrolysis dominates, and decomposition is enhanced as fuel temperature increases. There are two different routes that lead to the formation of solid deposits: decomposition of hydrocarbons to elemental carbon and hydrogen; polymerization/condensation of aromatics to form PAHs, also called carbonaceous deposits (Altin and Eser, 2004).

Oxygen is the driving force for low temperature thermal oxidative reactions and has a significant effect on deposit formation. Removal of oxygen can dramatically lower the rate of deposit formation (Taylor, 1974) or even eliminate the thermal oxidative surface deposition (Edwards and Liberio, 1994), leading to a more stable fuel that can be heated up to relatively high temperatures (around 773 K) before significant coking occurs (Ervin et al., 1998; Stewart, 1999). The impact of oxygen content on pyrolytic deposition has not been well understood. It was reported that the absence of dissolved oxygen could lead to increased surface deposition in the pyrolytic region probably due to the oxidative products (alcohols, aldehydes, etc) acting as radical scavengers or hydrogen donors (Edwards and Liberio, 1994). It was also reported, however, that deoxygenation had little effects on pyrolytic deposition (Edwards and Atria, 1995). Oxygen content also affects deposit morphology (Hazlett, 1991).

Hydroperoxides are the key intermediaries and play a crucial role in deposition.

Decomposition products of hydroperoxides appear to be important in the path to highly polar oxidation products with limited solubility (Hazlett, 1991; Hazlett, 1992). Aromatic and heteroaromatic compounds are also significantly involved in deposit formation (Hazlett, 1992).

Pressure exhibited a complicated effect on deposit formation (Taylor, 1974). Much of available data found no change or less deposition as pressure increased (Hazlett, 1992). Below the critical pressure, conversion increased as pressure increased; above the critical pressure, conversion decreased with increasing pressure. The large changes in product distributions with pressure occurred in the near-critical region (Yu and Eser, 1997a; Yu and Eser, 1997b), which was possibly due to unusual, high solubilities (Hazlett, 1992). However, recent study showed that the supercritical environment promotes unique reaction mechanisms and is necessary for the formation of large PAH deposits (Somers et al., 2007).

Much work on thermal oxidation stability has shown that trace amounts of sulfur and nitrogen compounds and other contaminants such as metals significantly enhance fuel degradation and are of major importance in deposition (Gül et al., 2006; Song et al., 1993). These elements were found in large concentrations in deposits compared to fresh fuels (Hazlett, 1991). A recent study showed that nitrogen and sulfur compounds were presented only in the liquid-phase product, but not in the solid phase deposits, indicating that they did not aggregate during solid formation (Venkataraman and Eser, 2008). In the pyrolysis regime, the gross hydrocarbon composition other than sulfur and nitrogen compounds played a key role in determine fuel stability (Song et al., 1993).

The nature and amount of carbonaceous deposition from the thermal decomposition of jet fuel were determined to be dependent on the substrate properties

and jet fuel composition (Eser et al., 2006). It was reported that stainless steel tubes formed more deposits than aluminum tubes (Hazlett, 1992). This result is probably due to the catalytic behavior of iron and iron-based alloys during carbon oxidation (Eser et al., 2006). Contradictorily, the deposit formed by reactions in the liquid phase and the surface played a negligible role in deposit formation (Venkataraman and Eser, 2008).

2.5 SUMMARY

Fuel temperature has a significant effect on fuel spray and combustion, and increase in fuel temperature leads to simultaneous reduction of PM and NO_x emissions. However, fuel coking at high temperature caused the failure of the hypergolic combustion system and restricts the implementation of high temperature fuel injection in diesel engines. Dissolved gases have demonstrated positive impacts on emission reductions in diesel engines. The clean diesel combustion technology using supercritical fluids proposed and under development at Syracuse University is a promising technology that incorporates both the high temperature effect and the dissolved gas effect and refines current technologies into a unique design that is simultaneously clean and efficient. However, the role of dissolved gases in preventing fuel coking needs to be further addressed.

As DF is complex hydrocarbon mixtures, simplified DFSs are often used in diesel engine research. A good DFS should represent DF both chemically and physically and be able to reproduce various characteristics of DF combustion. A variety of DFSs have been proposed, most of which are focusing on addressing chemical aspects of DF. Physical aspects of DFSs, e.g. thermophysical properties, were seldom addressed. Further studies

on this topic are necessary to advance the understanding of DFSs.

Fuel stability is one major issue that must be addressed in the development of the supercritical fuel combustion technology. However, limited work on thermal stability of DF could be found in the literature. Extensive work on jet fuels has revealed that two different mechanisms are involved in fuel degradation depending on fuel temperature, which is helpful to advance the understanding of thermal stability of DF.

CHAPTER III

DIESEL FUEL SURROGATES

3.1 INTRODUCTION

DF is a complex mixture of hundreds of hydrocarbons, while a DFS is composed of a small number of pure compounds to mimic certain characteristics of DF. These characteristics include both chemical characteristics (ignition behavior, molecular structure, flame temperature, etc.) and physical characteristics (volatility, density, viscosity, surface tension, diffusivity, heat capacity, thermal conductivity, etc.) (Pitz and Mueller, 2010). No single surrogate or surrogate mixture is able to account for all aspects of DF properties and to meet all requirements for modeling and simulation of the diesel fuel spray and combustion processes in diesel engines. Different surrogates are usually proposed for different applications. While these surrogates may have a good representation of DF chemically, the role of them in predicting physical properties has been less discussed. Therefore, it is necessary and valuable to evaluate DFSs in terms of the capability of predicting physical properties of DF.

In this chapter, DFSs used in previous studies are summarized and one DFS is proposed. The performance of these DFSs in predicting DF properties were evaluated. These properties are volatility, critical properties (T_c , P_c), and other thermophysical properties including density, viscosity, heat capacity and thermal conductivity. Volatility characterizes the tendency of a fuel to vaporize, which plays a significant role in fuel spray, atomization, and vaporization processes. Critical properties are key constants used

in many equations of state (EOS) and correlations to determine phase behavior and other thermophysical properties. Density, viscosity, heat capacity, and thermal conductivity are also major thermophysical properties required in the design and simulation of DF delivery and combustion processes.

Various techniques were applied to measure or estimate properties of DF and DFSs. Volatility was measured using the thermal gravimetric analysis (TGA) method (Li et al., 1996). Critical properties of DFSs were either obtained from literature or estimated using estimation techniques, depending on DFS compositions. Critical properties of DF were estimated using different correlation methods. Density, viscosity, heat capacity and thermal conductivity of DFSs were obtained from NIST databases (Ely and Huber, 2007; Lemmon et al., 2010), while those of DF were calculated using correlations based on experimental data (Kolev, 2007).

3.2 DEVELOPMENT OF DIESEL FUEL SURROGATES

A number of DFSs have been developed and used in previous studies. A summary of these surrogates is presented in **Table 3-1**. DFS-1 to DFS-5 are one-component surrogates selected from n-alkanes. N-alkanes were first selected as DFSs probably because alkanes are major components of DF and reaction mechanisms of n-alkanes were better understood than those of chemicals from other groups. With the advancement in studies on reaction mechanisms and kinetics, more compounds have been included in DFSs. DFS-6 to DFS-8 are two-component surrogates composed of 70% of n-alkanes and 30% of aromatic compounds by volume. Aromatics are added because they have great influence on soot formation. DFS-9 is a mixture of four compounds from n-alkane,

Table 3-1 Components and compositions of diesel fuel surrogates.

| DFSs | Components | Wt% | Vol% | Mol. Frac. | References |
|--------|-----------------------------------|------|------|------------|--|
| DFS-1 | n-heptane | 100 | 100 | 1.0 | (Curran et al., 1998) |
| DFS-2 | n-decane | 100 | 100 | 1.0 | (Barths et al., 1999) |
| DFS-3 | n-dodecane | 100 | 100 | 1.0 | (Sahetchian et al., 1995) |
| DFS-4 | n-tetradecane | 100 | 100 | 1.0 | (Hamosfakidis and Reitz, 2003) |
| DFS-5 | n-hexadecane | 100 | 100 | 1.0 | (Ristori et al., 2001) |
| DFS-6 | n-heptane | 65.2 | 70.0 | 0.63 | (Gustavsson and Golovitchev, 2003) |
| | toluene | 34.8 | 30.0 | 0.37 | |
| DFS-7 | n-decane | 63.1 | 70.0 | 0.63 | (Barths et al., 1999; Barths et al., 2000) |
| | 1-methylnaphthalene | 36.9 | 30.0 | 0.37 | |
| DFS-8 | n-decane | 66.5 | 70.0 | 0.60 | (Seshadri, 2003) |
| | o-xylene (m-xylene ^a) | 33.5 | 30.0 | 0.40 | |
| DFS-9 | n-hexadecane | 36.9 | 37.0 | 0.24 | (Dagaut, 2002) |
| | iso-octane | 22.9 | 25.0 | 0.29 | |
| | n-propylcyclohexane | 20.3 | 20.0 | 0.23 | |
| | n-propylbenzene | 20.0 | 18.0 | 0.24 | |
| DFS-10 | n-hexadecane | 30.0 | 30.2 | 0.16 | This work |
| | iso-octane | 20.0 | 22.0 | 0.22 | |
| | 1-methylcyclohexane | 30.0 | 30.4 | 0.38 | |
| | toluene | 15.0 | 13.5 | 0.20 | |
| | 1-methylnaphthalene | 5.0 | 3.9 | 0.04 | |

^a M-xylene was used in this work. *Italicized* indicates values calculated using densities provided in **Table 3-2**.

iso-alkane, cyclo-alkane, and aromatic groups, respectively. NIST (NIST, 2003) suggested six classes of hydrocarbons and their model compounds which are necessary to simulate real transportation fuels, as given in **Table 2-1**. However, DFSs composed of hydrocarbons from all suggested classes have not been developed. Following NIST's suggestion (NIST, 2003), DFS-10 is proposed in this study, which includes compounds from n-alkane (n-hexadecane), iso-alkane (iso-octane), cyclohexane (1-methylcyclohexane), 1-ring aromatic (toluene), and 2-ring aromatic (1-methylnaphthalene) groups, with weight percentages of 30%, 20%, 30%, 15%, and 5%, respectively. Properties of these ten surrogates were studied and a comparison with DF was made.

3.3 EVALUATION OF DIESEL FUEL SURROGATES

3.3.1 Determination of volatilities

Volatility is one important parameter for a fuel, which characterizes the tendency of the fuel to vaporize. Volatility is closely related to boiling temperature and vapor pressure. The higher volatility, the lower the boiling point. In conventional diesel engines, fuel volatility has a significant effect on spray characteristics, combustion efficiency and emission formation (Canaan et al., 1998; Sharma and Som, 2004). When an engine is operated under the supercritical conditions, however, fuel volatility becomes less important because fuel reaches the supercritical state upon injection and the vaporization step is eliminated in the injection and combustion processes. But fuel volatility still affects the overall fuel delivery and combustion process. Therefore, it is valuable to evaluate volatilities of DFSs.

Volatility of a pure fluid is normally characterized by a single boiling point and the associated vapor pressure, while that of a mixture is described by a mean boiling point and a distillation curve is usually measured. Several experimental techniques have been developed for determination of fuel volatility, one of which is the TGA method (Goodrum, 2002; Lang et al., 2001; Rudnick et al., 2006).

In this work, volatilities of DF and DFSs were evaluated by the TGA method. A thermogravimetric analyzer (TA Q500, TA Instruments) was used in the experiment. Nitrogen was used as the balance gas and the sample gas, the flow rates of which were 40.0 and 60.0 ml/min, respectively. 10 μ l (7-9 mg) samples were loaded in a regular platinum pan. The temperature program was set as: ramp 2 $^{\circ}$ C/min to 25 $^{\circ}$ C (initial temperature \sim 23 $^{\circ}$ C), ramp 10 $^{\circ}$ C/min to 250 $^{\circ}$ C, and then equilibrate at 23 $^{\circ}$ C. To minimize experimental uncertainties, measurements for all DFSs were done in a single continuous run.

N-heptane (certified, spectranalyzed), n-decane (99%, ASSAY), n-dodecane (99%, ASSAY), n-tetradecane (99+%), n-propylcyclohexane (MP Biomedicals), and 1-methylcyclohexane (99+%) were purchased from Fisher Scientific. Toluene (chromasolv plus, for HPLC), iso-octane (anhydrous, 99.8%), m-xylene (anhydrous, \geq 99%), n-hexadecane ($>$ 99%), 1-methylnaphthalene (95%), and n-propylbenzene (puriss., \geq 99.0%) were purchased from Sigma-Aldrich. No. 2 DF was purchased from a local gas station. These chemicals were used as received. Density data of these chemicals either provided by the manufacturers or obtained from online resources are given in **Table 3-2**.

Table 3-2 Densities of chemicals provided by the manufacturers.

| Chemicals | Density^a , kg/m³ |
|---------------------|---|
| n-heptane | <i>695</i> |
| n-decane | <i>735</i> |
| n-dodecane | <i>751</i> |
| n-tetradecane | <i>764</i> |
| n-hexadecane | <i>773</i> |
| toluene | 865 |
| 1-methylnaphthalene | 1001 |
| m-xylene | 864 |
| iso-octane | <i>709</i> |
| n-propylcyclohexane | <i>786</i> |
| n-propylbenzene | 862 |
| 1-methylcyclohexane | <i>770</i> |

^a Normal indicates values provided by the manufacturers; *italicized* indicates values adapted from ChemSpider (<http://www.chemspider.com>, accessed on February 3, 2011).

3.3.2 Estimation of critical properties

3.3.2.1 Critical properties of diesel fuel surrogates

Vapor-liquid critical temperatures and critical pressures for many pure hydrocarbons have been experimentally determined and reported in literature, while those for mixtures are still very limited (Etter and Kay, 1961; Hicks and Young, 1975; Smith and Watson, 1937; Smith et al., 1987). Experimental values are usually preferred when available. However, for compounds containing twelve or more carbons, even experimental values may not be reliable because they are unstable at high temperatures (API, 2006). In this work, critical properties of DFS-1 to DFS-5 are obtained from literature, while those of DFS-6 to DFS-10 are estimated using modeling techniques.

A great number of modeling techniques have been developed for estimating critical properties of pure fluids and mixtures. For pure fluids, the group contribution approach was mostly applied (Constantinou and Gani, 1994; Joback and Reid, 1987; Klincewicz and Reid, 1984; Lydersen, 1955; Marrero-Morejón and Pardillo-Fontdevila, 1999; Nannoolal et al., 2007). Evaluations of and reviews on these methods are available elsewhere (Poling et al., 2001; Spencer and Daubert, 1973). For mixtures, various approaches have been applied to develop correlations for critical properties. As categorized by Li and Kiran (Li and Kiran, 1990), these approaches include graphical approach, EOS approach, excess property approach, conformal solution approach, and thermodynamic potential approach. The EOS based methods (Abu-Eishah, 1999; Heidemann and Khalil, 1980; Michelsen, 1980; Michelsen, 1982; Stradi et al., 2001) are most reliable, while the group contribution methods (Li and Kiran, 1990) give rapid estimates (Poling et al., 2001). Reviews on calculation of mixture critical properties are also available elsewhere (Heidemann, 1994; Sadus, 1994).

In this work, the Li and Kiran equations (Li and Kiran, 1990) were used to estimate critical properties of binary DFSs, while the method for critical properties of defined mixtures suggested by the American Petroleum Institute (API) (API, 2006) was applied in multicomponent DFS systems. These two methods were chosen because they are simpler than other methods and they give rapid, reliable estimates.

The Li and Kiran method (Li and Kiran, 1990) was developed based on the group contribution method for pure fluids proposed by Klincewicz and Reid (Klincewicz and Reid, 1984), assuming that a given binary mixture of compound “A” and compound “B” is a pseudo-compound. The critical temperature ($T_{c,AB}$) and critical pressure ($P_{c,AB}$) of the pseudo-compound are then given as,

$$T_{c,AB} = \frac{T_{b,AB}}{0.567 + q_{T,AB} - q_{T,AB}^2} \quad (3-1)$$

$$P_{c,AB} = \frac{MW_{AB}}{(0.33 + q_{P,AB})^2} \quad (3-2)$$

where $T_{b,AB}$ is the pseudo boiling point, MW_{AB} is the average molecular weight, and $q_{T, AB}$, and $q_{P, AB}$ are the total group contributions. $T_{b,AB}$, MW_{AB} , $q_{T, AB}$, and $q_{P, AB}$ can be calculated as follows.

$$T_{b,AB} = sT_{b,A} + (1-s)T_{b,B} \quad (3-3)$$

$$MW_{AB} = x_A MW_A + x_B MW_B \quad (3-4)$$

$$q_{T,AB} = 0.5 \left[x_A q_{T,A} + x_B q_{T,B} \right] + 0.5 \left[x_A^2 q_{T,A} + x_B^2 q_{T,B} \right] + 3s(1-s)q_{T,ss} - 2v(1-v)q_{T,vv} \quad (3-5)$$

$$q_{P,AB} = 0.5 \left[x_A q_{P,A} + x_B q_{P,B} \right] + 0.5 \left[x_A^2 q_{P,A} + x_B^2 q_{P,B} \right] + 3s(1-s)q_{P,ss} - 2v(1-v)q_{P,vv} - x_A x_B \exp(0.091 - \omega_{AB}) |q_{P,A} - q_{P,B}| \quad (3-6)$$

where x_A and x_B are molar fractions of A and B, respectively; s and v are the critical surface increment fraction and the critical volume increment fraction, respectively; $q_{i,ss}$ and $q_{i,vv}$ represent the contributions from A-B and B-A types of interactions and subscript i indicates either T or P ; ω_{AB} is the mean acentric factor. s , v , $q_{i,ss}$, $q_{i,vv}$ and ω_{AB} are defined as follows

$$s = \frac{x_A q_{v,A}^{2/3}}{x_A q_{v,A}^{2/3} + x_B q_{v,B}^{2/3}} \quad (3-7)$$

$$v = \frac{x_A q_{v,A}}{x_A q_{v,A} + x_B q_{v,B}} \quad (3-8)$$

$$q_{i,ss} = \frac{2q_{i,A}q_{i,B}}{q_{i,A} + q_{i,B}} \quad (3-9)$$

$$q_{i,vv} = \frac{1}{8} \left(q_{i,A}^{1/3} + q_{i,B}^{1/3} \right)^3 \quad (3-10)$$

$$\omega_{AB} = x_A \omega_A + x_B \omega_B \quad (3-11)$$

where the subscript v indicates the critical volume increment; $q_{i,A}$ and $q_{i,B}$ are the total group contributions from the functional groups in A and B, respectively; ω_A and ω_B are the acentric factors for compounds A and B, respectively, and are obtained from literature. The total group contribution q for any compound is defined by

$$q = \sum_{j=1}^m n_j \Delta_j \quad (3-12)$$

where n_j and Δ_j are the number of and the critical property increment for the type j functional group, respectively, and m is the total number of functional groups in the compound.

The Li equation (Li, 1971) and the equation developed by Kreglewski and Kay (Kreglewski and Kay, 1969), suggested by API (API, 2006), were used to estimate critical temperatures and critical pressures of multicomponent DFSs, respectively. The Li equation (Li, 1971) reads,

$$T_{cm} = \sum_{i=1}^n \theta_i T_{ci} \quad (3-13)$$

where θ_i is the volumetric fraction of component i and can be calculated by

$$\theta_i = \frac{x_i V_{ci}}{\sum_{i=1}^n x_i V_{ci}} \quad (3-14)$$

The equation for critical pressure of a mixture is as follows (API, 2006; Kreglewski and Kay,

1969),

$$P_{cm} = P_{pc} \left[1 + (5.808 + 4.93\omega_m) \frac{T_{cm} - T_{pc}}{T_{pc}} \right] \quad (3-15)$$

where T_{pc} and P_{pc} are pseudocritical temperature and pseudocritical pressure, respectively, and ω_m is the mean acentric factor; they are given as follows

$$T_{pc} = \sum_{i=1}^n x_i T_{ci} \quad (3-16)$$

$$P_{pc} = \sum_{i=1}^n x_i P_{ci} \quad (3-17)$$

$$\omega_m = \sum_{i=1}^n x_i \omega_i \quad (3-18)$$

All critical constants (T_{ci} , P_{ci} , V_{ci}) and acentric factors (ω_i) are obtained from literature.

3.3.2.2 Critical properties of diesel fuel

Since no experimental data on critical properties of DF were found in the literature, modeling techniques were applied to estimate these properties. Due to the complexity of DF and unknown detailed composition information, the methods presented in the preceding section cannot be applied to diesel fuel. Fortunately, other correlation methods have been developed based on the availability of characteristic information of hydrocarbon mixtures, mainly boiling point and specific gravity. These methods fall in three categories (Korsten, 1998) (a) polynomial empirical equations, e.g., the API method

(API, 2006), and correlations proposed by Cavett (Cavett, 1962), Kesler and Lee (Kesler and Lee, 1976), and Brule et al. (Brule et al., 1982), (b) exponential empirical equations, e.g., correlations proposed by Riazi and Daubert (Riazi and Daubert, 1980), Sim and Daubert (Sim and Daubert, 1980), and Zhou (Zhou, 1984), and (c) equations based on the perturbation of a reference system, e.g., the Twu correlation (Twu, 1984). Except for the API method which uses the volumetric average boiling point, others require the mean average boiling point. A review on critical properties of hydrocarbon systems can be found elsewhere (Korsten, 1998). Some of these methods have been applied to estimate critical properties of some jet fuels and gave satisfactory predictions (Yu and Eser, 1995).

The methods used to estimate DF properties are described below.

1. API Method (API, 2006)

$$T_c = 186.16 + 1.6667\Theta - 0.7127 \times 10^{-3} \Theta^2 \quad (3-19)$$

$$\Theta = SG(T_v + 100.0) \quad (3-20)$$

where SG is the specific gravity (60 °F / 60 °F), T_v is the volumetric average boiling point, and both T_v and T_c are in °F. T_v can be estimated by averaging ASTM D86 distillation temperatures at 10, 30, 50, 70, and 90 vol % distillate points:

$$T_v = (T_{10} + T_{30} + T_{50} + T_{70} + T_{90})/5 \quad (3-21)$$

Critical pressure, P_c , can be obtained from Figure 4D2.1 in the API Technical Data Book, with the inputs of T_v , the ASTM slope (SL), and the API gravity (API) (API, 2006). SL and API are defined by

$$SL = \frac{T_{90} - T_{10}}{90 - 10} \quad (3-22)$$

$$API = 141.5/SG - 131.5 \quad (3-23)$$

2. Cavett Correlation (Cavett, 1962; Korsten, 1998)

$$\begin{aligned} T_c = & 768.07121 + 1.7133693T_b - 0.10834003 \times 10^{-2} T_b^2 - \\ & 0.89212579 \times 10^{-2} (API)T_b + 0.38890584 \times 10^{-6} T_b^3 + \\ & 0.53094920 \times 10^{-5} (API)T_b^2 + 0.32711600 \times 10^{-7} (API)^2 T_b^2 \end{aligned} \quad (3-24)$$

$$\begin{aligned} \log_{10} P_c = & 2.8290406 + 0.94120109 \times 10^{-3} T_b - 0.30474749 \times 10^{-5} T_b^2 \\ & - 0.20876110 \times 10^{-4} (API)T_b + 0.15184103 \times 10^{-8} T_b^3 \\ & + 0.11047899 \times 10^{-7} (API)T_b^2 + 0.13949619 \times 10^{-9} (API)^2 T_b^2 \\ & - 0.48271599 \times 10^{-7} (API)^2 T_b \end{aligned} \quad (3-25)$$

where T_c is in $^{\circ}\text{R}$, P_c is in psia, and T_b is the mean average boiling point in $^{\circ}\text{F}$. T_b can be calculated from T_v by the method recommended by API (API, 2006), given below

$$T_b = T_v - \Gamma \quad (3-26)$$

$$\ln \Gamma = -0.94402 - 0.00865(T_v - 32)^{0.6667} + 2.99791(SL)^{0.333} \quad (3-27)$$

3. Kesler and Lee Correlation (Kesler and Lee, 1976; Korsten, 1998)

$$\begin{aligned} T_c = & 341.7 + 811 \times SG + (0.4244 + 0.1174 \times SG) \times T_b \\ & + (0.4669 - 3.2623 \times SG) \times 10^5 / T_b \end{aligned} \quad (3-28)$$

$$\begin{aligned}
\ln P_c = & 8.3634 - \frac{0.0566}{SG} \\
& - \left(0.24244 + \frac{2.2898}{SG} + \frac{0.11857}{SG^2} \right) \times 10^{-3} T_b \\
& + \left(1.4685 + \frac{3.648}{SG} + \frac{0.47227}{SG^2} \right) \times 10^{-7} T_b^2 \\
& - \left(0.42019 + \frac{1.6977}{SG^2} \right) \times 10^{-10} T_b^3
\end{aligned} \tag{3-29}$$

where T_c and T_b are in $^{\circ}\text{R}$, and P_c is in psia.

4. Brule Correlation (Brule et al., 1982)

$$\begin{aligned}
T_c = & 429.138 + 0.886861T_b - 4.596433 \times 10^{-4} T_b^2 - \\
& 2.410089 \times 10^{-3} (API)T_b + 1.630489 \times 10^{-7} T_b^3 + \\
& 9.323778 \times 10^{-7} (API)T_b^2 - 1.430628 \times 10^{-8} (API)^2 T_b^2
\end{aligned} \tag{3-30}$$

where T_c is in K and T_b are in $^{\circ}\text{F}$. P_c is not available in this method.

5. Riazi and Daubert Correlation (Korsten, 1998; Riazi and Daubert, 1980)

$$T_c = 19.0623T_b^{0.58848} SG^{0.3596} \tag{3-31}$$

$$P_c = 5.53028 \times 10^6 T_b^{-2.3125} SG^{2.3201} \tag{3-32}$$

where T_c and T_b are in K, and P_c is in MPa.

6. Sim and Daubert Correlations (Korsten, 1998; Sim and Daubert, 1980)

$$\ln(1.8T_c) = 4.2009T_b^{0.08615} SG^{0.04614} \tag{3-33}$$

$$P_c = 6.1483 \times 10^6 T_b^{-2.3177} SG^{2.4853} \tag{3-34}$$

where T_c and T_b are in K, and P_c is in MPa.

7. **Zhou Correlation** (Korsten, 1998; Zhou, 1984)

$$T_c = 47.1126T_b^{0.42928} SG^{0.82944} \quad (3-35)$$

$$P_c = 356.971T_b^{-0.87273} SG^{1.93053} \quad (3-36)$$

where T_c and T_b are in °C, and P_c is in MPa.

8. **Twu Correlation** (Twu, 1984)

$$T_c = T_c^o \left[\frac{(1+2f_T)}{(1-2f_T)} \right]^2 \quad (3-37)$$

$$V_c = V_c^o \left[\frac{(1+2f_V)}{(1-2f_V)} \right]^2 \quad (3-38)$$

$$P_c = P_c^o (T_c/T_c^o)(V_c^o/V_c) \left[\frac{(1+2f_P)}{(1-2f_P)} \right]^2 \quad (3-39)$$

$$T_c^o = T_b / (0.533272 + 0.191017 \times 10^{-3} T_b + 0.779681 \times 10^{-7} T_b^2 - 0.284376 \times 10^{-10} T_b^3 + 0.959468 \times 10^{28} / T_b^{13}) \quad (3-40)$$

$$V_c^o = \left[1 - (0.419869 - 0.505839\alpha - 1.56436\alpha^3 - 9481.70\alpha^{14}) \right]^{-8} \quad (3-41)$$

$$P_c^o = (3.83354 + 1.19629\alpha^{1/2} + 34.8888\alpha + 36.1952\alpha^2 + 104.193\alpha^4)^2 \quad (3-42)$$

$$f_T = \Delta(SG)_T \left[-0.362456/T_b^{1/2} + (0.0398285 - 0.948125/T_b^{1/2}) \Delta(SG)_T \right] \quad (3-43)$$

$$f_V = \Delta(SG)_V [0.466590/T_b^{1/2} + (-0.182421 + 3.01721/T_b^{1/2})\Delta(SG)_V] \quad (3-44)$$

$$f_P = \Delta(SG)_P [2.53262 - 46.1955/T_b^{1/2} - 0.00127885T_b + (-11.4277 + 252.140/T_b^{1/2} + 0.00230535T_b)\Delta(SG)_P] \quad (3-45)$$

$$\alpha = 1 - T_b/T_c^o \quad (3-46)$$

$$\Delta(SG)_T = \exp\left[5\left((SG)^o - SG\right)\right] - 1 \quad (3-47)$$

$$\Delta(SG)_V = \exp\left[4\left((SG)^{o2} - SG^2\right)\right] - 1 \quad (3-48)$$

$$\Delta(SG)_P = \exp\left[0.5\left((SG)^o - SG\right)\right] - 1 \quad (3-49)$$

$$(SG)^o = 0.843593 - 0.128624\alpha - 3.36159\alpha^3 - 13749.5\alpha^{12} \quad (3-50)$$

where T_c and T_b are in °R, P_c in psia, and V_c in ft³ lb⁻¹ mol⁻¹.

3.3.3 Calculation of thermophysical properties

3.3.3.1 Thermophysical properties of diesel fuel surrogates

Two NIST software programs, i.e. REFPROP (Lemmon et al., 2010) and SUPERTRAPP (Ely and Huber, 2007), were applied to calculate thermophysical properties of DFSs, including density, viscosity, heat capacity, and thermal conductivity. A brief introduction of these two programs is given below.

“REFPROP is based on the most accurate pure fluid and mixture models currently available” (Lemmon et al., 2010). Three models are used for the thermodynamic properties of pure fluids: the modified Benedict-Webb-Rubin EOS (Jacobsen and Stewart, 1973), the Helmholtz EOS, and an extended corresponding states (ECS) model (Huber and Hanley, 1996). For mixture calculations, a departure function is applied to the mixing rules. Transport properties, i.e. viscosity and thermal conductivity, are modeled with either an ECS method or the friction theory method. A detailed description of the models is given in the manual of REFPROP V7.0 (Lemmon et al., 2002). REFPROP was initially developed for predictions of refrigerant properties, and later expanded to natural gas components and other species. The number of fluids and mixtures in this database is relatively small and the application for fuel properties estimation is limited.

SUPERTRAPP (Ely and Huber, 2007) is a robust interactive computer database for the prediction of thermodynamic and transport properties of pure fluids or mixtures of up to 20 components at temperatures and pressures up to 1000 K and 300 MPa, respectively. The predictive technique of it is based on the ECS method and the Peng-Robinson (PR) EOS (Friend and Huber, 1994; Huber and Hanley, 1996). Phase equilibrium problems are solved using the PR EOS, while transport properties are obtained by using the ECS method.

SUPERTRAPP has been successfully used to predict thermophysical properties of a variety of fluids and mixtures, including natural gas (Vesovic, 2001), natural gas and hydrogen mixtures (Hourri et al., 1982), jet fuel surrogates and mixtures (Cormier, 2001; Dounghthip et al., 2002; Ervin et al., 2003; Fan et al., 2006; Hirasaki and Mohanty, 2001; Huang et al., 2004; Senda et al., 2001), kerosene surrogate (Fan et al., 2006), ethane (Hirasaki and

Mohanty, 2001), organic fluid mixtures (Vijayaraghavan, 2003), and supercritical fuels (Helfrich, 2006; Huang et al., 2002; Micci and Long, 2000). Huang et al. (Huang et al., 2002) and Helfrich (Helfrich, 2006) applied it to calculate thermodynamic properties of supercritical jet fuels including JP-7, JP-8+100 and JP-10 in the temperature and pressure ranges of 273 to 998 K and 1 to 85 atm, respectively. The results indicated that thermodynamic property data were only reliable up to 810.7 K since the program does not take into account the effects of endothermic reactions occurring in the fuel (Helfrich, 2006).

REFPROP is first considered in this study due to the high accuracy and low uncertainty. Hydrocarbons of interest, which have been included in REFPROP, are n-heptane, n-decane, n-dodecane and toluene. Accordingly, densities, viscosities, heat capacities and thermal conductivities of DFS-1, DFS-2, and DFS-3 were calculated using REFPROP. Properties of the rest of DFSs, i.e. DFS-4 to DFS-10, were calculated by SUPERTRAPP.

3.3.3.2 Thermophysical properties of diesel fuel

Empirical correlations recommended by Kolev (Kolev, 2007) were used to estimate density, viscosity, heat capacity, and thermal conductivity of diesel fuel. These correlations are based on SIEMEMS data and good for estimation at temperatures from 293.15-393.15 K and pressures up to 240 MPa. They are given below.

Density in kg/m³ is correlated by

$$\rho = \sum_{i=1}^3 \left(\sum_{j=1}^3 a_{ij} T^{j-1} \right) P^{i-1} \quad (3-51)$$

$$A = \begin{bmatrix} 828.59744 & 0.63993 & -0.00216 \\ 8.65679 \times 10^{-7} & -5.93672 \times 10^{-9} & 1.56678 \times 10^{-11} \\ -7.59052 \times 10^{-16} & 8.99915 \times 10^{-18} & -2.77890 \times 10^{-20} \end{bmatrix} \quad (3-52)$$

Kinematic viscosity in m²/s is correlated by

$$\log_{10} (10^6 \nu) = \sum_{i=1}^2 \left(\sum_{j=1}^3 b_{ij} T^{j-1} \right) P^{i-1} \quad (3-53)$$

$$B = \begin{bmatrix} 8.67271 & -0.04287 & 5.31710 \times 10^{-5} \\ 5.38000 \times 10^{-8} & -2.78208 \times 10^{-10} & 3.74529 \times 10^{-13} \end{bmatrix} \quad (3-54)$$

Heat capacity in J/kg.K is correlated by

$$c_p = \sum_{i=1}^5 \left(\sum_{j=1}^3 c_{ij} T^{j-1} \right) \left(\frac{P}{10^5} \right)^{i-1} \quad (3-55)$$

$$C = \begin{bmatrix} -977.16186 & 14.025100 & -0.01374 \\ 2.22361 \times 10^{-4} & -1.62143 \times 10^{-4} & 2.23214 \times 10^{-9} \\ -1.96181 \times 10^{-9} & 2.03748 \times 10^{-7} & -1.78571 \times 10^{-14} \\ 4.15000 \times 10^{-14} & -7.54100 \times 10^{-11} & 4.03897 \times 10^{-28} \\ -3.48714 \times 10^{-18} & 1.00688 \times 10^{-14} & -1.47911 \times 10^{-31} \end{bmatrix} \quad (3-56)$$

Thermal conductivity in W/m.K is correlated by

$$k = \sum_{i=1}^3 \left(\sum_{j=1}^3 d_{ij} T^{j-1} \right) P^{i-1} \quad (3-57)$$

$$D = \begin{bmatrix} 0.13924 & 3.78253 \times 10^{-5} & -2.89732 \times 10^{-7} \\ 6.27425 \times 10^{-11} & 6.08052 \times 10^{-13} & 3.64777 \times 10^{-16} \\ -1.38756 \times 10^{-19} & -2.57608 \times 10^{-22} & -2.70893 \times 10^{-24} \end{bmatrix} \quad (3-58)$$

In Eqs. (3-51), (3-53), (3-55) and (3-57), T and p are in K and Pa, respectively.

3.4 RESULTS AND DISCUSSIONS

3.4.1 Comparison of volatilities

Fig. 3-1 presents original TGA curves for DF and DFSs, demonstrating very different volatility characteristics. Curves for DFS-1 and DFS-6 are not shown in the figure because they are so volatile that they completely vaporized during the loading stage and no TGA curves were obtained. The initial weights of DFS-8 to DFS-10 at 25 °C were much lower than those of others due to weight loss during the loading stage, indicating high volatilities. Weight loss before data recording changes sample compositions and hence brings uncertainties to the measurements. For DF, it is noticed that although it has a boiling point range of 150-370 °C (ConocoPhillips, 2007), it completely vaporized below 200 °C. The reason is that the DF sample was loaded in an open pan and vaporized in a flowing flow environment. This effect could be reduced by using a closed pan with a laser-drilled hole (Goodrum, 2002).

Since the initial weights were different, TGA curves are normalized by dividing the corresponding initial weights. Results are plotted in **Fig. 3-2**. From **Fig. 3-1** and **Fig. 3-2**, it is found that DFS-1, DFS-2, and DFS-6 to DFS-10 were more volatile than DF, while DFS-3 to DFS-5 vaporized slower initially and then faster than DF. These results indicate that none of these DFSs has volatility close to DF.

3.4.2 Comparison of critical properties

Critical temperatures and pressures of DFS-1 to DFS-5 were adapted from literature, critical temperatures and pressures of DFS-6 to DFS-8 were calculated using the group contribution method given by Eqs. (3-1) to (3-12), critical temperatures and

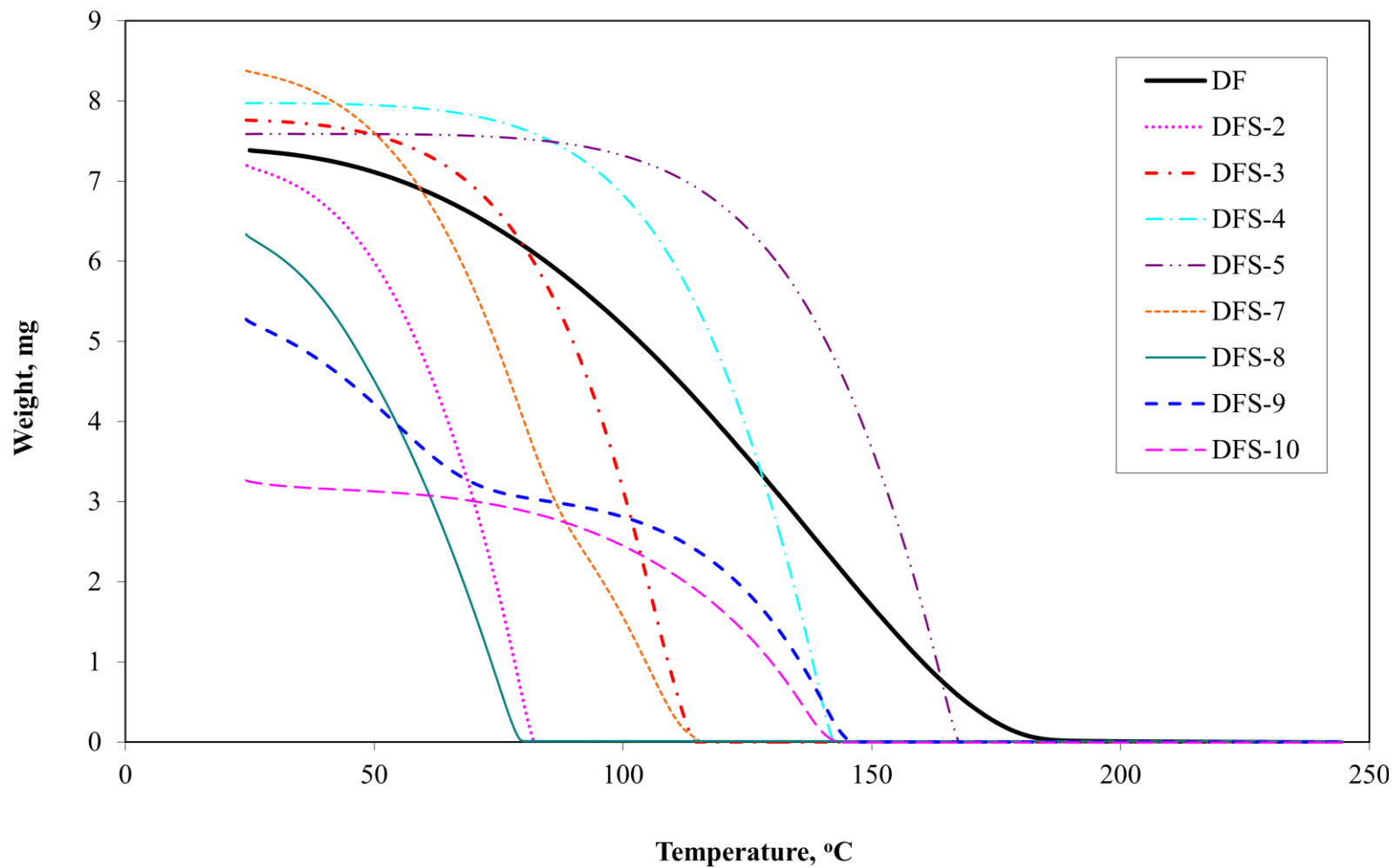


Fig. 3-1 Original TGA curves for DF and DFSs.

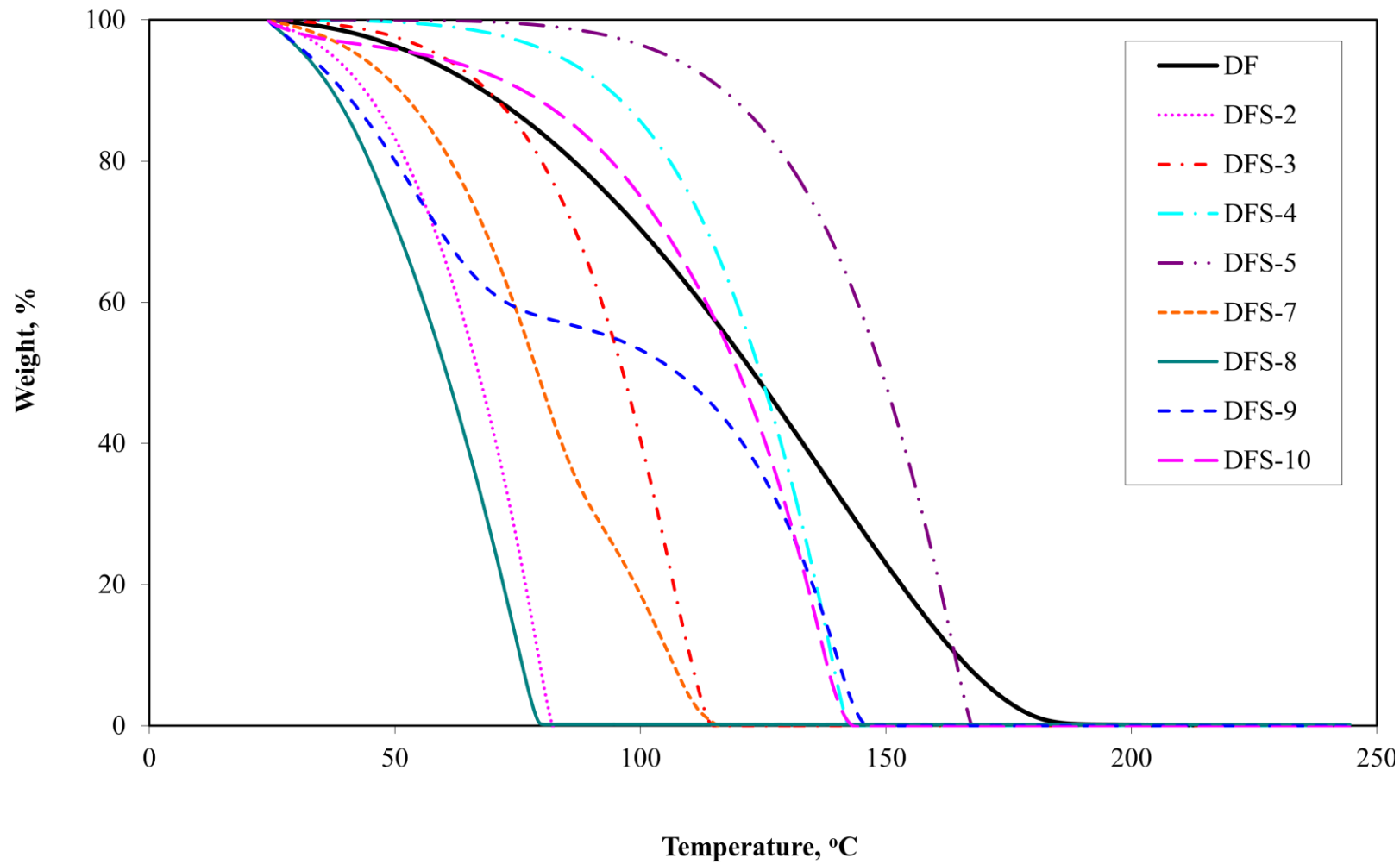


Fig. 3-2 Normalized TGA curves for DF and DFSs.

critical pressures of DFS-9 and DFS-10 were calculated using API methods given by Eqs. (3-13) to (3-18), and those of DF were estimated using empirical correlations given by Eqs. (3-19) to (3-50). Constants for DFS compounds used in the calculations are given in **Table 3-3**. Lydersen's group contributions for critical properties (Gupta, 2003; Lydersen, 1955) are given in **Table 3-4**. Distillation curve data for DF and density of DF were adapted from Smith et al. (Smith et al., 2008) and are presented in **Table 3-5** and **Table 3-6**, respectively. Critical pressure of DF was not obtained by the API method because temperature was out of range.

Estimated critical properties for DFSs and DF are presented in **Table 3-7** and **Table 3-8**, respectively. Results are also plotted in **Fig. 3-3**. **Table 3-7** shows that critical temperatures of these DFSs vary significantly from 540.2 K for DFS-1 to 723.0 K for DFS-5, while critical pressures are in a range of 1.40 – 4.03 MPa. **Table 3-8** shows that all empirical correlations give very close estimates of critical temperatures and pressures for DF, which are 739-754 K and 1.72-1.96 MPa, respectively. It is easily seen that critical temperatures of all DFSs are lower than those of DF. A lower critical temperature could lead to a design of the fuel delivery system where real DF only reaches the subcritical state upon injection. Therefore, care must be taken in choosing a DFS for supercritical fuel combustion applications. Critical pressure is another important parameter in determining the critical state. However, it is not that important in engine design because injection pressure is much higher than the critical pressure. **Fig. 3-3** shows that DFS-5 has a best estimate of critical temperature and pressure of DF. Therefore, better results would be expected when n-hexadecane is used as a DFS in engine experiments and simulations.

Table 3-3 Constants for DFS compounds ^a.

| Name | Formula | MW | T_c | P_c | $\rho_c^{\#}$ | V_c | T_b | Z_c | ω |
|----------------------------------|---------------------------------|---------|---------------|--------------|---------------|---------------|---------------|--------------|--------------|
| | | g/mol | K | MPa | g/ml | ml/mol | K | | |
| toluene | C ₇ H ₈ | 92.141 | 591.75 | 4.108 | <i>0.292</i> | 316.00 | <i>383.79</i> | <i>0.264</i> | <i>0.264</i> |
| 1-methylcyclohexane | C ₇ H ₁₄ | 98.188 | 572.19 | 3.471 | <i>0.267</i> | 368.00 | <i>374.09</i> | <i>0.268</i> | <i>0.235</i> |
| n-heptane | C ₇ H ₁₆ | 100.204 | 540.20 | 2.740 | <i>0.234</i> | 428.00 | <i>371.57</i> | 0.261 | <i>0.350</i> |
| m-xylene | C ₈ H ₁₀ | 106.167 | 617.00 | 3.541 | <i>0.283</i> | 375.00 | <i>412.34</i> | <i>0.259</i> | <i>0.327</i> |
| iso-octane | C ₈ H ₁₈ | 114.231 | 543.90 | 2.570 | <i>0.243</i> | 469.70 | <i>372.39</i> | <i>0.266</i> | <i>0.304</i> |
| n-propylbenzene | C ₉ H ₁₂ | 120.194 | 638.35 | 3.200 | <i>0.273</i> | 440.00 | <i>432.35</i> | <i>0.265</i> | <i>0.345</i> |
| n-propylcyclohexane [§] | C ₉ H ₁₈ | 126.240 | 639.16 | 2.807 | <i>0.265</i> | 477.19 | 429.91 | <i>0.252</i> | <i>0.260</i> |
| n-decane | C ₁₀ H ₂₂ | 142.285 | 617.70 | 2.110 | <i>0.228</i> | 624.00 | <i>447.30</i> | <i>0.256</i> | <i>0.490</i> |
| 1-methylnaphthalene | C ₁₁ H ₁₀ | 142.200 | 772.00 | 3.600 | <i>0.308</i> | 462.00 | <i>517.84</i> | 0.259 | <i>0.348</i> |
| n-dodecane | C ₁₂ H ₂₆ | 170.338 | 658.00 | 1.820 | <i>0.226</i> | 754.00 | <i>489.48</i> | <i>0.251</i> | <i>0.576</i> |
| n-tetradecane | C ₁₄ H ₃₀ | 198.392 | 693.00 | 1.570 | <i>0.222</i> | 894.00 | <i>526.76</i> | <i>0.244</i> | <i>0.644</i> |
| n-hexadecane | C ₁₆ H ₃₄ | 226.446 | 723.00 | 1.400 | <i>0.219</i> | 1034.00 | <i>559.98</i> | <i>0.241</i> | <i>0.718</i> |

^a Unless otherwise noted, all values presented in the table are adapted from Poling et al (Poling et al., 2001). Normal is a value from experiments; *italicized* is a value calculated from other values in the table; **bold** is an estimated value. [#] Values are calculated in this work. [§] Values are from

Table 3-4 Group Contributions for critical properties.

| | | - CH ₃ | - CH ₂ - | = CH | = C - | | | |
|--------------------------------|---------------------------------|-------------------------|---------------------|----------|-----------|-------------------------|---------------------------|------------------------------|
| Group types^a | | | | | | | | |
| ΔT, K | | 0.020 | 0.020 | 0.011 | 0.011 | | | |
| ΔP, bar | | 0.227 | 0.227 | 0.154 | 0.154 | | | |
| ΔV, ml/mol | | 55 | 55 | 37 | 36 | | | |
| Name | Formula | Number of groups | | | | q_T, K | q_p, bar | q_v, ml/mol |
| toluene | C ₇ H ₈ | 1 | 0 | 5 | 1 | 0.086 | 1.151 | 276 |
| n-heptane | C ₇ H ₁₆ | 2 | 5 | 0 | 0 | 0.140 | 1.589 | 385 |
| m-xylene | C ₈ H ₁₀ | 2 | 0 | 4 | 2 | 0.106 | 1.378 | 330 |
| n-decane | C ₁₀ H ₂₂ | 2 | 8 | 0 | 0 | 0.200 | 2.270 | 550 |
| 1-methylnaphthalene | C ₁₁ H ₁₀ | 1 | 0 | 7 | 3 | 0.130 | 1.767 | 422 |

^a Lydersen's group contributions (Gupta, 2003; Lydersen, 1955).

Table 3-5 Distillation curve data for DF^a.

| Distillate vol% | T, °C | T, °F |
|-----------------|-------|-------|
| 10 | 248.6 | 479.5 |
| 30 | 269.7 | 517.5 |
| 50 | 289.2 | 552.6 |
| 70 | 308.3 | 586.9 |
| 75 | 313.5 | 596.3 |
| 80 | 319.8 | 607.6 |
| 85 | 327.5 | 621.5 |
| 90 ^b | 334.3 | 633.7 |

^a Data adapted from (Smith et al., 2008).

^b Value extrapolated using data at 75, 80, and 85 vol%.

Table 3-6 Density of DF at 0.1 MPa^a.

| T, °C | Density, g/ml |
|-------------------|---------------|
| 15.5 ^b | 0.85745 |
| 20 | 0.8543 |
| 25 | 0.8507 |
| 30 | 0.8473 |

^a Data adapted from (Smith et al., 2008).

^b Extrapolated value.

Table 3-7 Critical temperatures and critical pressures of DFSs.

| DFS | T_c, K | P_c, Mpa |
|------------|-------------------------|---------------------------|
| DFS-1 | 540.2 | 2.74 |
| DFS-2 | 617.7 | 2.11 |
| DFS-3 | 658.0 | 1.82 |
| DFS-4 | 693.0 | 1.57 |
| DFS-5 | 723.0 | 1.40 |
| DFS-6 | 560.1 | 3.52 |
| DFS-7 | 664.2 | 2.65 |
| DFS-8 | 624.2 | 3.06 |
| DFS-9 | 652.1 | 3.13 |
| DFS-10 | 627.2 | 4.03 |

Table 3-8 Critical temperature and critical pressure of DF.

| Methods | T_c, K | P_c, MPa |
|-----------------|-------------------------|---------------------------|
| API | 753.5 | n/a |
| Cavett | 746.4 | 1.85 |
| Kesler & Lee | 740.3 | 1.82 |
| Brule | 744.1 | n/a |
| Riazi & Daubert | 745.6 | 1.72 |
| Sim & Daubert | 738.6 | 1.81 |
| Zhou | 742.5 | 1.91 |
| Twu | 749.0 | 1.96 |

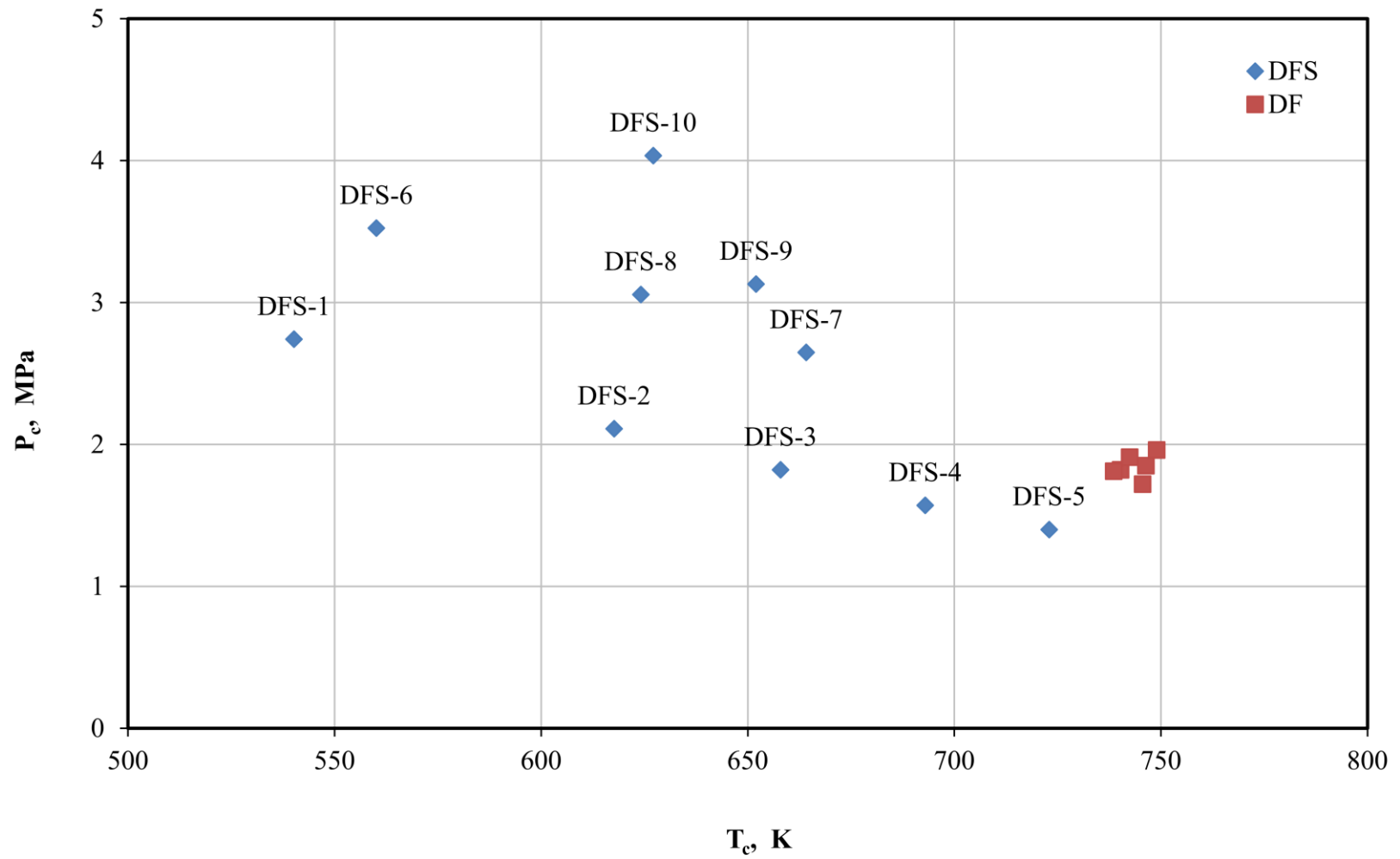


Fig. 3-3 Critical temperatures and pressures of DFSs and DF.

3.4.3 Comparison of thermophysical properties

For comparison, densities, viscosities, heat capacities, and thermal conductivities of DFSs and DF were calculated at 300-800 K and 10, 30, 50, and 100 MPa. Properties of DFS-1, DFS-2, and DFS-3 were calculated using REFPROP (Lemmon et al., 2010). The upper temperature limits for DFS-1, DFS-2 and DFS-3 are 600, 670, and 700 K, respectively. Properties of DFS-4 to DFS-10 were calculated by SUPERTRAPP (Ely and Huber, 2007). Although SUPERTRAPP has an extensive database, n-propylcyclohexane is not included in the original program. It was added as a new component with parameters given in **Table 3-3**. The required parameters include the critical temperature, the critical pressure, the critical volume, the normal boiling point, and the acentric factor. DF properties were obtained using empirical correlations (Kolev, 2007). As mentioned in section 3.2.3.1, those empirical correlations are good for temperatures up to 393.15 K.

Density, heat capacity, viscosity, and thermal conductivity of DFSs and DF at 30 MPa are plotted in **Fig. 3-4** to **Fig. 3-7**, respectively. Results for 10, 50, and 100 MPa are available in Appendix A. It is clearly demonstrated in **Fig. 3-4** to **Fig. 3-7** that these DFSs exhibit significantly different behavior in predicting DF properties. For example, DFS-7 gives best predictions of density of DF as shown in **Fig. 3-4**, but it shows poor fit for thermal conductivity of DF as show in **Fig. 3-7**. For a better comparison, average absolute deviations (AAD) are calculated by

$$AAD\% = \frac{1}{n} \sum_{i=1}^n \left(\frac{|y_i - z_i|}{z_i} \times 100 \right) \quad (3-59)$$

where y is properties of DFSs, z is properties of DF, and n is number of data points. Results are presented in **Fig. 3-8** to **Fig. 3-11** and also available in Appendix A.

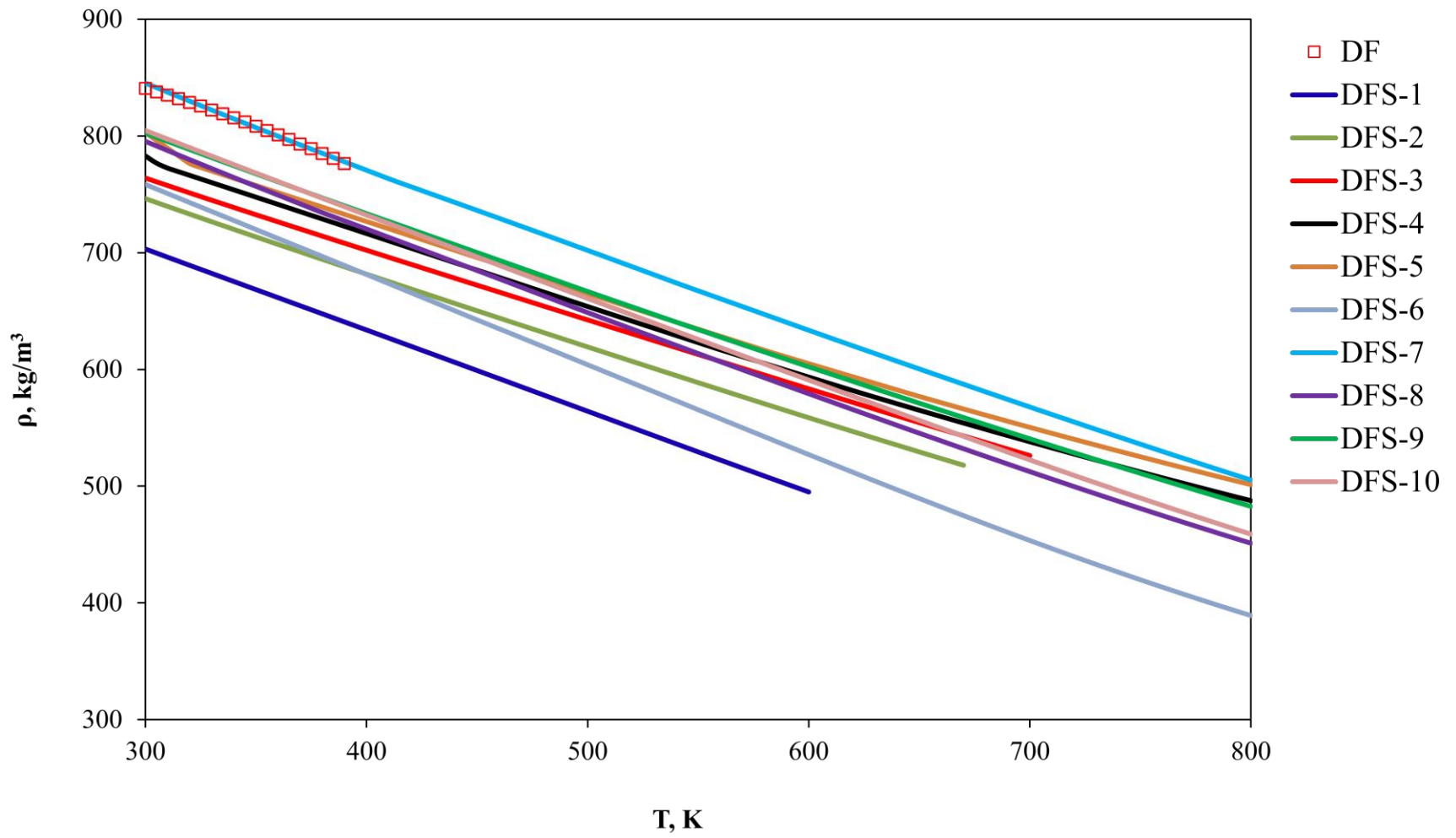


Fig. 3-4 Densities of DFSs and DF at 30 MPa.

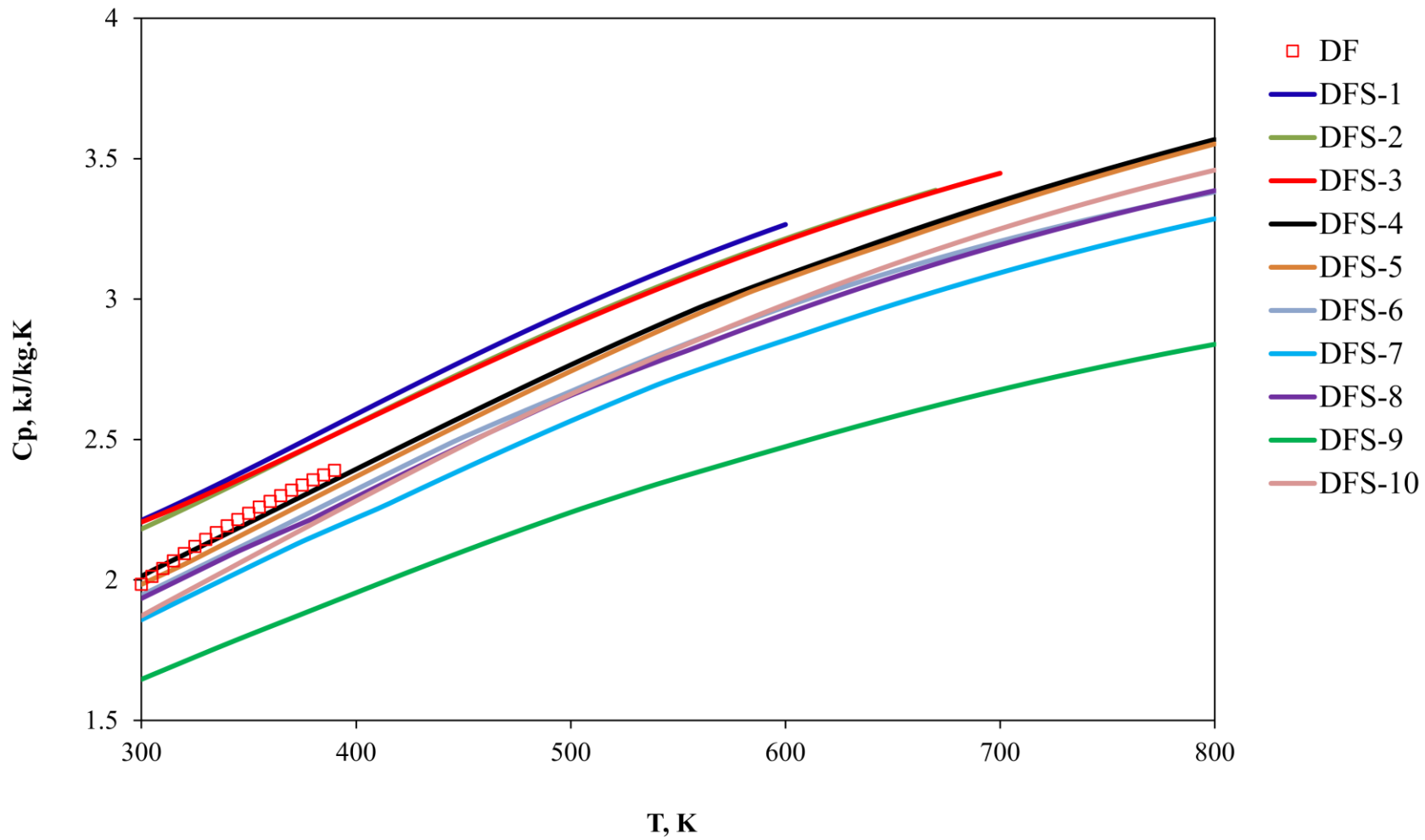


Fig. 3-5 Heat capacities of DFSs and DF at 30 MPa.

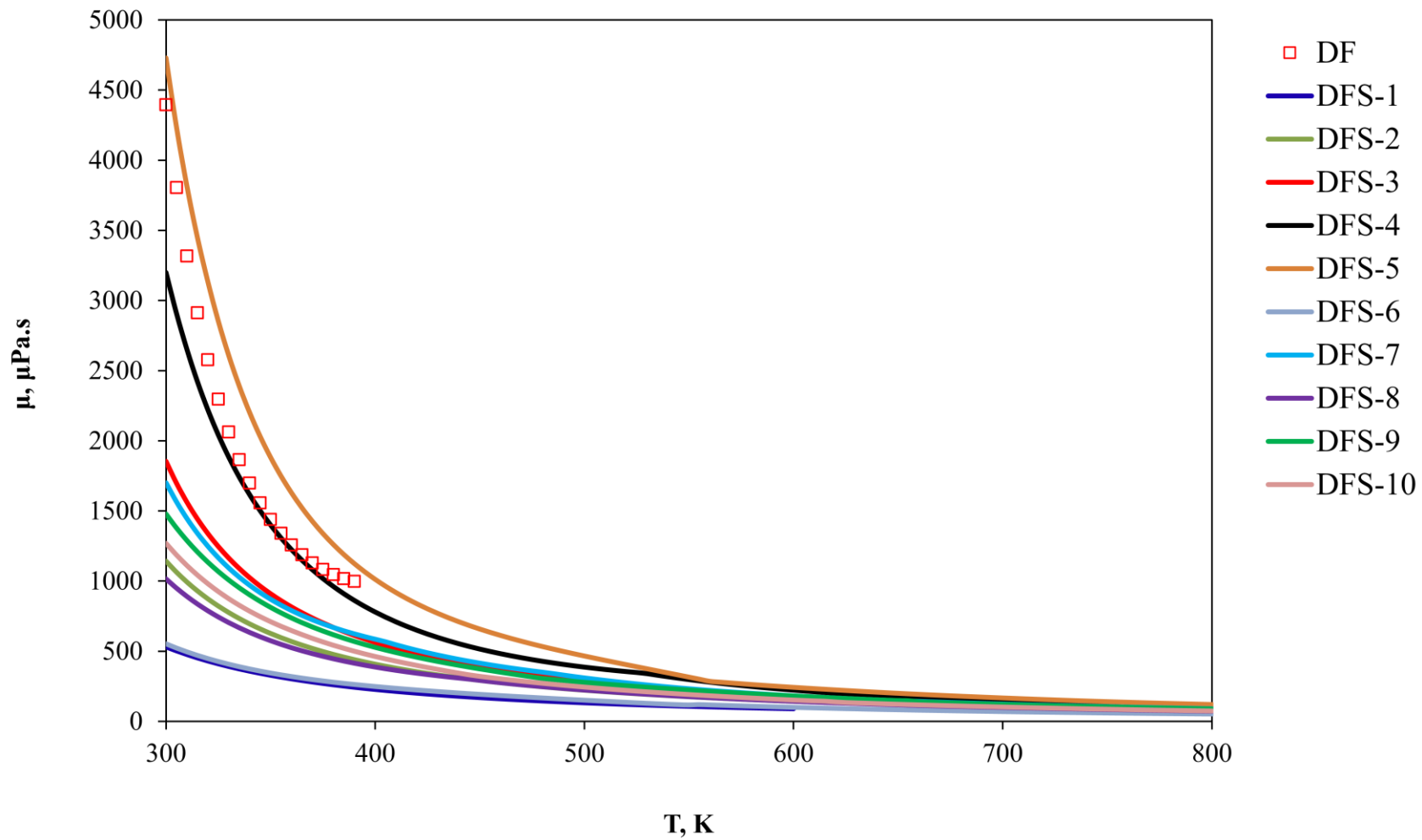


Fig. 3-6 Viscosities of DFSs and DF at 30 MPa.

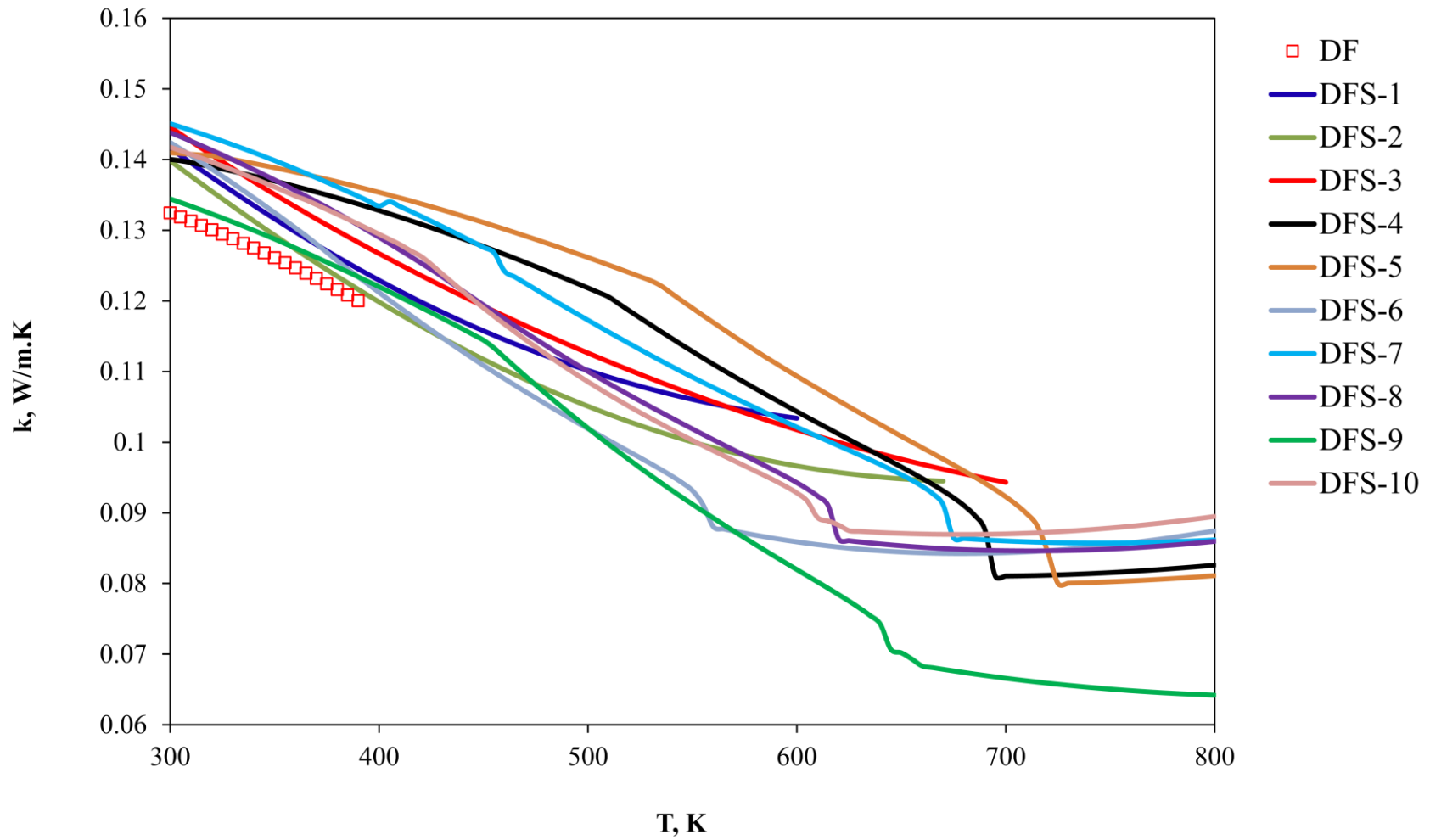


Fig. 3-7 Thermal conductivities of DFSs and DF at 30 MPa.

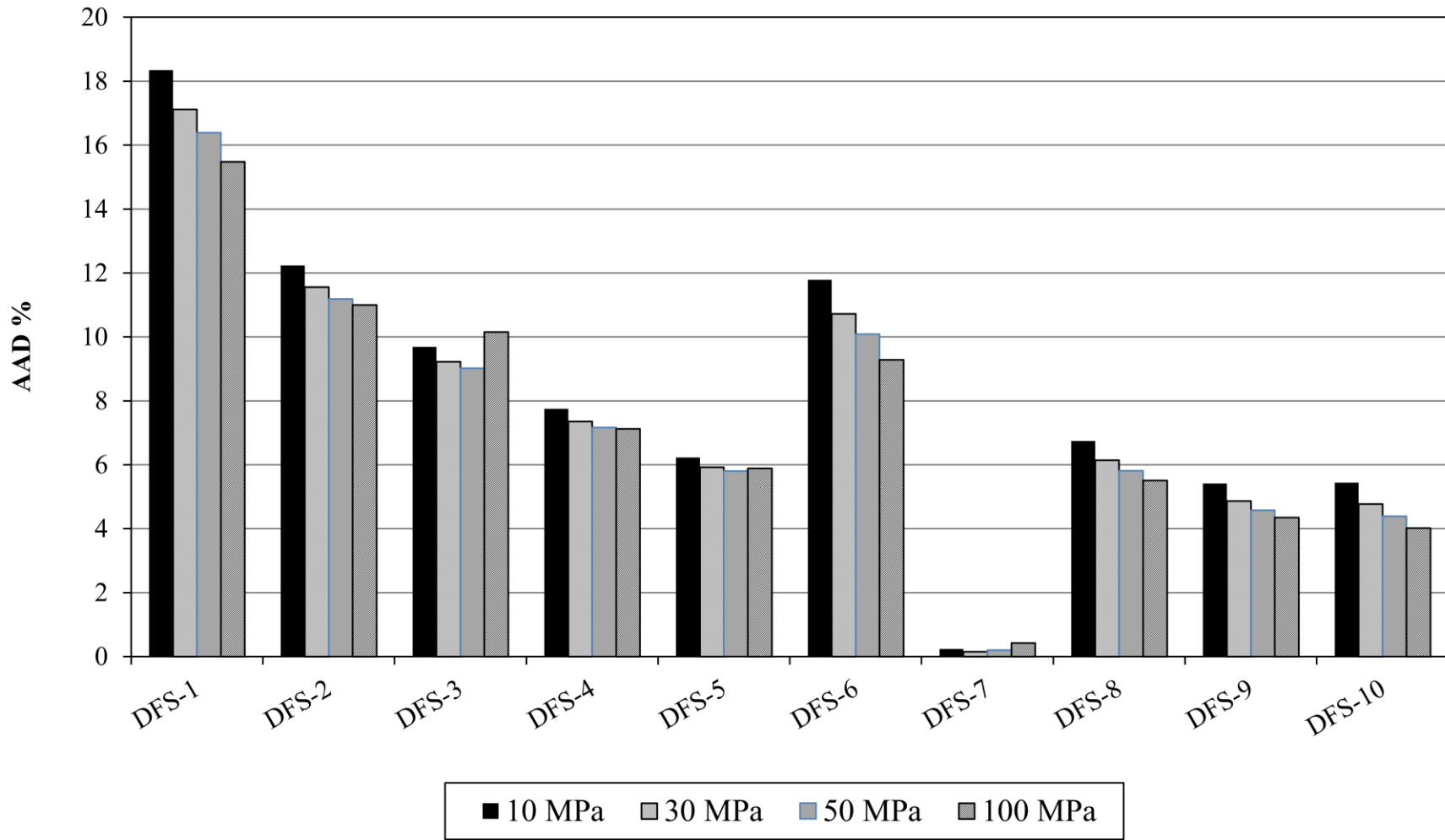


Fig. 3-8 Comparison of DFS's capability in predicting DF density.

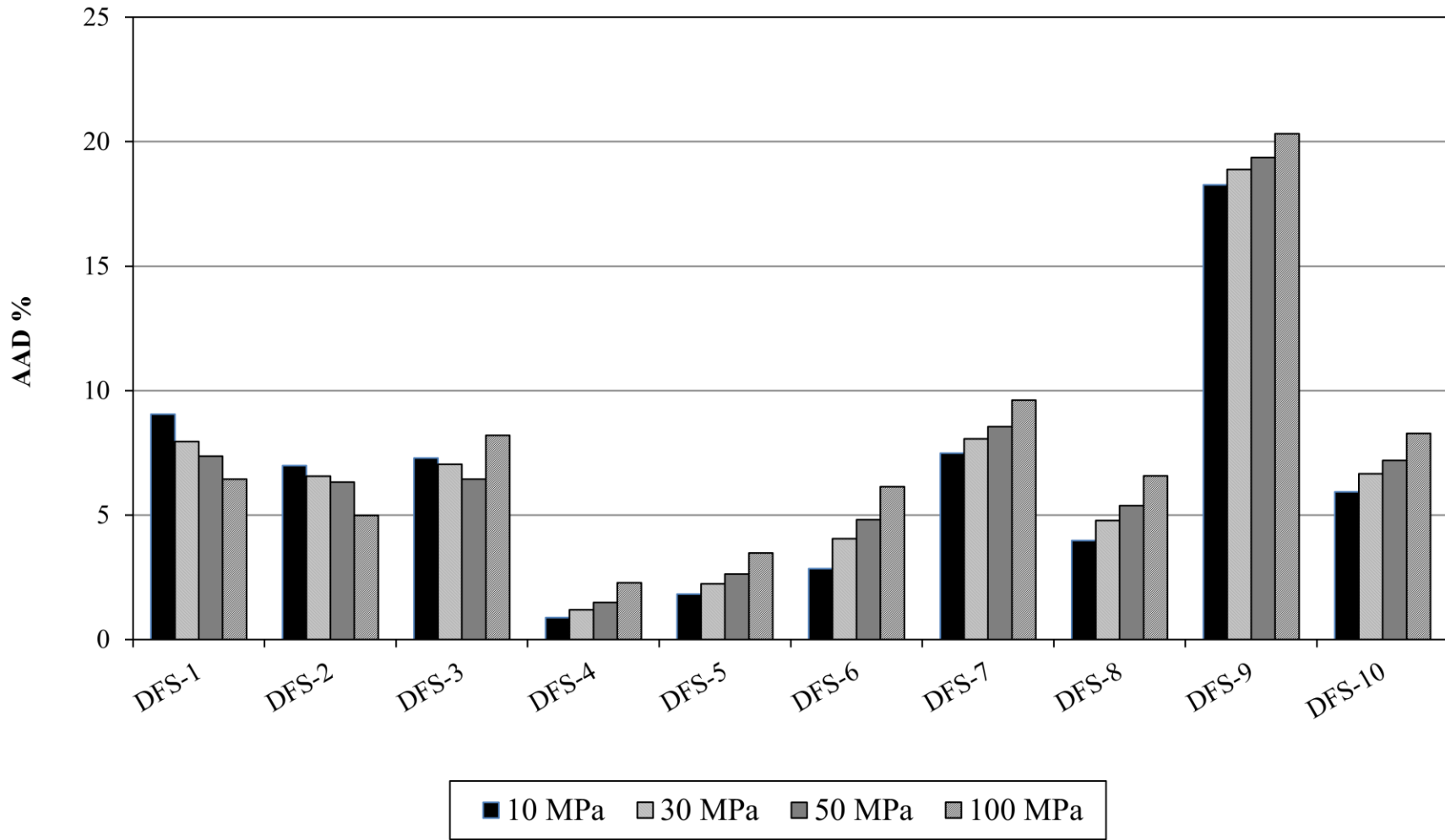


Fig. 3-9 Comparison of DFS's capability in predicting DF heat capacity.

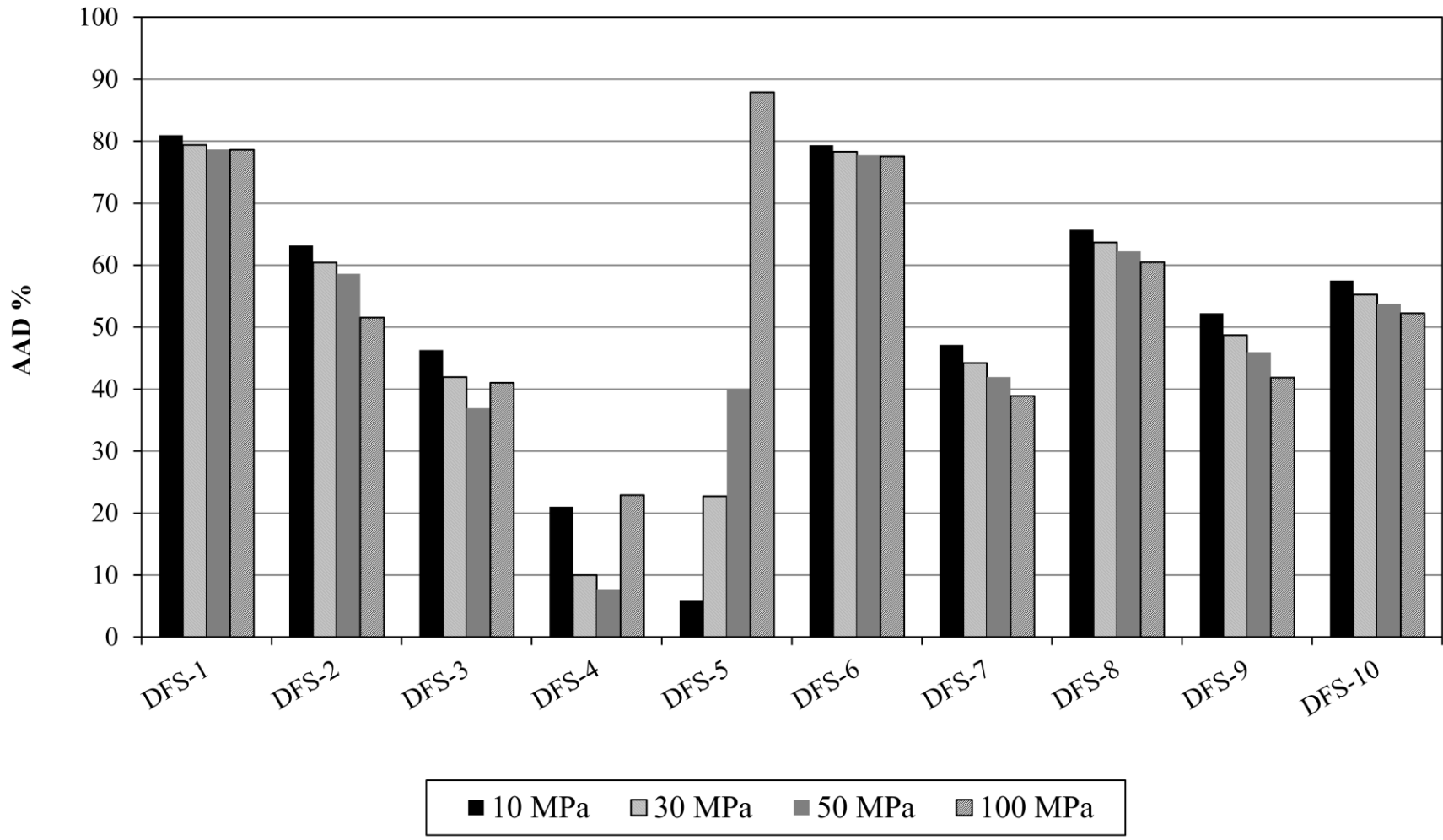


Fig. 3-10 Comparison of DFS's capability in predicting DF viscosity.

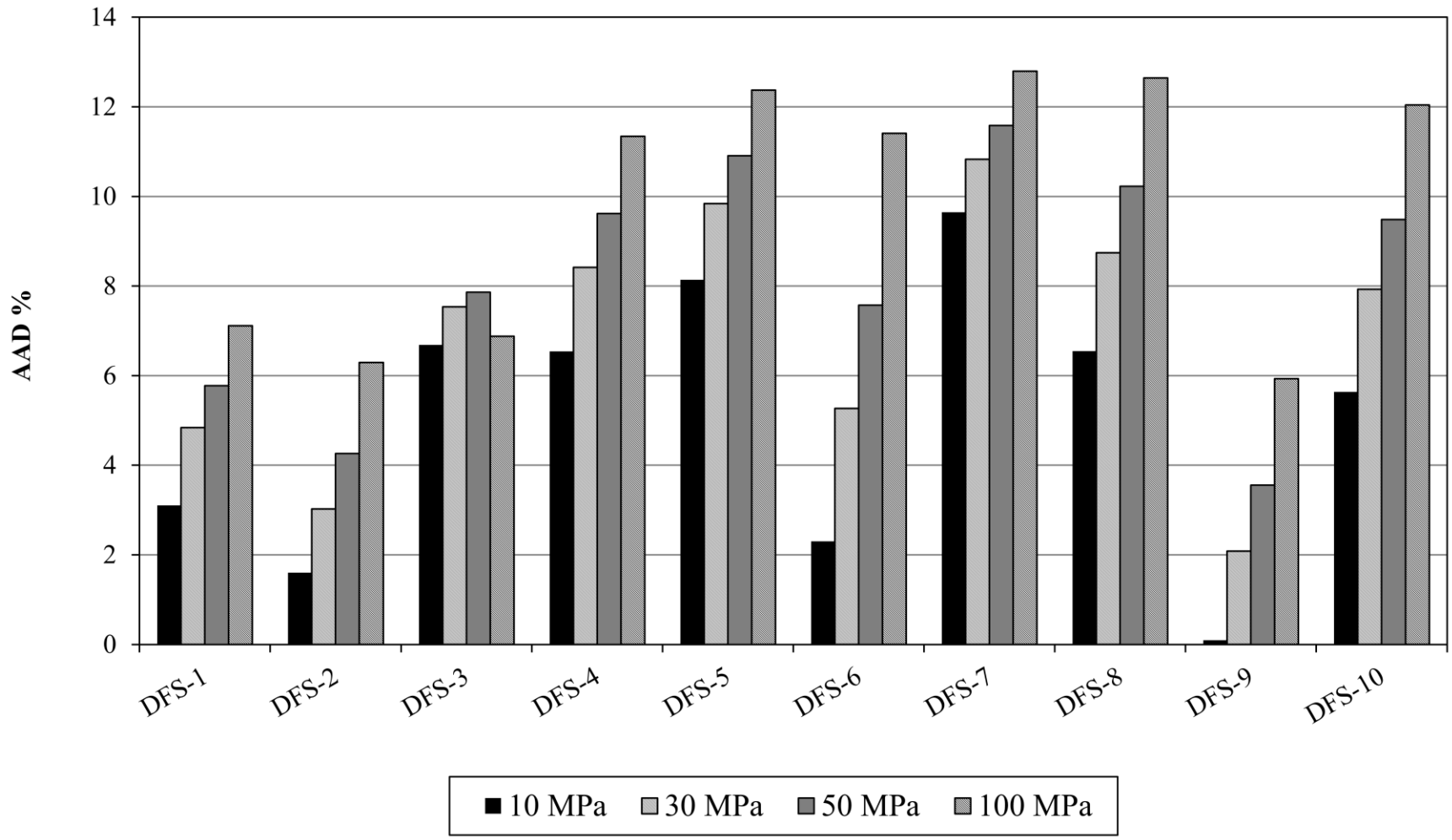


Fig. 3-11 Comparison of DFS's capability in predicting DF thermal conductivity.

Fig. 3-8 shows that DFS-7 gives best predictions of density of DF with AAD% less than 1% which is significantly lower than those of other DFSs. For most DFSs, the predictions are improved with reduced AAD values as pressure increases. For heat capacity, as shown in **Fig. 3-9**, DFS-4 gives best predictions followed by DFS-5. For viscosity, AADs for all DFSs except DFS-4 at 50 MPa and DFS-5 at 10 MPa are above 10%, and DFS-4 gives a relatively better overall predictions, as illustrated in **Fig. 3-10**. For thermal conductivity, DFS-9 gives a relatively better results as shown in **Fig. 3-11**. The DFS-10 proposed for this study has AAD% of less than 8% for density and heat capacity and 12% for thermal conductivity but exceeds 50% for viscosity for all pressures studied. These results lead to the conclusion that none of these DFSs are able to represent DF in terms of predicting all thermophysical properties of interest. Different DFSs are suggested to obtain different properties from these results.

3.5 CONCLUSIONS

Physical properties of DFSs are important parameters required for diesel engine design and simulation. The capabilities of ten DFSs in representing DF physical properties were evaluated. These properties include volatility, critical points, density, viscosity, heat capacity, and thermal conductivity. Volatility was measured using the TGA method, while other properties were estimated using various modeling techniques. As volatility is closely related to fuel compositions, it is not surprising that no simplified DFSs have volatility close to DF. However, it is not a big issue in the supercritical fuel system because fuel has already reached the supercritical state upon injection and hence volatility would have no effect on spray behavior. The critical point of DFS-5 is closest to

the estimated critical point of DF which is 739-754 K and 1.72-1.96 MPa. This suggests that DFS-5 may be considered where critical properties are key parameters. DFS-7 gives best predictions of density of DF with AAD% less than 1% which is significantly lower than those of other DFSs. DFS-4 gives overall best predictions of heat capacity and viscosity, while DFS-9 gives a relatively better results for thermal conductivity. Therefore, it is concluded that none of these DFSs are able to represent all thermophysical properties of DF. Different DFSs are suggested to obtain different properties.

CHAPTER IV

DIFFUSIVITY MEASUREMENTS¹

4.1 INTRODUCTION

Diffusivities are important parameters required for modeling of the multiphase fuel/diluents mixing processes and for simulation of spray atomization and combustion processes. This chapter describes experimental and modeling work on diffusion coefficients of diesel fuel and surrogate components in SCCO₂ over a wide range of temperature and pressure. DF was treated as one fluid, and CO₂ was chosen as a model compound for EGR. Experimental uncertainties are also extensively discussed.

Diffusivity data obtained in this work are also useful for design of other supercritical fluid processes. Knowledge of thermophysical properties of SCFs and other species involved in SCF systems is crucial to advancing the SCF technology and to developing SCF processes. Binary diffusion coefficients are one such property that needs further investigation. Although binary diffusion coefficients in SCFs have been studied since the 1960s (Funazukuri et al., 2004), experimental data are still very limited (Suárez et al., 1998). Moreover, the accuracy of data from various sources has seldom been justified. A comparison of diffusion coefficients of benzene in SCCO₂ from various sources showed large variations especially when the density of CO₂ is below the critical value.

¹ The majority of this chapter is written based on two published papers: (1) Lin, R., Tavlarides, L.L., 2010. Diffusion coefficients of diesel fuel and surrogate compounds in supercritical carbon dioxide, *The Journal of Supercritical Fluids* 52(1), 47-55 and (2) Lin, R., Tavlarides, L.L., 2010. Determination of diffusion coefficients by supercritical fluid chromatography: Effects of mobile phase mean velocity and column orientation, *Journal of Chromatography A* 1217 (26), 4454-4462. Copyright permissions are attached in Appendix E.

These variations largely resulted from experimental errors. Therefore, a better understanding of those aspects that influence uncertainties of measurements of binary diffusion coefficients in SCFs is of practical importance.

Besides, among fluid thermophysical properties, molecular binary diffusion coefficients are less understood than others due to both theoretical challenges and experimental difficulties. The accuracy of estimates for gases based on the Chapman-Enskog theory is around 10%, while that for liquids based on the Stokes-Einstein equation or its empirical correlations is about 20% (Cussler, 2009). These estimates help to solve only the routine problems (Cussler, 2009). Limitations exist, for example, in the field of diesel engine combustion where mass diffusion can limit the combustion rates (Farrell et al., 2007), and the information on mass diffusion coefficients is less reliable (Harstad and Bellan, 2004). Therefore, the current study is also intended to make contributions to advance the fundamentals of fluid thermophysical properties.

4.2 THEORETICAL BACKGROUND

4.2.1 Taylor dispersion analysis

Among all experimental techniques (Cussler, 2009) developed to date for determination of diffusion coefficients, the Taylor (or Taylor-Aris) dispersion method, also known as the chromatographic technique (Bruno, 1994; Funazukuri et al., 2004; Funazukuri et al., 2006; Liong et al., 1991; Roth, 1991) or the peak broadening technique, has been mostly applied in SCF systems. The Taylor dispersion phenomenon was first observed by Griffiths back to the early 1910s (Griffiths, 1910). During the investigation of the behavior of a short fluorescein solution pulse injected into a laminar water flow in a

capillary tube, Griffiths found that the colored pulse expanded symmetrically about the center which moved in a mean velocity of the liquid. In early 1950s, Taylor (Taylor, 1953; Taylor, 1954) experimentally confirmed Griffiths' observation and first developed the theoretical description of the phenomenon. Following Taylor's work, Aris (Aris, 1956) improved the theoretical analysis which formed a theoretical basis for Taylor dispersion towards the measurement of molecular diffusivity. A complete analysis of the theory was given by Alizadeh et al. (Alizadeh et al., 1980). Detailed descriptions of the theory can also be found elsewhere (Matthews, 1986; Pratt and Wakeham, 1975).

Applications of this method to the measurements of diffusion coefficients in SCFs were substantially investigated and a number of reviews were published (Bruno, 1994; Funazukuri et al., 2004; Funazukuri et al., 2006; Liong et al., 1991). Recent applications of this technique include determination of diffusion coefficients of various organic compounds in SCCO₂ (Pizarro et al., 2009a; Pizarro et al., 2009b). Although this method has been widely used, the reliability of its application in near-critical regions is still under debate and needs further investigations due to anomalous diffusivity behavior (Ago and Nishiumi, 1999; Funazukuri et al., 2000; Kong et al., 2008; Levelt Sengers et al., 1993; Nishiumi et al., 1996; Nishiumi and Kubota, 2007; Yang et al., 2000).

The idealized Taylor dispersion experiment for the measurement of molecular diffusivity is illustrated in **Fig. 4-1**. In a circular straight tube of infinite length and uniform cross section, a fully-developed laminar flow is maintained and the velocity field is defined by

$$u(r) = 2U \left(1 - \frac{r^2}{R^2} \right) \quad (4-1)$$

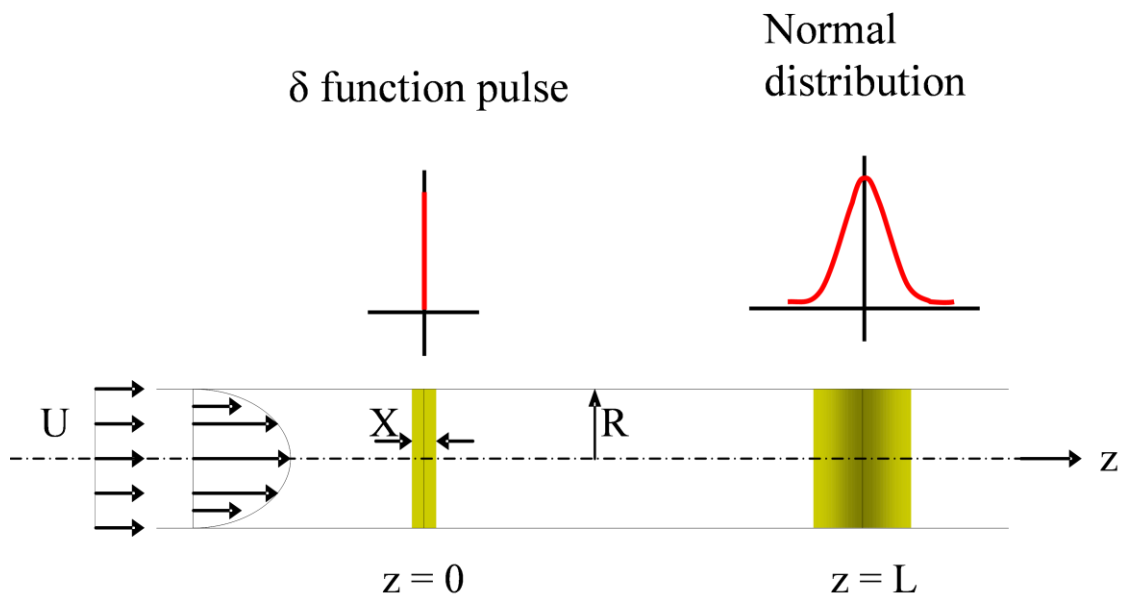


Fig. 4-1 The idealized Taylor dispersion experiment. U is the mean velocity, R is the radius of the dispersion column, L is the length of the dispersion column, and X is the width of the solute pulse.

where U and R are the mobile phase mean velocity and the pipe radius, respectively. Assume a δ -function pulse is injected into the flow at position $z = 0$. As the solute pulse moves along the tube, due to the combined action of forced convection and molecular diffusion, it disperses symmetrically about the cross section which moves at the mean flow velocity. If time is long enough, a concentration gradient that follows the Gaussian distribution is formed.

The mathematical analysis starts with the continuity equation. In the cylindrical coordinate system, the continuity equation for one component in terms of concentration C which is a function of time (t), length (z), and pipe radius (r) is given by

$$D_{12} \left[\frac{1}{r} \frac{\partial}{\partial r} \left(r \frac{\partial C}{\partial r} \right) + \frac{\partial^2 C}{\partial z^2} \right] = u \frac{\partial C}{\partial z} + \frac{\partial C}{\partial t} \quad (4-2)$$

where D_{12} is the binary molecular diffusion coefficient of solute 1 in solvent 2.

Several assumptions are followed in this analysis. D_{12} is assumed constant and independent of the concentration, no chemical reactions are considered, the fluid is incompressible, and the flow is the fully-developed laminar flow. Practically, it is more convenient to measure the mean concentration (C_m) over any cross section than to measure the concentration at any point. The mean concentration is defined by

$$C_m = \frac{1}{\pi R^2} \int_0^R C \cdot (2\pi r) \cdot dr \quad (4-3)$$

Accordingly, Eq. (4-2) can be reduced to the one-dimension diffusion equation

$$K \frac{\partial^2 C_m}{\partial x^2} = \frac{\partial C_m}{\partial t} \quad (4-4)$$

where,

$$K = D_{12} + \frac{R^2 U^2}{48 D_{12}} \quad (4-5)$$

K is the apparent diffusion coefficient also called the dispersion coefficient. Applying the similarity method by using dimensional analysis, a solution to Eq. (4-4) can be found in the form

$$C_m(x, t) = \frac{M}{\pi R^2 \sqrt{4\pi K t}} \exp\left[-x^2/4Kt\right] \quad (4-6)$$

where M is the total amount of solute injected into the tube.

The Taylor dispersion analysis is provided in detail in Appendix B.

4.2.2 Analysis of experimental data

To obtain the molecular diffusion coefficient D_{12} , the moment method was applied to process experimental data (Matthews, 1986). Zero and normalized first and second moments are the sum function (S), the center of the gravity (\bar{t}), and the variance (σ^2), respectively. They are defined by

$$S = \int_0^{\infty} C_m dt \quad (4-7)$$

$$\bar{t} = \frac{1}{S} \int_0^{\infty} C_m t dt \quad (4-8)$$

$$\sigma^2 = \frac{1}{S} \int_0^{\infty} (t - \bar{t})^2 C_m dt \quad (4-9)$$

Inserting Eq. (4-6) into Eqs. (4-7) - (4-9) and performing the integrations, we get (Pratt and Wakeham, 1975)

$$\bar{t} = \frac{L}{U} \left(1 + \frac{2K}{UL} \right) \quad (4-10)$$

$$\sigma^2 = \left(\frac{L}{U} \right)^2 \left(\frac{8K^2}{U^2 L^2} + \frac{2K}{UL} \right) \quad (4-11)$$

where L is the length of the diffusion column. With the substitution of Eq. (4-5), it can be shown that (Alizadeh et al., 1980)

$$D_{12} = \frac{R^2 \bar{t}}{24\sigma^2} \quad (4-12)$$

providing the following two conditions are satisfied

$$\frac{D_{12} \bar{t}}{R^2} > 10 \quad (4-13)$$

$$\frac{UR}{D_{12}} > 700 \quad (4-14)$$

Eq. (4-12) is the final working equation for measurement of binary molecular diffusion coefficient by using the Taylor dispersion technique.

To evaluate experimental uncertainties, curve-fitting errors between elution profiles measured in the experiments and those calculated by the Eq. (4-6) were estimated by (Funazukuri et al., 2006)

$$\mathcal{E} = \left[\frac{\int_{t_1}^{t_2} (C_{m,exp} - C_{m,cal})^2 dt}{\int_{t_1}^{t_2} C_{m,exp}^2 dt} \right]^{1/2} \quad (4-15)$$

where subscripts *exp* and *cal* indicate experimental data and calculated values given by

Eq. (4-6). In this work, t_1 and t_2 were times at 1% peak height of elution profiles.

4.3 EXPERIMENTAL

4.3.1 Materials

Benzene (99%), toluene (CHROMASOLV Plus, for HPLC, $\geq 99.9\%$), m-xylene (anhydrous, $\geq 99\%$), 1-hexadecene (99%) and 1-methylnaphthalene (95%) were purchased from Sigma-Aldrich, Inc. and used without further purification. Hexane (OPTIMA) was supplied by Fisher Scientific, Inc. No.2 diesel fuel was purchased from a local gas station. Liquid CO₂ (industrial) was supplied by Airgas, Inc. 1-hexadecene instead of n-hexadecane was used because n-hexadecane is not sensitive to UV-vis light.

4.3.2 Experimental setup

Design of the Taylor dispersion experiment has been well described in the literature (Funazukuri et al., 2000a; Matthews, 1986; Umezawa and Nagashima, 1992). The experimental setup is mainly composed of five parts: a pump for mobile phase delivery, a valve for sample injection, a diffusion column, a temperature control unit, and a concentration profile detector. **Fig. 4-2** shows schematic diagrams of three different setups used in this study. Three stainless steel tubes (Small Parts, Inc., I.D.0.762 mm \times 30.4 m, I.D.0.508 mm \times 30.48 m, and I.D.0.254 mm \times 30.48 m) were used as diffusion columns. The tubes were coiled in a diameter of 0.2 m and installed either vertically in a gas chromatography (GC) oven (HP 5890) (**Fig. 4-2 A and B**) or horizontally in a water bath (**Fig. 4-2 C**). Liquid CO₂ was delivered by a syringe pump (ISCO 100D or 260D). A second stainless steel tube was located in a water bath to pre-heat the mobile phase.

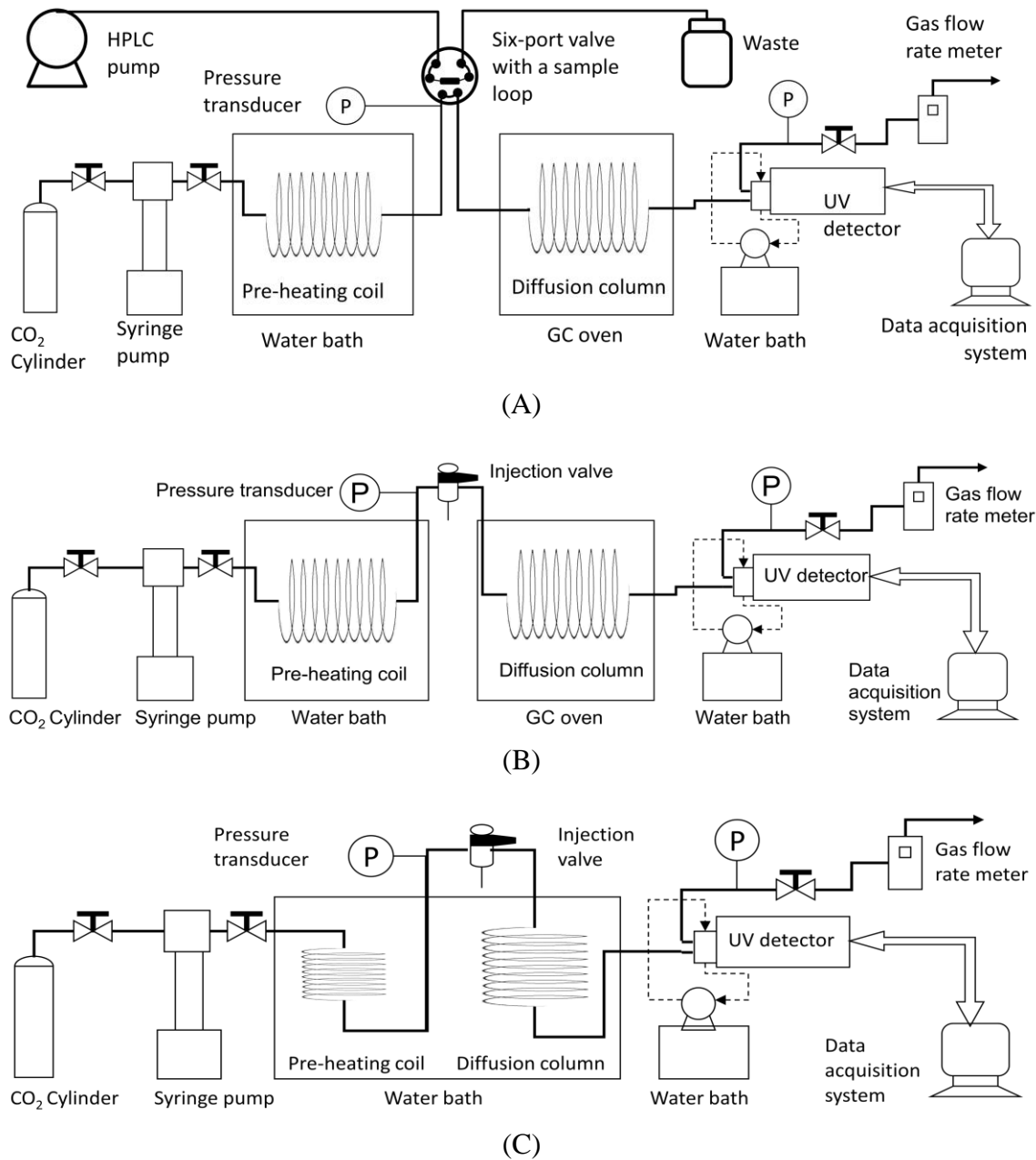


Fig. 4-2 Schematic diagrams of experimental setups for measurement of diffusion coefficients using the Taylor dispersion method. (A) A six-port injection valve was used and a column was vertically installed in a GC oven; (B) A manual injection valve was used and a column was vertically installed in a GC oven; (C) A manual injection valve was used and a column was horizontally installed in a water bath.

Samples were loaded through either a six-port valve (Rheodyne 7010, 5 μ L) (**Fig. 4-2 A**) or a manual injection valve (Rheodyne 7520, 0.5 μ L) (**Fig. 4-2 B and C**). When the six-port valve was used, an HPLC pump (Dynamex, Model SD-1) was used to deliver samples. Pressures were controlled by the syringe pump, and flow rates were controlled by a manual valve after the second pressure transducer and measured by a digital flowmeter (Fisher Scientific, Model 520). A dual-wavelength UV-vis detector (Thermo Electron, Model 205) equipped with a high-pressure flow cell (Thermo Electron, Model 9550-150) with an illuminated volume of 0.25 μ L was used to monitor elution profiles out of the diffusion column. Elution profiles and pressure data were recorded by a data acquisition system (LabVIEW, National Instruments).

4.3.3 Experimental conditions and procedure

The system was warmed up to reach experimental conditions and then stabilized for about two hours before each run. CO₂ was delivered by the syringe pump at constant pressure mode to minimize pressure fluctuations. Pressure fluctuations for all runs were controlled within ± 0.02 MPa. Pressure drops along the diffusion column varied with flow rates and were less than 1.0% of working pressure for all runs. Flow rates were monitored by the digital flow rate meter and controlled by a manual valve within 3% of set points with the exception of a maximum value of 7.0 % which occurred in the critical region of CO₂. Samples were injected continuously in an interval of 12-20 min, depending on pressure, temperature and flow rate conditions, to avoid peak overlapping. All temperature measurements were within ± 0.1 K of set points. The maximum working temperatures of the injection valve and the UV-vis detector flow cell are 353.15 and

313.15 K, respectively. As measurements went above these temperature limits, the injection valve and the detector were thermally stabilized at their maximum working temperatures.

The experiment mainly includes three sections. First, various combinations of diffusion columns and injection volumes were tried and diffusion coefficients of benzene in SCCO₂ were measured to examine the performance of the setup in getting accurate diffusivity data. Second, diffusion coefficients of diesel fuel and surrogate compounds including benzene, toluene, m-xylene, 1-hexadecene and 1-methylnaphthalene were measured. Finally, diffusion coefficients of benzene in SCCO₂ were measured in a wide range of experimental conditions to examine experimental uncertainties.

In the second part of this experiment, the retention time for all experimental conditions varied from 60 to 90 min with a velocity range of 0.006-0.008 m/s close to the one reported previously (Kong et al., 2008), and the laminar flow condition was satisfied with $Re < 50$. UV absorbance spectra of benzene, toluene, m-xylene, 1-hexadecene, 1-methylnaphthalene and diesel fuel were measured and optimal wavelength ranges for each species were determined by measuring diffusion coefficients at 313.15 K and 10 MPa with varying wavelengths. In the third part, experiments were conducted at 313.15 and 333.15 K and 9-15 MPa. The dual-wavelength of 230 and 235 nm determined in the second part of this experiment was used.

4.4 EXPERIMENTAL UNCERTAINTIES

4.4.1 Sources of experimental uncertainties

Diffusion coefficient measurement by the Taylor dispersion method is based on

the analysis of idealized Taylor dispersion behavior in a straight pipe. Any departures from the ideal case in real experiments result in uncertainties in the measurements. **Fig. 4-3** shows schematically difference between the ideal (**Fig. 4-3A**) and the real (**Fig. 4-3B**) Taylor dispersion experiments. In the ideal experiment, a δ -function type solute pulse is introduced in a laminar flow inside a straight cylindrical pipe. Under the combined action of bulk convection and molecular diffusion, the pulse disperses symmetrically, forming a Gaussian distributed concentration profile. The average cross-sectional concentration measured at the end of the pipe can be approximated by Eq. (4-6) with negligible error (Funazukuri et al., 2000a). In practice, however, a coiled dispersion column is usually applied to minimize space usage and for better temperature control. Moreover, an approximately rectangular pulse is injected instead of a δ -function type one, and the concentration of the effluent at the end of tube is averaged over a finite detection volume. These departures of the real experiment from the ideal one result in significant experimental uncertainties. Alizadeh *et al.* (Alizadeh et al., 1980) classified and examined these departures in four groups: sample injection, diffusion column geometry, concentration measurement, and fluid properties. In addition, flow conditions and P-T control (Bueno et al., 1993), dead volume (Bueno et al., 1993), and wall adsorption (Umezawa and Nagashima, 1992) may also contribute to experimental uncertainties.

4.4.2 Peak tailing

Peak tailing can cause large errors in diffusion coefficient measurement by the Taylor dispersion method. Umezawa and Nagashima (Umezawa and Nagashima, 1992) and van de Ven-Lucassen et al. (van de Ven-Lucassen et al., 1997) claimed that peak tailing is

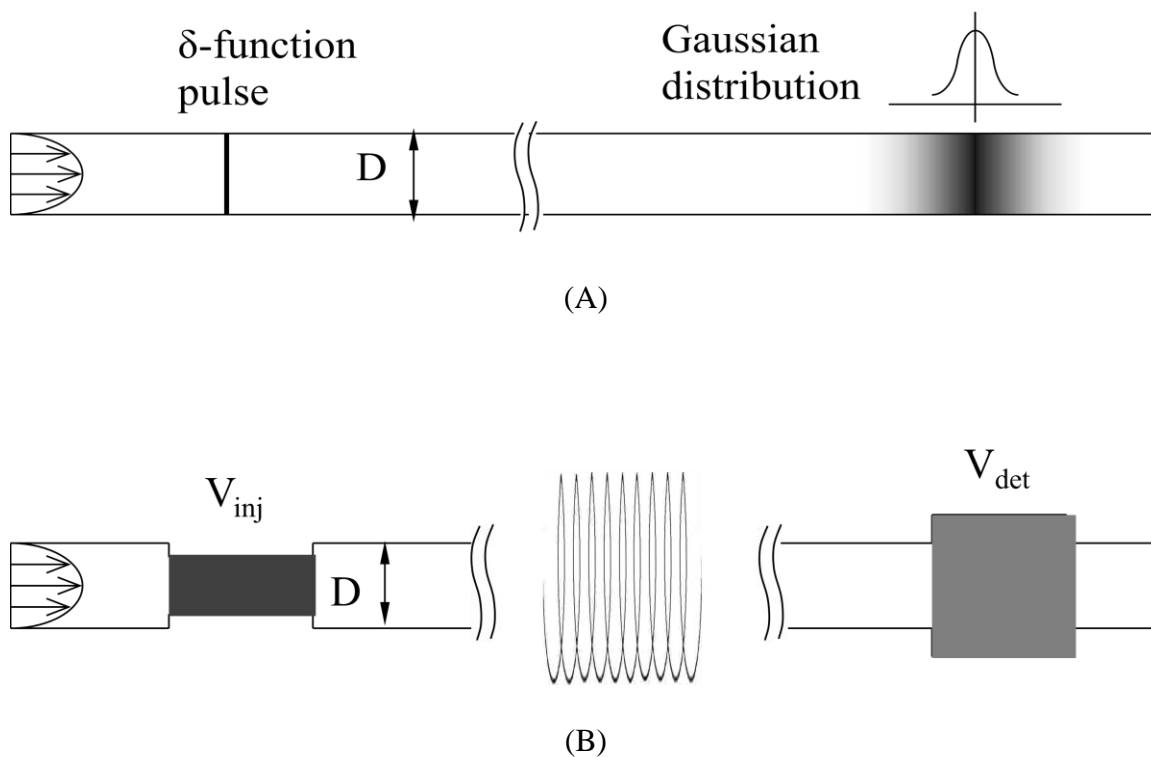


Fig. 4-3 Comparison of ideal and real Taylor dispersion experiments for diffusion coefficient measurements. (A): A straight cylindrical tube is used as a diffusion column; (B): A coiled cylindrical tube is used as a diffusion column. D : diameter of diffusion columns; V_{inj} : injection volume; V_{det} : detection volume.

due to adsorption of solute onto the wall of the diffusion column. Umezawa and Nagashima (Umezawa and Nagashima, 1992) further pointed out that this effect becomes more significant in the low density range where the solvent power of CO₂ is low.

4.4.3 Effect of sample injection

In real experiments, it is impossible to inject a δ -function pulse (**Fig. 4-3A**). However, a rectangular pulse (**Fig. 4-3B**) is produced if the sample instantaneously fills the rectangle upon injection. Alizadeh et al (Alizadeh et al., 1980) made corrections in the moment analysis by means of a perturbation treatment to account for the influence of the rectangular pulse on diffusion coefficient measurement. Bruno (Bruno, 1994) suggested that the error associated with non- δ -function pulse can be minimized by using a diffusion tube volume that is large with respect to the volume of the rectangular pulse.

A new dimensionless parameter, φ , was proposed in this study to characterize the effect of the finite injection volume. φ is defined by the ratio of equivalent length of the sample injected over the column diameter as follows

$$\varphi = \frac{L_{e,inj}}{D} \quad (4-16)$$

$$L_{e,inj} = \frac{V_{inj}}{A} \quad (4-17)$$

where $L_{e,inj}$ is the equivalent length of the sample injected, A is the cross-section area of the diffusion column, and V_{inj} is the injection volume. A literature survey shows a wide range of φ values from 0.25 to greater than 100. Different combinations of V_{inj} and D were examined to determine an optimal range of φ in which the influence of the finite

injection volume is minimized and can be neglected.

4.4.4 Effect of concentration measurement

The accuracy of diffusion coefficient measurements is directly proportional to the accuracy of concentration measurements. There are two aspects involved in concentration measurements which lead to measurement uncertainty: detector volume and detector linearity. The influence of detector volume is independent of the type of detector used, while detector linearity varies from one to another. A comprehensive theoretical analysis addressing the effect of finite detector volume was reported elsewhere (Alizadeh et al., 1980). A finite detector volume results in a concentration profile of which each point is actually an averaged value over a finite length of the column. Similar to the treatment of the injection volume, an equivalent length of the detector volume was introduced to characterize this effect. The new parameter is defined by

$$L_{e,\text{det}} = \frac{V_{\text{det}}}{A} \quad (4-18)$$

where V_{det} is the detector volume. The higher the $L_{e,\text{det}}$ value is, the greater is the systemic error. In this work, $L_{e,\text{det}} = 2.5D$.

Different types of detectors have different linear ranges. Linearity of the UV detector used in the work depends on both solute concentration and the wavelength chosen. Also, the optimal linear range varies with wavelength. **Fig. 4-4** demonstrates the effect of detector linearity on the accuracy of diffusion coefficient measurements. Assuming a linearity limit of absorbance unit (AU) AU=1, as concentration increases above the limit, the detector gives a lower value (experimental data) than what it should

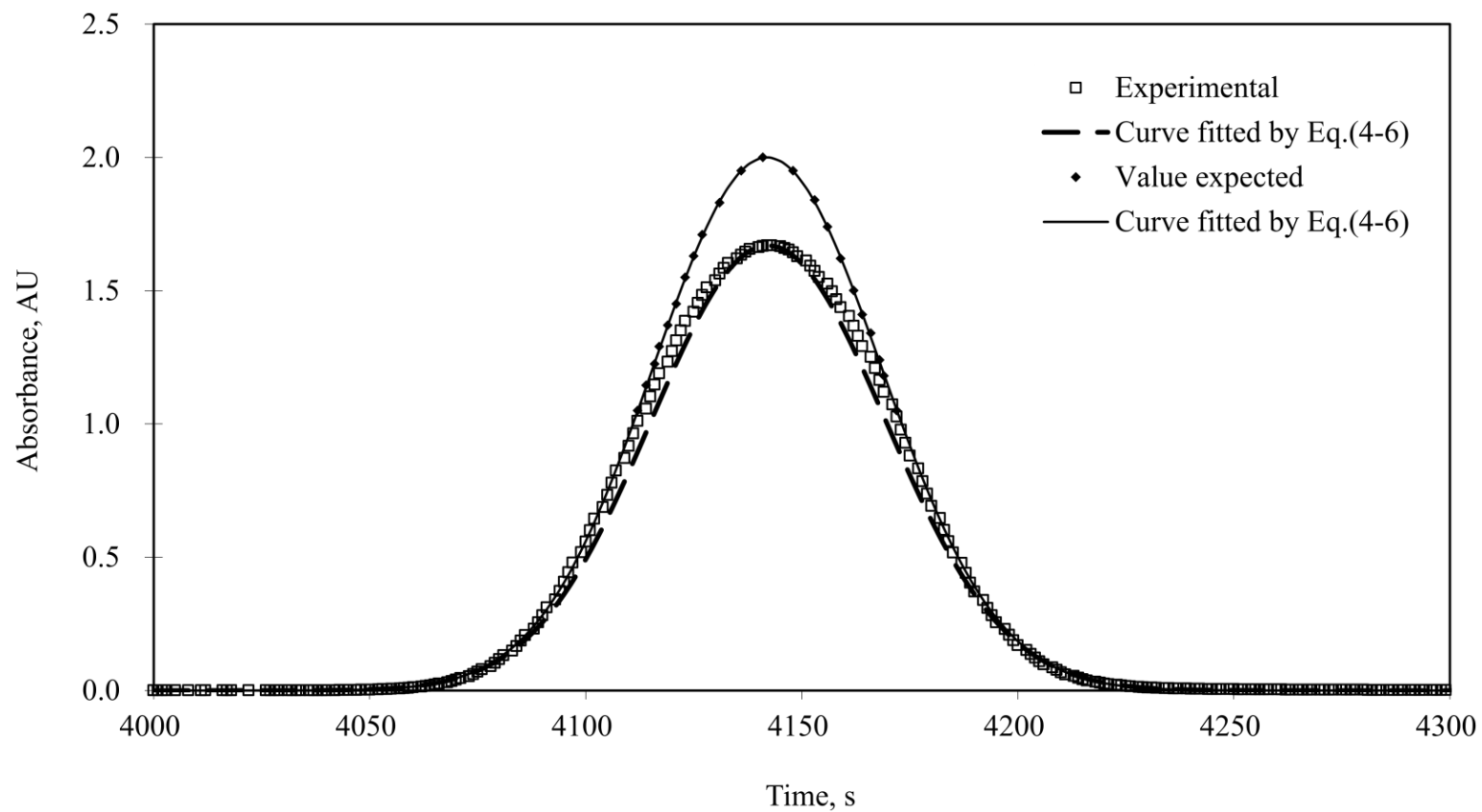


Fig. 4-4 Demonstration of the effect of detector linearity on the accuracy of diffusion coefficient measurements. Open squares (\square): data measured in this work for 1-methylnaphthalene at 353.15 K and 15 MPa; Filled diamonds (\blacklozenge): data manipulated for demonstration only.

be (data manipulated for demonstration only), leading to a lower diffusion coefficient ($15.5 \times 10^{-9} \text{ m}^2/\text{s}$). Under the same experimental conditions, the better linearity gives a higher diffusion coefficient value. Diffusion coefficients are theoretically independent of wavelength. Therefore, the optimal wavelength should be chosen where constant diffusion coefficients were obtained (Funazukuri et al., 2004).

In this work, UV absorption spectra of diesel fuel and all surrogate compounds were measured. The effect of wavelength on diffusivity measurements was examined by measuring diffusion coefficients using different wavelengths, and the optimal wavelength ranges for each species were determined.

4.4.5 Effect of column geometry and orientation

It is well known that coiling of a tube brings centrifugal forces on flowing fluids, which creates secondary flows that can influence the dispersion process. The effect of tube curvature on the laminar dispersion of solute in a circular tube has been extensively studied (Alizadeh et al., 1980; Erdogan and Chatwin, 1967; Janssen, 1976; Nunge et al., 1972). Erdogan and Chatwin (Erdogan and Chatwin, 1967) treated the problem in a similar analytical way as Taylor (Taylor, 1953; Taylor, 1954) did for straight tubes using the velocity distribution of Dean (Dean, 1927; Dean, 1928) and predicted that the dispersion coefficient is always reduced by the curvature for all common liquids and most gases if the radius of the curvature is sufficiently large. Nunge *et al.* (Nunge et al., 1972), employing the velocity distribution of Topakoglu (Topakoglu, 1967), extended the previous analysis to small curvature and found that the dispersion coefficient may be increased substantially by curvature in low Reynolds number flows. The authors (Nunge et al., 1972)

attributed this behavior to the opposing impacts of the asymmetric axial velocity distribution, which tends to increase dispersion, and the secondary flow, which decreases the dispersion by creating a transverse mixing. Employing results of the previous study, Alizadeh *et al.* (Alizadeh et al., 1980) established conditions under which the effects of curvature are negligible, which provided a useful guide for the design of experiment for diffusivity measurements.

A dimensionless group, $De\sqrt{Sc}$, has been successfully formulated and applied to characterize the effect of curvature (Alizadeh et al., 1980; Bueno et al., 1993). The Dean number (De) and the Schmidt number (Sc) are defined as

$$De = Re \sqrt{R/R_c} \quad (4-19)$$

$$Sc = \frac{\mu}{\rho D_{12}} \quad (4-20)$$

where Re is the Reynolds number, R is the radius of the column, R_c is the radius of the diffusion column coil, and μ and ρ are viscosity and density of the solvent, respectively.

The secondary flow effects become negligible providing the following restriction is satisfied (Alizadeh et al., 1980; Funazukuri et al., 2000a; Liong et al., 1991)

$$De\sqrt{Sc} < \chi \quad (4-21)$$

Various χ values were reported in the literature including 4.5 (Alizadeh et al., 1980), 8 (Funazukuri et al., 2000a), and 10 (Liong et al., 1991). In this work, χ was less than 7.5.

All studies referred above were based on the assumptions that the mobile phase was incompressible and the density of the solute/mobile phase mixture was constant and independent of solute concentration. When the density of the solute differs from that of

the mobile phase and the density of the mixture depends on solute concentration, which is inevitably encountered in most SCF systems, the problem becomes much more complicated. Density gradients induce buoyancy forces which may cause significant uncertainties in diffusivity measurements. Reejhsinghani *et al.* (Reejhsinghani *et al.*, 1966) observed the impact of density difference on dispersion in horizontal tubes. Erdogan and Chatwin (Erdogan and Chatwin, 1967) also studied this issue and concluded that the effect of buoyancy forces was related to the magnitude of Peclet numbers. Buoyancy effects have also been recognized in other transport property measurements (Laesecke *et al.*, 1999).

Coiled columns used in diffusion coefficient experiments were usually installed either horizontally (Ago and Nishiumi, 1999; Funazukuri *et al.*, 2000b; Lai and Tan, 1995; Pizarro *et al.*, 2009a; Yang *et al.*, 2000) or vertically (Bueno *et al.*, 1993; Fu *et al.*, 2000; Funazukuri and Nishimoto, 1996; Nishiumi *et al.*, 1996) depending on the temperature control instrument used. Less attention, however, has been given to the understanding of the impact of column orientation on measurements of diffusion coefficients in supercritical fluids. In studying diffusion coefficients of benzene in SCCO₂, Funazukuri and Nishimoto (Funazukuri and Nishimoto, 1996) found that diffusion coefficients measured using the horizontally-installed column were higher than those measured using the vertically-installed one. Nishiumi *et al.* (Nishiumi *et al.*, 1996) studied the effect of column orientation on diffusion coefficients of acetone in SCCO₂ at 314.25 K and various pressures. Their results showed a good agreement with Funazukuri and Nishimoto's findings (Funazukuri and Nishimoto, 1996) when pressure was less than 17 MPa. For pressures above 17 MPa, the effect of column orientation was reduced. The authors further pointed out that a vertical orientation should be avoided due to complicated

buoyancy effects especially near the critical point. In supercritical fluid systems, the impact of column orientation may become more significant due to substantial density difference between injected samples and SCFs. Further investigations are necessary to address this issue.

In this work, the effect of column orientation was examined. Diffusion coefficients of benzene in SCCO₂ were measured using a column either vertically-installed in the GC oven (**Fig. 4-2B**) or horizontally-installed in the water bath (**Fig. 4-2C**).

4.4.6 Effect of mean velocity

The mean velocity, U , is an important parameter that practically affects diffusion coefficient measurements, although diffusion coefficients are theoretically independent of U . A typical relationship between measured diffusion coefficients and U is shown in **Fig. 4-5** (Bueno et al., 1993; Funazukuri et al., 1991; Funazukuri et al., 1989; Mantell et al., 2003; Yang et al., 2000). As U is reduced from a high level, the measured diffusion coefficient decreases initially and then reaches a constant value which is the real value of diffusion coefficient. The increase of measured diffusion coefficient with increasing U is known as a consequence of the secondary flow effects due to tube coiling. Therefore, accurate diffusion coefficients can be determined only within a limited range of U . This limited range within which measured diffusion coefficients are independent of U is defined in this work as the *optimal velocity range* (OVR). Various OVRs were reported in the literature (Bueno et al., 1993; Fu et al., 2000; Funazukuri et al., 1991; Funazukuri and Nishimoto, 1996; Funazukuri et al., 1989; Lai and Tan, 1995; Mantell et al., 2003). However, no information is available about whether or not the OVR is affected by other operation

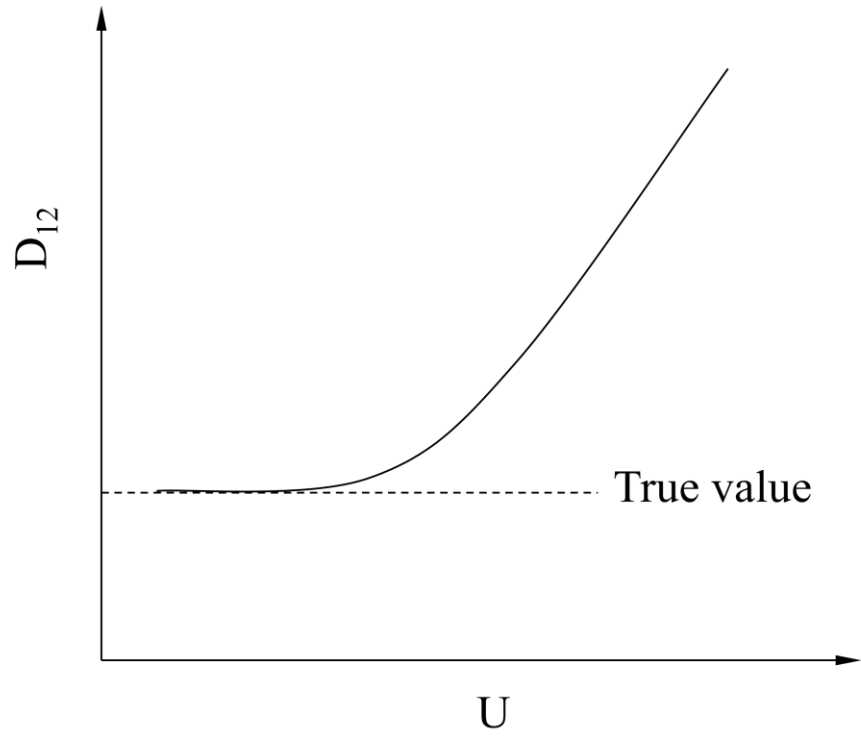


Fig. 4-5 Typical relationship between measured diffusion coefficient and U .

conditions.

In this work, the effect of mean velocity was examined. Diffusion coefficients of benzene in SCCO₂ were measured over a wide velocity range. A new D₁₂-U relationship pattern diagram was generalized based on the current findings.

4.5 MODELING OF EXPERIMENTAL DATA USING PREDICTIVE

CORRELATIONS

Three predictive correlations were evaluated with diffusion coefficients measured in this work, including Wilke-Chang (Poling et al., 2001), Scheibel (Scheibel, 1954) and He-Yu (He and Yu, 1998). Data were also fitted by $D_{12}/T - \mu$ (Funazukuri et al., 2006) and $D_{12}/\sqrt{T} - \rho$ correlations.

The Wilke-Chang correlation (Poling et al., 2001) given in Eq. (4-22) is a semi-empirical modification of the Stokes-Einstein relation and has been widely employed for diffusion coefficient estimation:

$$D_{12} = 7.4 \times 10^{-15} \frac{T (\psi MW_2)^{1/2}}{\mu_2 V_{1,b}^{0.6}} \quad (4-22)$$

where MW_2 is the molecular weight of the solvent in g/mol, μ_2 is the viscosity of the solvent in Pa.s, ψ is a dimensionless association factor of the solvent, and $V_{1,b}$ is the molar volume in $10^{-6} \text{ m}^3/\text{mol}$ of the solute at its normal boiling temperature. $V_{1,b}$ can be estimated from the critical volume by the Tyn and Calus method (Poling et al., 2001)

$$V_b = 0.285 V_c^{1.048} \quad (4-23)$$

where subscript c indicates the critical point.

The Scheibel correlation (Scheibel, 1954) reads

$$D_{12} = 8.2 \times 10^{-15} \frac{T \left(1 + \left(\frac{3V_{2,b}}{V_{1,b}} \right)^{2/3} \right)}{\mu_2 V_{1,b}^{1/3}} \quad (4-24)$$

where $V_{2,b}$ is the molar volume of solvent at its normal boiling temperature.

The Hu-Yu correlation (He and Yu, 1998) has the following form

$$D_{12} = B \times 10^{-9} \left(\frac{T}{MW_1} \right)^{1/2} \exp \left(- \frac{0.3887V_{2,c}}{V_2 - 0.23V_{2,c}} \right) \quad (4-25)$$

$$B = 14.882 + 0.0059081 \frac{T_{2,c} V_{2,c}}{MW_2} + 2.0821 \times 10^{-6} \left(\frac{T_{2,c} V_{2,c}}{MW_2} \right)^2 \quad (4-26)$$

The $D_{12}/T - \mu$ correlation given by Eq. (4-27) is valid for various compounds at supercritical conditions (Funazukuri et al., 2006):

$$\frac{D_{12}}{T} = \beta \mu_2^\gamma \quad (4-27)$$

The $D_{12}/\sqrt{T} - \rho$ correlation proposed in this work has a form very similar to the $D_{12}/T - \mu$ correlation:

$$\frac{D_{12}}{\sqrt{T}} = \zeta \rho_2^\xi \quad (4-28)$$

where ρ_2 is the density of SCCO₂ in kg/m³. β and γ in Eq. (4-27) and ζ and ξ in Eq. (4-28) are constants to be fitted by experimental data. Units of other variables in Eqs. (4-23) - (4-28) are the same as described for Eq. (4-22).

4.6 RESULTS AND DISCUSSIONS

4.6.1 Physical properties

Physical properties of CO₂ used in this work were calculated using the NIST Chemistry WebBook (Linstrom and Mallard, 2009). Properties used in modeling of experimental data are given in **Table 4-1**. Density of CO₂ is also presented as a function of pressure in **Fig. 4-6**. Also presented in this figure is density of benzene provided by the supplier. Highlighted by red diamonds in **Fig. 4-6** are conditions where diffusivities of benzene in SCCO₂ were measured to understand experimental uncertainties.

4.6.2 Validation of the apparatus

Before acquiring data for diesel fuel and surrogate compounds, diffusion coefficients of benzene in SCCO₂ were measured under different conditions and compared with data from literature to validate the reliability of the apparatus assembled in this work. Data presented in this section were obtained using the 0.508 mm I.D. column in the vertical orientation. **Fig. 4-7** shows diffusion coefficients of benzene in SCCO₂ as a function of the density of CO₂. A good agreement with literature data (Bueno et al., 1993; Funazukuri and Nishimoto, 1996; Levelt Sengers et al., 1993; Sassi et al., 1987; Suárez et al., 1993; Swaid and Schneider, 1979) validates the reliability of the measurements in this study. All literature data presented in **Fig. 4-7** are listed in Appendix C.

4.6.3 Diffusion coefficients of diesel fuel and surrogate compounds in SCCO₂

Diffusion coefficients of benzene, toluene, m-xylene, 1-hexadecene, 1-methyl-

Table 4-1 Physical properties of CO₂ as a function of temperature and pressure.

| T, K | P, MPa | ρ , kg/m ³ | V, 10 ⁻⁶ m ³ /mol | μ , 10 ⁻⁵ Pa · s |
|---------------------|-------------------|----------------------------|---|---------------------------------|
| 304.13 ^a | 7.38 ^a | 467.60 | 94.12 | n/a |
| 313.15 | 10 | 628.61 | 70.01 | 4.78 |
| 313.15 | 20 | 839.81 | 52.40 | 7.83 |
| 313.15 | 30 | 909.89 | 48.37 | 9.38 |
| 333.15 | 10 | 289.95 | 151.79 | 2.38 |
| 333.15 | 15 | 604.09 | 72.85 | 4.61 |
| 333.15 | 20 | 723.68 | 60.81 | 6.00 |
| 333.15 | 30 | 829.71 | 53.04 | 7.68 |
| 353.15 | 10 | 221.60 | 198.60 | 2.20 |
| 353.15 | 15 | 427.15 | 103.03 | 3.25 |
| 353.15 | 20 | 593.89 | 74.10 | 4.60 |
| 353.15 | 30 | 745.60 | 59.03 | 6.38 |
| 373.15 | 10 | 188.56 | 233.39 | 2.18 |
| 373.15 | 20 | 480.53 | 91.58 | 3.72 |
| 373.15 | 30 | 661.87 | 66.49 | 5.40 |

^a Critical point.

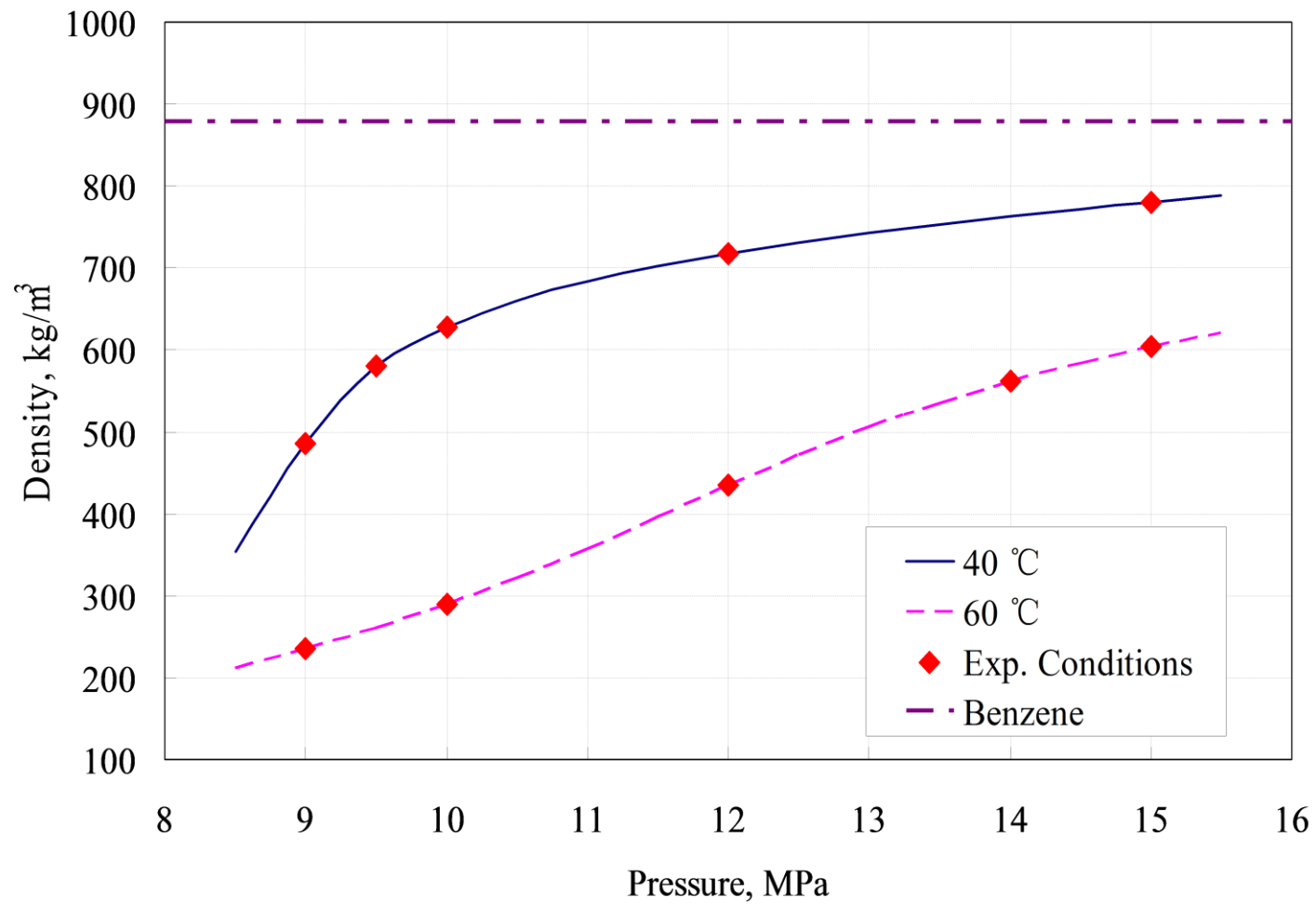


Fig. 4-6 Density of benzene and CO₂ as a function of pressure.

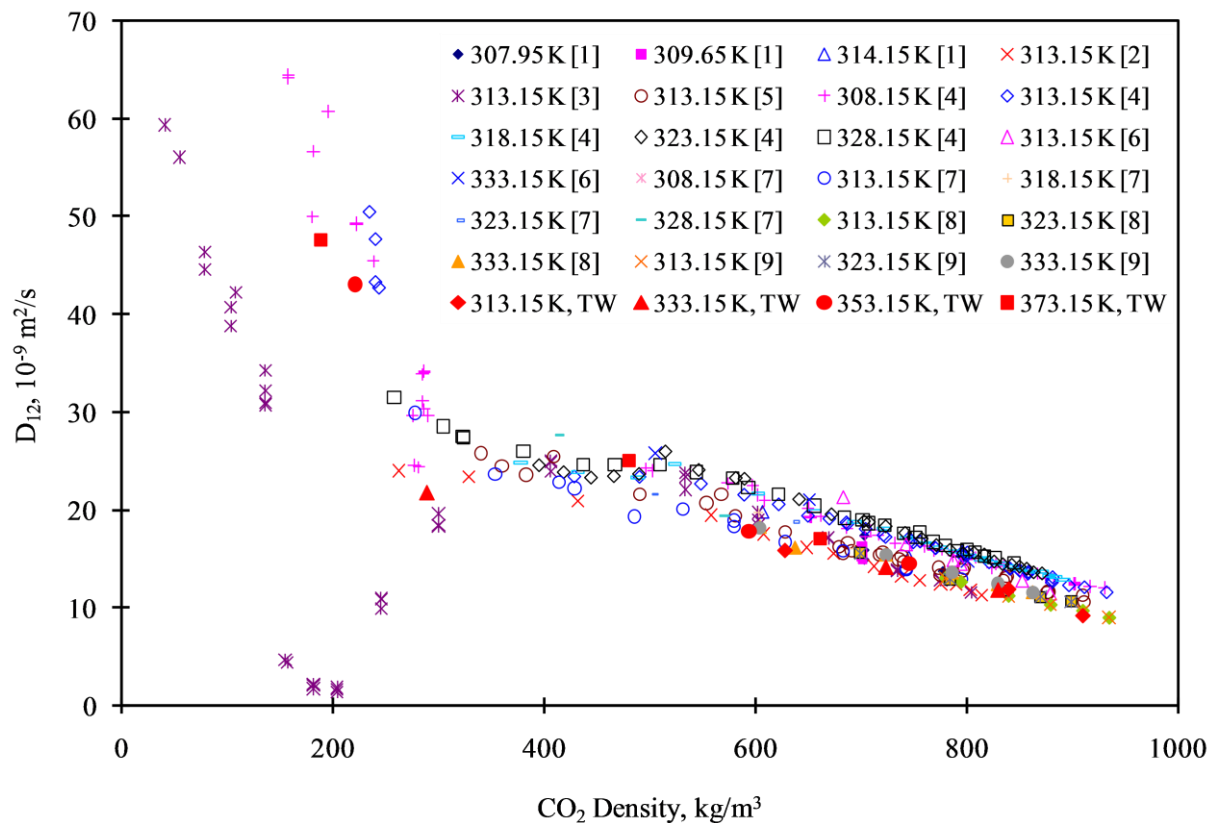


Fig. 4-7 Diffusion coefficients of benzene in SCCO_2 as a function of the density of CO_2 : a comparison with literature data. References: [1] (Levelt Sengers et al., 1993), [2] (Ago and Nishiumi, 1999), [3] (Nishiumi and Kubota, 2007), [4] (Funazukuri et al., 2001), [5] (Funazukuri and Nishimoto, 1996), [6] (Sassiat et al., 1987), [7] (Swaid and Schneider, 1979), [8] (Suárez et al., 1993), and [9] (Bueno et al., 1993). TW: This Work.

naphthalene and diesel fuel in SCCO₂ were measured at 313.15-373.15 K and 10-30 MPa using the 0.508 mm I.D. column in the vertical orientation. Results are presented in **Table 4-2** and **Table 4-3**, showing that diffusion coefficients increased with increasing temperature but decreasing pressure. Under the same conditions, diffusion coefficients decreased with increasing molecular weight in the order of benzene, toluene, m-xylene, 1-methylnaphthalene, and then 1-hexadecene. Measured diffusion coefficients of diesel fuel were generally lower than those of all other compounds largely due to its mixture characteristics.

Diffusion coefficients and their corresponding errors evaluated by Eq. (4-15) are plotted as a function of the density of CO₂ in **Fig. 4-8**, illustrating that both diffusion coefficients and curve-fitting errors generally increased with decreasing density of CO₂. However, when the density of CO₂ reduced across the critical density, measured diffusion coefficients dropped, associated with a significant increase in curve-fitting errors as shown for 1-methylnaphthalene, 1-hexadecene and diesel fuel in **Fig. 4-8**. Furthermore, diffusivities could not be obtained for these compounds at lower CO₂ densities due to significant peak tailing. For benzene, toluene and m-xylene, the same behavior is expected as shown previously (Nishiumi and Kubota, 2007) followed by large rebound in diffusivity values as the density of CO₂ moves below 300 kg/m³. This abnormality is largely due to the reduced solubilities of these solutes in SCCO₂ and shows the difficulty in measuring diffusion coefficients near critical regions by the Taylor dispersion method. Thus, a better understanding of phase equilibria of solute-solvent systems is helpful for an improved design of Taylor dispersion experiments. Also, this abnormality may be improved by reducing injection volume or using a larger-diameter diffusion column.

Table 4-2 Diffusion coefficients of benzene, toluene, m-xylene, 1-hexadecene, 1-methylnaphthalene and diesel fuel in SCCO₂ at 313.15 and 333.15 K and 10-30 MPa.

| P MPa | D ₁₂ , 10 ⁻⁹ m ² /s | | | | | | | |
|---------------------|--|-------|-------|------|----------|-------|-------|------|
| | 313.15 K | | | | 333.15 K | | | |
| | Avg. | Max. | Min. | Std. | Avg. | Max. | Min. | Std. |
| Benzene | | | | | | | | |
| 10 | 15.24 | 16.53 | 14.00 | 0.95 | 21.73 | 22.64 | 20.35 | 0.97 |
| 20 | 11.86 | 12.30 | 11.15 | 0.53 | 14.09 | 14.82 | 13.46 | 0.56 |
| 30 | 9.10 | 9.32 | 8.80 | 0.18 | 11.75 | 11.97 | 11.39 | 0.27 |
| Toluene | | | | | | | | |
| 10 | 13.25 | 14.70 | 12.12 | 1.10 | 21.51 | 22.81 | 20.76 | 1.13 |
| 20 | 11.24 | 11.59 | 10.80 | 0.35 | 12.83 | 13.41 | 12.35 | 0.44 |
| 30 | 9.07 | 9.46 | 8.63 | 0.42 | 10.58 | 11.35 | 10.03 | 0.61 |
| m-Xylene | | | | | | | | |
| 10 | 12.78 | 14.07 | 12.14 | 0.68 | 19.08 | 20.34 | 17.67 | 1.17 |
| 20 | 10.57 | 11.57 | 9.98 | 0.75 | 11.97 | 12.38 | 11.56 | 0.34 |
| 30 | 8.13 | 8.51 | 7.92 | 0.28 | 10.02 | 10.26 | 9.91 | 0.16 |
| 1-Hexadecene | | | | | | | | |
| 10 | 8.81 | 11.2 | 7.12 | 1.29 | | | | |
| 15 | | | | | 11.82 | 13.22 | 10.52 | 1.35 |
| 20 | 7.94 | 9.02 | 6.85 | 0.89 | 9.92 | 10.14 | 9.51 | 0.36 |
| 30 | 5.48 | 5.82 | 5.17 | 0.33 | 7.32 | 7.65 | 7.08 | 0.28 |
| 1-Methylnaphthalene | | | | | | | | |
| 10 | 11.11 | 11.77 | 10.76 | 0.57 | | | | |
| 15 | | | | | 12.57 | 13.11 | 11.88 | 0.51 |
| 20 | 9.37 | 9.80 | 8.99 | 0.34 | 10.65 | 10.73 | 10.59 | 0.07 |
| 30 | 7.26 | 7.62 | 6.81 | 0.38 | 8.88 | 8.99 | 8.82 | 0.07 |
| Diesel fuel | | | | | | | | |
| 10 | 8.71 | 9.37 | 8.10 | 0.64 | | | | |
| 15 | | | | | 10.19 | 10.28 | 10.12 | 0.08 |
| 20 | 7.41 | 7.48 | 7.35 | 0.06 | 8.98 | 9.20 | 8.84 | 0.17 |
| 30 | 6.05 | 6.08 | 6.00 | 0.05 | 7.39 | 7.48 | 7.27 | 0.11 |

Table 4-3 Diffusion coefficients of benzene, toluene, m-xylene, 1-hexadecene, 1-methylnaphthalene and diesel fuel in SCCO₂ at 353.15 and 373.15 K and 10-30 MPa.

| P MPa | D ₁₂ , 10 ⁻⁹ m ² /s | | | | | | | |
|---------------------|--|-------|-------|------|----------|-------|-------|------|
| | 353.15 K | | | | 373.15 K | | | |
| | Avg. | Max. | Min. | Std. | Avg. | Max. | Min. | Std. |
| Benzene | | | | | | | | |
| 10 | 41.59 | 43.45 | 37.35 | 2.85 | 47.55 | 52.31 | 43.60 | 4.30 |
| 20 | 17.80 | 18.96 | 16.99 | 0.89 | 25.07 | 26.47 | 23.86 | 1.39 |
| 30 | 14.50 | 15.03 | 14.06 | 0.49 | 17.08 | 17.93 | 15.95 | 0.93 |
| Toluene | | | | | | | | |
| 10 | 32.99 | 35.69 | 30.08 | 2.47 | 44.67 | 45.83 | 42.49 | 1.89 |
| 20 | 16.72 | 18.93 | 14.95 | 1.92 | 23.29 | 24.07 | 22.61 | 0.61 |
| 30 | 13.44 | 14.39 | 12.90 | 0.66 | 16.30 | 17.09 | 15.10 | 0.94 |
| m-Xylene | | | | | | | | |
| 10 | 32.11 | 34.01 | 30.59 | 1.57 | 37.74 | 40.38 | 35.12 | 2.25 |
| 20 | 16.86 | 19.74 | 15.47 | 1.56 | 22.87 | 24.65 | 21.70 | 1.25 |
| 30 | 12.38 | 13.11 | 11.87 | 0.59 | 15.36 | 16.13 | 14.75 | 0.66 |
| 1-Hexadecene | | | | | | | | |
| 10 | | | | | | | | |
| 15 | 13.23 | 14.85 | 11.89 | 1.22 | | | | |
| 20 | 13.08 | 13.86 | 11.93 | 1.02 | 14.75 | 15.32 | 13.71 | 0.73 |
| 30 | 9.26 | 10.88 | 8.63 | 0.95 | 12.29 | 12.85 | 11.60 | 0.64 |
| 1-Methylnaphthalene | | | | | | | | |
| 10 | | | | | | | | |
| 15 | 14.78 | 15.77 | 13.35 | 1.02 | | | | |
| 20 | 13.15 | 14.33 | 12.52 | 0.83 | 17.12 | 19.13 | 15.41 | 1.96 |
| 30 | 10.97 | 11.35 | 10.64 | 0.36 | 13.09 | 13.91 | 12.19 | 0.82 |
| Diesel fuel | | | | | | | | |
| 10 | | | | | | | | |
| 15 | 10.45 | 11.29 | 9.51 | 0.89 | | | | |
| 20 | 11.88 | 11.97 | 11.65 | 0.15 | 13.80 | 14.04 | 13.41 | 0.34 |
| 30 | 8.75 | 8.91 | 8.63 | 0.11 | 10.74 | 11.00 | 10.41 | 0.24 |

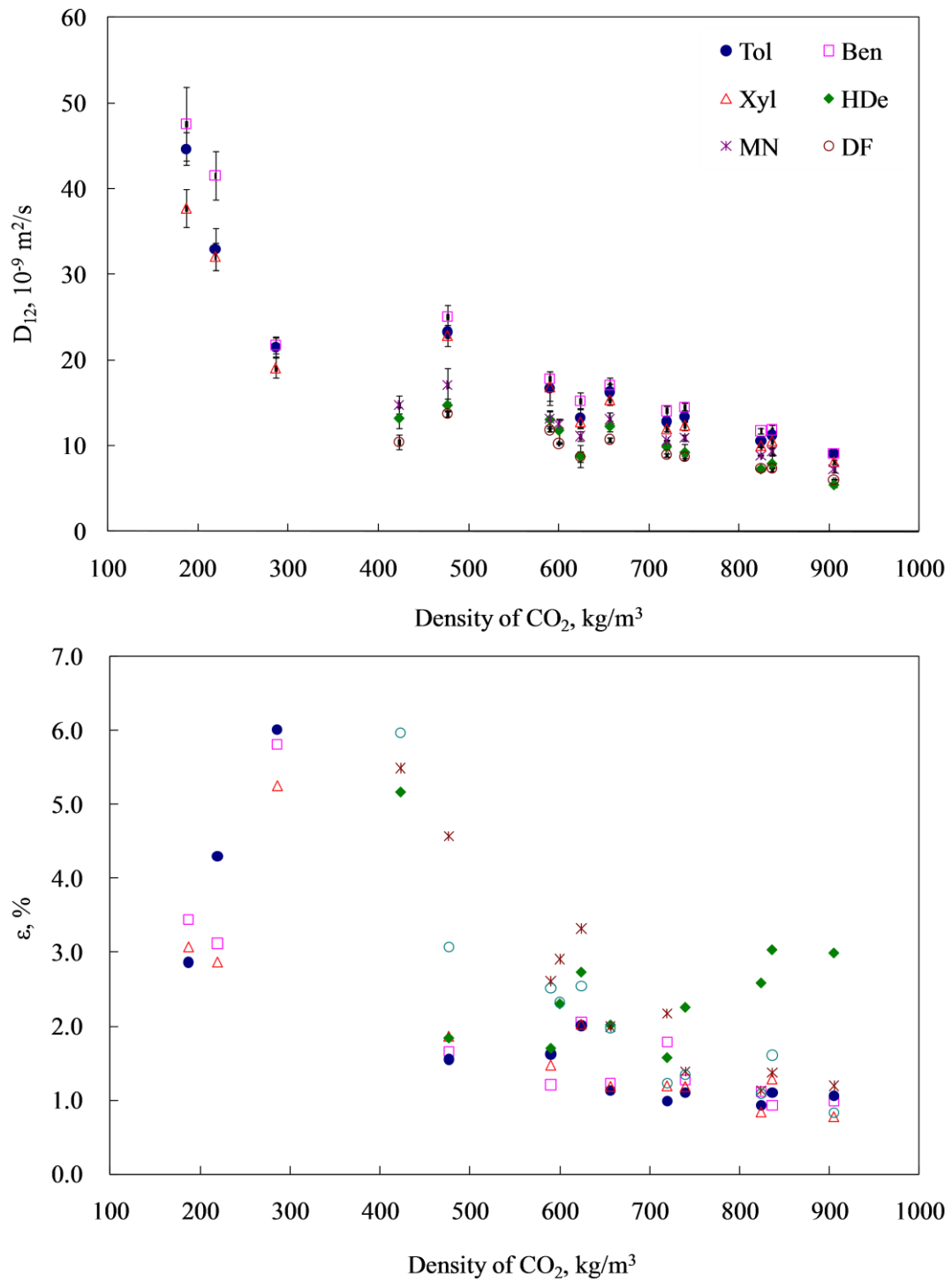


Fig. 4-8 Diffusion coefficients of benzene, toluene, m-xylene, 1-hexadecene, 1-methylnaphthalene and diesel fuel in SCCO_2 (top) and corresponding curve-fitting errors (bottom) as a function of the density CO_2 . Errors bars indicate standard deviation.

4.6.4 Modeling of experimental data using predictive correlations

As described in section 4.5, five predictive correlations were evaluated using data obtained in this work. They are Wilke-Chang, Scheibel, He-Yu, $D_{12}/T - \mu$ and $D_{12}/\sqrt{T} - \rho$ correlations. Properties of pure compounds used in this evaluation are given in **Table 4-4**. Diffusion data with $\varepsilon > 5\%$ were excluded from these evaluations. **Fig. 4-9** plots diffusion coefficients as a function of T/μ , showing a near linear relationship between them. However, this relationship with non-zero intersections was found to be slightly different than the Stokes-Einstein relation, and agrees with observations reported in the literature (Silva et al., 2004). Results of calculations are presented in **Table 4-5**. It was found that the He-Yu correlation had the best prediction performance with AAD of ~ 6.5 - 12.5% followed by the Wilke-Chang correlations. The Scheibel correlation had worst predicting capability with AAD% $> 20\%$ except for 1-hexadecene. The performance of the Wilke-Chang correlation could be improved considerably by varying ψ values. Results also show that the $D_{12}/T - \mu$ correlation fitted the data better than did the $D_{12}/\sqrt{T} - \rho$ correlation with AAD of ~ 3 - 7.5% .

A comparison of predicted and measured D_{12} of benzene in CO_2 is presented in **Fig. 4-10**. It shows that the $D_{12}/T - \mu$ and $D_{12}/\sqrt{T} - \rho$ correlations give best predictions. The Wilke-Chang and Scheibel correlations predict higher values than measured ones, while the He-Yu correlation gives higher predictions when D_{12} is below $\sim 30 \times 10^{-9} \text{ m}^2/\text{s}$ but lower predictions when D_{12} is above $\sim 30 \times 10^{-9} \text{ m}^2/\text{s}$.

Table 4-4 Properties for pure compounds.

| Species | MW kg/kmol | V_c $10^{-6} \text{ m}^3/\text{mol}$ | V_b $10^{-6} \text{ m}^3/\text{mol}$ |
|---------------------|---------------|---|---|
| Carbon Dioxide | 44.01 | 94.12 ^a | 33.36 |
| Benzene | 78.11 | 256.00 ^b | 95.21 |
| Toluene | 92.14 | 316.00 ^b | 118.72 |
| m-Xylene | 106.17 | 375.00 ^b | 142.05 |
| 1-Hexadecene | 224.43 | 978.00 ^c | 387.90 |
| 1-Methylnaphthalene | 142.20 | 462.00 ^b | 176.76 |

^a Data from NIST (Linstrom and Mallard, 2009). ^b Data from Poling et al. (Poling et al., 2001).

^c Data from Wakeham et al. (Wakeham et al., 2002).

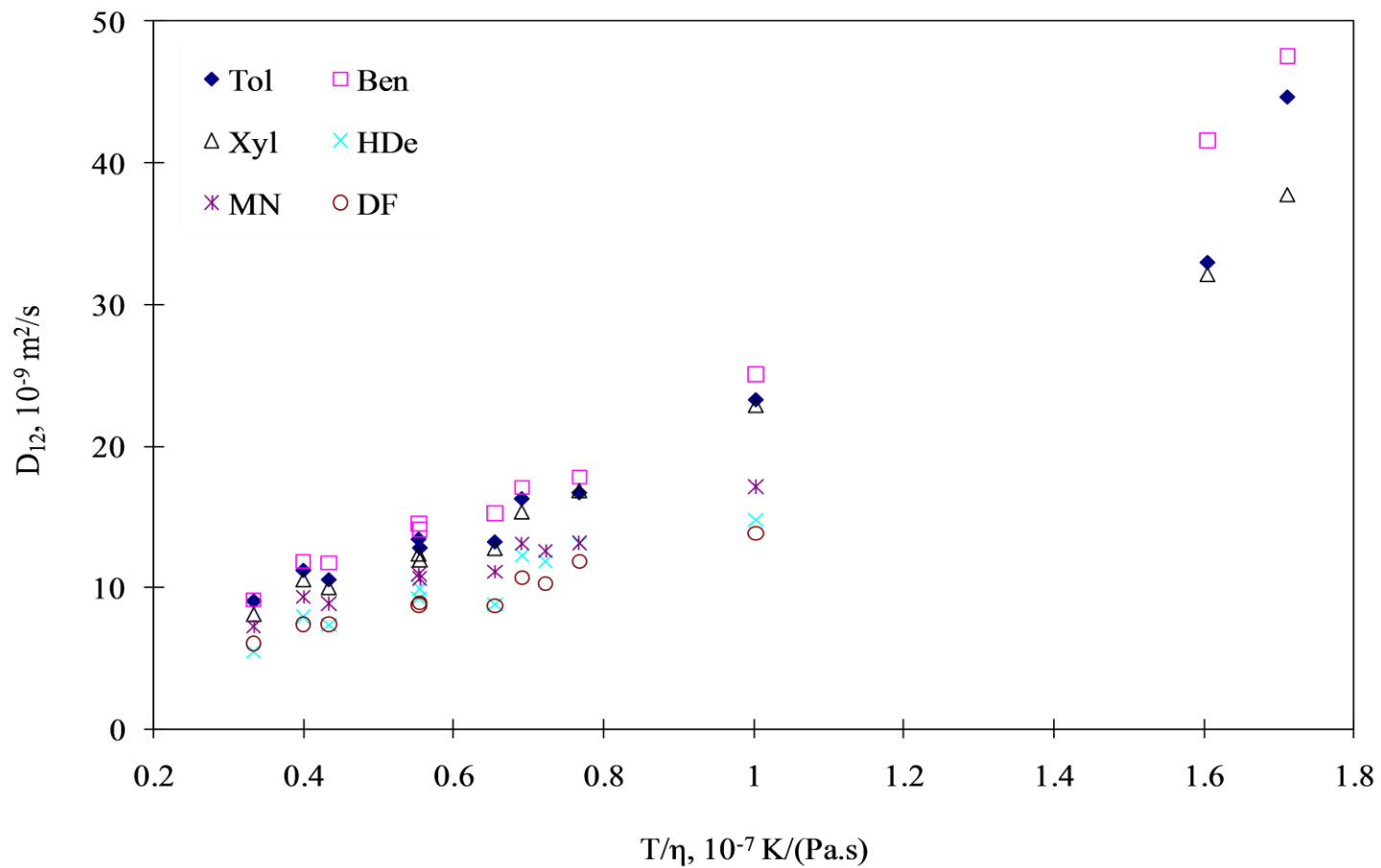


Fig. 4-9 D_{12} - T/η correlation for diffusion coefficients of benzene, toluene, m-xylene, 1-hexadecene, 1-methylnaphthalene and diesel fuel in SCCO_2 .

Table 4-5 Results of modeling of diffusion coefficients by predictive correlations.

| Species | Wilke-Chang | | | Scheibel | He-Yu | D ₁₂ /T-μ | | | D ₁₂ /T ^{0.5} -ρ | | |
|---------------------|---------------|------|----------|----------|-------|----------------------|-------|------|--------------------------------------|-------|------|
| | AAD% (ψ=1) | ψ | AAD % | AAD% | AAD% | β×10 ¹⁴ | γ | AAD% | ζ×10 ⁷ | ξ | AAD% |
| Benzene | 18.66 | 0.67 | 5.80 | 28.96 | 12.06 | 3.29 | -0.97 | 5.70 | 3.31 | -0.92 | 5.84 |
| Toluene | 14.70 | 0.70 | 8.32 | 24.42 | 10.31 | 5.07 | -0.90 | 6.96 | 2.14 | -0.87 | 7.34 |
| M-xylene | 11.72 | 0.74 | 6.93 | 20.47 | 9.38 | 4.88 | -0.90 | 4.87 | 1.77 | -0.85 | 8.59 |
| 1-Hexadecene | 22.07 | 1.39 | 8.35 | 10.10 | 6.56 | 6.89 | -0.81 | 7.26 | 24.9 | -1.29 | 9.47 |
| 1-Methylnaphthalene | 13.99 | 0.69 | 10.21 | 21.93 | 9.14 | 26.5 | -0.65 | 3.33 | 6.73 | -1.07 | 4.19 |
| Diesel fuel | | | | | | 20.9 | -0.65 | 3.70 | 5.92 | -1.08 | 4.89 |

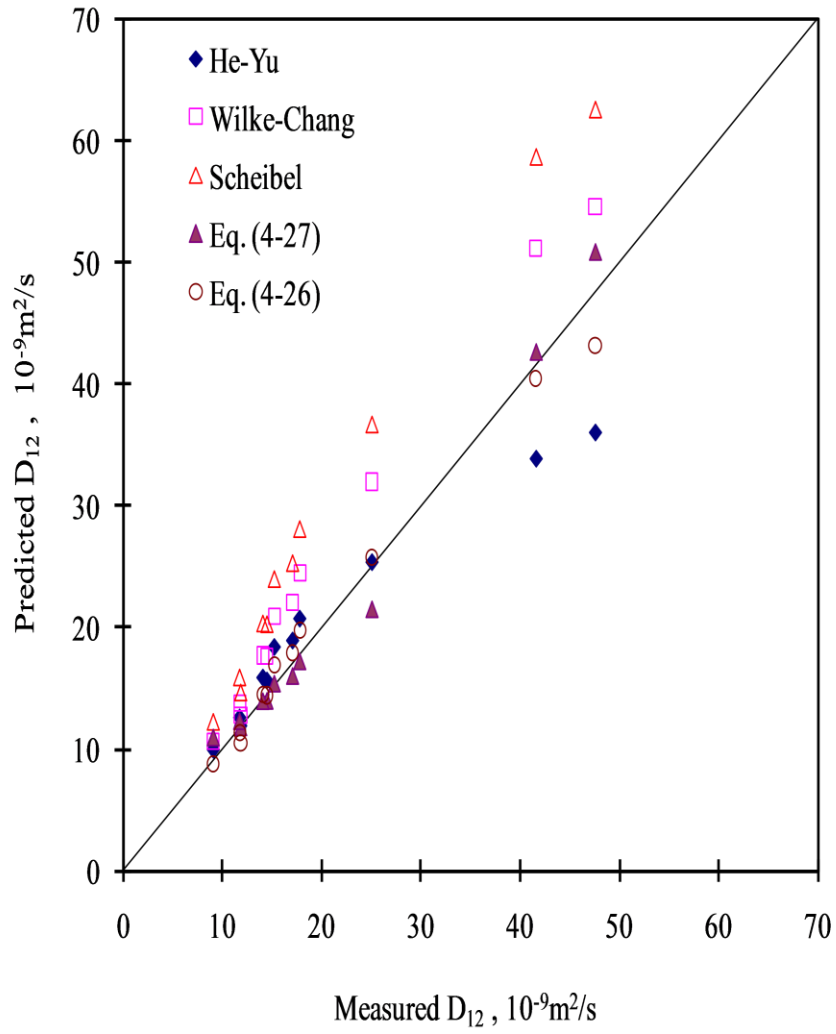


Fig. 4-10 A comparison of predicted and measured D_{12} of benzene in CO_2 .

4.6.5 Experimental uncertainties

4.6.5.1 Peak tailing

Significant peak tailings were observed in this work, especially for 1-hexadecene, 1-methylnaphthalene and diesel fuel, when the density of SCCO₂ was below the critical value. Examples of peak tailing are illustrated in **Fig. 4-11**. The formation of peak tailing is likely the consequence of the combined effects of reduced solubility and wall absorption. As the density of CO₂ decreases, solubilities of these species in CO₂ decrease. At relatively low density, CO₂ is unable to quickly solubilize the injected sample, leading to a multiphase flow in the diffusion column for a non-negligible period of time. The sample phase is more likely to stick to the wall and hence, peak tailing forms. Significant peak tailing was also observed for benzene in the near-critical region of CO₂ (**Fig. 4-12** top). As pressure increased and hence solubility of benzene in CO₂ increased, peak tailing reduced significantly (**Fig. 4-12** middle) and then disappeared (**Fig. 4-12** bottom). Strategies to minimize the solubility effect include pre-solubilizing a sample (Fu et al., 2000) and reducing injection volume. The effect of injection volume will be further discussed in section 4.6.5.3.

Temperature gradients along the column, especially in the injection valve and the detector regions, may also result in peak tailing. **Fig. 4-13** shows that when the injection valve, the detector and connections to the column were not insulated, temperature gradients induced significant peak deformation.

Peak tailing significantly affects the accuracy of diffusivity measurements. Therefore, in this study, the experimental apparatus was carefully designed and built to minimize peak tailing and/or deformation.

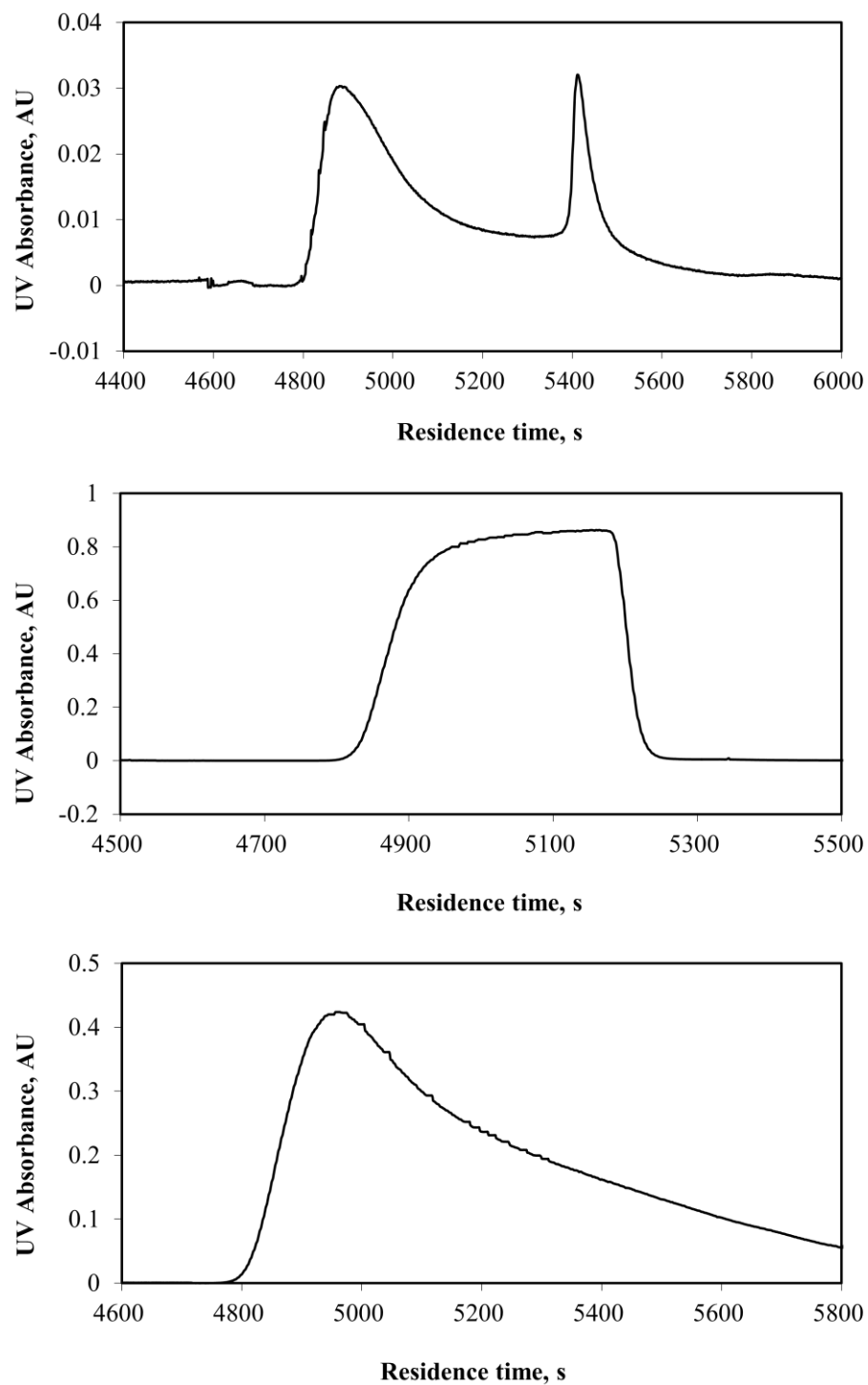


Fig. 4-11 Typical peak tailing of 1-hexadecene (top), 1-methylnaphthalene (middle) and diesel fuel (bottom) observed at 333.15 K and 10 MPa using the 0.508 mm column in the vertical orientation.

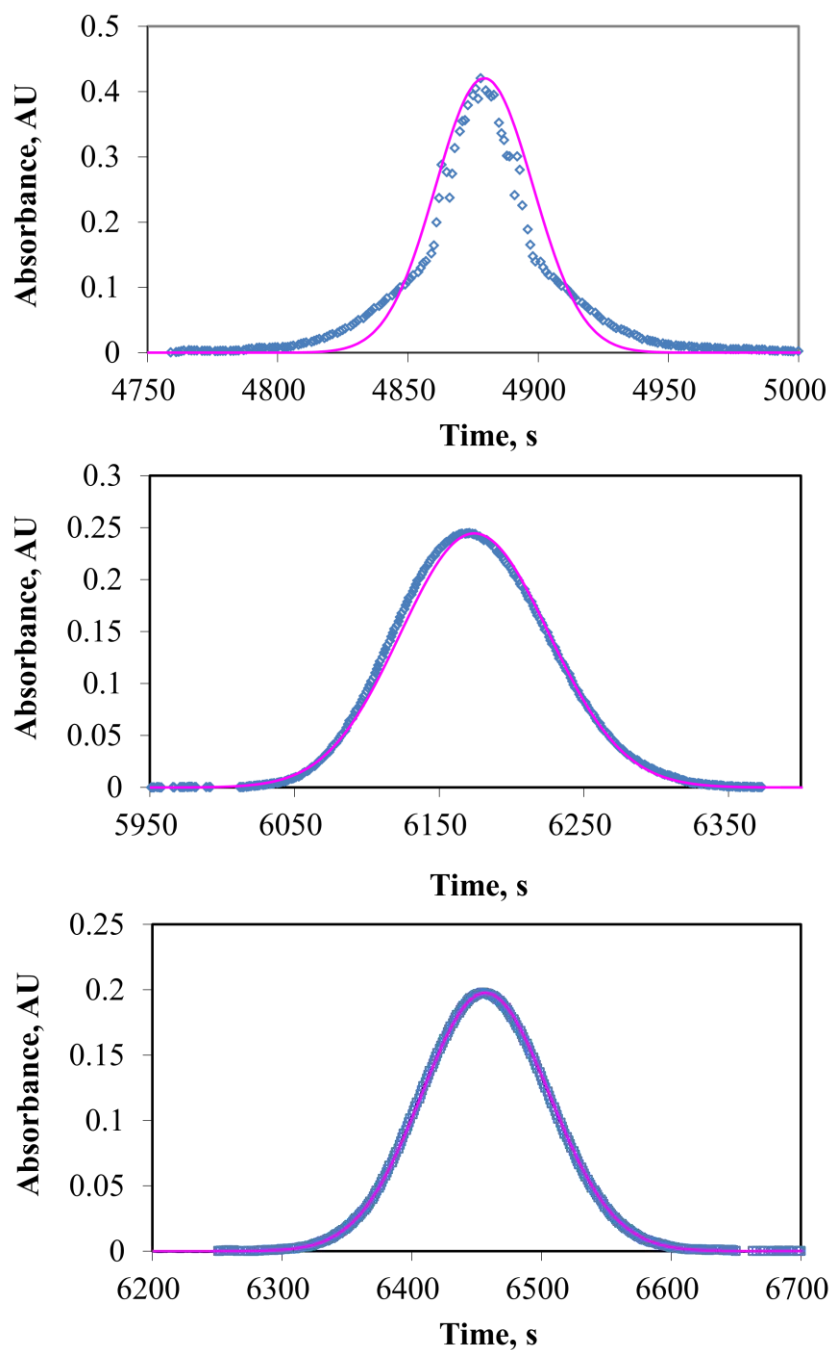


Fig. 4-12 The effect of pressure on the shape of benzene dispersion peaks. Open blue diamonds: experimental data; solid red lines: predictions by Eq. (4-6). Benzene dispersion peaks were obtained at 313.15 K and 7.5 (top), 8.5 (middle), and 10 (bottom) MPa using the 0.508 mm I.D. column in the vertical orientation.

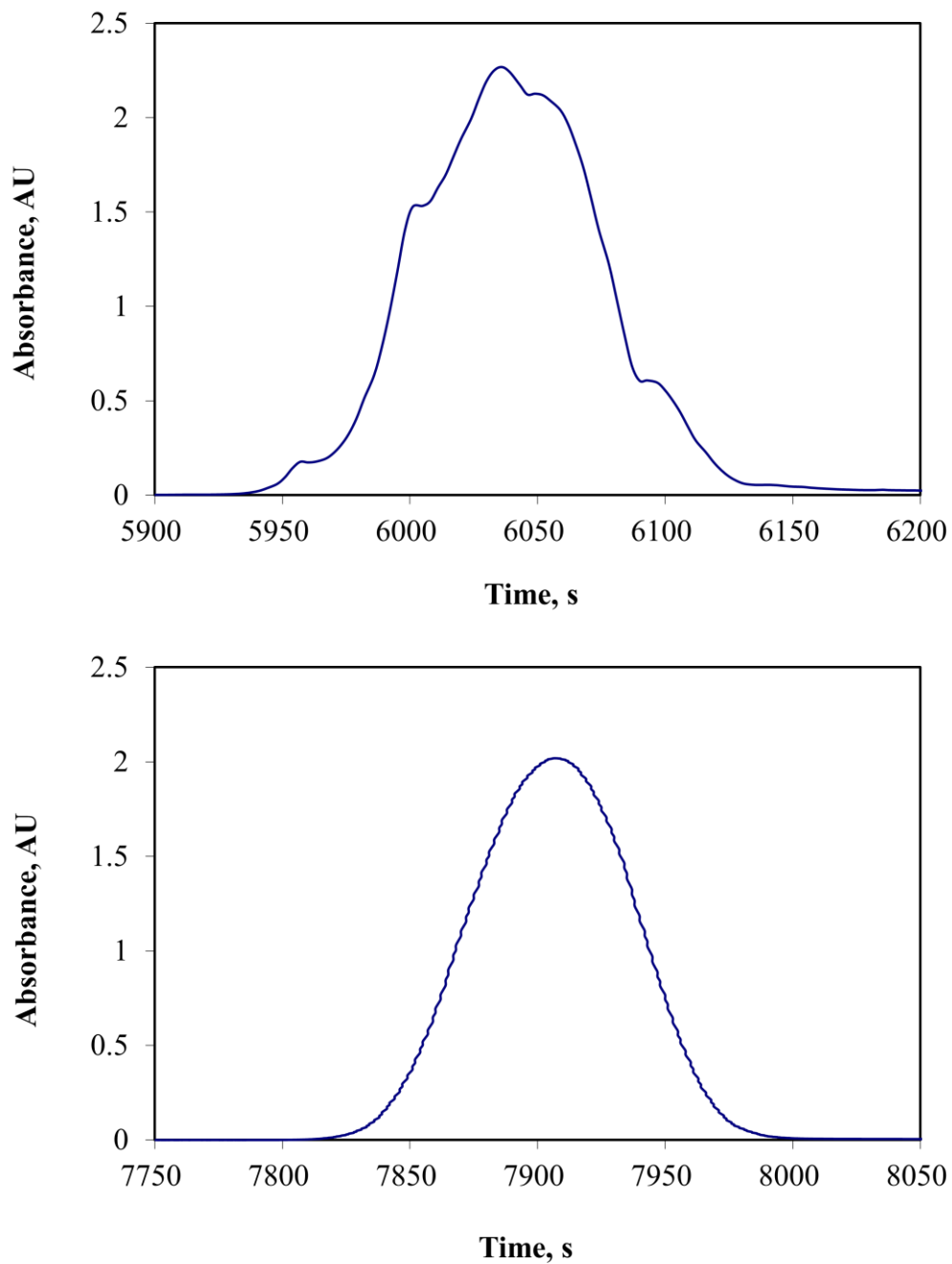


Fig. 4-13 The effect of temperature gradients in the injection and the detection regions on the shape of benzene dispersion peaks. Peaks were obtained at 313.15 K and 10 MPa using the 0.508 mm I.D. column in the vertical orientation. Top: connections were not insulated; bottom: connections were insulated.

4.6.5.2 Effect of wavelength

Linearity of a UV detector depends on wavelength. For the same species, different wavelengths may exhibit different linear ranges. An optimal wavelength is such that absorbance of any point in a dispersion peak falls in the linear range. Funazukuri et al. (Funazukuri et al., 2004) selected the optimal wavelength for any compound within a range where constant diffusion coefficients were obtained. A new hypothesis was proposed in this work: an optimal wavelength for any compound is such that the measured diffusion coefficient is maximized. This hypothesis was validated in the following way. First, spectra of species of interest were determined. Second, diffusion coefficients were measured using different wavelengths. Finally, diffusion coefficients were measured using different initial concentration and different wavelengths.

Each chemical has different UV light sensitivity, which depends on the type of chemical bonds within the chemical and varies with wavelength. **Fig. 4-14** shows an example of UV absorbance spectra determined in this work. As experimental conditions change, concentration profiles change and hence, UV absorbance spectra show some different shapes as shown in **Fig. 4-16** as compared to **Fig. 4-14** for 1-methylnaphthalene. **Fig. 4-15** and **Fig. 4-16** demonstrate the effect of wavelength on diffusion coefficients. Experimental data were obtained at 313.15 K and 10 MPa using the 0.508 mm column in the vertical orientation. It was found that diffusion coefficients of benzene, toluene and m-xylene exhibit very similar patterns of wavelength dependence due to similar molecular structures. They achieve near constant values in the wavelength ranges where the first half of the spectrum peaks are located and decrease when the wavelength moves below or beyond the ranges. This finding agrees well with observation for benzene by

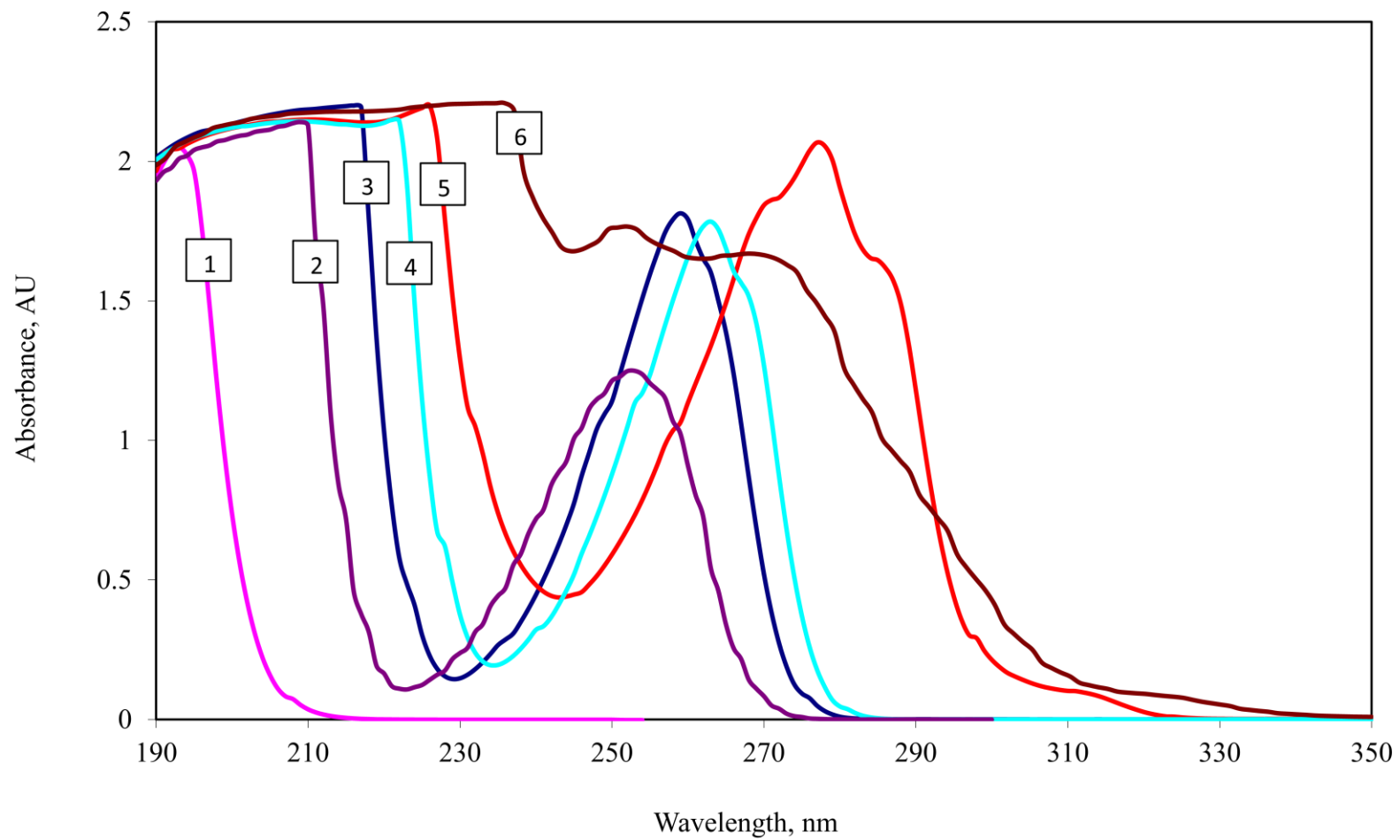


Fig. 4-14 Typical UV absorbance spectra of benzene (2), toluene (3), m-xylene (4), 1-hexadecene (1), 1-methylnaphthalene (5) and diesel fuel (6).

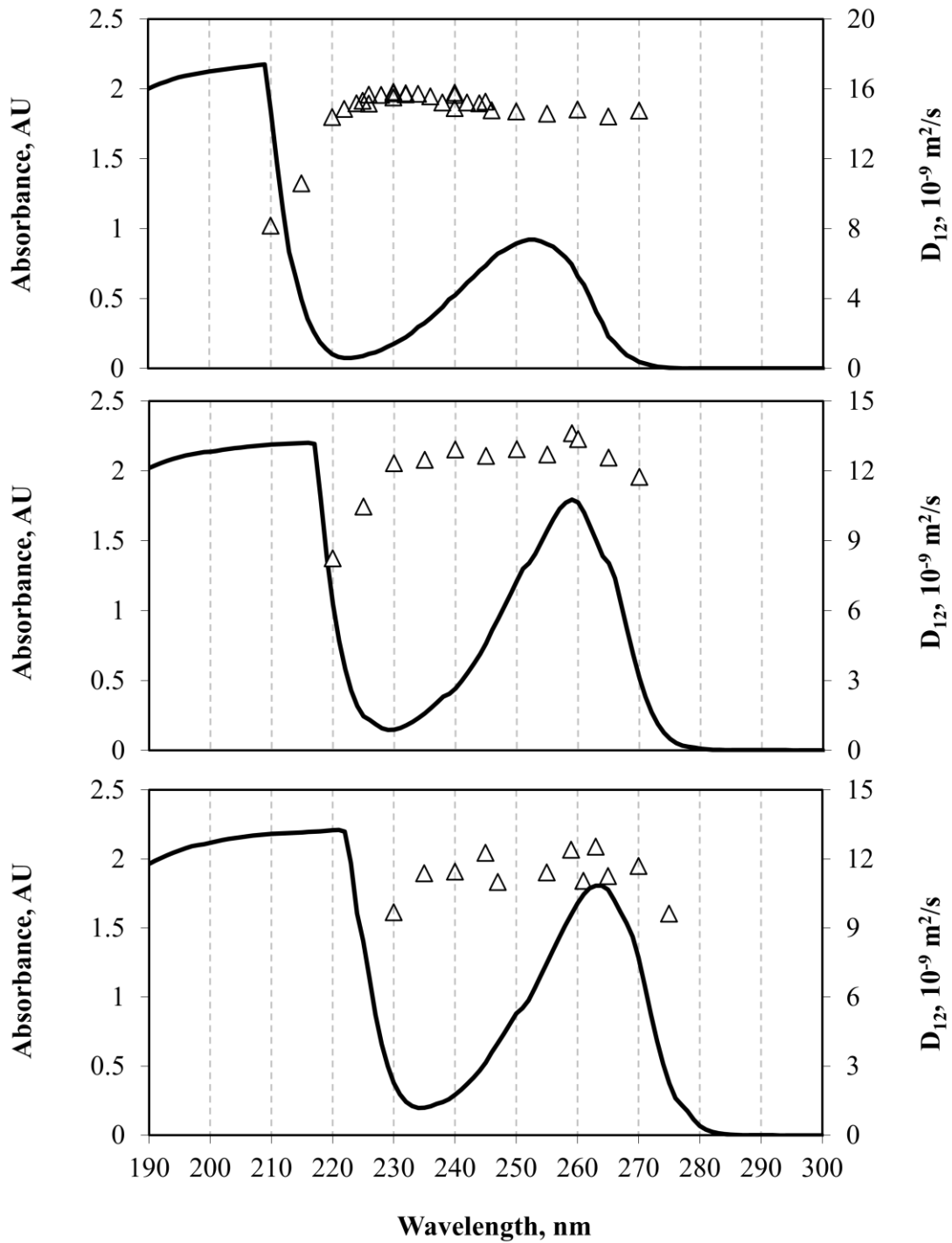


Fig. 4-15 Effect of wavelength on diffusion coefficients of benzene (top), toluene (middle) and m-xylene (bottom). Experiments were conducted at 313.15 K and 10 MPa. Solid lines: spectra; triangles: diffusion coefficients.

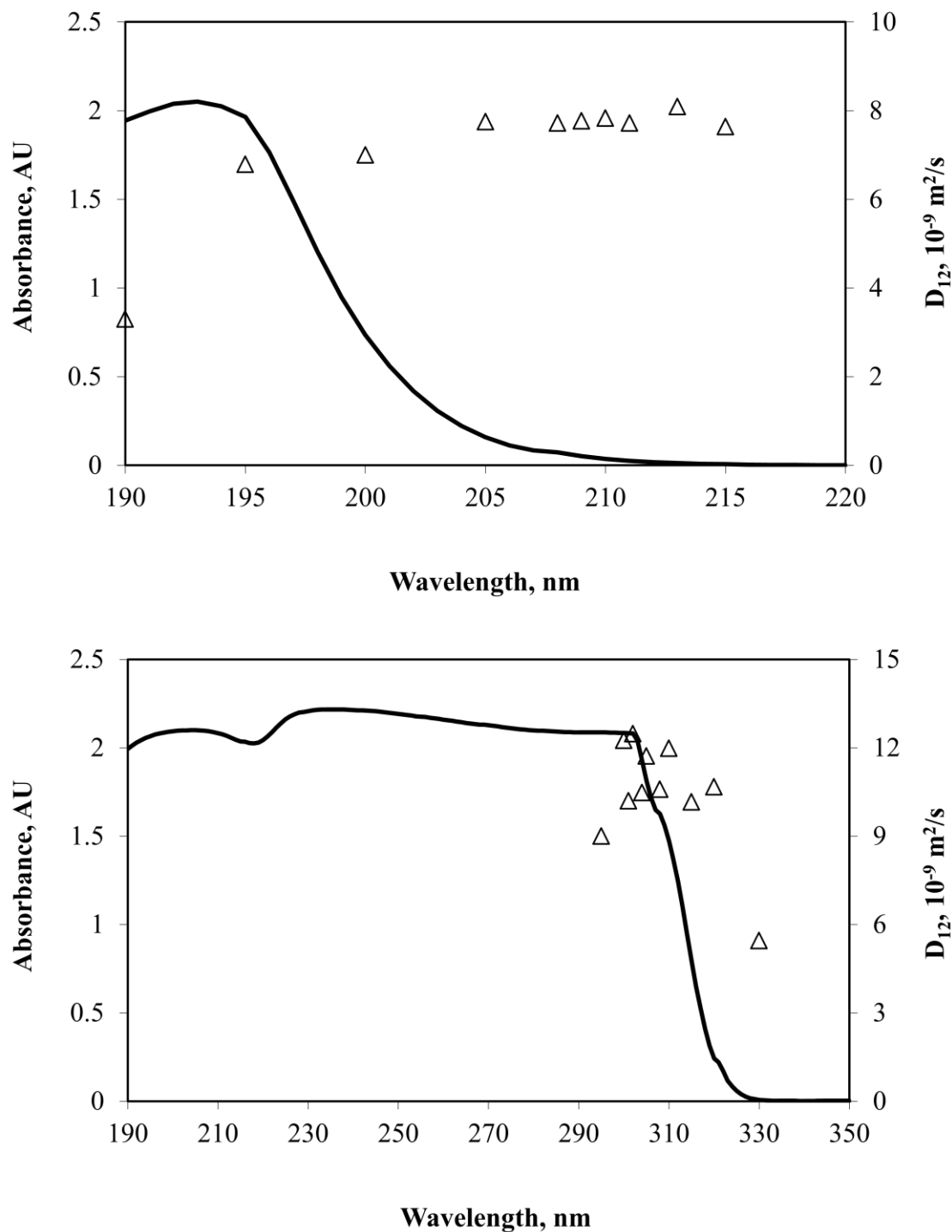


Fig. 4-16 Effect of wavelength on diffusion coefficients of 1-hexadecene (top) and 1-methylnaphthalene (bottom). Experiments were conducted at 313.15 K and 10 MPa. Solid lines: spectra; triangles: diffusion coefficients.

Funazukuri et al. (Funazukuri et al., 2001). The diffusion coefficient of 1-hexadecene increased as wavelength increased and reached near constant beyond 205 nm, while that of 1-methylnaphthalene presented a maximum value at the wavelength where a sharp decrease in the absorbance unit occurred. Wavelength dependence of diffusivity of DF was not determined due to the complex mixture nature of DF. It is worth pointing out that diffusion coefficients presented in **Fig. 4-15** and **Fig. 4-16** were obtained in more than one set of experiments using the single-wavelength detection mode. This results in discernable data fluctuations as shown, in particular, for m-xylene and 1-methylnaphthalene.

In order to further verify the criteria used to determine optimal wavelengths, dispersion peaks of benzene injected as solutions in hexane with varying concentrations were measured. The ratio of peak area over residence time, which is directly proportional to the mass of benzene injected, is plotted as a function of benzene concentration in **Fig. 4-17**. The best linearity was found at 230 nm followed by 240 nm. Further verification was done by using the dual-wavelength detection mode and similar results were obtained. Accordingly, it is concluded that when a UV detector is used in diffusion coefficient measurements, the maximum value found at the wavelength where the best linearity is achieved is closest to the true diffusion coefficients. **Table 4-6** summarizes optimal wavelength ranges determined in this work. Also listed in this table are the wavelengths used in the dual-wavelength mode to obtain data presented in other sections of this chapter.

4.6.5.3 Effect of sample injection

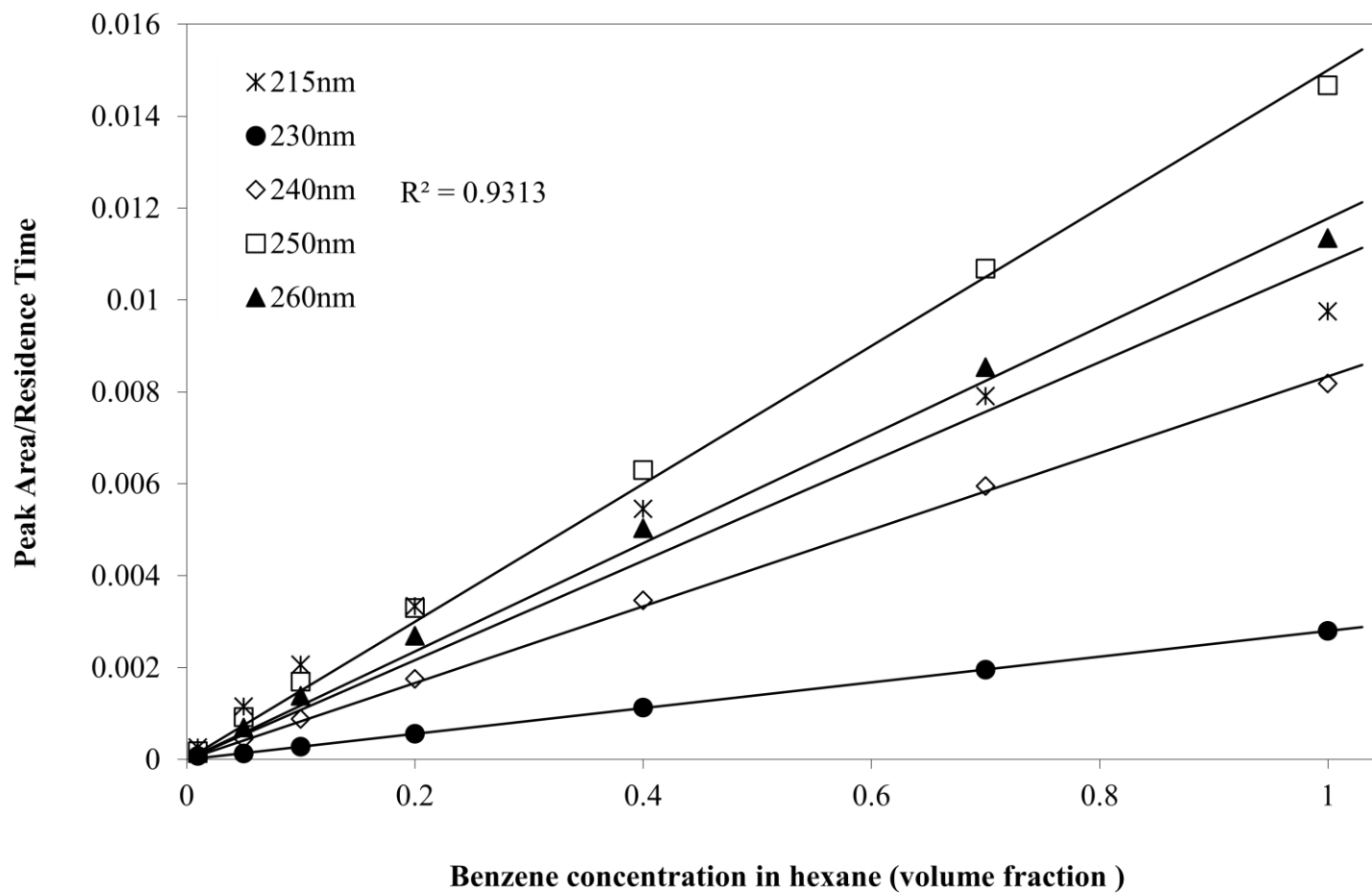


Fig. 4-17 Detector linearity for benzene at various wavelengths.

Table 4-6 Optimal ranges of wavelength determined and wavelengths used in the experiments.

| Species | Wavelength, nm | | |
|---------------------|----------------|-------------|-------------|
| | Optimal range | λ_1 | λ_2 |
| Benzene | 230-235 | 230 | 235 |
| Toluene | 235-240 | 235 | 240 |
| m-Xylene | 235-240 | 235 | 240 |
| 1-Hexadecene | 205-215 | 210 | 215 |
| 1-Methylnaphthalene | 305-315 | 310 | 305 |
| Diesel fuel | 280-290 | 290 | 285 |

As described in section 4.4.3, different combinations of V_{inj} and D , giving a wide range of ϕ values, were examined to determine an optimal range of ϕ in which the influence of the finite injection volume is minimized and can be neglected. These combinations are listed in **Table 4-7**.

Diffusion coefficients of benzene in SCCO₂ at 313.15 K and 10 MPa were measured using these different combinations to reveal the effect of ϕ . In the experiment, columns were vertically installed. Results are presented in **Fig. 4-18**, demonstrating a significant effect of ϕ on diffusion coefficient measurements. As ϕ increased from 1.4 to 4.9, measured diffusion coefficients decreased slightly associated with a small increase in curve-fitting errors. However, as ϕ further increased to 38.9, significant reduction of measured diffusion coefficients was observed associated with a substantial increase in curve-fitting errors. When the 5 μ L injection volume was used, which gives a ϕ value of 388.5, no normal dispersion peaks were obtained. Reduction of measured diffusion coefficients with increasing ϕ is mainly due to the violation of the δ -function-pulse injection assumption and the solubilization effect as mentioned in section 4.6.5.1. As ϕ increases, the equivalent length, L_e , increases, which makes the initial conditions away from the delta-function-pulse assumption. On the other hand, it takes longer time for the sample to be solubilized by the mobile phase, which results in non-negligible peak tailing.

Therefore, it can be concluded that ϕ is an effective parameter to characterize the effect of sample injection. The smaller the ϕ value, the more accurate the measurements. ϕ values can be minimized by either reducing the injection volume or increasing the column diameter. Also, the results suggest that a ϕ value below 5 would give good accuracy.

Table 4-7 Different combinations of V_{inj} and D examined in this study.

| V_{inj} , μL | D , mm | φ |
|---------------------------|----------|-----------|
| 0.5 | 0.762 | 1.4 |
| 0.5 | 0.508 | 4.9 |
| 0.5 | 0.254 | 38.9 |
| 5 | 0.254 | 388.5 |

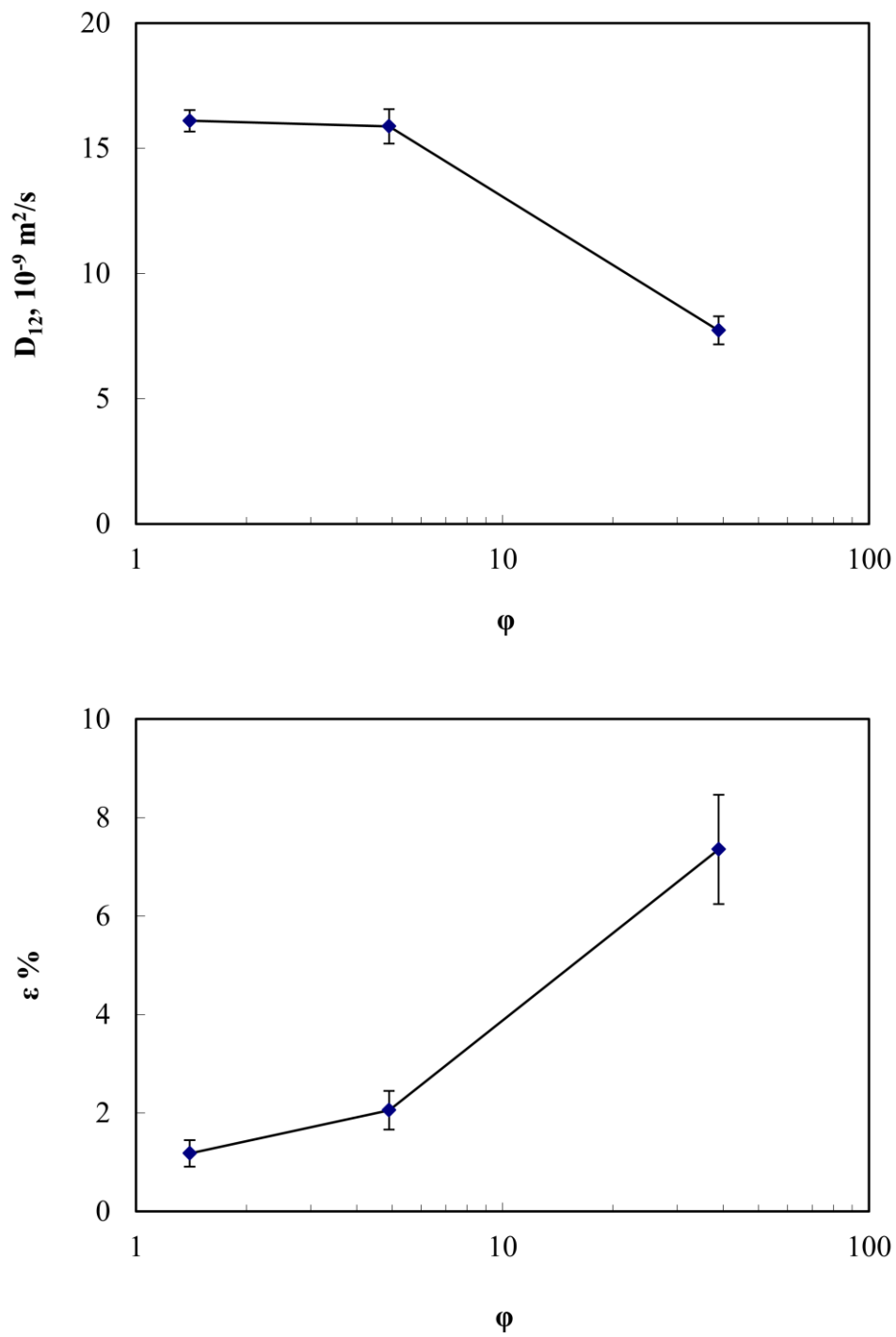


Fig. 4-18 Effect of ϕ on diffusion coefficients (top) and curve-fitting errors (bottom). Error bars represent standard deviation. Experimental data are for benzene and were obtained at 313.15 K and 10 MPa using vertically installed columns.

4.6.5.4 Effect of the mean velocity

To advance the understanding of the effect of the mean velocity on diffusion coefficient measurements, diffusion coefficients of benzene in SCCO₂ at given T-P conditions were measured using different mean velocities from 0.002–0.025 m/s. Experiments were conducted at 313.15 and 333.15 K and 9–15 MPa using the I.D. 0.762 mm column. The column was vertically installed in the GC oven. Results are plotted in **Fig. 4-19** and **Fig. 4-20** and also presented in Appendix D.

Fig. 4-19 presents measured diffusion coefficients (top) of benzene in SCCO₂ and corresponding curve-fitting errors (bottom) as a function of U at 313.15 K for the vertical orientation. At 15 MPa, as U reduced, measured diffusion coefficients decreased and then reached a constant value, which was in a good agreement with previous findings (Bueno et al., 1993; Funazukuri et al., 1991; Funazukuri et al., 1989; Mantell et al., 2003; Yang et al., 2000) as demonstrated in **Fig. 4-5**. As pressure reduced down toward 9.5 MPa, diffusion coefficients increased and the D_{12} curves moved upward accordingly. Different to the pattern shown in **Fig. 4-5**, however, measured diffusion coefficients decreased further when U reduced below ~ 0.005 m/s. As pressure decreased, the U at which the decline started to occur increased, leading to a narrower OVR within which accurate diffusion coefficients could be determined. At 9 MPa, measured diffusion coefficients increased with increasing U in the entire velocity range, which implies that diffusion coefficients cannot be determined accurately under these conditions when the column is installed vertically. Moreover, curve-fitting errors increased significantly at low U , for example, from $\sim 1\%$ to $\sim 3.5\%$ at 10 MPa, as shown in **Fig. 4-19**, which implies that disturbance to the ideal Taylor dispersion became more pronounced as U decreased.

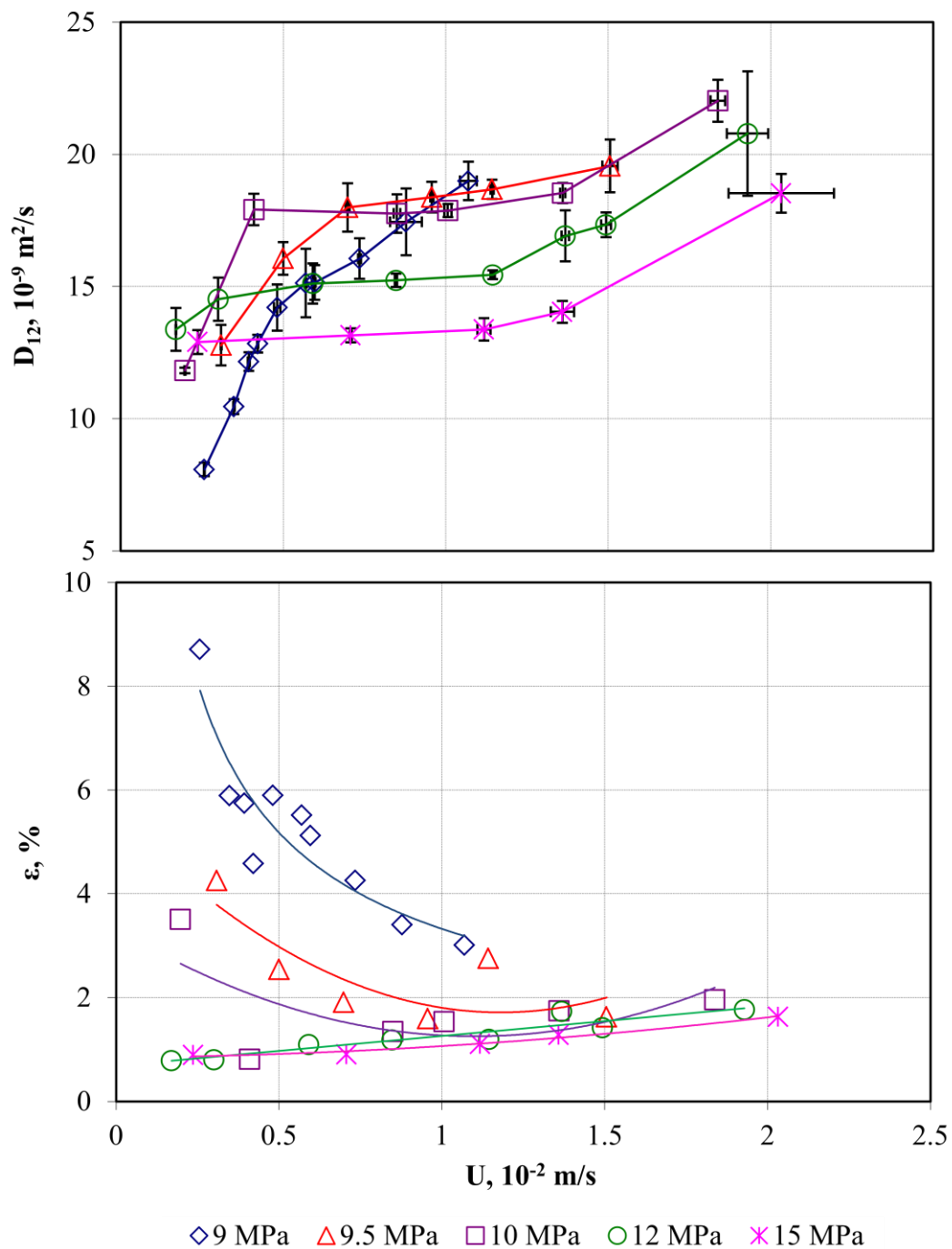


Fig. 4-19 Measured diffusion coefficients (top) of benzene in SCCO₂ and corresponding curve-fitting errors (bottom) as a function of the mean velocity at 313.15 K for the vertical orientation. The solid lines in the top figure connect the data points. The solid lines in the bottom figure are trend lines.

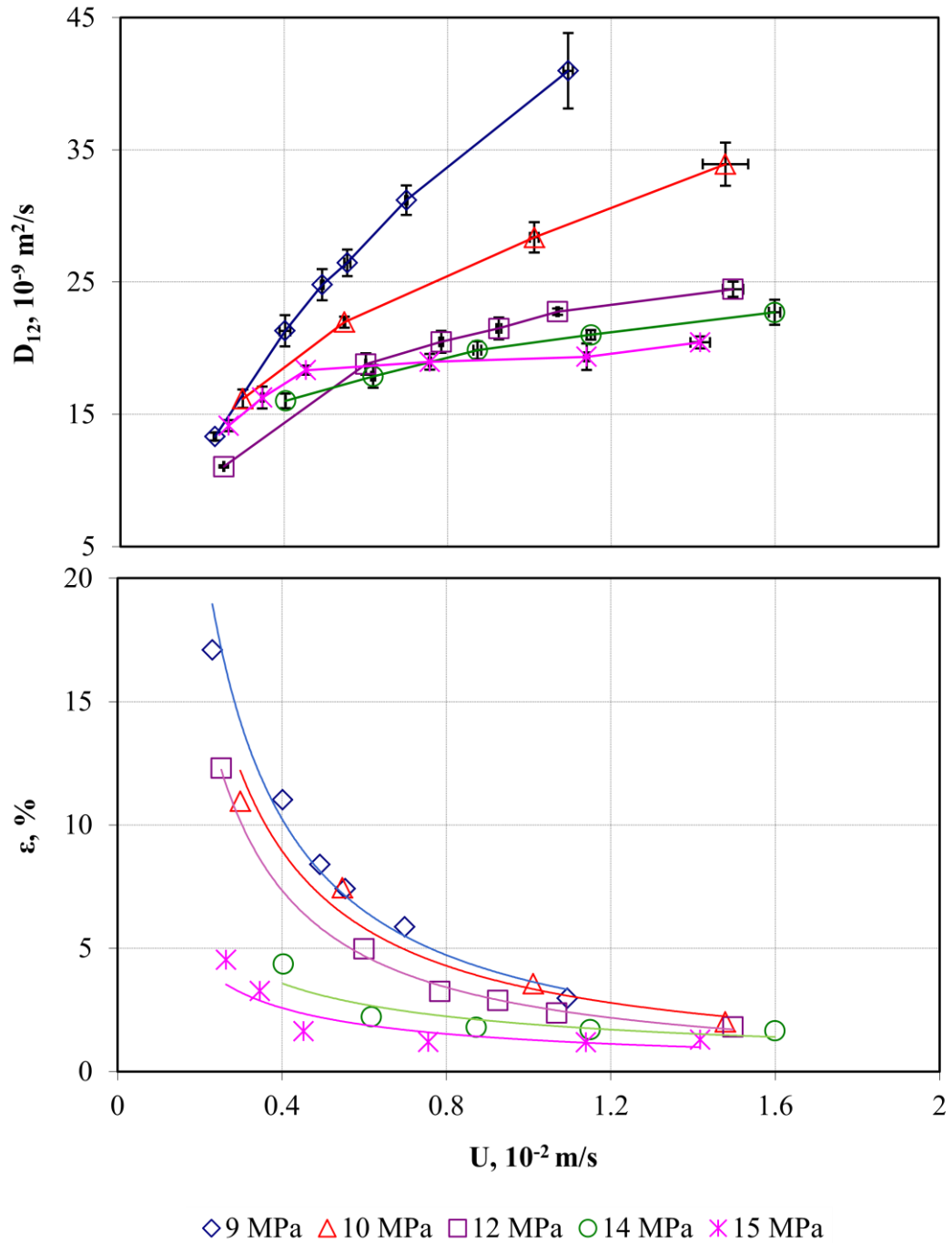


Fig. 4-20 Measured diffusion coefficients (top) of benzene in SCCO_2 and corresponding curve-fitting errors (bottom) as a function of the mean velocity at 333.15 K for the vertical orientation. The solid lines in the top figure connect the data points. The solid lines in the bottom figure are trend lines.

Similar D_{12} - U - P behavior was observed at 333.15 K as shown in **Fig. 4-20**. By comparing two sets of data obtained at different temperatures for the same column orientation, it was found that the increase in temperature required a higher pressure to achieve an OVR. Both reducing pressure and increasing temperature result in lower CO_2 density and hence higher density difference between the SCCO_2 phase and the sample phase. Therefore, care must be taken in diffusion coefficient measurements when the density difference between the mobile phase and the sample phase is relatively high and the column is vertically installed.

In brief, results obtained in this set of experiments where the column was installed vertically disclosed two new phenomena. First, significant decline of measured diffusion coefficients occurred when U was relatively low. Second, measured diffusion coefficients were dependent on U in the entire velocity range at relatively low mobile phase density ($< 580 \text{ kg/m}^3$). Accordingly, it may be concluded that accurate diffusion coefficients can be determined only within a limited range of operating conditions, when the column is in the vertical position.

New phenomena observed in the vertically-installed column are believed to be the consequence of the combined effects of buoyancy forces induced by density difference between benzene and SCCO_2 and secondary flows due to tube curvature. In a horizontal straight tube, as Reejhsinghani *et al.* (Reejhsinghani et al., 1966) explained, the density difference has two effects. On one hand, the axial density gradient causes an axial pressure gradient and hence a change in the axial velocity distribution which may increase the dispersion and is critical in calculating dispersion coefficients (Nunge et al., 1972). On the other hand, the radial variation of density can also induce secondary flows.

When the tube is coiled but still in horizontal position, the secondary flows are enhanced by superimposition of the effects of radial density variation and tube curvature, while the buoyancy effects are insignificant for the buoyancy forces are perpendicular to the axial velocity. When the coil is placed vertically, however, the buoyancy forces become parallel to the axial velocity plane, which is claimed to be the main cause of the reduction of measured diffusion coefficients especially when the density difference is significant and U is relatively low. To support this explanation, the column was moved from the GC oven and placed horizontally in the water bath where the preheating coil was located. Experiments were repeated under the same temperature and pressure conditions. Results and discussions are presented in the following sections.

4.6.5.5 Effect of column orientation

Diffusion coefficients and corresponding curve-fitting errors obtained at 313.15 and 333.15 K for the horizontal orientation are presented in **Fig. 4-21** and **Fig. 4-22**, respectively, demonstrating very similar D_{12} - U - P behavior as observed for the vertical orientation. For a better comparison, data obtained at the same T-P conditions for both orientations are plotted in the same figure and presented in **Fig. 4-23** to **Fig. 4-32**. It was found that at 40 °C and 9 MPa (**Fig. 4-23**) and 60 °C and 9-14 MPa (**Fig. 4-28** to **Fig. 4-31**), OVRs appeared to be associated with substantial increase of measured diffusion coefficients and significant reduction of curve-fitting errors, when the column was switched from vertical to horizontal orientation. This suggests that under these temperature and pressure conditions, the vertical position of a column should be avoided in diffusion coefficient measurements when using the chromatographic technique.

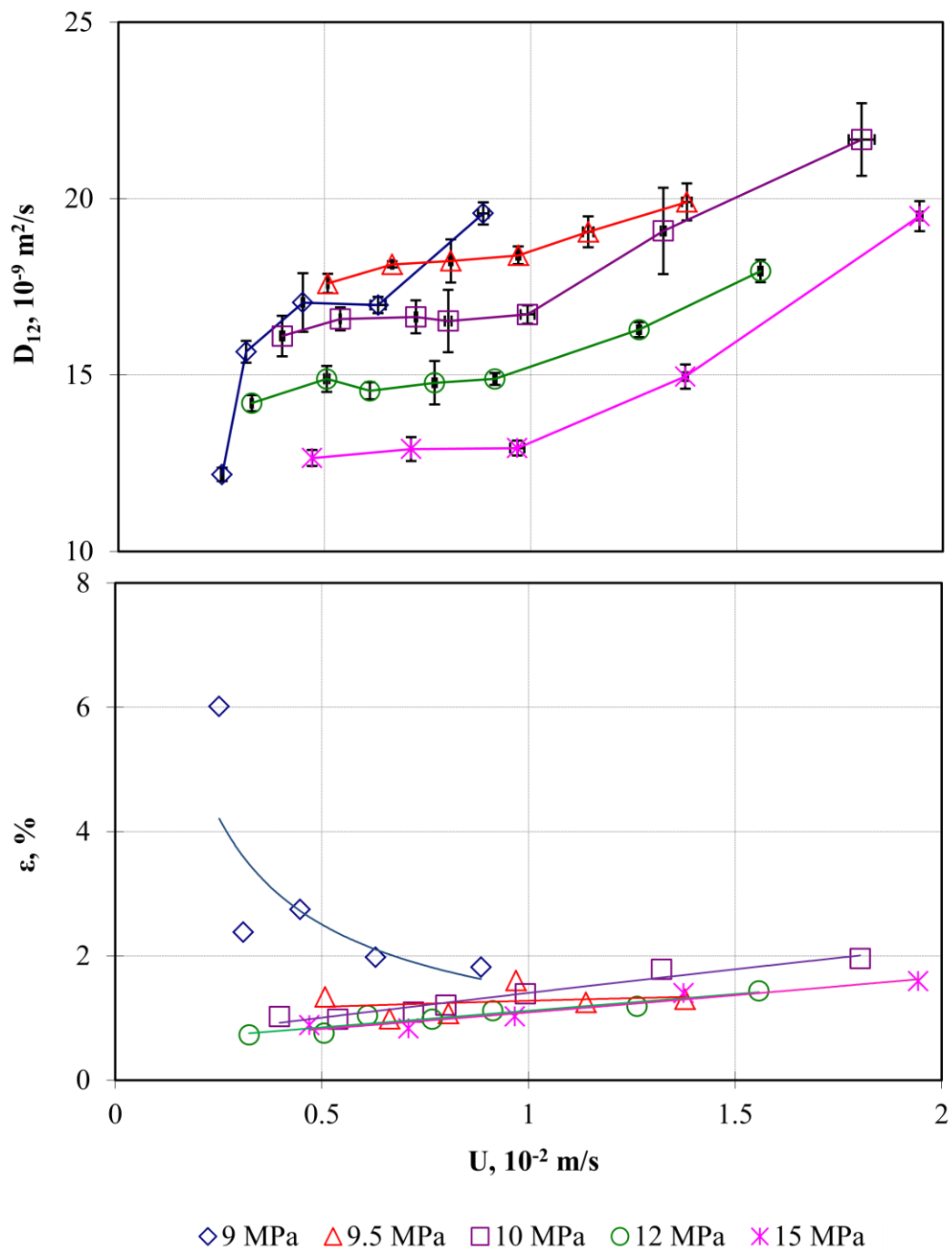


Fig. 4-21 Measured diffusion coefficients (top) of benzene in SCCO₂ and corresponding curve-fitting errors (bottom) as a function of the mean velocity at 313.15 K for the horizontal orientation. The solid lines in the top figure connect the data points. The solid lines in the bottom figure are trend lines.

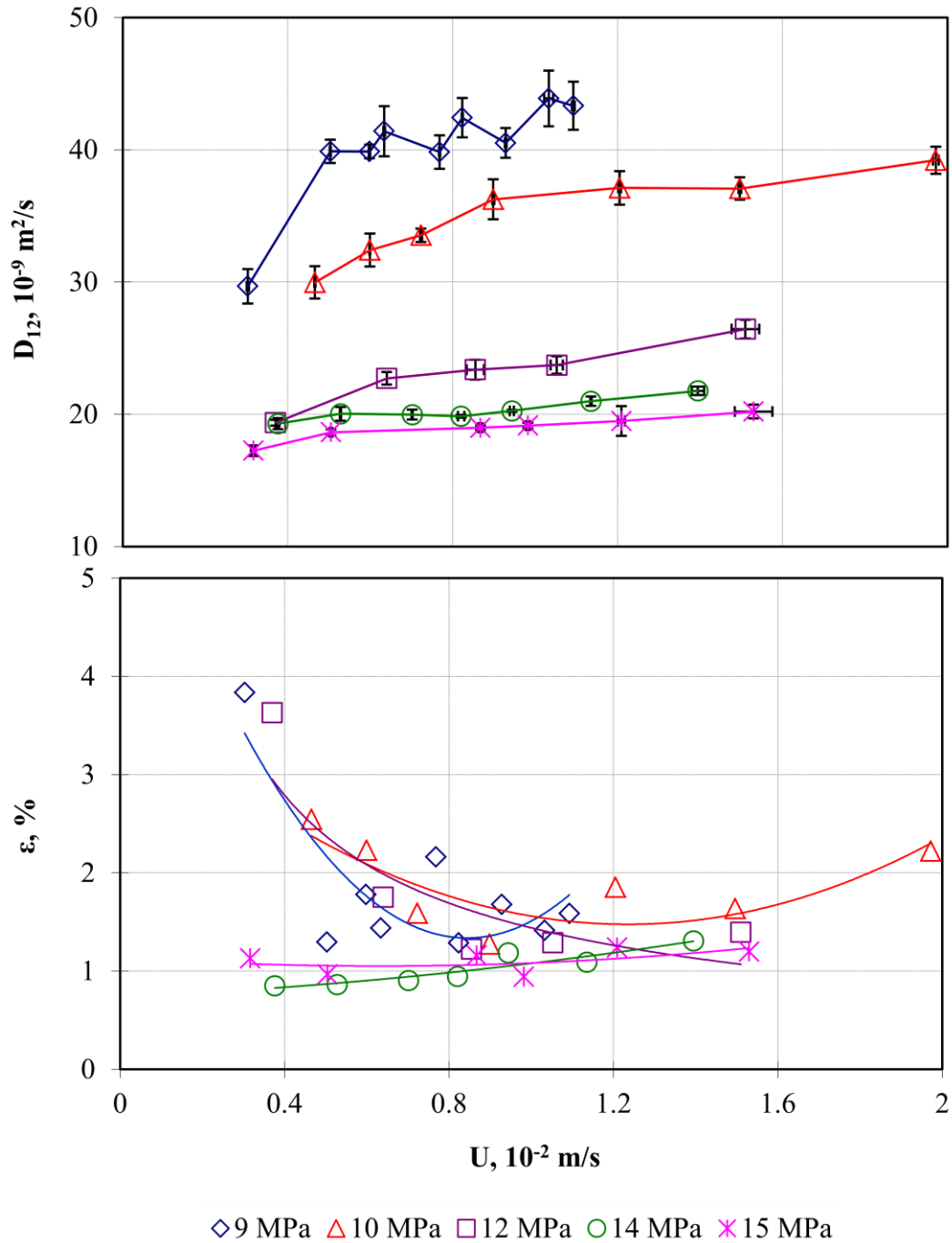


Fig. 4-22 Measured diffusion coefficients (top) of benzene in SCCO₂ and corresponding curve-fitting errors (bottom) as a function of the mean velocity at 333.15 K for the horizontal orientation. The solid lines in the top figure connect the data points. The solid lines in the bottom figure are trend lines.

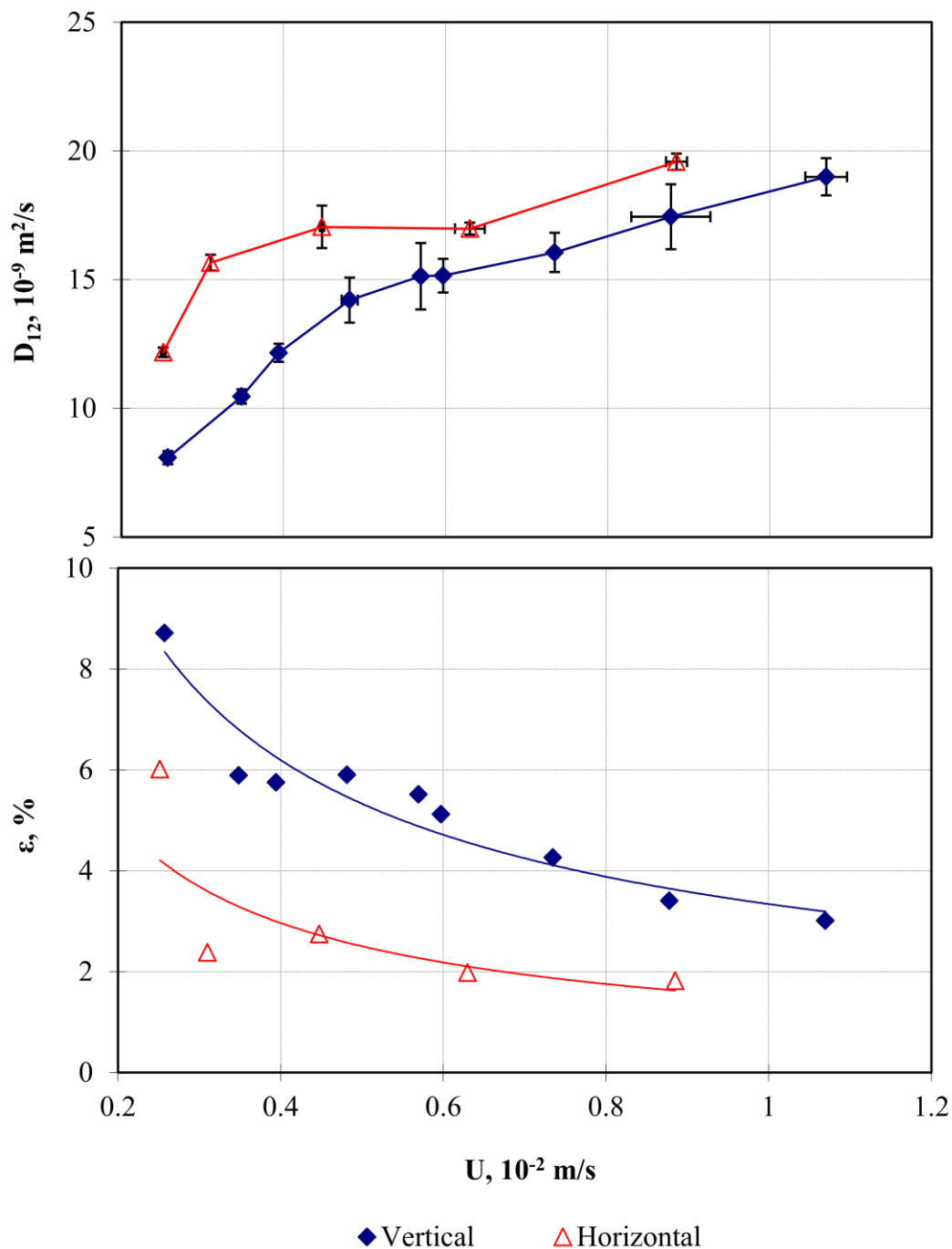


Fig. 4-23 Measured diffusion coefficients of benzene in SCCO₂ (top) and corresponding curve-fitting errors (bottom) at 313.15 K and 9 MPa for both vertical and horizontal column orientations. The solid lines in the top figure connect the data points. The solid lines in the bottom figure are trend lines.

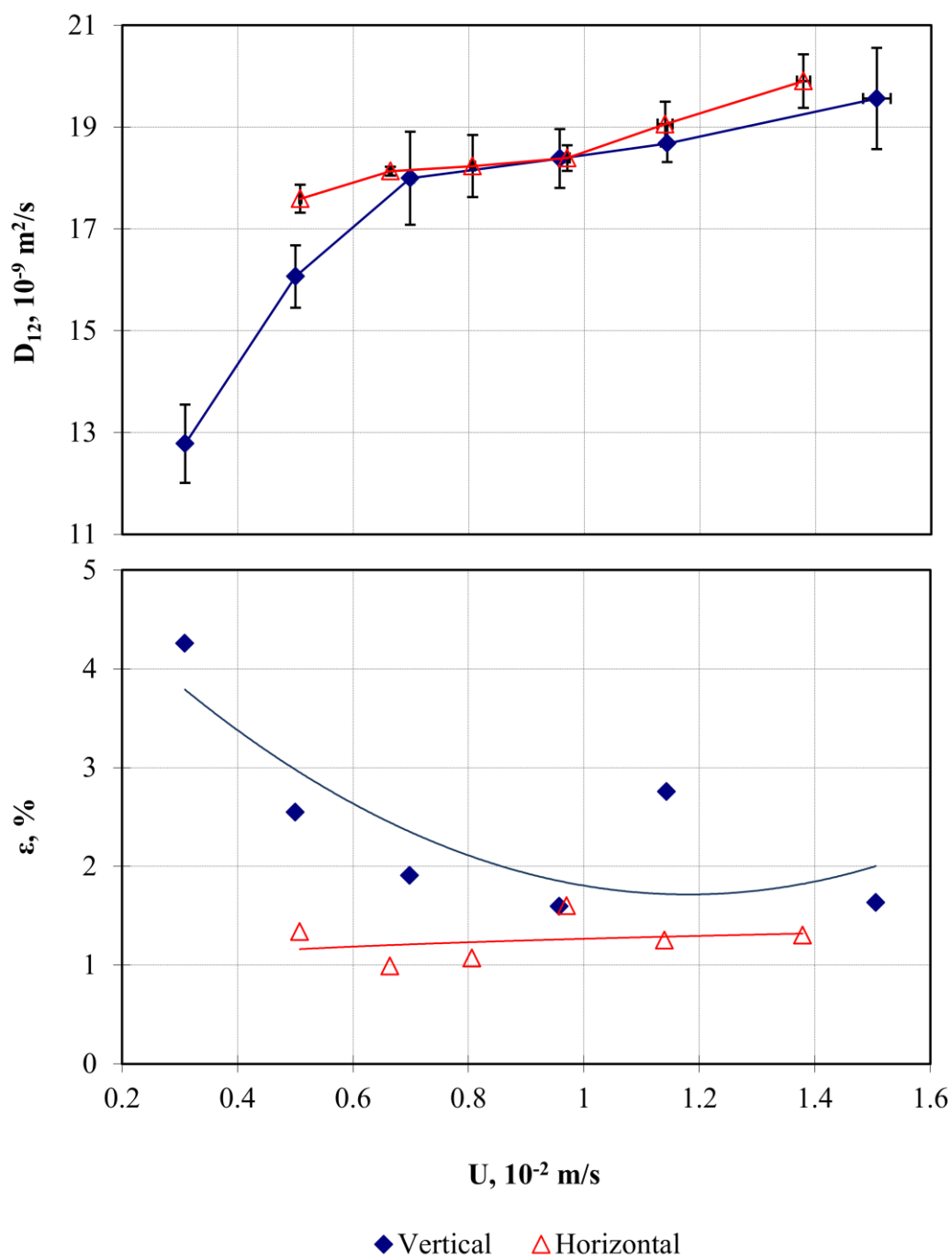


Fig. 4-24 Measured diffusion coefficients of benzene in SCCO₂ (top) and corresponding curve-fitting errors (bottom) at 313.15 K and 9.5 MPa for both vertical and horizontal column orientations.

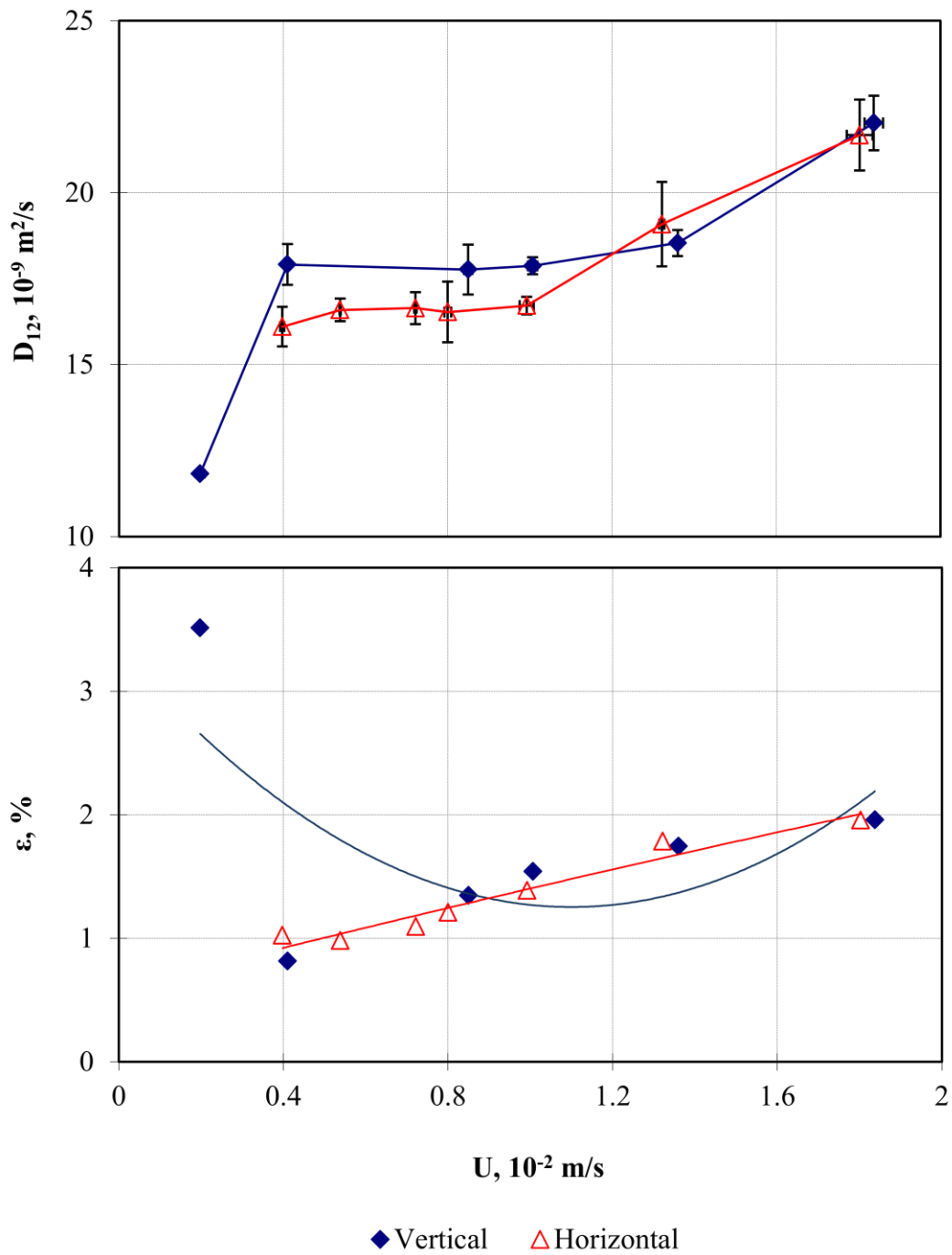


Fig. 4-25 Measured diffusion coefficients of benzene in SCCO₂ (top) and corresponding curve-fitting errors (bottom) at 313.15 K and 10 MPa for both vertical and horizontal column orientations.

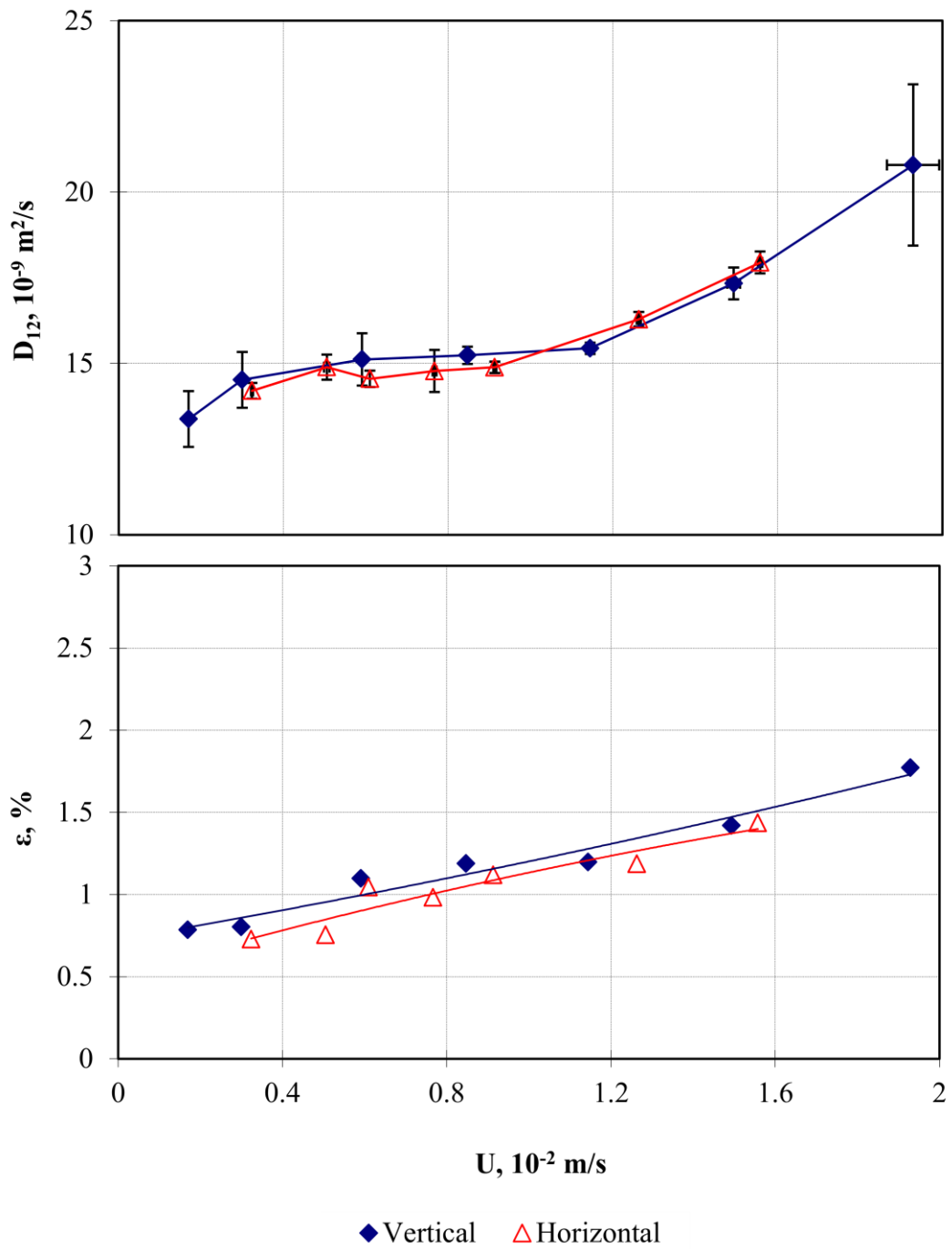


Fig. 4-26 Measured diffusion coefficients of benzene in SCCO₂ (top) and corresponding curve-fitting errors (bottom) at 313.15 K and 12 MPa for both vertical and horizontal column orientations.

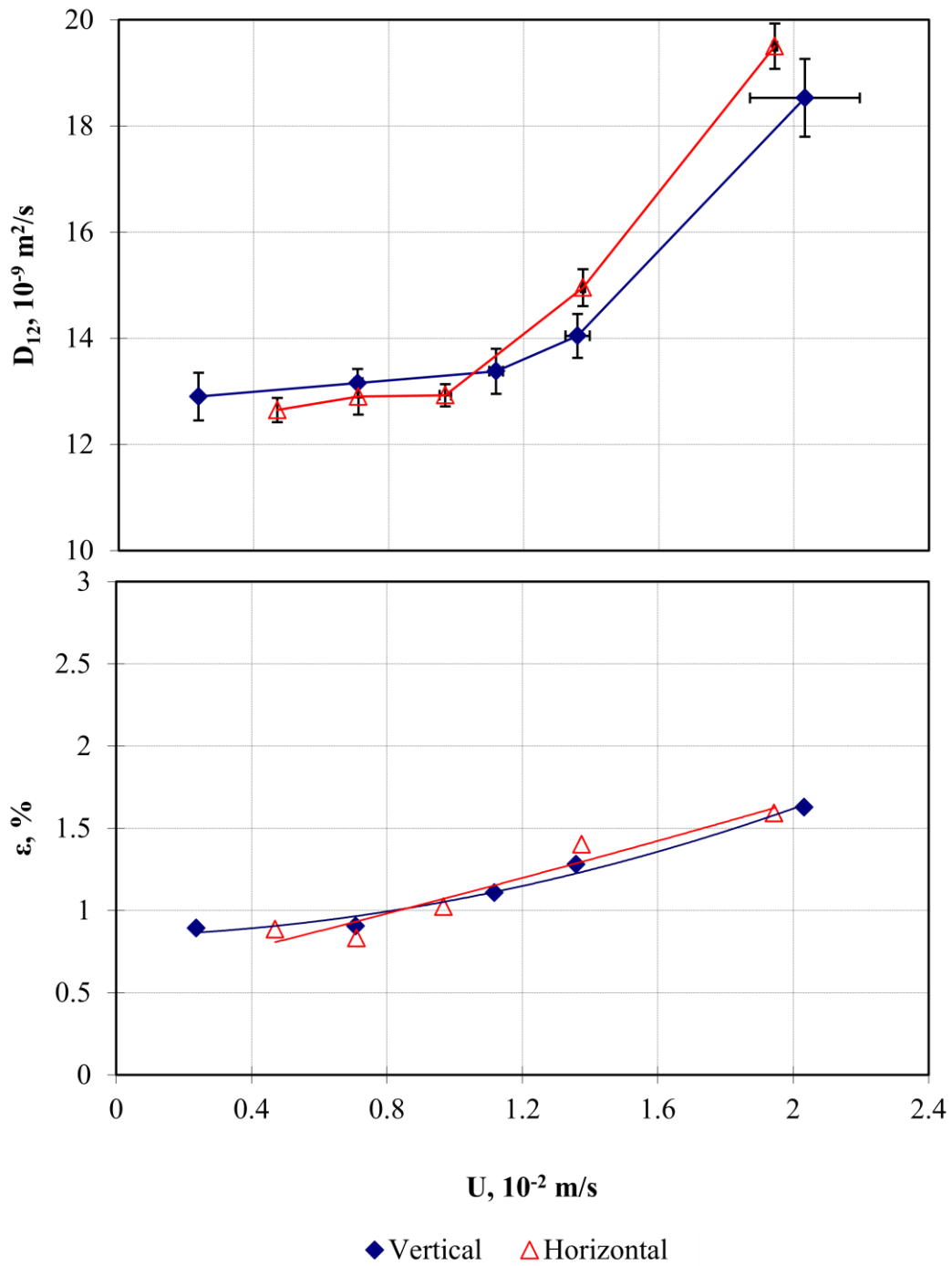


Fig. 4-27 Measured diffusion coefficients of benzene in SCCO₂ (top) and corresponding curve-fitting errors (bottom) at 313.15 K and 15 MPa for both vertical and horizontal column orientations.

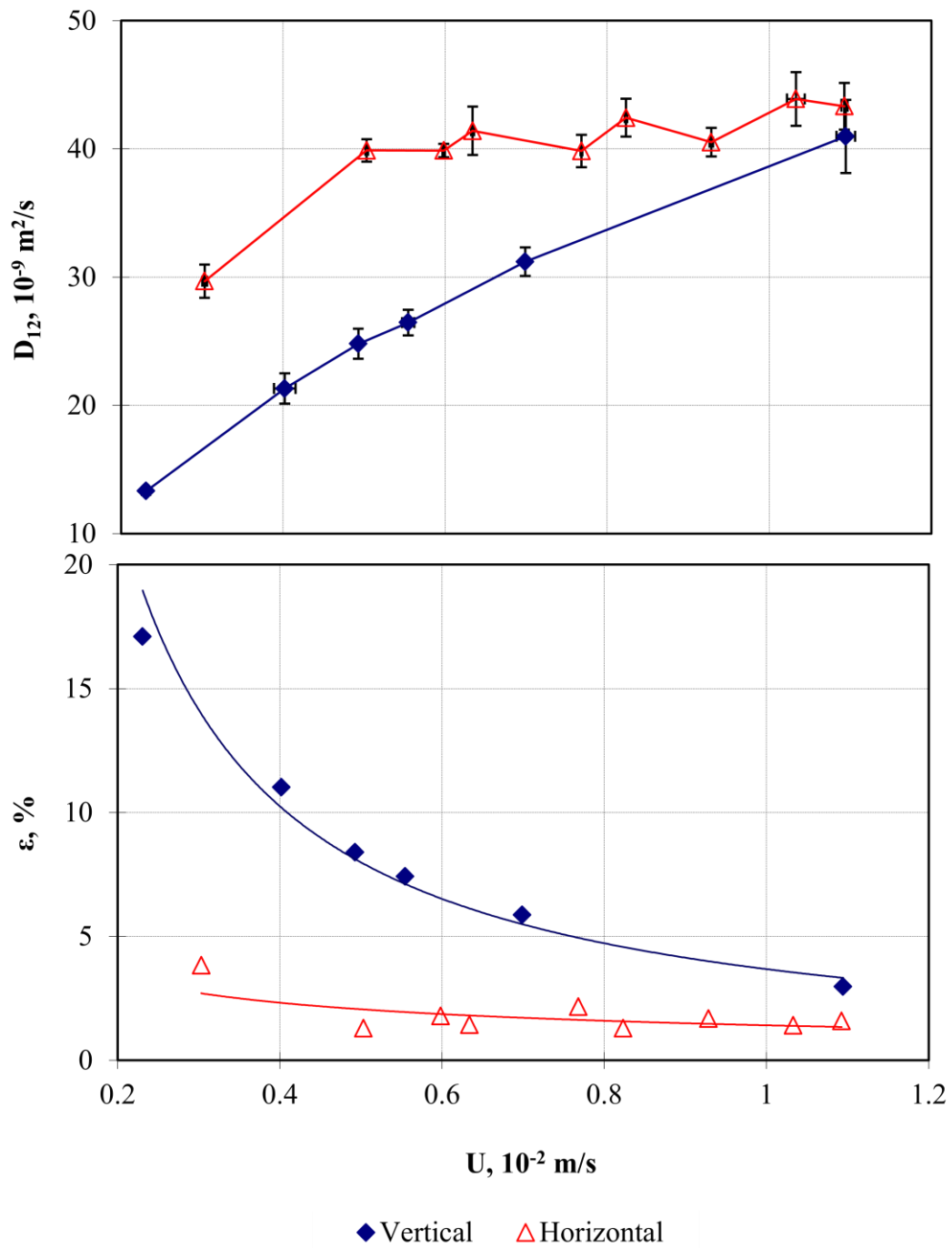


Fig. 4-28 Measured diffusion coefficients of benzene in SCCO₂ (top) and corresponding curve-fitting errors (bottom) at 333.15 K and 9 MPa for both vertical and horizontal column orientations.

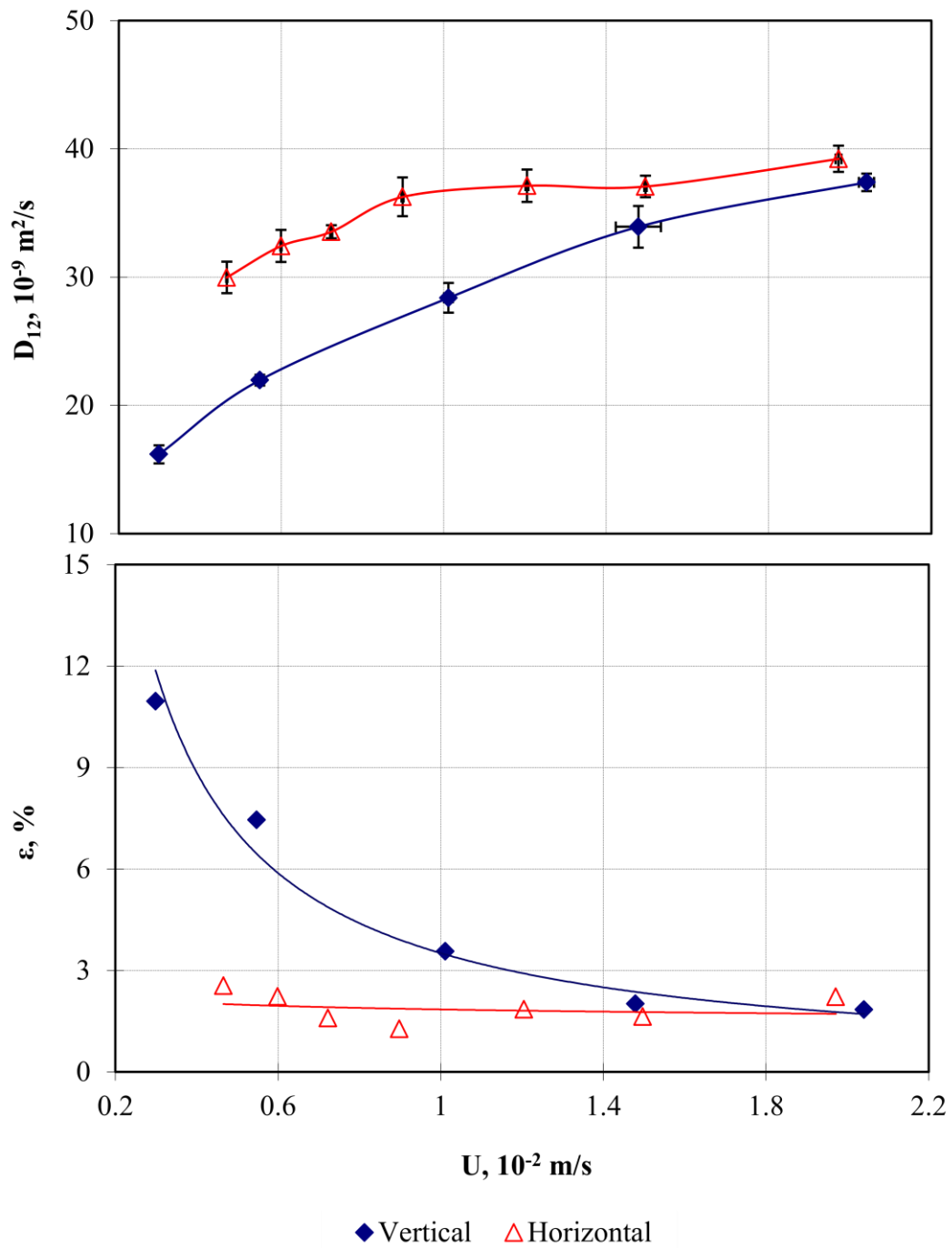


Fig. 4-29 Measured diffusion coefficients of benzene in SCCO₂ (top) and corresponding curve-fitting errors (bottom) at 333.15 K and 10 MPa for both vertical and horizontal column orientations.

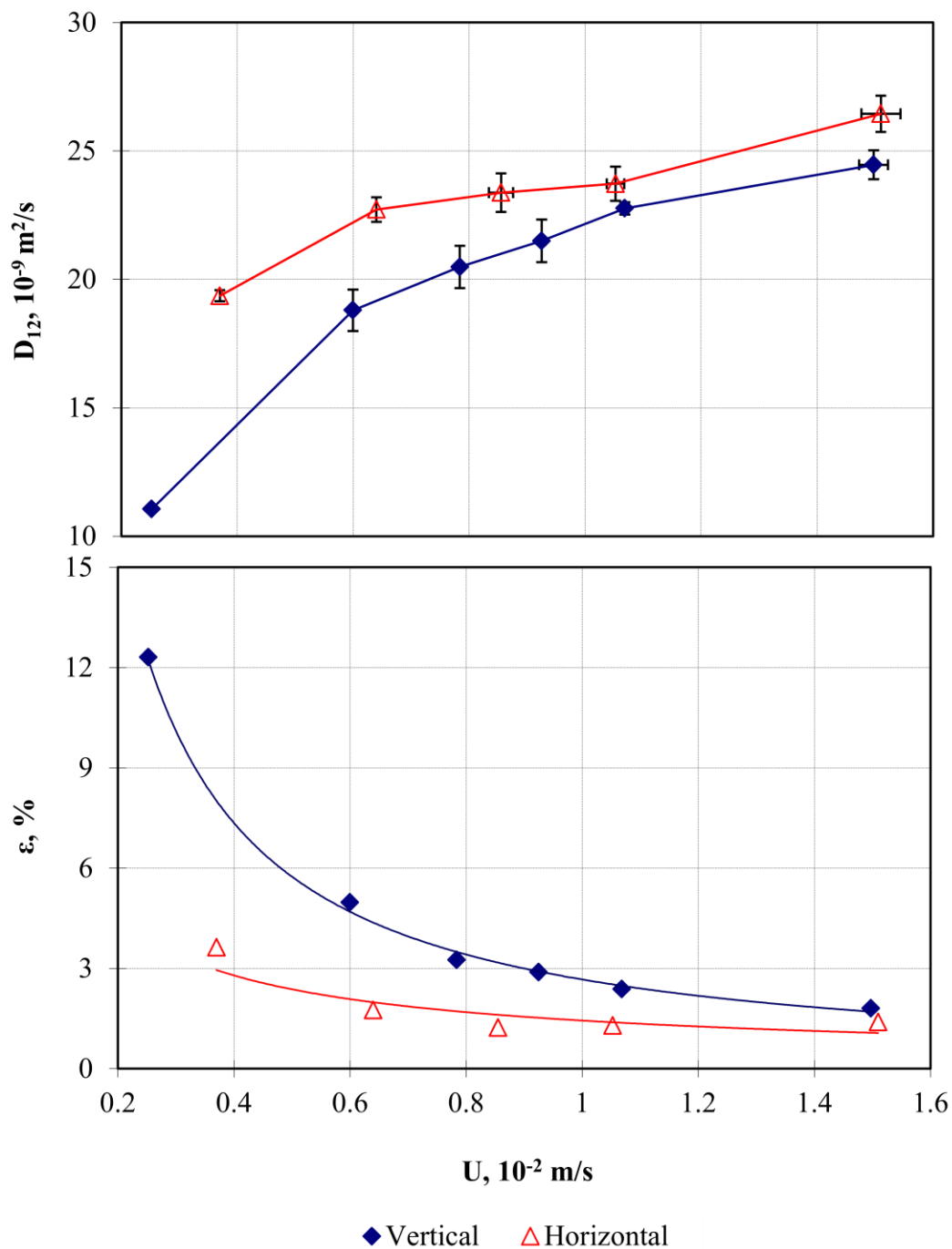


Fig. 4-30 Measured diffusion coefficients of benzene in SCCO₂ (top) and corresponding curve-fitting errors (bottom) at 333.15 K and 12 MPa for both vertical and horizontal column orientations.

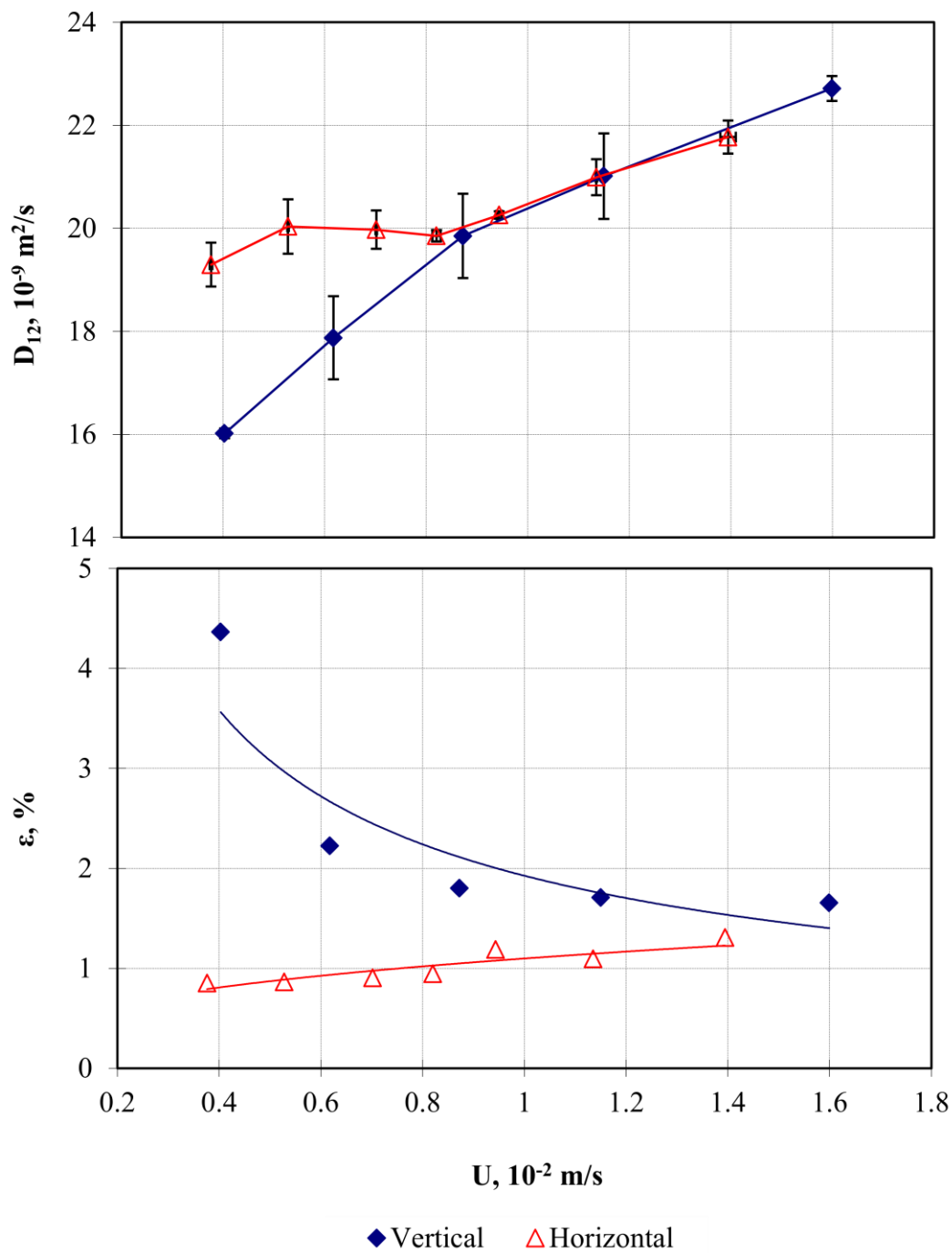


Fig. 4-31 Measured diffusion coefficients of benzene in SCCO₂ (top) and corresponding curve-fitting errors (bottom) at 333.15 K and 14 MPa for both vertical and horizontal column orientations.

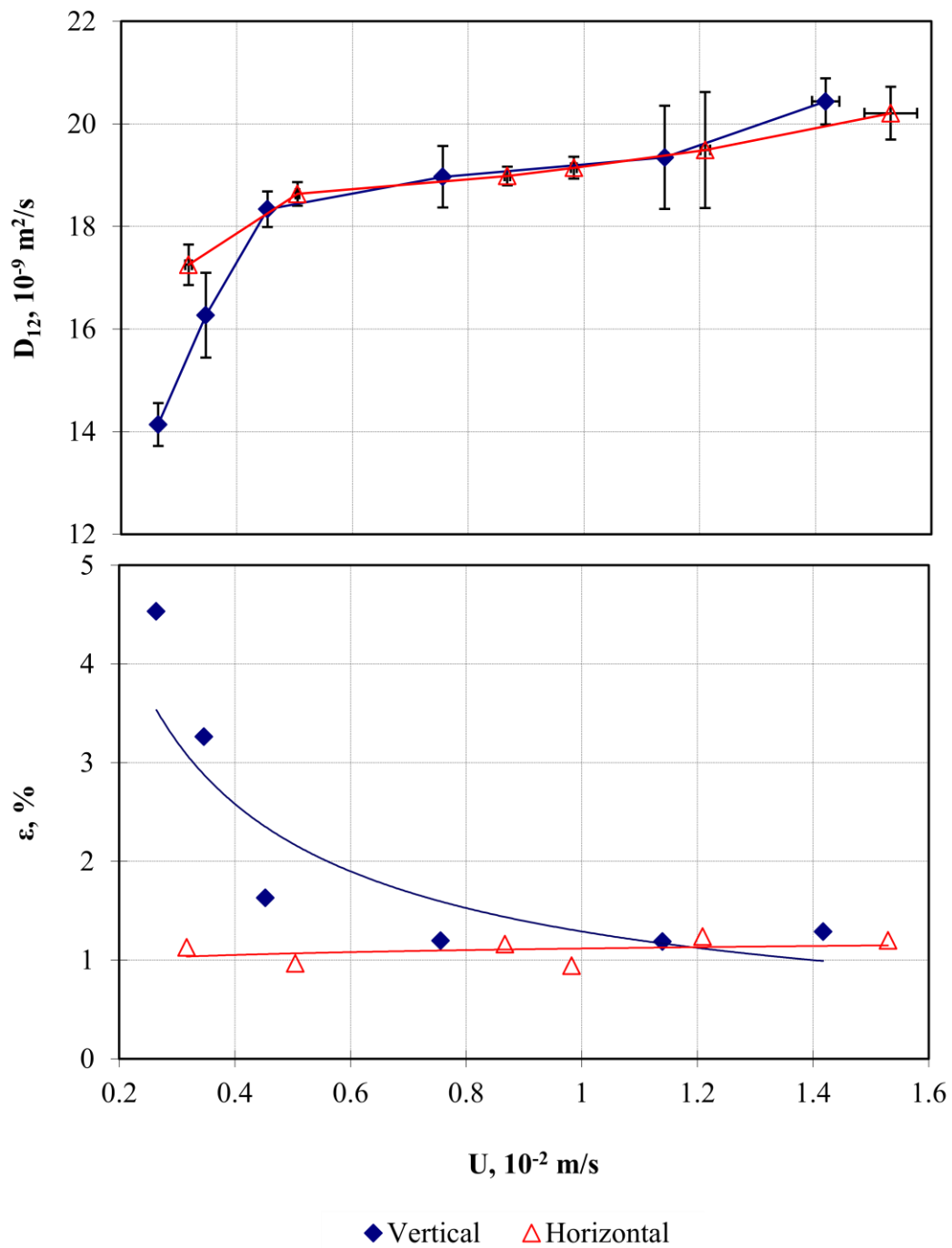


Fig. 4-32 Measured diffusion coefficients of benzene in SCCO_2 (top) and corresponding curve-fitting errors (bottom) at 333.15 K and 15 MPa for both vertical and horizontal column orientations.

Moreover, improvements were found to be much more significant at the low U end that favors the buoyancy effects as shown in **Fig. 4-23**, **Fig. 4-24**, and **Fig. 4-28** to **Fig. 4-32**. These results strongly support the argument that the buoyancy forces due to density difference play an important role in dispersion and may significantly influence diffusion coefficient measurements. Finally, as clearly demonstrated in **Fig. 4-28** to **Fig. 4-32**, the difference between two D_{12} curves decreased as pressure (or density) increased. This can be explained by the competing relationship between the buoyancy forces and the inertial forces. Higher pressure results in lower density difference and higher viscosity, which reduces the impact of the buoyancy forces on the dispersion process.

Diffusion coefficients of benzene in SCCO₂ were determined by averaging measured values within OVRs. Under those conditions where no OVR existed for the vertical orientation, diffusion coefficients were interpolated at U of 0.008 m/s (333.15 °C, 9-14 MPa) (**Fig. 4-28** to **Fig. 4-32**). Results are plotted in **Fig. 4-33** as a function of CO₂ density, more explicitly demonstrating the non-negligible impact of column orientation on diffusion coefficient measurements. It was found that when CO₂ density was below ~ 580 kg/m³, diffusion coefficients obtained when the column was installed horizontally were higher than those determined when the column was in the vertical position. Higher CO₂ density beyond that value resulted in opposite outcomes, which is contradictory to previous findings (Funazukuri and Nishimoto, 1996). Further investigations are required to address this issue. Additionally, the difference between two sets of data decreased as CO₂ density increased.

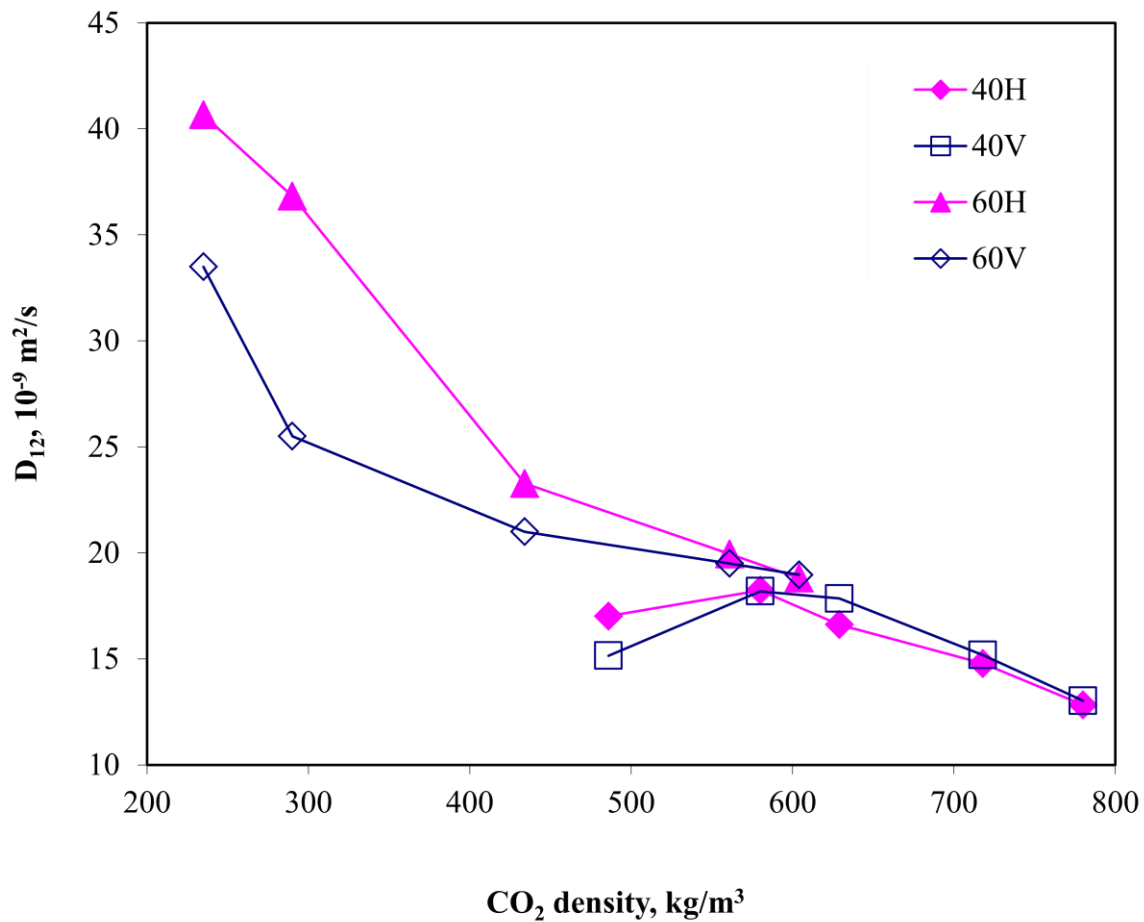


Fig. 4-33 Comparison of diffusion coefficients obtained in vertically- and horizontally-installed columns. V: vertical; H: horizontal. The solid lines connect the data points.

4.6.5.6 A new generalized D_{12} - U pattern diagram

A new pattern diagram of D_{12} - U relationship was generalized based on current results and is presented in **Fig. 4-34**. The new pattern diagram is divided into three regions, I, II and III. Regions II and III at ρ_2 and ρ_3 are identical to the pattern shown in **Fig. 4-5**. In regions I and III, measured diffusion coefficients increase as U increases, while in region II, they stay constant at ρ_2 and ρ_3 . As density decreases, both regions I and III expand and region II shrinks, and finally, regions I and III merge together and region II disappears. Since accurate measurements of diffusion coefficients can only be possible in region II, measurements at ρ_1 will likely result in substantial uncertainties. Therefore, when measurements of diffusion coefficients in SCFs cover a wide range of SCF density, it is highly recommended to identify region II at both maximum and minimum densities to make sure that the U used is within region II, especially when a column is installed vertically.

Formation of the new D_{12} - U pattern can be interpreted by the combined action of the buoyancy effects induced by density gradients and the secondary flow effects due to tube curvature. It is well understood that increasing U enhances the secondary flow effects but weakens the buoyancy effects. At low U (region I), the buoyancy effects dominate, while at high U (region III), the secondary flow effects dominate. The combined impact of both factors is minimized in region II and measured diffusion coefficients are independent of U and represent the true diffusion coefficients. More specifically, as U increases in region I, the effect of buoyancy forces on laminar flow reduces gradually and consequently, the measured diffusion coefficient moves toward the true value. When U enters region II, the buoyancy forces become negligible compared to

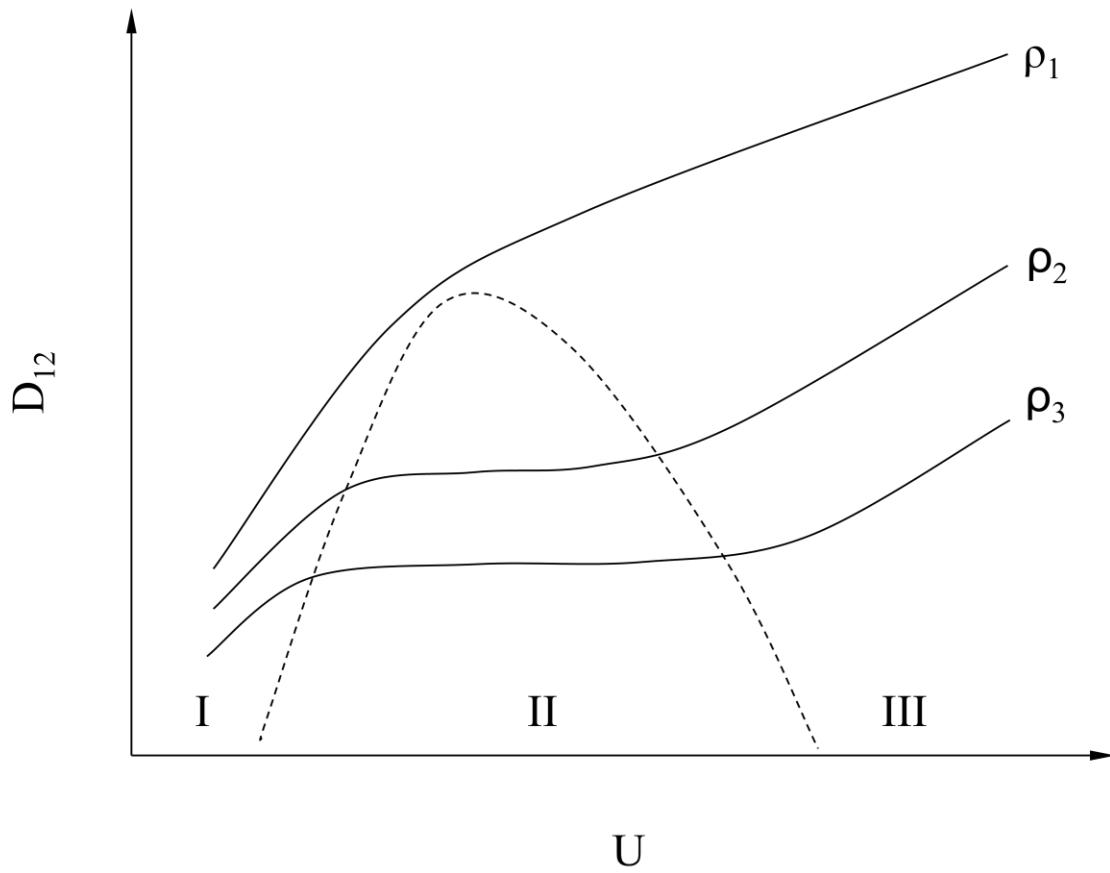


Fig. 4-34 Generalized relationship between measured diffusion coefficients and the mean velocity. The solid lines indicate D_{12} - U curves at different densities ($\rho_1 < \rho_2 < \rho_3$); the dash line indicates the boundary among regions I, II, and III.

the inertial forces, while the centrifugal forces are still too small to create effective secondary flows. This results in constant measured diffusion coefficient values. As U enters into region III, however, the centrifugal forces produce secondary flows that are strong enough to affect the dispersion process, leading to higher measured diffusion coefficients.

4.7 CONCLUSIONS

In this chapter, diffusion coefficients of diesel fuel and surrogate compounds (toluene, m-xylene, 1-hexadecene and 1-methylnaphthalene) in SCCO₂ were determined by the Taylor dispersion method at temperatures up to 373.15 K and pressures up to 30 MPa. Results were correlated by Wilke-Chang, Scheibel, He-Yu, $D_{12}/T - \mu$ and $D_{12}/\sqrt{T} - \rho$ correlations. Among three predictive correlations, the He-Yu correlation had the best capability of predicting diffusion coefficients in SCCO₂. The prediction performance of the Wilke-Chang correlation could be improved considerably by varying the association factor ψ . Diffusion coefficients of diesel fuel surrogate compounds in SCCO₂ were best fitted by the $D_{12}/T - \mu$ correlation with AAD% < 8%.

The Taylor dispersion method encountered difficulty in measuring diffusion coefficients near the critical point of CO₂ due to reduced solvent power of SCCO₂. This difficulty may be improved by reducing injection volume or by increasing inner diameter of the diffusion column.

Diffusion coefficients of benzene in SCCO₂ were measured at 40 and 60 °C and 9-15 MPa covering a wide range of CO₂ densities (235-780kg/m³). Sources of

uncertainties including detector linearity, sample injection, mobile phase mean velocity, and column orientation were discussed. Some key points are outlined below.

A new dimensionless parameter was proposed to account for the impact of finite injection volume and to guide experimental design.

The linearity of the UV detector is crucial to the accuracy of diffusion coefficient measurements by the Taylor dispersion method. It was found that the best linearity results in maximum diffusion coefficients and that the wavelength which gives maximum diffusion coefficients should be selected for dispersion peak detection.

Diffusion coefficient measurements by the Taylor dispersion method were significantly affected by U . Measured diffusion coefficients decreased dramatically as U decreased at very low U , which differs substantially from the well-known D_{12} - U relationship. This implies that low U will likely bring significant experimental errors. Measured diffusion coefficients increased with increasing U over the entire velocity ranges and no OVRs were located at relatively low CO_2 density, when the column was installed vertically. Significant improvement was achieved when the column was switched from vertical to horizontal position. Thus, it is concluded that accurate diffusion coefficients can only be determined using a horizontally installed column when mobile phase density is relatively low and density difference is large.

A new generalized D_{12} - U pattern was proposed, which is comprised of three regions, I, II and III, dominated by buoyancy forces, inertial forces, and centrifugal forces, respectively. At relatively low density, regions I and III merge together and region II disappears. Good care must be taken when conducting experiments under such conditions to assure measurements are made in constant D_{12} - U region II.

Column orientation affects diffusion coefficient measurements mainly by enhancing or weakening the buoyancy effects. When density difference is substantial and the column is installed vertically, alternate upward and downward flow along the column will significantly enhance the buoyancy effects, leading to lower measured diffusion coefficients.

When CO₂ density was below ~ 580 kg/m³, diffusion coefficients obtained when the column was horizontally installed were higher than those obtained when the same column was vertically installed. When CO₂ density was above that value, opposite outcomes resulted. These differences decreased, as CO₂ density increased.

CHAPTER V

THERMAL STABILITY OF DIESEL FUEL

5.1 INTRODUCTION

Thermal stability of DF is one major issue that needs to be addressed in the development of the supercritical fuel combustion technology because this new technology requires DF to be delivered near or above the critical temperature which is 740-755 K (or 467-482 °C) as estimated in Chapter III. It is generally understood that fuel stability reduces as fuel temperature increases. Previous studies on the hypergolic combustion demonstrated significant fuel coking at high fuel temperatures, which caused the failure of the system (Scharnweber, 1984). When a fuel is thermally stressed at relatively high temperatures, fuel compositions and other chemical properties will change, which have a direct impact on fuel combustion. Also, significantly high fuel temperatures will produce solid deposits, which will block the delivery system. The new solution proposed by Tavlarides and Anitescu is to use diluents to prevent fuel coking (Tavlarides and Anitescu, 2009).

This chapter reports the experimental studies on thermal stability of DF. The major objectives are to address the impacts of temperature, residence time, and CO₂ contents on thermal stability of DF. CO₂ was used as an EGR surrogate to dilute DF in this study. Three different experiments were designed and conducted, i.e. batch thermal stressing of DF, batch thermal stressing of DF/CO₂ mixtures, and continuous thermal stressing of DF and DF/CO₂ mixtures. The upper temperature limit above which

significant degradation occurs was determined. The role of CO₂ in preventing DF coking is discussed.

5.2 EXPERIMENTAL

5.2.1 Batch thermal stressing of DF

The first experiment was batch thermal stressing of DF to reveal the effects of temperature and residence time on thermal stability of DF. **Fig. 5-1** (bottom) shows a schematic diagram of the experimental setup. A high pressure stainless steel tee (Autoclave Engineers) (**Fig. 5-1** upper right) was used as the thermal stressing cell. The volume of the cell was ca. 0.6 ml. A thermocouple (T2) was connected to the cell to monitor inside temperature. The cell was placed inside a GC oven (HP 5890) to achieve constant temperatures required for the experiment. A second thermocouple (T1) was used to monitor the oven temperature. Both thermocouples were connected to a data acquisition system (LabVIEW, National Instruments). To capture solid deposits formed during the thermal stressing experiment, a stainless steel sheet (**Fig. 5-1** upper left) was added to the cell in each run. The metal sheets were washed by hexane before adding to the vessel. After experiments, they were rinsed by hexane, dried in air at room temperature, and then analyzed by the Scanning Electron Microscope (SEM) method. Since pressure inside the cell was not monitored during the experiments, it was necessary to estimate the maximum pressures at different DF loading amount to make sure that the actual pressures would be within the pressure limit of interest, which was 60 MPa. To do so, a P-T- ρ diagram of DFS-7, as shown in **Fig. 5-2**, was constructed to guide the design because DFS-7 gives best predictions of DF density as demonstrated in the Chapter III.

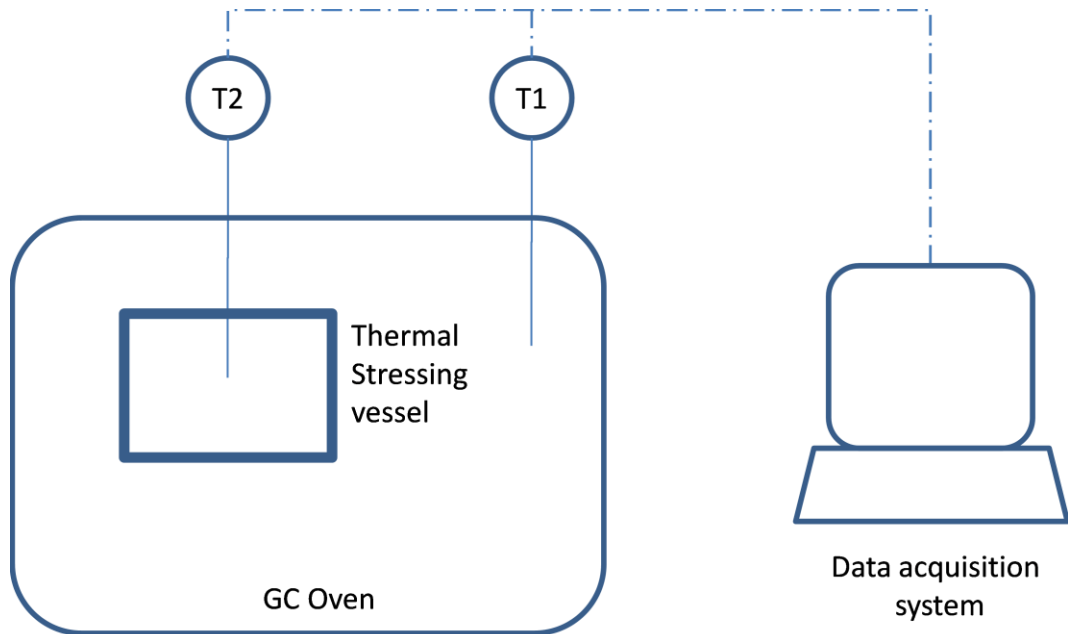
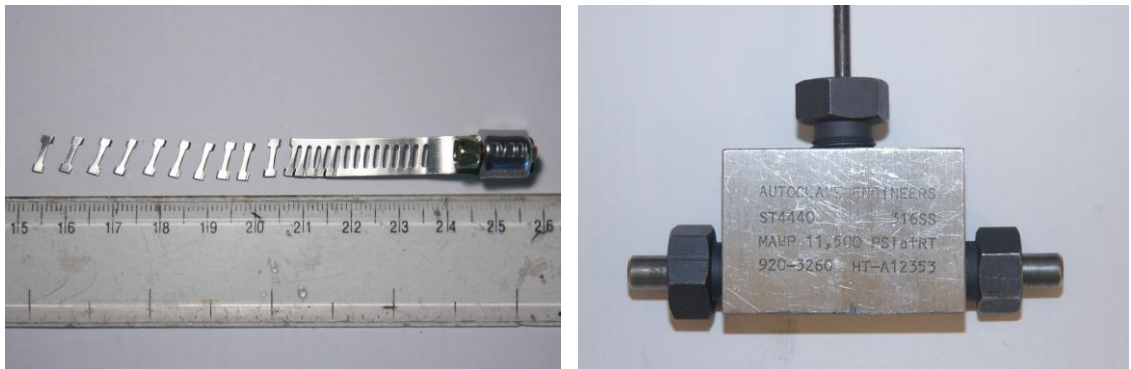


Fig. 5-1 Experimental setup for batch thermal stressing of DF. Top left: stainless steel sheets used to capture solid deposits; Top right: a photo of the thermal stressing cell; T1 and T2: outside and inside temperatures of the cell.

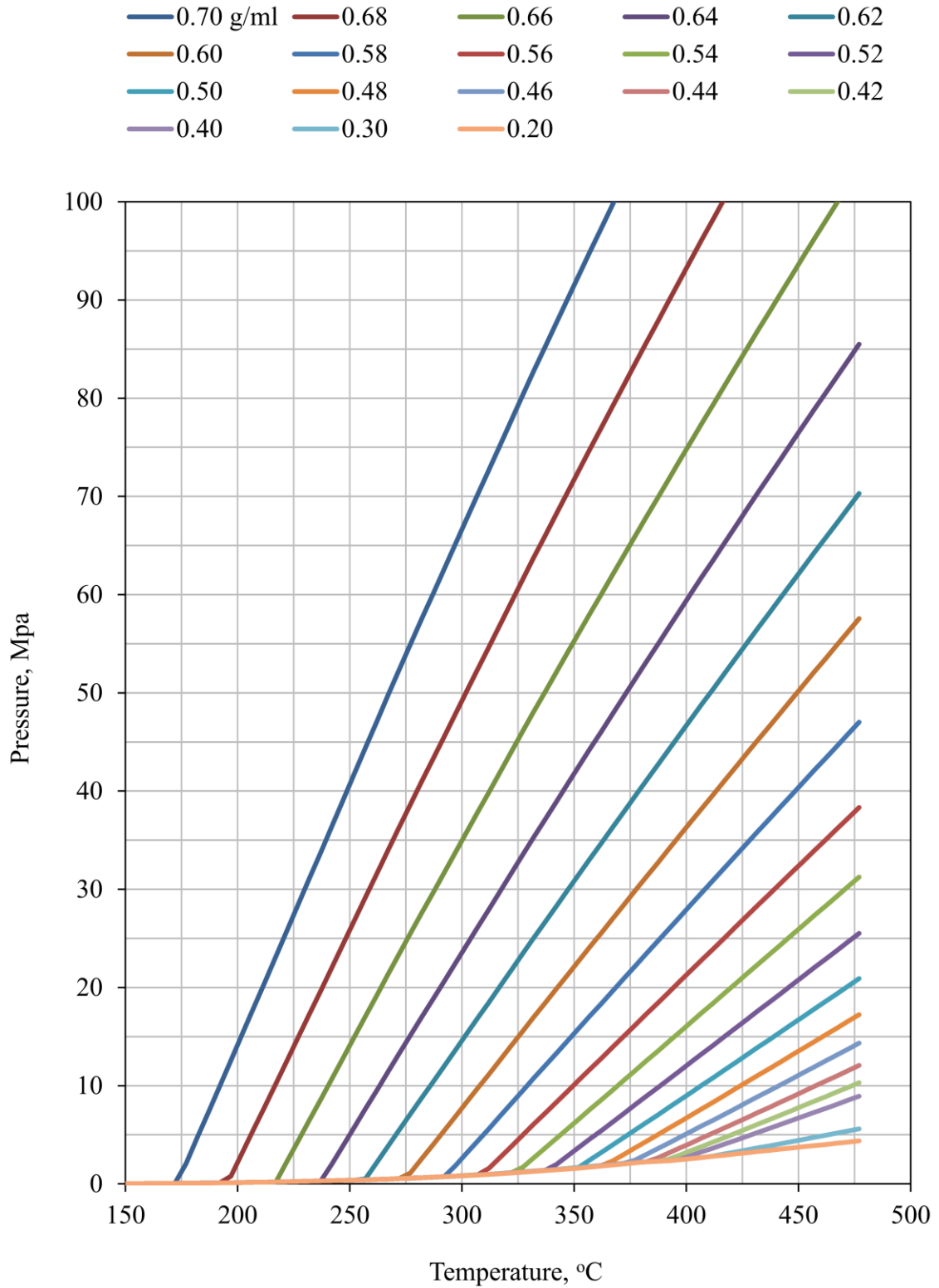


Fig. 5-2 A pressure-temperature-density diagram for DFS-7.

No. 2 DF was purchased from a local gas station and used as received. The density of the fuel at room temperature measured in this work was 0.835 ± 0.004 g/ml. Accordingly, 0.45 ml DF was added to the vessel in each run, giving a bulk density of 0.626 g/ml, and the pressure found in **Fig. 5-2** at 440 °C is below 60 MPa.

Experimental conditions are given in **Table 5-1**. Tests were first performed at 200-440 °C for a residence time of 10-15 min to determine the temperature range where significant degradation of DF starts to occur. The rest of the experiments were conducted based on these tests. **Fig. 5-3** presents an example of temperature history obtained in the experiments. The residence time is defined as the duration of the isothermal stage as illustrated in **Fig. 5-3** excluding the heating and cooling stages. **Fig. 5-3** also shows excellent temperature control of the GC oven.

DF was manually added into the vessel. As described in section 2.3, oxygen exhibits significant impact on fuel stability. Therefore, to eliminate O₂ from air, DF was loaded in CO₂ environment for most runs. Several runs were made with samples prepared in air for comparison and to demonstrate the effect of O₂. Thermal stressing of pure compounds, i.e. n-hexadecane, 1-methylnaphthalene and butylbenzene, were also conducted to explain DF color change after thermal stressing. N-hexadecane (>99%), 1-methylnaphthalene (95%), butylbenzene (>99%) were purchased from Sigma-Aldrich and used as received.

5.2.2 Batch thermal stressing of DF/CO₂ mixtures

The second experiment was batch thermal stressing of DF/CO₂ mixtures to understand the effect of CO₂ on thermal stability of DF and the role of CO₂ in preventing

Table 5-1 Conditions for batch thermal stressing of DF.

| T, °C | Residence time, min | | | | | | |
|------------------|---------------------|----|----|-----|-----|-----|-----|
| | 10 | 30 | 60 | 120 | 180 | 300 | 600 |
| 200 ^a | × | | | | | | |
| 300 | × | | | | | | × |
| 400 | × | × | × | | × | × | × |
| 410 | | × | | | | | |
| 420 | | × | × | × | | | |
| 430 | | × | | | | | |
| 440 | × | × | | × | | | |

^a Actual residence time was 15 min.

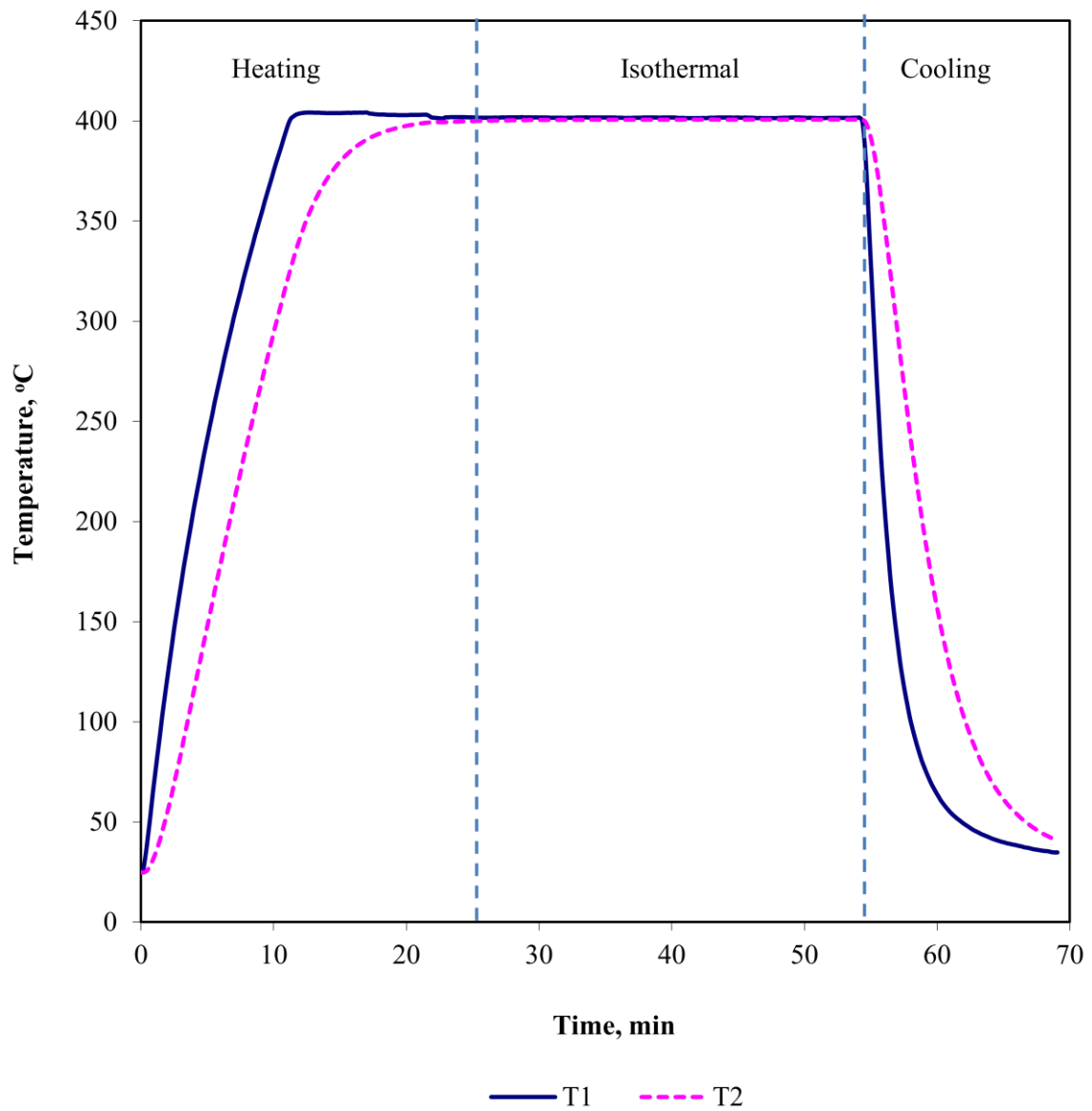


Fig. 5-3 An example of temperature history for batch thermal stressing of DF. T1: temperature of the GC oven; T2: temperature of DF inside the cell.

DF coking. A schematic diagram of the experimental setup is shown in **Fig. 5-4**. A high pressure stainless steel cross (High Pressure Equipment Co.) was machined and used as a thermal stressing cell. The total volume of the cell was ca. 2 ml. DF and CO₂ were added to the vessel by a syringe pump (ISCO 260D) and an HPLC pump (Dynamex, Model SD-1), respectively. A second syringe pump (ISCO 100D) was used to pump hexane to wash the vessel after each run. A thermocouple (T2) and a pressure transducer (P) were connected to the cell to monitor inside temperature and pressure, respectively. A second thermocouple (T1) was attached to outside wall of the cell. Both the thermocouples and the pressure transducer were connected to a data acquisition system (LabVIEW, National Instruments). The cell was heated by a heating tape (Briskheat), and temperature was controlled by a percentage control unit (Briskheat, TP0941-000) which is not shown in **Fig. 5-4**. An example of T-P history is given in **Fig. 5-5**.

In this experiment, a known amount of DF was first added into to the cell, and then CO₂ was added by pressurizing the cell with CO₂ to a desired pressure. Experimental conditions are given in **Table 5-2**. Two sets of experiments were conducted. In the first set of experiments, i.e. runs 1-5, the amount of DF was 1.7 ml for all runs, while the amount of CO₂ varied by changing pressure from 0-4.83 MPa (or 0-700 psi). It is obvious that in a constant volume system, the system pressure increases with increase in initial CO₂ pressure while keeping the amount of DF constant. To reduce pressure, the amount of DF needs to be reduced. Thus, the second set of runs, i.e. 1-a to 3-b, followed, where the amount of DF was varying from 1.6 to 1.2 ml and the initial CO₂ pressure was either 0 or 4.83 MPa. The thermal stressing temperature was 440 °C for both sets, while the residence times were 30 and 45 min for the first and the second, respectively. These

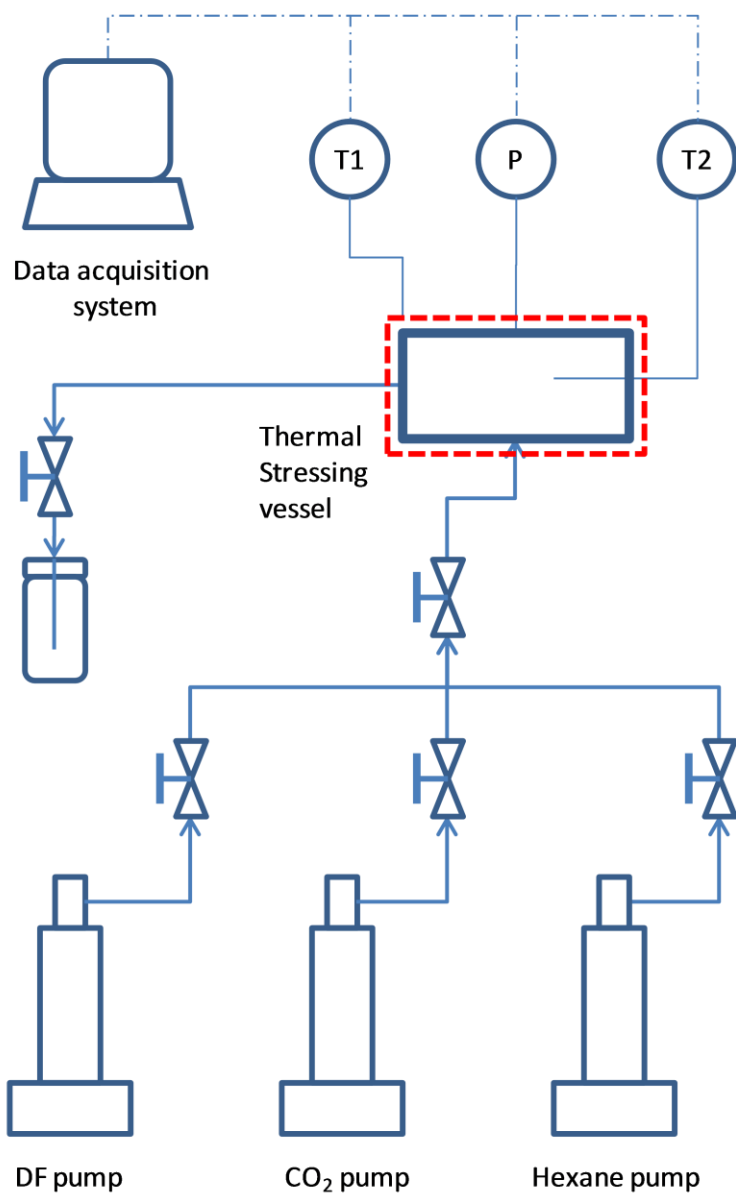


Fig. 5-4 A schematic diagram for the experimental setup for batch thermal stressing of DF/CO₂ mixtures. T1 and T2: thermocouples; P: pressure transducer; Red dash square: heating tape.

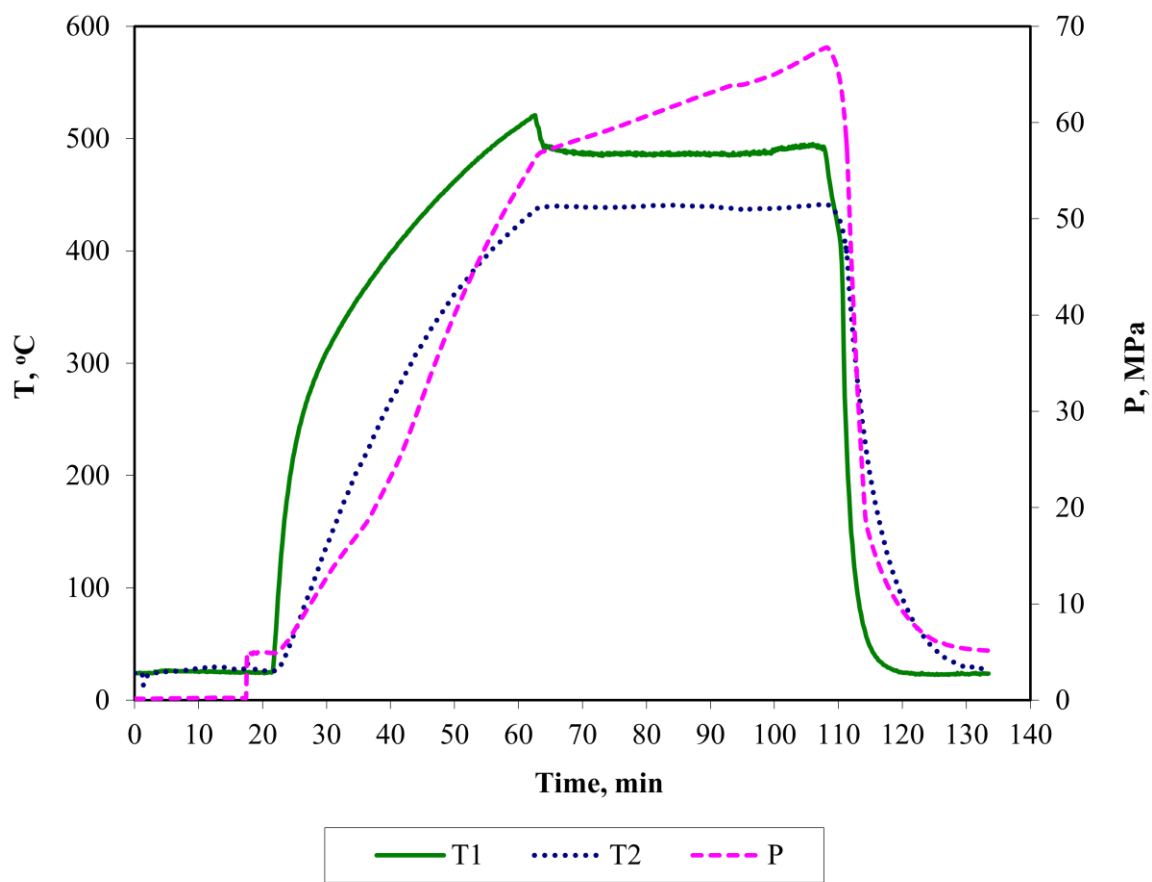


Fig. 5-5 An example of temperature/pressure history for batch thermal stressing of DF/CO₂ mixtures (run 1-b). T1: outside wall temperature of the vessel; T2: temperature of DF inside the vessel.

Table 5-2 Conditions for batch thermal stressing of DF/CO₂ mixtures.

| Run | DF, ml | CO₂, MPa | T, °C | τ, min |
|------------------|---------------|----------------------------|--------------|---------------|
| 1 | 1.7 | 0 | 440 | 30 |
| 2 | 1.7 | 2.76 | 440 | 30 |
| 3 | 1.7 | 3.45 | 440 | 30 |
| 4 | 1.7 | 4.14 | 440 | 30 |
| 5 | 1.7 | 4.83 | 440 | 30 |
| 1-a | 1.6 | 0 | 440 | 45 |
| 1-b | 1.6 | 4.83 | 440 | 45 |
| 2-a | 1.4 | 0 | 440 | 45 |
| 2-b | 1.4 | 4.83 | 440 | 45 |
| 3-a | 1.2 | 0 | 440 | 45 |
| 3-b | 1.2 | 4.83 | 440 | 45 |
| 4-b ^a | 1.0 | 4.83 | n/a | n/a |

^a The apparatus was incidentally overheated and damaged during the experiment.

two sets of runs were designed to demonstrate not only the effect of CO₂ but also the effect of pressure on thermal stability of DF.

5.2.3 Continuous thermal stressing of DF and DF/CO₂ mixtures

The major drawback of both batch experiments described in the preceding sections is that they are not able to eliminate the pressure effect because pressure cannot be controlled in the batch systems. Accordingly, continuous isobaric thermal stressing experiments were designed and conducted. A schematic diagram of the experimental setup is presented in **Fig. 5-6**. Thermal stressing was accomplished in a stainless steel coil (I.D. 1.524 mm, 18.3 m), the main coil shown in **Fig. 5-6**, which was located in the GC oven. CO₂ and DF were continuously delivered by a syringe pump (ISO 260D) and an HPLC pump (Dynamex, Model SD-1), respectively. The fuel, either DF or DF/CO₂ mixtures, was preheated before entering the main coil by a heating tape (Briskheat) controlled by a percentage control unit (Briskheat, TP0941-000). After thermal stressing, it was cooled down to room temperature in a water bath (Fisher Scientific) before entering a micro-filter (4200 series, Norman Filter). The 3-micron filter was installed to capture solid deposits formed in the process. A back pressure regulator (Swagelok) was located after the filter to control the system pressure. Preheating temperature (T1), GC oven temperature (T3), outlet temperatures of the preheating coil (T2) and the main coil (T4), and inlet (P1) and outlet (P2) pressures of the filter were monitored and recorded by the data acquisition system (LabVIEW, National Instruments).

The hypothesis of this experiment is that if fuel coking occurs, deposits will accumulate inside the filter and the pressure drop (P1-P2) through the filter will increase.

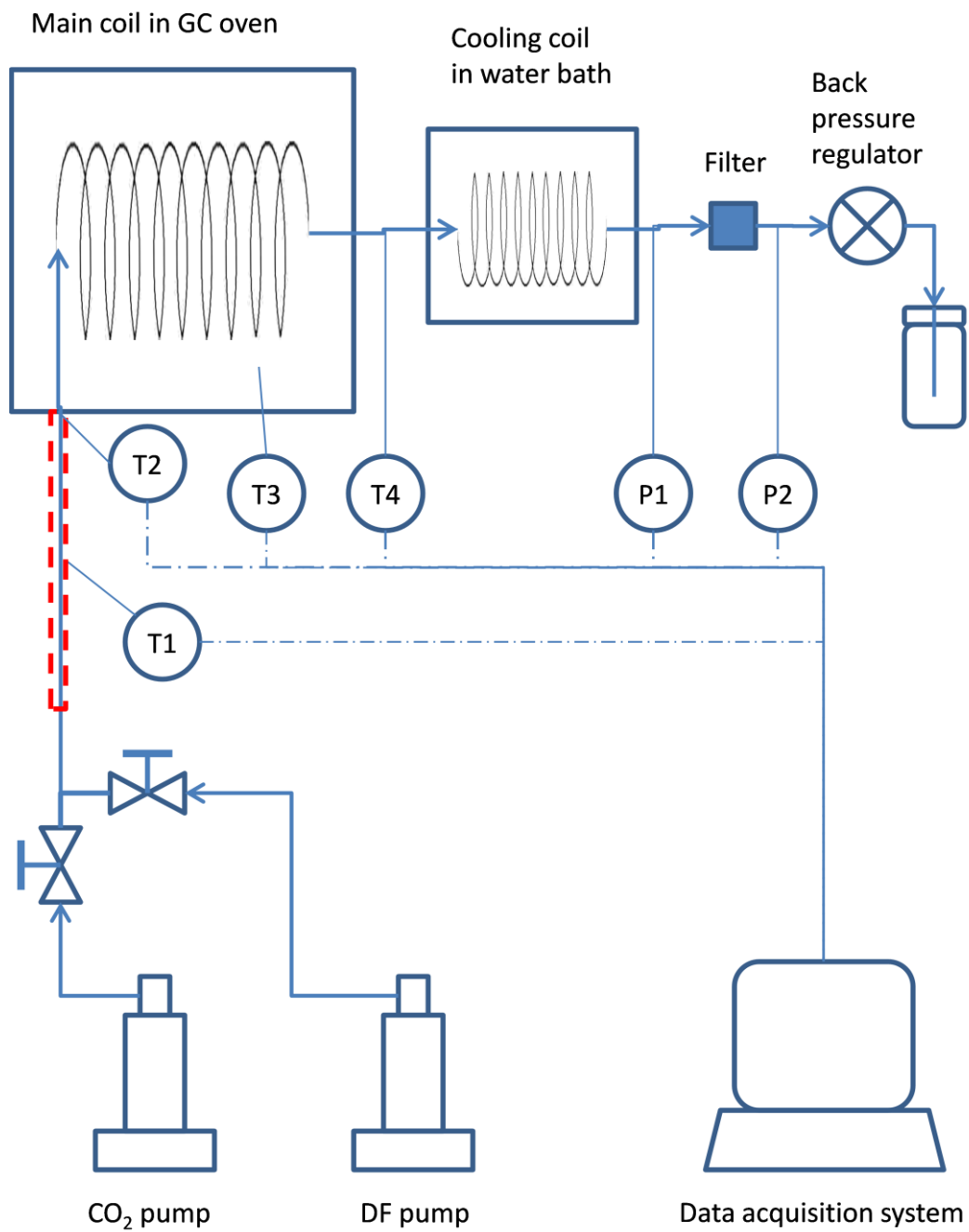


Fig. 5-6 A schematic diagram of the experimental setup for continuous thermal stressing of DF and DF/CO₂ mixtures. Red dash square indicates the heating tape.

If CO₂ were able to prevent DF coking, the rate of pressure drop increase would be reduced. Thus, through monitoring the pressure drop, it would be possible to characterize thermal stability of DF under different temperature and pressure conditions, with or without CO₂.

Experimental conditions for both DF and the DF/CO₂ mixture follow. Temperatures of the GC oven and the water bath were set at 440 and 20 °C, respectively. Fuels were preheated to about 350 °C. Pressure was set at 30 MPa. Flow rates for both pumps were determined based on a 30-min residence time, assuming a steady state at 440 °C and 30 MPa throughout the main coil. Consequently, pump flow rates for DF in the DF experiment and for DF and CO₂ in the DF/CO₂ experiment were 0.7339, 0.6309 and 0.0617 ml/min, respectively. Details of calculation are given in **Table 5-3**. Duration of each experiment was about 12 hr to ensure that change in pressure drop was captured. Samples were collected in one hour intervals and analyzed by GC-MS.

5.2.4 Fuel characterization

Fuel characterization includes four aspects: color, chemical composition, volatility, and solid deposits. Color change was analyzed simply by visual observation and recorded by digital photography. Chemical compositions were characterized by GC-MS. Volatility was measured using the TGA method described in section 3.2.1. Solid deposits captured by the metal sheets were analyzed by SEM.

A suitable GC-MS method was developed for DF analysis by trying different temperature programs. Key parameters for this method are presented in **Table 5-4**. Unless stated, all samples were prepared by diluting 2 µl fuel in 1 ml hexane, which gave

Table 5-3 Determination of pump flow rates for a given residence time of 30 minutes.

| | | |
|--|---------------------------------------|-----------------|
| Thermal stressing coil configuration | | |
| Inner diameter, mm | 1.524 | |
| Length, m | 18.3 | |
| Volume, ml | 33.36 | |
| DF/CO ₂ mixture composition | DF | CO ₂ |
| wt% | 90 | 10 |
| Density ^a , g/ml | 25 °C, 30 MPa | 440 °C, 30 MPa |
| DF | 0.847 | 0.559 |
| DF/CO ₂ mixture | 0.892 | 0.534 |
| CO ₂ | 0.963 | |
| Residence time, min | 30 | |
| Average volumetric flow rate, ml/min | 33.36 / 30 = <u>1.112</u> | |
| Mass flow rate, g/min | | |
| DF | 1.112 * 0.559 = <u>0.6216</u> | |
| DF/CO ₂ mixture | 1.112 * 0.534 = <u>0.5938</u> | |
| DF | 0.5938 * 0.9 = <u>0.5344</u> | |
| CO ₂ | 0.5938 * 0.1 = <u>0.0594</u> | |
| Pump flow rate, ml/min | | |
| DF | 0.6216 / 0.847 = <u>0.7339</u> | |
| DF/CO ₂ mixture | | |
| DF | 0.5344 / 0.847 = <u>0.6309</u> | |
| CO ₂ | 0.0594 / 0.963 = <u>0.0617</u> | |

^a Values are obtained from SUPERTRAPP. DFS-7 is used.

Table 5-4 Equipment, chemicals and key parameters for the GC-MS method.

| | |
|---------------------------|---|
| GC | HP 6790 |
| MS | HP 5971 |
| Column | HP-1MS Crosslinked methyl siloxane 30m × 0.25mm × 0.25 μm |
| Carrier gas | Helium |
| Solvent | Hexane |
| Injection volume | 1.0 μl |
| Injector temperature | 260 °C |
| Detector temperature | 285 °C |
| Oven Program | |
| Initial temperature | 45 °C |
| Initial time | 3 min |
| Temperature increase rate | 1 °C/min |
| Final temperature | 270 °C |
| Final time | 5 min |
| Column flow rate | |
| Head pressure | 8 psi |
| Linear velocity | 30 cm/s |
| Column flow rate | 0.9 ml/min |
| Solvent delay | 4 min |

good peak resolutions.

Fig. 5-7 shows an example of chromatographs obtained in this work. It is clearly seen that the abundances of C14 through C25 were reduced and those of C9 through C12 were increased when the fuel was stressed at 440 °C, which indicates occurrence of significant fuel degradation. However, when degradation is not that significant or when stressing temperatures vary in a relatively narrow range, the shape of chromatographs will look very similar, making it very difficult to do analysis qualitatively, not to mention quantitatively, due to the complexity of DF compositions. Accordingly, a new method for GC-MS data analysis is proposed in this work, which is able to effectively characterize fuel degradation. The procedure of this method is as follows:

- (1) Obtain peak area through automatic integration of chromatographs. A sample of integrated chromatograph of fresh DF is illustrated in **Fig. 5-8**.
- (2) Calculate percentage of peak area (*PPA*) using the equation below:

$$(PPA)_i = \frac{A_i}{\sum A_i} \times 100\% \quad (4-29)$$

where A_i is the area of peak i .

- (3) Calculate *PPA* change of stressed DF by

$$\Delta(PPA) = (PPA)_{Stressed\ DF} - (PPA)_{Fresh\ DF} \quad (4-30)$$

A positive $\Delta(PPA)$ value means increase in the concentration of the corresponding component when DF is thermally stressed.

- (4) Plot $\Delta(PPA)$ versus GC retention time and then add a linear trend line. A negative slope of the trend line indicates fuel degradation. The greater negative the slope, the more significant the degradation.

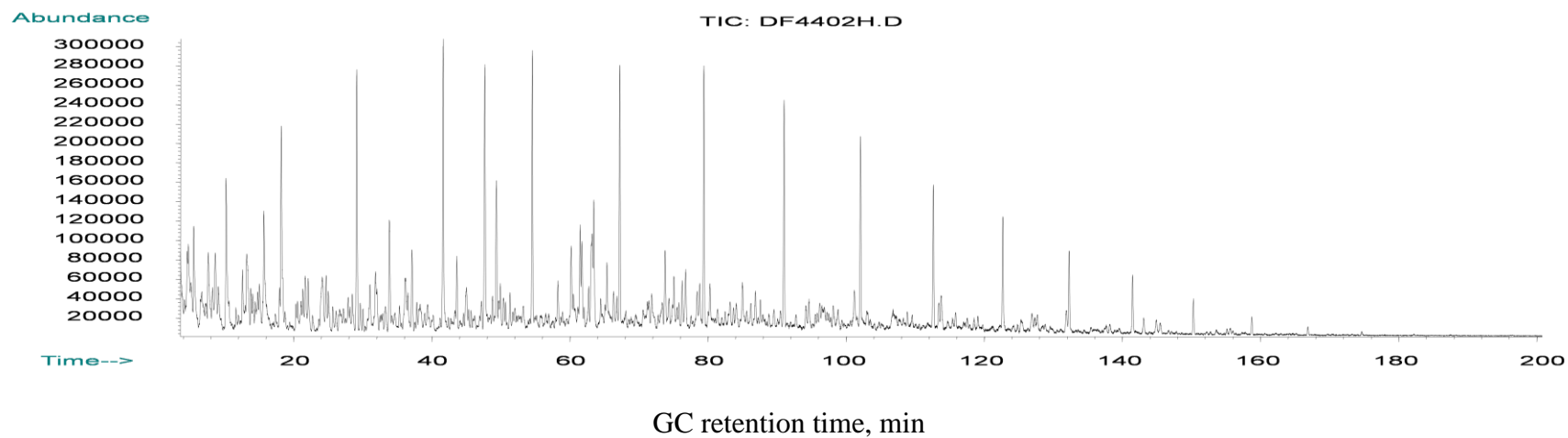
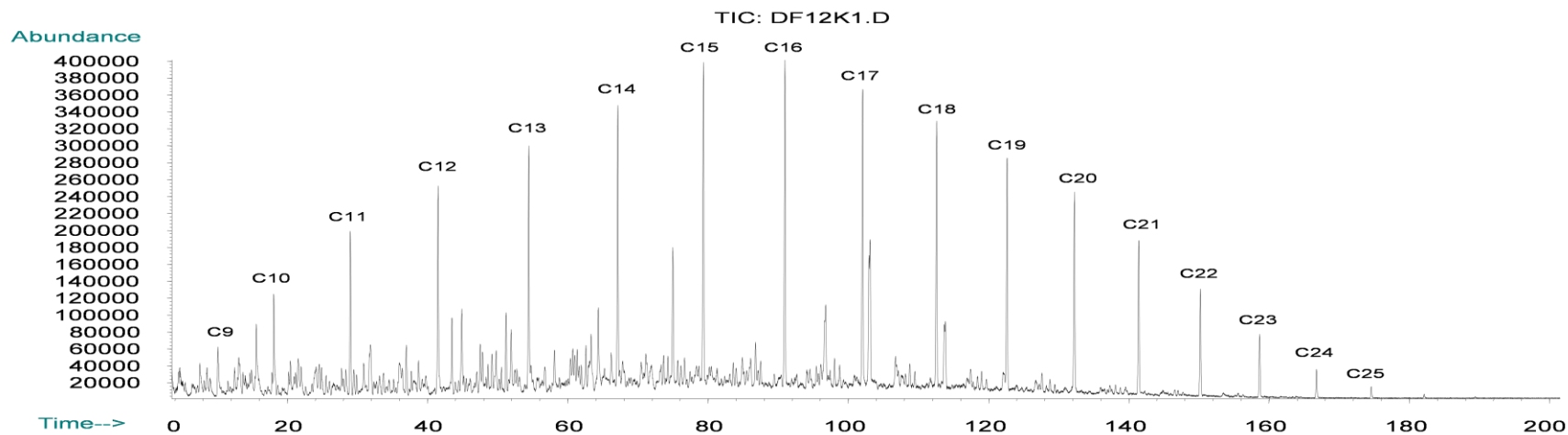


Fig. 5-7 Chromatographs of fresh DF (top) and DF stressed at 440 °C for 2 hours (bottom). C9 through C25 indicate normal alkanes.

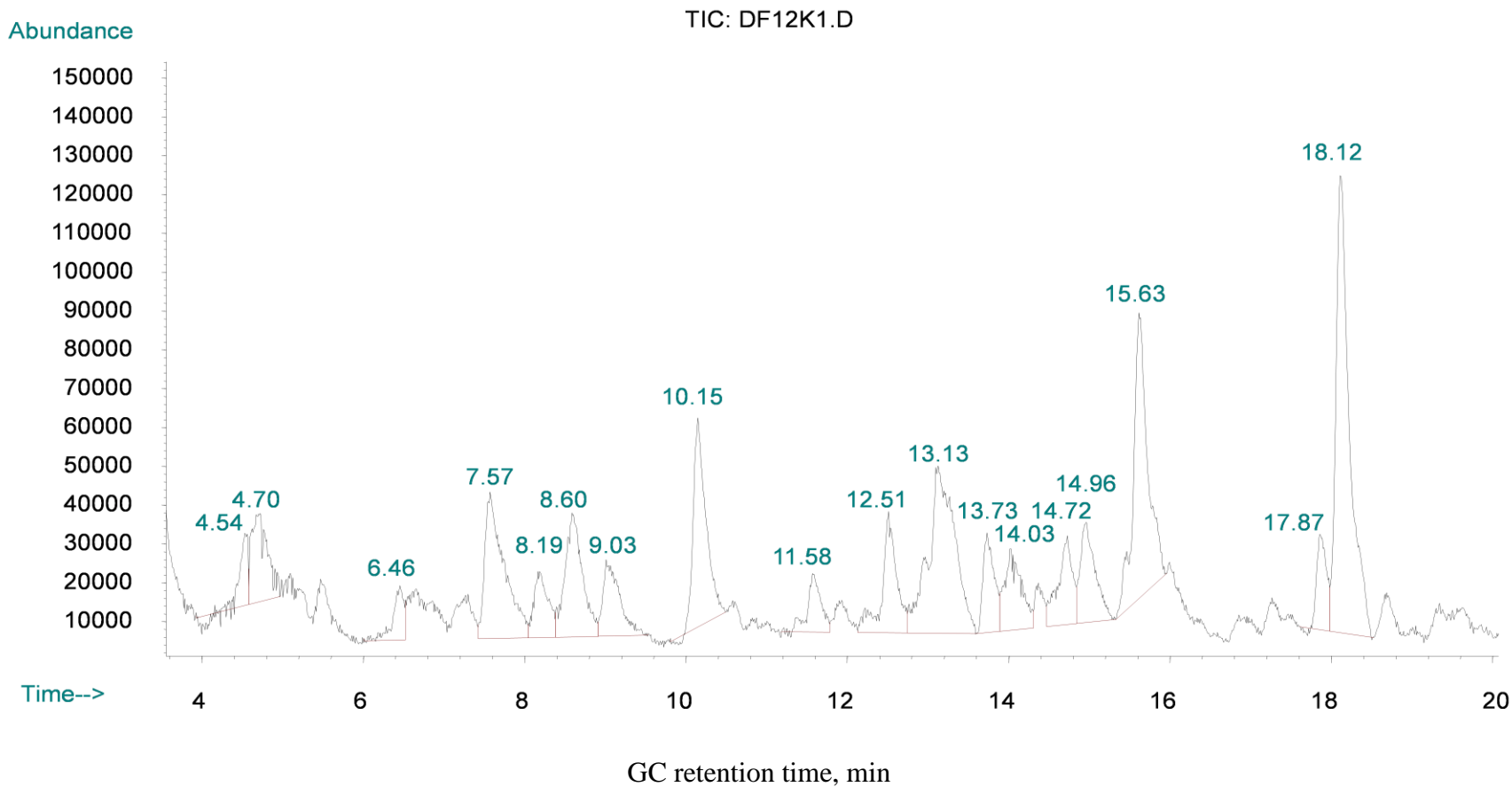


Fig. 5-8 Part of integrated chromatograph of fresh DF. Numbers above peaks indicate actual retention time. Horizontal and inclined red lines indicate base lines, while vertical red lines indicate integration boundaries between two peaks.

5.3 RESULTS AND DISCUSSION

5.3.1 Validation of the $\Delta(PPA)$ analysis

To demonstrate the feasibility of the $\Delta(PPA)$ analysis in characterizing fuel degradation, chromatographs of fresh DF of different initial concentrations were measured and analyzed. Horizontal trend lines were expected because theoretically, $\Delta(PPA)$ values for fresh DF equal to zero. Samples were prepared by diluting 1, 2 and 3 μl DF in 1 ml hexane, giving DF concentrations of 1000, 2000 and 3000 ppm, respectively. The 2000 ppm sample was used as a reference to provide values for $(PPA)_{\text{Fresh DF}}$ in Eq. (5-2). Results are presented in **Fig. 5-9 (top)**, showing that although variations of $\Delta(PPA)$ values occurred over the retention time range, near horizontal trend lines were obtained for both samples as expected. $\Delta(PPA)$ variations were mainly due to systematic errors, and it is reasonable to argue that the effect of such variations on the slope of the trend line is negligible.

Next, chromatographs of two thermally stressed DF samples were analyzed; results are shown in **Fig. 5-9** as well. When stressed at 400 °C for 10 min, DF showed no color change, indicating negligible fuel degradation. Increasing temperature to 440 °C resulted in slight color change. The $\Delta(PPA)$ analysis of these two chromatographs gave a horizontal trend line for 400 °C and a slightly inclined trend line with a negative slope for 440 °C, which agreed well with color changes. Accordingly, it is confident to conclude that the linear trend line of $\Delta(PPA)$ is capable of capturing overall changes in fuel compositions and the slope of the trend line is an effective parameter for characterizing fuel degradation. A greater negative slope corresponds to more significant degradation.

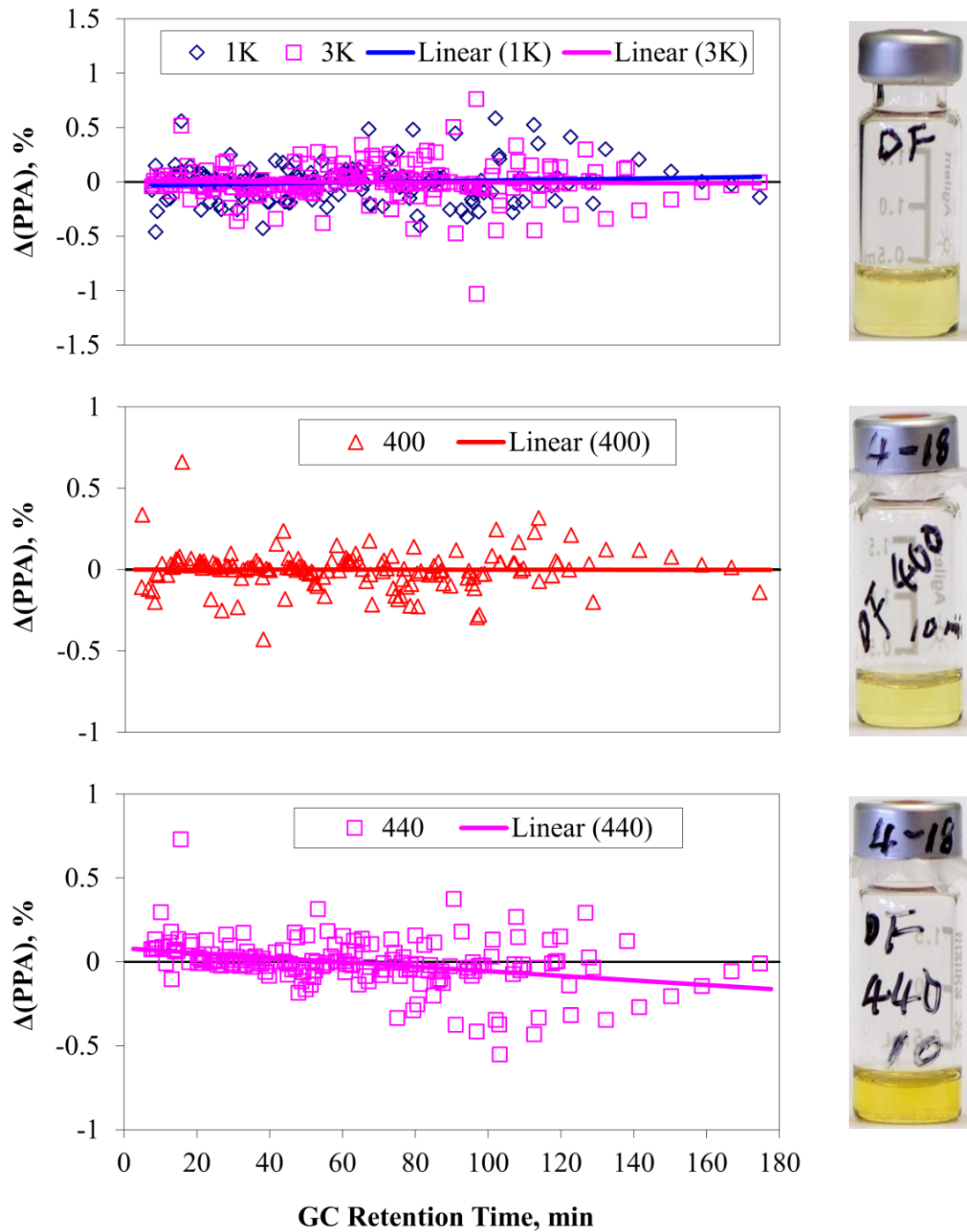


Fig. 5-9 $\Delta(PPA)$ analysis of chromatographs of fresh DF (top) and DF stressed at 400 °C (middle) and 440 °C (bottom). The residence time was 10 min for both temperatures. 1K and 3K indicate DF concentrations of 1000 and 3000 ppm, respectively.

5.3.2 Batch thermal stressing of DF

5.3.2.1 *Color change*

Thermal degradation of hydrocarbon fuels is always associated with color change. In order to have a better idea of the main cause of color change, three pure compounds were thermally stressed. They were n-hexadecane from the n-alkane group and 1-methylnaphthalene and butylbenzene from the aromatic group. **Fig. 5-10** shows that at the same stressing temperature, color changes were most significant for butylbenzene followed by 1-methylnaphthalene and then n-hexadecane. **Fig. 5-11** to **Fig. 5-13** show chromatographs of these three compounds, which further confirm that these chemicals are unstable at 440 °C. The thermal stabilities are in the order: n-hexadecane < butylbenzene < 1-methylnaphthalene. Thermal stressing of n-hexadecane at 440 °C produced large amount of both low MW and high MW n-alkanes and isomers. Although n-hexadecane is less stable, color change is not as strong as aromatics. Thermal stressing of 1-methylnaphthalene at the same time produced significant amounts of four-ring aromatics, while the products from butylbenzene were mainly single- and double-ring aromatics. Therefore, it is reasonable to conclude that color change during thermal stressing of DF is mainly caused by formation of multiple-ring aromatics and color is a simple, effective indicator of fuel stability.

5.3.2.2 *Effect of O₂*

As described in Section 5.2.1, the cell was partially loaded to ensure a mild system pressure, which inevitably caused trapping of air when samples were prepared in air environment. Previous studies have shown the effect of O₂ on thermal stability of

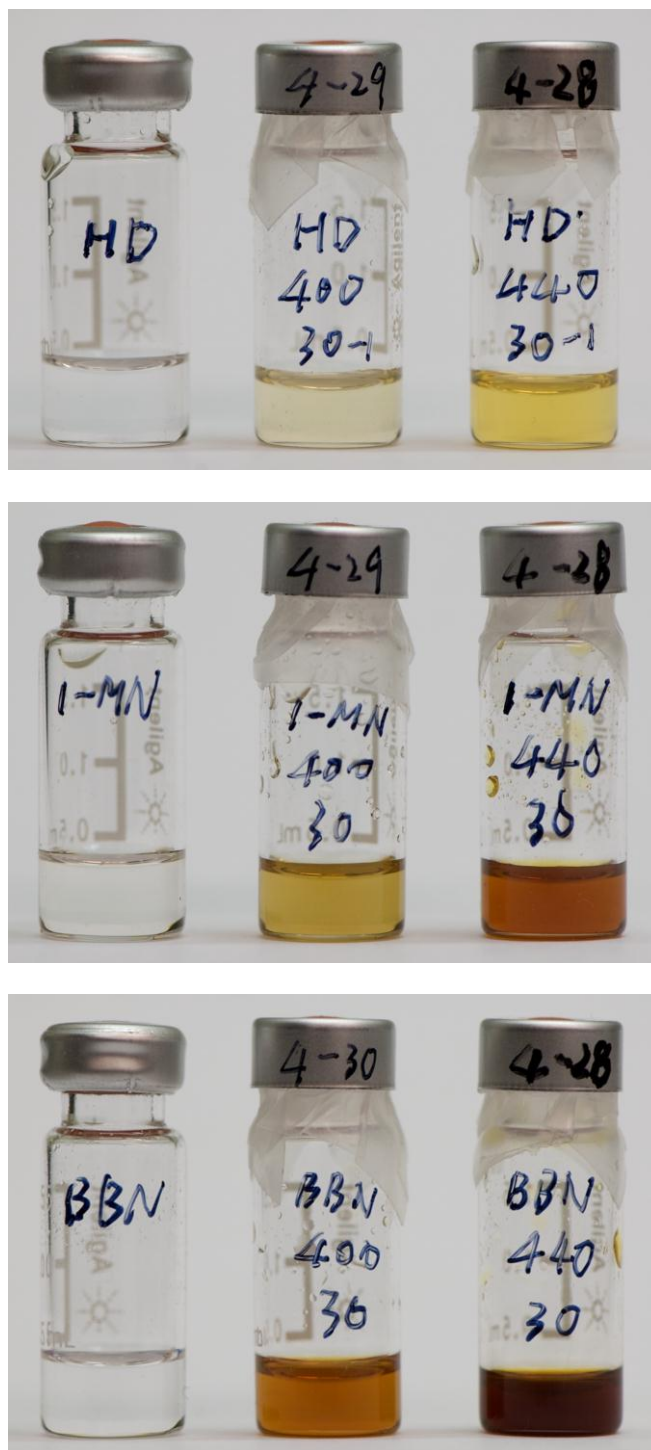


Fig. 5-10 Thermal stressing of n-hexadecane (top), 1-methylnaphthalene (middle), and butylbenzene (bottom) at 400 and 440 °C for 30 min.

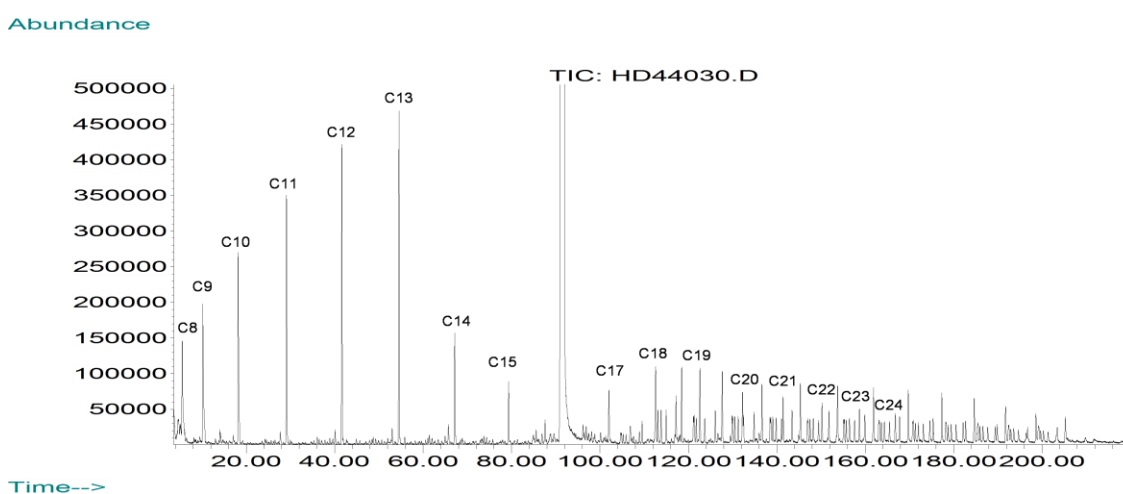
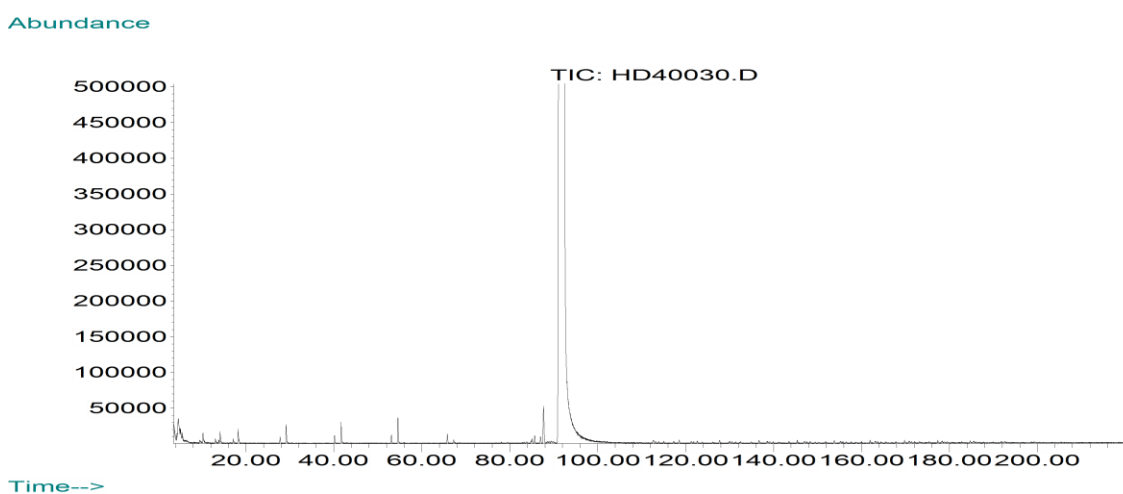
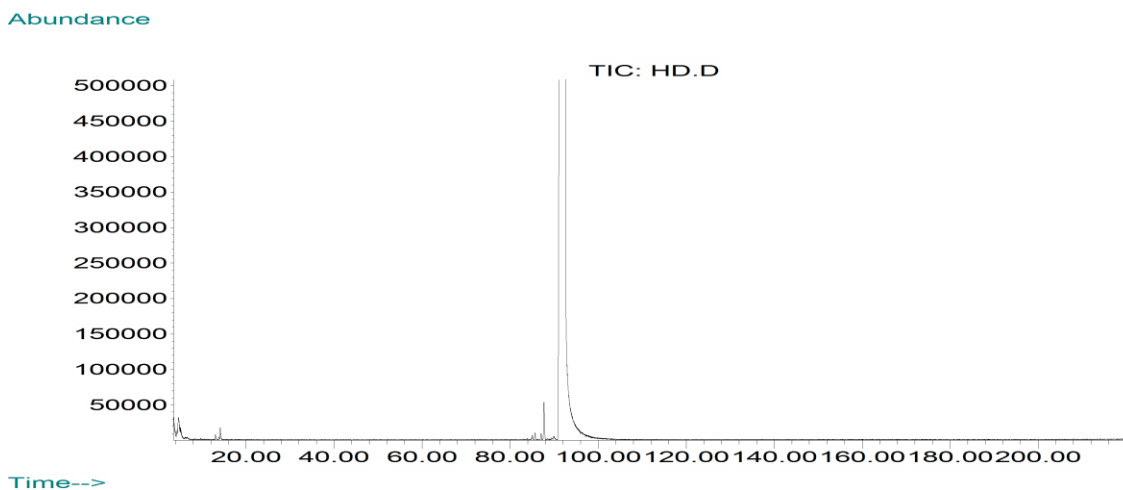


Fig. 5-11 Chromatographs of n-hexadecane. Top: fresh; middle: 400 °C, 30 min; bottom: 440 °C, 30 min.

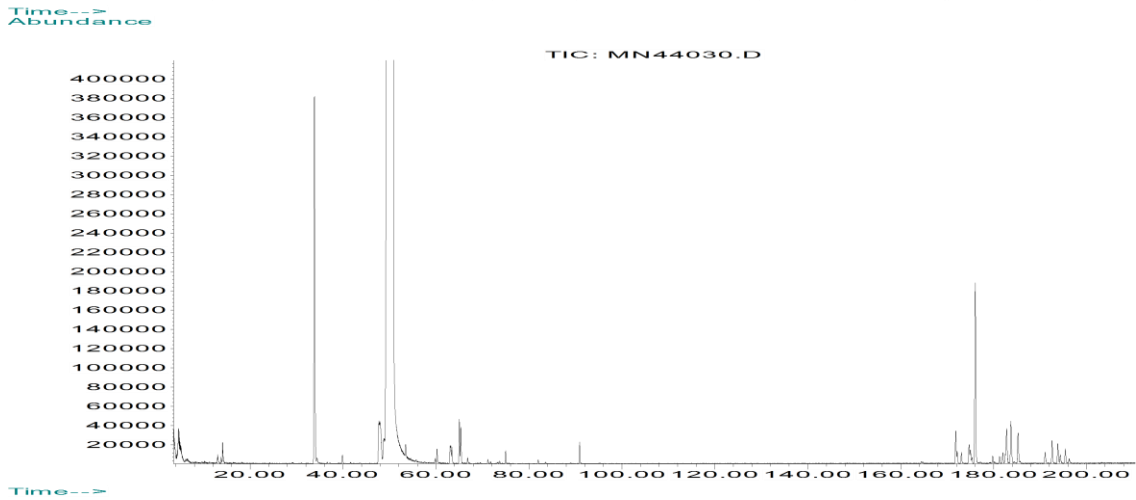
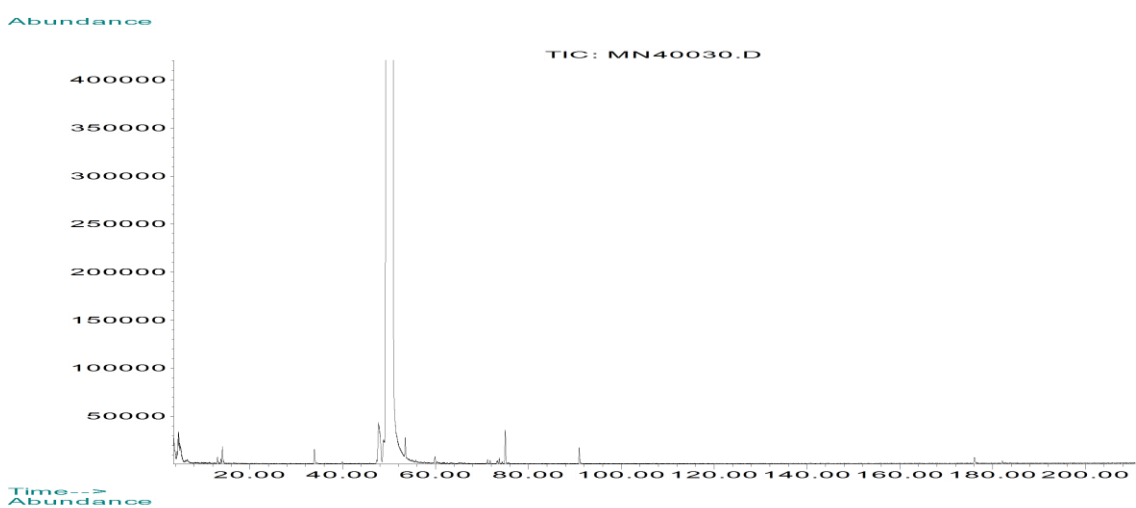
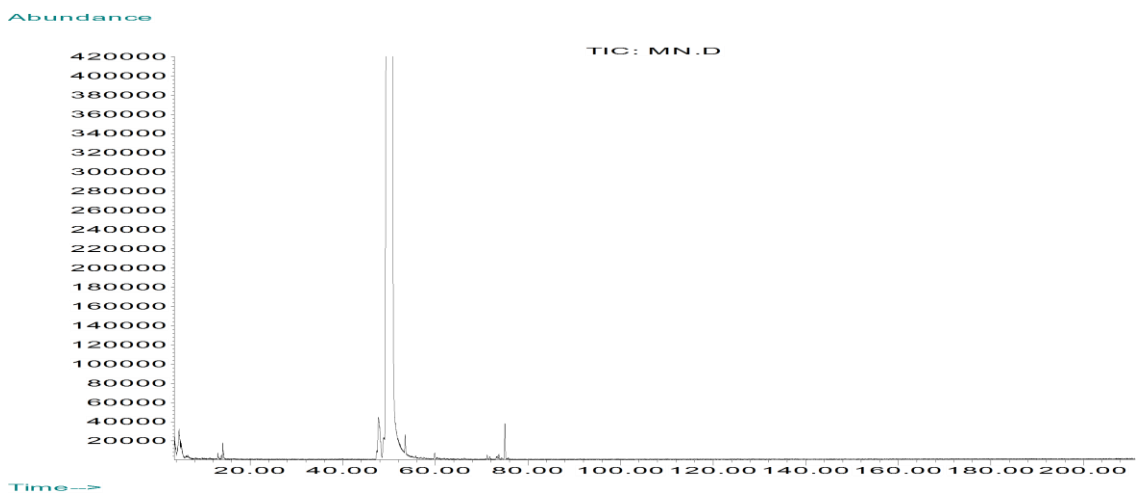


Fig. 5-12 Chromatographs of 1-methylnaphthalene. Top: fresh; middle: 400 °C, 30 min; bottom: 440 °C, 30 min.

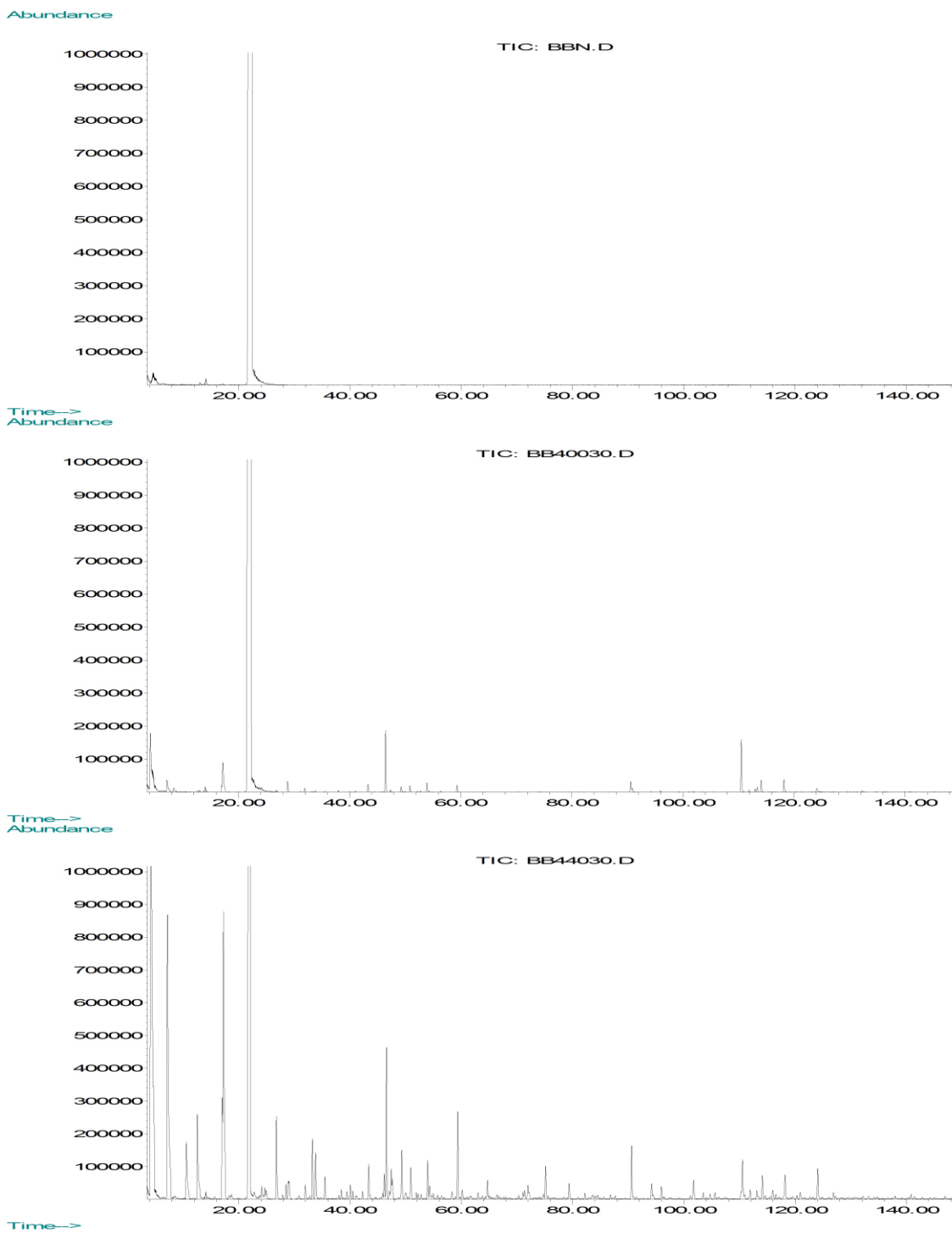


Fig. 5-13 Chromatographs of butylbenzene. Top: fresh; middle: 400 °C, 30 min; bottom: 440 °C, 30 min.

fuels (Edwards and Liberio, 1994; Ervin et al., 1998; Hazlett, 1991; Stewart, 1999; Taylor, 1974). To demonstrate the effect of trace amounts of O₂ from air on thermal stability of diesel fuel, samples were prepared both in air and in CO₂ environments and then thermally stressed under the same conditions. As shown in **Fig. 5-14**, no effect of O₂ was observed at 300 °C simply because the temperature was not high enough to have noticeable fuel degradation. At 400 and 440 °C, great color enhancements were observed when air was trapped in the cell, and the effect became greater as temperature increased. This leads to the conclusion that DF is less stable with the present of O₂.

Results of $\Delta(PPA)$ analysis are presented in **Fig. 5-15**, showing that at both 400 and 440 °C, the slope of the $\Delta(PPA)$ trend line increased with the presence of O₂. Based on the hypothesis of the $\Delta(PPA)$ analysis, this leads to a contrary conclusion that DF is more stable with the presence of O₂. Therefore, with the presence of O₂, either color or the slope of the $\Delta(PPA)$ trend line or both are invalid as indicators of fuel thermal stability. One possible explanation is that the present of O₂ results in different reaction mechanisms and hence different product distributions, which is beyond the scope of this discussion. In the rest of experiments, samples were prepared in the CO₂ environment.

Oxygen is the driving force for low temperature thermal oxidative reactions and has a significant effect on deposit formation. Removal of oxygen can dramatically lower the rate of deposit formation (Taylor, 1974) or even eliminate the thermal oxidative surface deposition (Edwards and Liberio, 1994), leading to a more stable fuel that can be heated up to relatively high temperatures (around 773 K) before significant coking occurs (Ervin et al., 1998; Stewart, 1999). The impact of oxygen content on pyrolytic deposition has not been well understood. It was reported that the absence of dissolved oxygen could lead to

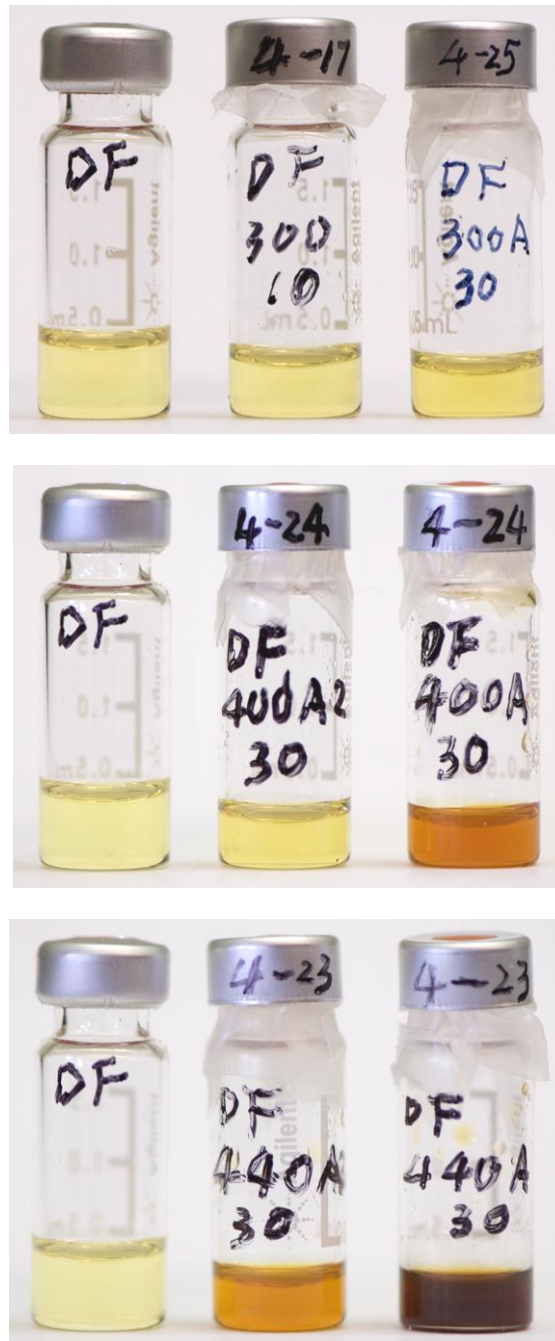


Fig. 5-14 Effect of trace amounts of O₂ on thermal stability of DF. Left column: fresh DF; middle column: samples prepared in CO₂ environment, no air trapped; right column: samples prepared in air environment. Top: 300 °C; middle: 400 °C; bottom: 440 °C.

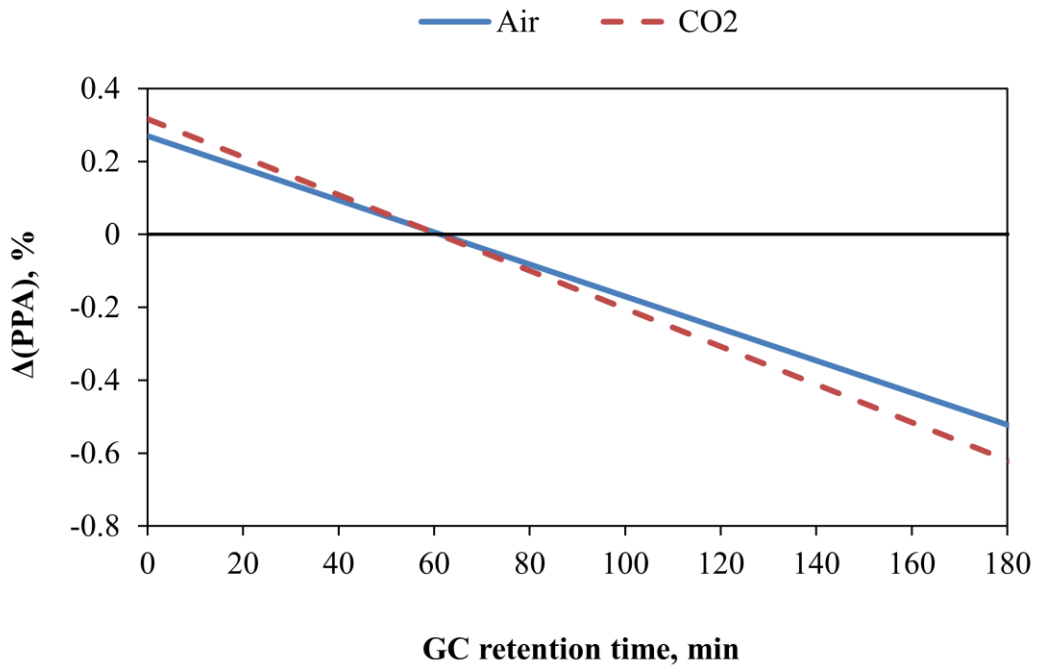
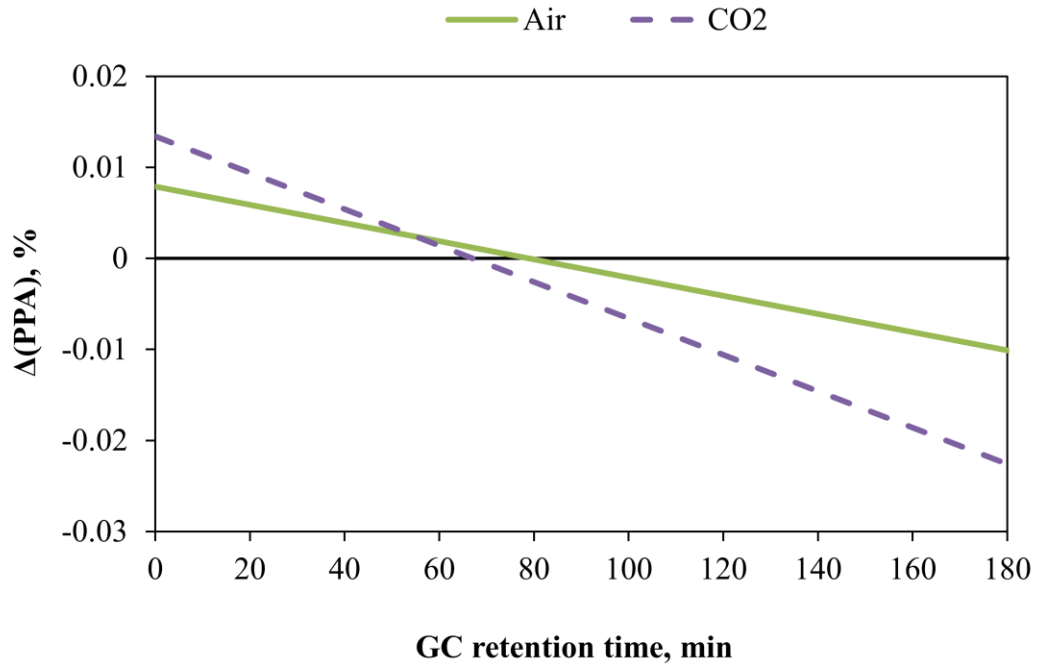


Fig. 5-15 $\Delta(\text{PPA})$ analysis for stressed DF. Top: 400 °C; bottom: 440 °C. “Air” and “CO₂” represent DF samples prepared in air and CO₂ environments, respectively.

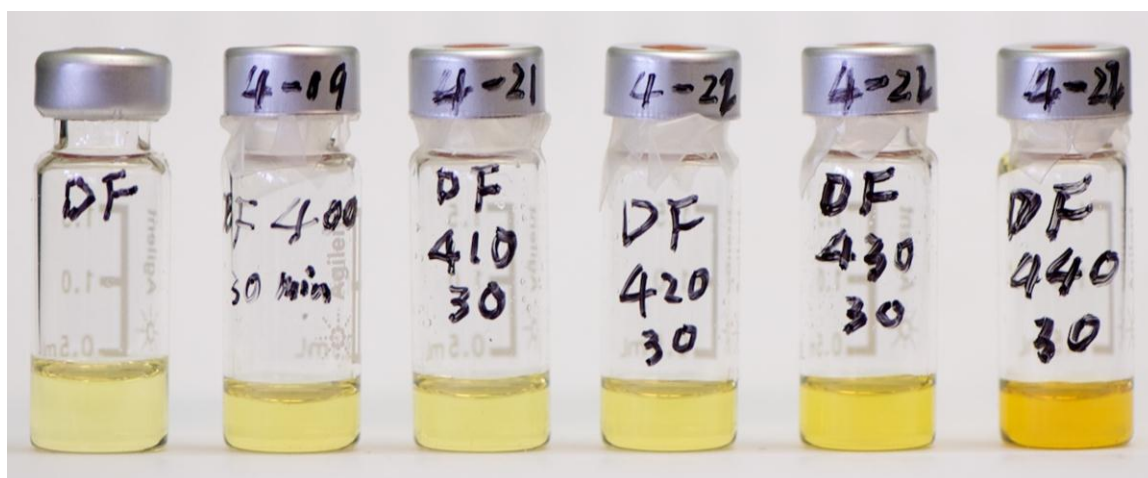
increased surface deposition in the pyrolytic region probably due to the oxidative products (alcohols, aldehydes, etc) acting as radical scavengers or hydrogen donors (Edwards and Liberio, 1994). It was also reported, however, that deoxygenation had little effect on pyrolytic deposition (Edwards and Atria, 1995). Oxygen content also affects deposit morphology (Hazlett, 1991).

5.3.2.3 Effect of temperature

To determine the temperature range where significant reduction of thermal stability of DF occurs, experiments were initially conducted in a relative broad temperature range from 200-440 °C for a residence time of 10-15 min. It was found that noticeable color change did not occur until the temperature increased to 440 °C, as shown in **Fig. 5-16** (top). This result narrowed the temperature range down to 400-440 °C. Since the color change was very slight, a longer residence time was desired. Thus, the residence time was increased to 30 min in the second set of experiments. As shown in **Fig. 5-16** (bottom), fuel color remained nearly the same from 400-420 °C and then was gradually enhanced as temperature increased from 420-440 °C. Results from the $\Delta(PPA)$ analysis presented in **Fig. 5-17** agreed well with color change; slope of the $\Delta(PPA)$ trend line dropped at 420 °C and then reduced further as temperature increased to 440 °C. Selected results from TGA are presented in **Fig. 5-18**. It is seen that volatility of DF remained almost the same when DF was heated up to 420 °C and stressed for 30 min. As temperature further increased to 440 °C, volatility change was observed. Increase in weight loss at $T < \sim 120$ °C suggests formation of low MW components due to fuel decomposition, while increase in weight percentage at $T > 190$ °C indicates formation of



Fresh DF 200-15 300-10 400-10 440-10



Fresh DF 400-30 410-30 420-30 430-30 440-30

Fig. 5-16 Changes in DF color at different stressing temperatures from 200-440 °C. The first and the second numbers indicate stressing temperature and residence time, respectively.

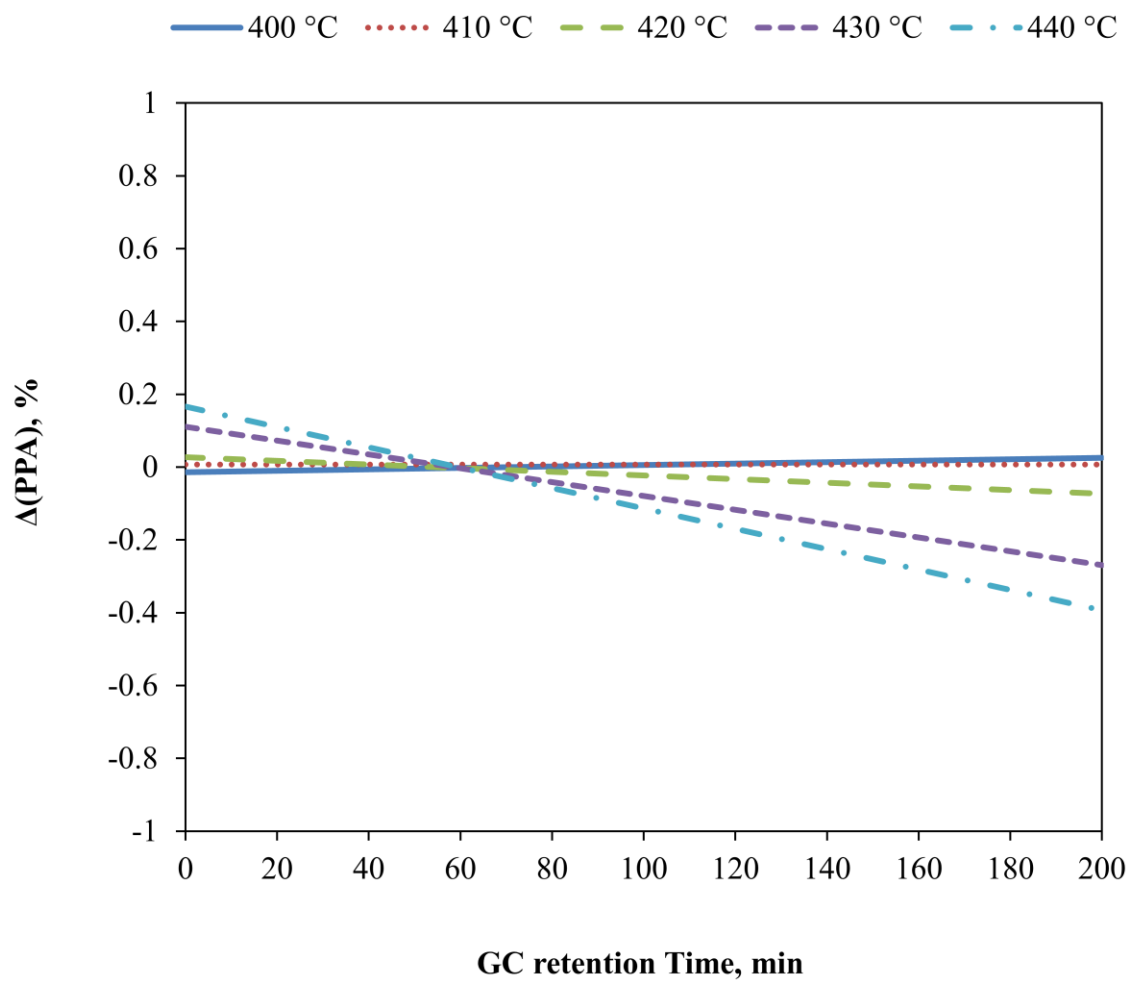


Fig. 5-17 $\Delta(\text{PPA})$ analysis for DF thermally stressed at 400-440 °C for 30 min.

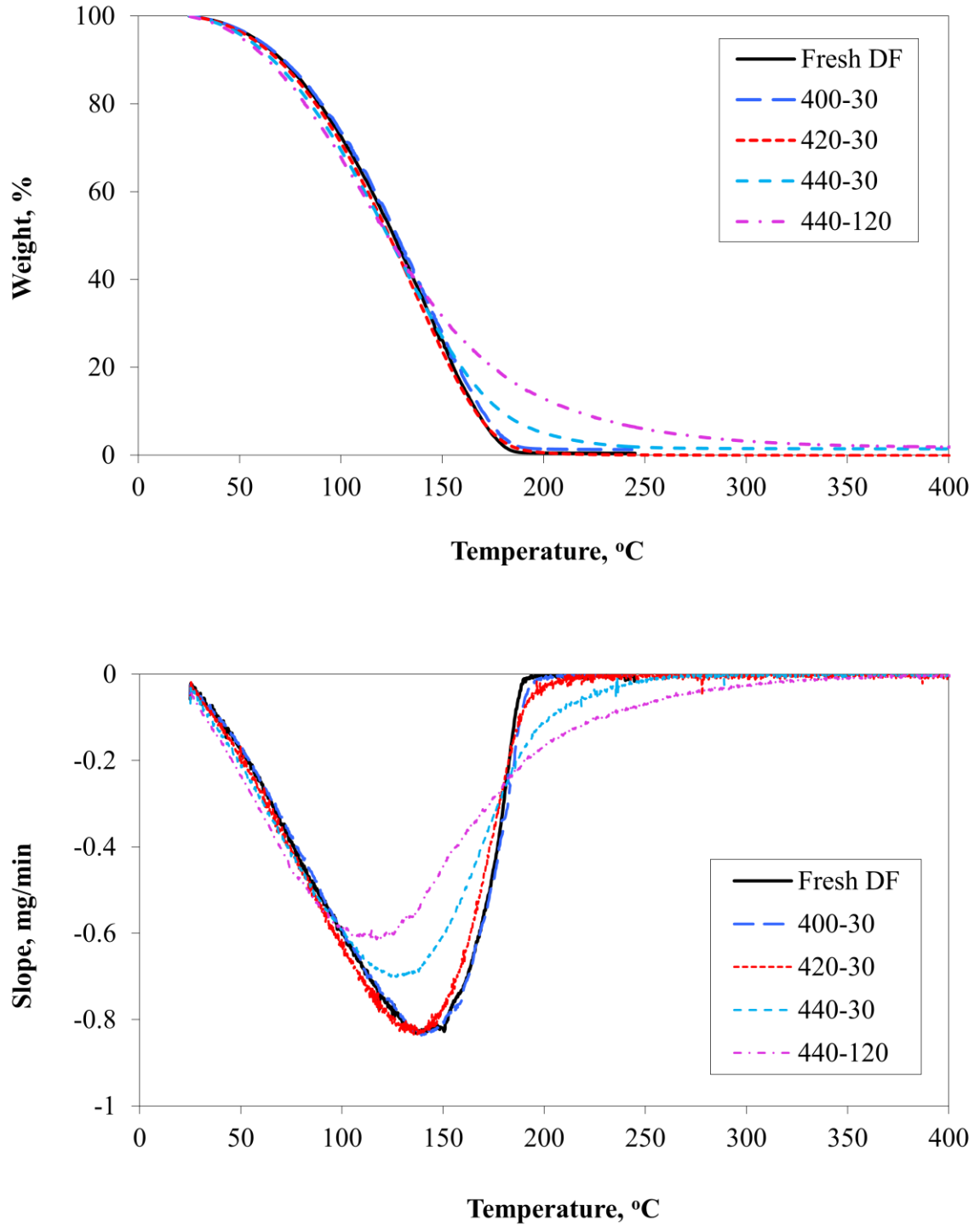


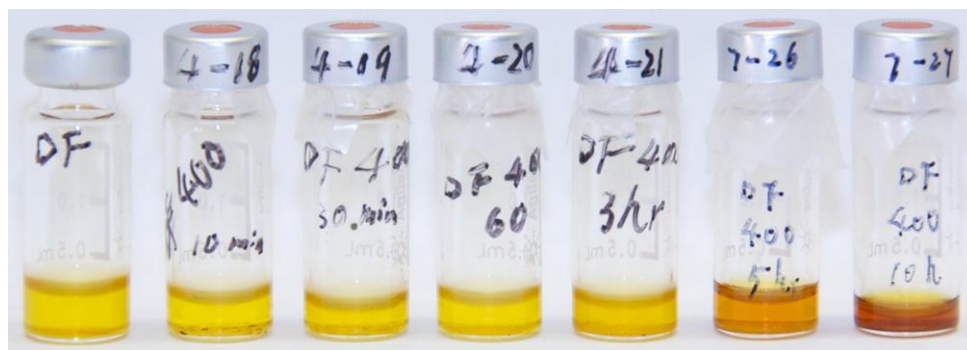
Fig. 5-18 TGA curves (top) and the corresponding slope curves (bottom) for DF thermally stressed at 400-440 °C.

large MW compounds, mainly aromatics which further form solid deposits. Volatility change became more significant at 440 °C when the residence time was increased to 2 hours. The effect of residence time is further discussed in the next section.

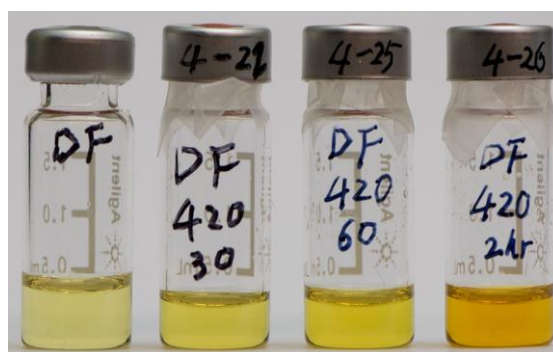
Accordingly, it can be concluded that 420 °C is an upper temperature limit below which temperature shows negligible effect on thermal stability of DF when residence time is relatively short (< 30 min). When temperature is above 420 °C, discernable reduction of thermal stability of DF occurs and becomes more significant with increasing temperature.

5.3.2.4 Effect of residence time

When an engine runs, the residence time of fuel in the fuel line from the fuel tank to the injector is very short. However, during the start-up and shut-down stages, fuel residuals may experience a long residence time at high temperature. Although results presented in the preceding section show that DF was still quite stable when thermally stressed at 440 °C for 10 min, it is valuable to explore much longer residence time. Accordingly, residence time was extended to as high as 10 hours, as given in **Table 5-1**. Fuel color change is illustrated in **Fig. 5-19**, and results from $\Delta(PPA)$ analyses are shown in **Fig. 5-20** and **Fig. 5-21**. At 300 °C for 10 hours, color was slightly enhanced, but the slope of the $\Delta(PPA)$ trend line remained nearly zero as shown in **Fig. 5-21**, indicating very good thermal stability at this condition. At 400 °C, no color changes were observed within 60 min. As residence time increased from 60 min to 300 min, DF Color increased associated with a gradual drop of the slope of the $\Delta(PPA)$ trend line as shown in **Fig. 5-21**. When residence time was greater than 300 min up to 600 min, color was not changing



Fresh DF 400-10 400-30 400-60 400-180 400-300 400-600



Fresh DF 420-30 420-60 420-120



Fresh DF 440-10 440-30 440-120

Fig. 5-19 Changes in DF color at 400, 420 and 440 °C for varying residence time. The first and the second numbers indicate stressing temperature and residence time, respectively.

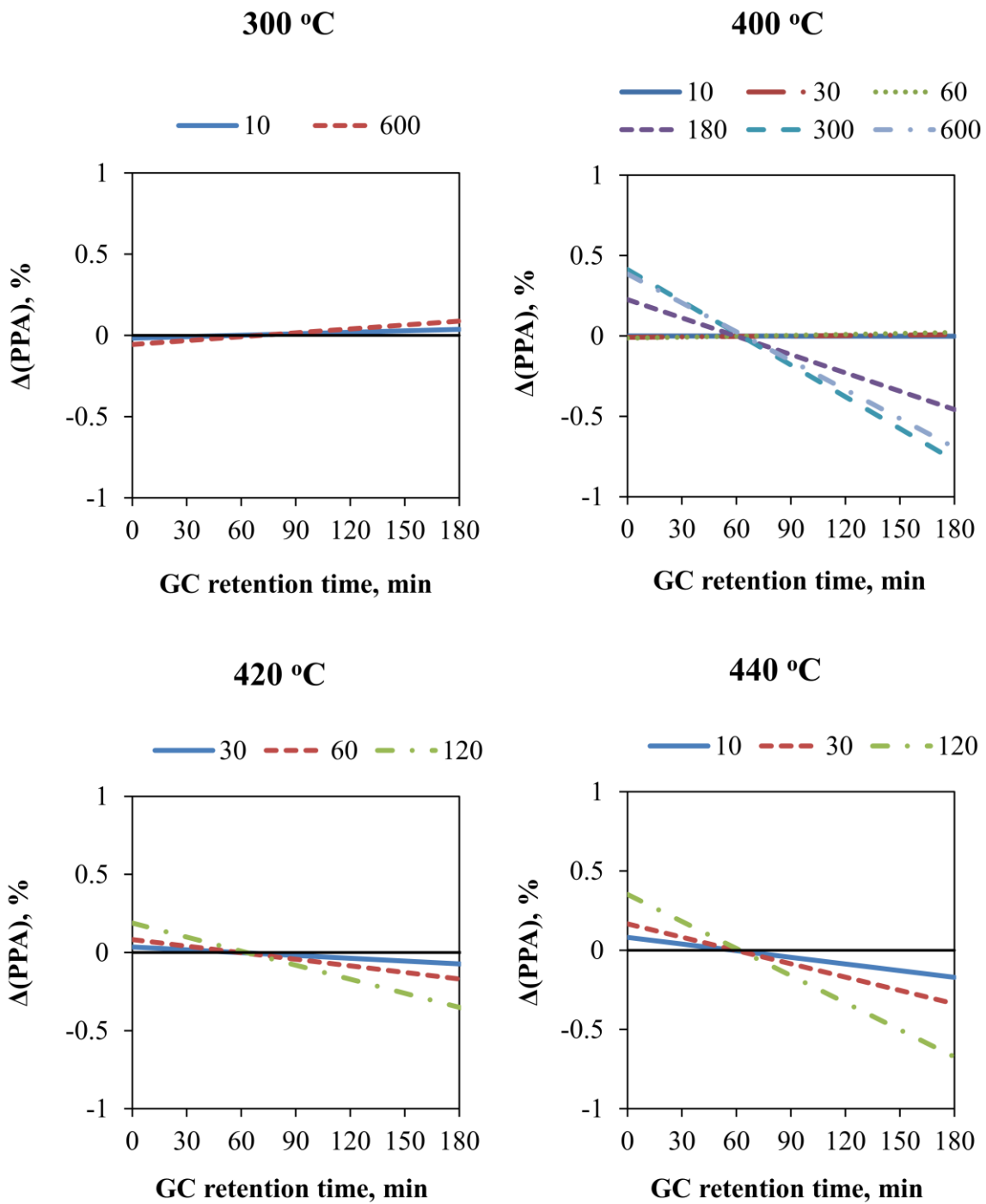


Fig. 5-20 $\Delta(PPA)$ analysis of stressed Changes in DF color at 300, 400, 420 and 440 °C for varying residence time. The first and the second numbers in legend indicate stressing temperature and residence time, respectively.

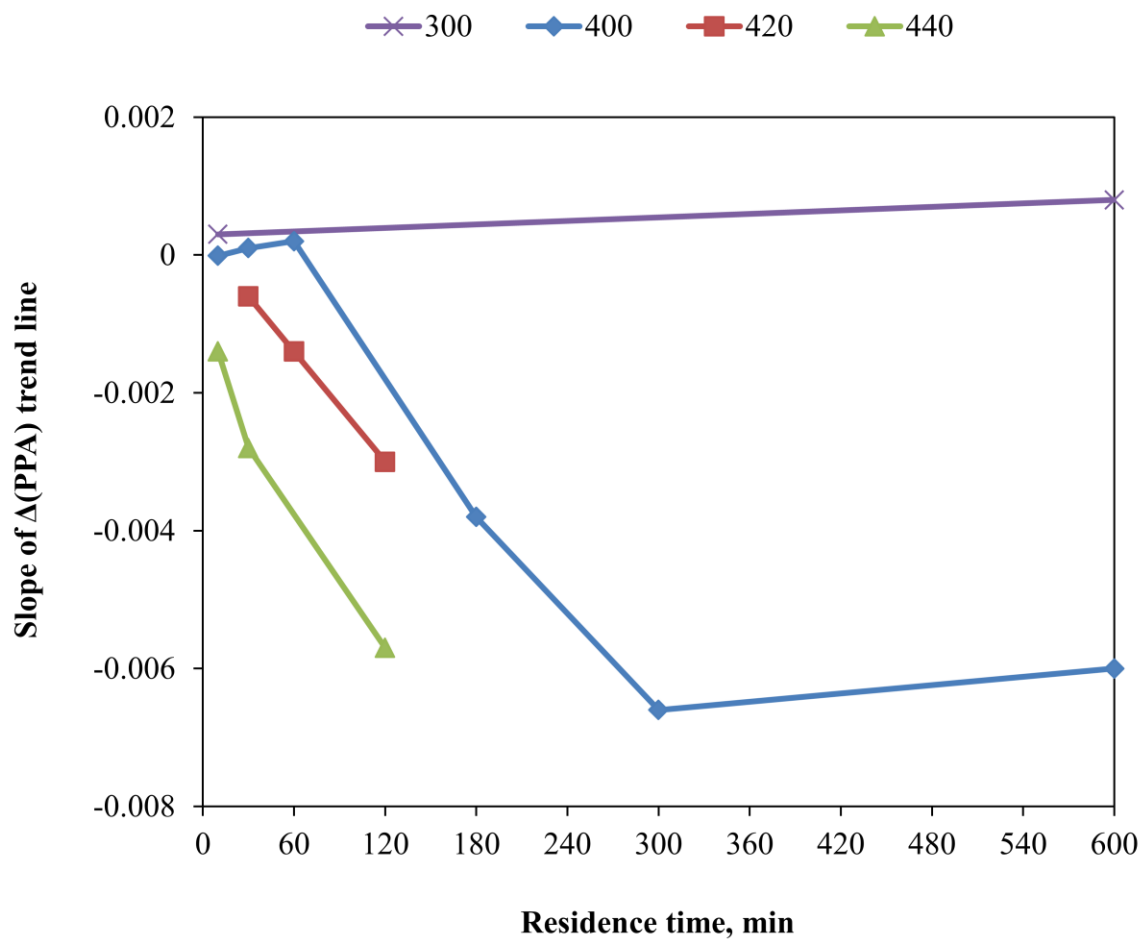


Fig. 5-21 Slope of $\Delta(PPA)$ trend lines as a function residence time at 300, 400, 420, and 440 °C.

and the slope remained almost constant as well. At 420 and 440 °C, both color change and slope drop indicate that DF stability decreased as residence time increased. Significant degradation occurred at 440 °C for a 2-hour stressing period. These results reveal the impact of residence time on thermal stability of DF. More significantly, a targeted region in the temperature- residence time domain for engine operation was identified, which is 400-420 °C and < 60 min.

5.3.2.5 Formation of solid deposits

Fig. 5-22 shows SEM photos of solid deposits accumulated on stainless steel sheets when DF was thermally stressed at 300, 400 and 440 °C for a residence time of 2 to 10 hours. Long residence time was chosen, on the one hand, to see the effect on fuel stability as discussed in the preceding section, and on the other hand, to produce discernable amounts of solid deposits. As shown in **Fig. 5-22** (top right), large ring-type deposits with ring diameter as large as 3 μm were formed when DF was heated to 300 °C for a 10-hour duration. Similar structure was observed at 400 °C for the same residence time as shown in **Fig. 5-22** (middle right), but the size was slightly smaller. Reducing the residence time to 300 min at 400 °C resulted in much smaller size. As temperature increased to 440 °C, a substantial number of deposits were produced. A closer look (**Fig. 5-22** bottom right) shows crystal-like structures of solid deposits, the diameters of which are of the order of magnitude of 100nm. The different morphologies of solid deposits obtained at different stressing temperatures imply different mechanisms of deposit formation, further studies on deposit formation mechanisms would be valuable to development of strategies for preventing DF coking.

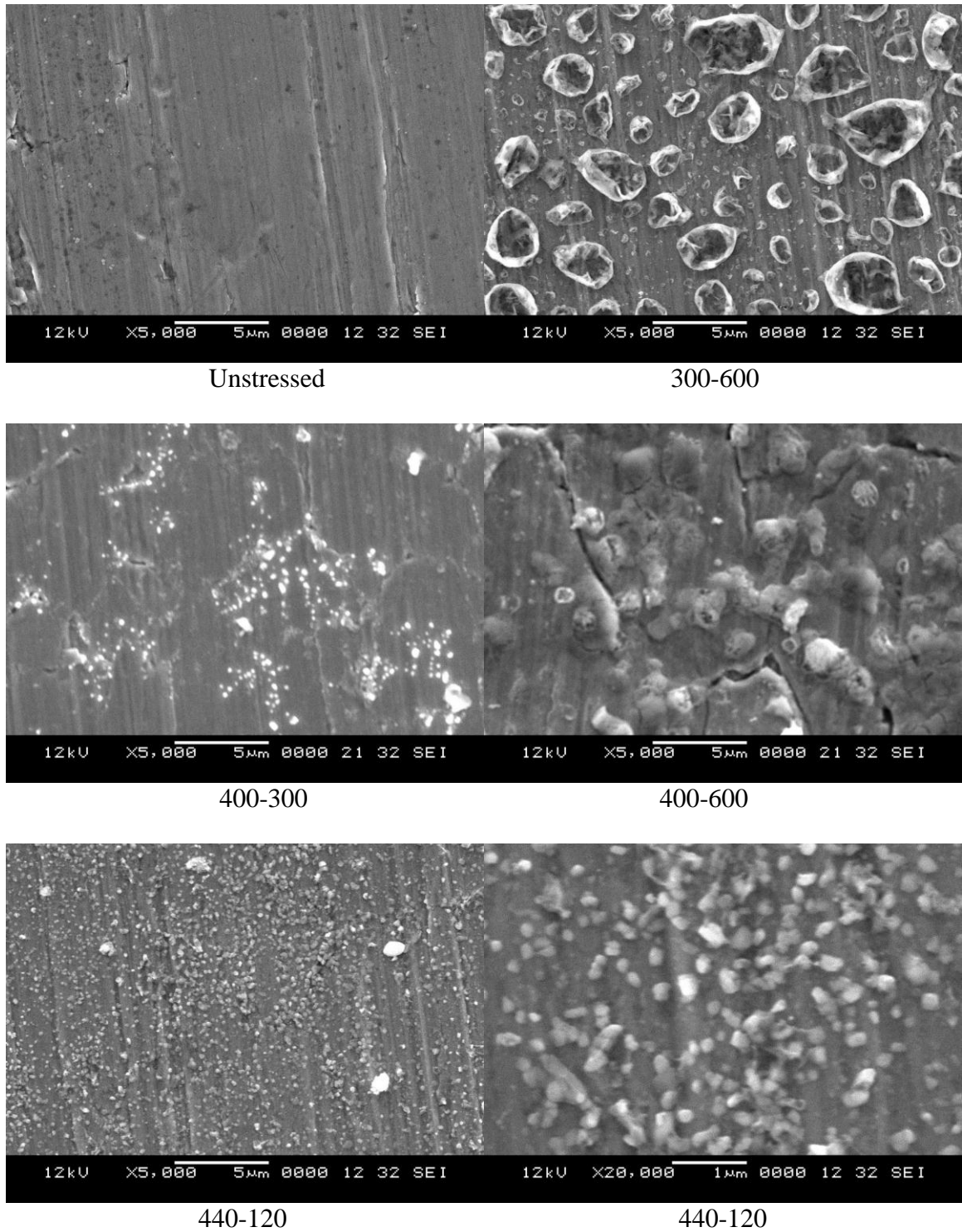


Fig. 5-22 SEM analysis of DF solid deposits. The first and the second numbers indicate stressing temperature and residence time, respectively.

5.3.3 Batch thermal stressing of DF/CO₂ mixtures

Fig. 5-23 shows photos of samples collected in the first set of runs, i.e. runs 1-5 in **Table 5-2**. Weak enhancement in sample color was observed from run 2 through run 5. However, the color of samples from runs 2-5 was slightly lighter than that from run 1, which is a good sign that addition of CO₂ might prevent fuel degradation. Samples were analyzed by GC-MS and the $\Delta(PPA)$ analysis of chromatographs was performed. Results of the $\Delta(PPA)$ analysis are presented **Fig. 5-24**. The slopes of the trend lines became more negative from run 1 through run 5, indicating that addition of CO₂ did not reduce but enhanced fuel degradation.

Degradation mainly refers to breakdown of large molecules, while coking is associated with production of PAHs. Some PAH precursors identified by GC-MS are given in **Table 5-5**; they are naphthalene (A1), 2-methylnaphthalene (A2), 1-methylnaphthalene (A3), and 1, 4, 5-trimethylnaphthalene (A4). As shown in **Fig. 5-25**, concentrations of these compounds increased, when DF was thermally stressed no matter how much CO₂ was added. A1 demonstrated a continuous growing trend from runs 1 through 5, while A2-A4 were nearly constant for all runs despite small variations. TGA results are presented in **Fig. 5-26**. It can be seen that at $T < 100$ °C, the curves for runs 1 and 2 are almost identical. As initial CO₂ pressure increased from 2.76 to 3.45 MPa (from run 2 to run 3), the rate of weight loss increased slightly, but further increase in initial CO₂ pressure (run 4 and 5) made no difference. The increase in weight loss indicates a larger amount of low MW molecules. At $T = 100-180$ °C, the slopes of TGA curves for runs 3-5 are generally greater than those for runs 1 and 2. These results suggest that in the current system, addition of CO₂ slightly promotes fuel degradation.

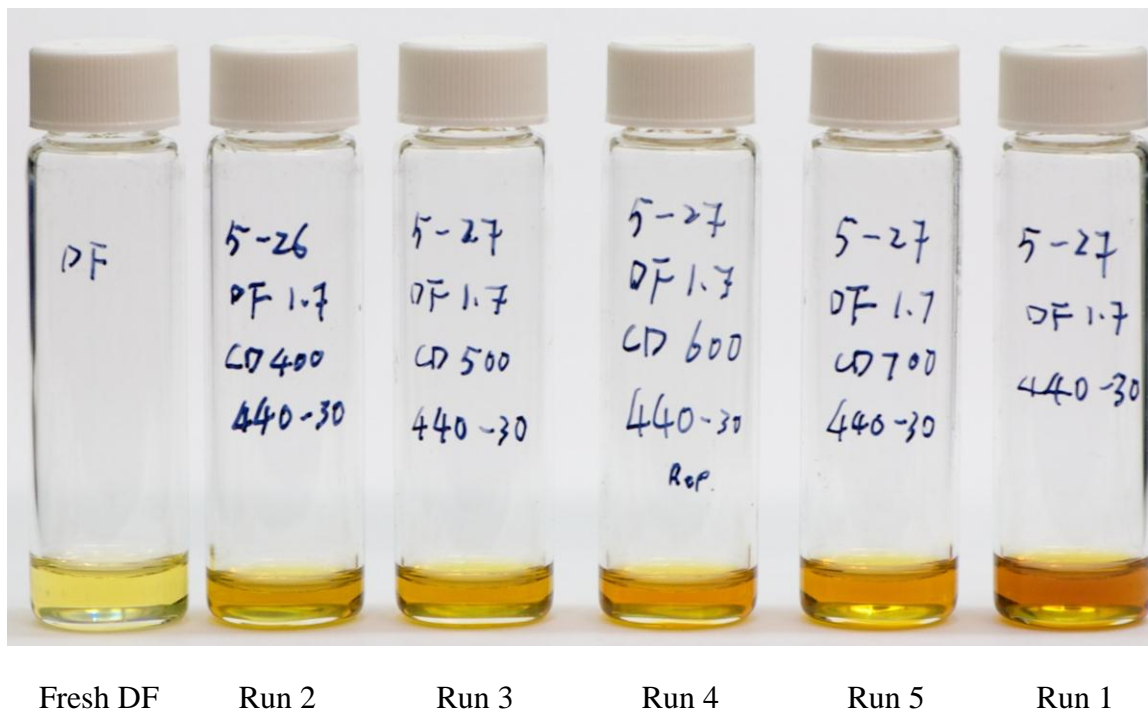


Fig. 5-23 Photos of DF samples collected in batch thermal stressing of DF/CO₂ mixtures.

Conditions for runs 1-5 are indicated on the bottles and also given in **Table 5-2**.

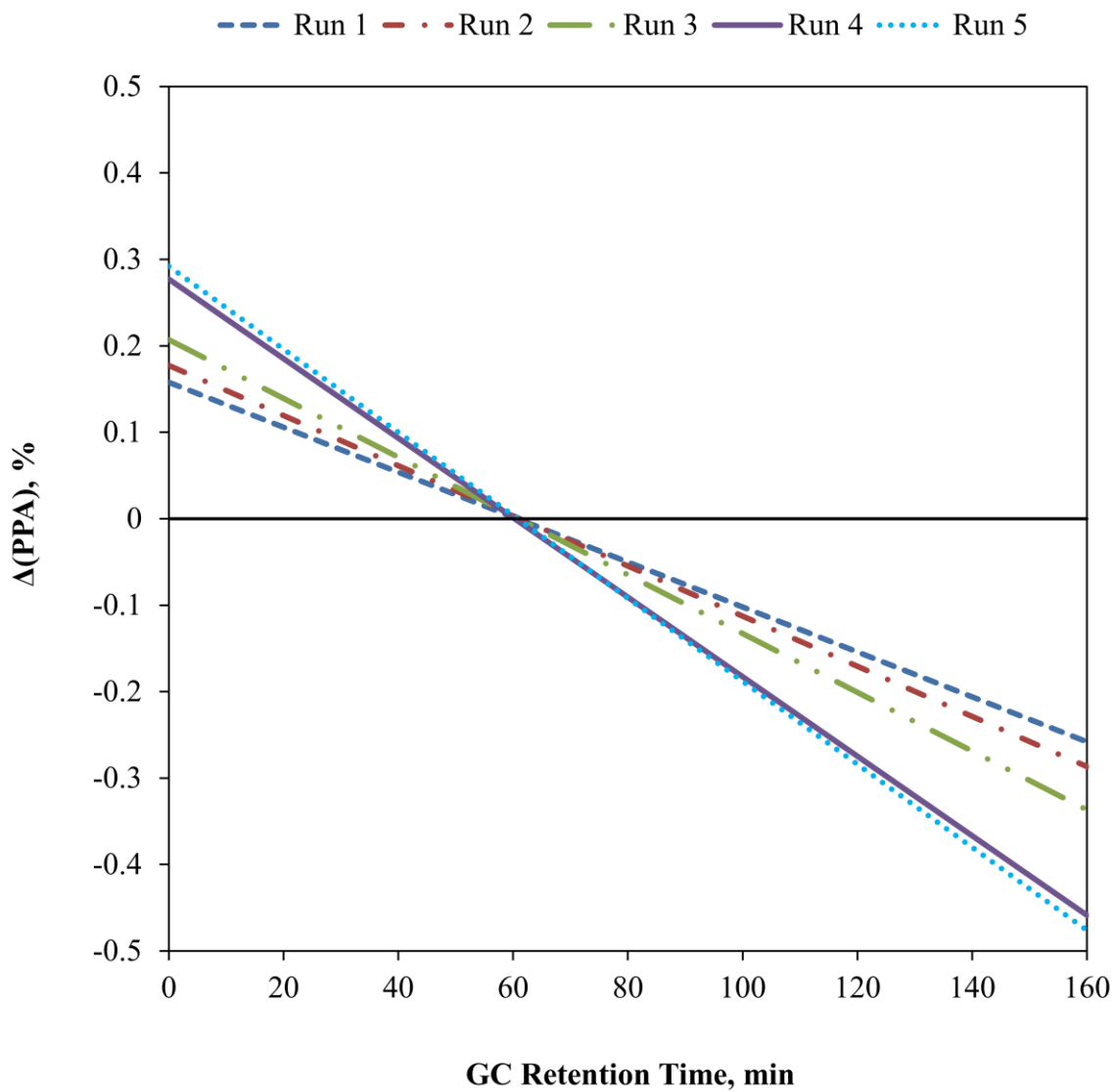
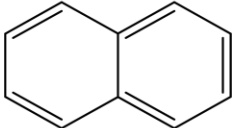
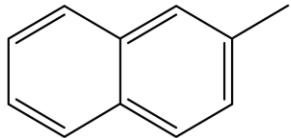
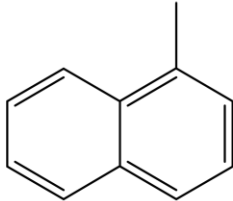
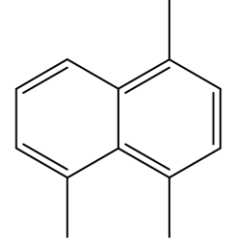


Fig. 5-24 $\Delta(\text{PPA})$ analysis for runs 1-5 of batch thermal stressing of DF/ CO_2 mixtures.

Table 5-5 Examples of precursors of PAHs identified by GC-MS.

| No. | GC retention time, min | Name | Molecular structure |
|-----|------------------------|-----------------------------|---|
| A1 | 33.78 | Naphthalene |  |
| A2 | 47.58 | 2-methyl-naphthalene |  |
| A3 | 49.27 | 1-methyl-naphthalene |  |
| A4 | 73.70 | 1,4,5-trimethyl-naphthalene |  |

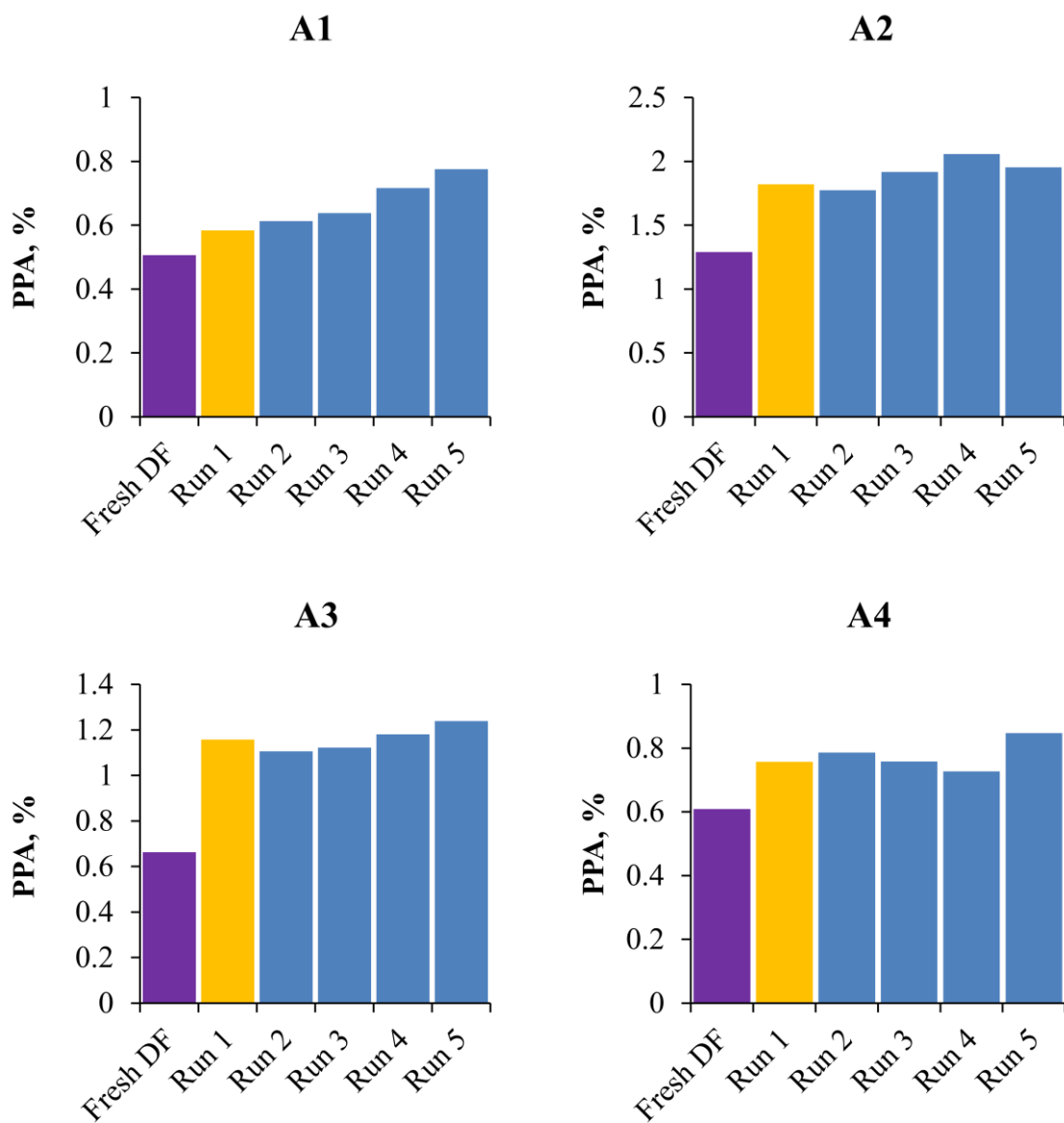


Fig. 5-25 Changes in concentration of PAH precursors in runs 1-5. A1: naphthalene; A2: 2-methylnaphthalene; A3: 1-methylnaphthalene; A3: 1, 4, 5-trimethylnaphthalene.

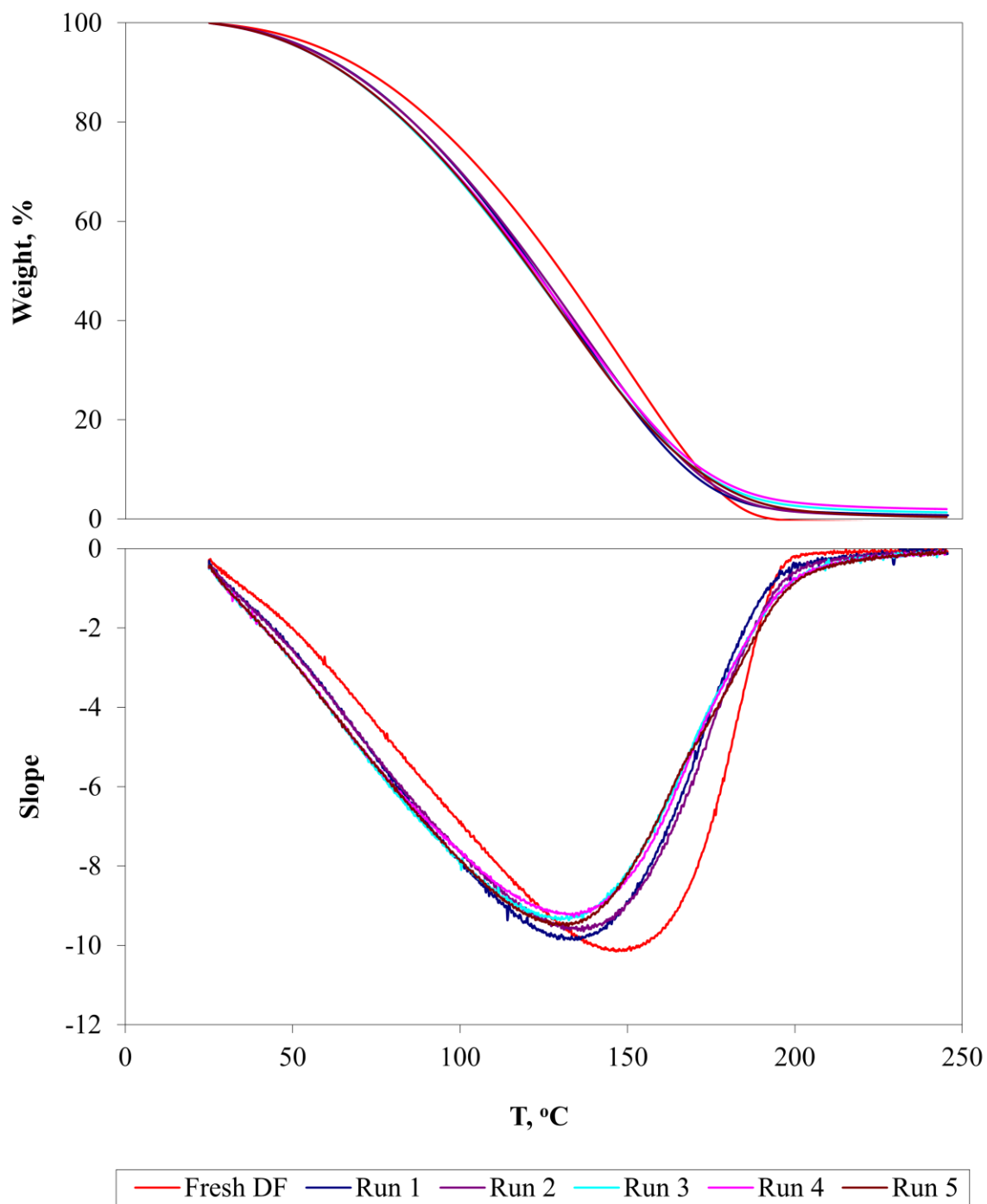


Fig. 5-26 TGA curves for fresh DF and thermally stressed DF from runs 1-5. Top: original TGA curves; bottom: slope curves.

It can be concluded from the above analysis that in the isochoric system, when the amount of fuel remained the same, addition of CO₂ did not improve thermal stability of the fuel. However, one factor that has not been taken into consideration is pressure. **Fig. 5-27** plots thermal stressing P-T diagrams for these runs, demonstrating significant increase in final stressing pressures with increasing initial CO₂ pressure from run 1 through run 5. The T-P histories of these runs are given in Appendix D. The final pressure for run 5 was 30-35 Mpa, which was almost one-order-of-magnitude higher than that for run 1. Thus, it is reasonable to argue that the enhancement in fuel degradation might be due to the significant increase in pressure.

To lower final stressing pressure at a given initial pressure, the amount of DF has to be reduced. Accordingly, in the second set of runs, three DF loads, i.e. 1.6, 1.4 and 1.2 ml, were studied, with or without the presence of CO₂. When CO₂ was added, the initial pressure was 4.83 MPa for all loads as shown in **Table 5-2**. P-T diagrams for this set of runs are plotted in **Fig. 5-28**. T-P histories are attached in Appendix D. **Fig. 5-29** plots $\Delta(PPA)$ trend lines and **Fig. 5-30** illustrates changes in concentrations of PAH precursors A1-A4. It is clearly demonstrated that both the slopes of trend lines and the concentrations of A1-A4 increased for all DF loads when CO₂ was added. These results are similar to those from the first set of runs and further confirm the apparent negative effect of CO₂. Since the pressure effect could not be differentiated in the isochoric system, continuous isobaric thermal stressing experiments were carried out, results from which are presented in the next section.

During the last run, i.e. 4-b in **Table 5-2**, 1.0 ml DF was added and the cell was initially pressurized to 4.83 MPa. The cell was heated, cooled, and then heated again to

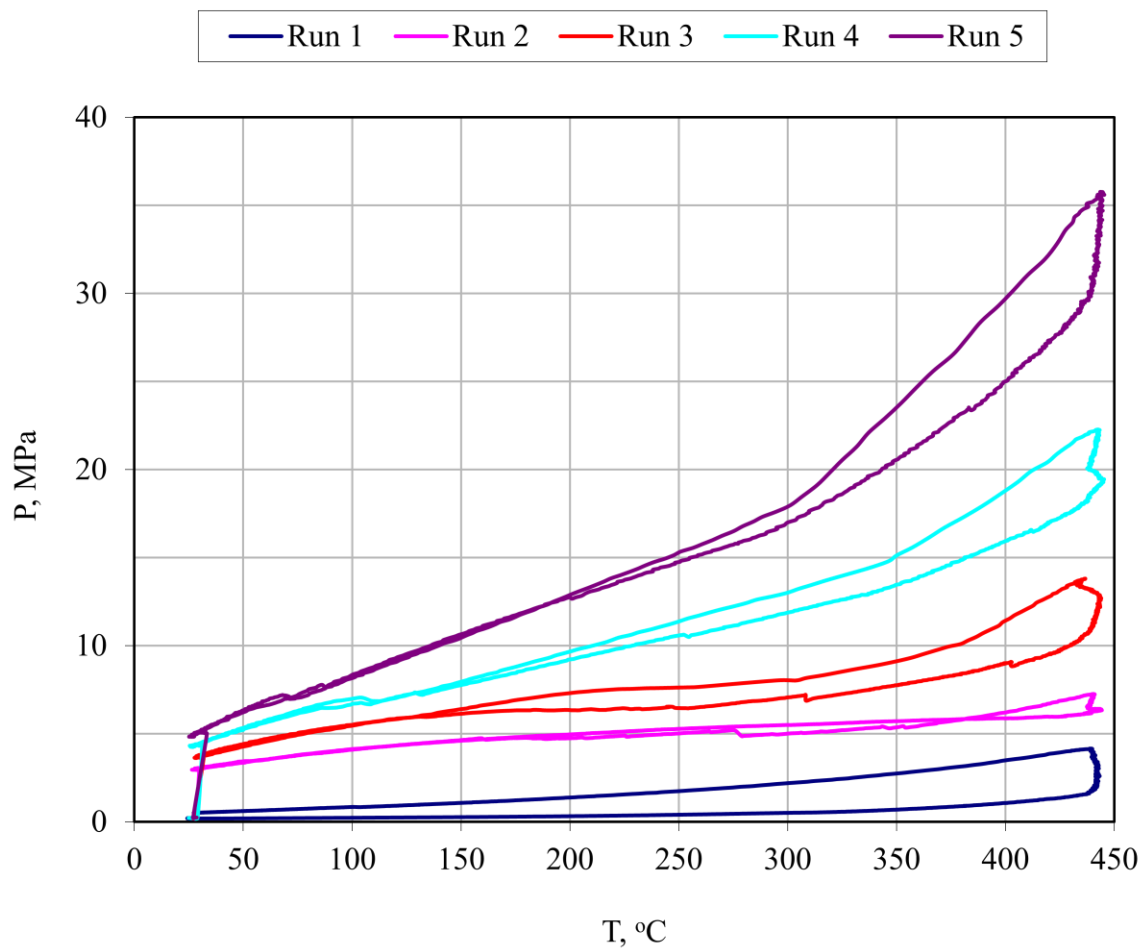


Fig. 5-27 P-T diagrams for batch thermal stressing of DF/CO₂ mixtures: Runs 1-5.

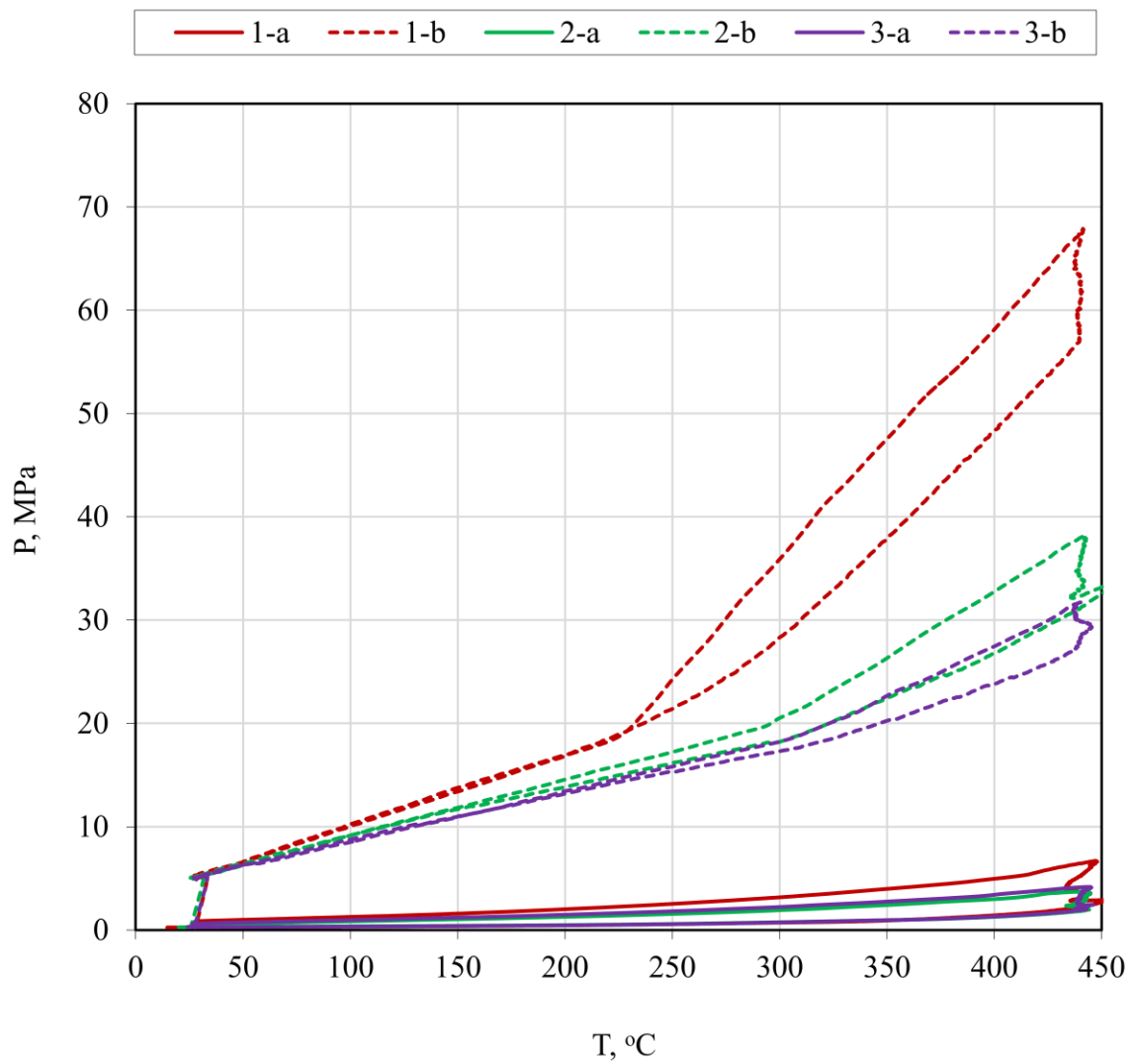


Fig. 5-28 P-T diagrams for batch thermal stressing of DF and DF/CO₂ mixtures: Runs 1-a – 3-b.

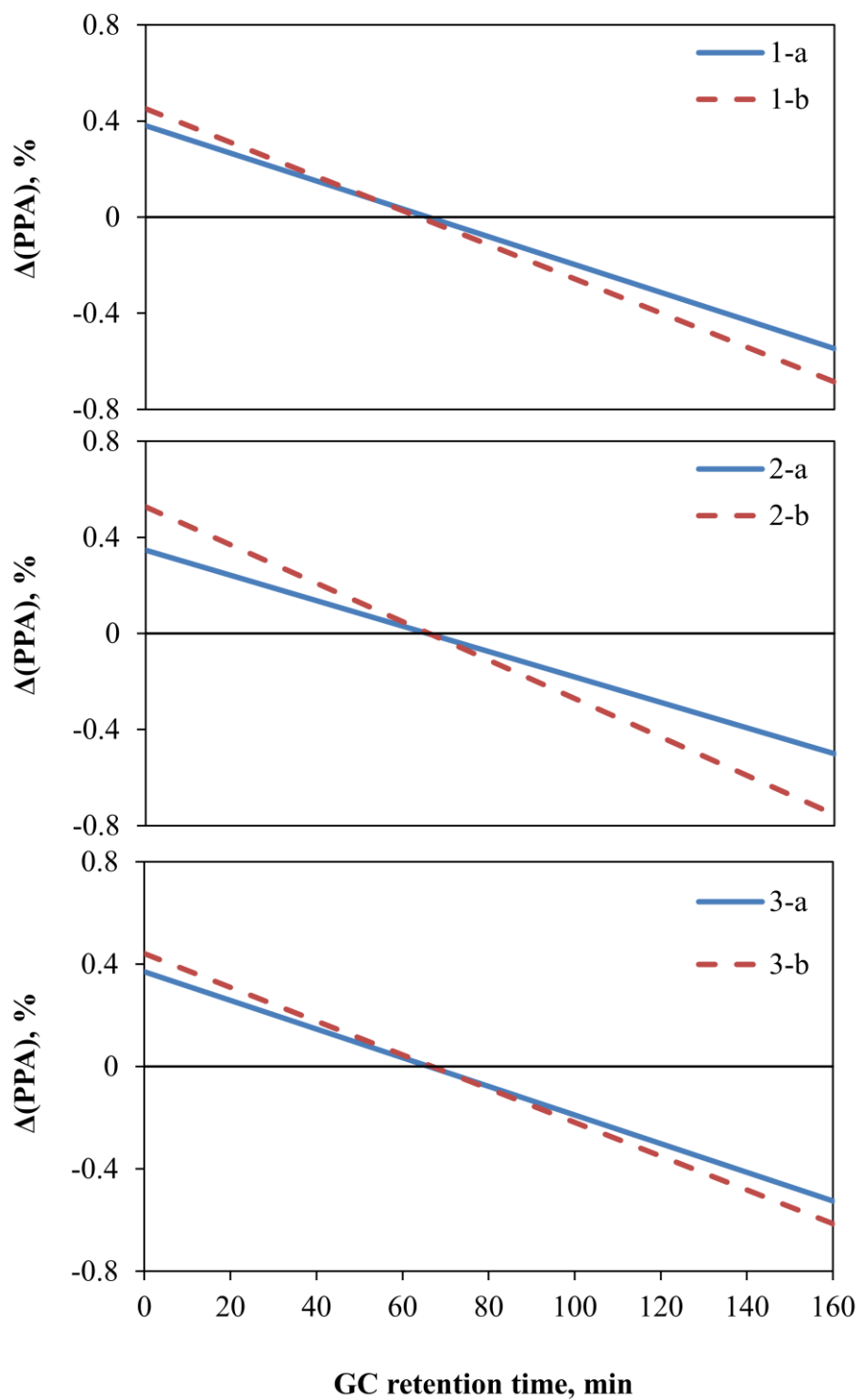


Fig. 5-29 $\Delta(\text{PPA})$ analysis for samples from runs 1-a – 3-b of batch thermal stressing of DF/CO₂ mixtures.

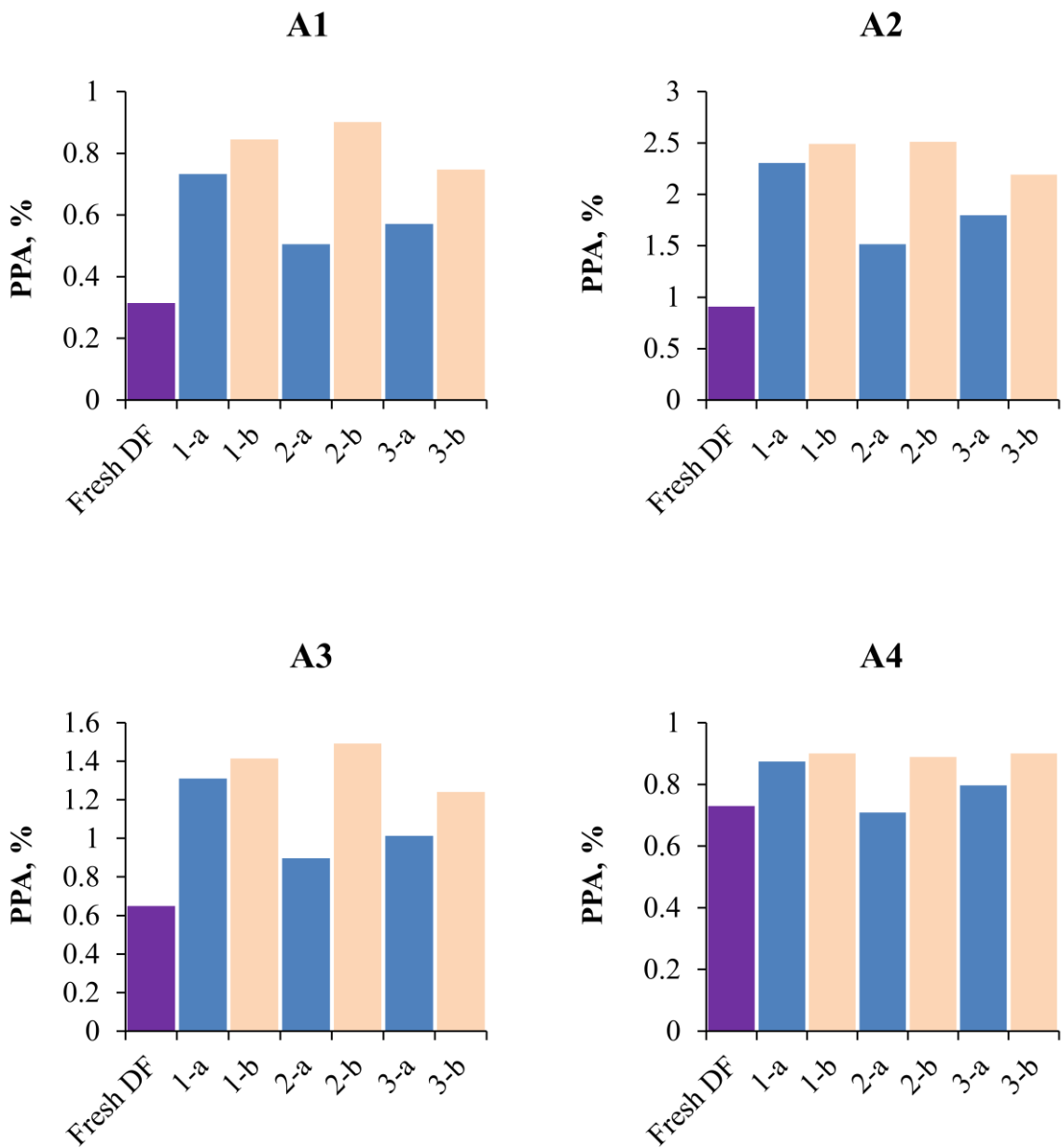


Fig. 5-30 Changes in concentration of PAH precursors in runs 1-a - 3-b.

check the repeatability of the T-P curve. Unfortunately, during the repeated heating stage, the cell was incidentally overheated to above 600 °C as shown in **Fig. 5-31** (bottom). Interesting results were obtained from this “accident”.

In the P-T diagram shown in **Fig. 5-32**, the P-T curves from first run are slightly above the second heating curve. This was probably caused by the dead volume effect; the repeated run was more homogeneous than the first one. Slope changes were observed at about 300 °C for both runs, indicating the occurrence of phase transition from gas-liquid to supercritical. More interestingly, a second slope change occurred at about 470 °C during the second heating stage, which was caused by production of large amounts of gas components due to significant thermal degradation. Also, significant amount of solid deposits was generated. This “accident” reveals the temperature range where significant thermal decomposition occurs.

5.3.4 Continuous thermal stressing of DF and the DF/CO₂ mixture

Fig. 5-33 shows temperature and pressure histories for both DF and DF/CO₂ experiments. Both experiments continued for about 13 hours including the heating and cooling processes. As shown in **Fig. 5-33** (top), for DF, the experiment reached the steady state at around 70 min; T1, T2, T3 and T4 were 461.1 ± 2.5 , 356.6 ± 1.2 , 431.6 ± 1.3 and 235.3 ± 2.1 °C, respective, and P1 and P2 were 29.96 ± 0.12 and 29.89 ± 0.12 MPa, respectively. T3 was slightly lower than the setting temperature which was 440 °C because the thermocouple was close to the inlet of the coil. T4 was much lower because the thermocouple was located outside the GC oven. Unfortunately, at 442 min, one syringe of the HPLC pump malfunctioned, leading to a reduced flow rate. Consequently,

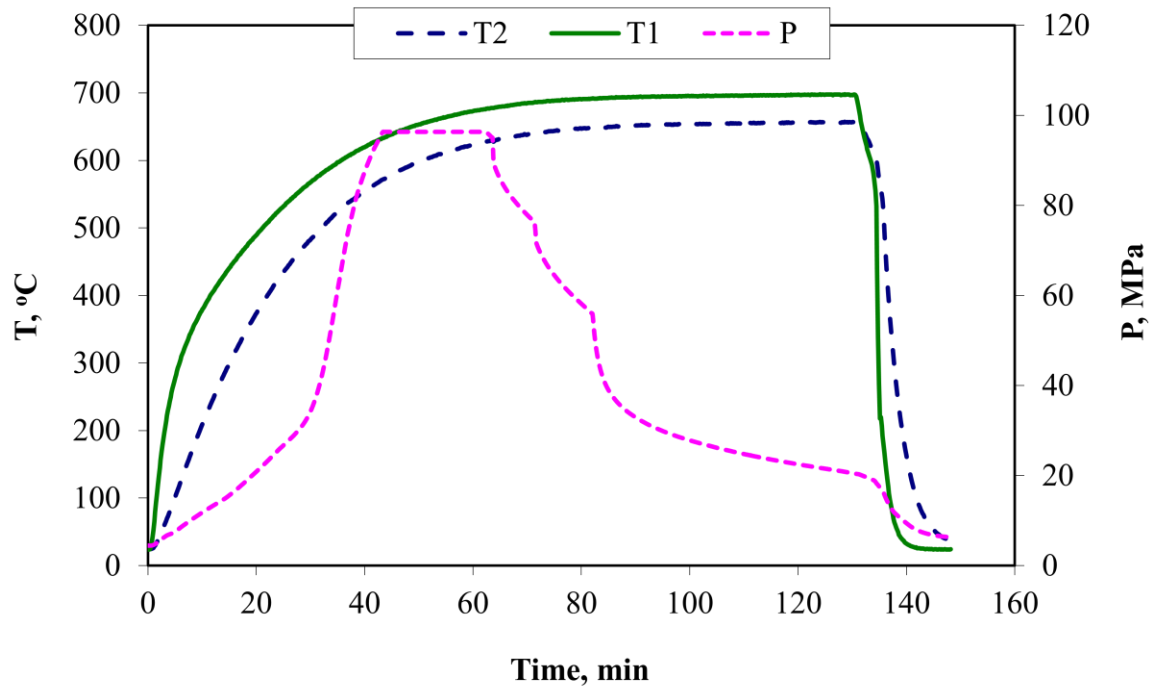
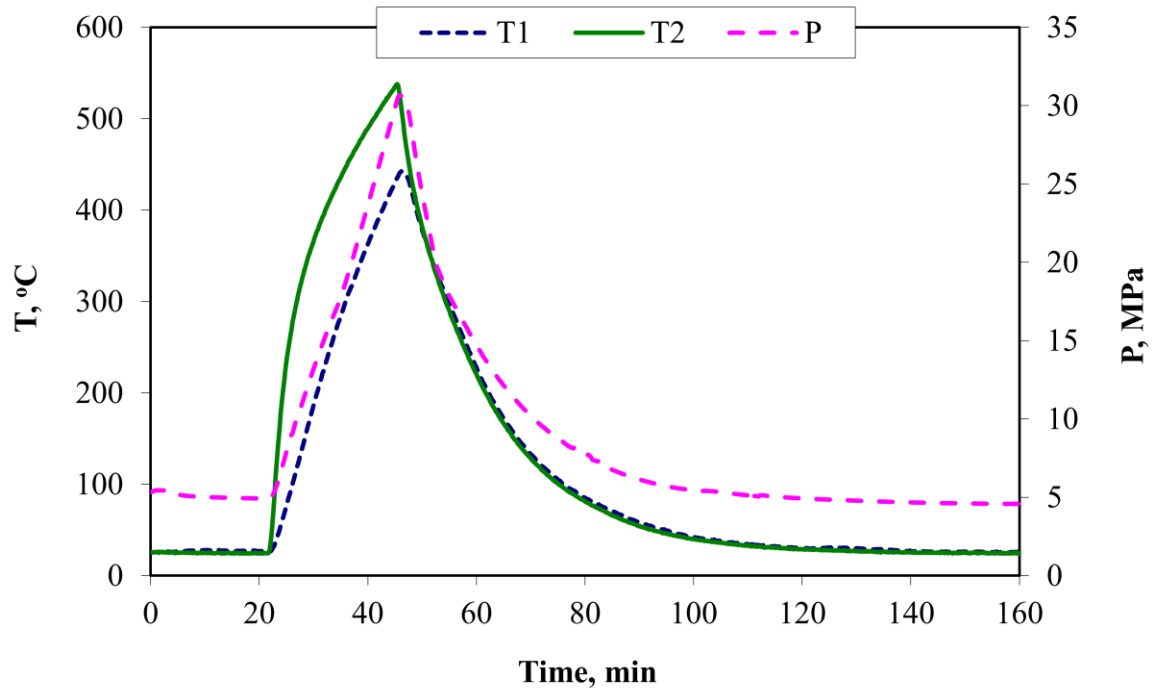


Fig. 5-31 Temperature and pressure history for run 4-b. Top: first run; bottom: repeated run.

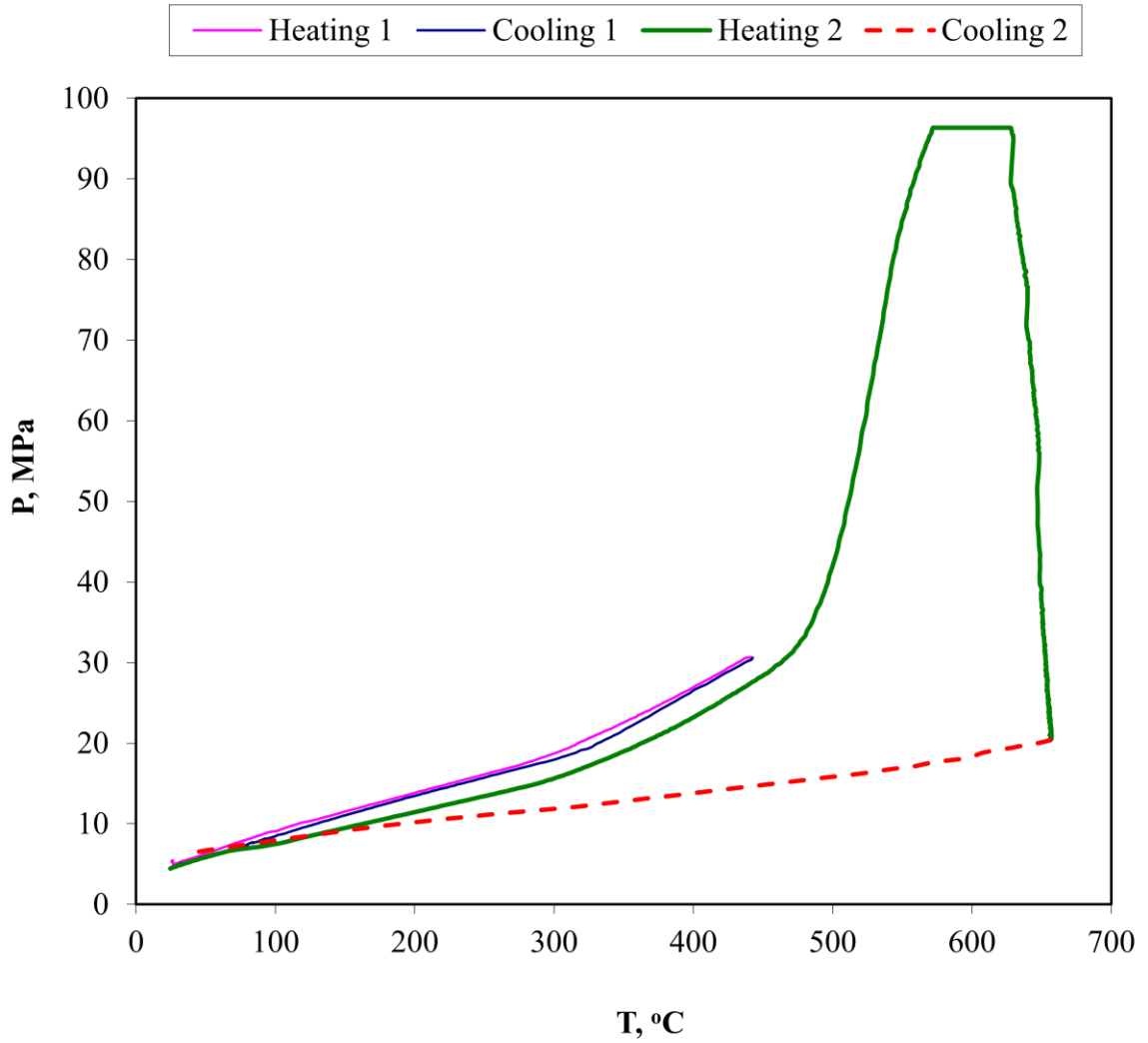


Fig. 5-32 A P-T diagram for run 4-b. Dash line circles highlight regions where slope changes occur.

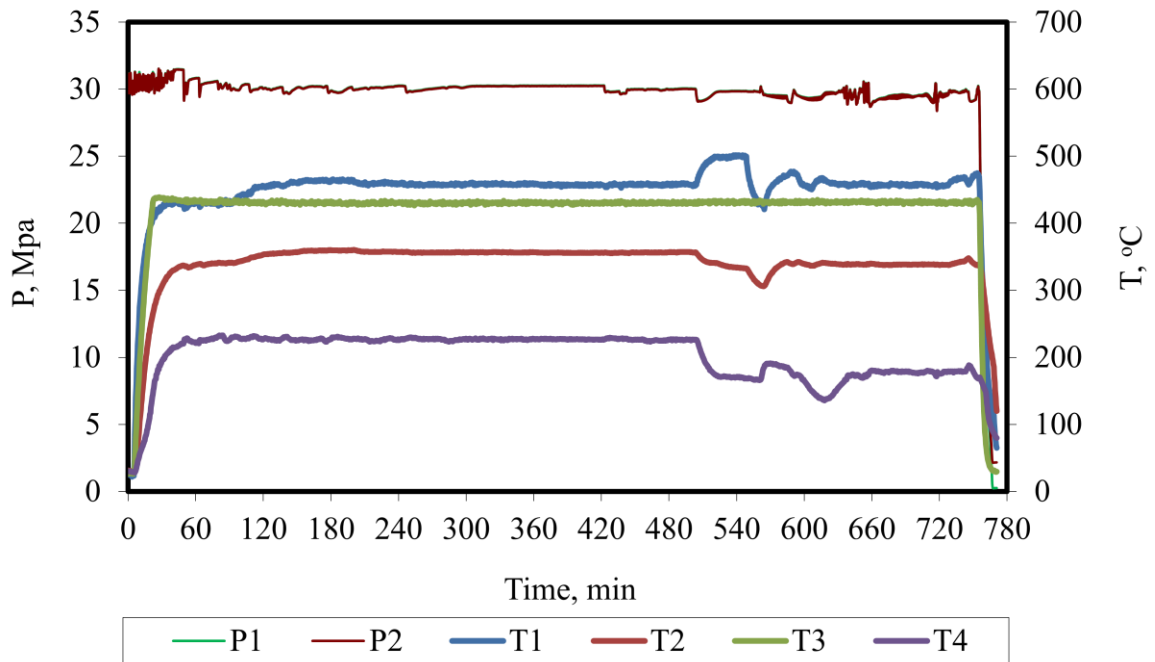
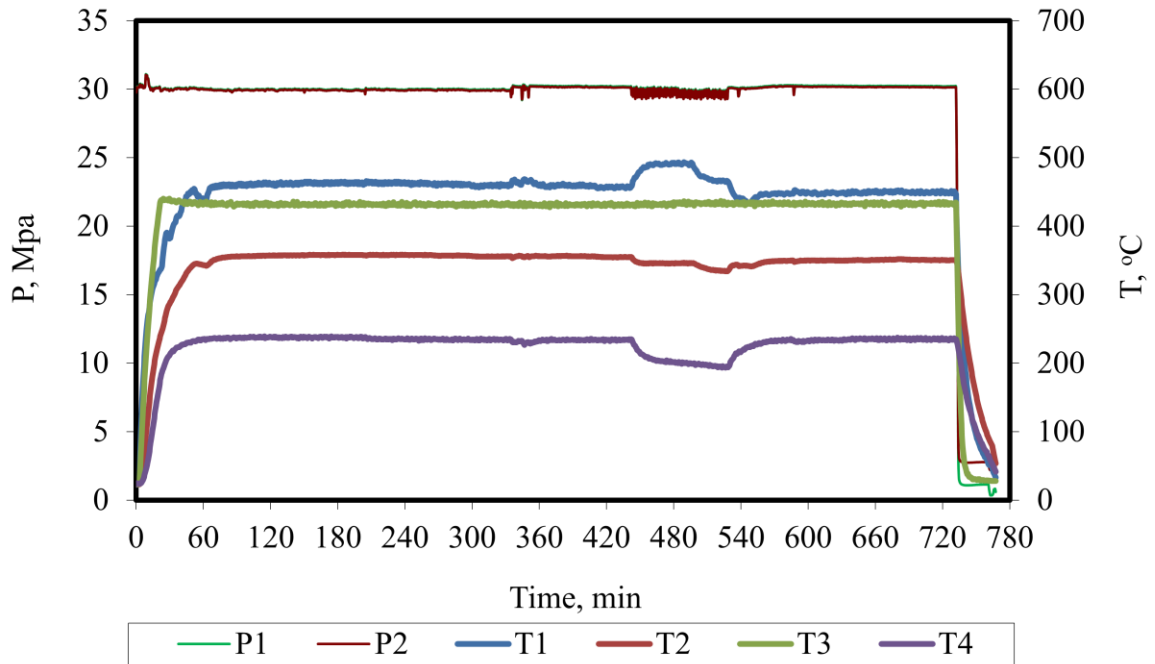


Fig. 5-33 Temperature and pressure history for continuous thermal stressing of DF (top) and the DF/CO₂ mixture (bottom). DF:CO₂ = 9:1 by mass.

T1 increased significantly up to 490 °C, T2 reduced slightly to 345 °C, and T4 continuously reduced to 195 °C until the pump returned to normal at 528 min. Temperature adjustment occurred at 496 min. Reduced flow rate resulted in increase in residence time, which promoted fuel degradation, and as a consequent more gas products were produced, which was evidenced by vibrations in the pressure profiles.

As shown in **Fig. 5-33** (bottom), for the DF/CO₂ mixture, it took longer time, about 2 hours, for the experiment to reach the steady state due to the difficulty in pressure control of the initially inhomogeneous two-phase flow. At the steady state, T1, T2, T3 and T4 were 458.6 ± 2.3 , 356.8 ± 1.2 , 430.3 ± 1.2 and 226.8 ± 1.3 °C, respectively, and P1 and P2 were 30.10 ± 0.16 and 30.07 ± 0.16 MPa, respectively. Compared to the DF experiment, T4 was slightly lower, which can be explained by a lower heat capacity of the DF/CO₂ mixture. Similar malfunctioning occurred in the HPLC pump at 504 min but the pump did not return to normal afterward, causing significant fuel degradation.

Fig. 5-34 shows photos of DF samples collected in one hour interval for a 12 hr period. Similar color changes were observed for both experiments, indicating occurrence of fuel degradation. Darkening of sample # 9 (**Fig. 5-34** top) for the DF experiment and samples # 10-12 (**Fig. 5-34** bottom) for the DF/CO₂ experiment agreed well with the temperature profiles shown in **Fig. 5-33**. For the DF experiment, when the HPLC pump returned to normal, the color of the stressed fuel changed back to normal as shown by sample # 10-12 in **Fig. 5-34** top. This did not occur in the DF/CO₂ experiment and the color of the stressed fuel remained dark brown as illustrated by samples # 10-12 in **Fig. 5-34** bottom.

Fig. 5-35 records changes in the pressure drop across the micro-filter during the

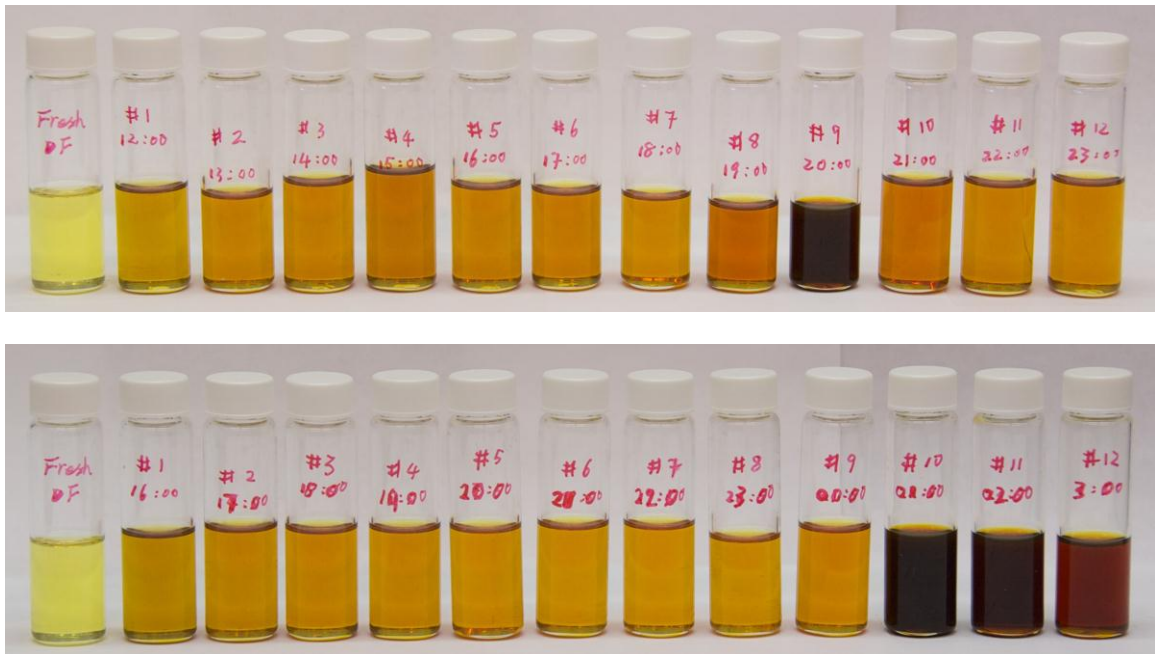


Fig. 5-34 Photos of DF samples collected in thermal stressing of DF (top) and the DF/CO₂ mixture (bottom). Left to right: 0 through 12 hours.

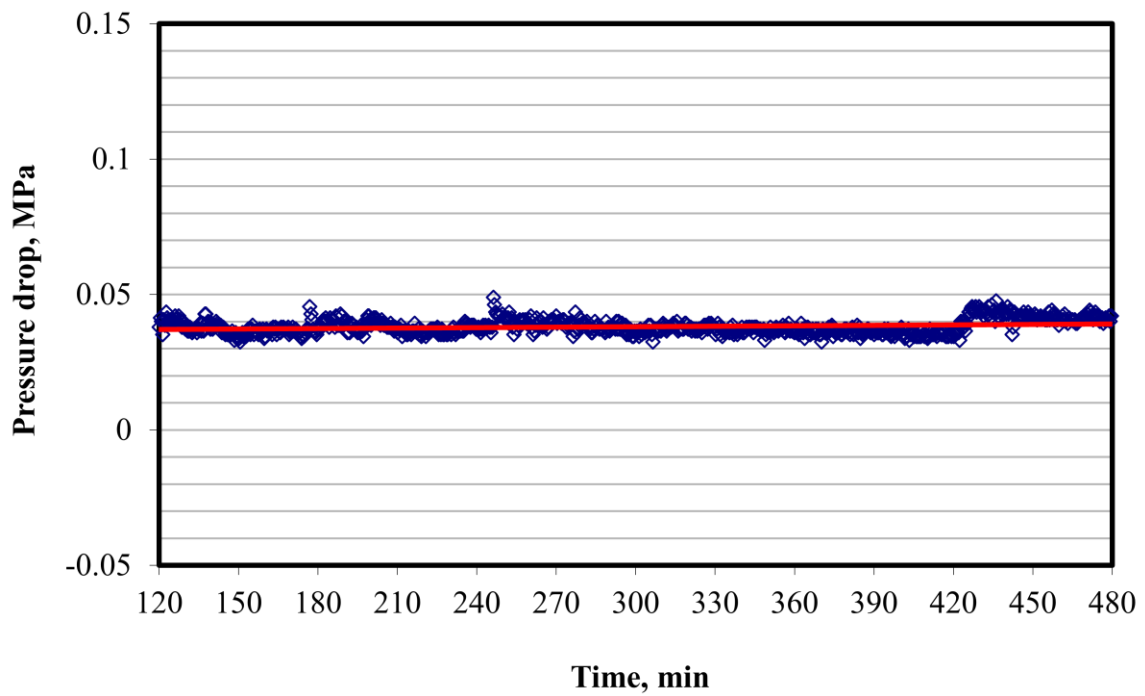
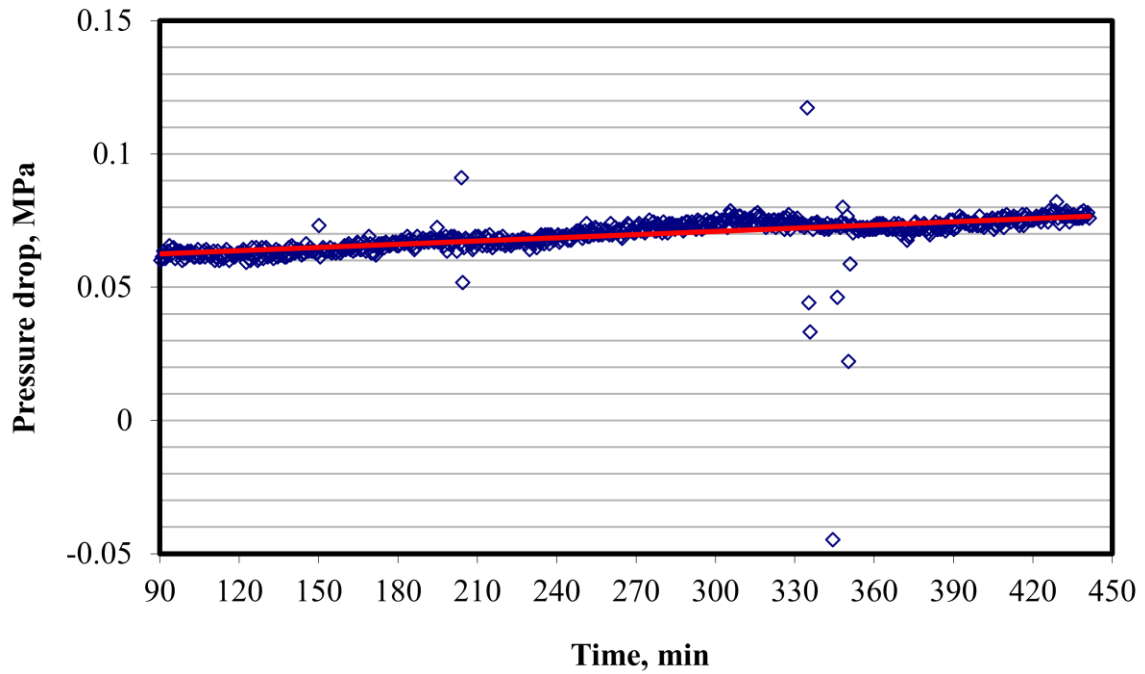


Fig. 5-35 Changes in pressure drop across the micro-filter during continuous thermal stressing of DF (top) and the DF/CO₂ mixture (bottom). Red lines are linear trend lines.

steady state from 90-440 min for DF (top) and from 120-480 min for the DF/CO₂ mixture (bottom). It is seen that in the DF experiment, the pressure drop increased about 30 % from 0.06 to 0.078 MPa, while in the DF/CO₂ experiment, despite some variations, the pressure drop remained constant at 0.04 MPa. This suggests two possibilities: CO₂ was able to reduce fuel degradation and prevent coking; addition of CO₂ increased solubilization capability of the fuel mixture and hence prevented accumulation of solid deposits within the filter.

Fig. 5-36 through **Fig. 5-38** present results from the Δ (PPA) analysis of chromatographs. As shown in **Fig. 5-38**, the slopes of sample #1 from both runs are higher than others, while the slopes of sample # 9 from the DF run and samples # 10-12 from the DF/CO₂ run are much lower than others, which agrees well with visual observation as shown in **Fig. 5-34**. In the nearly steady state, i.e samples # 2-8 & 10-12 from the DF run and samples # 2-9 from the DF/CO₂ run, the slopes are in the same level, despite some small variations. Similar patterns were observed for variations of PAH precursor concentration as shown in **Fig. 5-39**. In the nearly steady state, concentrations of A1-A3 are nearly constant and the same for both runs, while variations are observed for A4 and A4 for the DF run is slightly higher than that for the DF/CO₂ run. These results indicate that addition of CO₂ did not effectively reduced fuel degradation under current experimental conditions.

Results from analysis of pressure drop across the filter and analysis of DF chromatographs suggest that CO₂ might not effectively prevent fuel degradation but was able to reduce accumulation of solid deposits along the flow path due the solubilization effect. One explanation of these phenomena is that addition of CO₂ reduces the critical

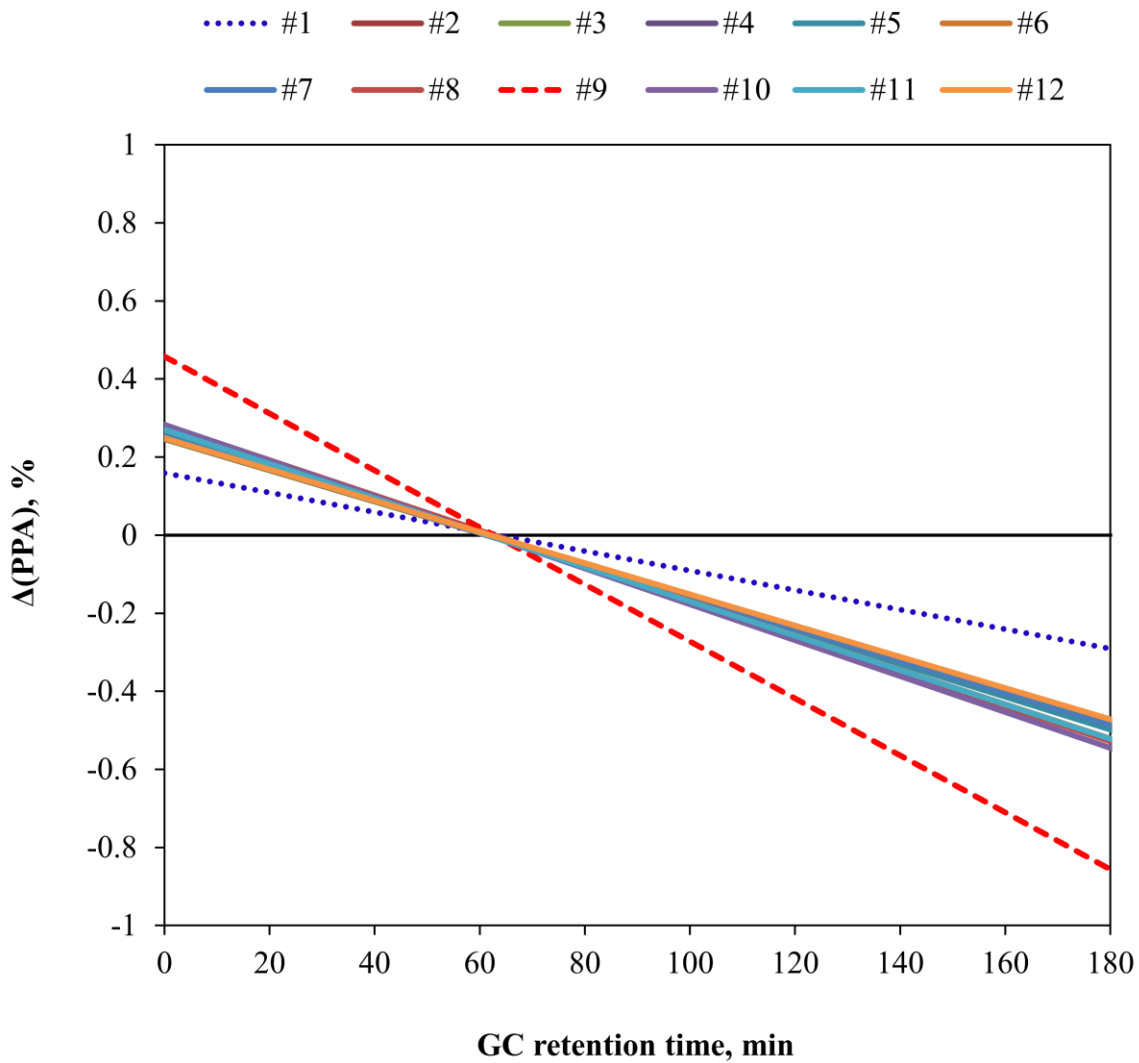


Fig. 5-36 $\Delta(PPA)$ analysis for DF samples collected during thermal stressing of DF.

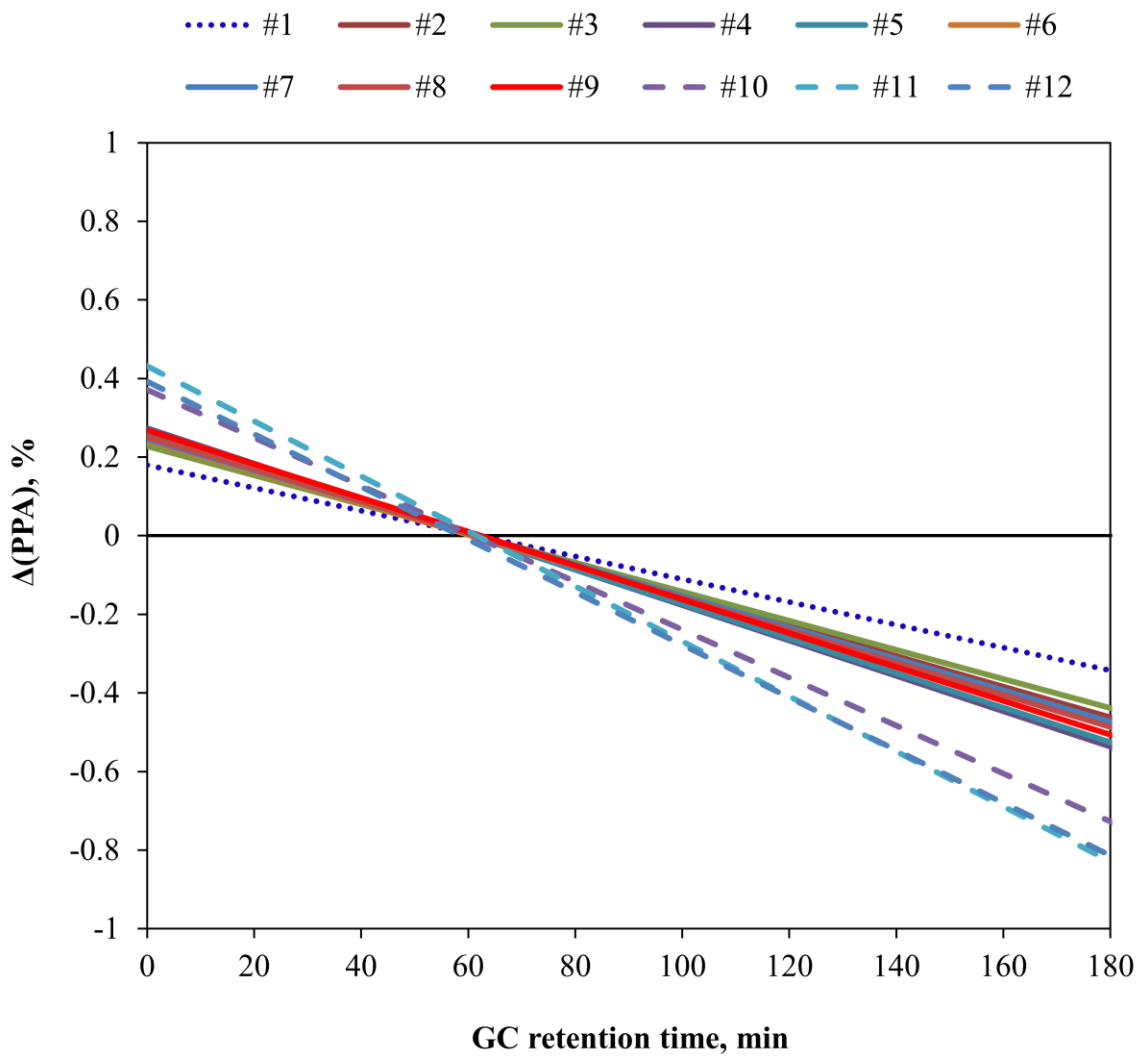


Fig. 5-37 $\Delta(PPA)$ analysis for DF samples collected during thermal stressing of the DF/CO₂ mixture.

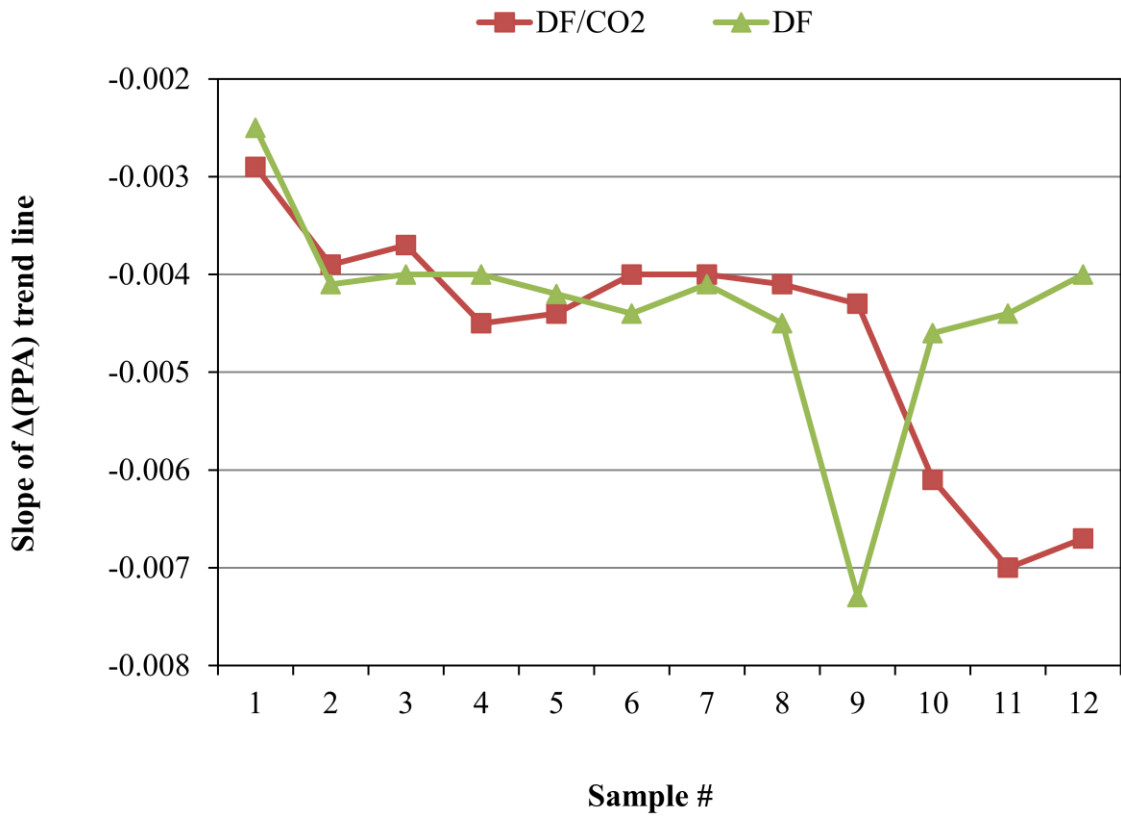


Fig. 5-38 Slopes of $\Delta(PPA)$ trend lines.

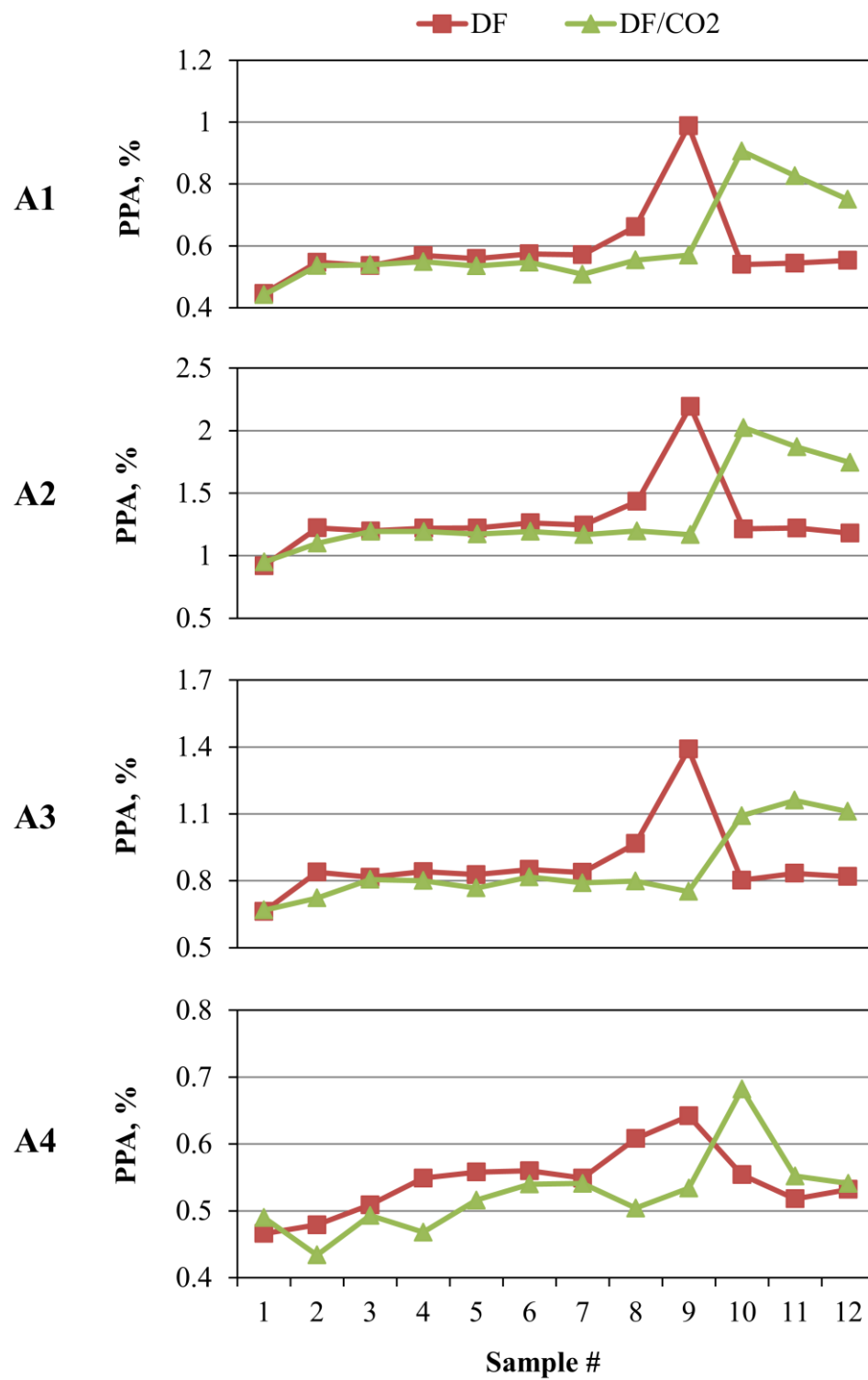


Fig. 5-39 Variations of concentrations of PAH precursors in thermal stressing of DF and the DF/CO₂ mixture.

temperature of the fuel mixture, bringing the fuel from liquid state to the supercritical state. For a rough estimate, Eq. (3-16) is used to obtain pseudocritical temperatures of DF/CO₂ mixtures at varying compositions. Some constants required for the calculation include critical temperatures and molecular weights of both DF and CO₂. Molecular weight of DF is calculated by Eq. (5-3) suggested by API (API, 2006), while other constants are described in Chapter III.

$$MW = 20.486[\exp(1.165 \times 10^{-4} T_b - 7.78712 SG + 1.1582 \times 10^{-3} T_b SG)] T_b^{1.26007} SG^{4.98308} \quad (4-31)$$

where T_b is in °R. With $T_b = 1000.4$ °R and $SG = 0.85745$ from Chapter III, it gives $MW = 221$ g/mol. Critical temperatures at varying compositions are presented in **Table 5-6**. It is shown that addition of 10 wt% of CO₂ reduces the critical point from 472 to 314 °C, a value much lower than the thermal stressing temperature which was 440 °C.

5.4 CONCLUSIONS

Thermal stability of DF is one major concern of the development of supercritical fuel combustion technology. Fuel degradation, on the one hand, directly influences fuel combustion and combustion efficiency. On the other hand, it leads to solid deposits, which could eventually block the fuel delivery system, causing failure of diesel engines. Therefore, a better understanding of DF thermal stability is desired.

Three experiments were designed and conducted in this work to explore the impacts of temperature, residence time and CO₂ on thermal stability of DF. They were batch thermal stressing of DF, batch thermal stressing of DF/CO₂ mixtures, and continuous thermal stressing of DF and the DF/CO₂ mixture. Stressed DF samples were

Table 5-6 Pseudocritical points of DF/CO₂ mixtures.

| Wt % | | Molar ratio, x | | T _c , °C |
|------|-----------------|------------------|-----------------|---------------------|
| DF | CO ₂ | DF | CO ₂ | |
| 100 | 0 | 1.00 | 0.00 | 472.0 |
| 95 | 5 | 0.79 | 0.21 | 379.7 |
| 90 | 10 | 0.64 | 0.36 | 313.9 |
| 85 | 15 | 0.53 | 0.47 | 264.7 |
| 80 | 20 | 0.44 | 0.56 | 226.4 |
| 75 | 25 | 0.37 | 0.63 | 195.8 |
| 70 | 30 | 0.32 | 0.68 | 170.9 |
| 65 | 35 | 0.27 | 0.73 | 150.1 |
| 60 | 40 | 0.23 | 0.77 | 132.5 |
| 55 | 45 | 0.20 | 0.80 | 117.4 |
| 50 | 50 | 0.17 | 0.83 | 104.3 |
| 45 | 55 | 0.14 | 0.86 | 92.9 |
| 40 | 60 | 0.12 | 0.88 | 82.8 |
| 35 | 65 | 0.10 | 0.90 | 73.9 |
| 30 | 70 | 0.08 | 0.92 | 65.9 |
| 25 | 75 | 0.06 | 0.94 | 58.7 |
| 20 | 80 | 0.05 | 0.95 | 52.1 |
| 15 | 85 | 0.03 | 0.97 | 46.2 |
| 10 | 90 | 0.02 | 0.98 | 40.8 |
| 5 | 95 | 0.01 | 0.99 | 35.9 |
| 0 | 100 | 0.00 | 1.00 | 31.3 |

characterized by GC-MS and TGA methods. Solid deposits were analyzed using SEM.

It was found that DF exhibited very good thermal stability up to 420 °C for a residence time of 30 min. As temperature increased further from 420 °C, thermal stability of DF dropped and degradation accelerated. The higher the temperature, the more significant fuel degradation. At 400 °C, DF remained stable for a residence time as high as 60 min. These results suggest that 400-420 °C can be an optimal temperature range for supercritical fuel delivery.

Two different morphologies and structures of solid deposits were observed. At relative low temperature (300-400 °C), deposits had ring structure and the size was as large as 1 µm. At high temperature (440 °C), increasing amount of crystal-like deposits were captured on the stainless steel sheet. The size of these “crystals” was in the order of magnitude of 100 nm. The difference in solid structures was likely due to different reaction mechanisms that lead to formation of solid deposits.

CO₂ was not able to chemically reduce fuel degradation and hence to prevent fuel coking. However, a constant instead of increasing pressure drop across the fuel filter with addition of CO₂ in DF implies that CO₂ was able to reduce accumulation of solid deposits along the pipe line. This is well explained by enhanced solvent capacity due to a reduced critical temperature of the fuel mixture with addition of CO₂.

Finally, a new method based on GC analysis, named the $\Delta(PPA)$ analysis, was proposed in this work for characterization of DF thermal stability. When degradation occurs, a negative slope of the $\Delta(PPA)$ trend line is obtained. A greater negative slope indicates more significant fuel degradation.

CHAPTER VI

CONCLUSIONS

The clean diesel combustion technology using supercritical fluids incorporates two innovative concepts: injecting diesel fuel under the supercritical condition which is above 400 °C and using EGR/CO₂ to prevent fuel coking. Implementation of this technology in conventional diesel engines requires not only technological innovations but also a deep understanding of fuel science. This study has been conducted to address some important issues related to fuel properties which were encountered in this project but had not been well explored in the literature yet. These issues include development of DFSs, diffusivity measurements, and thermal stability of DF. Both modeling and experimental techniques have been employed in this study.

DFSs are often used in engine simulations and experimentations to mimic DF. In this study, ten DFSs were evaluated in terms of the ability to predict DF physical properties including volatility, critical points, density, viscosity, heat capacity, and thermal conductivity. It was found that none of these DFSs are able to predict all properties of interest. Different DFSs are suggested to obtain different properties. The critical temperatures of all DFSs are lower than that of DF with DFS-5 giving a closest value. The estimated critical temperatures of DFS-5 and DF are 723 K and 739-754 K, respectively. These estimates suggest that DFS-5 is a good surrogate candidate when critical properties are important. DFS-7 gives best predictions of density of DF with AAD% less than 1%, DFS-4 gives best predictions of both heat capacity and viscosity, while

DFS-9 gives relatively better results for thermal conductivity. These surrogates may be used to have rough estimates of DF properties, when no experimental data are available. This work on DFS has provided the first evaluation of the capability of DFSs in predicting DF thermophysical properties and a guideline for DFS selection.

Diffusivity is one important parameter required for modeling of fuel-diluent and fuel-air mixing. Lack of experimental data in the literature motivated the study on diffusivities of DF and surrogate compounds in SCCO₂. Measurements were done by the Taylor dispersion method at temperatures and pressures up to 373.15 K and 30 MPa, respectively. Experimental data were correlated by Wilke-Chang, Scheibel, He-Yu, $D_{12}/T-\mu$ and $D_{12}/\sqrt{T}-\rho$ correlations. It was found that among the first three predictive correlations, the He-Yu correlation had the best capability of predicting diffusion coefficients in SCCO₂. The $D_{12}/T-\mu$ correlation had the best overall performance with AAD% < 8%.

Experimental uncertainties in the diffusivity measurement experiments caused by sample injection, detector linearity, mobile phase mean velocity, and column orientation have been studied. It was found that the effect of sample injection volume could be characterized by a new dimensionless parameter ϕ proposed in this work, which is defined by the ratio of equivalent length of injection volume over column diameter. Measured diffusion coefficients decreased as ϕ increased. A ϕ value below 5 is suggested for a better design of Taylor dispersion experiments. Measured diffusion coefficients were significantly affected by the mean velocity. The current results lead to a new generalized D_{12} -U- ρ pattern diagram which is comprised of three regions, I, II and III, dominated by buoyancy forces, inertial forces, and centrifugal forces, respectively. At

relatively low density, regions I and III merge together and region II disappears. Accurate diffusion coefficients can only be determined in the region II. Column orientation affects diffusion coefficient measurements mainly by enhancing or weakening the buoyancy effects. When the density difference between the injected sample and the mobile phase is substantial and the column is installed vertically, alternate upward and downward flow along the column will significantly enhance the buoyancy effects, leading to lower measured diffusion coefficients. The horizontal position is preferred especially when the density difference between the solute and the solvent is relatively large.

The work on diffusivity measurements has provided significant advances by expanding the data base for diffusivities of hydrocarbons in SCFs and by improving the understanding of experimental uncertainties.

Both batch and continuous thermal stressing experiments have been conducted to demonstrate the impacts of temperature, residence time and CO₂ on thermal stability of DF. It was found that thermal stability of DF generally decreases as temperature and residence time increase. At 400 °C, DF remained stable for a residence time as high as 60 min. At 420 °C, DF exhibited very good stability for a residence time of 30 min. Above 420 °C, thermal stability of DF dropped and degradation accelerated. The higher the temperature, the more significant fuel degradation. These results suggest that 400-420 °C can be an optimal temperature range for supercritical fuel delivery. CO₂ was able to reduce accumulation of solid deposits along the pipe line due to the enhanced solvent capacity. However, it was found that CO₂ was not likely to be able to chemically reduce fuel degradation.

Two different morphologies and structures of solid deposits were observed. At

relative low temperature (300-400 °C), deposits had ring structures and their sizes were as large as 1 μm. At high temperature (440 °C), increasing amounts of crystal-like deposits were captured on the stainless steel sheet. The sizes of these “crystals” were in the order of magnitude of 100 nm. The difference in solid structures was likely due to different reaction mechanisms that lead to formation of solid deposits.

The work on thermal stability has resulted in some important observations, improved the understanding of the impacts of process conditions on fuel stability, and provided conditions where the supercritical fuel combustion could work.

CHAPTER VII

FUTURE WORK

To date, research has not been focused on the challenges associated with supercritical fuel combustion. Thus, there are numerous opportunities for innovations and breakthroughs in fuel science and technologies that could allow fuels to be consumed in a greener, more efficient way. Research is needed to develop reliable, accurate fuel property database for applications in modeling, simulation, and design of conventional and supercritical fuel delivery and combustion systems. Research is also required to advance the understanding of the impacts of fuel temperature and diluents on spray behavior, fuel degradation, coke formation, and combustion efficiency. Some of the key areas recommended for further investigations are provide below:

1. Thermophysical properties of fuels

Improve equipment and develop methodology for measuring fuel properties.

Reliable data depend on reliable instrumentation and experimentation. Equipment and instruments developed to date for measuring thermophysical properties are mostly limited for low temperature and/or low pressure applications. Measuring fuel properties at high temperature and high pressure is still a big challenge. Research is needed to improve current equipment and/or develop new equipment and methods to enable acquisition of fuel properties under severe conditions.

Improve fuel property models. Predictive fuel property models and correlations are essential to engineering applications. With acquisition of new experimental data,

current theoretical models and empirical/semi-empirical correlations need to be improved to cover a broader range of operation conditions.

Develop fuel property database. The long-term goal of research on fuel properties would be to develop a fuel property database to support R&D of advanced fuel and combustion systems including supercritical fuel combustion systems. Such properties include density, viscosity, heat capacity, heat of vaporization, thermal conductivity, thermal diffusivity, mass diffusivity, volatility, and many others. Furthermore, the database should include fuels manufactured from a variety of feedstock, both petroleum and biomass, as biofuels will play a major role in future global energy supplies.

2. Thermal stability of fuels

Advance the understanding of the impacts of EGR on fuel stability. Preliminary batch thermal stressing experiments of DF with trapped air have demonstrated effects of air on thermal stability of DF. Since EGR contains certain amounts of O₂, N₂ and water, research is needed to reveal the impacts of these species on thermal stability of DF. Also, optimal temperature and pressure conditions and the optimal amount of EGR/CO₂ need to be determined.

Develop fuel coking and solid deposit formation mechanisms. Two different morphologies of solid deposits were observed at different stressing temperatures in this work, which implies different fuel coking and solid deposit formation mechanisms. A better understanding of the mechanisms would benefit the development of new strategies for prevention of fuel coking. It is also valuable to investigate the effects of CO₂ and EGR on formation of solid deposits.

Determine thermal stability of biofuel and fuel/biofuel blends. Biofuel will play an

important role in future energy supplies, and supercritical fuel combustion is not limited to diesel fuel. Thus, thermal stability of biofuel and fuel/biofuel blends and the impacts of compositions of fuel blends on thermal stability need to be addressed.

3. Supercritical fuel combustion

One issue has been overlooked in design of the supercritical fuel combustion process is the impact of fuel degradation on combustion. Fuel degradation at high temperatures involves not only formation of solid deposits but also changes in chemical compositions. Changes in fuel composition would further influence volatility and cetane number. These properties are of primary importance in determining ignition quality and combustion efficiency. Thus, the impacts of fuel temperature and high-temperature induced fuel degradation on fuel combustion behavior must be addressed in the development of the clean diesel combustion technology using supercritical fluids.

APPENDIX A

DENSITIES, HEAT CAPACITIES, VISCOSITIES, AND THERMAL CONDUCTIVITIES OF DF AND DFSs

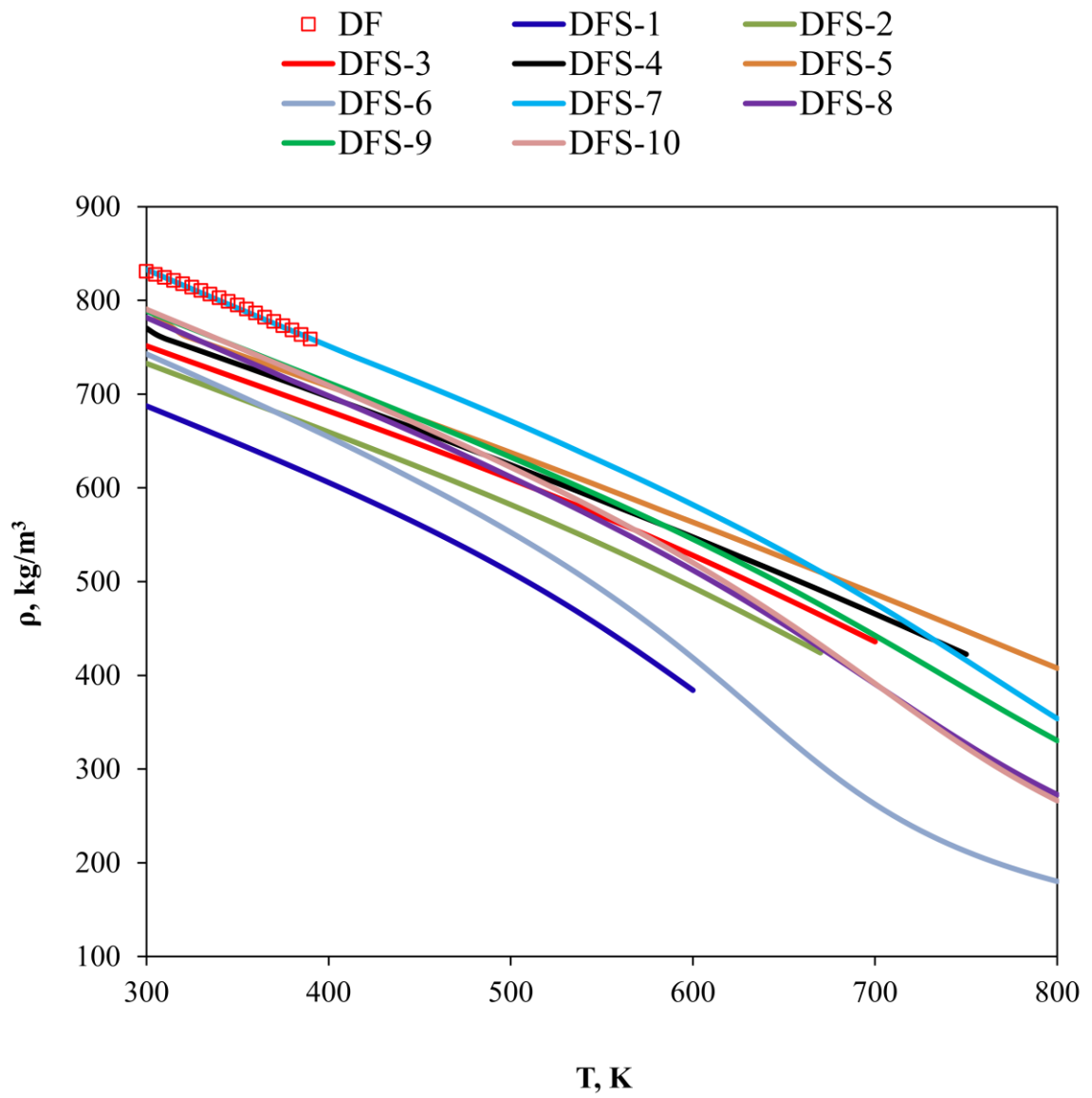


Fig. A-1 Densities of DFSs and DF at 10 MPa.

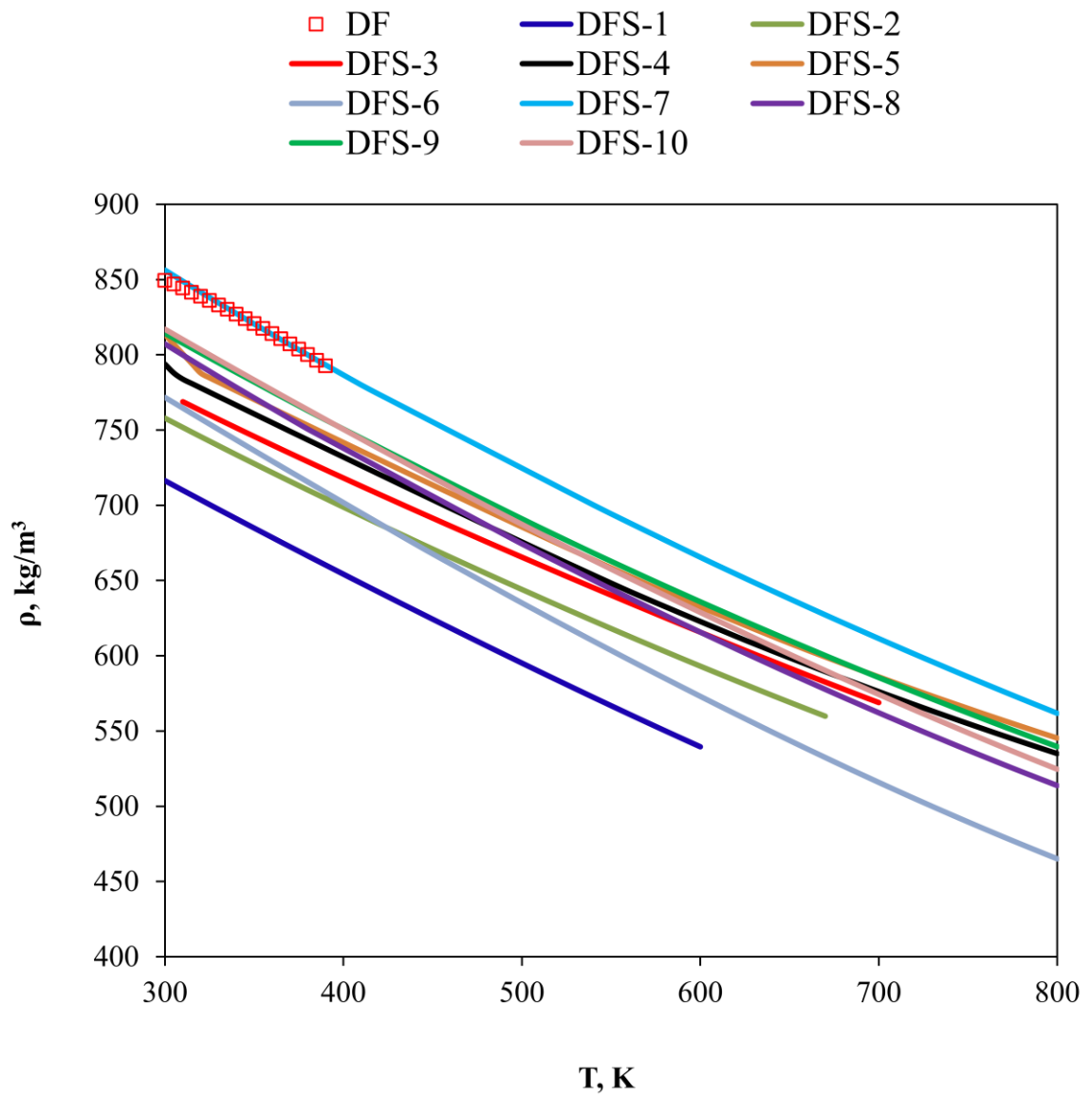


Fig. A-2 Densities of DFSs and DF at 50 MPa.

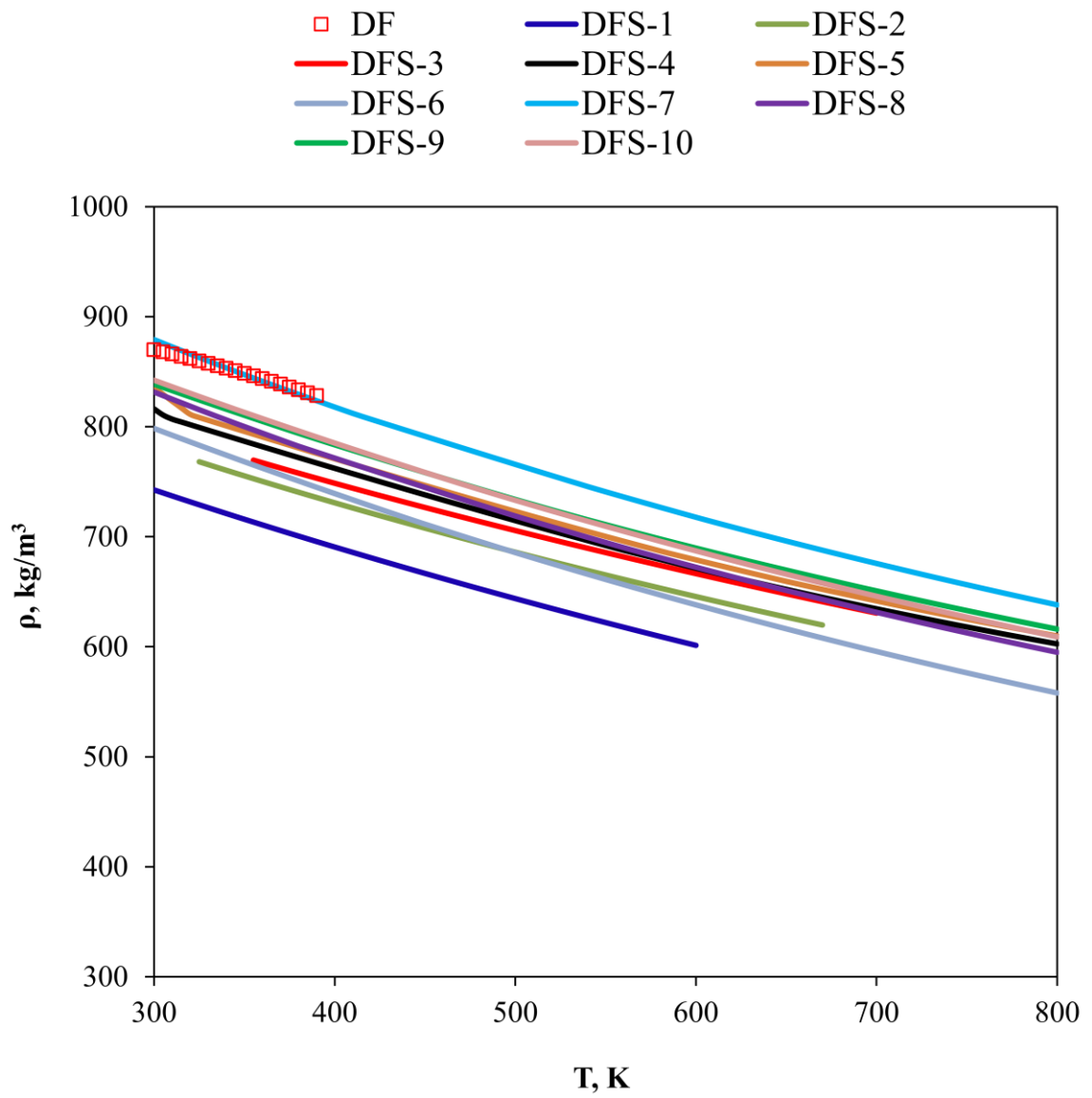


Fig. A-3 Densities of DFSs and DF at 100 MPa.

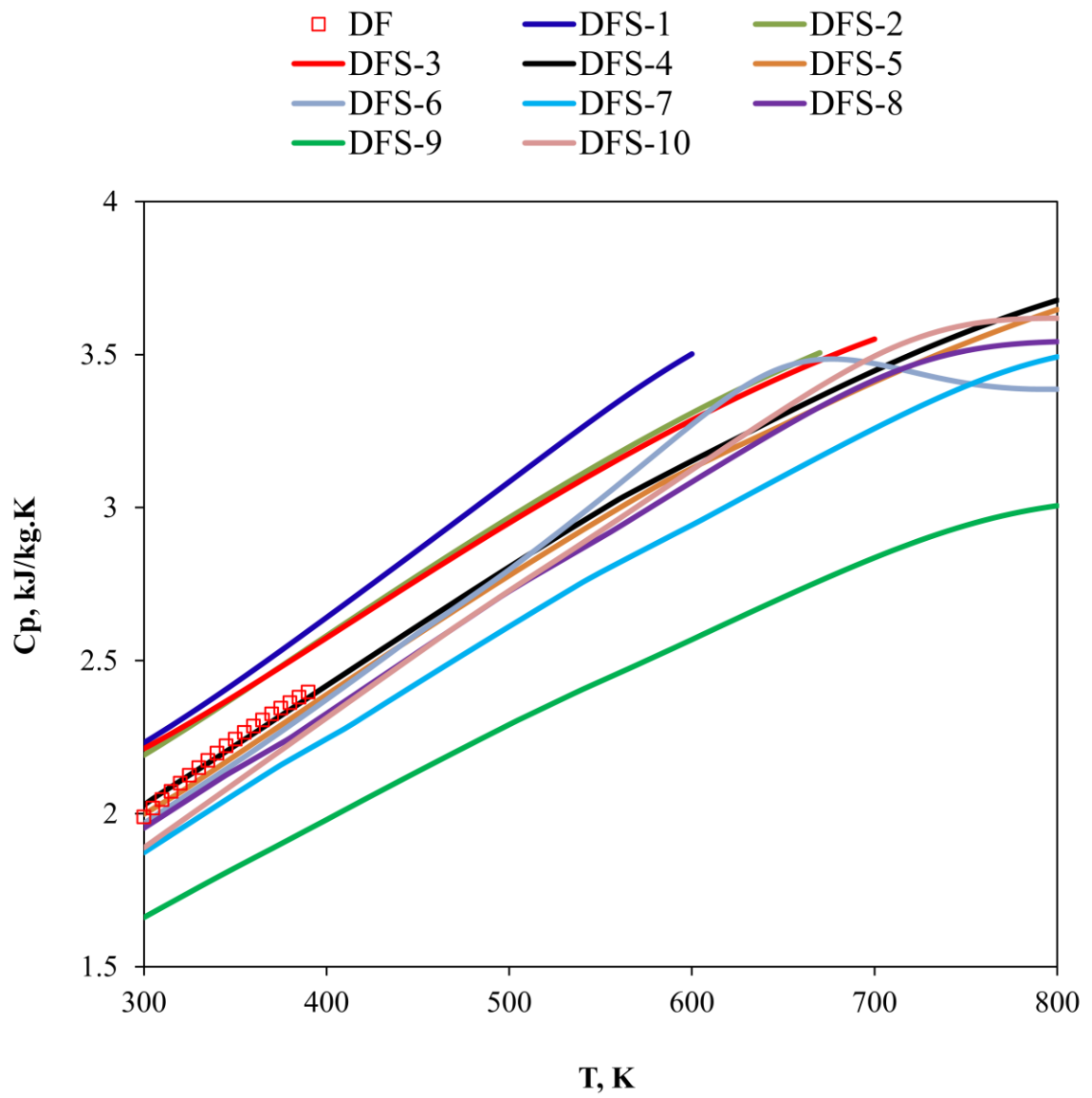


Fig. A-4 Heat capacities of DFSs and DF at 10 MPa.

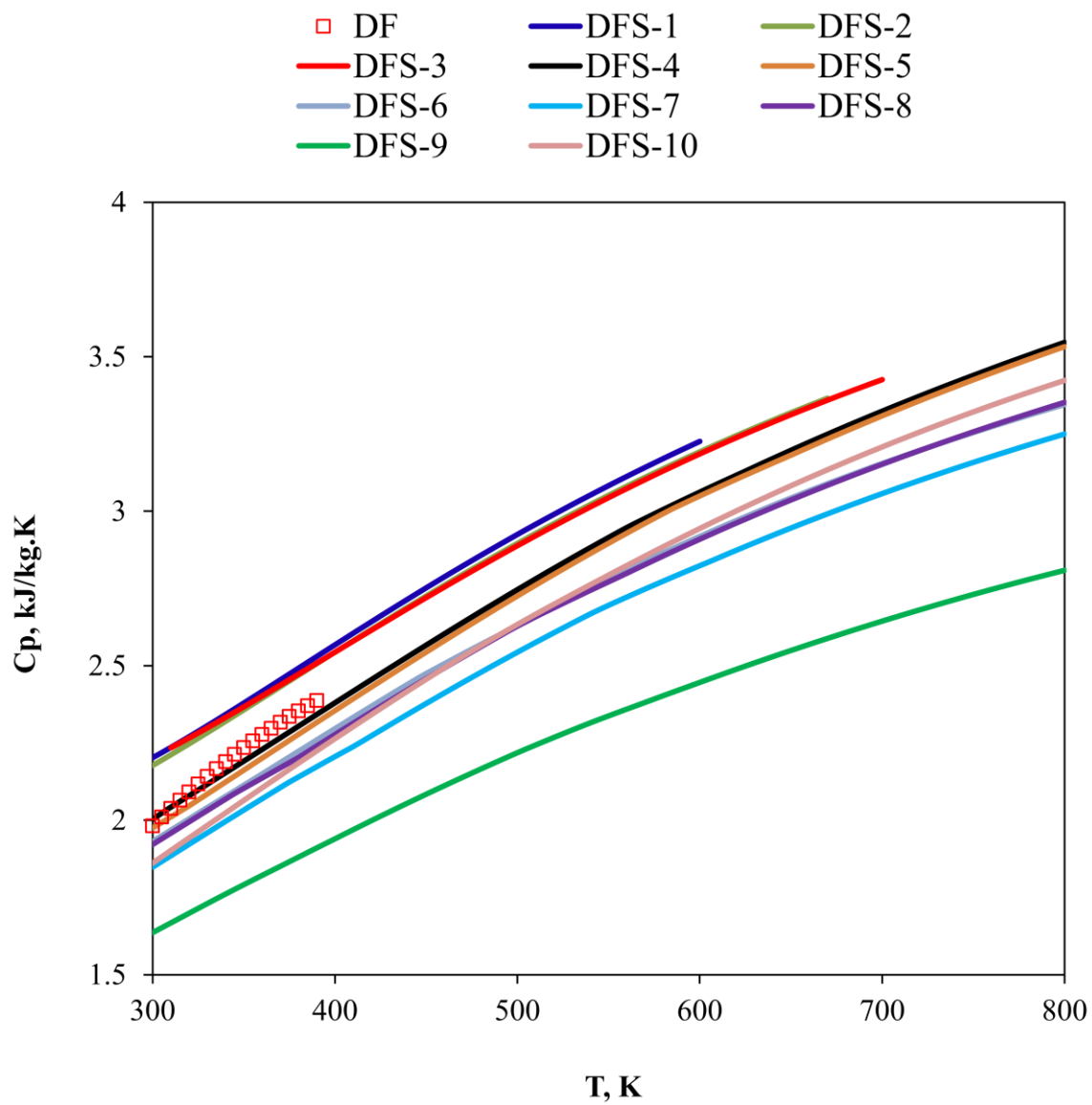


Fig. A-5 Heat capacities of DFSs and DF at 50 MPa.

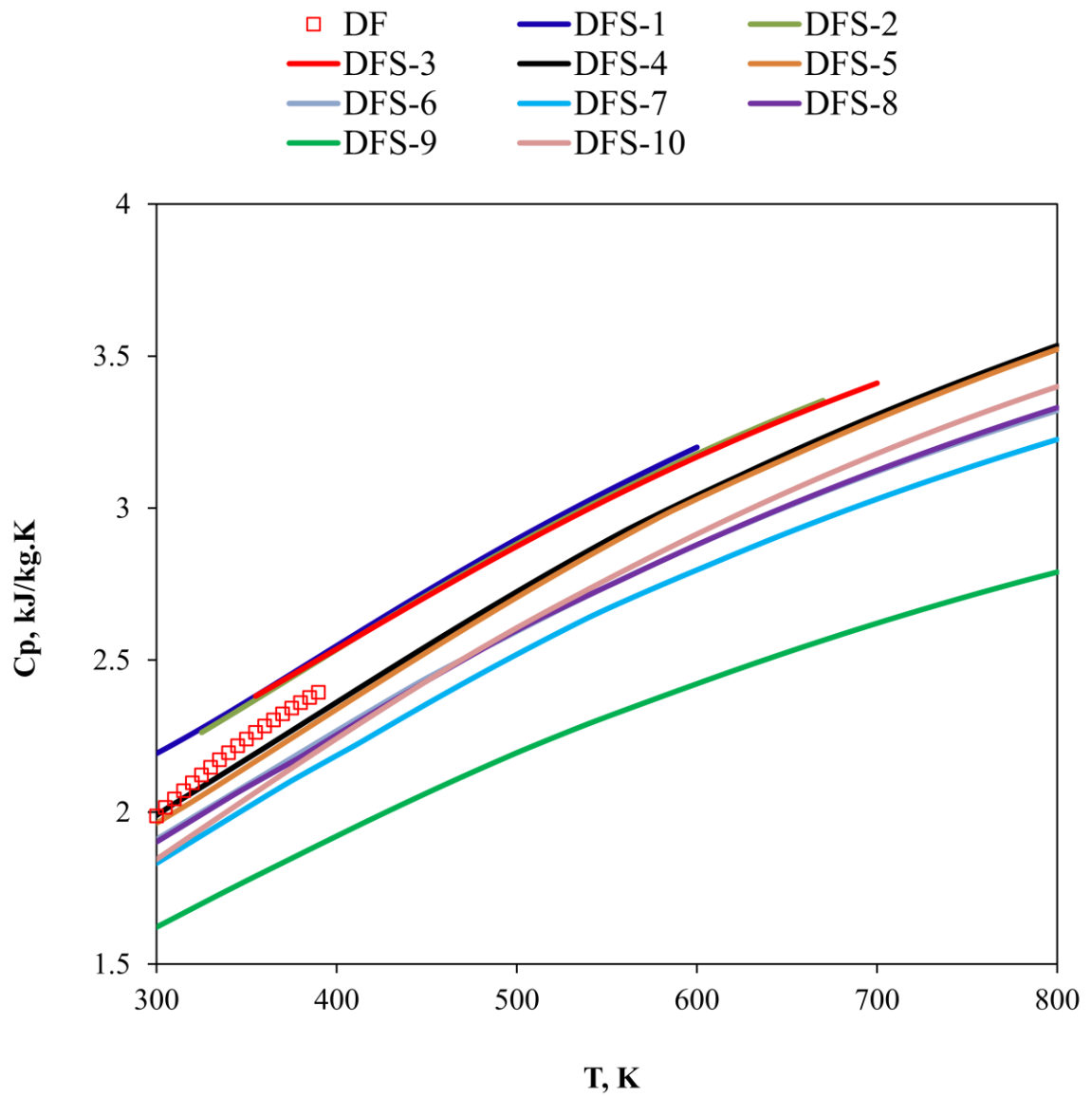


Fig. A-6 Heat capacities of DFSs and DF at 100 MPa.

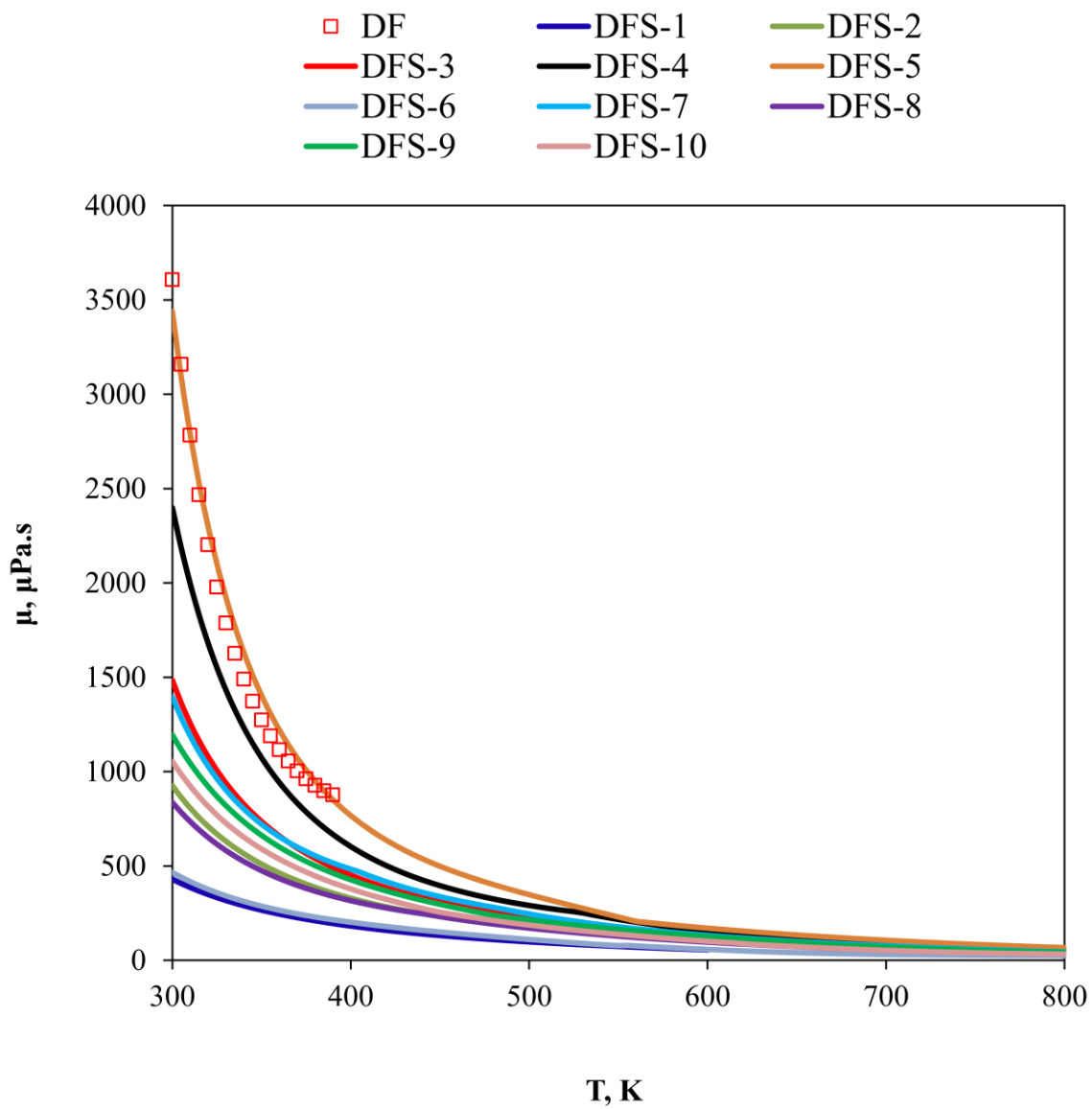


Fig. A-7 Viscosities of DFSs and DF at 10 MPa.

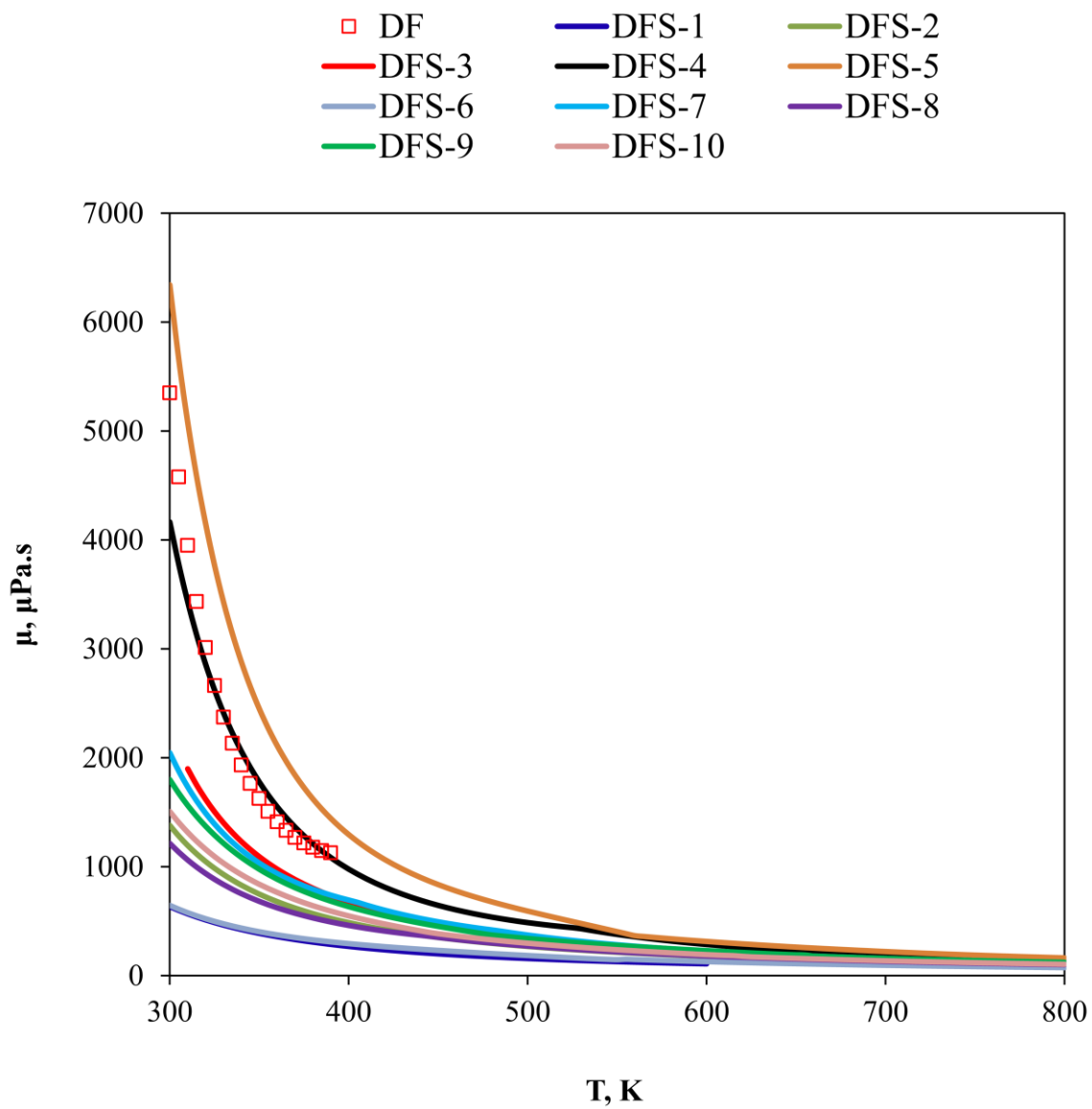


Fig. A-8 Viscosities of DFSs and DF at 50 MPa.

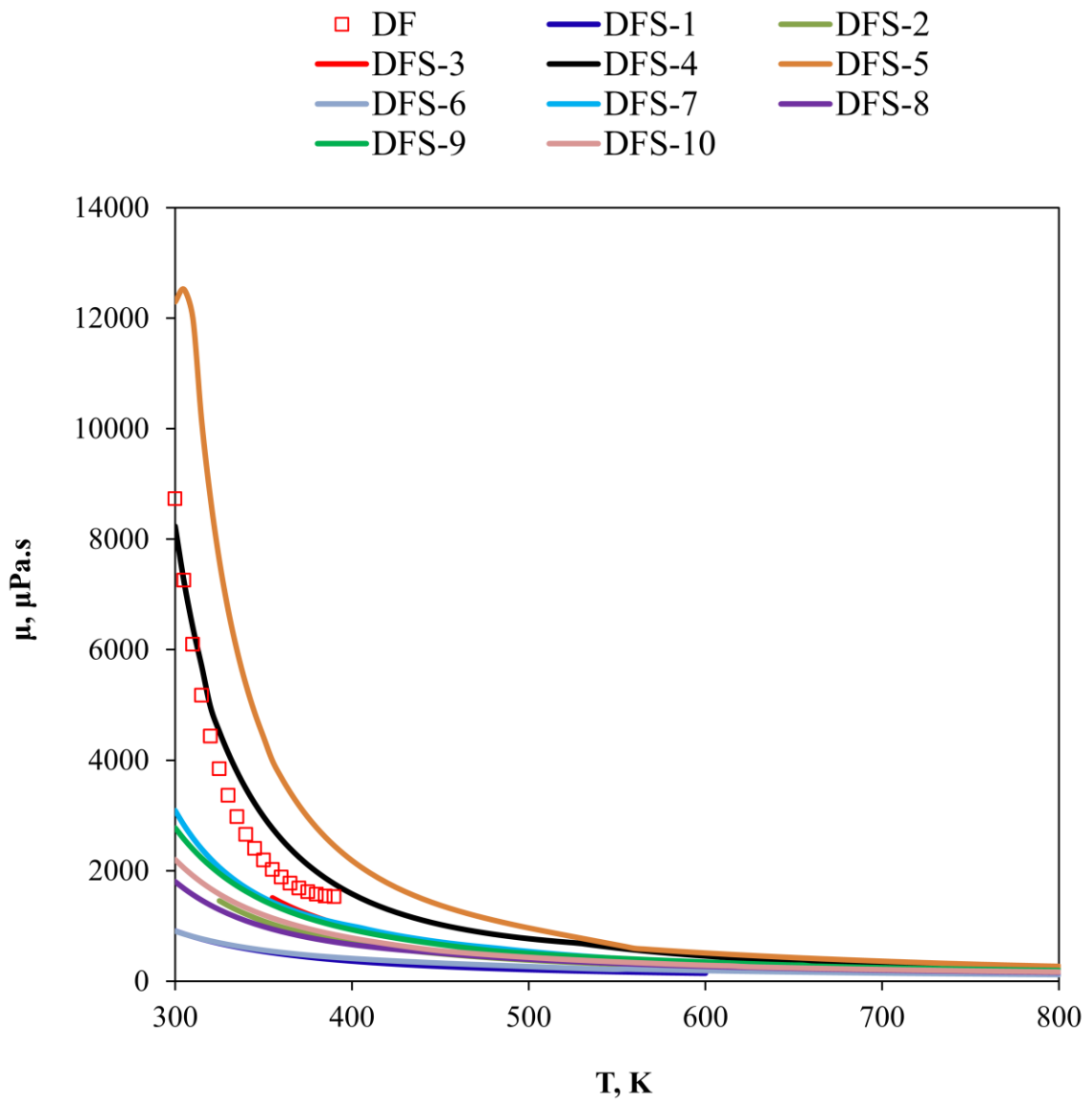


Fig. A-9 Viscosities of DFSs and DF at 100 MPa.

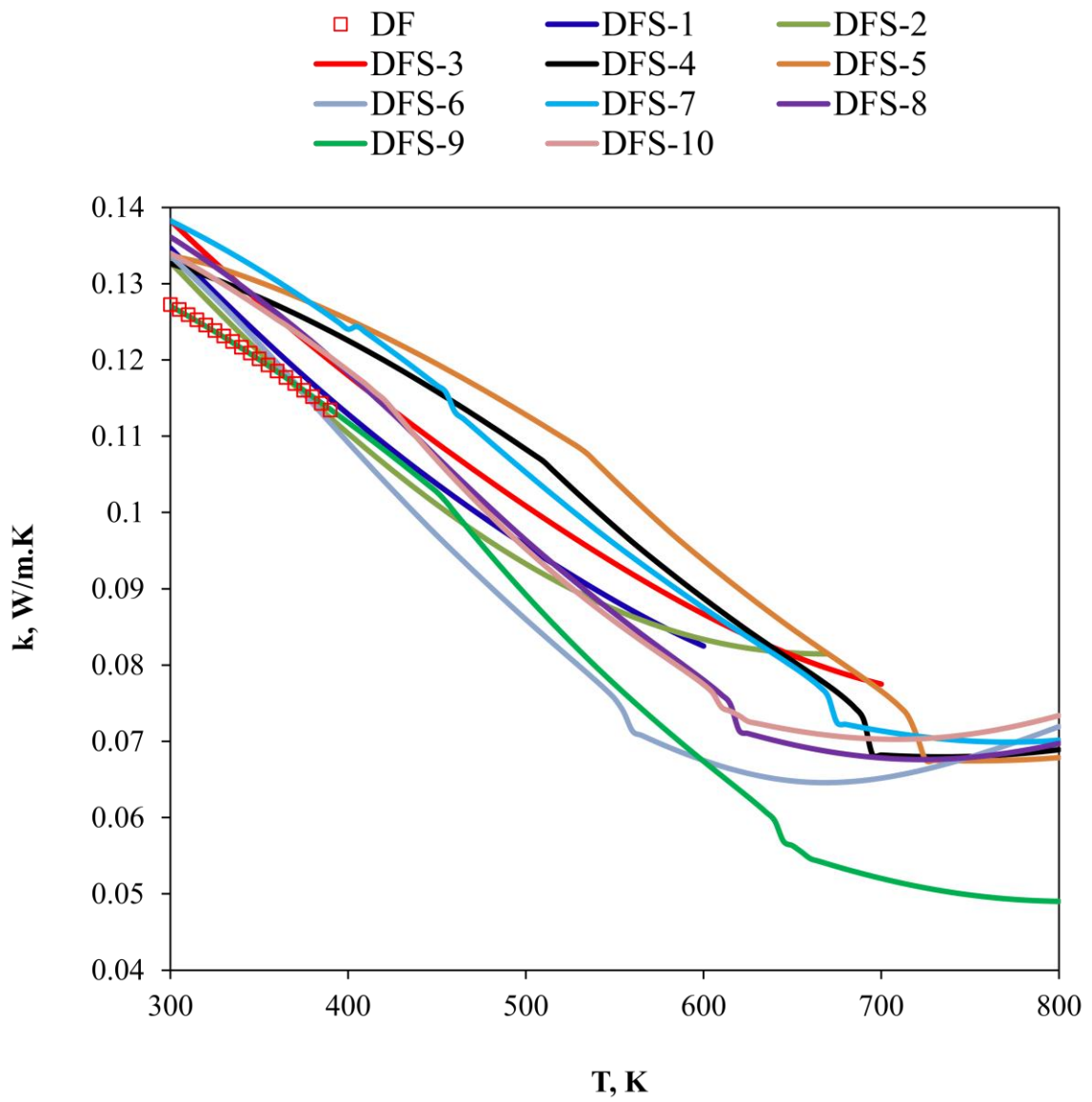


Fig. A-10 Thermal conductivities of DFSs and DF at 10 MPa.

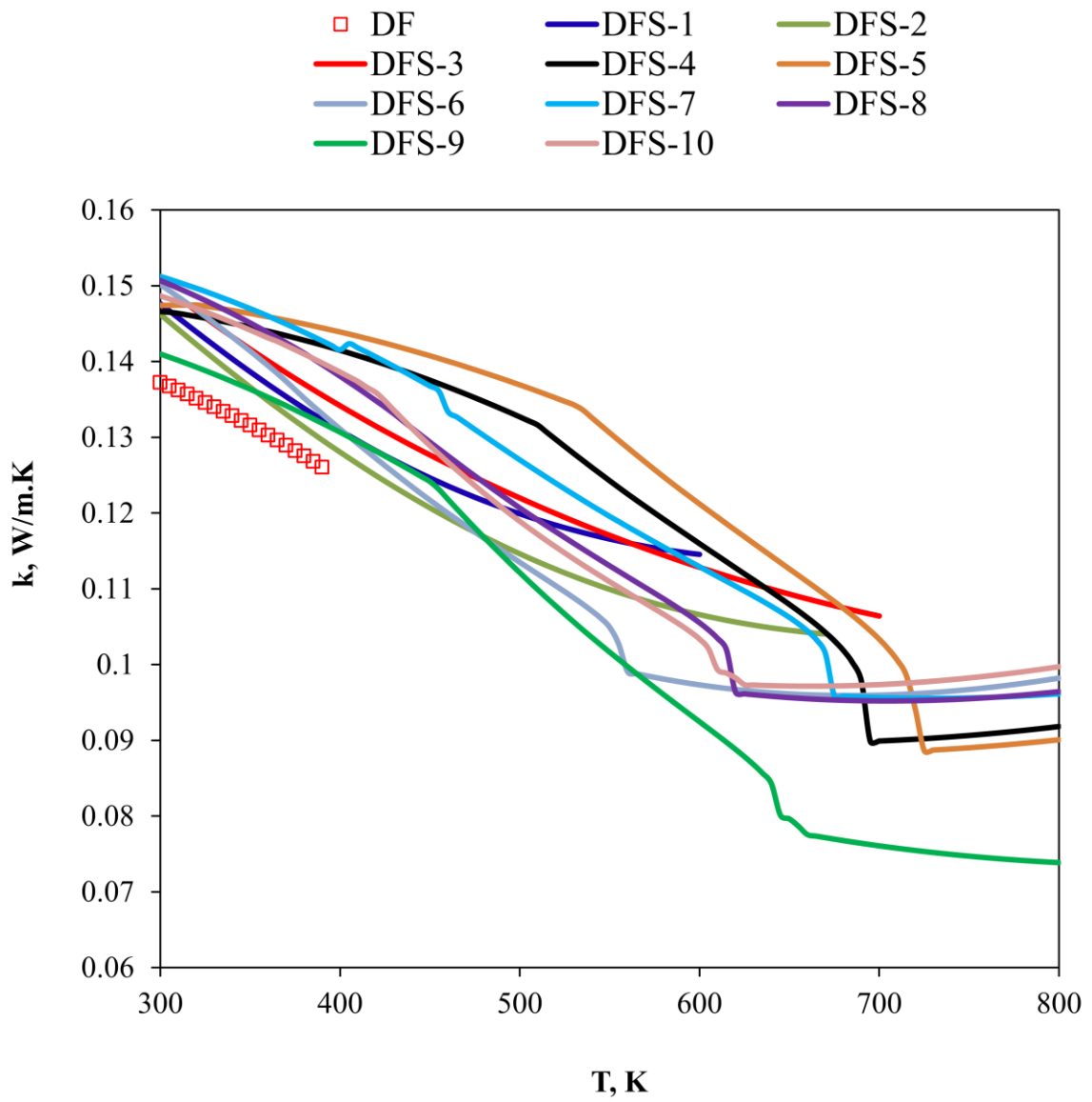


Fig. A-11 Thermal conductivities of DFSs and DF at 50 MPa.

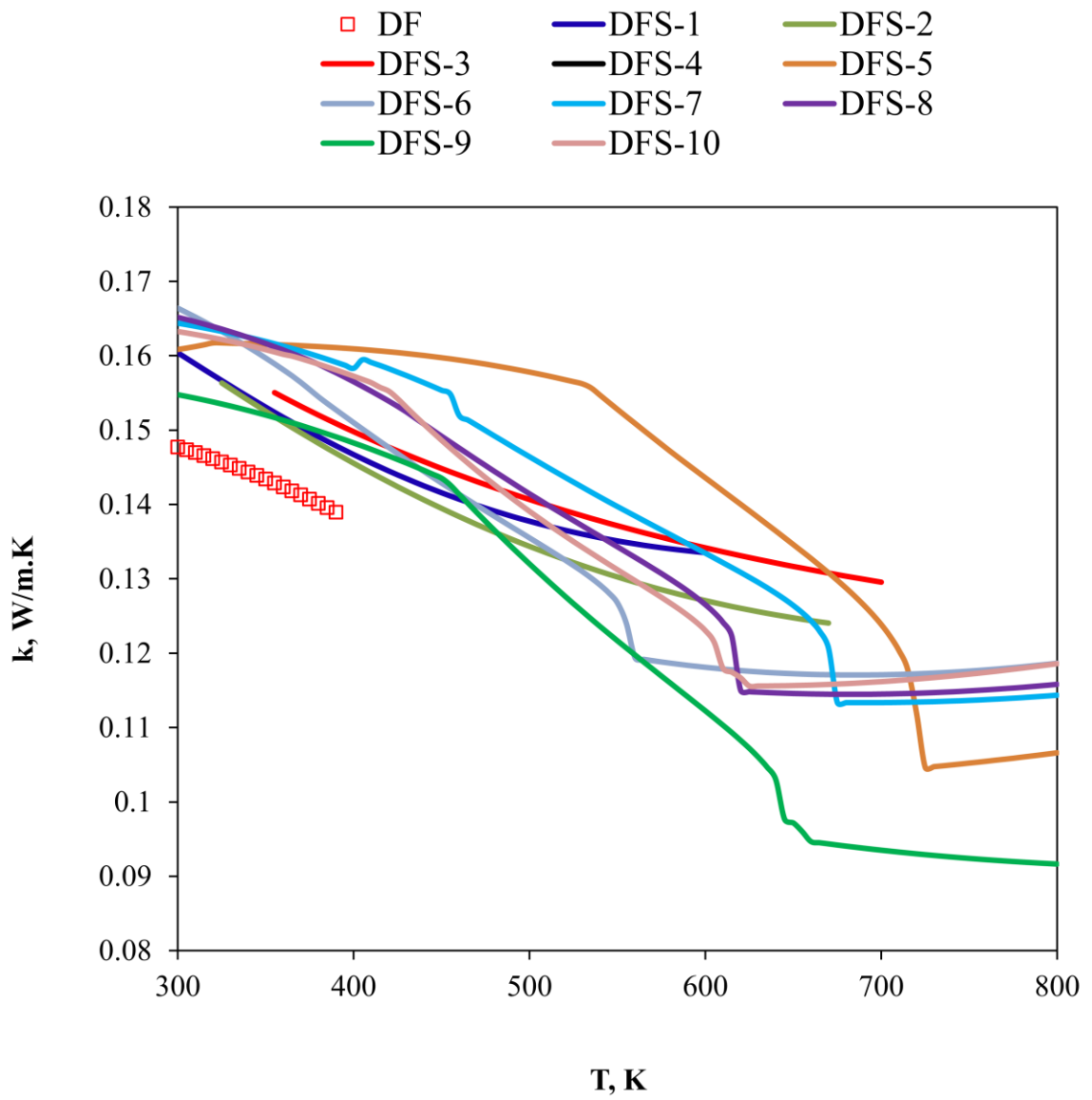


Fig. A-12 Thermal conductivities of DFSs and DF at 100 MPa.

Table A-1 AAD% in prediction of density and heat capacity of DF.

| P, MPa | 10.0 | 30.0 | 50.0 | 100.0 |
|---------------|------|------|------|-------|
| Density | | | | |
| DFS-1 | 18.3 | 17.1 | 16.4 | 15.5 |
| DFS-2 | 12.2 | 11.6 | 11.2 | 11.0 |
| DFS-3 | 9.7 | 9.2 | 9.0 | 10.2 |
| DFS-4 | 7.8 | 7.4 | 7.2 | 7.1 |
| DFS-5 | 6.2 | 5.9 | 5.8 | 5.9 |
| DFS-6 | 11.8 | 10.7 | 10.1 | 9.3 |
| DFS-7 | 0.2 | 0.2 | 0.2 | 0.4 |
| DFS-8 | 6.7 | 6.1 | 5.8 | 5.5 |
| DFS-9 | 5.4 | 4.9 | 4.6 | 4.3 |
| DFS-10 | 5.4 | 4.8 | 4.4 | 4.0 |
| Heat Capacity | | | | |
| DFS-1 | 9.1 | 7.9 | 7.4 | 6.4 |
| DFS-2 | 7.0 | 6.6 | 6.3 | 5.0 |
| DFS-3 | 7.3 | 7.0 | 6.4 | 8.2 |
| DFS-4 | 0.9 | 1.2 | 1.5 | 2.3 |
| DFS-5 | 1.8 | 2.2 | 2.6 | 3.5 |
| DFS-6 | 2.8 | 4.0 | 4.8 | 6.1 |
| DFS-7 | 7.5 | 8.1 | 8.5 | 9.6 |
| DFS-8 | 4.0 | 4.8 | 5.4 | 6.6 |
| DFS-9 | 18.3 | 18.9 | 19.4 | 20.3 |
| DFS-10 | 5.9 | 6.7 | 7.2 | 8.3 |

Table A-2 AAD% in prediction of thermal conductivity and viscosity of DF.

| P, MPa | 10.0 | 30.0 | 50.0 | 100.0 |
|----------------------|------|------|------|-------|
| Thermal conductivity | | | | |
| DFS-1 | 3.1 | 4.8 | 5.8 | 7.1 |
| DFS-2 | 1.6 | 3.0 | 4.3 | 6.3 |
| DFS-3 | 6.7 | 7.5 | 7.9 | 6.9 |
| DFS-4 | 6.5 | 8.4 | 9.6 | 11.3 |
| DFS-5 | 8.1 | 9.8 | 10.9 | 12.4 |
| DFS-6 | 2.3 | 5.3 | 7.6 | 11.4 |
| DFS-7 | 9.6 | 10.8 | 11.6 | 12.8 |
| DFS-8 | 6.5 | 8.7 | 10.2 | 12.6 |
| DFS-9 | 0.1 | 2.1 | 3.6 | 5.9 |
| DFS-10 | 5.6 | 7.9 | 9.5 | 12.0 |
| Viscosity | | | | |
| DFS-1 | 81.0 | 79.4 | 78.6 | 78.6 |
| DFS-2 | 63.2 | 60.4 | 58.6 | 51.6 |
| DFS-3 | 46.3 | 42.0 | 36.9 | 41.1 |
| DFS-4 | 21.0 | 10.0 | 7.7 | 22.9 |
| DFS-5 | 5.8 | 22.7 | 39.9 | 87.9 |
| DFS-6 | 79.4 | 78.3 | 77.7 | 77.6 |
| DFS-7 | 47.1 | 44.2 | 42.0 | 38.9 |
| DFS-8 | 65.7 | 63.7 | 62.2 | 60.5 |
| DFS-9 | 52.2 | 48.7 | 46.0 | 41.9 |
| DFS-10 | 57.5 | 55.2 | 53.7 | 52.2 |

APPENDIX B

TAYLOR DISPERSION ANALYSIS*

The mathematical analysis of Taylor dispersion starts with the continuity equation. In the cylindrical coordinate system, the continuity equation for one component in terms of its concentration C which is a function of time (t), length (z), and pipe radius (r) is given by

$$D_{12} \left[\frac{1}{r} \frac{\partial}{\partial r} \left(r \frac{\partial C}{\partial r} \right) + \frac{\partial^2 C}{\partial z^2} \right] = u \frac{\partial C}{\partial z} + \frac{\partial C}{\partial t} \quad (\text{B-1})$$

where D_{12} is the binary molecular diffusion coefficient of solute 1 in solvent 2 and u is the flow velocity given by

$$u(r) = 2U \left(1 - \frac{r^2}{R^2} \right) \quad (\text{B-2})$$

Inserting Eq. (B-2), Eq. (B-1) becomes

$$D_{12} \left[\frac{1}{r} \frac{\partial}{\partial r} \left(r \frac{\partial C}{\partial r} \right) + \frac{\partial^2 C}{\partial z^2} \right] = 2U \left[1 - \left(\frac{r}{R} \right)^2 \right] \frac{\partial C}{\partial z} + \frac{\partial C}{\partial t} \quad (\text{B-3})$$

As described in Section 4.2.1, the pulse disperses about a plane which moves at a constant mean velocity U , so it is more convenient in the treatment to transfer the static z – coordinate to such a coordinate that moves with the mean velocity of the flow. Thus, we define

* This analysis is based on the work of Taylor (1953;1954), Aris (1956), Alizadeh et al. (1980), Matthews (1986) and Pratt and Wakeham (1975). No citations are placed in the context.

$$x = z - Ut \quad (\text{B-4})$$

Accordingly,

$$dx = dz - Udt \quad (\text{B-5})$$

$$u'(x, r) = u(z, r) - U \quad (\text{B-6})$$

Consequently, Eq. (B-3) can be rewritten as

$$D_{12} \left[\frac{1}{r} \frac{\partial}{\partial r} \left(r \frac{\partial C}{\partial r} \right) + \frac{\partial^2 C}{\partial x^2} \right] = U \left[1 - 2 \left(\frac{r}{R} \right)^2 \right] \frac{\partial C}{\partial x} + \frac{\partial C}{\partial t} \quad (\text{B-7})$$

Generally, the transfer of solute along the tube by molecular diffusion is much smaller than by convection generated by the bulk flow. It is reasonable to assume,

therefore, that $\frac{\partial^2 C}{\partial x^2}$ is insignificant compared with $\frac{1}{r} \frac{\partial}{\partial r} \left(r \frac{\partial C}{\partial r} \right)$. Also, we assume that

$\frac{\partial C}{\partial x}$ is independent of r and $\frac{\partial C}{\partial t} = 0$. Thus, the continuity equation Eq. (B-7) can be

simplified as

$$D_{12} \frac{1}{r} \frac{\partial}{\partial r} \left(r \frac{\partial C}{\partial r} \right) = U \left[1 - 2 \left(\frac{r}{R} \right)^2 \right] \frac{\partial C}{\partial x} \quad (\text{B-8})$$

The boundary conditions for Eq. (B-8) are as follows,

$$\left. \frac{\partial C}{\partial r} \right|_{r=R} = 0 \quad (\text{B-9})$$

$$C(x, 0) = C' \quad (\text{B-10})$$

To solve Eq. (B-8), let

$$C = ar^4 + br^3 + cr^2 + dr + e \quad (\text{B-11})$$

Taking the first and second derivatives with r , it becomes

$$\frac{\partial C}{\partial r} = 4ar^3 + 3br^2 + 2cr + d \quad (\text{B-12})$$

$$\frac{\partial^2 C}{\partial r^2} = 12ar^2 + 6br + 2c \quad (\text{B-13})$$

Solving Eqs. (B-8) - (B-13), the parameters in Eq. (B-11) are obtained

$$a = -\frac{1}{8R^2} \frac{U}{D_{12}} \frac{\partial C}{\partial x} \quad (\text{B-14})$$

$$b = 0 \quad (\text{B-15})$$

$$c = \frac{1}{4} \frac{U}{D_{12}} \frac{\partial C}{\partial x} \quad (\text{B-16})$$

$$d = 0 \quad (\text{B-17})$$

$$e = C' \quad (\text{B-18})$$

Thus, a solution to Eq. (B-8) has the following form

$$C = C' + \frac{R^2 U}{4D_{12}} \frac{\partial C'}{\partial x} \left[\left(\frac{r}{R} \right)^2 - \frac{1}{2} \left(\frac{r}{R} \right)^4 \right] \quad (\text{B-19})$$

In practice, however, it is more convenient to measure the mean concentration (C_m) over any cross section than to measure the concentration (C') in the center of the tube at $r=0$. C_m is defined by

$$C_m = \frac{1}{\pi R^2} \int_0^R C \cdot (2\pi r) \cdot dr \quad (\text{B-20})$$

Substitute Eq. (B-19) into Eq. (B-20) and perform the integration, it gives

$$C_m = C' + \frac{1}{3} \frac{R^2 U}{4D_{12}} \frac{\partial C'}{\partial x} \quad (\text{B-21})$$

Eq. (B-21) can be rewritten in the form

$$C' = C_m - \frac{1}{3} \frac{R^2 U}{4D_{12}} \frac{\partial C_m}{\partial x} \quad (\text{B-22})$$

Substitute Eq. (B-22) into Eq. (B-19) and it gives

$$C = C_m + \frac{R^2 U}{4D_{12}} \frac{\partial C_m}{\partial x} \left[-\frac{1}{3} + \left(\frac{r}{R}\right)^2 - \frac{1}{2} \left(\frac{r}{R}\right)^4 \right] \quad (\text{B-23})$$

Similarly, the continuity Eq. (B-7) can be averaged by multiplying it by $\frac{2r}{R_2}$ and

integrating from 0 to R . This results

$$D_{12} \frac{\partial^2 C_m}{\partial x^2} + \frac{4U}{R^4} \frac{\partial}{\partial x} \left(\int_0^R C r^3 dr \right) - U \frac{\partial C_m}{\partial t} = \frac{\partial C_m}{\partial t} \quad (\text{B-24})$$

Eq. (B-24) can be reduced to the following form by inserting Eq. (B-23)

$$\left(D_{12} + \frac{R^2 U^2}{48D_{12}} \right) \frac{\partial^2 C_m}{\partial x^2} = \frac{\partial C_m}{\partial t} \quad (\text{B-25})$$

or

$$K \frac{\partial^2 C_m}{\partial x^2} = \frac{\partial C_m}{\partial t} \quad (\text{B-26})$$

where,

$$K = D_{12} + \frac{R^2 U^2}{48 D_{12}} \quad (\text{B-27})$$

Eq. (B-26) is known as the one-dimension diffusion equation. K is the apparent diffusion coefficient or called dispersion coefficient. To solve Eq. (B-26), the following initial and boundary conditions are applied

$$C_m(x,0) = \frac{M}{\pi R^2 X} \delta(x) \quad (\text{B-28})$$

$$C_m(\infty, t) = 0 \quad (\text{B-29})$$

where M is the total amount of solute injected, X is the length of the tube occupied by the solute, and $\delta(x)$ is defined by

$$\delta(x) = \begin{cases} +\infty & x = 0 \\ 0 & x \neq 0 \end{cases} \quad (\text{B-30})$$

The similarity method based on dimensional analysis is applied to solve Eq. (B-26). The first step in this analysis is to identify important variables and their dimensions. It is obvious in Eq. (B-26) that C_m is a function of position (x) and time (t). Also, C_m depends on apparent diffusion coefficient (K) and the initial condition. The variables involved in the problem and their dimensions are summarized in Table B-1. Dimension characteristics of mass, length, and time are indicated by M , L , and T , respectively. A is the cross section area of the diffusion column.

Since the mean concentration distribution depends on position, time, diffusion coefficient, and the initial amount of solute, C_m is written as a function of these variables in the following form

Table B-1 Variables and Dimensions.

| Variables | Symbols | Dimensions |
|---|----------------|-------------------|
| Mean concentration | C_m | M/L^3 |
| Initial amount of solute per cross section area | $\frac{M}{A}$ | M/L^2 |
| Apparent Diffusion coefficient | K | L^2/T |
| Position | x | L |
| Time | t | T |

$$C_m = f\left(\frac{M}{A}, K, x, t\right) \quad (\text{B-31})$$

or

$$C_m = \left(\frac{M}{A}\right)^h K^i x^j t^k \quad (\text{B-32})$$

Comparing dimensions of both sides of Eq. (B-32), it gives

$$M/L^3 = (M/L^2)^h (L^2/T)^i L^j T^k \quad (\text{B-33})$$

which results

$$h = 1 \quad (\text{B-34})$$

$$j = -1 - 2i \quad (\text{B-35})$$

$$k = i \quad (\text{B-36})$$

So,

$$\begin{aligned} C_m &= \frac{M}{A} K^i x^{-(1+2i)} t^i \\ &= \frac{M}{Ax} \left(\frac{Kt}{x^2}\right)^i \\ &= \frac{M}{A\sqrt{Kt}} \left(\frac{x}{\sqrt{Kt}}\right)^{-(1+2i)} \end{aligned} \quad (\text{B-37})$$

The dimensional analysis indicates that the solution to Eq. (B-26) is of the form

$$C_m = \frac{M}{A\sqrt{Kt}} f\left(\frac{x}{\sqrt{Kt}}\right) \quad (\text{B-38})$$

with the function f to be determined from the initial and boundary conditions. It is worth pointing out that f is only a function of the dimensionless group $\frac{x}{\sqrt{Kt}}$.

Next, a new variable is introduced in the form,

$$\eta = \frac{x}{\sqrt{Kt}} \quad (\text{B-39})$$

Accordingly, both initial and boundary conditions become,

$$f(\pm\infty) = 0 \quad (\text{B-40})$$

Taking derivatives of η and C_m with t and x , it gives

$$\frac{\partial \eta}{\partial t} = -\frac{\eta}{2t} \quad (\text{B-41})$$

$$\frac{\partial \eta}{\partial x} = \frac{1}{\sqrt{Kt}} \quad (\text{B-42})$$

$$\begin{aligned} \frac{\partial C_m}{\partial t} &= \frac{\partial}{\partial t} \left[\frac{M}{A\sqrt{Kt}} f(\eta) \right] \\ &= \frac{M}{A\sqrt{Kt}} \frac{\partial f}{\partial \eta} \frac{\partial \eta}{\partial t} + f \frac{\partial}{\partial t} \left(\frac{M}{A\sqrt{Kt}} \right) \\ &= \frac{M}{A\sqrt{Kt}} \frac{\partial f}{\partial \eta} \left(-\frac{\eta}{2t} \right) - \frac{1}{2t} f \frac{M}{A\sqrt{Kt}} \\ &= -\frac{M}{2At\sqrt{Kt}} \left(f + \eta \frac{\partial f}{\partial \eta} \right) \end{aligned} \quad (\text{B-43})$$

$$\begin{aligned}\frac{\partial C_m}{\partial x} &= \frac{M}{A\sqrt{Kt}} \frac{\partial f}{\partial \eta} \frac{\partial \eta}{\partial x} \\ &= \frac{M}{A\sqrt{Kt}} \frac{\partial f}{\partial \eta} \frac{1}{\sqrt{Kt}}\end{aligned}\quad (\text{B-44})$$

$$\begin{aligned}\frac{\partial^2 C_m}{\partial x^2} &= \frac{M}{AKt} \frac{\partial^2 f}{\partial \eta^2} \frac{\partial \eta}{\partial x} \\ &= \frac{M}{AKt\sqrt{Kt}} \frac{\partial^2 f}{\partial \eta^2}\end{aligned}\quad (\text{B-45})$$

Inserting Eqs. (B-43) and (B-45), Eq. (B-26) becomes

$$K \frac{M}{AKt\sqrt{Kt}} \frac{\partial^2 f}{\partial \eta^2} = -\frac{M}{2At\sqrt{Kt}} \left(f + \eta \frac{\partial f}{\partial \eta} \right) \quad (\text{B-46})$$

which can be further simplified as

$$\frac{\partial^2 f}{\partial \eta^2} + \frac{1}{2} \left(f + \eta \frac{\partial f}{\partial \eta} \right) = 0 \quad (\text{B-47})$$

The dimensional analysis has successfully reduced the two-variable partial differential equation to a one-variable ordinary differential equation.

To solve Eq. (B-47), the equation is first rearranged to have the following form

$$\frac{\partial^2 f}{\partial \eta^2} + \frac{1}{2} \frac{\partial(f\eta)}{\partial \eta} = 0 \quad (\text{B-48})$$

which can then be rewritten as an exact differential equation

$$\frac{d}{d\eta} \left(\frac{df}{d\eta} + \frac{1}{2} f\eta \right) = 0 \quad (\text{B-49})$$

Applying boundary conditions and integrating once, it gives

$$\frac{df}{d\eta} + \frac{1}{2} f\eta = 0 \quad (\text{B-50})$$

A solution to Eq. (B-50) can be easily found of the form

$$f(\eta) = \alpha \exp\left(-\frac{1}{4}\eta^2\right) \quad (\text{B-51})$$

where α is a constant to be determined.

A mass balance gives

$$\begin{aligned} M &= \int_V C_m(x, t) dV \\ &= \int_{-\infty}^{+\infty} \int_0^R C_m dx (2\pi r) dr \\ &= \int_{-\infty}^{+\infty} \int_0^R \frac{Mf}{A\sqrt{D_{12}t}} (\sqrt{D_{12}t} d\eta) (2\pi r) dr \\ &= \frac{2M}{R^2} \int_0^R r dr \int_{-\infty}^{+\infty} f d\eta \end{aligned} \quad (\text{B-52})$$

Therefore,

$$\int_{-\infty}^{+\infty} f d\eta = 1 \quad (\text{B-53})$$

Inserting Eq. (B-51), Eq. (B-53) reads

$$\int_{-\infty}^{+\infty} \alpha \exp\left(-\frac{1}{4}\eta^2\right) d\eta = 1 \quad (\text{B-54})$$

Rearranging the equation, it gives

$$\int_{-\infty}^{+\infty} \exp\left[-\left(\frac{\eta}{2}\right)^2\right] d\left(\frac{\eta}{2}\right) = \frac{1}{2\alpha} \quad (\text{B-55})$$

The integration on the left side of Eq. (B-55) can be calculated in the following way. Let $x = \frac{\eta}{2} = y$, the integration equals to B as

$$B = \int_{-\infty}^{+\infty} \exp(-x^2) dx = \int_{-\infty}^{+\infty} \exp(-y^2) dy \quad (\text{B-56})$$

So,

$$\begin{aligned} B^2 &= \int_{-\infty}^{+\infty} \exp(-x^2) dx \int_{-\infty}^{+\infty} \exp(-y^2) dy \\ &= \int_{-\infty}^{+\infty} \int_{-\infty}^{+\infty} \exp(-x^2) \exp(-y^2) dx dy \end{aligned} \quad (\text{B-57})$$

Changing Cartesian coordinates to polar coordinates, Eq. (B-57) becomes

$$B^2 = \int_0^{2\pi} \int_0^{\infty} \exp(-r^2) r dr d\theta = \pi \quad (\text{B-58})$$

Thus,

$$\alpha = \frac{1}{2\sqrt{\pi}} \quad (\text{B-59})$$

Finally, the expression for C_m reads

$$C_m(x, t) = \frac{M}{\pi R^2 \sqrt{4\pi Kt}} \exp[-x^2/4Kt] \quad (\text{B-60})$$

APPENDIX C

LITERATURE DATA

Table C-1 Diffusion Coefficients of Benzene in CO₂.

| T, K | P, MPa | ρ, kg/m³ | D₁₂, 10⁹ m²/s | Ref.* |
|-------------|---------------|--|---|--------------|
| 307.95 | 9.68 | 702.86 | 14.90 | 1 |
| 307.95 | 9.68 | 702.86 | 15.90 | 1 |
| 307.95 | 9.68 | 702.86 | 17.40 | 1 |
| 307.95 | 12.46 | 777.77 | 13.70 | 1 |
| 309.65 | 10.24 | 701.36 | 15.30 | 1 |
| 309.65 | 10.24 | 701.36 | 16.20 | 1 |
| 309.65 | 10.25 | 701.76 | 14.90 | 1 |
| 314.15 | 10.00 | 606.55 | 19.80 | 1 |
| 314.15 | 13.53 | 745.62 | 15.10 | 1 |
| 313.15 | 7.86 | 263.00 | 24.02 | 2 |
| 313.15 | 8.37 | 329.44 | 23.39 | 2 |
| 313.15 | 8.81 | 431.99 | 20.86 | 2 |
| 313.15 | 9.35 | 558.75 | 19.47 | 2 |
| 313.15 | 9.76 | 608.41 | 17.52 | 2 |
| 313.15 | 10.30 | 648.82 | 16.15 | 2 |
| 313.15 | 10.79 | 674.42 | 15.55 | 2 |
| 313.15 | 11.82 | 712.44 | 14.25 | 2 |
| 313.15 | 12.81 | 738.70 | 13.20 | 2 |
| 313.15 | 13.61 | 755.84 | 12.75 | 2 |
| 313.15 | 14.71 | 775.58 | 12.45 | 2 |
| 313.15 | 15.69 | 790.56 | 12.38 | 2 |
| 313.15 | 16.67 | 803.75 | 11.82 | 2 |
| 313.15 | 17.56 | 814.53 | 11.28 | 2 |
| 313.15 | 2.21 | 41.49 | 59.33 | 3 |
| 313.15 | 2.84 | 55.23 | 56.06 | 3 |
| 313.15 | 3.82 | 79.00 | 46.39 | 3 |
| 313.15 | 3.82 | 79.00 | 44.60 | 3 |
| 313.15 | 4.70 | 103.68 | 40.69 | 3 |
| 313.15 | 4.70 | 103.68 | 38.82 | 3 |
| 313.15 | 4.85 | 108.30 | 42.22 | 3 |
| 313.15 | 5.68 | 136.68 | 30.73 | 3 |
| 313.15 | 5.68 | 136.68 | 30.97 | 3 |
| 313.15 | 5.68 | 136.68 | 34.27 | 3 |
| 313.15 | 5.68 | 136.68 | 32.21 | 3 |
| 313.15 | 6.14 | 155.13 | 4.72 | 3 |
| 313.15 | 6.19 | 157.29 | 4.38 | 3 |
| 313.15 | 6.71 | 181.98 | 1.73 | 3 |
| 313.15 | 6.71 | 181.98 | 2.05 | 3 |
| 313.15 | 6.71 | 181.98 | 2.19 | 3 |
| 313.15 | 7.11 | 204.67 | 1.87 | 3 |

| T, K | P, MPa | ρ, kg/m³ | D_{12}, 10⁹ m²/s | Ref.* |
|-------------|---------------|--|--|--------------|
| 313.15 | 7.11 | 204.67 | 1.66 | 3 |
| 313.15 | 7.11 | 204.67 | 1.41 | 3 |
| 313.15 | 7.68 | 246.24 | 9.86 | 3 |
| 313.15 | 7.68 | 246.24 | 10.94 | 3 |
| 313.15 | 7.68 | 246.24 | 10.82 | 3 |
| 313.15 | 8.18 | 300.29 | 18.44 | 3 |
| 313.15 | 8.18 | 300.29 | 18.34 | 3 |
| 313.15 | 8.18 | 300.29 | 19.61 | 3 |
| 313.15 | 8.72 | 406.53 | 24.90 | 3 |
| 313.15 | 8.72 | 406.53 | 25.04 | 3 |
| 313.15 | 8.72 | 406.53 | 23.90 | 3 |
| 313.15 | 9.21 | 534.02 | 22.05 | 3 |
| 313.15 | 9.21 | 534.02 | 23.82 | 3 |
| 313.15 | 9.21 | 534.02 | 23.40 | 3 |
| 313.15 | 9.70 | 602.58 | 18.94 | 3 |
| 313.15 | 9.70 | 602.58 | 18.42 | 3 |
| 313.15 | 9.70 | 602.58 | 19.72 | 3 |
| 313.15 | 10.68 | 669.27 | 17.12 | 3 |
| 313.15 | 10.68 | 669.27 | 17.20 | 3 |
| 313.15 | 10.68 | 669.27 | 17.10 | 3 |
| 313.15 | 12.64 | 734.66 | 13.88 | 3 |
| 313.15 | 12.64 | 734.66 | 13.78 | 3 |
| 313.15 | 12.64 | 734.66 | 13.87 | 3 |
| 313.15 | 14.70 | 775.42 | 12.87 | 3 |
| 313.15 | 14.70 | 775.42 | 12.81 | 3 |
| 313.15 | 14.70 | 775.42 | 12.85 | 3 |
| 313.15 | 16.71 | 804.26 | 11.56 | 3 |
| 313.15 | 16.71 | 804.26 | 11.52 | 3 |
| 313.15 | 16.71 | 804.26 | 11.55 | 3 |
| 308.15 | 5.99 | 158.31 | 64.11 | 4 |
| 308.15 | 5.99 | 158.31 | 64.42 | 4 |
| 308.15 | 6.43 | 181.28 | 49.96 | 4 |
| 308.15 | 6.44 | 181.86 | 56.63 | 4 |
| 308.15 | 6.67 | 196.00 | 60.73 | 4 |
| 308.15 | 7.03 | 222.56 | 49.18 | 4 |
| 308.15 | 7.03 | 222.56 | 49.28 | 4 |
| 308.15 | 7.21 | 238.91 | 45.42 | 4 |
| 308.15 | 7.52 | 275.85 | 29.64 | 4 |
| 308.15 | 7.53 | 277.33 | 24.53 | 4 |
| 308.15 | 7.56 | 281.92 | 24.37 | 4 |
| 308.15 | 7.58 | 285.12 | 31.10 | 4 |
| 308.15 | 7.58 | 285.12 | 33.84 | 4 |
| 308.15 | 7.59 | 286.76 | 34.08 | 4 |
| 308.15 | 7.59 | 286.76 | 34.23 | 4 |

| T, K | P, MPa | ρ, kg/m³ | D_{12}, 10⁹ m²/s | Ref.* |
|-------------|---------------|--|--|--------------|
| 308.15 | 7.59 | 286.76 | 30.28 | 4 |
| 308.15 | 7.61 | 290.15 | 29.65 | 4 |
| 308.15 | 8.11 | 497.21 | 24.24 | 4 |
| 308.15 | 8.12 | 503.39 | 24.01 | 4 |
| 308.15 | 8.30 | 574.13 | 22.70 | 4 |
| 308.15 | 8.41 | 597.53 | 22.53 | 4 |
| 308.15 | 8.44 | 602.75 | 21.52 | 4 |
| 308.15 | 8.44 | 602.75 | 21.53 | 4 |
| 308.15 | 8.48 | 609.13 | 20.96 | 4 |
| 308.15 | 8.85 | 650.45 | 20.18 | 4 |
| 308.15 | 8.87 | 652.12 | 19.27 | 4 |
| 308.15 | 8.88 | 652.94 | 19.22 | 4 |
| 308.15 | 9.00 | 662.13 | 19.35 | 4 |
| 308.15 | 9.41 | 686.98 | 18.14 | 4 |
| 308.15 | 9.79 | 704.53 | 17.20 | 4 |
| 308.15 | 9.92 | 709.75 | 17.92 | 4 |
| 308.15 | 10.10 | 716.48 | 17.44 | 4 |
| 308.15 | 10.59 | 732.49 | 16.63 | 4 |
| 308.15 | 11.08 | 746.03 | 16.55 | 4 |
| 308.15 | 11.66 | 759.83 | 16.23 | 4 |
| 308.15 | 12.11 | 769.30 | 15.88 | 4 |
| 308.15 | 12.53 | 777.38 | 15.99 | 4 |
| 308.15 | 13.11 | 787.55 | 15.29 | 4 |
| 308.15 | 13.57 | 794.95 | 15.71 | 4 |
| 308.15 | 13.94 | 800.53 | 14.87 | 4 |
| 308.15 | 14.48 | 808.18 | 15.09 | 4 |
| 308.15 | 15.75 | 824.27 | 14.03 | 4 |
| 308.15 | 16.10 | 828.31 | 14.45 | 4 |
| 308.15 | 16.70 | 834.92 | 14.27 | 4 |
| 308.15 | 18.16 | 849.56 | 13.85 | 4 |
| 308.15 | 19.03 | 857.48 | 13.37 | 4 |
| 308.15 | 20.16 | 867.03 | 13.52 | 4 |
| 308.15 | 21.09 | 874.37 | 13.02 | 4 |
| 308.15 | 22.13 | 882.08 | 12.94 | 4 |
| 308.15 | 25.14 | 902.09 | 12.44 | 4 |
| 308.15 | 25.18 | 902.34 | 12.56 | 4 |
| 308.15 | 25.18 | 902.34 | 12.36 | 4 |
| 308.15 | 27.72 | 917.10 | 12.17 | 4 |
| 308.15 | 30.29 | 930.56 | 12.04 | 4 |
| 313.15 | 7.55 | 235.44 | 50.47 | 4 |
| 313.15 | 7.62 | 241.13 | 47.69 | 4 |
| 313.15 | 7.62 | 241.13 | 43.31 | 4 |
| 313.15 | 7.66 | 244.51 | 42.72 | 4 |
| 313.15 | 8.80 | 429.10 | 23.44 | 4 |

| T, K | P, MPa | ρ, kg/m³ | D_{12}, 10⁹ m²/s | Ref.* |
|-------------|---------------|--|--|--------------|
| 313.15 | 9.02 | 490.71 | 23.41 | 4 |
| 313.15 | 9.29 | 548.82 | 22.70 | 4 |
| 313.15 | 9.58 | 589.70 | 21.58 | 4 |
| 313.15 | 9.92 | 622.36 | 20.60 | 4 |
| 313.15 | 10.32 | 650.02 | 19.43 | 4 |
| 313.15 | 10.70 | 670.22 | 19.14 | 4 |
| 313.15 | 11.07 | 686.37 | 18.76 | 4 |
| 313.15 | 11.09 | 687.16 | 18.58 | 4 |
| 313.15 | 11.57 | 704.51 | 18.09 | 4 |
| 313.15 | 12.13 | 721.43 | 17.45 | 4 |
| 313.15 | 12.20 | 723.36 | 17.27 | 4 |
| 313.15 | 13.11 | 745.47 | 17.16 | 4 |
| 313.15 | 13.22 | 747.84 | 16.90 | 4 |
| 313.15 | 13.30 | 749.53 | 16.72 | 4 |
| 313.15 | 13.62 | 756.04 | 16.80 | 4 |
| 313.15 | 14.40 | 770.38 | 16.16 | 4 |
| 313.15 | 14.42 | 770.72 | 16.12 | 4 |
| 313.15 | 16.08 | 796.00 | 15.71 | 4 |
| 313.15 | 16.11 | 796.40 | 15.31 | 4 |
| 313.15 | 16.12 | 796.54 | 15.40 | 4 |
| 313.15 | 16.13 | 796.68 | 15.31 | 4 |
| 313.15 | 16.16 | 797.08 | 15.38 | 4 |
| 313.15 | 16.43 | 800.66 | 15.68 | 4 |
| 313.15 | 18.16 | 821.27 | 14.68 | 4 |
| 313.15 | 20.08 | 840.56 | 14.05 | 4 |
| 313.15 | 20.16 | 841.30 | 14.02 | 4 |
| 313.15 | 21.17 | 850.28 | 13.88 | 4 |
| 313.15 | 21.18 | 850.37 | 13.81 | 4 |
| 313.15 | 22.12 | 858.17 | 13.53 | 4 |
| 313.15 | 22.15 | 858.41 | 13.71 | 4 |
| 313.15 | 25.17 | 880.64 | 12.62 | 4 |
| 313.15 | 25.19 | 880.78 | 12.85 | 4 |
| 313.15 | 25.27 | 881.32 | 13.16 | 4 |
| 313.15 | 27.71 | 896.80 | 12.33 | 4 |
| 313.15 | 30.28 | 911.41 | 12.13 | 4 |
| 313.15 | 34.48 | 932.41 | 11.62 | 4 |
| 318.15 | 9.28 | 378.02 | 24.79 | 4 |
| 318.15 | 9.60 | 431.98 | 23.89 | 4 |
| 318.15 | 9.94 | 489.07 | 23.33 | 4 |
| 318.15 | 10.18 | 523.64 | 24.65 | 4 |
| 318.15 | 11.00 | 603.15 | 21.70 | 4 |
| 318.15 | 11.96 | 656.01 | 19.91 | 4 |
| 318.15 | 13.01 | 693.95 | 18.76 | 4 |
| 318.15 | 14.03 | 721.18 | 18.06 | 4 |

| T, K | P, MPa | ρ, kg/m³ | D_{12}, 10⁹ m²/s | Ref.* |
|-------------|---------------|--|--|--------------|
| 318.15 | 15.08 | 743.52 | 17.13 | 4 |
| 318.15 | 16.05 | 760.81 | 16.64 | 4 |
| 318.15 | 17.00 | 775.53 | 16.19 | 4 |
| 318.15 | 17.98 | 788.98 | 15.71 | 4 |
| 318.15 | 19.06 | 802.23 | 15.34 | 4 |
| 318.15 | 20.06 | 813.33 | 14.98 | 4 |
| 318.15 | 20.56 | 818.52 | 15.11 | 4 |
| 318.15 | 21.07 | 823.60 | 14.66 | 4 |
| 318.15 | 22.03 | 832.64 | 14.54 | 4 |
| 318.15 | 23.03 | 841.42 | 14.29 | 4 |
| 318.15 | 24.08 | 850.03 | 13.91 | 4 |
| 318.15 | 25.00 | 857.14 | 13.76 | 4 |
| 318.15 | 25.96 | 864.17 | 13.67 | 4 |
| 318.15 | 27.07 | 871.87 | 13.69 | 4 |
| 318.15 | 27.98 | 877.87 | 13.29 | 4 |
| 318.15 | 29.03 | 884.48 | 13.17 | 4 |
| 318.15 | 30.18 | 891.38 | 12.91 | 4 |
| 323.15 | 10.09 | 395.11 | 24.56 | 4 |
| 323.15 | 10.28 | 418.40 | 23.85 | 4 |
| 323.15 | 10.49 | 444.33 | 23.30 | 4 |
| 323.15 | 10.67 | 465.96 | 23.45 | 4 |
| 323.15 | 10.88 | 489.83 | 23.67 | 4 |
| 323.15 | 11.12 | 514.79 | 25.96 | 4 |
| 323.15 | 11.47 | 546.39 | 24.08 | 4 |
| 323.15 | 11.95 | 581.51 | 23.27 | 4 |
| 323.15 | 12.08 | 589.68 | 23.18 | 4 |
| 323.15 | 13.13 | 641.47 | 21.10 | 4 |
| 323.15 | 14.00 | 672.17 | 19.57 | 4 |
| 323.15 | 15.13 | 702.91 | 18.87 | 4 |
| 323.15 | 15.33 | 707.60 | 18.79 | 4 |
| 323.15 | 16.07 | 723.50 | 18.35 | 4 |
| 323.15 | 17.06 | 741.92 | 17.68 | 4 |
| 323.15 | 18.03 | 757.58 | 17.09 | 4 |
| 323.15 | 19.00 | 771.45 | 16.44 | 4 |
| 323.15 | 20.00 | 784.29 | 15.95 | 4 |
| 323.15 | 21.09 | 796.94 | 15.60 | 4 |
| 323.15 | 22.05 | 807.12 | 15.66 | 4 |
| 323.15 | 23.05 | 816.93 | 15.48 | 4 |
| 323.15 | 24.07 | 826.24 | 14.77 | 4 |
| 323.15 | 25.03 | 834.44 | 14.49 | 4 |
| 323.15 | 26.09 | 842.95 | 14.44 | 4 |
| 323.15 | 27.06 | 850.29 | 14.25 | 4 |
| 323.15 | 28.01 | 857.12 | 14.04 | 4 |
| 323.15 | 28.96 | 863.63 | 13.67 | 4 |

| T, K | P, MPa | ρ, kg/m³ | D_{12}, 10⁹ m²/s | Ref.* |
|-------------|---------------|--|--|--------------|
| 323.15 | 30.19 | 871.64 | 13.56 | 4 |
| 328.15 | 9.05 | 258.54 | 31.50 | 4 |
| 328.15 | 9.74 | 304.92 | 28.54 | 4 |
| 328.15 | 9.98 | 323.47 | 27.49 | 4 |
| 328.15 | 9.99 | 324.27 | 27.40 | 4 |
| 328.15 | 10.64 | 380.86 | 26.00 | 4 |
| 328.15 | 11.24 | 437.73 | 24.66 | 4 |
| 328.15 | 11.56 | 467.26 | 24.60 | 4 |
| 328.15 | 12.07 | 509.99 | 24.64 | 4 |
| 328.15 | 12.55 | 544.21 | 23.88 | 4 |
| 328.15 | 13.14 | 578.38 | 23.25 | 4 |
| 328.15 | 13.43 | 593.50 | 22.31 | 4 |
| 328.15 | 14.10 | 622.40 | 21.59 | 4 |
| 328.15 | 15.08 | 655.94 | 20.40 | 4 |
| 328.15 | 16.13 | 684.31 | 19.19 | 4 |
| 328.15 | 16.90 | 701.72 | 18.94 | 4 |
| 328.15 | 17.16 | 707.10 | 18.65 | 4 |
| 328.15 | 17.99 | 722.90 | 18.40 | 4 |
| 328.15 | 19.03 | 740.28 | 17.62 | 4 |
| 328.15 | 19.78 | 751.49 | 17.15 | 4 |
| 328.15 | 20.06 | 755.44 | 17.70 | 4 |
| 328.15 | 21.03 | 768.26 | 16.72 | 4 |
| 328.15 | 21.99 | 779.82 | 16.38 | 4 |
| 328.15 | 23.03 | 791.29 | 15.84 | 4 |
| 328.15 | 23.96 | 800.78 | 15.98 | 4 |
| 328.15 | 24.68 | 807.69 | 15.71 | 4 |
| 328.15 | 25.75 | 817.35 | 15.28 | 4 |
| 328.15 | 26.83 | 826.46 | 15.17 | 4 |
| 328.15 | 29.23 | 844.80 | 14.54 | 4 |
| 313.15 | 8.43 | 340.20 | 25.80 | 5 |
| 313.15 | 8.53 | 360.21 | 24.50 | 5 |
| 313.15 | 8.63 | 383.16 | 23.60 | 5 |
| 313.15 | 8.73 | 409.28 | 25.40 | 5 |
| 313.15 | 9.02 | 490.71 | 21.60 | 5 |
| 313.15 | 9.32 | 553.90 | 20.70 | 5 |
| 313.15 | 9.41 | 567.80 | 21.60 | 5 |
| 313.15 | 9.51 | 581.27 | 19.40 | 5 |
| 313.15 | 10.00 | 628.61 | 17.70 | 5 |
| 313.15 | 10.90 | 679.30 | 16.20 | 5 |
| 313.15 | 11.00 | 683.52 | 15.60 | 5 |
| 313.15 | 11.10 | 687.56 | 16.60 | 5 |
| 313.15 | 11.20 | 691.43 | 15.80 | 5 |
| 313.15 | 12.00 | 717.76 | 15.40 | 5 |
| 313.15 | 12.10 | 720.60 | 15.60 | 5 |

| T, K | P, MPa | ρ, kg/m³ | D_{12}, 10⁹ m²/s | Ref.* |
|-------------|---------------|--|--|--------------|
| 313.15 | 12.70 | 736.10 | 14.90 | 5 |
| 313.15 | 12.80 | 738.47 | 15.30 | 5 |
| 313.15 | 12.90 | 740.78 | 14.70 | 5 |
| 313.15 | 14.60 | 773.76 | 14.10 | 5 |
| 313.15 | 14.70 | 775.42 | 13.30 | 5 |
| 313.15 | 16.10 | 796.27 | 13.80 | 5 |
| 313.15 | 16.20 | 797.62 | 14.10 | 5 |
| 313.15 | 19.50 | 835.05 | 12.80 | 5 |
| 313.15 | 19.70 | 836.98 | 13.00 | 5 |
| 313.15 | 19.80 | 837.93 | 13.20 | 5 |
| 313.15 | 19.90 | 838.87 | 11.70 | 5 |
| 313.15 | 24.50 | 876.03 | 11.50 | 5 |
| 313.15 | 24.60 | 876.73 | 11.60 | 5 |
| 313.15 | 24.70 | 877.42 | 11.60 | 5 |
| 313.15 | 30.00 | 909.89 | 11.30 | 5 |
| 313.15 | 30.20 | 910.97 | 10.60 | 5 |
| 313.15 | 11.00 | 683.52 | 21.30 | 6 |
| 313.15 | 13.00 | 743.04 | 16.50 | 6 |
| 313.15 | 15.50 | 787.81 | 14.90 | 6 |
| 313.15 | 16.00 | 794.90 | 14.50 | 6 |
| 313.15 | 21.50 | 853.08 | 12.80 | 6 |
| 313.15 | 25.00 | 879.49 | 11.50 | 6 |
| 333.15 | 13.00 | 505.35 | 25.80 | 6 |
| 333.15 | 16.50 | 651.70 | 21.00 | 6 |
| 333.15 | 26.50 | 800.93 | 14.80 | 6 |
| 308.15 | 11.00 | 743.95 | 14.60 | 7 |
| 308.15 | 13.00 | 785.70 | 13.70 | 7 |
| 313.15 | 8.00 | 277.90 | 29.90 | 7 |
| 313.15 | 8.50 | 353.91 | 23.70 | 7 |
| 313.15 | 8.75 | 414.84 | 22.80 | 7 |
| 313.15 | 8.80 | 429.10 | 22.20 | 7 |
| 313.15 | 9.00 | 485.50 | 19.30 | 7 |
| 313.15 | 9.20 | 532.04 | 20.10 | 7 |
| 313.15 | 9.50 | 580.01 | 18.30 | 7 |
| 313.15 | 9.50 | 580.01 | 18.90 | 7 |
| 313.15 | 10.00 | 628.61 | 16.70 | 7 |
| 313.15 | 11.00 | 683.52 | 15.80 | 7 |
| 313.15 | 13.00 | 743.04 | 13.90 | 7 |
| 313.15 | 13.00 | 743.04 | 14.00 | 7 |
| 313.15 | 16.00 | 794.90 | 12.90 | 7 |
| 318.15 | 11.00 | 603.15 | 19.70 | 7 |
| 318.15 | 13.00 | 693.65 | 16.00 | 7 |
| 323.15 | 11.00 | 502.64 | 21.60 | 7 |
| 323.15 | 13.00 | 636.12 | 18.80 | 7 |

| T, K | P, MPa | ρ, kg/m³ | D_{12}, 10⁹ m²/s | Ref.* |
|-------------|---------------|--|--|--------------|
| 328.15 | 11.00 | 414.90 | 27.60 | 7 |
| 328.15 | 13.00 | 571.33 | 19.40 | 7 |
| 313.15 | 15.00 | 780.23 | 13.00 | 8 |
| 313.15 | 16.00 | 794.90 | 12.60 | 8 |
| 313.15 | 20.00 | 839.81 | 11.20 | 8 |
| 313.15 | 25.00 | 879.49 | 10.30 | 8 |
| 313.15 | 30.00 | 909.89 | 9.70 | 8 |
| 313.15 | 35.00 | 934.81 | 9.00 | 8 |
| 323.15 | 15.00 | 699.75 | 15.60 | 8 |
| 323.15 | 20.00 | 784.29 | 12.90 | 8 |
| 323.15 | 25.00 | 834.19 | 11.70 | 8 |
| 323.15 | 30.00 | 870.47 | 11.10 | 8 |
| 323.15 | 35.00 | 899.23 | 10.60 | 8 |
| 333.15 | 15.00 | 604.09 | 18.20 | 8 |
| 333.15 | 16.00 | 637.50 | 16.10 | 8 |
| 333.15 | 20.00 | 723.68 | 15.40 | 8 |
| 333.15 | 25.00 | 786.55 | 13.60 | 8 |
| 333.15 | 30.00 | 829.71 | 12.40 | 8 |
| 333.15 | 35.00 | 862.94 | 11.60 | 8 |
| 313.15 | 15.00 | 780.23 | 12.99 | 9 |
| 313.15 | 20.00 | 839.81 | 11.20 | 9 |
| 313.15 | 25.00 | 879.49 | 10.27 | 9 |
| 313.15 | 30.00 | 909.89 | 9.67 | 9 |
| 313.15 | 35.00 | 934.81 | 9.01 | 9 |
| 323.15 | 15.00 | 699.75 | 15.58 | 9 |
| 323.15 | 20.00 | 784.29 | 12.97 | 9 |
| 323.15 | 25.00 | 834.19 | 11.72 | 9 |
| 323.15 | 30.00 | 870.43 | 11.10 | 9 |
| 323.15 | 35.00 | 899.23 | 10.58 | 9 |
| 333.15 | 15.00 | 604.09 | 18.18 | 9 |
| 333.15 | 20.00 | 723.68 | 15.40 | 9 |
| 333.15 | 25.00 | 786.55 | 13.60 | 9 |
| 333.15 | 30.00 | 829.71 | 12.44 | 9 |
| 333.15 | 35.00 | 862.94 | 11.57 | 9 |

* 1 (Levelt Sengers et al., 1993), 2 (Ago and Nishiumi, 1999), 3 (Nishiumi and Kubota, 2007), 4 (Funazukuri et al., 2001), 5 (Funazukuri and Nishimoto, 1996), 6 (Sassiat et al., 1987), 7 (Swaid and Schneider, 1979), 8 (Suárez et al., 1993), and 9 (Bueno et al., 1993).

APPENDIX D

EXPERIMENTAL DATA

D-1

MEASURED DIFFUSION COEFFICIENTS OF BENZENE IN CO₂

Table D-1 Measured diffusion coefficients of benzene in CO₂ and curve-fitting errors as a function of mobile phase mean velocity: 40 °C, 9-9.5 MPa, vertical coil.

| Avg_U (cm/s) | StD_U (cm/s) | Avg_D₁₂ (10 ⁻⁹ m ² /s) | StD_D₁₂ (10 ⁻⁹ m ² /s) | Avg_ε (%) |
|------------------------|------------------------|---|---|---------------------|
| 9 MPa | | | | |
| 0.26 | 0.00 | 8.08 | 0.25 | 8.71 |
| 0.35 | 0.00 | 10.46 | 0.28 | 5.89 |
| 0.39 | 0.00 | 12.16 | 0.35 | 5.75 |
| 0.48 | 0.01 | 14.21 | 0.88 | 5.90 |
| 0.57 | 0.00 | 15.13 | 1.29 | 5.52 |
| 0.60 | 0.00 | 15.15 | 0.65 | 5.12 |
| 0.73 | 0.00 | 16.06 | 0.76 | 4.26 |
| 0.88 | 0.05 | 17.45 | 1.26 | 3.40 |
| 1.07 | 0.03 | 19.00 | 0.72 | 3.01 |
| 9.4 MPa | | | | |
| 0.21 | 0.00 | 10.64 | 0.26 | 7.62 |
| 0.40 | 0.00 | 14.64 | 0.52 | 3.08 |
| 0.54 | 0.00 | 15.28 | 0.83 | 2.43 |
| 0.73 | 0.01 | 16.52 | 0.55 | 1.77 |
| 0.91 | 0.00 | 17.79 | 0.83 | 1.53 |
| 1.10 | 0.00 | 18.45 | 0.30 | 1.82 |
| 1.25 | 0.01 | 19.23 | 0.83 | 2.47 |
| 9.5 MPa | | | | |
| 0.31 | 0.00 | 12.78 | 0.77 | 4.26 |
| 0.50 | 0.00 | 16.06 | 0.61 | 2.55 |
| 0.70 | 0.01 | 18.00 | 0.92 | 1.91 |
| 0.96 | 0.01 | 18.38 | 0.58 | 1.60 |
| 1.14 | 0.00 | 18.68 | 0.36 | 2.76 |
| 1.51 | 0.02 | 19.56 | 1.00 | 1.63 |

Table D-2 Measured diffusion coefficients of benzene in CO₂ and curve-fitting errors as a function of mobile phase mean velocity: 40 °C, 10-15 MPa, vertical coil.

| Avg_U (cm/s) | StD_U (cm/s) | Avg_D₁₂ (10 ⁻⁹ m ² /s) | StD_D₁₂ (10 ⁻⁹ m ² /s) | Avg_ε (%) |
|------------------------|------------------------|---|---|---------------------|
| 10 MPa | | | | |
| 0.20 | 0.00 | 11.83 | 0.11 | 3.51 |
| 0.41 | 0.00 | 17.91 | 0.59 | 0.82 |
| 0.85 | 0.01 | 17.77 | 0.73 | 1.35 |
| 1.01 | 0.01 | 17.87 | 0.25 | 1.54 |
| 1.36 | 0.01 | 18.54 | 0.38 | 1.74 |
| 1.84 | 0.02 | 22.03 | 0.79 | 1.96 |
| 12 MPa | | | | |
| 0.17 | 0.00 | 13.38 | 0.81 | 0.79 |
| 0.30 | 0.00 | 14.52 | 0.81 | 0.80 |
| 0.59 | 0.00 | 15.12 | 0.76 | 1.10 |
| 0.85 | 0.00 | 15.24 | 0.25 | 1.19 |
| 1.14 | 0.01 | 15.44 | 0.17 | 1.20 |
| 1.49 | 0.02 | 17.34 | 0.47 | 1.42 |
| 1.93 | 0.06 | 20.79 | 2.35 | 1.77 |
| 15 MPa | | | | |
| 0.24 | 0.00 | 12.90 | 0.45 | 0.89 |
| 0.71 | 0.00 | 13.15 | 0.27 | 0.90 |
| 1.12 | 0.02 | 13.38 | 0.42 | 1.11 |
| 1.36 | 0.04 | 14.05 | 0.41 | 1.28 |
| 2.03 | 0.16 | 18.53 | 0.73 | 1.63 |

Table D-3 Measured diffusion coefficients of benzene in CO₂ and curve-fitting errors as a function of mobile phase mean velocity: 40 °C, 9-10 MPa, horizontal coil.

| Avg_U (cm/s) | StD_U (cm/s) | Avg_D₁₂ (10 ⁻⁹ m ² /s) | StD_D₁₂ (10 ⁻⁹ m ² /s) | Avg_ε (%) |
|------------------------|------------------------|---|---|---------------------|
| 9 MPa | | | | |
| 0.25 | 0.00 | 12.18 | 0.19 | 6.01 |
| 0.31 | 0.00 | 15.66 | 0.31 | 2.38 |
| 0.45 | 0.00 | 17.05 | 0.83 | 2.75 |
| 0.63 | 0.02 | 16.98 | 0.23 | 1.98 |
| 0.89 | 0.01 | 19.58 | 0.31 | 1.82 |
| 9.4 MPa | | | | |
| 0.32 | 0.00 | 16.55 | 0.75 | 1.87 |
| 0.58 | 0.00 | 17.38 | 0.59 | 1.25 |
| 0.87 | 0.01 | 18.02 | 0.69 | 1.38 |
| 1.15 | 0.01 | 19.28 | 0.12 | 2.16 |
| 9.5 MPa | | | | |
| 0.51 | 0.00 | 17.59 | 0.27 | 1.34 |
| 0.66 | 0.00 | 18.13 | 0.09 | 0.99 |
| 0.81 | 0.00 | 18.23 | 0.61 | 1.07 |
| 0.97 | 0.00 | 18.39 | 0.25 | 1.60 |
| 1.14 | 0.01 | 19.06 | 0.44 | 1.25 |
| 1.38 | 0.01 | 19.90 | 0.53 | 1.30 |
| 10 MPa | | | | |
| 0.40 | 0.01 | 16.10 | 0.57 | 1.02 |
| 0.54 | 0.00 | 16.59 | 0.33 | 0.98 |
| 0.72 | 0.00 | 16.64 | 0.47 | 1.09 |
| 0.80 | 0.01 | 16.53 | 0.88 | 1.21 |
| 0.99 | 0.02 | 16.72 | 0.26 | 1.39 |
| 1.32 | 0.01 | 19.08 | 1.23 | 1.79 |
| 1.80 | 0.03 | 21.68 | 1.03 | 1.96 |

Table D-4 Measured diffusion coefficients of benzene in CO₂ and curve-fitting errors as a function of mobile phase mean velocity: 40 °C, 12 & 15 MPa, horizontal coil.

| Avg_U (cm/s) | StD_U (cm/s) | Avg_D₁₂ (10 ⁻⁹ m ² /s) | StD_D₁₂ (10 ⁻⁹ m ² /s) | Avg_ε (%) |
|------------------------|------------------------|---|---|---------------------|
| 12 MPa | | | | |
| 0.32 | 0.00 | 14.20 | 0.23 | 0.73 |
| 0.51 | 0.01 | 14.89 | 0.37 | 0.75 |
| 0.61 | 0.00 | 14.55 | 0.24 | 1.04 |
| 0.77 | 0.00 | 14.78 | 0.62 | 0.98 |
| 0.91 | 0.00 | 14.89 | 0.17 | 1.12 |
| 1.26 | 0.00 | 16.29 | 0.21 | 1.19 |
| 1.56 | 0.01 | 17.95 | 0.32 | 1.44 |
| 15 MPa | | | | |
| 0.47 | 0.00 | 12.65 | 0.23 | 0.88 |
| 0.71 | 0.00 | 12.90 | 0.34 | 0.83 |
| 0.97 | 0.02 | 12.93 | 0.21 | 1.02 |
| 1.38 | 0.01 | 14.95 | 0.35 | 1.40 |
| 1.94 | 0.01 | 19.50 | 0.43 | 1.59 |

Table D-5 Measured diffusion coefficients of benzene in CO₂ and curve-fitting errors as a function of mobile phase mean velocity: 60 °C, 9-15 MPa, vertical coil.

| Avg_U (cm/s) | StD_U (cm/s) | Avg_D ₁₂ (10 ⁻⁹ m ² /s) | StD_D ₁₂ (10 ⁻⁹ m ² /s) | Avg_ε (%) |
|-----------------|-----------------|---|---|--------------|
| 9 MPa | | | | |
| 0.23 | 0.00 | 13.31 | 0.29 | 17.10 |
| 0.40 | 0.01 | 21.31 | 1.18 | 11.01 |
| 0.49 | 0.00 | 24.80 | 1.17 | 8.39 |
| 0.55 | 0.01 | 26.46 | 1.00 | 7.41 |
| 0.70 | 0.00 | 31.20 | 1.11 | 5.86 |
| 1.09 | 0.01 | 40.98 | 2.85 | 2.97 |
| 10 MPa | | | | |
| 0.30 | 0.00 | 16.18 | 0.70 | 10.96 |
| 0.55 | 0.00 | 21.97 | 0.42 | 7.45 |
| 1.01 | 0.01 | 28.38 | 1.16 | 3.56 |
| 1.48 | 0.06 | 33.93 | 1.63 | 2.01 |
| 2.04 | 0.02 | 37.39 | 0.68 | 1.84 |
| 12 MPa | | | | |
| 0.25 | 0.00 | 11.05 | 0.09 | 12.31 |
| 0.60 | 0.00 | 18.80 | 0.81 | 4.98 |
| 0.78 | 0.00 | 20.48 | 0.82 | 3.26 |
| 0.93 | 0.01 | 21.50 | 0.83 | 2.89 |
| 1.07 | 0.00 | 22.76 | 0.24 | 2.38 |
| 1.50 | 0.03 | 24.46 | 0.57 | 1.81 |
| 14 MPa | | | | |
| 0.40 | 0.00 | 16.02 | 0.55 | 4.36 |
| 0.62 | 0.01 | 17.87 | 0.86 | 2.23 |
| 0.87 | 0.01 | 19.85 | 0.66 | 1.80 |
| 1.15 | 0.01 | 21.01 | 0.37 | 1.71 |
| 1.60 | 0.01 | 22.72 | 0.94 | 1.66 |
| 15 MPa | | | | |
| 0.26 | 0.00 | 14.14 | 0.42 | 4.53 |
| 0.35 | 0.00 | 16.27 | 0.83 | 3.26 |
| 0.45 | 0.00 | 18.34 | 0.35 | 1.63 |
| 0.76 | 0.00 | 18.97 | 0.60 | 1.20 |
| 1.14 | 0.01 | 19.35 | 1.00 | 1.19 |
| 1.42 | 0.02 | 20.44 | 0.45 | 1.29 |

Table D-6 Measured diffusion coefficients of benzene in CO₂ and curve-fitting errors as a function of mobile phase mean velocity: 60 °C, 9-12 MPa, horizontal coil.

| Avg_U (cm/s) | StD_U (cm/s) | Avg_D₁₂ (10 ⁻⁹ m ² /s) | StD_D₁₂ (10 ⁻⁹ m ² /s) | Avg_ε (%) |
|------------------------|------------------------|---|---|---------------------|
| 9 MPa | | | | |
| 0.30 | 0.00 | 29.68 | 1.30 | 3.84 |
| 0.50 | 0.00 | 39.88 | 0.88 | 1.30 |
| 0.60 | 0.00 | 39.87 | 0.52 | 1.78 |
| 0.63 | 0.00 | 41.41 | 1.89 | 1.44 |
| 0.77 | 0.00 | 39.84 | 1.27 | 2.16 |
| 0.82 | 0.00 | 42.43 | 1.48 | 1.29 |
| 0.93 | 0.00 | 40.53 | 1.12 | 1.68 |
| 1.03 | 0.01 | 43.89 | 2.10 | 1.41 |
| 1.09 | 0.00 | 43.33 | 1.82 | 1.59 |
| 10 MPa | | | | |
| 0.47 | 0.00 | 29.97 | 1.22 | 2.54 |
| 0.60 | 0.00 | 32.42 | 1.25 | 2.23 |
| 0.72 | 0.00 | 33.54 | 0.51 | 1.59 |
| 0.90 | 0.00 | 36.26 | 1.51 | 1.27 |
| 1.20 | 0.00 | 37.12 | 1.26 | 1.85 |
| 1.50 | 0.00 | 37.07 | 0.85 | 1.64 |
| 1.97 | 0.01 | 39.22 | 1.03 | 2.22 |
| 12 MPa | | | | |
| 0.37 | 0.00 | 19.36 | 0.22 | 3.63 |
| 0.64 | 0.00 | 22.72 | 0.48 | 1.75 |
| 0.86 | 0.02 | 23.38 | 0.75 | 1.23 |
| 1.05 | 0.02 | 23.73 | 0.66 | 1.29 |
| 1.51 | 0.03 | 26.45 | 0.71 | 1.40 |

Table D-7 Measured diffusion coefficients of benzene in CO₂ and curve-fitting errors as a function of mobile phase mean velocity: 60 °C, 14 & 15 MPa, horizontal coil.

| Avg_U (cm/s) | StD_U (cm/s) | Avg_D₁₂ (10 ⁻⁹ m ² /s) | StD_D₁₂ (10 ⁻⁹ m ² /s) | Avg_ε (%) |
|------------------------|------------------------|---|---|---------------------|
| 14 MPa | | | | |
| 0.38 | 0.00 | 19.29 | 0.43 | 0.85 |
| 0.53 | 0.00 | 20.03 | 0.53 | 0.86 |
| 0.70 | 0.00 | 19.97 | 0.37 | 0.90 |
| 0.82 | 0.01 | 19.85 | 0.11 | 0.95 |
| 0.94 | 0.00 | 20.26 | 0.07 | 1.19 |
| 1.14 | 0.00 | 20.99 | 0.35 | 1.09 |
| 1.39 | 0.02 | 21.77 | 0.32 | 1.31 |
| 15 MPa | | | | |
| 0.32 | 0.01 | 17.25 | 0.39 | 1.13 |
| 0.50 | 0.00 | 18.64 | 0.23 | 0.97 |
| 0.87 | 0.01 | 18.99 | 0.18 | 1.16 |
| 0.98 | 0.01 | 19.15 | 0.21 | 0.94 |
| 1.21 | 0.01 | 19.49 | 1.13 | 1.24 |
| 1.53 | 0.05 | 20.21 | 0.51 | 1.20 |

D-2

**TEMPERATURE & PRESSURE HISTORIES FOR BATCH THERMAL STRESSING
OF DF/CO₂ MIXTURES**

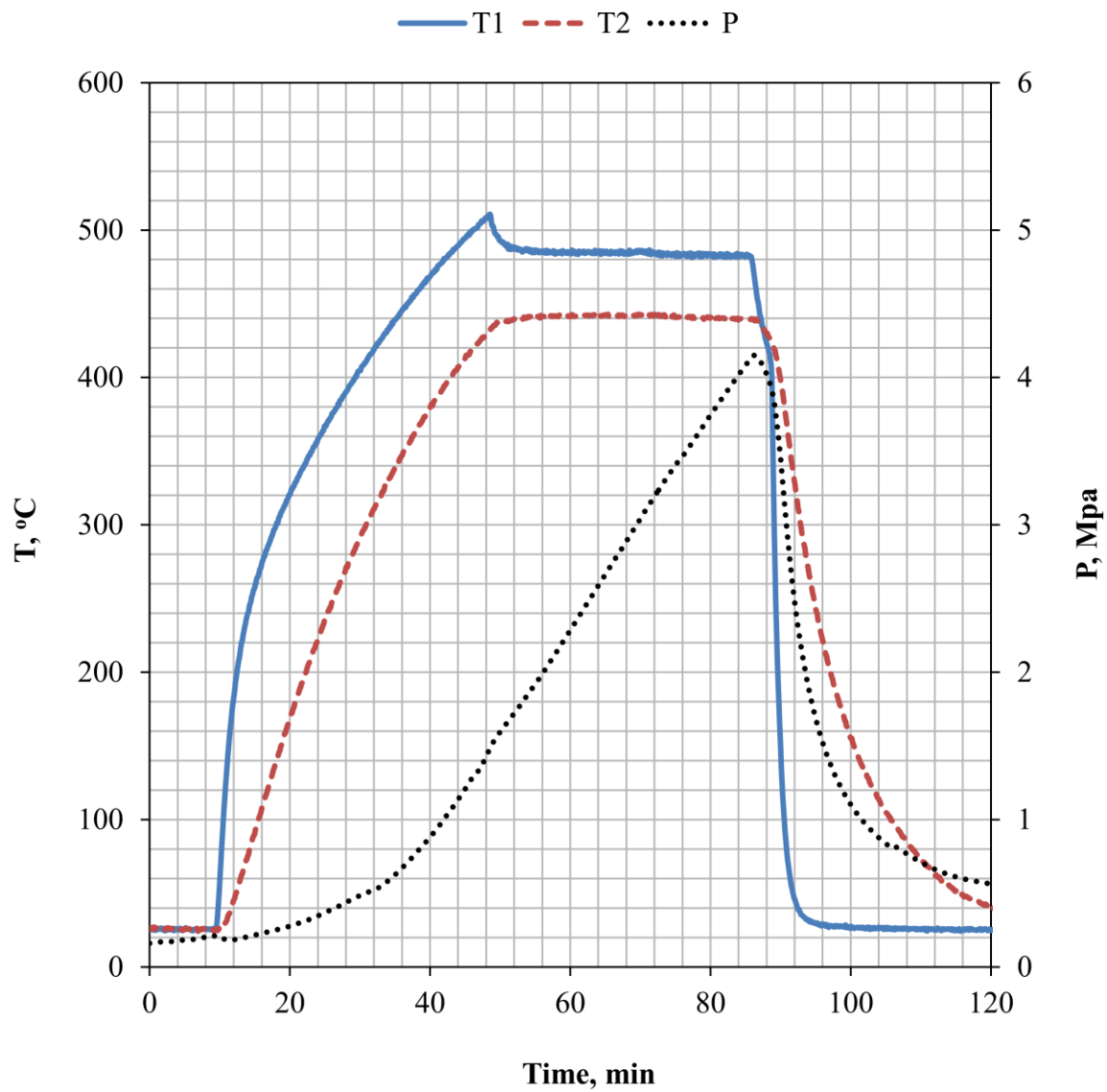


Fig. D-1 T-P history for batch thermal stressing of DF/CO₂ mixtures: Run 1.

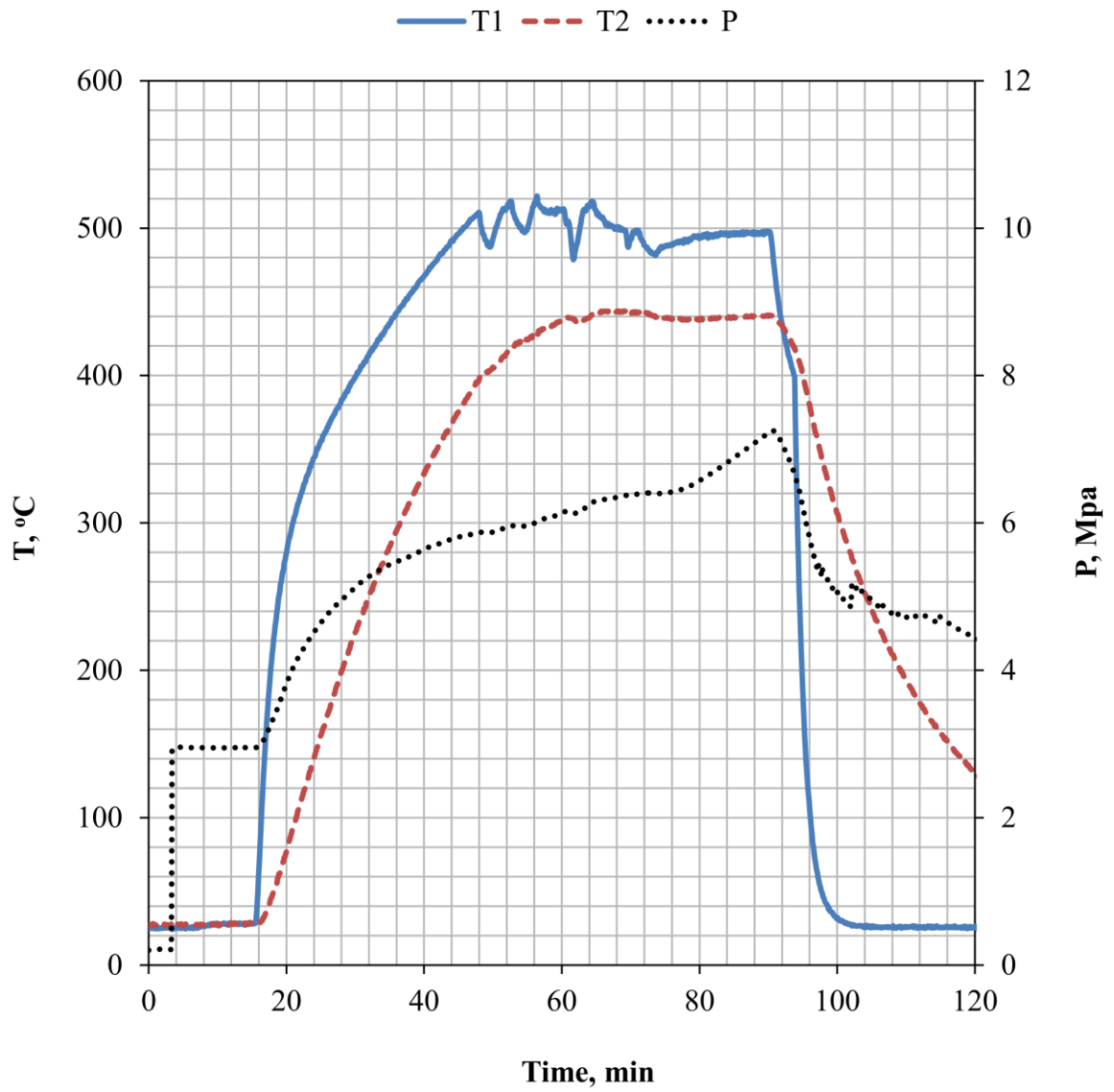


Fig. D-2 T-P history for batch thermal stressing of DF/CO₂ mixtures: Run 2.

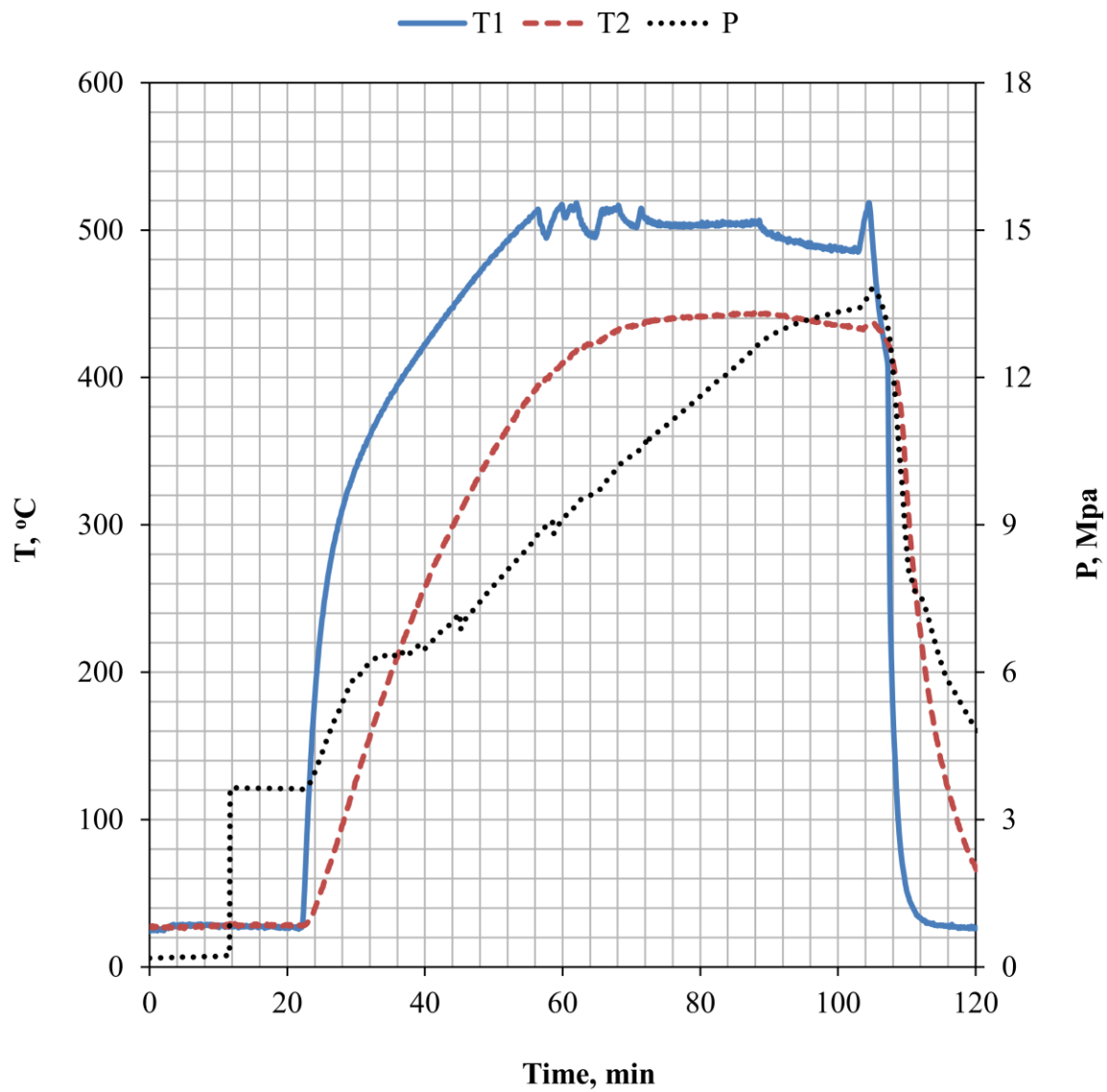


Fig. D-3 T-P history for batch thermal stressing of DF/CO₂ mixtures: Run 3.

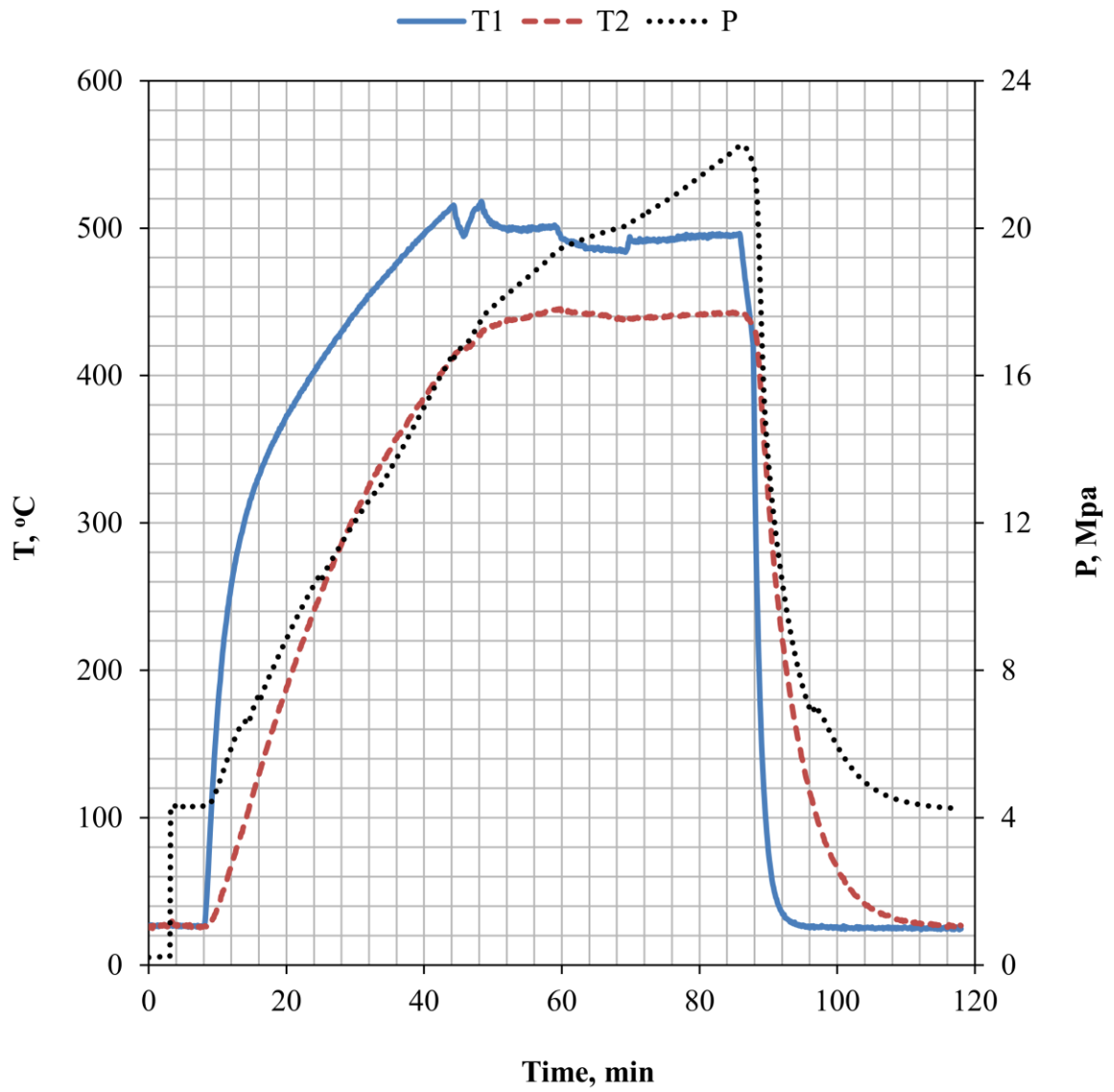


Fig. D-4 T-P history for batch thermal stressing of DF/CO₂ mixtures: Run 4.

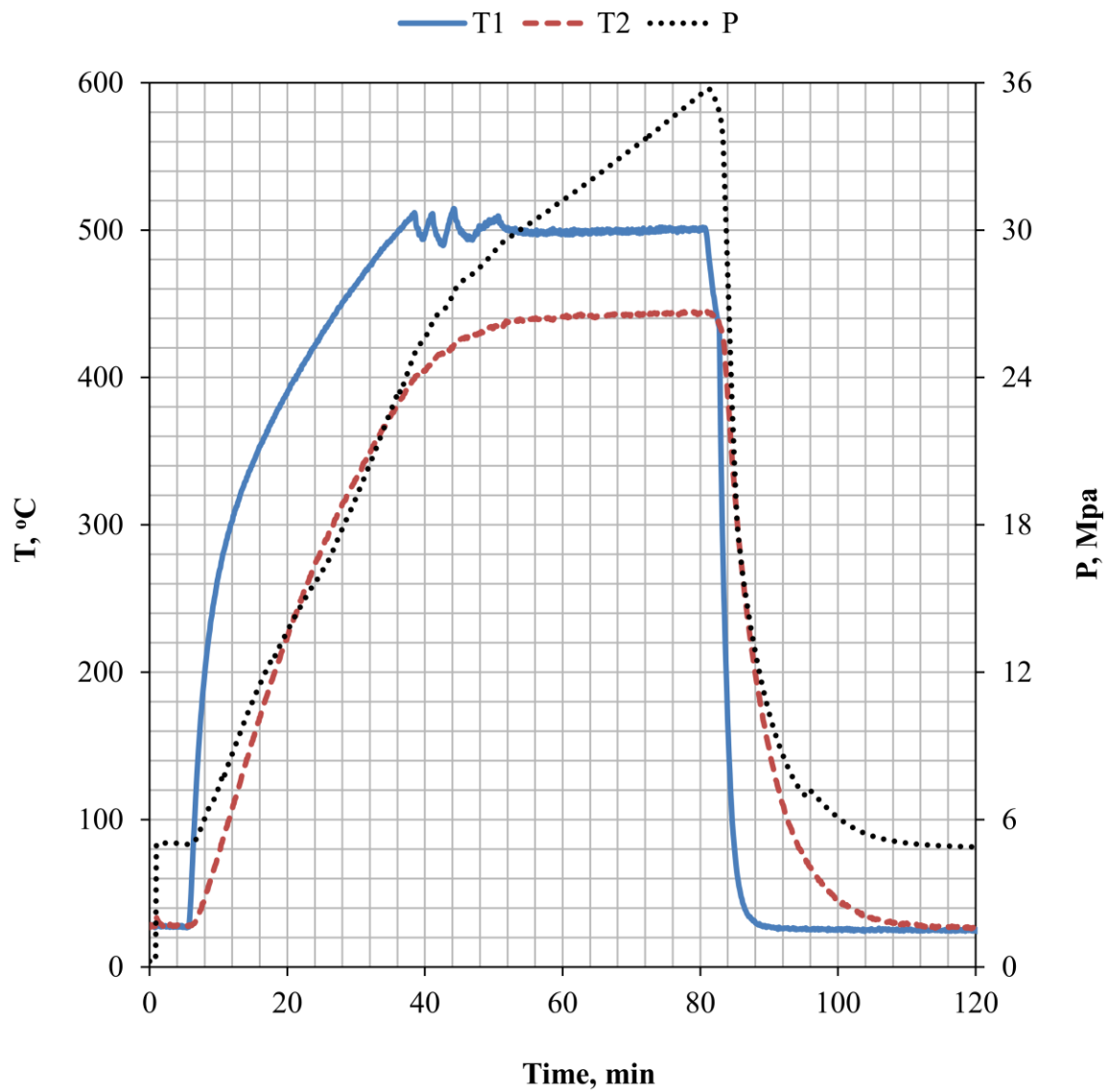


Fig. D-5 T-P history for batch thermal stressing of DF/CO₂ mixtures: Run 5.

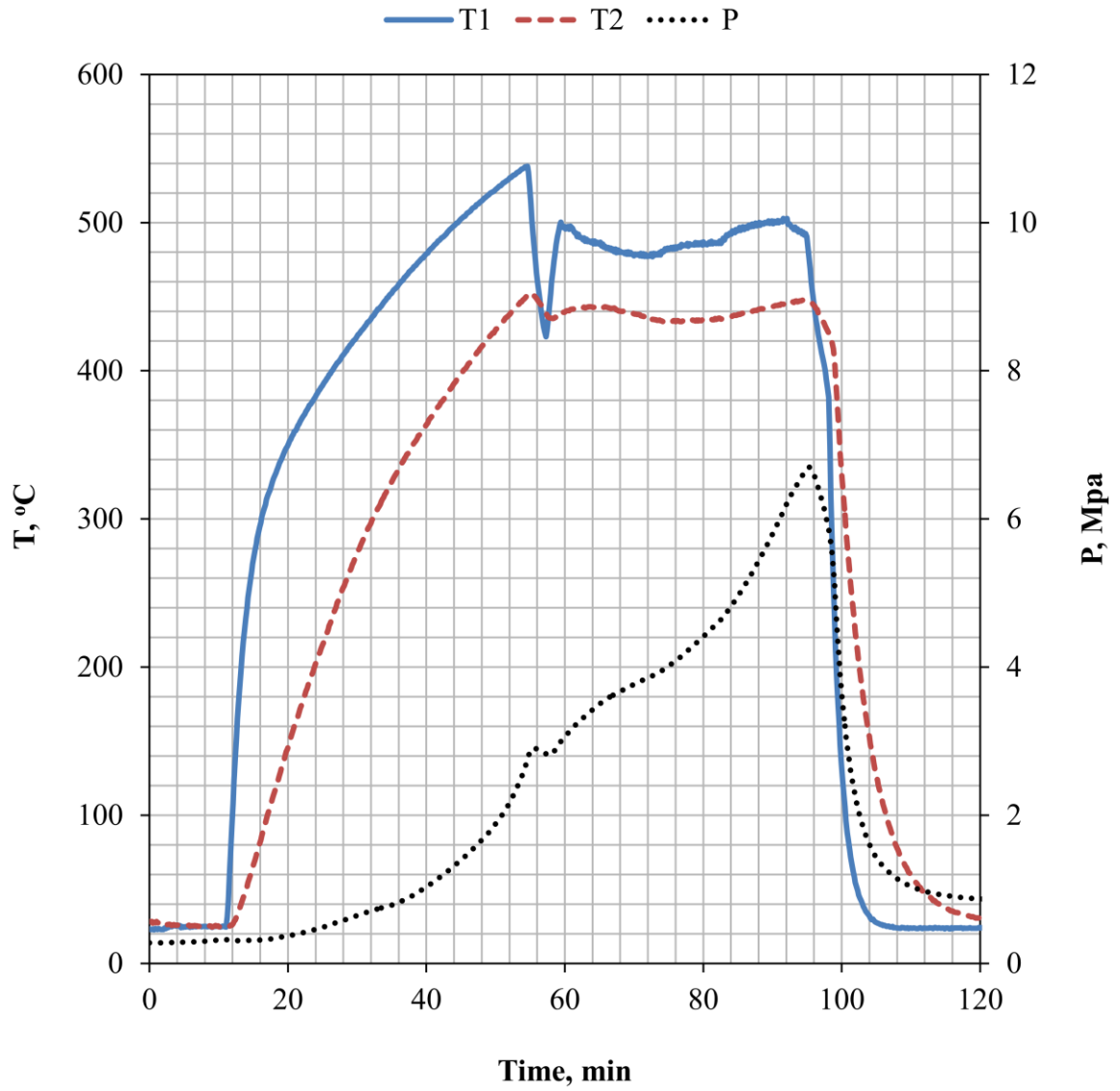


Fig. D-6 T-P history for batch thermal stressing of DF/CO₂ mixtures: Run 1-a.

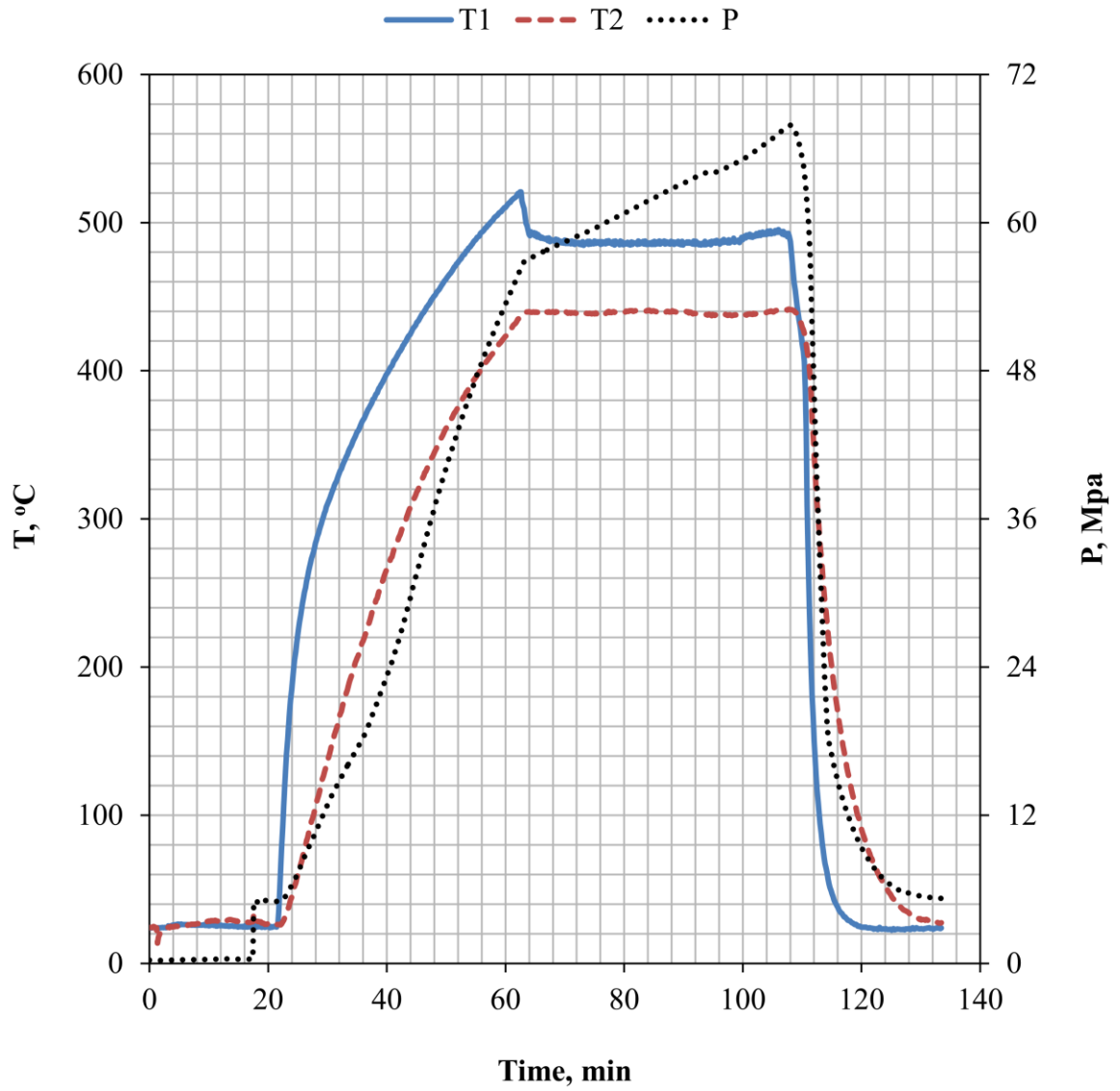


Fig. D-7 T-P history for batch thermal stressing of DF/CO₂ mixtures: Run 1-b.

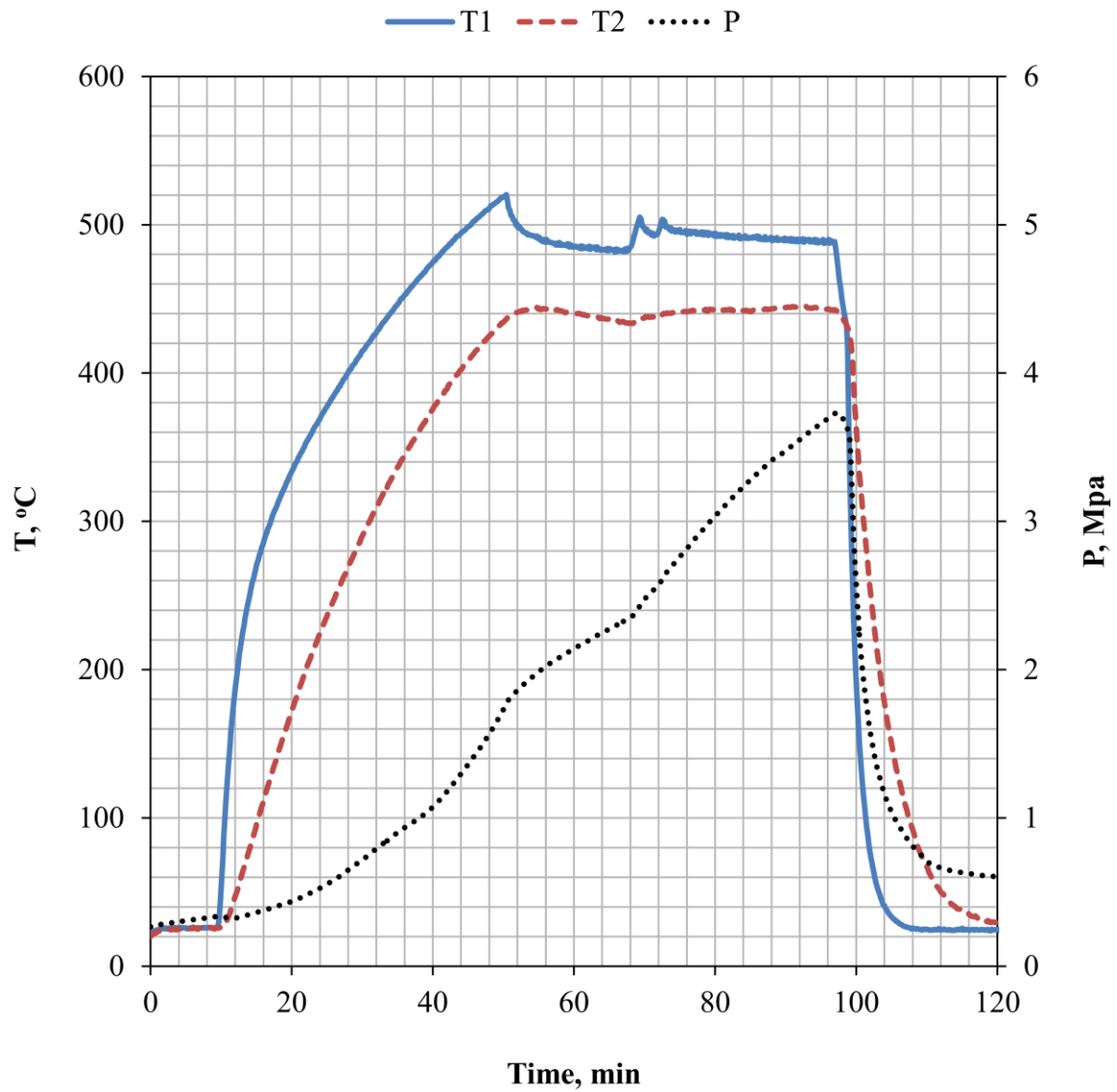


Fig. D-8 T-P history for batch thermal stressing of DF/CO₂ mixtures: Run 2-a.

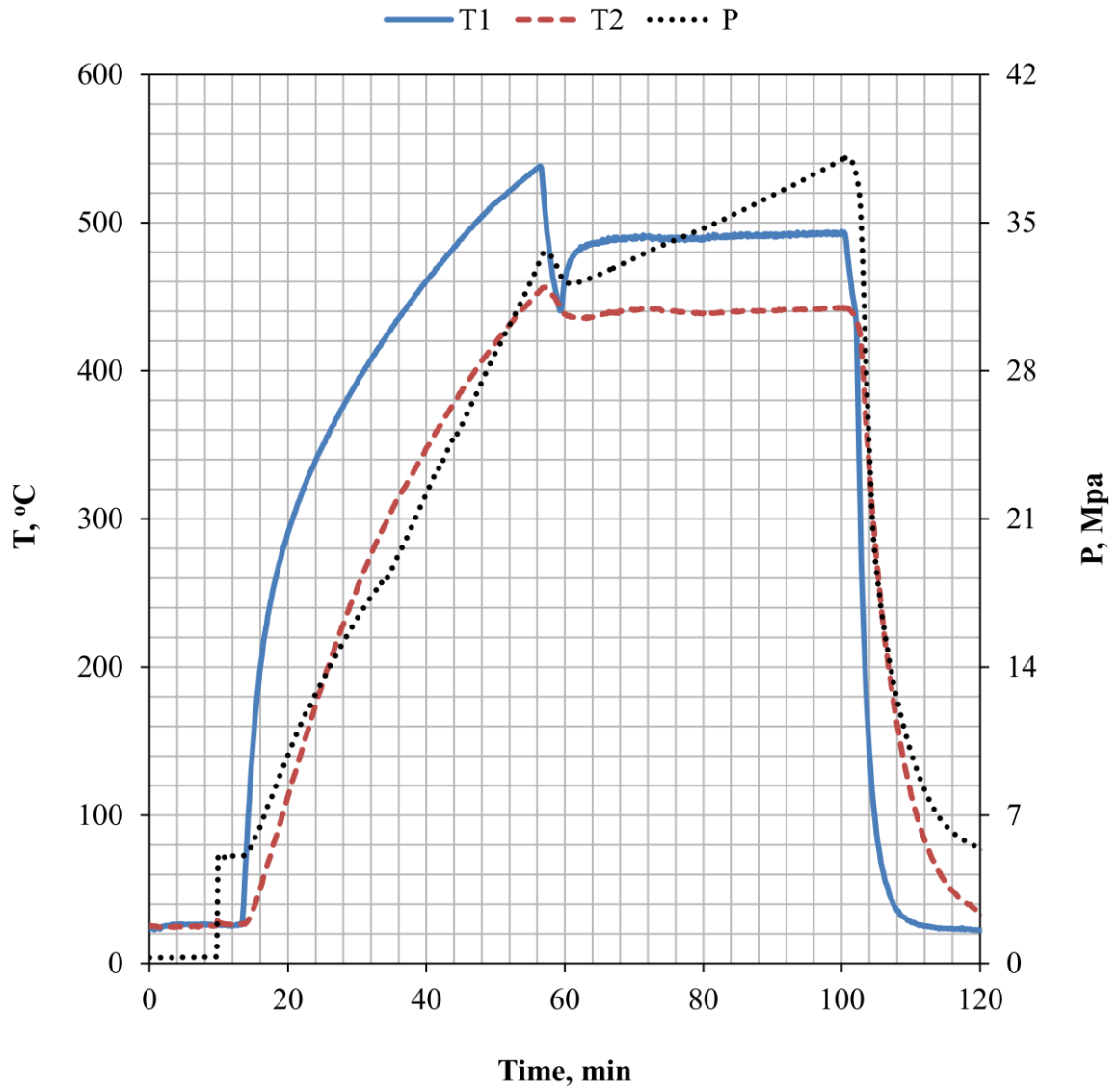


Fig. D-9 T-P history for batch thermal stressing of DF/CO₂ mixtures: Run 2-b.

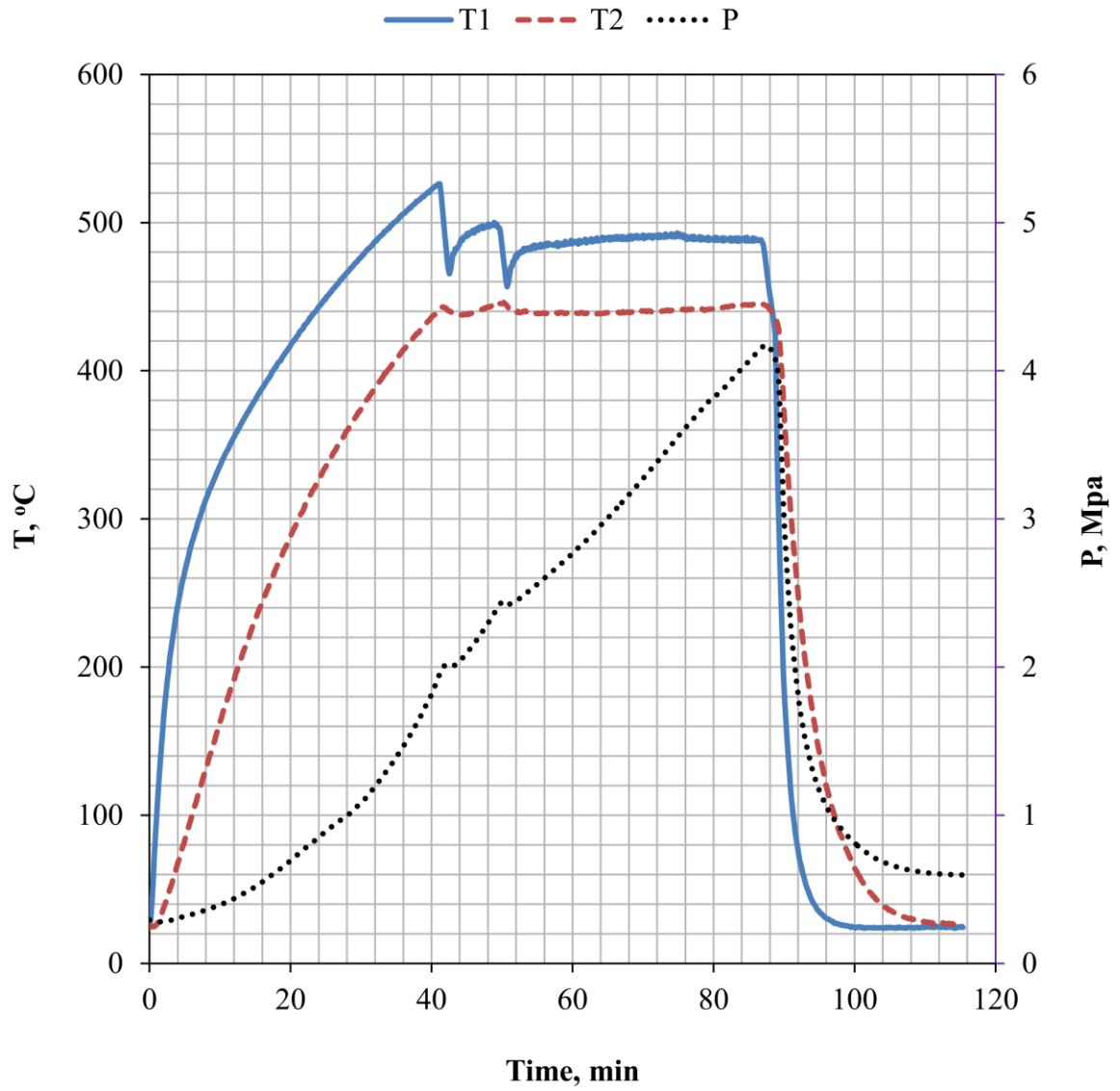


Fig. D-10 T-P history for batch thermal stressing of DF/CO₂ mixtures: Run 3-a.

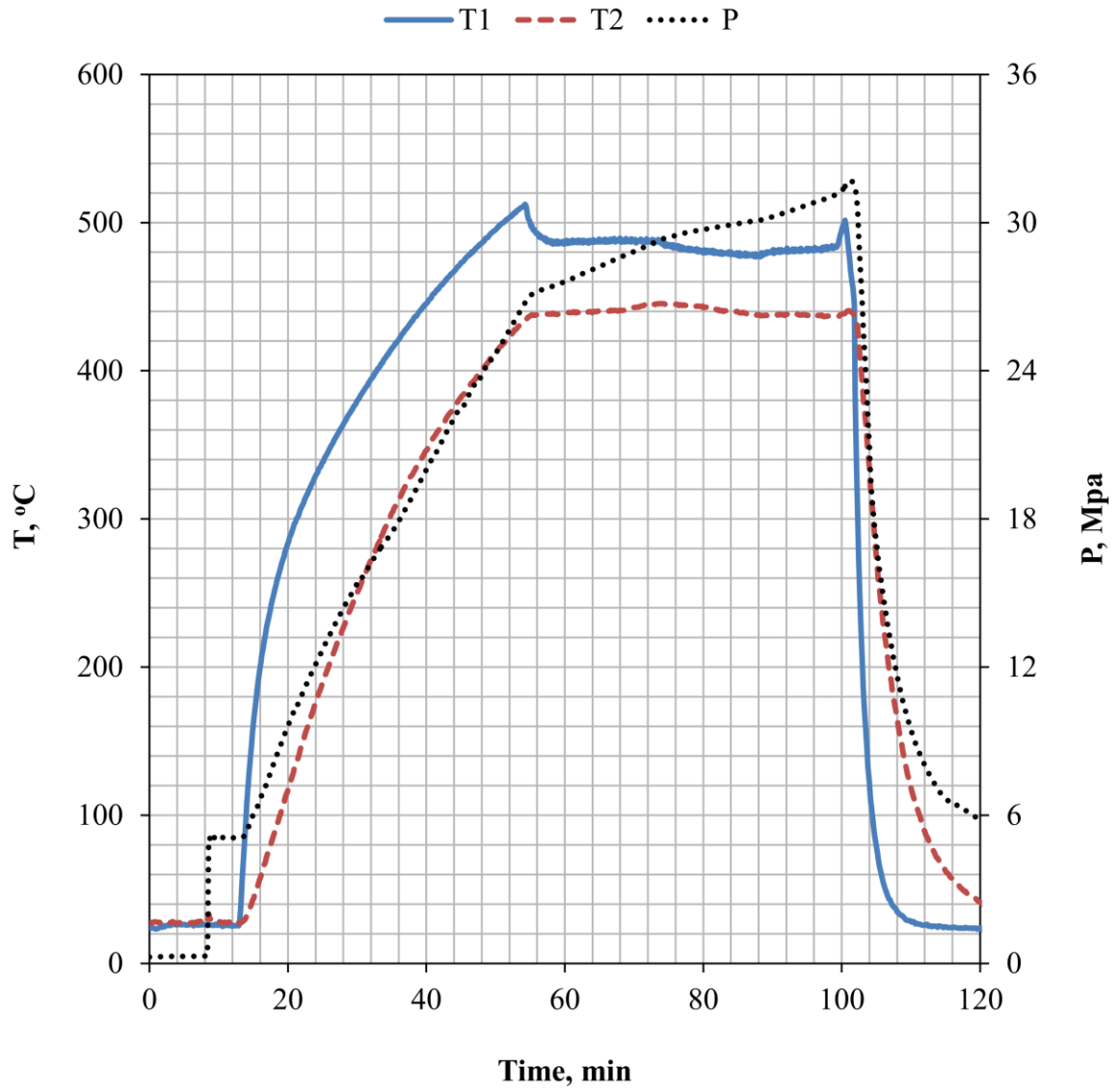


Fig. D-11 T-P history for batch thermal stressing of DF/CO₂ mixtures: Run 3-b.

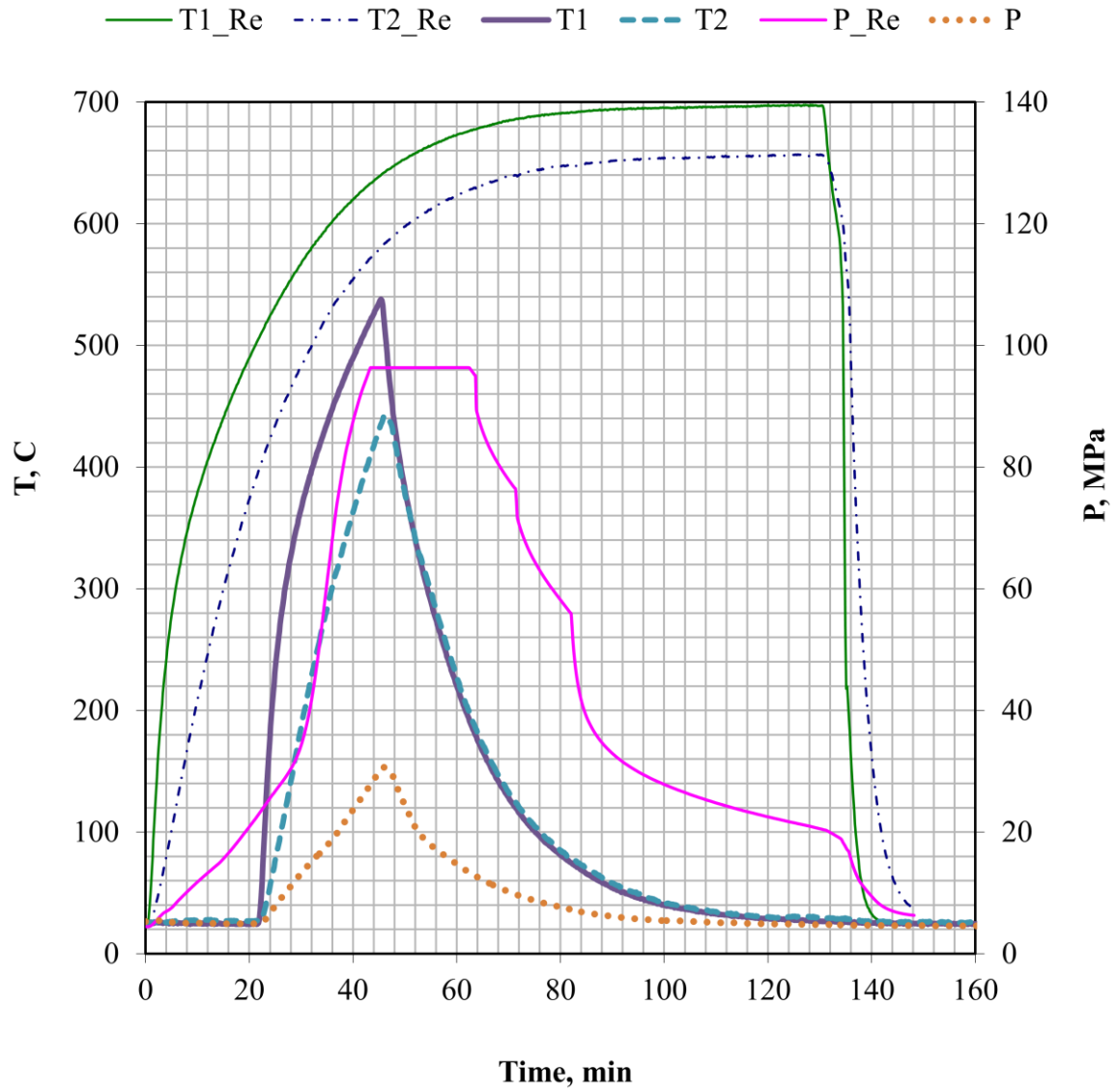


Fig. D-12 T-P history for batch thermal stressing of DF/CO₂ mixtures: Run 4-b.

D-3

GC-MS REPORTS FOR FRESH DF*

* Reports for thermally stressed DF are not attached in this dissertation, but are available in the lab at 411 Link Hall, Syracuse University, Syracuse, NY 13244.

Table D-8 GC-MS report for fresh DF –
sample1 (S1)

| Pk | R.T. | Height | Area | %Tot |
|----|--------|--------|----------|-------|
| 1 | 4.539 | 18150 | 1121326 | 0.108 |
| 2 | 4.7 | 22495 | 3151013 | 0.303 |
| 3 | 6.452 | 13844 | 1258940 | 0.121 |
| 4 | 7.569 | 37569 | 6250472 | 0.601 |
| 5 | 8.193 | 17026 | 2077827 | 0.2 |
| 6 | 8.596 | 31307 | 4817301 | 0.463 |
| 7 | 9.029 | 17777 | 2815152 | 0.271 |
| 8 | 10.146 | 53412 | 5753413 | 0.553 |
| 9 | 11.586 | 14197 | 1546713 | 0.149 |
| 10 | 12.512 | 30799 | 3721783 | 0.358 |
| 11 | 13.126 | 42673 | 9784436 | 0.941 |
| 12 | 13.73 | 25448 | 2408108 | 0.231 |
| 13 | 14.022 | 21052 | 2981545 | 0.287 |
| 14 | 14.726 | 22484 | 2769198 | 0.266 |
| 15 | 14.958 | 25484 | 3346463 | 0.322 |
| 16 | 15.622 | 72224 | 9047023 | 0.87 |
| 17 | 17.867 | 24012 | 1995746 | 0.192 |
| 18 | 18.119 | 117233 | 13794502 | 1.326 |
| 19 | 20.243 | 25419 | 2228298 | 0.214 |
| 20 | 20.495 | 38037 | 4220714 | 0.406 |
| 21 | 21.028 | 20771 | 2676963 | 0.257 |
| 22 | 21.25 | 25881 | 2901140 | 0.279 |
| 23 | 21.612 | 42026 | 6703721 | 0.644 |
| 24 | 22.025 | 33185 | 4623547 | 0.444 |
| 25 | 23.565 | 13581 | 1914005 | 0.184 |
| 26 | 24.169 | 33181 | 8107706 | 0.779 |
| 27 | 24.612 | 34969 | 5473168 | 0.526 |
| 28 | 24.934 | 32163 | 4072592 | 0.391 |
| 29 | 25.578 | 23124 | 2507718 | 0.241 |
| 30 | 26.052 | 15955 | 2198455 | 0.211 |
| 31 | 26.615 | 12236 | 2635413 | 0.253 |
| 32 | 27.803 | 27701 | 2686028 | 0.258 |
| 33 | 28.397 | 26525 | 3347158 | 0.322 |
| 34 | 29.041 | 192728 | 18906998 | 1.817 |
| 35 | 29.545 | 30381 | 3553973 | 0.342 |
| 36 | 29.937 | 24479 | 2448404 | 0.235 |
| 37 | 30.954 | 37445 | 6961154 | 0.669 |
| 38 | 31.921 | 59721 | 12859883 | 1.236 |
| 39 | 32.384 | 15312 | 1389192 | 0.134 |
| 40 | 33.209 | 23261 | 3771847 | 0.363 |
| 41 | 33.763 | 26525 | 3757469 | 0.361 |
| 42 | 34.558 | 18062 | 2815768 | 0.271 |
| 43 | 35.223 | 18234 | 2882860 | 0.277 |
| 44 | 36.018 | 38967 | 9396914 | 0.903 |
| 45 | 36.451 | 32478 | 4396244 | 0.423 |
| 46 | 37.025 | 59315 | 6917828 | 0.665 |
| 47 | 37.739 | 27732 | 2878112 | 0.277 |
| 48 | 38.051 | 15834 | 4460385 | 0.429 |
| 49 | 38.766 | 36933 | 4647243 | 0.447 |
| 50 | 39.3 | 14098 | 1896196 | 0.182 |
| 51 | 39.783 | 16492 | 1931379 | 0.186 |
| 52 | 41.555 | 241182 | 26349134 | 2.533 |
| 53 | 43.538 | 88828 | 9455752 | 0.909 |
| 54 | 44.021 | 13235 | 1890504 | 0.182 |
| 55 | 44.484 | 15587 | 1875338 | 0.18 |
| 56 | 44.937 | 97639 | 12852843 | 1.235 |
| 57 | 45.229 | 20611 | 1999903 | 0.192 |
| 58 | 45.571 | 16793 | 1960872 | 0.188 |
| 59 | 46.135 | 16610 | 3625711 | 0.349 |
| 60 | 47.071 | 25369 | 3194907 | 0.307 |
| 61 | 47.554 | 57859 | 7170625 | 0.689 |
| 62 | 47.897 | 49371 | 5879254 | 0.565 |
| 63 | 48.672 | 33578 | 3743407 | 0.36 |
| 64 | 49.236 | 45899 | 6133318 | 0.59 |
| 65 | 49.83 | 49526 | 7962771 | 0.765 |
| 66 | 50.585 | 29154 | 3297788 | 0.317 |
| 67 | 51.239 | 94373 | 9202217 | 0.885 |
| 68 | 51.621 | 15750 | 1711407 | 0.165 |
| 69 | 51.964 | 73302 | 10308357 | 0.991 |
| 70 | 52.487 | 26851 | 3805266 | 0.366 |
| 71 | 52.789 | 27225 | 3176300 | 0.305 |
| 72 | 54.48 | 289048 | 29851574 | 2.87 |
| 73 | 54.803 | 30248 | 3633307 | 0.349 |
| 74 | 55.688 | 16029 | 2427580 | 0.233 |
| 75 | 56.755 | 29567 | 4624279 | 0.445 |
| 76 | 58.145 | 46289 | 6256805 | 0.601 |
| 77 | 58.819 | 12819 | 1206393 | 0.116 |
| 78 | 60.41 | 30551 | 3511474 | 0.338 |
| 79 | 60.742 | 42185 | 5519155 | 0.531 |
| 80 | 61.034 | 37219 | 4570262 | 0.439 |
| 81 | 61.376 | 43839 | 4563032 | 0.439 |

| Pk | R.T. | Height | Area | %Tot | Pk | R.T. | Height | Area | %Tot |
|-----|--------|--------|----------|-------|-----|---------|--------|----------|-------|
| 82 | 61.638 | 25265 | 2911967 | 0.28 | 125 | 96.107 | 27731 | 4191955 | 0.403 |
| 83 | 61.96 | 27302 | 2681984 | 0.258 | 126 | 96.771 | 99187 | 20449117 | 1.966 |
| 84 | 62.624 | 51573 | 5868747 | 0.564 | 127 | 97.405 | 21261 | 2888741 | 0.278 |
| 85 | 63.138 | 33422 | 5749612 | 0.553 | 128 | 98.04 | 35071 | 4092208 | 0.393 |
| 86 | 63.359 | 65214 | 9788868 | 0.941 | 129 | 98.764 | 26797 | 3890885 | 0.374 |
| 87 | 64.376 | 93609 | 14085600 | 1.354 | 130 | 100.878 | 8988 | 1034361 | 0.099 |
| 88 | 65.262 | 15203 | 2589460 | 0.249 | 131 | 102.056 | 350422 | 38657310 | 3.716 |
| 89 | 66.228 | 35926 | 4623472 | 0.444 | 132 | 102.972 | 150909 | 15891791 | 1.528 |
| 90 | 67.155 | 332633 | 32490079 | 3.123 | 133 | 103.103 | 168952 | 16265632 | 1.564 |
| 91 | 67.446 | 18970 | 2115259 | 0.203 | 134 | 106.727 | 35356 | 7383152 | 0.71 |
| 92 | 67.859 | 28902 | 4597708 | 0.442 | 135 | 107.15 | 17396 | 2038581 | 0.196 |
| 93 | 70.497 | 30910 | 5812997 | 0.559 | 136 | 108.771 | 27099 | 3195044 | 0.307 |
| 94 | 70.899 | 17745 | 2329135 | 0.224 | 137 | 109.486 | 19571 | 1925360 | 0.185 |
| 95 | 71.161 | 39318 | 7517945 | 0.723 | 138 | 112.596 | 312836 | 34272981 | 3.295 |
| 96 | 71.936 | 26859 | 7977458 | 0.767 | 139 | 113.694 | 74522 | 7123288 | 0.685 |
| 97 | 73.325 | 29272 | 5597194 | 0.538 | 140 | 113.834 | 79594 | 8249557 | 0.793 |
| 98 | 73.698 | 40138 | 5050959 | 0.486 | 141 | 117.438 | 22695 | 3252341 | 0.313 |
| 99 | 74.292 | 38712 | 4776432 | 0.459 | 142 | 118.425 | 15630 | 1812918 | 0.174 |
| 100 | 75.007 | 165032 | 22600720 | 2.173 | 143 | 118.999 | 21405 | 2439940 | 0.235 |
| 101 | 75.711 | 34053 | 5261108 | 0.506 | 144 | 122.089 | 21321 | 4719978 | 0.454 |
| 102 | 76.164 | 27024 | 4022099 | 0.387 | 145 | 122.643 | 274187 | 30071548 | 2.891 |
| 103 | 76.668 | 36325 | 5024616 | 0.483 | 146 | 127.616 | 21548 | 2522793 | 0.243 |
| 104 | 77.443 | 19092 | 2664627 | 0.256 | 147 | 128.753 | 16098 | 2086008 | 0.201 |
| 105 | 78.379 | 25857 | 6724945 | 0.646 | 148 | 132.237 | 234992 | 26733844 | 2.57 |
| 106 | 78.721 | 25819 | 3760412 | 0.361 | 149 | 141.407 | 180874 | 19564638 | 1.881 |
| 107 | 79.366 | 383447 | 42280793 | 4.064 | 150 | 150.196 | 126189 | 13303776 | 1.279 |
| 108 | 80.211 | 25080 | 3514102 | 0.338 | 151 | 158.632 | 72828 | 7870060 | 0.757 |
| 109 | 80.493 | 25691 | 6099628 | 0.586 | 152 | 166.756 | 33855 | 3613990 | 0.347 |
| 110 | 81.308 | 23033 | 4267198 | 0.41 | 153 | 174.558 | 13675 | 1449160 | 0.139 |
| 111 | 83.604 | 29085 | 3249278 | 0.312 | End | | | | |
| 112 | 84.006 | 22260 | 2954412 | 0.284 | | | | | |
| 113 | 84.892 | 34685 | 6800908 | 0.654 | | | | | |
| 114 | 85.516 | 19342 | 2789523 | 0.268 | | | | | |
| 115 | 86.09 | 33522 | 6971416 | 0.67 | | | | | |
| 116 | 86.785 | 52645 | 6476707 | 0.623 | | | | | |
| 117 | 87.117 | 19317 | 2323692 | 0.223 | | | | | |
| 118 | 87.51 | 30705 | 3949769 | 0.38 | | | | | |
| 119 | 89.463 | 16491 | 2651875 | 0.255 | | | | | |
| 120 | 90.983 | 384278 | 42414579 | 4.077 | | | | | |
| 121 | 94.114 | 22558 | 3361766 | 0.323 | | | | | |
| 122 | 94.536 | 22716 | 4222259 | 0.406 | | | | | |
| 123 | 95.442 | 25754 | 3836129 | 0.369 | | | | | |
| 124 | 95.744 | 17549 | 1950705 | 0.188 | | | | | |

Table D-9 GC-MS report for fresh DF – sample 2 (S2)

| Pk | R.T. | Height | Area | %Tot |
|----|-------|--------|---------|-------|
| 1 | 4.693 | 5167 | 1167192 | 0.363 |
| 2 | 7.541 | 8154 | 1077576 | 0.335 |
| 3 | 8.578 | 4930 | 1038496 | 0.323 |

| Pk | R.T. | Height | Area | %Tot | Pk | R.T. | Height | Area | %Tot |
|----|--------|--------|---------|-------|----|--------|--------|---------|-------|
| 4 | 10.118 | 10038 | 1402375 | 0.436 | 47 | 50.578 | 7179 | 715965 | 0.223 |
| 5 | 12.483 | 4943 | 580062 | 0.18 | 48 | 51.253 | 22146 | 2200296 | 0.684 |
| 6 | 13.097 | 10329 | 1943662 | 0.604 | 49 | 51.977 | 26738 | 3680494 | 1.144 |
| 7 | 13.711 | 4896 | 410682 | 0.128 | 50 | 52.501 | 10679 | 1341356 | 0.417 |
| 8 | 15.593 | 21760 | 3532992 | 1.098 | 51 | 52.813 | 9927 | 1136092 | 0.353 |
| 9 | 17.858 | 6546 | 528337 | 0.164 | 52 | 53.165 | 7479 | 1064689 | 0.331 |
| 10 | 18.089 | 19512 | 2520142 | 0.783 | 53 | 54.483 | 60882 | 6281817 | 1.952 |
| 11 | 20.223 | 6319 | 637420 | 0.198 | 54 | 54.815 | 8390 | 717305 | 0.223 |
| 12 | 20.485 | 7899 | 1086260 | 0.338 | 55 | 55.641 | 5851 | 786919 | 0.245 |
| 13 | 21.219 | 7803 | 783044 | 0.243 | 56 | 56.748 | 10575 | 1522741 | 0.473 |
| 14 | 21.572 | 11192 | 1759531 | 0.547 | 57 | 58.167 | 15209 | 2127024 | 0.661 |
| 15 | 22.004 | 8933 | 1226862 | 0.381 | 58 | 60.422 | 12701 | 1254120 | 0.39 |
| 16 | 24.098 | 8379 | 2213638 | 0.688 | 59 | 60.754 | 19111 | 2341505 | 0.728 |
| 17 | 24.581 | 9785 | 1365309 | 0.424 | 60 | 61.035 | 11795 | 1642250 | 0.51 |
| 18 | 24.903 | 5880 | 809160 | 0.251 | 61 | 61.378 | 17732 | 1702476 | 0.529 |
| 19 | 27.782 | 7811 | 823813 | 0.256 | 62 | 61.639 | 11348 | 1305400 | 0.406 |
| 20 | 28.385 | 8378 | 1042330 | 0.324 | 63 | 61.972 | 7156 | 704839 | 0.219 |
| 21 | 29.03 | 37936 | 3771377 | 1.172 | 64 | 62.636 | 11147 | 1390906 | 0.432 |
| 22 | 29.543 | 8534 | 965265 | 0.3 | 65 | 63.149 | 14862 | 2515979 | 0.782 |
| 23 | 29.935 | 7561 | 674296 | 0.21 | 66 | 63.36 | 24701 | 3491540 | 1.085 |
| 24 | 30.942 | 10122 | 1378310 | 0.428 | 67 | 64.397 | 24477 | 4661130 | 1.449 |
| 25 | 31.898 | 17887 | 3518268 | 1.093 | 68 | 65.273 | 9716 | 2684724 | 0.834 |
| 26 | 33.166 | 6031 | 896695 | 0.279 | 69 | 66.249 | 15541 | 2231955 | 0.694 |
| 27 | 33.76 | 8127 | 1011967 | 0.315 | 70 | 67.175 | 75461 | 7765231 | 2.413 |
| 28 | 36.115 | 12609 | 2634391 | 0.819 | 71 | 67.447 | 8036 | 936514 | 0.291 |
| 29 | 36.457 | 8609 | 1050838 | 0.327 | 72 | 67.88 | 11668 | 1463910 | 0.455 |
| 30 | 37.031 | 15030 | 1673034 | 0.52 | 73 | 68.111 | 8643 | 967481 | 0.301 |
| 31 | 37.736 | 6407 | 756134 | 0.235 | 74 | 70.506 | 10163 | 1789213 | 0.556 |
| 32 | 38.038 | 3848 | 478413 | 0.149 | 75 | 70.919 | 6674 | 789204 | 0.245 |
| 33 | 38.772 | 10143 | 1186056 | 0.369 | 76 | 71.171 | 14493 | 2684542 | 0.834 |
| 34 | 39.809 | 6419 | 872844 | 0.271 | 77 | 71.915 | 11170 | 3091258 | 0.961 |
| 35 | 41.55 | 52177 | 6048562 | 1.88 | 78 | 72.65 | 4992 | 555614 | 0.173 |
| 36 | 43.523 | 24641 | 3453926 | 1.073 | 79 | 73.325 | 11522 | 2467539 | 0.767 |
| 37 | 44.942 | 35833 | 4491941 | 1.396 | 80 | 73.707 | 17522 | 2349423 | 0.73 |
| 38 | 45.234 | 5994 | 506695 | 0.157 | 81 | 74.311 | 13700 | 2469584 | 0.768 |
| 39 | 46.13 | 5541 | 980043 | 0.305 | 82 | 74.734 | 9165 | 1380124 | 0.429 |
| 40 | 47.096 | 9114 | 1016427 | 0.316 | 83 | 75.025 | 47177 | 6299144 | 1.958 |
| 41 | 47.569 | 24366 | 2927478 | 0.91 | 84 | 75.72 | 12268 | 2184956 | 0.679 |
| 42 | 47.891 | 18120 | 1985913 | 0.617 | 85 | 76.173 | 18915 | 2699672 | 0.839 |
| 43 | 48.686 | 10715 | 1152319 | 0.358 | 86 | 76.686 | 22484 | 3413489 | 1.061 |
| 44 | 49.25 | 15570 | 2088414 | 0.649 | 87 | 77.481 | 9531 | 1346848 | 0.419 |
| 45 | 49.823 | 11134 | 2144608 | 0.667 | 88 | 77.723 | 7314 | 689891 | 0.214 |
| 46 | 50.286 | 6577 | 664172 | 0.206 | 89 | 78.357 | 16686 | 3881013 | 1.206 |

| Pk | R.T. | Height | Area | %Tot |
|-----|--------|--------|----------|-------|
| 90 | 78.719 | 17151 | 2377691 | 0.739 |
| 91 | 79.373 | 104978 | 11272932 | 3.503 |
| 92 | 79.957 | 7444 | 824688 | 0.256 |
| 93 | 80.219 | 14097 | 1835342 | 0.57 |
| 94 | 80.521 | 9745 | 1223646 | 0.38 |
| 95 | 81.326 | 7626 | 1116851 | 0.347 |
| 96 | 81.92 | 5955 | 746580 | 0.232 |
| 97 | 82.393 | 7689 | 1055711 | 0.328 |
| 98 | 83.128 | 8130 | 1136353 | 0.353 |
| 99 | 83.601 | 10966 | 1224831 | 0.381 |
| 100 | 84.013 | 11895 | 1594770 | 0.496 |
| 101 | 84.919 | 17458 | 2996472 | 0.931 |
| 102 | 85.553 | 6597 | 993326 | 0.309 |
| 103 | 86.117 | 12493 | 2603274 | 0.809 |
| 104 | 86.801 | 16385 | 2301439 | 0.715 |
| 105 | 87.133 | 7317 | 815914 | 0.254 |
| 106 | 87.526 | 9253 | 1059186 | 0.329 |
| 107 | 89.65 | 19086 | 2875755 | 0.894 |
| 108 | 90.425 | 8058 | 1804994 | 0.561 |
| 109 | 90.998 | 107535 | 11392724 | 3.541 |
| 110 | 92.679 | 9983 | 1501056 | 0.467 |
| 111 | 94.138 | 12594 | 1833851 | 0.57 |
| 112 | 94.541 | 15092 | 2414715 | 0.75 |
| 113 | 95.477 | 8968 | 1507045 | 0.468 |
| 114 | 95.759 | 6253 | 738600 | 0.23 |
| 115 | 96.131 | 10812 | 1452753 | 0.451 |
| 116 | 96.775 | 28847 | 6371307 | 1.98 |
| 117 | 97.128 | 5347 | 607875 | 0.189 |
| 118 | 98.034 | 10241 | 1288876 | 0.401 |
| 119 | 98.768 | 8599 | 1679060 | 0.522 |
| 120 | 99.332 | 6678 | 1632211 | 0.507 |
| 121 | 101.2 | 5198 | 1184821 | 0.368 |
| 122 | 102.05 | 96407 | 10917106 | 3.393 |
| 123 | 102.97 | 46533 | 5538514 | 1.721 |
| 124 | 103.12 | 52495 | 4641527 | 1.443 |
| 125 | 106.71 | 12807 | 2689516 | 0.836 |
| 126 | 107.14 | 8448 | 1234768 | 0.384 |
| 127 | 108.77 | 8491 | 1371082 | 0.426 |
| 128 | 109.48 | 6850 | 1133027 | 0.352 |
| 129 | 111.74 | 5174 | 962642 | 0.299 |
| 130 | 112.6 | 85838 | 9492242 | 2.95 |
| 131 | 113.33 | 5925 | 749638 | 0.233 |
| 132 | 113.69 | 27422 | 2998787 | 0.932 |

| Pk | R.T. | Height | Area | %Tot |
|-----|--------|--------|---------|-------|
| 133 | 113.83 | 26815 | 2639290 | 0.82 |
| 134 | 117.43 | 7339 | 938941 | 0.292 |
| 135 | 118.41 | 5663 | 825006 | 0.256 |
| 136 | 119.01 | 6415 | 1045058 | 0.325 |
| 137 | 122.1 | 7200 | 1480219 | 0.46 |
| 138 | 122.64 | 79068 | 8592977 | 2.671 |
| 139 | 126.8 | 5887 | 1090844 | 0.339 |
| 140 | 127.61 | 8592 | 1093341 | 0.34 |
| 141 | 132.23 | 66029 | 7349723 | 2.284 |
| 142 | 141.4 | 45942 | 4956062 | 1.54 |
| 143 | 150.19 | 29831 | 3184493 | 0.99 |
| 144 | 158.62 | 16995 | 1713286 | 0.532 |
| 145 | 166.74 | 6050 | 661231 | 0.205 |
| End | | | | |

Table D-10 GC-MS report for fresh DF – sample 3 (S3)

| Pk | R.T. | Height | Area | %Tot |
|----|--------|--------|---------|-------|
| 1 | 4.733 | 3963 | 514178 | 0.206 |
| 2 | 7.582 | 9806 | 1419608 | 0.568 |
| 3 | 8.628 | 7261 | 1035362 | 0.414 |
| 4 | 10.168 | 11951 | 1379055 | 0.552 |
| 5 | 12.543 | 7032 | 901629 | 0.361 |
| 6 | 13.147 | 13351 | 2868986 | 1.148 |
| 7 | 13.751 | 7241 | 567595 | 0.227 |
| 8 | 15.643 | 27218 | 4424711 | 1.77 |
| 9 | 17.898 | 8507 | 724199 | 0.29 |
| 10 | 18.15 | 25273 | 3128706 | 1.252 |
| 11 | 20.263 | 7347 | 638379 | 0.255 |
| 12 | 20.515 | 9142 | 1170955 | 0.468 |
| 13 | 21.27 | 8958 | 1039850 | 0.416 |
| 14 | 21.632 | 13947 | 2060162 | 0.824 |
| 15 | 22.045 | 12069 | 1330855 | 0.532 |
| 16 | 24.017 | 10390 | 2536386 | 1.015 |
| 17 | 24.651 | 12619 | 1771887 | 0.709 |
| 18 | 24.963 | 7869 | 929472 | 0.372 |
| 19 | 27.822 | 8989 | 904356 | 0.362 |

| Pk | R.T. | Height | Area | %Tot | Pk | R.T. | Height | Area | %Tot |
|----|--------|--------|---------|-------|-----|--------|--------|----------|-------|
| 20 | 28.436 | 11465 | 1300522 | 0.52 | 63 | 64.397 | 26841 | 4342995 | 1.737 |
| 21 | 29.07 | 43109 | 4412394 | 1.765 | 64 | 65.303 | 8528 | 1296266 | 0.519 |
| 22 | 29.563 | 10718 | 1230151 | 0.492 | 65 | 66.249 | 15283 | 1689890 | 0.676 |
| 23 | 29.965 | 8287 | 745675 | 0.298 | 66 | 67.195 | 84846 | 8342317 | 3.337 |
| 24 | 31.002 | 13224 | 1740205 | 0.696 | 67 | 67.457 | 7287 | 726769 | 0.291 |
| 25 | 31.918 | 21053 | 2640192 | 1.056 | 68 | 67.869 | 6891 | 478817 | 0.192 |
| 26 | 31.968 | 20748 | 1747679 | 0.699 | 69 | 67.92 | 6971 | 322034 | 0.129 |
| 27 | 33.216 | 7375 | 597304 | 0.239 | 70 | 70.547 | 11667 | 1863456 | 0.745 |
| 28 | 33.78 | 10542 | 1264746 | 0.506 | 71 | 71.191 | 14230 | 2843016 | 1.137 |
| 29 | 36.105 | 12384 | 2702239 | 1.081 | 72 | 71.935 | 9415 | 2553576 | 1.022 |
| 30 | 36.487 | 7288 | 654540 | 0.262 | 73 | 73.697 | 13935 | 1522746 | 0.609 |
| 31 | 37.071 | 15721 | 1773012 | 0.709 | 74 | 74.331 | 10523 | 1134260 | 0.454 |
| 32 | 37.776 | 6201 | 578358 | 0.231 | 75 | 75.035 | 42250 | 5116112 | 2.047 |
| 33 | 38.792 | 12521 | 836110 | 0.334 | 76 | 75.73 | 8563 | 908860 | 0.364 |
| 34 | 38.833 | 11829 | 657446 | 0.263 | 77 | 76.183 | 12873 | 1554539 | 0.622 |
| 35 | 41.58 | 59264 | 6333864 | 2.534 | 78 | 76.686 | 16469 | 1908986 | 0.764 |
| 36 | 43.553 | 26712 | 2773627 | 1.11 | 79 | 77.451 | 5267 | 639749 | 0.256 |
| 37 | 44.952 | 37004 | 4589473 | 1.836 | 80 | 78.357 | 11255 | 1906653 | 0.763 |
| 38 | 47.106 | 8593 | 967099 | 0.387 | 81 | 78.749 | 11913 | 1420730 | 0.568 |
| 39 | 47.579 | 29140 | 3224256 | 1.29 | 82 | 79.383 | 97613 | 10246878 | 4.099 |
| 40 | 47.921 | 18430 | 1926442 | 0.771 | 83 | 80.229 | 11042 | 1267409 | 0.507 |
| 41 | 48.706 | 10347 | 1020125 | 0.408 | 84 | 80.521 | 7126 | 793729 | 0.318 |
| 42 | 49.27 | 16069 | 1658536 | 0.663 | 85 | 83.631 | 8933 | 954823 | 0.382 |
| 43 | 49.864 | 11882 | 1621344 | 0.649 | 86 | 84.043 | 8441 | 1100567 | 0.44 |
| 44 | 50.608 | 7520 | 690020 | 0.276 | 87 | 84.909 | 14600 | 1065402 | 0.426 |
| 45 | 51.263 | 25260 | 2437865 | 0.975 | 88 | 84.959 | 13106 | 701092 | 0.28 |
| 46 | 52.007 | 28118 | 3476939 | 1.391 | 89 | 86.107 | 10174 | 1251554 | 0.501 |
| 47 | 52.541 | 8428 | 1108651 | 0.444 | 90 | 86.811 | 13937 | 1775060 | 0.71 |
| 48 | 52.802 | 8277 | 752688 | 0.301 | 91 | 87.536 | 9171 | 900863 | 0.36 |
| 49 | 54.513 | 67640 | 6924174 | 2.77 | 92 | 89.639 | 17499 | 2540351 | 1.016 |
| 50 | 54.835 | 7794 | 719524 | 0.288 | 93 | 91.008 | 93366 | 10268919 | 4.108 |
| 51 | 56.798 | 8850 | 1224596 | 0.49 | 94 | 94.148 | 8041 | 1057628 | 0.423 |
| 52 | 58.157 | 15142 | 1503216 | 0.601 | 95 | 94.511 | 7535 | 951480 | 0.381 |
| 53 | 60.431 | 13332 | 1496923 | 0.599 | 96 | 95.457 | 6220 | 681271 | 0.273 |
| 54 | 60.784 | 18291 | 2198378 | 0.879 | 97 | 96.121 | 7023 | 914553 | 0.366 |
| 55 | 61.045 | 11858 | 1530957 | 0.612 | 98 | 96.644 | 21319 | 2269653 | 0.908 |
| 56 | 61.398 | 19701 | 1969874 | 0.788 | 99 | 96.805 | 23517 | 2261629 | 0.905 |
| 57 | 61.639 | 14827 | 1625175 | 0.65 | 100 | 98.043 | 8451 | 828765 | 0.332 |
| 58 | 61.981 | 8525 | 817415 | 0.327 | 101 | 102.07 | 89595 | 9461537 | 3.785 |
| 59 | 62.636 | 13289 | 1674378 | 0.67 | 102 | 102.98 | 41235 | 4224707 | 1.69 |
| 60 | 63.028 | 14869 | 1565033 | 0.626 | 103 | 103.12 | 46963 | 4429772 | 1.772 |
| 61 | 63.159 | 18119 | 1599018 | 0.64 | 104 | 106.75 | 5779 | 637705 | 0.255 |
| 62 | 63.38 | 27627 | 3898526 | 1.56 | 105 | 106.86 | 1938 | 30209 | 0.012 |

| Pk | R.T. | Height | Area | %Tot | Pk | R.T. | Height | Area | %Tot |
|-----|--------|--------|---------|-------|----|--------|--------|----------|-------|
| 106 | 112.6 | 79982 | 8383743 | 3.354 | 25 | 21.184 | 25445 | 3152255 | 0.117 |
| 107 | 113.71 | 23017 | 2235723 | 0.894 | 26 | 22.05 | 32538 | 4358888 | 0.162 |
| 108 | 113.84 | 21504 | 1816005 | 0.726 | 27 | 22.523 | 61090 | 10244419 | 0.382 |
| 109 | 122.65 | 70682 | 6714264 | 2.686 | 28 | 22.705 | 72221 | 7898134 | 0.294 |
| 110 | 132.23 | 58698 | 6387358 | 2.555 | 29 | 23.067 | 89283 | 11111798 | 0.414 |
| 111 | 141.4 | 45071 | 4912582 | 1.965 | 30 | 23.43 | 76854 | 8957394 | 0.334 |
| 112 | 150.19 | 29439 | 3241998 | 1.297 | 31 | 24.054 | 51599 | 5807786 | 0.216 |
| 113 | 158.62 | 15460 | 1539120 | 0.616 | 32 | 24.497 | 34396 | 4475517 | 0.167 |
| End | | | | | 33 | 25 | 23186 | 5473616 | 0.204 |
| | | | | | 34 | 26.148 | 62030 | 6223828 | 0.232 |
| | | | | | 35 | 26.41 | 32565 | 3258173 | 0.121 |
| | | | | | 36 | 26.763 | 58293 | 6978362 | 0.26 |
| | | | | | 37 | 27.427 | 492344 | 44154915 | 1.645 |
| | | | | | 38 | 27.85 | 70024 | 7768709 | 0.289 |
| | | | | | 39 | 28.253 | 53066 | 5275034 | 0.196 |
| | | | | | 40 | 29.239 | 75994 | 9300185 | 0.346 |
| | | | | | 41 | 30.136 | 139530 | 26379553 | 0.982 |
| | | | | | 42 | 30.679 | 42483 | 3704252 | 0.138 |
| | | | | | 43 | 31.042 | 35424 | 3956747 | 0.147 |
| | | | | | 44 | 31.515 | 51953 | 8291342 | 0.309 |
| | | | | | 45 | 31.978 | 61386 | 7790353 | 0.29 |
| | | | | | 46 | 32.834 | 42003 | 6491409 | 0.242 |
| | | | | | 47 | 33.458 | 39869 | 4241776 | 0.158 |
| | | | | | 48 | 34.284 | 112269 | 21449937 | 0.799 |
| | | | | | 49 | 34.667 | 82898 | 8965317 | 0.334 |
| | | | | | 50 | 35.251 | 157789 | 15567727 | 0.58 |
| | | | | | 51 | 35.966 | 75710 | 6591973 | 0.246 |
| | | | | | 52 | 36.388 | 42135 | 8825002 | 0.329 |
| | | | | | 53 | 36.892 | 84383 | 12416745 | 0.462 |
| | | | | | 54 | 37.456 | 43850 | 6863125 | 0.256 |
| | | | | | 55 | 37.889 | 52282 | 13223226 | 0.492 |
| | | | | | 56 | 39.741 | 662950 | 68872081 | 2.565 |
| | | | | | 57 | 40.456 | 22753 | 3077143 | 0.115 |
| | | | | | 58 | 41.695 | 193665 | 23964210 | 0.893 |
| | | | | | 59 | 42.591 | 32449 | 3083108 | 0.115 |
| | | | | | 60 | 42.973 | 231943 | 25751816 | 0.959 |
| | | | | | 61 | 43.356 | 37630 | 2807199 | 0.105 |
| | | | | | 62 | 44.192 | 35856 | 4848985 | 0.181 |
| | | | | | 63 | 44.866 | 25851 | 4091026 | 0.152 |
| | | | | | 64 | 45.118 | 65939 | 6970919 | 0.26 |
| | | | | | 65 | 45.571 | 140548 | 15795668 | 0.588 |
| | | | | | 66 | 45.893 | 120444 | 12743361 | 0.475 |
| | | | | | 67 | 46.538 | 43410 | 4163393 | 0.155 |

Table D-11 GC-MS report for fresh DF – sample 4 (S4)

| Pk | R.T. | Height | Area | %Tot |
|----|--------|--------|----------|-------|
| 1 | 5.89 | 27151 | 3003283 | 0.112 |
| 2 | 6.051 | 22911 | 2402287 | 0.089 |
| 3 | 6.917 | 59747 | 8410519 | 0.313 |
| 4 | 7.863 | 54787 | 6882764 | 0.256 |
| 5 | 8.276 | 37299 | 4415618 | 0.164 |
| 6 | 9.333 | 95495 | 9907056 | 0.369 |
| 7 | 10.652 | 35665 | 3657650 | 0.136 |
| 8 | 11.538 | 64699 | 8134800 | 0.303 |
| 9 | 11.961 | 70802 | 5257830 | 0.196 |
| 10 | 12.092 | 93936 | 16664907 | 0.621 |
| 11 | 12.676 | 74175 | 6926080 | 0.258 |
| 12 | 12.938 | 77502 | 9199763 | 0.343 |
| 13 | 13.613 | 50215 | 5385554 | 0.201 |
| 14 | 13.844 | 48897 | 6462107 | 0.241 |
| 15 | 14.458 | 159717 | 22506429 | 0.838 |
| 16 | 14.831 | 33027 | 3374752 | 0.126 |
| 17 | 16.603 | 54884 | 4855040 | 0.181 |
| 18 | 16.845 | 282744 | 27614405 | 1.028 |
| 19 | 18.879 | 62999 | 4851180 | 0.181 |
| 20 | 19.13 | 85891 | 8943743 | 0.333 |
| 21 | 19.644 | 43515 | 6169259 | 0.23 |
| 22 | 19.825 | 55797 | 5834228 | 0.217 |
| 23 | 20.157 | 90971 | 15118102 | 0.563 |
| 24 | 20.6 | 71756 | 10359348 | 0.386 |

| Pk | R.T. | Height | Area | %Tot | Pk | R.T. | Height | Area | %Tot |
|-----|--------|--------|----------|-------|-----|--------|---------|-----------|-------|
| 68 | 46.759 | 85723 | 10132548 | 0.377 | 111 | 68.8 | 46067 | 5248628 | 0.195 |
| 69 | 47.293 | 110404 | 12781726 | 0.476 | 112 | 69.072 | 99103 | 19686466 | 0.733 |
| 70 | 47.696 | 46033 | 6437670 | 0.24 | 113 | 69.797 | 78075 | 18434283 | 0.687 |
| 71 | 47.948 | 120978 | 11508783 | 0.429 | 114 | 70.542 | 26415 | 2986984 | 0.111 |
| 72 | 48.683 | 79303 | 7848486 | 0.292 | 115 | 70.824 | 29916 | 4055436 | 0.151 |
| 73 | 49.337 | 232062 | 23660620 | 0.881 | 116 | 71.146 | 70737 | 7457146 | 0.278 |
| 74 | 49.7 | 45383 | 4591488 | 0.171 | 117 | 71.287 | 61063 | 5150559 | 0.192 |
| 75 | 49.971 | 166555 | 20661527 | 0.77 | 118 | 71.65 | 76261 | 11856212 | 0.442 |
| 76 | 50.485 | 65519 | 10606923 | 0.395 | 119 | 72.274 | 85208 | 16210196 | 0.604 |
| 77 | 50.777 | 69021 | 8568016 | 0.319 | 120 | 72.999 | 443706 | 54819068 | 2.042 |
| 78 | 51.139 | 51401 | 7181842 | 0.267 | 121 | 73.674 | 88789 | 11078163 | 0.413 |
| 79 | 52.559 | 797203 | 81539362 | 3.037 | 122 | 73.986 | 69258 | 8182385 | 0.305 |
| 80 | 52.992 | 34456 | 5381337 | 0.2 | 123 | 74.499 | 77291 | 14380135 | 0.536 |
| 81 | 53.546 | 32623 | 3002179 | 0.112 | 124 | 75.365 | 52220 | 8605579 | 0.321 |
| 82 | 53.838 | 48467 | 6748012 | 0.251 | 125 | 76.11 | 62477 | 9403129 | 0.35 |
| 83 | 54.301 | 40520 | 5876310 | 0.219 | 126 | 76.523 | 67230 | 13091557 | 0.488 |
| 84 | 54.674 | 62560 | 7826062 | 0.291 | 127 | 77.339 | 1066015 | 112050856 | 4.173 |
| 85 | 54.915 | 58386 | 5278059 | 0.197 | 128 | 78.013 | 54293 | 7886429 | 0.294 |
| 86 | 55.741 | 25700 | 2831733 | 0.105 | 129 | 78.336 | 46599 | 8023674 | 0.299 |
| 87 | 56.134 | 126765 | 16954690 | 0.631 | 130 | 79.181 | 47960 | 11099734 | 0.413 |
| 88 | 56.838 | 45813 | 5133796 | 0.191 | 131 | 81.497 | 65230 | 8498400 | 0.317 |
| 89 | 58.006 | 36187 | 7053536 | 0.263 | 132 | 81.96 | 49998 | 7213361 | 0.269 |
| 90 | 58.308 | 93014 | 9825405 | 0.366 | 133 | 82.806 | 60640 | 8650676 | 0.322 |
| 91 | 58.671 | 107396 | 16354762 | 0.609 | 134 | 83.068 | 44723 | 3785197 | 0.141 |
| 92 | 59.033 | 85953 | 12890171 | 0.48 | 135 | 83.451 | 52345 | 6100891 | 0.227 |
| 93 | 59.295 | 83052 | 10716250 | 0.399 | 136 | 84.075 | 72548 | 13951977 | 0.52 |
| 94 | 59.476 | 82262 | 9406913 | 0.35 | 137 | 84.739 | 131832 | 14418005 | 0.537 |
| 95 | 59.97 | 77625 | 7946701 | 0.296 | 138 | 85.102 | 38440 | 4756198 | 0.177 |
| 96 | 60.675 | 132999 | 12441141 | 0.463 | 139 | 85.444 | 74288 | 8183771 | 0.305 |
| 97 | 60.856 | 64580 | 5821892 | 0.217 | 140 | 87.367 | 36839 | 3309675 | 0.123 |
| 98 | 61.017 | 74817 | 6578221 | 0.245 | 141 | 88.213 | 35572 | 8100330 | 0.302 |
| 99 | 61.228 | 103237 | 11345878 | 0.423 | 142 | 88.938 | 1055297 | 111649945 | 4.158 |
| 100 | 61.39 | 106527 | 12014030 | 0.447 | 143 | 89.885 | 29749 | 3417293 | 0.127 |
| 101 | 62.034 | 33375 | 4162795 | 0.155 | 144 | 90.348 | 38242 | 7120174 | 0.265 |
| 102 | 62.407 | 289237 | 28625708 | 1.066 | 145 | 91.929 | 48431 | 8073803 | 0.301 |
| 103 | 63.131 | 35563 | 6494035 | 0.242 | 146 | 92.291 | 57233 | 7642651 | 0.285 |
| 104 | 64.068 | 70453 | 10272026 | 0.383 | 147 | 93.328 | 72527 | 8543436 | 0.318 |
| 105 | 65.175 | 875625 | 93263750 | 3.474 | 148 | 93.63 | 45286 | 5164331 | 0.192 |
| 106 | 65.8 | 94319 | 17349341 | 0.646 | 149 | 94.053 | 69820 | 11423089 | 0.425 |
| 107 | 66.515 | 24498 | 2540438 | 0.095 | 150 | 94.547 | 215685 | 23191666 | 0.864 |
| 108 | 66.817 | 16925 | 2925413 | 0.109 | 151 | 94.708 | 271019 | 32971767 | 1.228 |
| 109 | 68.317 | 71611 | 9698781 | 0.361 | 152 | 95.342 | 57923 | 8210553 | 0.306 |
| 110 | 68.538 | 42365 | 3491907 | 0.13 | 153 | 95.966 | 95218 | 9066594 | 0.338 |

| Pk | R.T. | Height | Area | %Tot |
|-----------|-------------|---------------|-------------|-------------|
| 154 | 96.671 | 64580 | 7044015 | 0.262 |
| 155 | 98.775 | 48438 | 6123904 | 0.228 |
| 156 | 99.974 | 992518 | 107086390 | 3.988 |
| 157 | 100.88 | 417690 | 38745334 | 1.443 |
| 158 | 101.031 | 479377 | 46984593 | 1.75 |
| 159 | 104.595 | 91963 | 8934039 | 0.333 |
| 160 | 104.726 | 83857 | 9977874 | 0.372 |
| 161 | 105.048 | 48174 | 5195554 | 0.194 |
| 162 | 105.491 | 41845 | 10452822 | 0.389 |
| 163 | 106.055 | 43700 | 6267657 | 0.233 |
| 164 | 106.68 | 75874 | 8697064 | 0.324 |
| 165 | 107.384 | 51188 | 5602344 | 0.209 |
| 166 | 109.549 | 27873 | 5760786 | 0.215 |
| 167 | 110.496 | 888395 | 94842669 | 3.532 |
| 168 | 111.573 | 194139 | 22473568 | 0.837 |
| 169 | 111.734 | 197587 | 18973304 | 0.707 |
| 170 | 114.795 | 32541 | 3639673 | 0.136 |
| 171 | 115.309 | 59330 | 11680506 | 0.435 |
| 172 | 116.295 | 39308 | 5372250 | 0.2 |
| 173 | 116.859 | 54545 | 7253644 | 0.27 |
| 174 | 117.574 | 33265 | 4274430 | 0.159 |
| 175 | 119.96 | 57763 | 12627205 | 0.47 |
| 176 | 120.524 | 796041 | 83127691 | 3.096 |
| 177 | 124.481 | 44367 | 7334783 | 0.273 |
| 178 | 125.438 | 63190 | 7413825 | 0.276 |
| 179 | 126.082 | 26190 | 4257647 | 0.159 |
| 180 | 126.616 | 44688 | 5518450 | 0.206 |
| 181 | 127.291 | 27332 | 2789035 | 0.104 |
| 182 | 130.1 | 665126 | 71200663 | 2.652 |
| 183 | 135.094 | 27668 | 2915075 | 0.109 |
| 184 | 136.635 | 25752 | 3172393 | 0.118 |
| 185 | 139.263 | 525730 | 55446529 | 2.065 |
| 186 | 148.023 | 367096 | 36435044 | 1.357 |
| 187 | 156.44 | 218289 | 22096865 | 0.823 |
| 188 | 164.556 | 99079 | 9950850 | 0.371 |
| 189 | 172.339 | 45474 | 4662945 | 0.174 |
| End | | | | |

D-4

Δ (PPA) ANALYSES FOR THERMALLY STRESSED DF

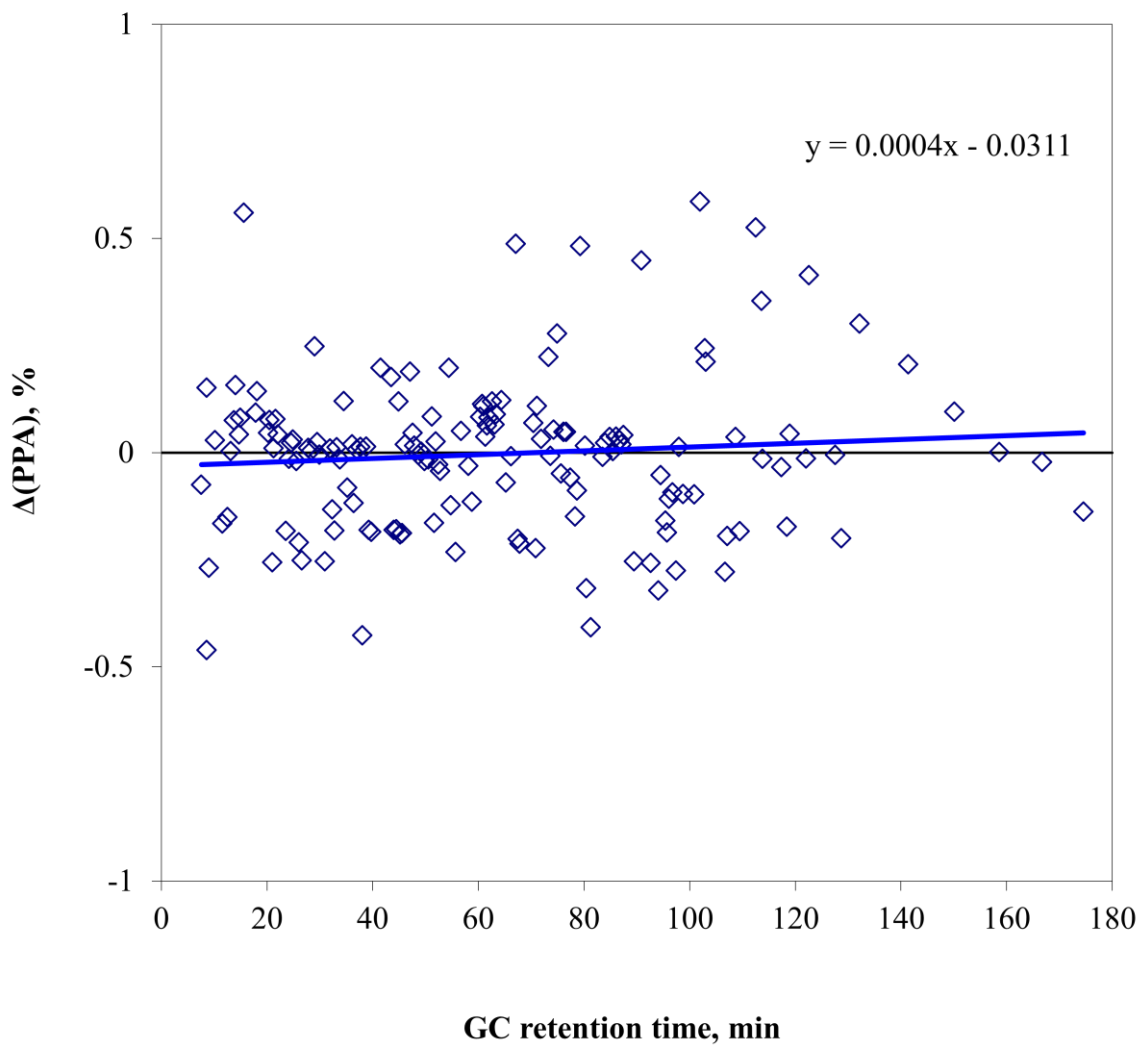


Fig. D-13 $\Delta(\text{PPA})$ for fresh DF (1000ppm, S1).

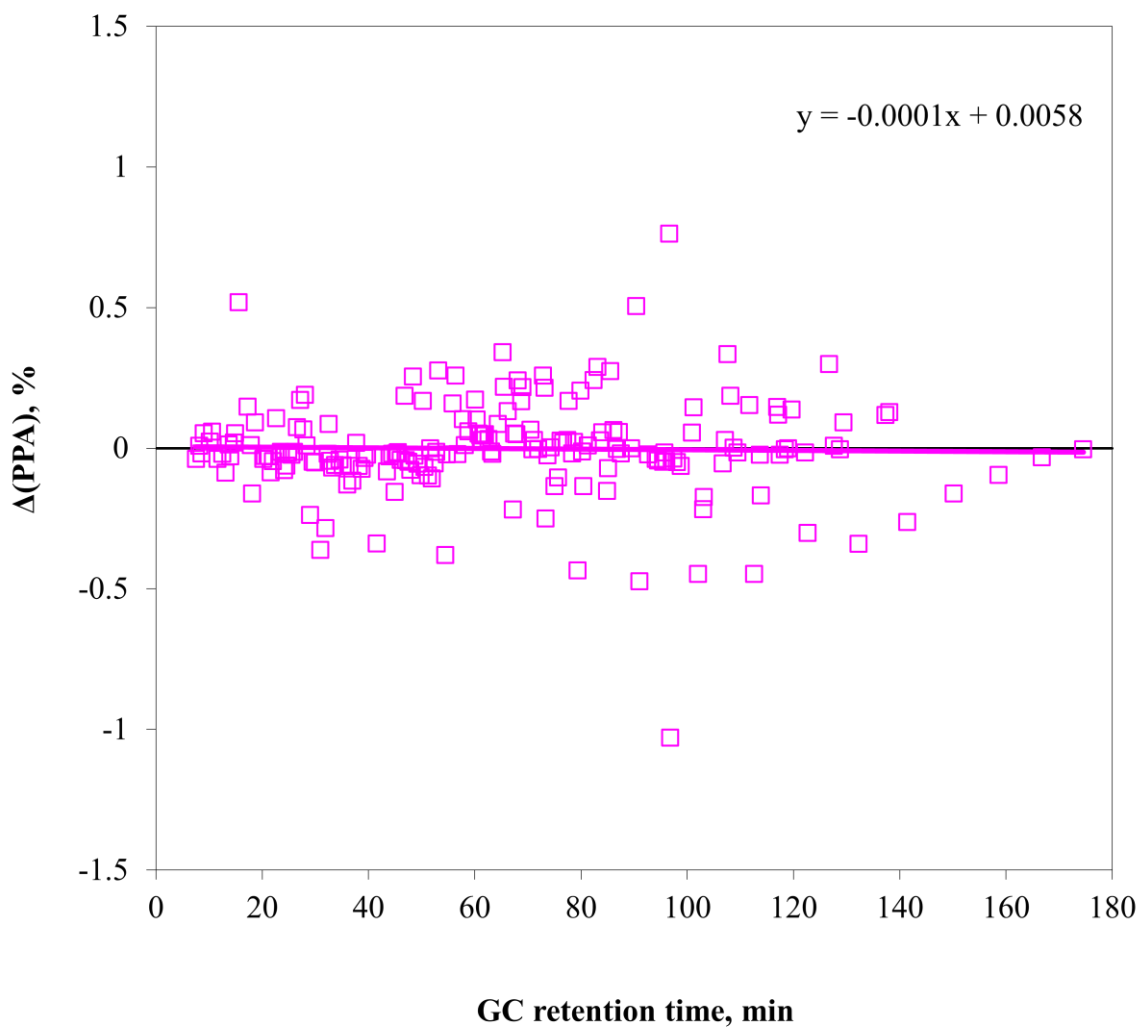


Fig. D-14 $\Delta(\text{PPA})$ for fresh DF (3000ppm, S1).

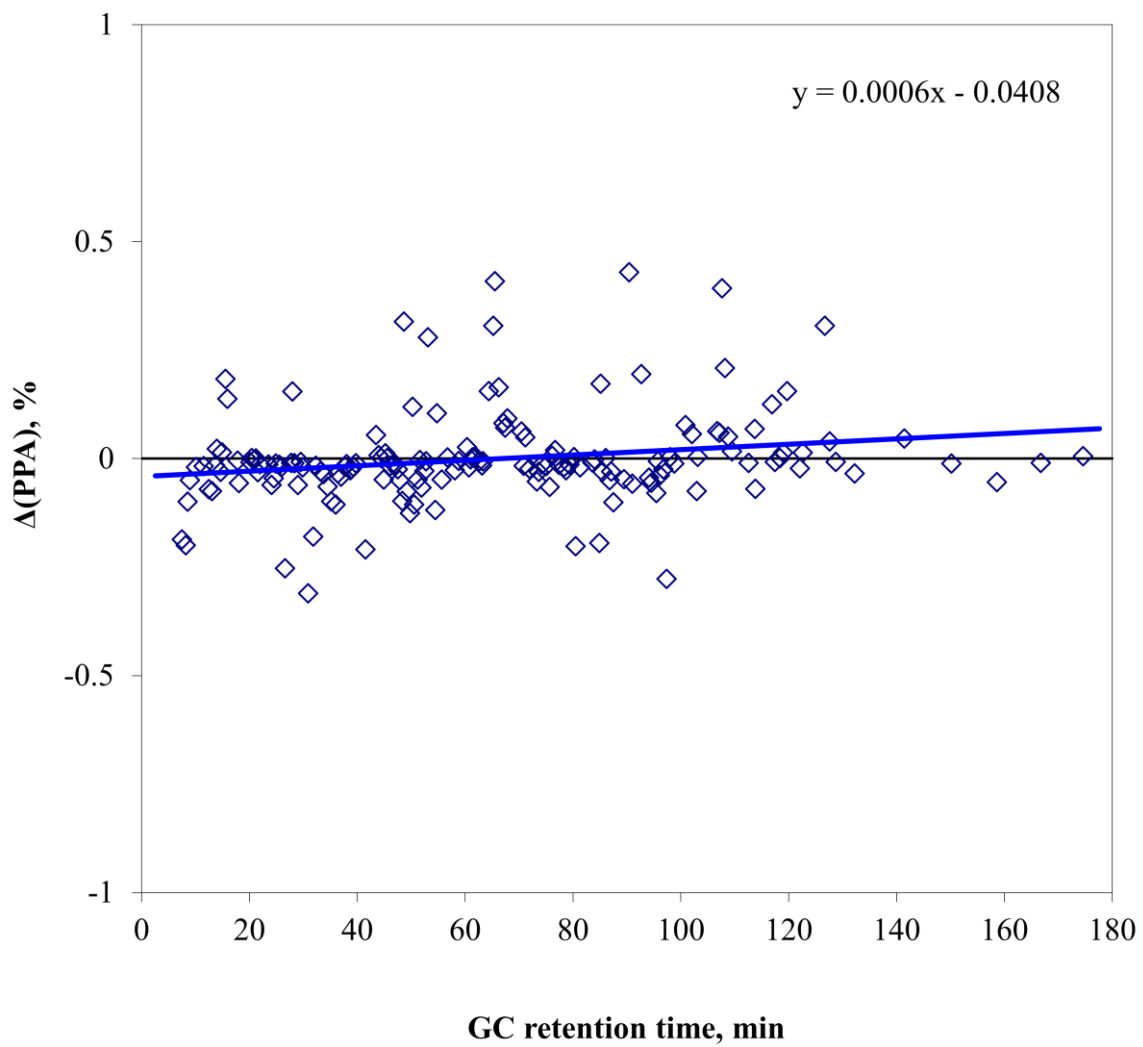


Fig. D-15 $\Delta(\text{PPA})$ for thermally stressed DF (200 °C, 15 min, DF, S1).

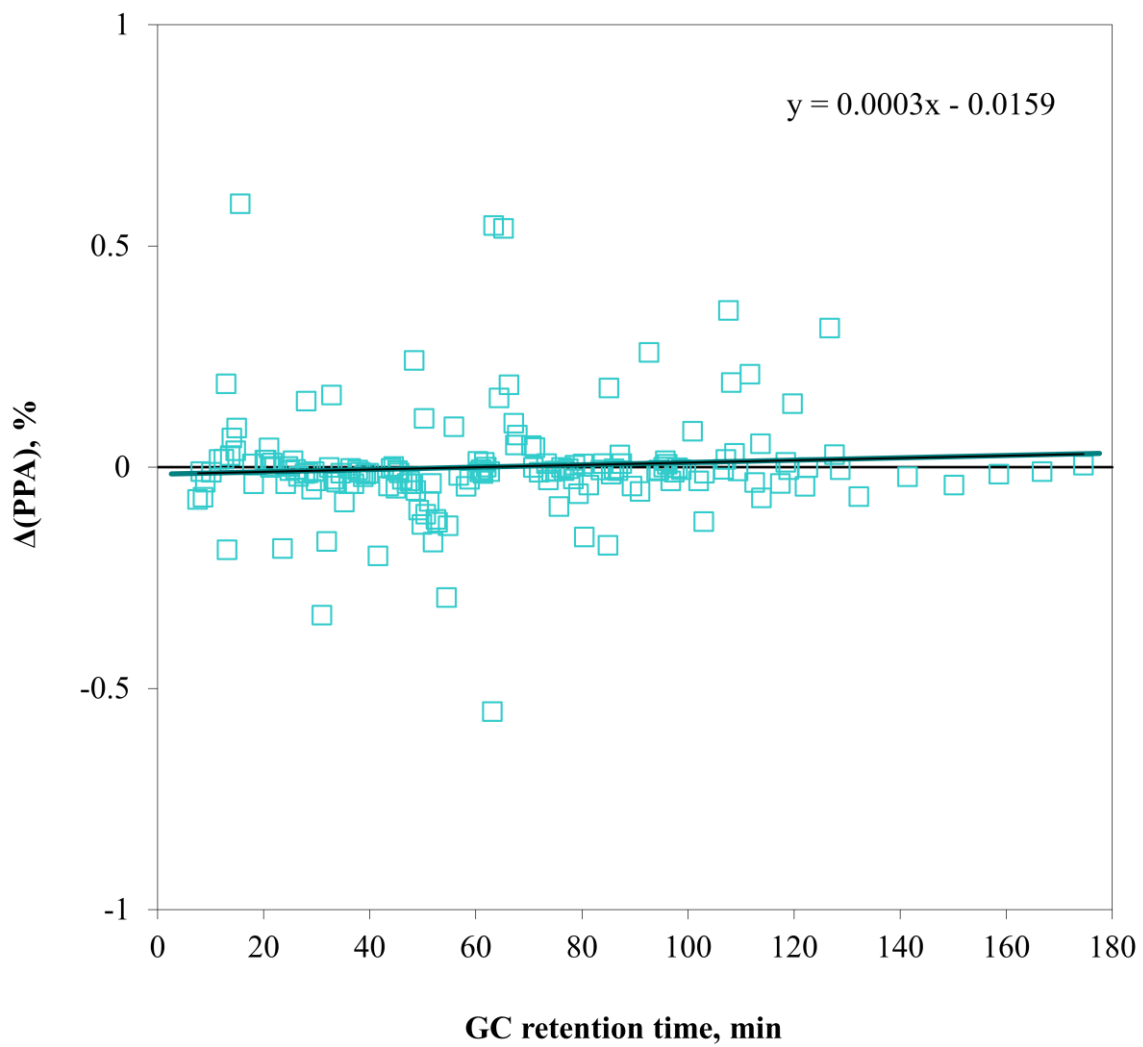


Fig. D-16 $\Delta(\text{PPA})$ for thermally stressed DF (300 °C, 10 min, DF, S1).

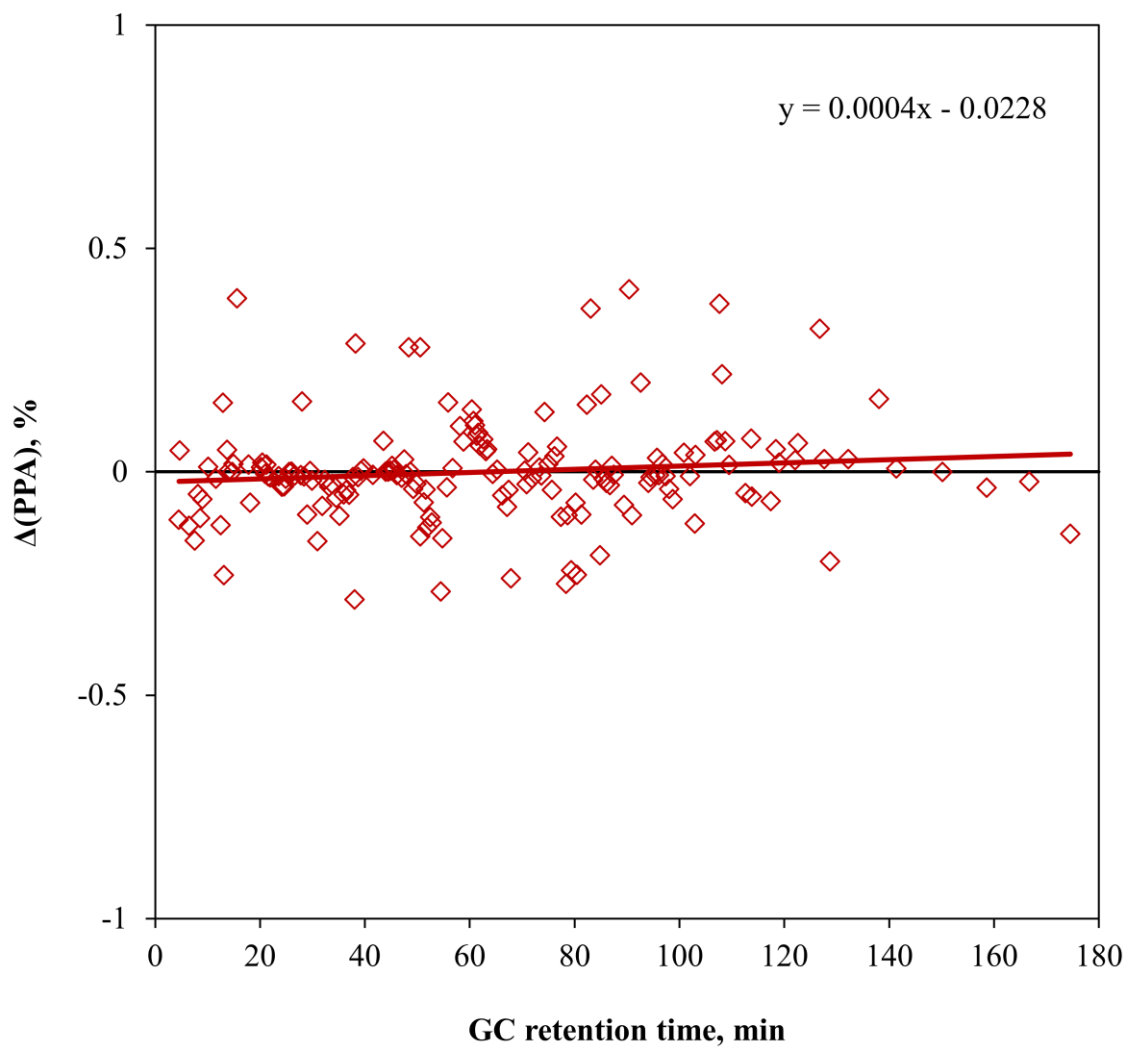


Fig. D-17 Δ(PPA) for thermally stressed DF (300 °C, 30 min, DF, w/air, S1).

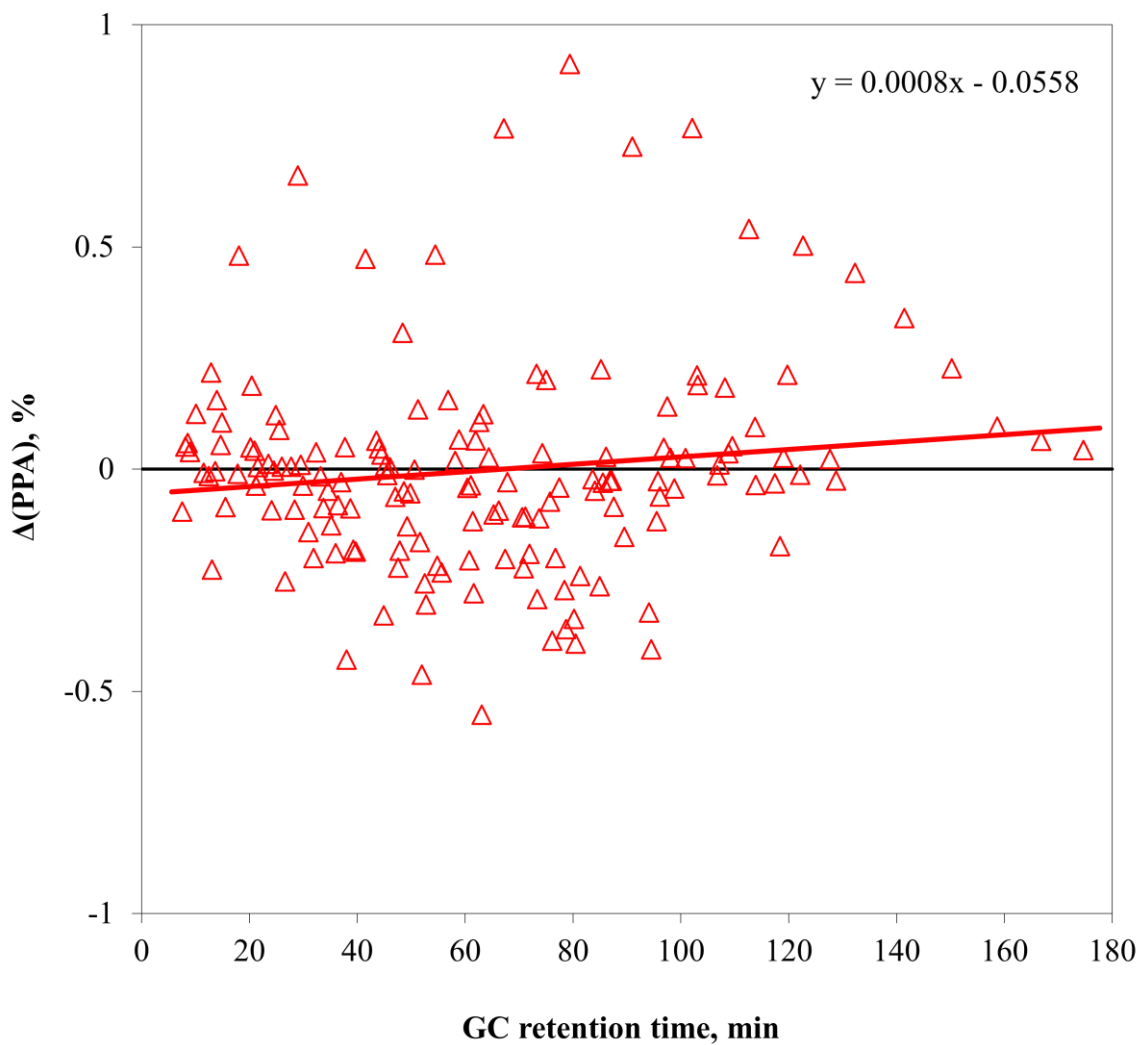


Fig. D-18 $\Delta(\text{PPA})$ for thermally stressed DF (300 °C, 600 min, DF, S1).

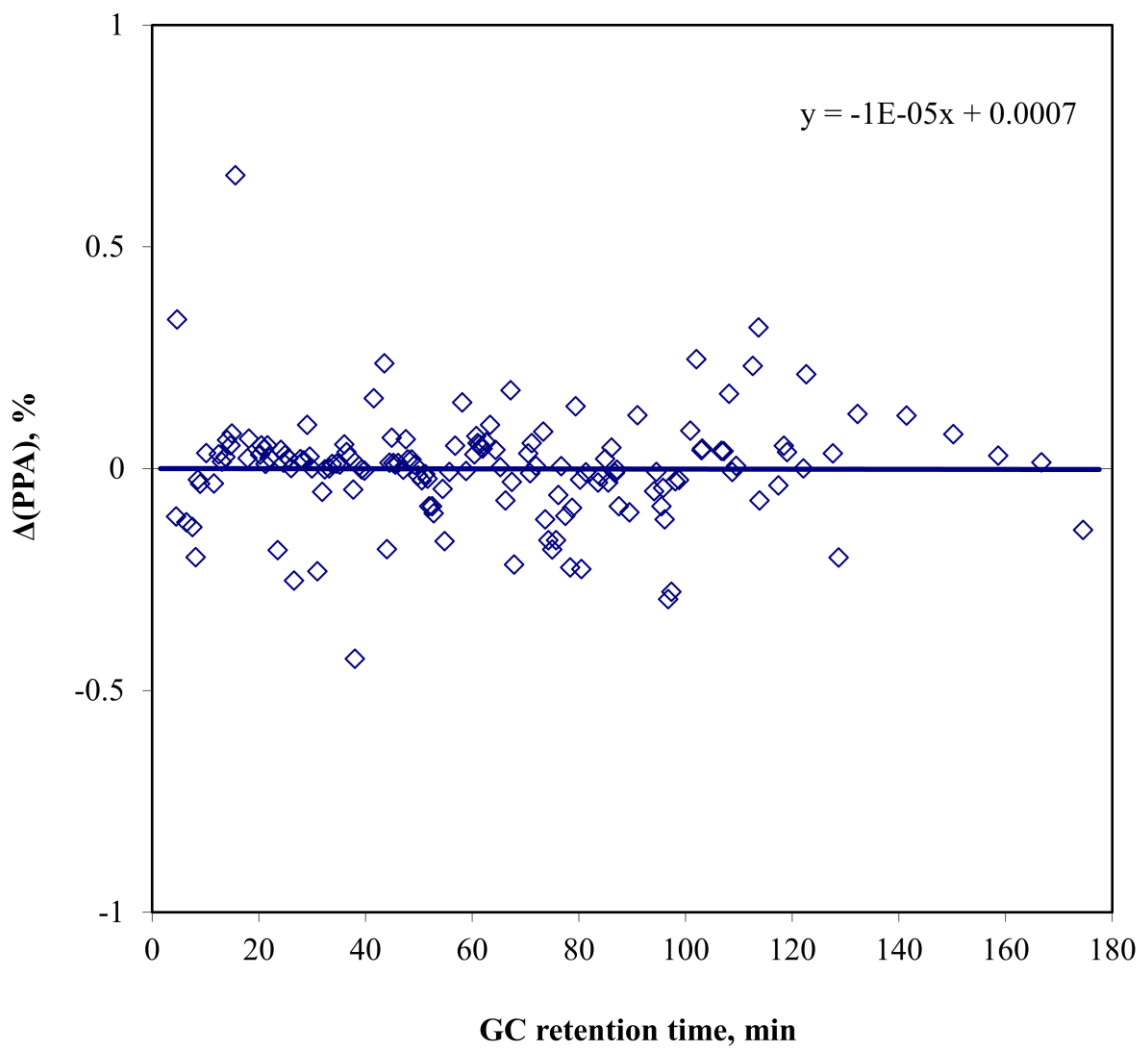


Fig. D-19 $\Delta(\text{PPA})$ for thermally stressed DF (400 °C, 10 min, DF, S1).

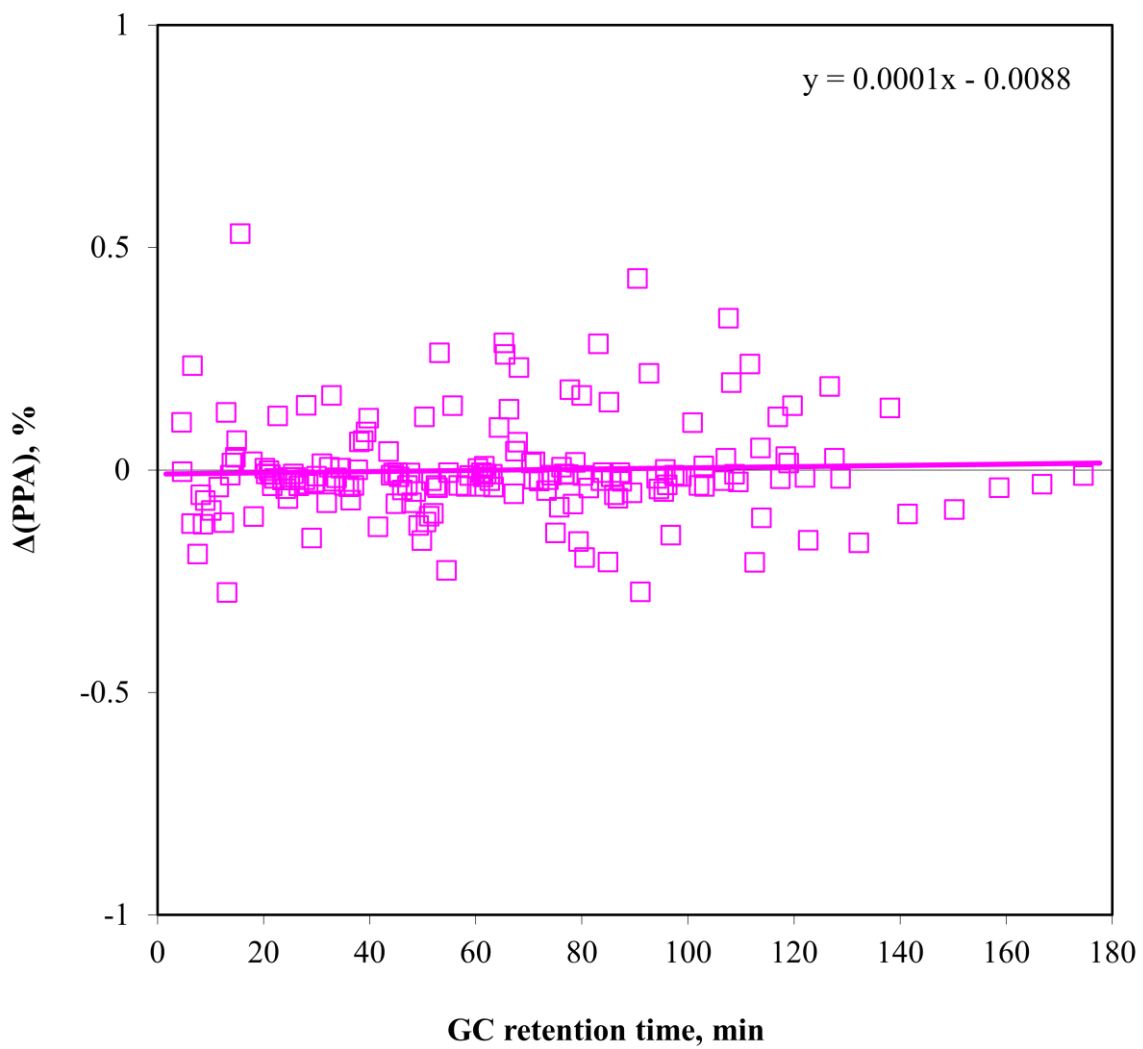


Fig. D-20 $\Delta(\text{PPA})$ for thermally stressed DF (400 °C, 30 min, DF, S1).

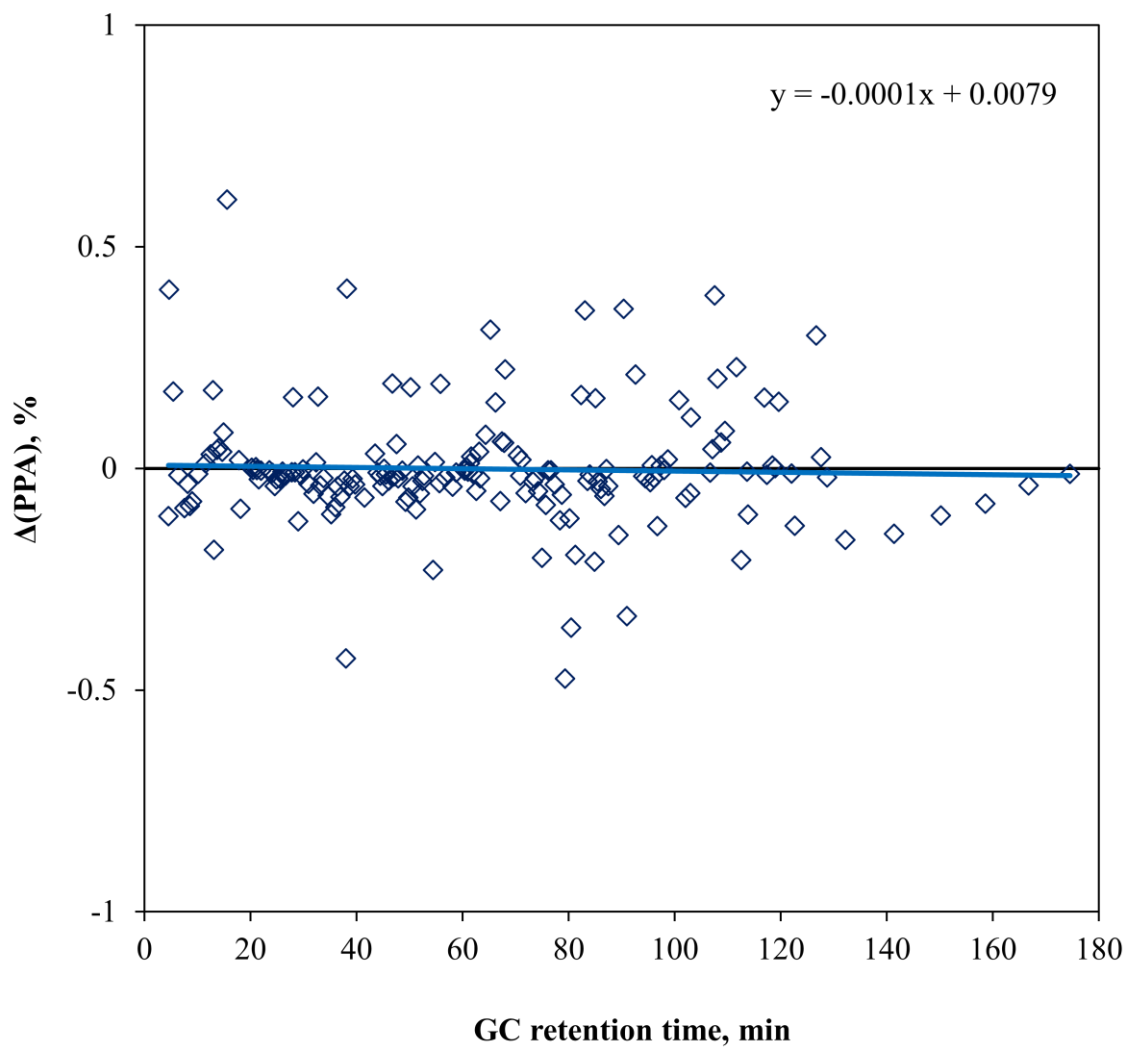


Fig. D-21 $\Delta(\text{PPA})$ for thermally stressed DF (400 °C, 30 min, DF, w/o air, S1).

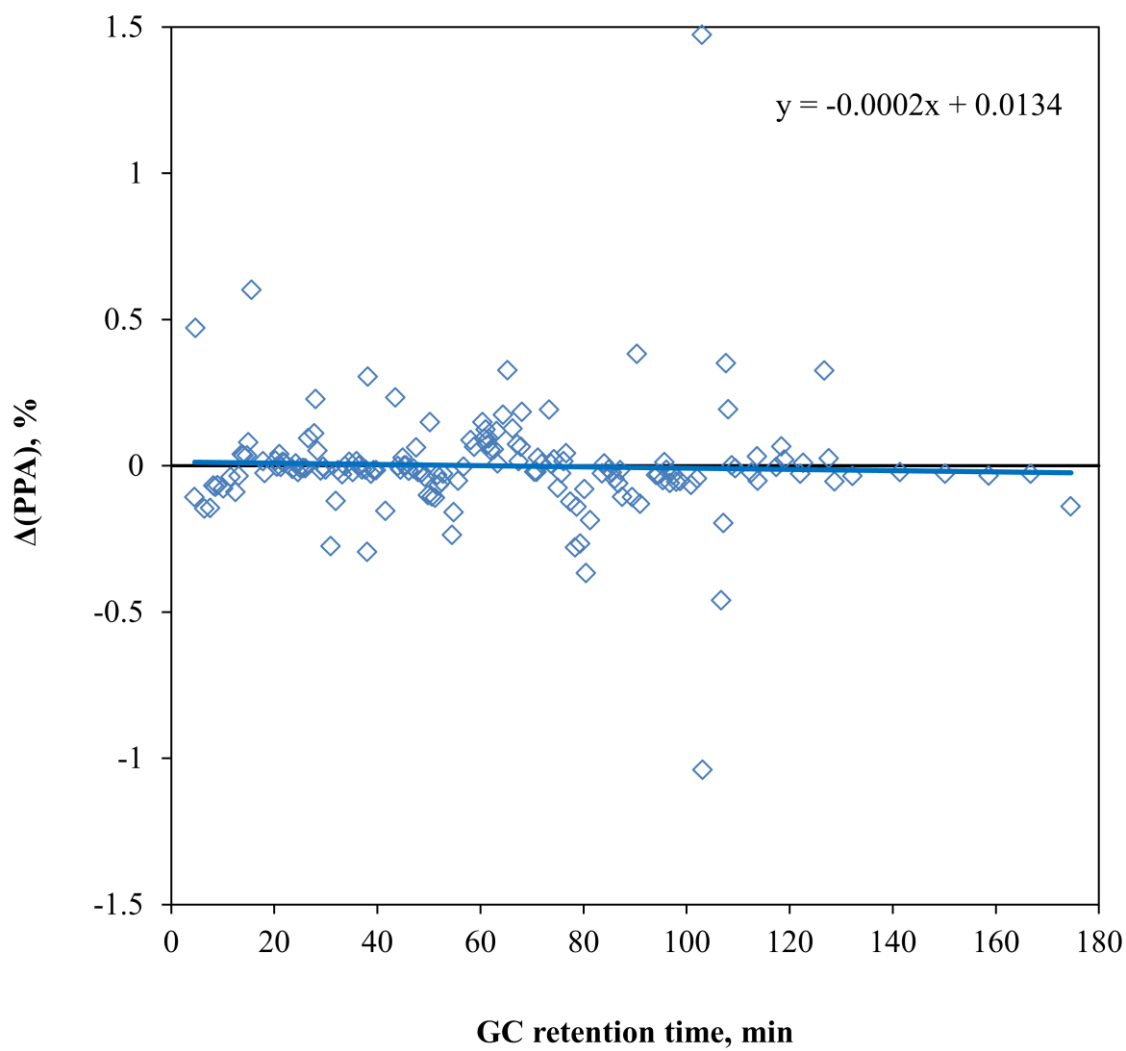


Fig. D-22 $\Delta(\text{PPA})$ for thermally stressed DF (400 °C, 30 min, DF, w/ air, S1).

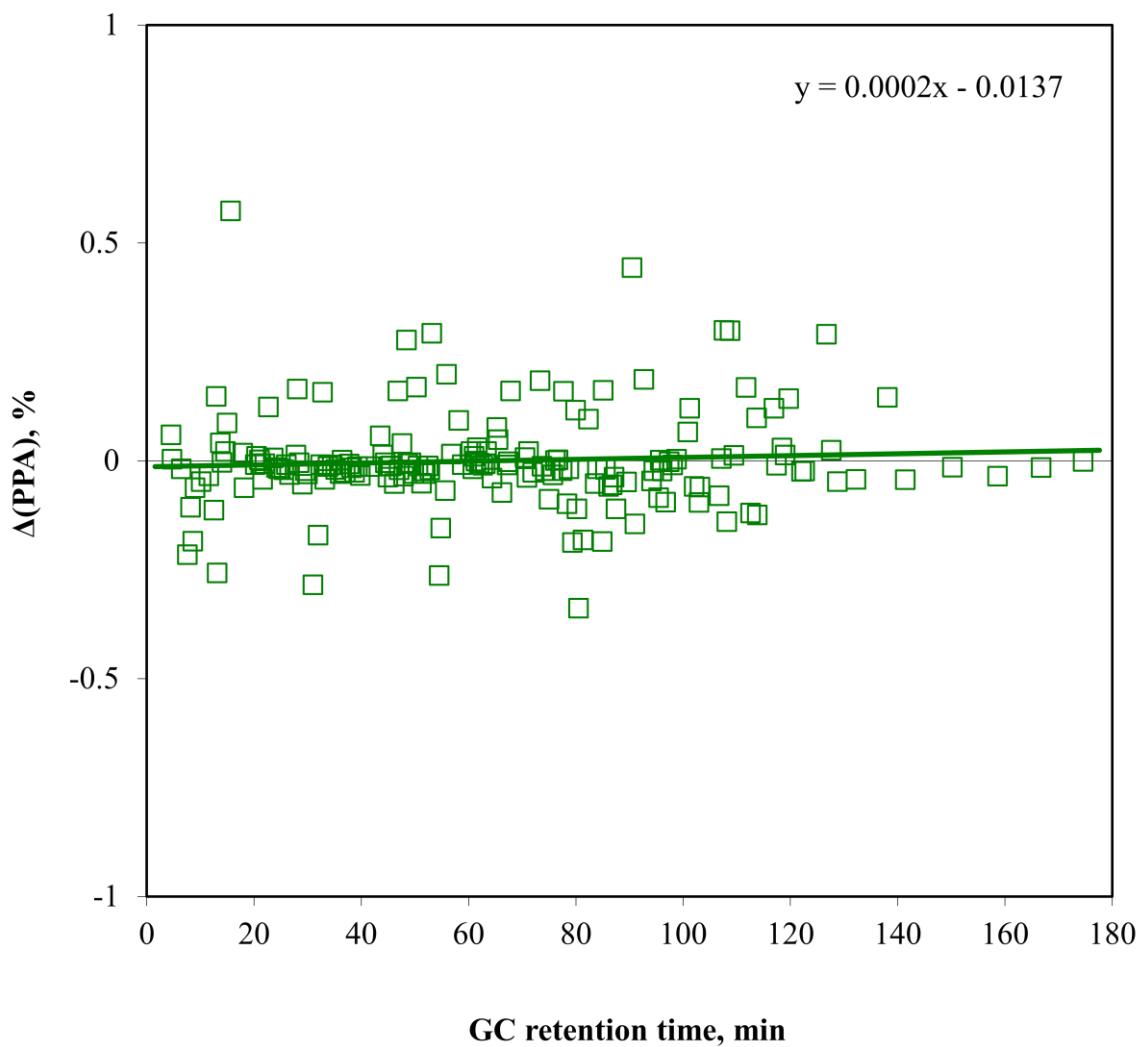


Fig. D-23 $\Delta(\text{PPA})$ for thermally stressed DF (400 °C, 60 min, DF, S1).

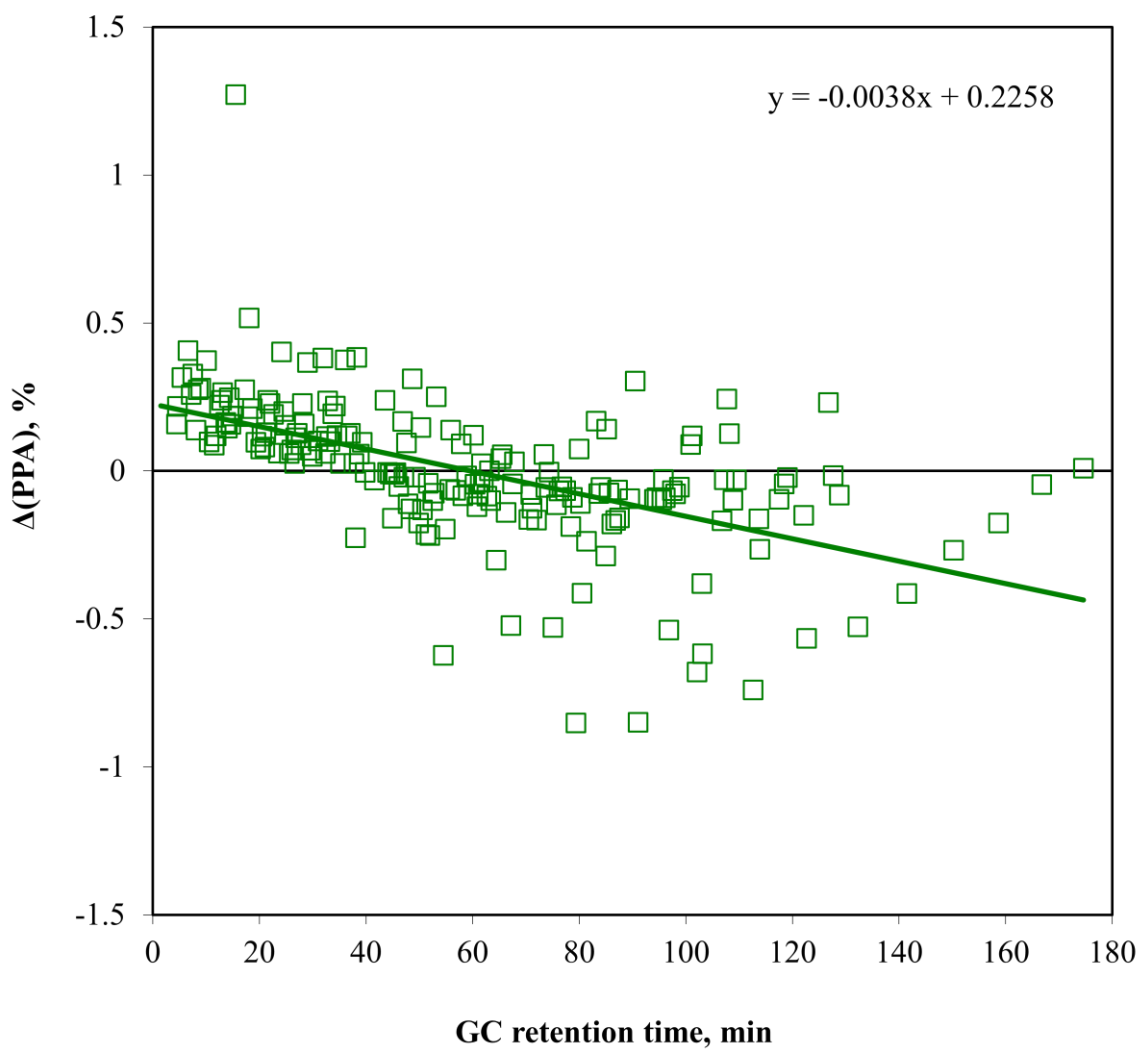


Fig. D-24 $\Delta(\text{PPA})$ for thermally stressed DF (400 °C, 180 min, DF, S1).

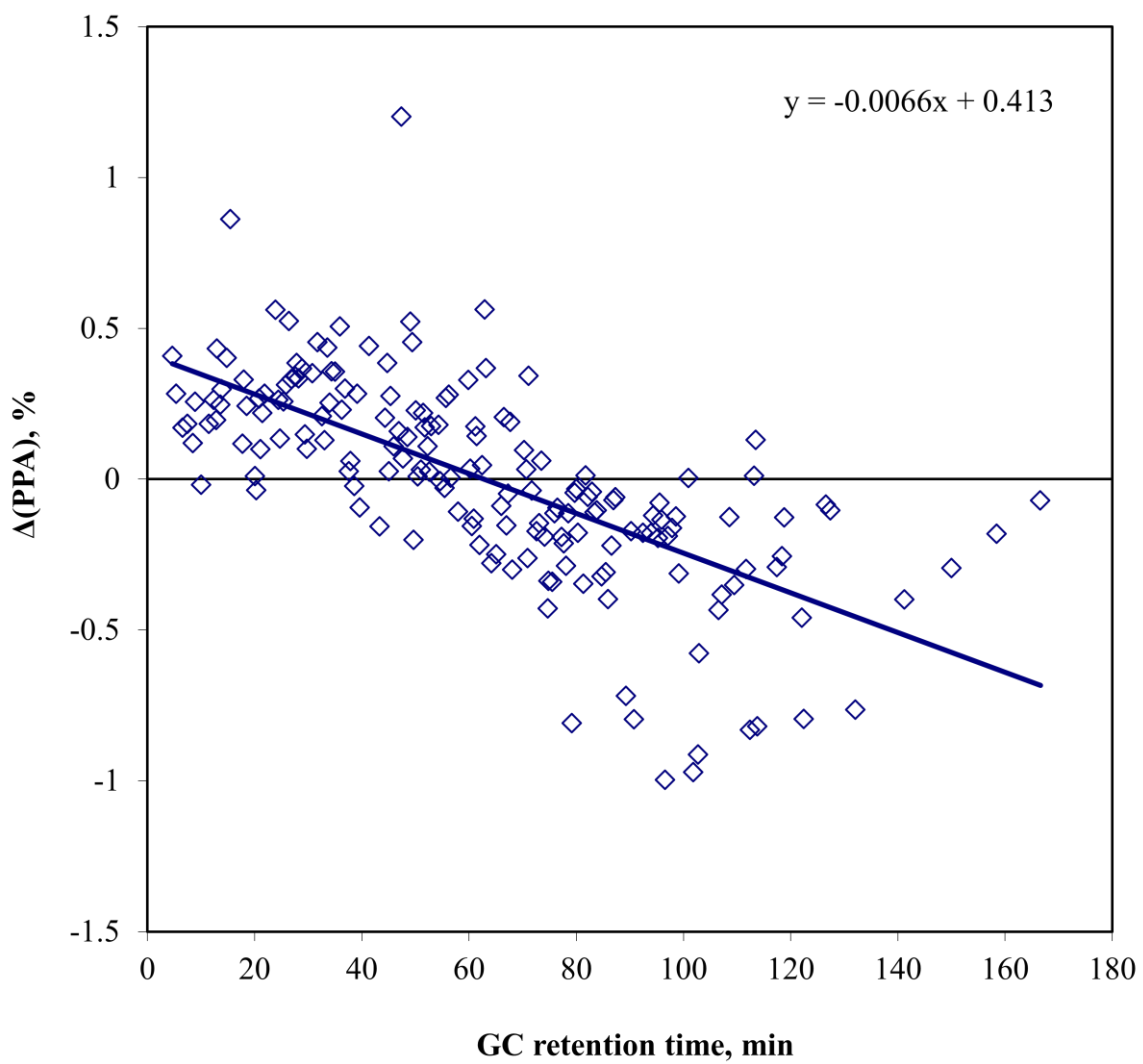


Fig. D-25 $\Delta(\text{PPA})$ for thermally stressed DF (400 °C, 300 min, DF, S1).

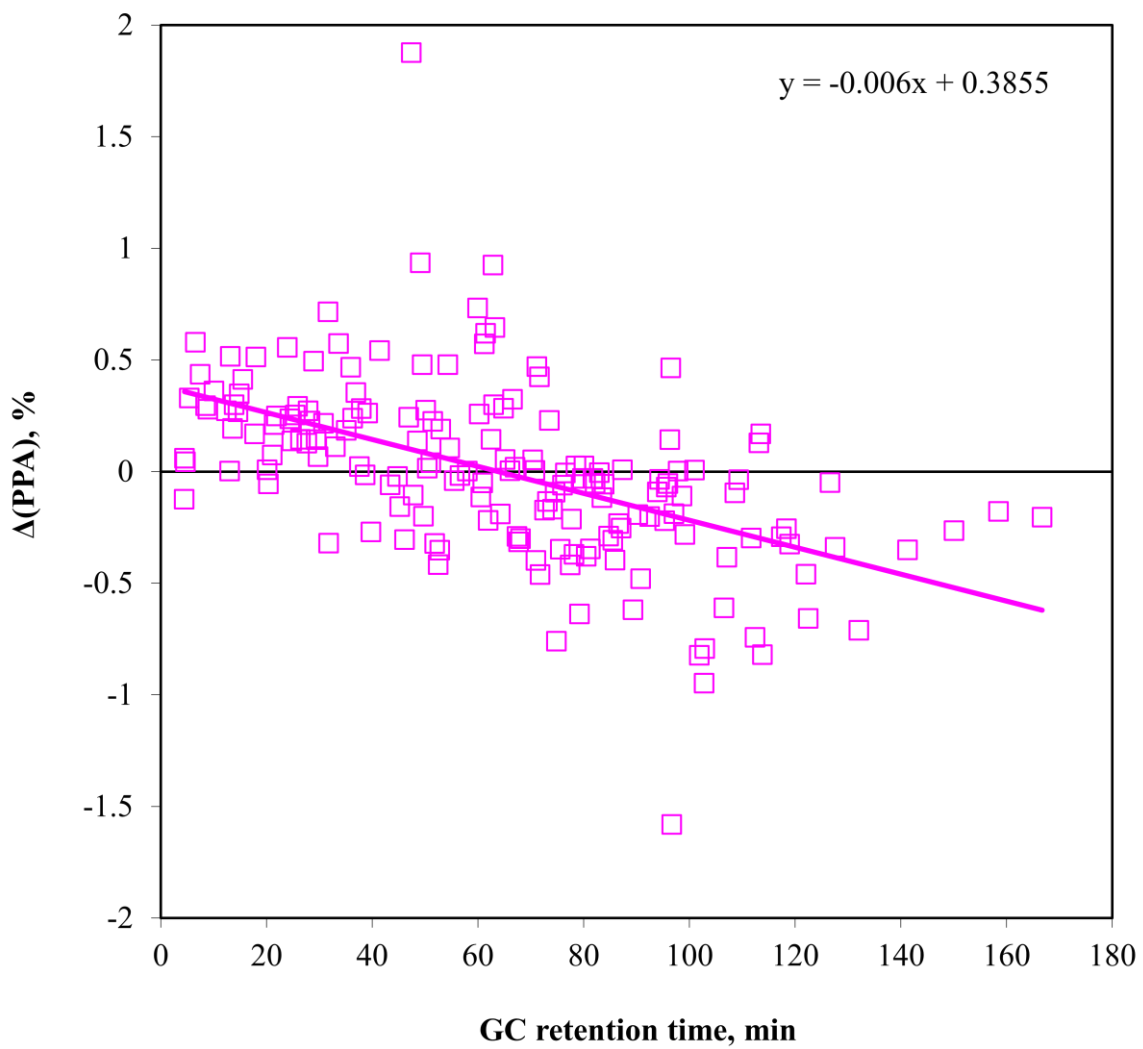


Fig. D-26 $\Delta(\text{PPA})$ for thermally stressed DF (400 °C, 600 min, DF, S1).

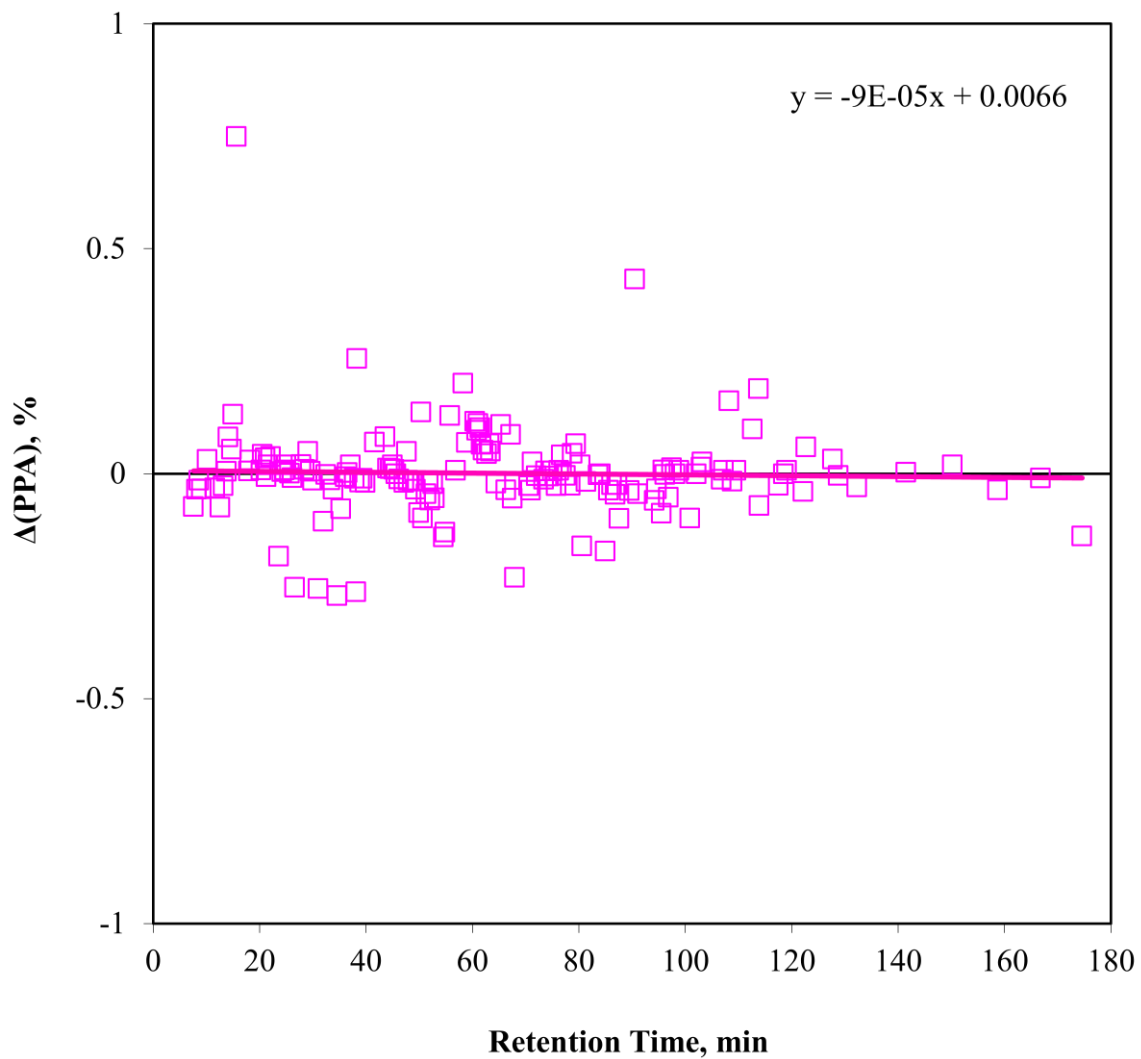


Fig. D-27 $\Delta(\text{PPA})$ for thermally stressed DF (410 °C, 30 min, DF, S1).

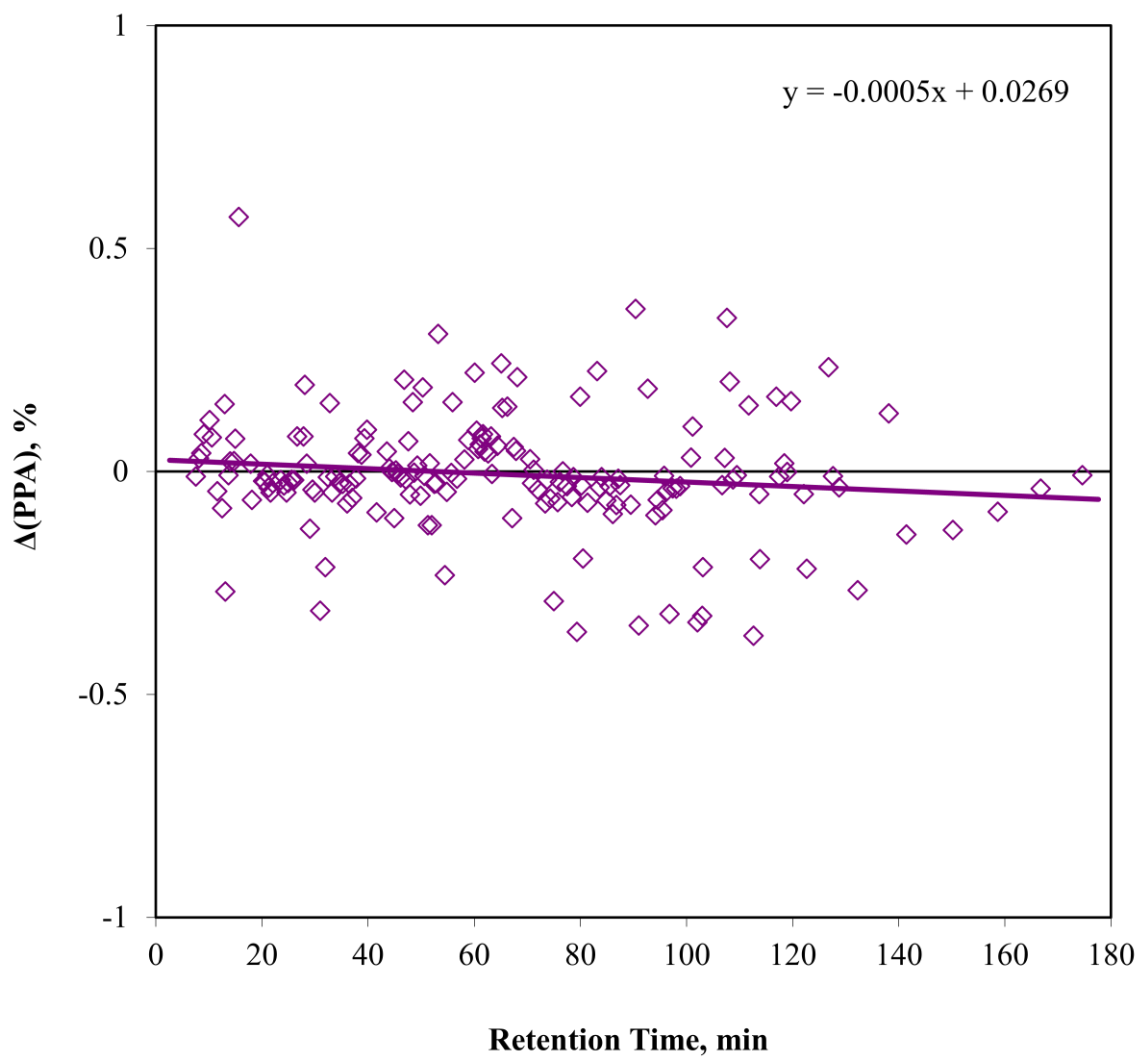


Fig. D-28 $\Delta(\text{PPA})$ for thermally stressed DF (420 °C, 30 min, DF, S1).

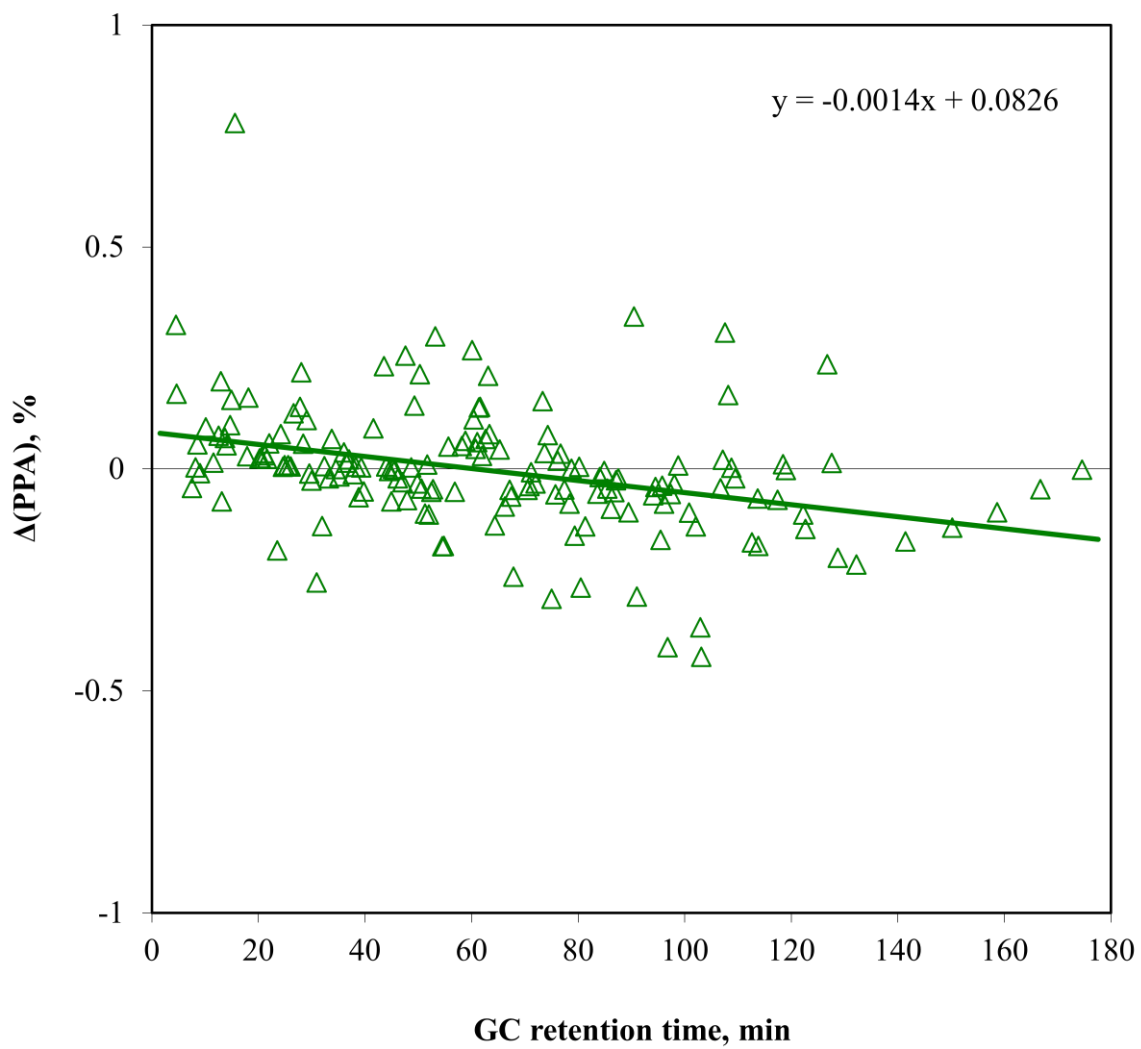


Fig. D-29 $\Delta(\text{PPA})$ for thermally stressed DF (420 °C, 60 min, DF, S1).

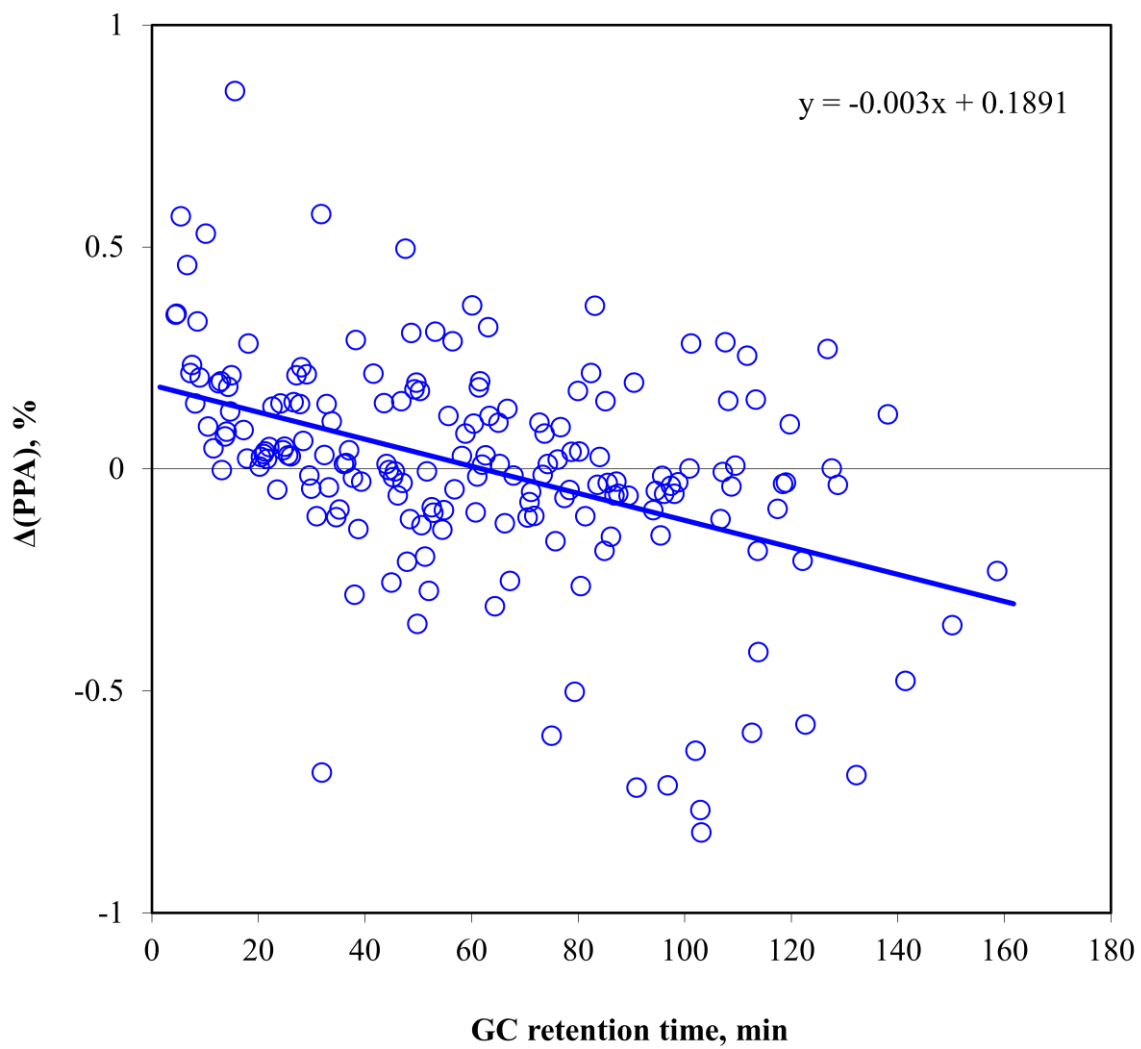


Fig. D-30 $\Delta(\text{PPA})$ for thermally stressed DF (420 °C, 120 min, DF, S1).

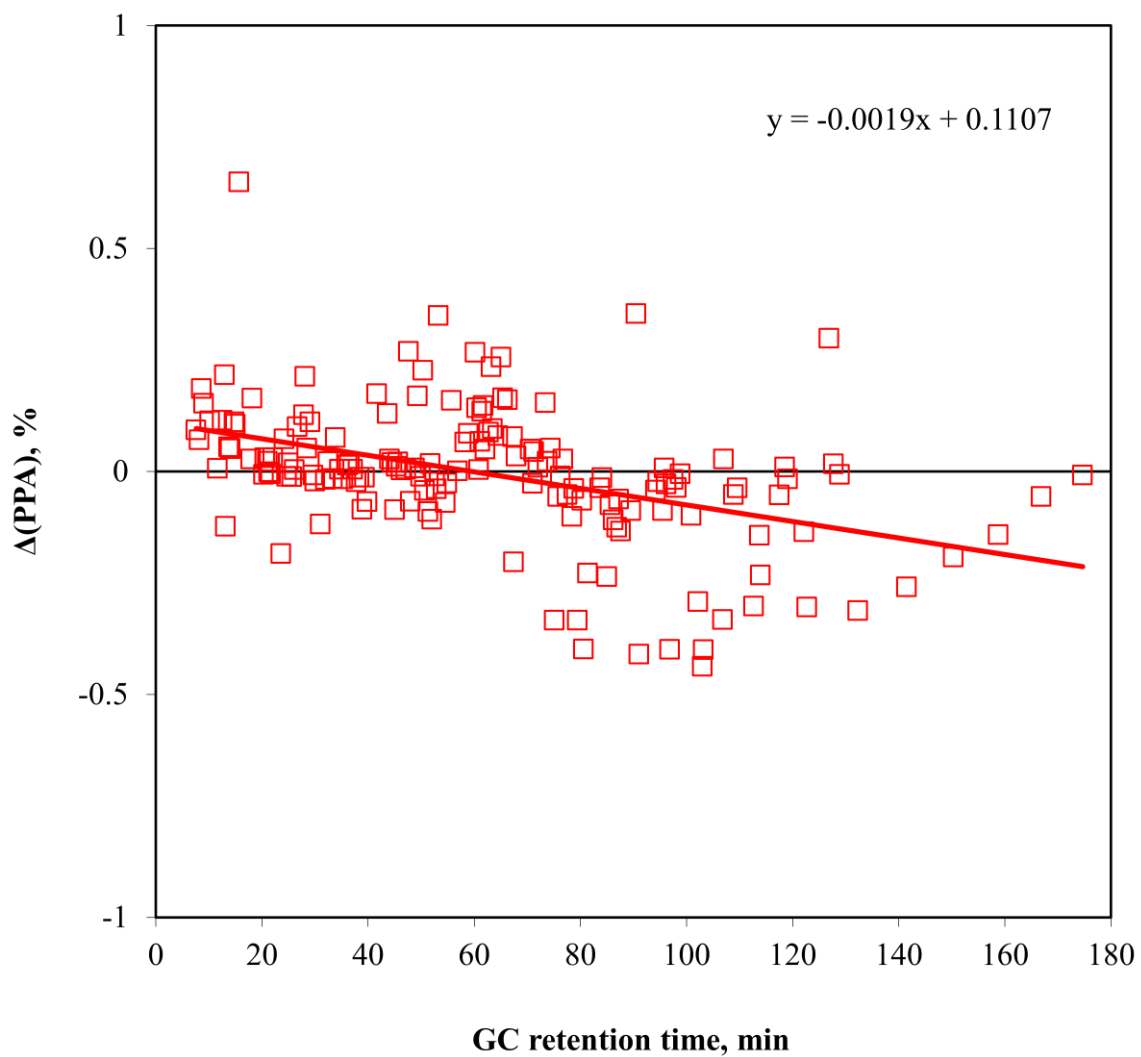


Fig. D-31 $\Delta(\text{PPA})$ for thermally stressed DF (430 °C, 30 min, DF, S1).

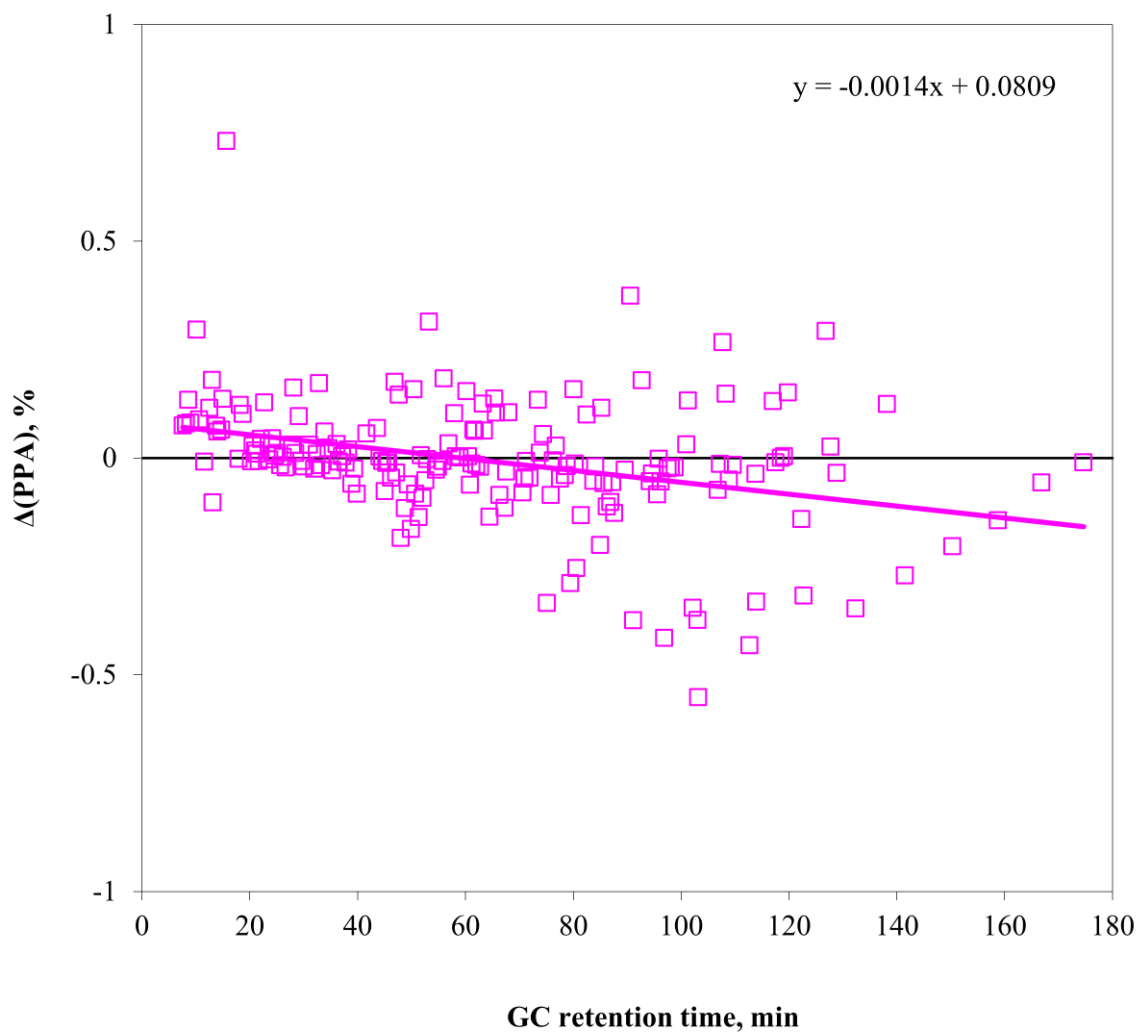


Fig. D-32 $\Delta(\text{PPA})$ for thermally stressed DF (440 °C, 10 min, DF, S1).

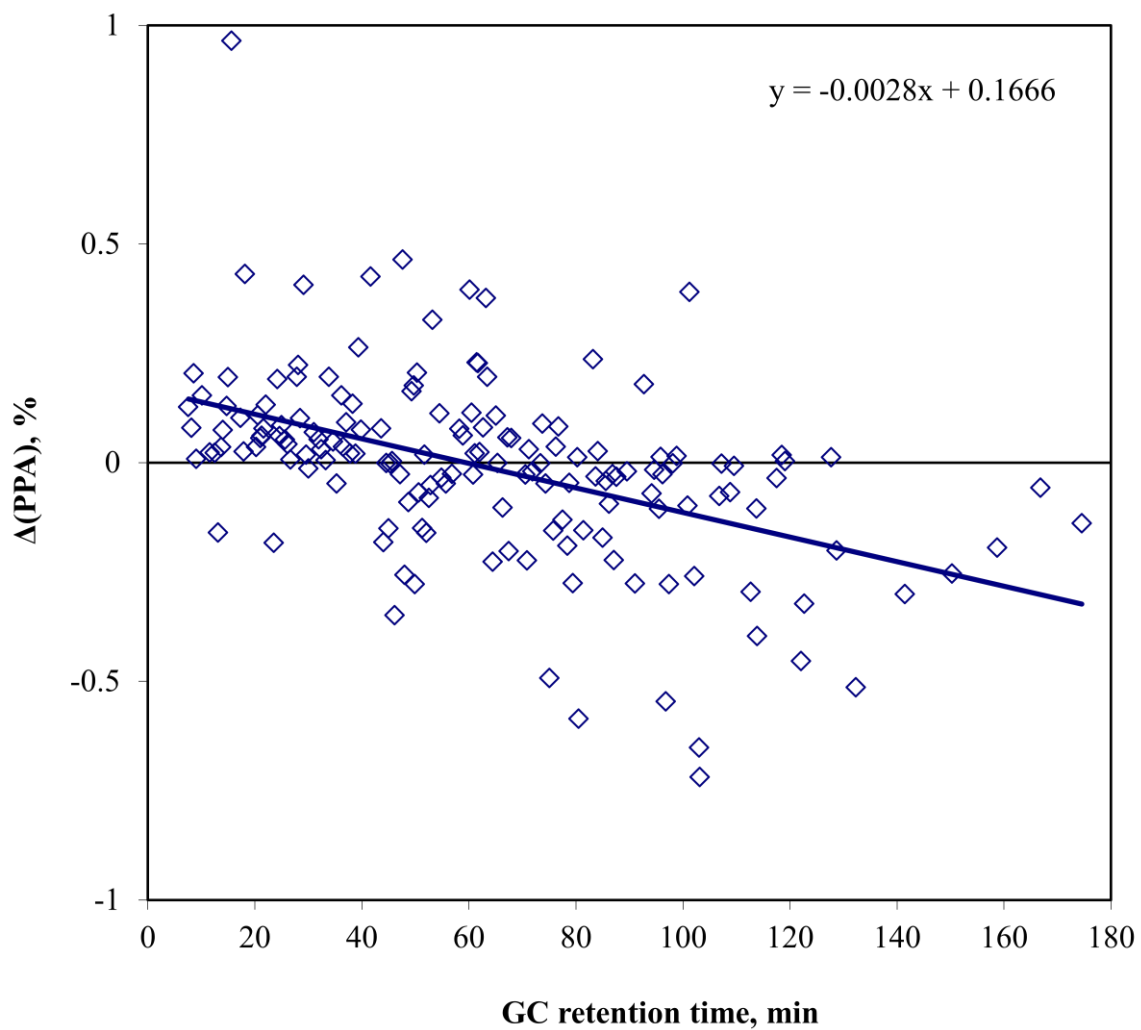


Fig. D-33 $\Delta(\text{PPA})$ for thermally stressed DF (440 °C, 30 min, DF, S1).

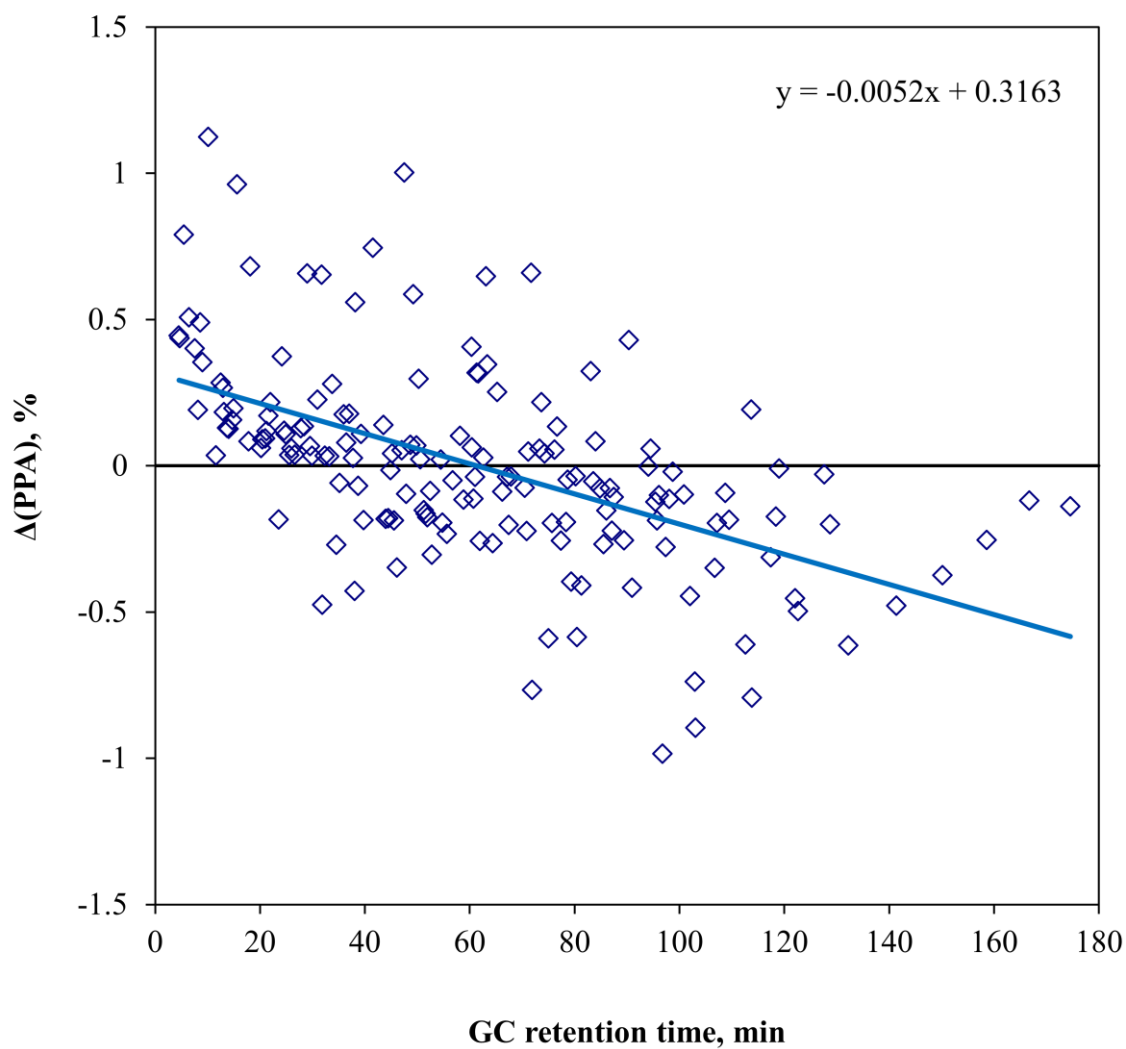


Fig. D-34 $\Delta(\text{PPA})$ for thermally stressed DF (440 °C, 30 min, DF, w/o air, S1).

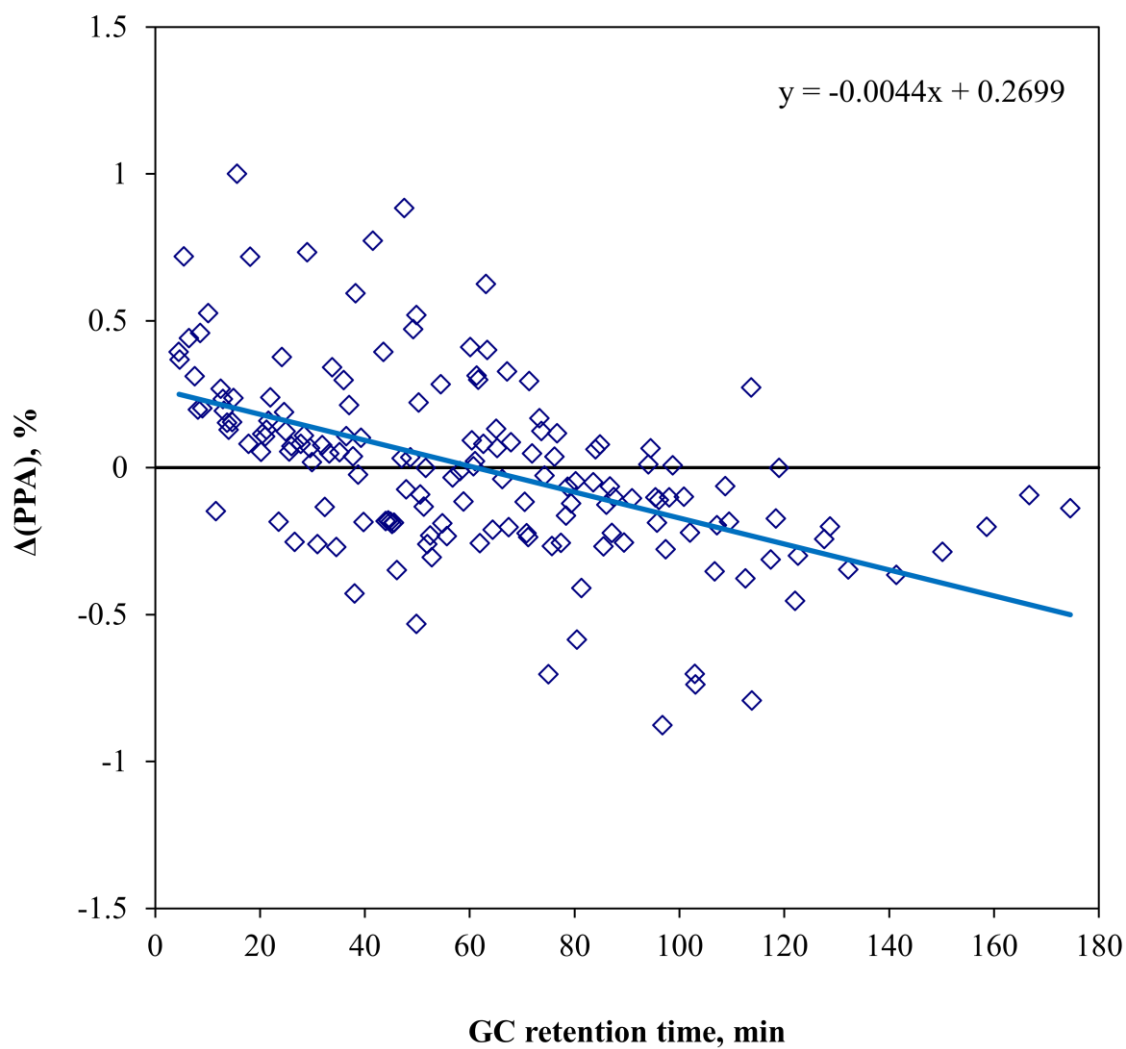


Fig. D-35 $\Delta(\text{PPA})$ for thermally stressed DF (440 °C, 30 min, DF, w/ air, S1).

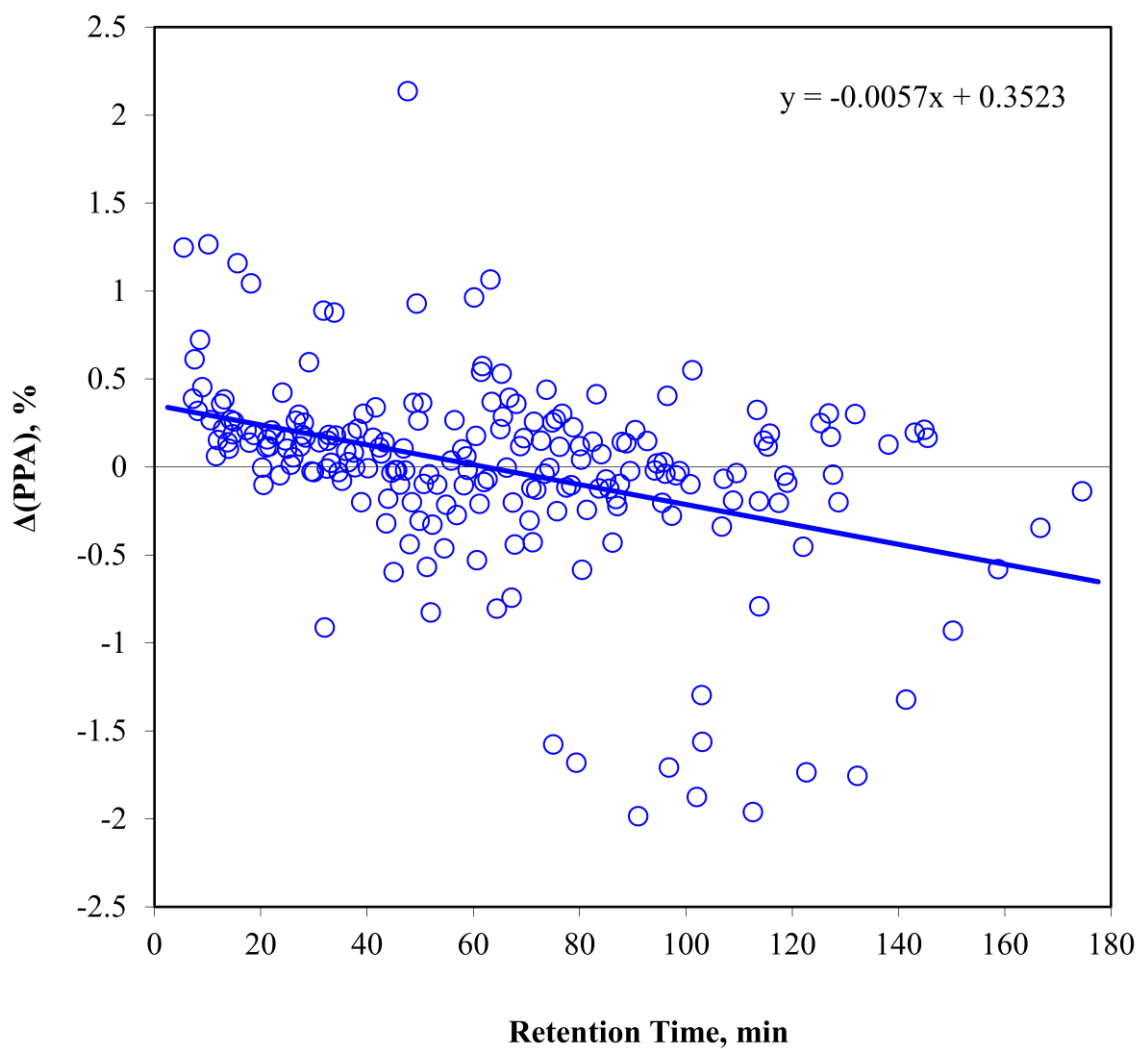


Fig. D-36 $\Delta(\text{PPA})$ for thermally stressed DF (440 °C, 120 min, DF, S1).

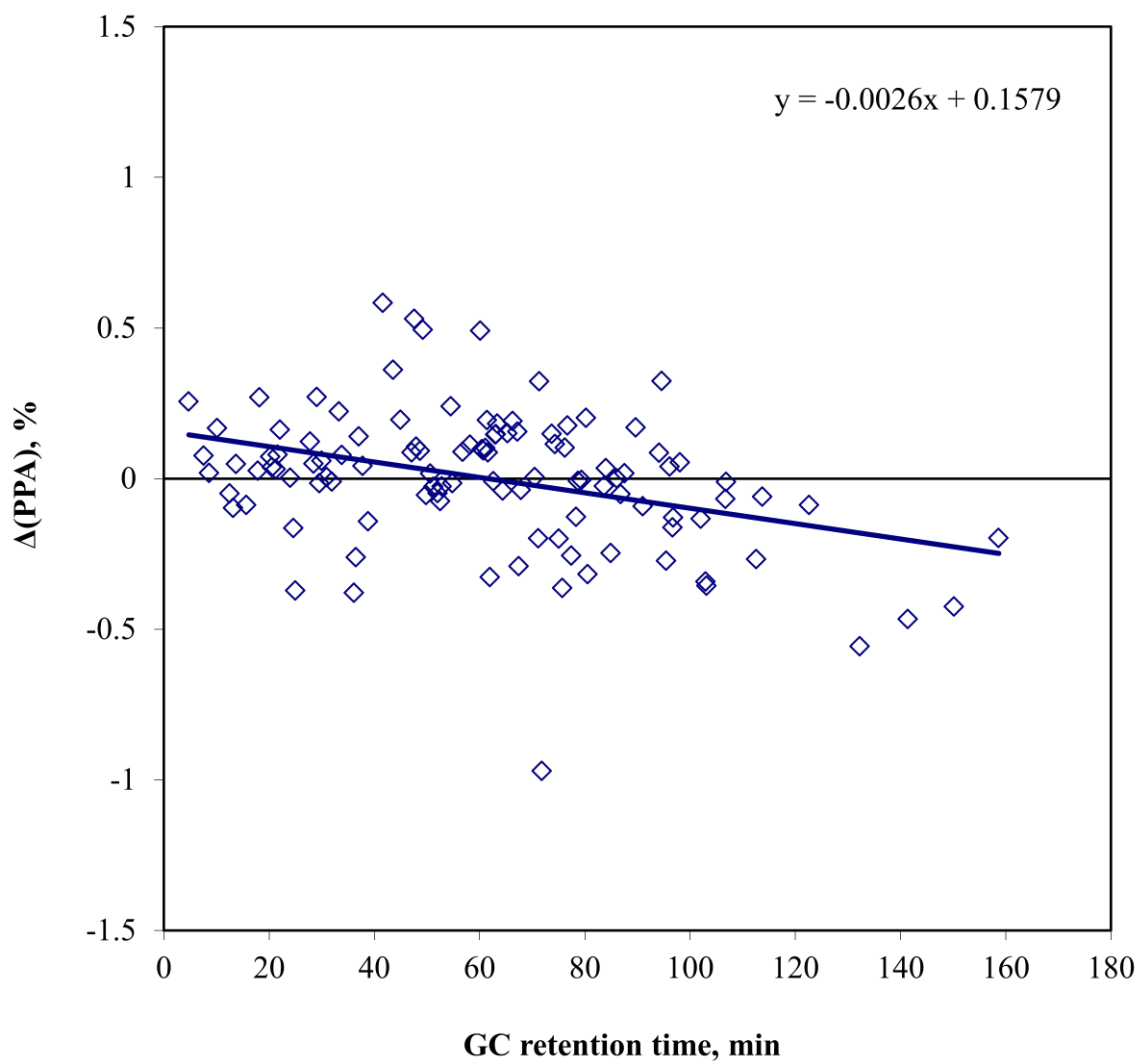


Fig. D-37 $\Delta(\text{PPA})$ for thermally stressed DF (DF/CO₂ run 1, S3).

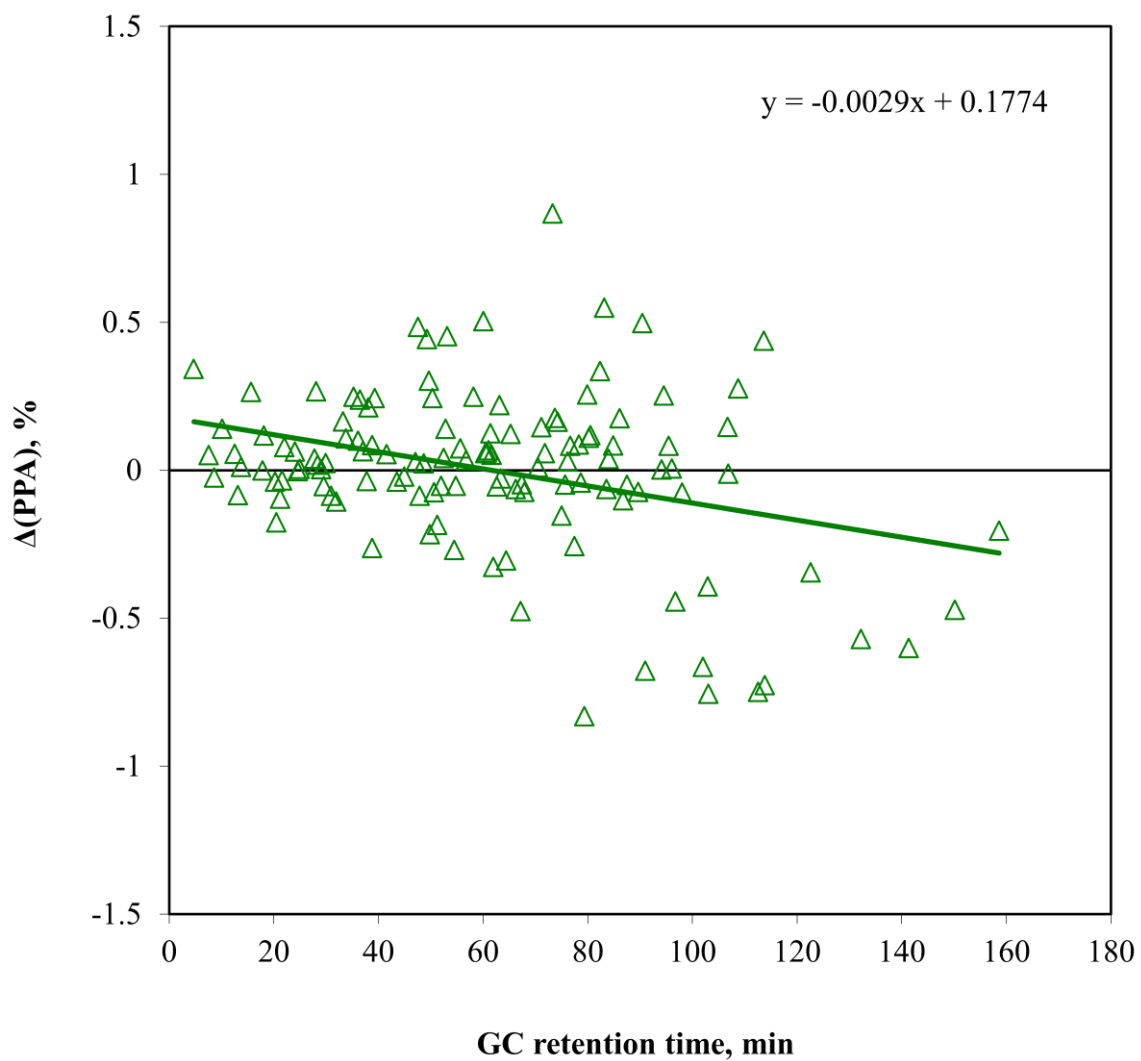


Fig. D-38 $\Delta(\text{PPA})$ for thermally stressed DF (DF/ CO_2 run 2, S3).

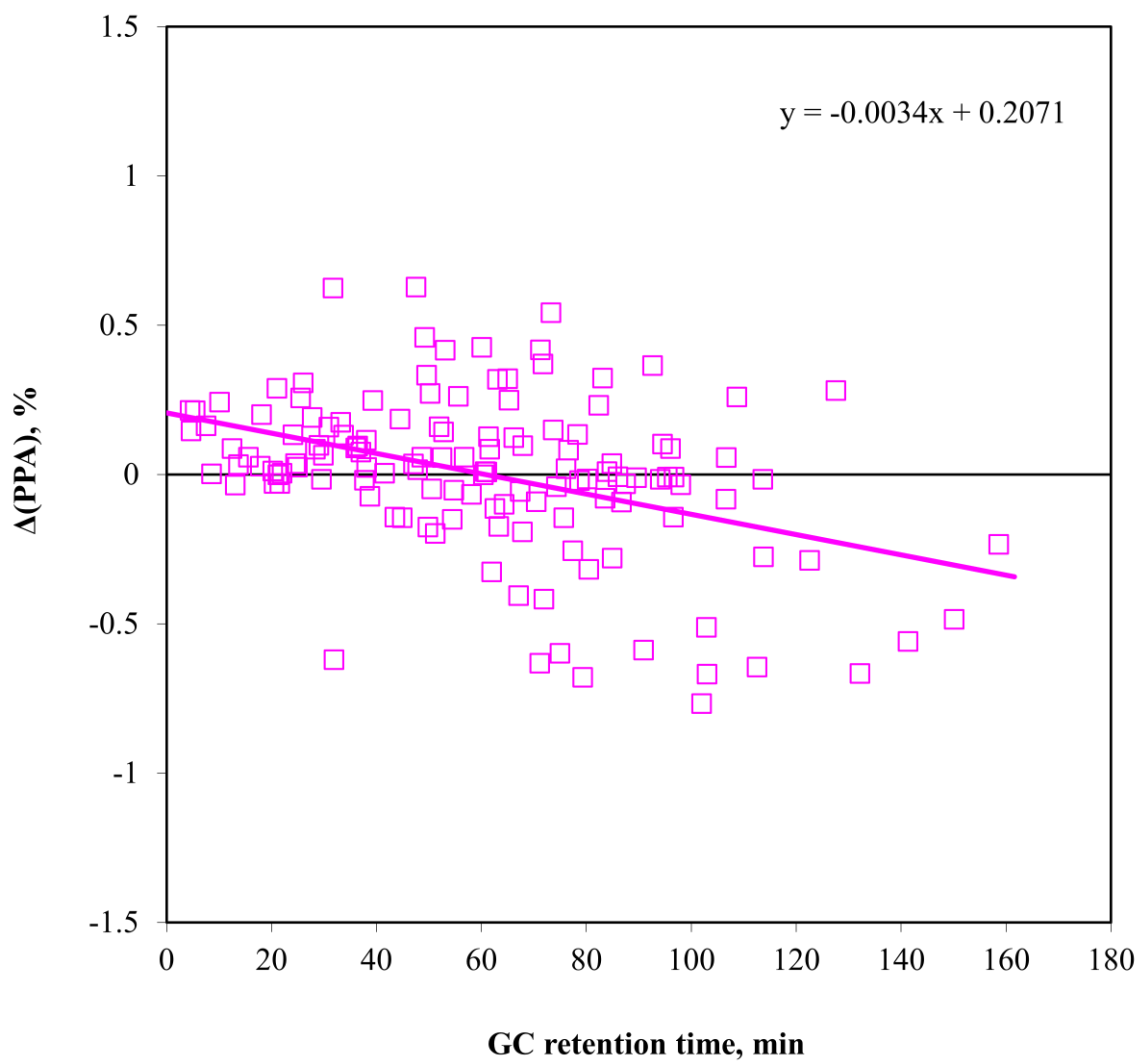


Fig. D-39 $\Delta(\text{PPA})$ for thermally stressed DF (DF/ CO_2 run 3, S3).

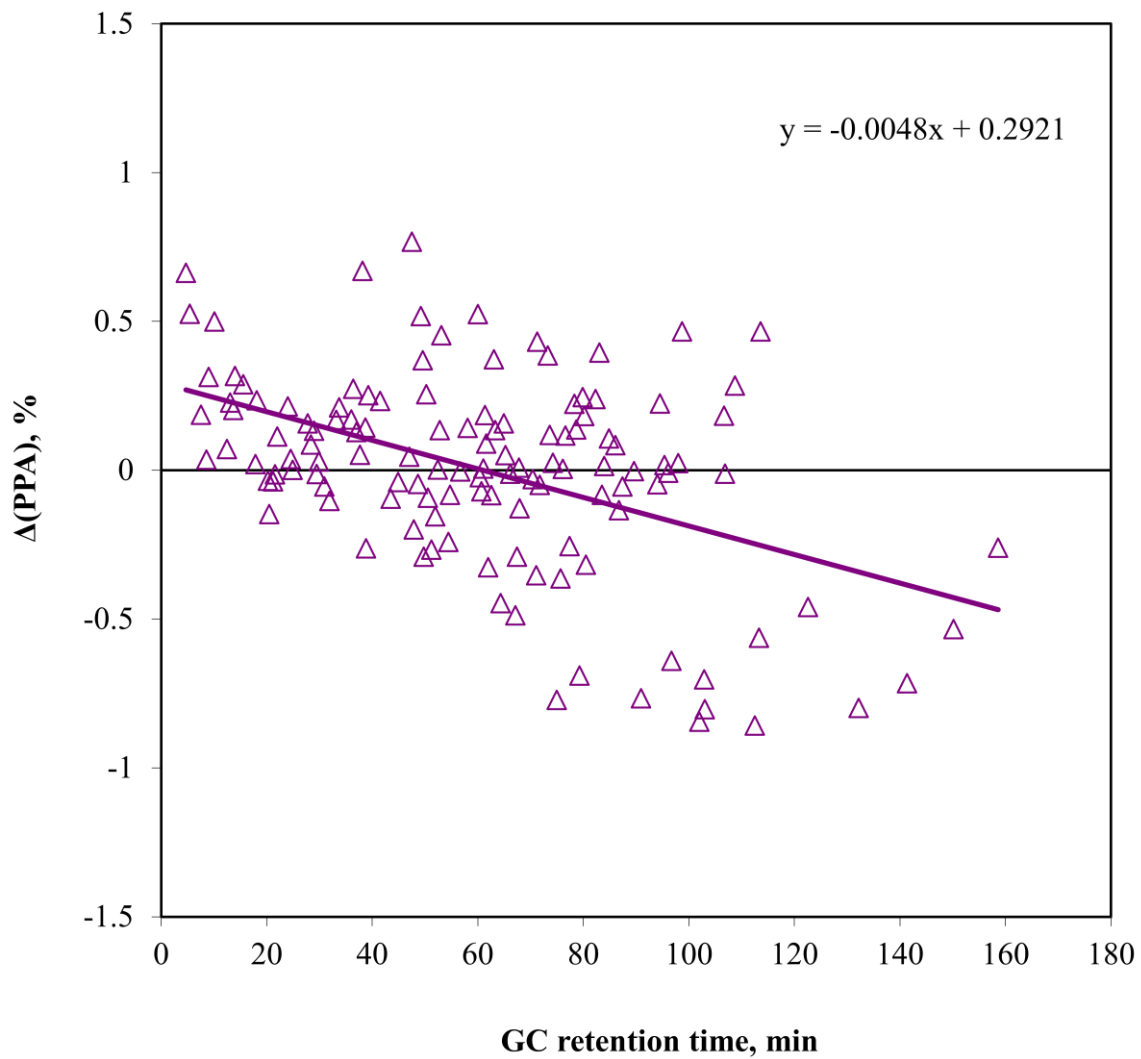


Fig. D-40 $\Delta(\text{PPA})$ for thermally stressed DF (DF/CO₂ run 4, S3).

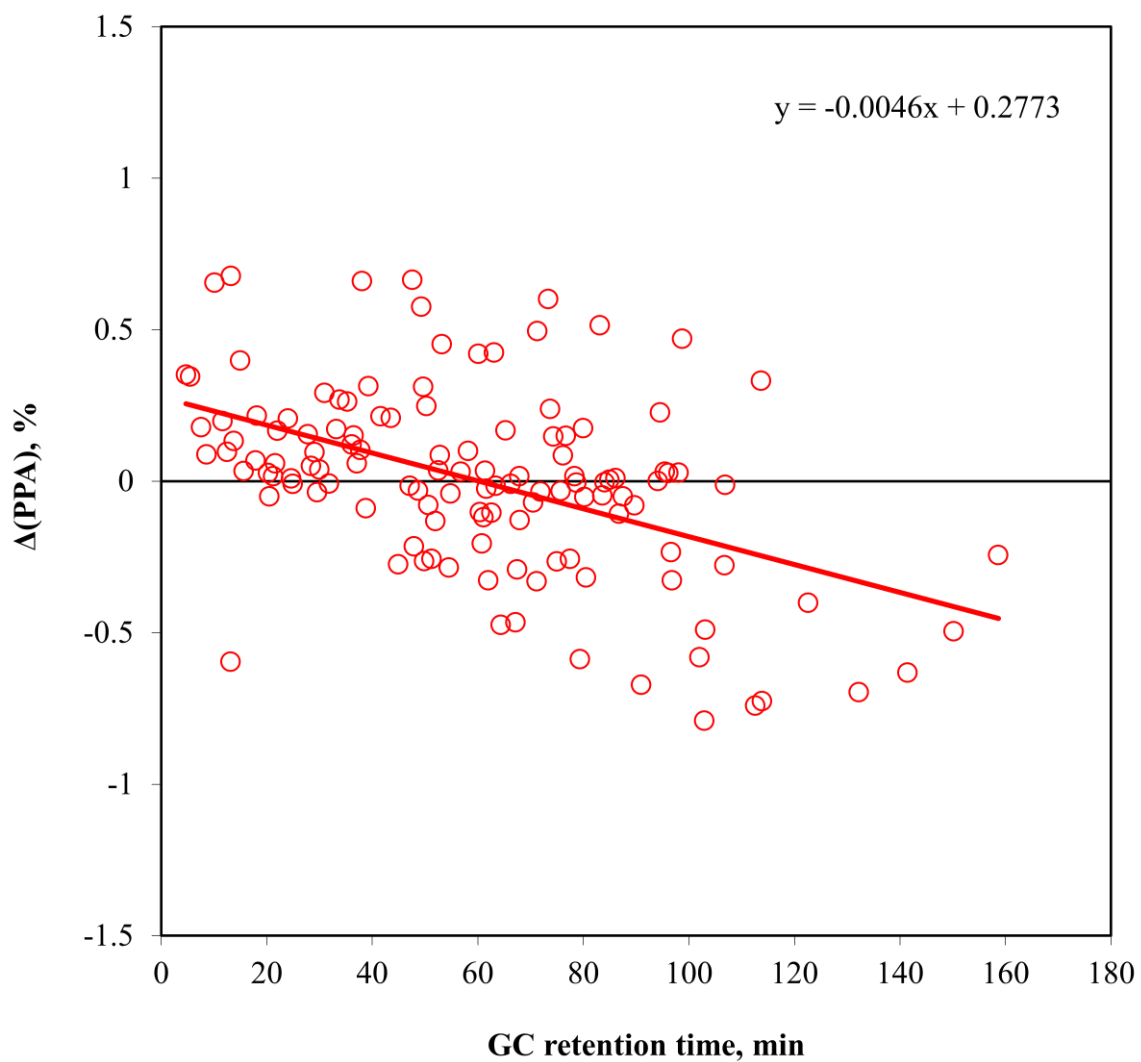


Fig. D-41 $\Delta(\text{PPA})$ for thermally stressed DF (DF/ CO_2 run 5, S3).

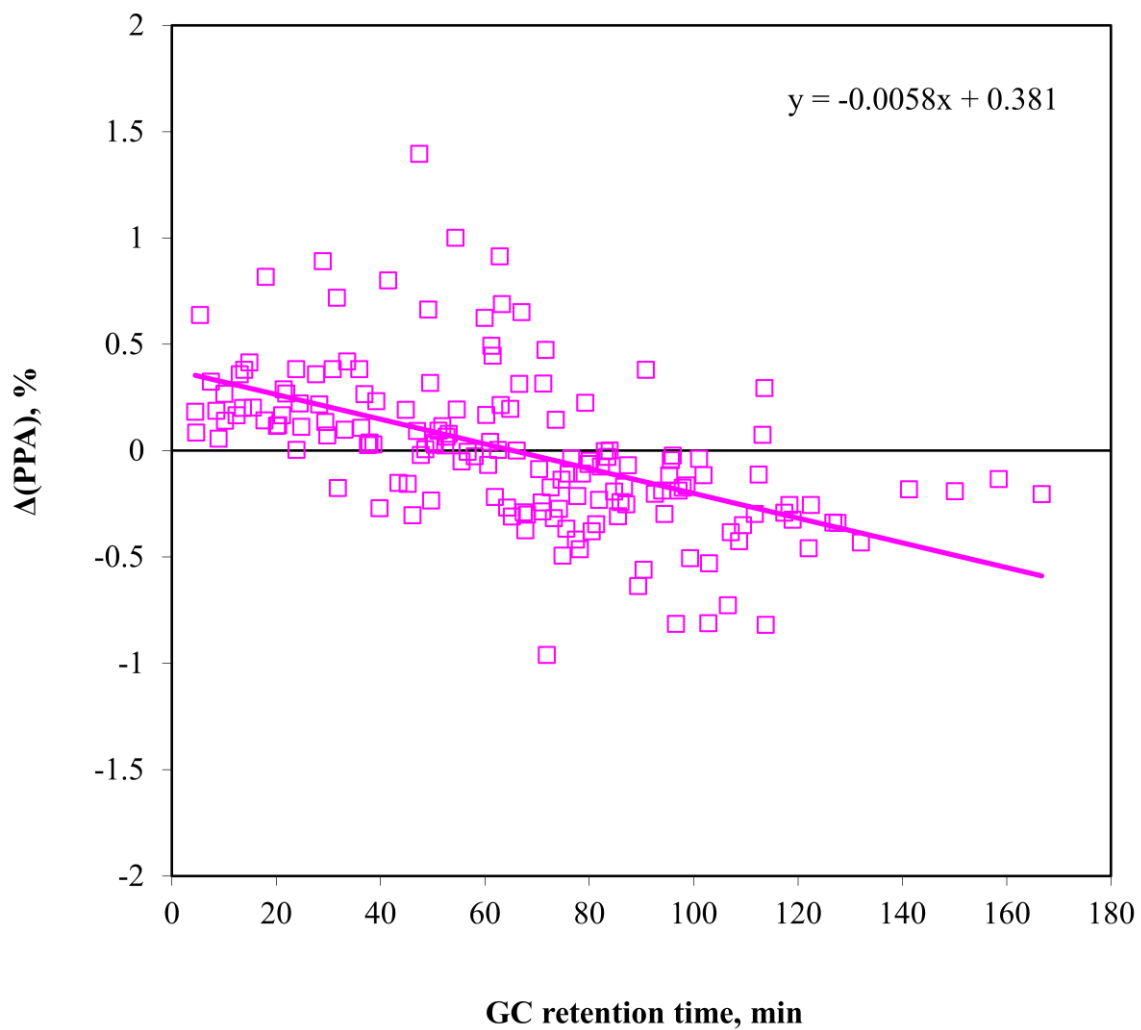


Fig. D-42 $\Delta(\text{PPA})$ for thermally stressed DF (DF/ CO_2 run 1-a, S2).

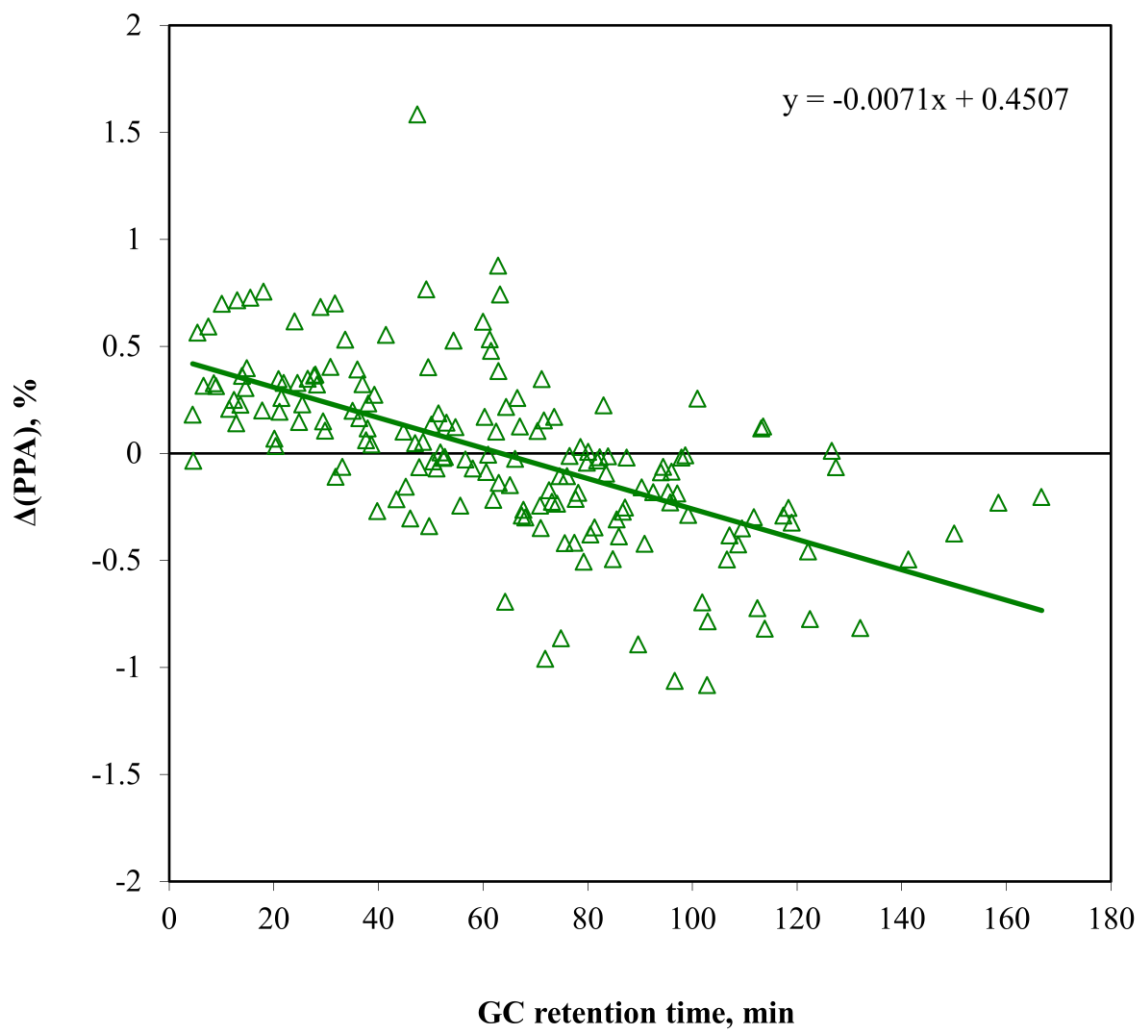


Fig. D-43 $\Delta(\text{PPA})$ for thermally stressed DF (DF/ CO_2 run 1-b, S2).

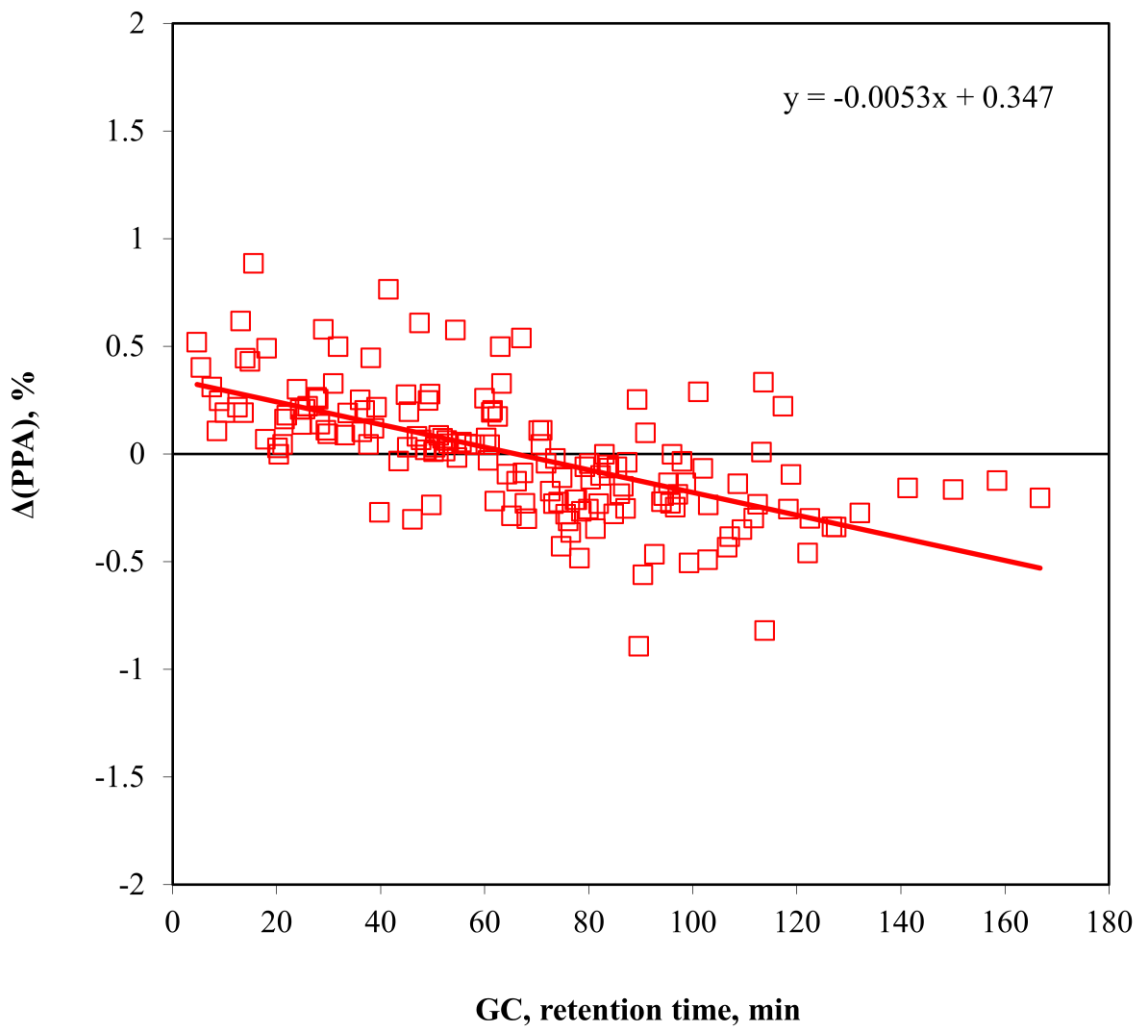


Fig. D-44 $\Delta(\text{PPA})$ for thermally stressed DF (DF/ CO_2 run 2-a, S2).

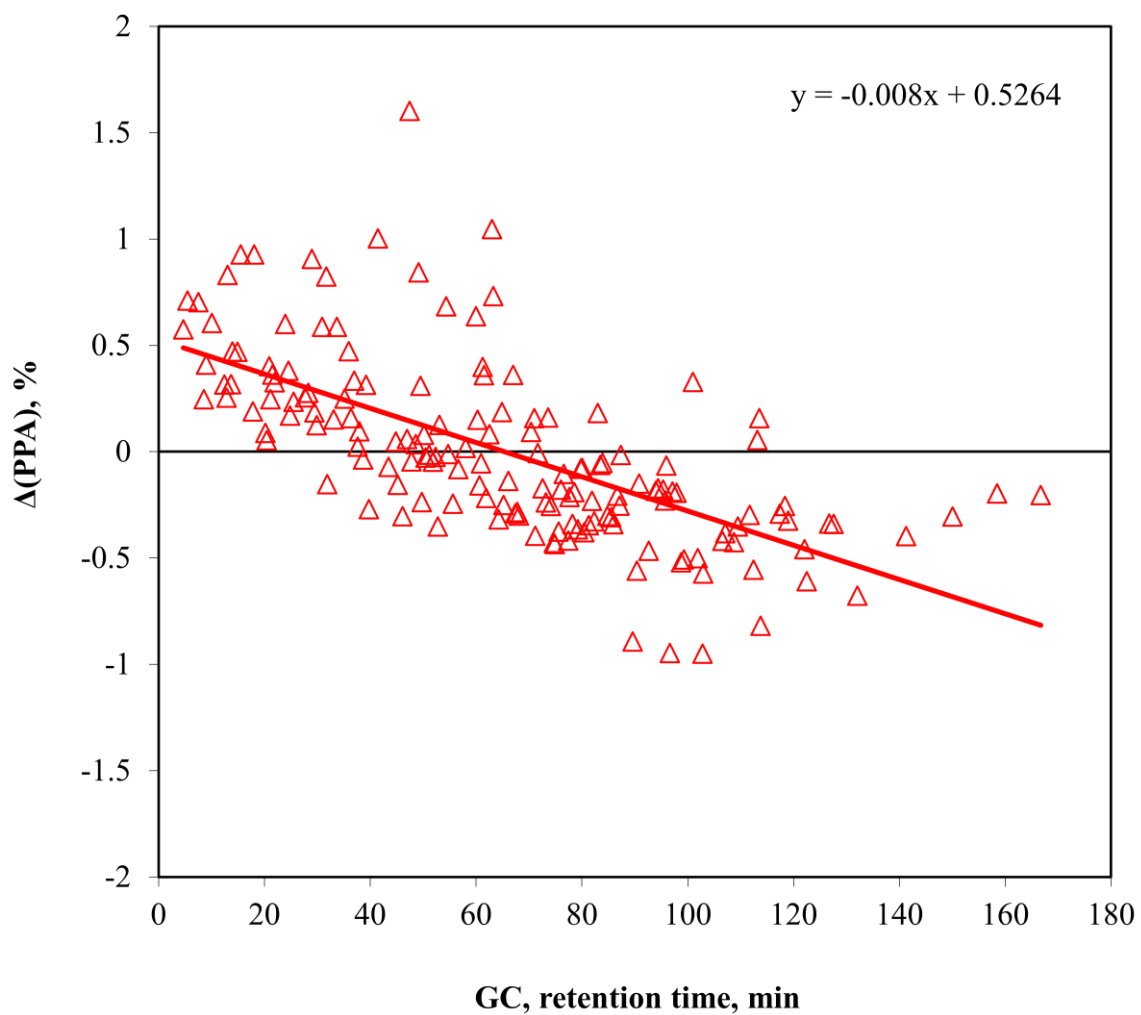


Fig. D-45 $\Delta(\text{PPA})$ for thermally stressed DF (DF/CO₂ run 2-b, S2).

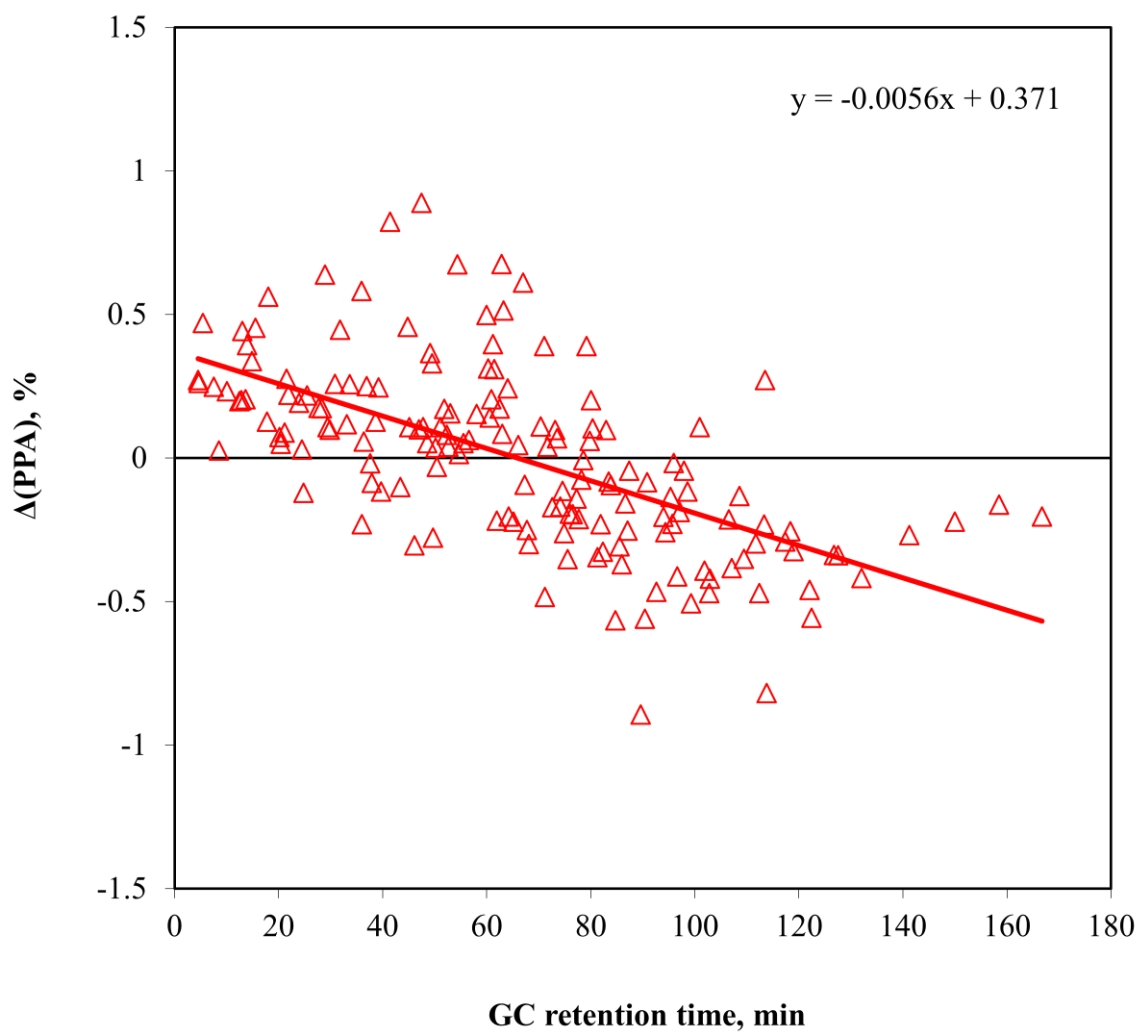


Fig. D-46 $\Delta(\text{PPA})$ for thermally stressed DF (DF/CO₂ run 3-a, S2).

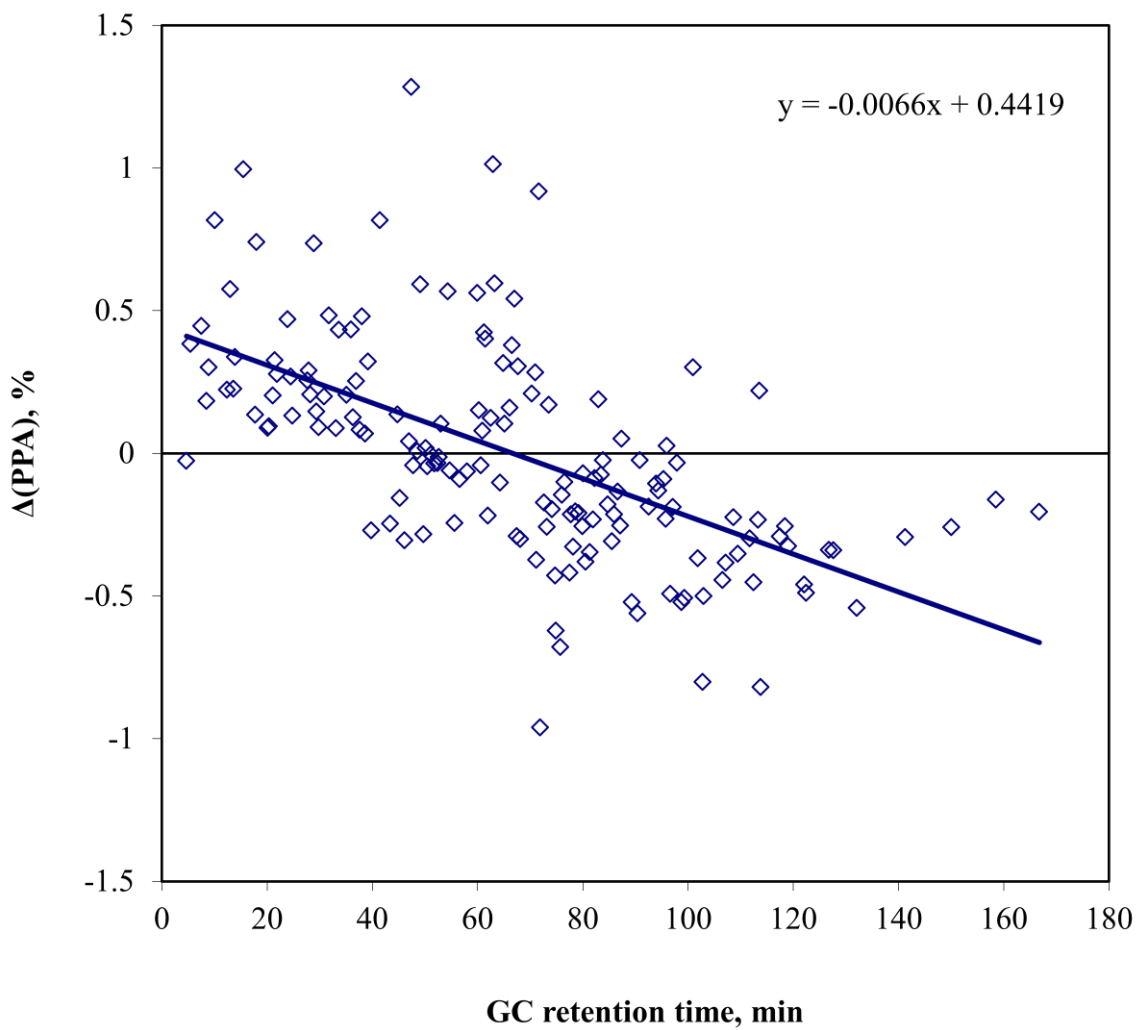


Fig. D-47 $\Delta(\text{PPA})$ for thermally stressed DF (DF/ CO_2 run 3-b, S2).

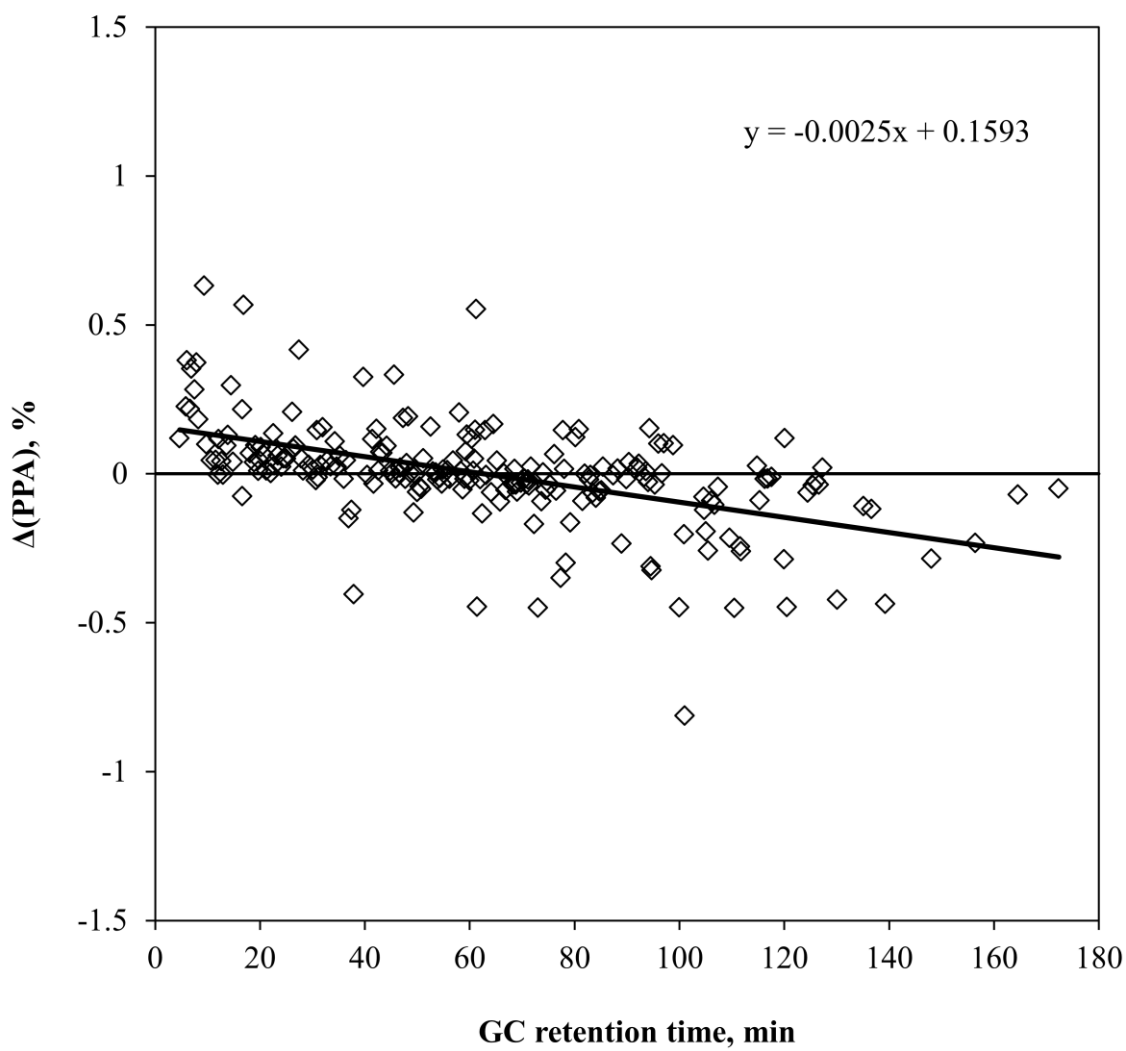


Fig. D-48 $\Delta(\text{PPA})$ for thermally stressed DF (Continuous, DF, #1, S4).

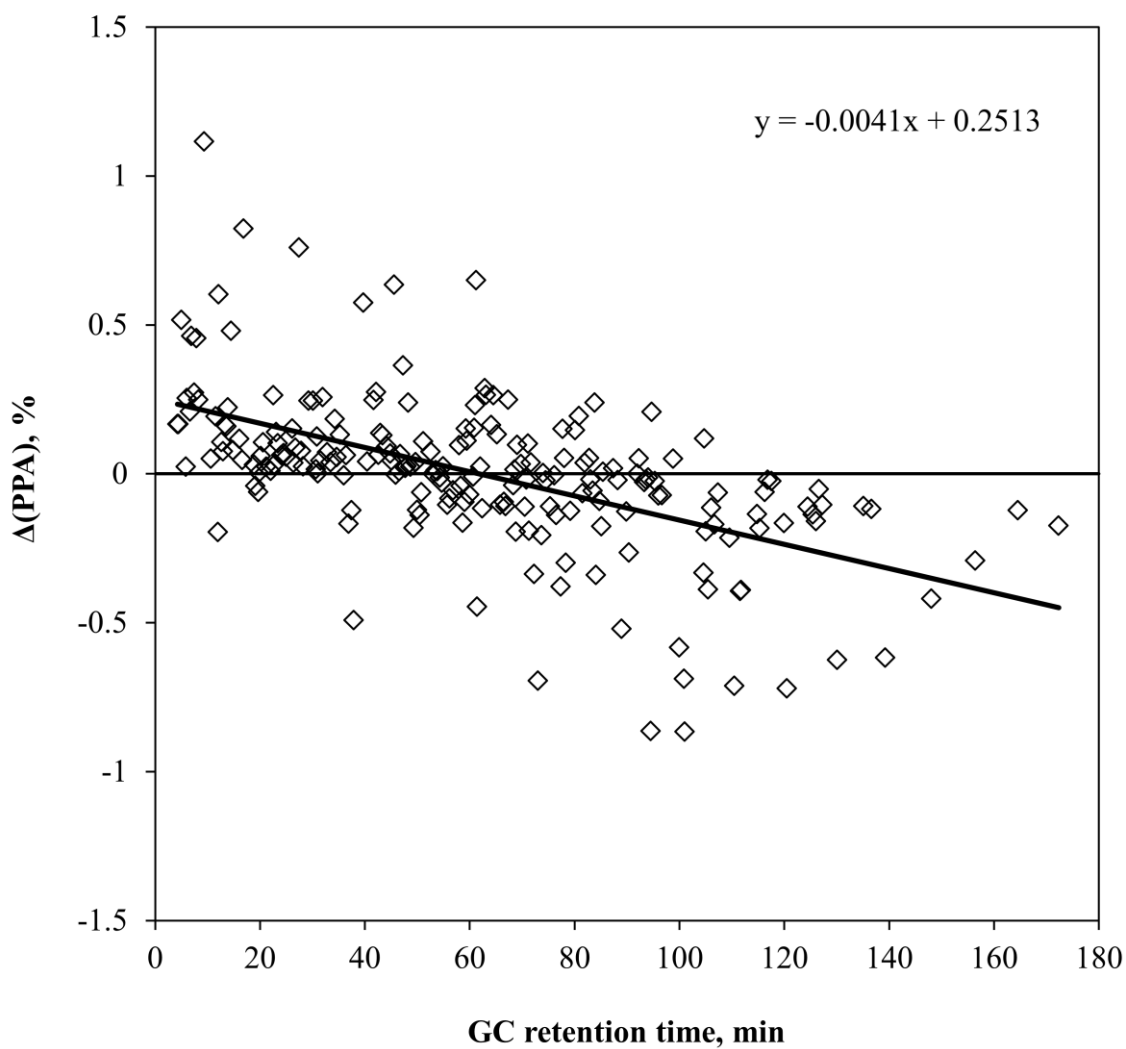


Fig. D-49 $\Delta(\text{PPA})$ for thermally stressed DF (Continuous, DF, #2, S4).

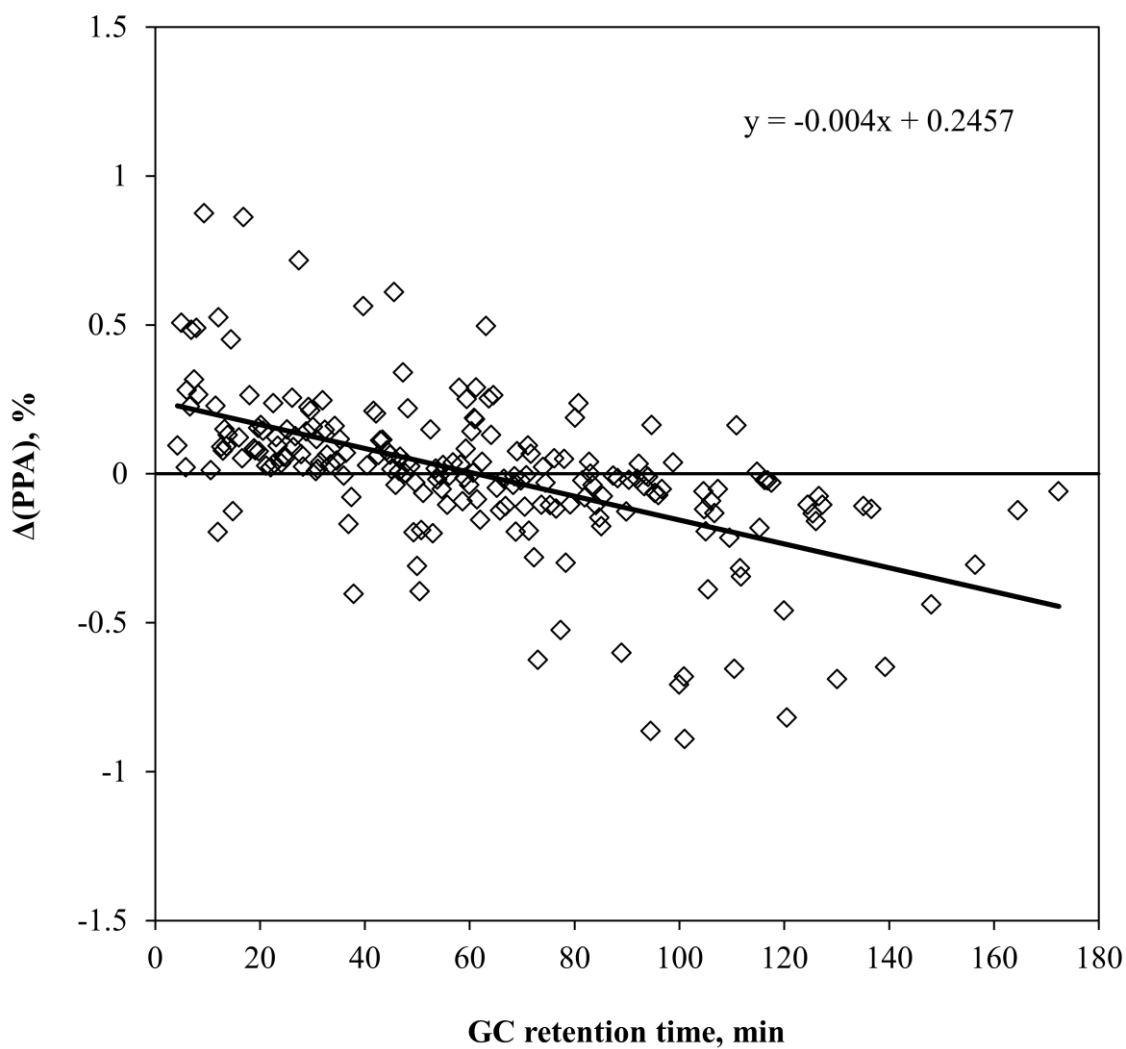


Fig. D-50 $\Delta(\text{PPA})$ for thermally stressed DF (Continuous, DF, #3, S4).

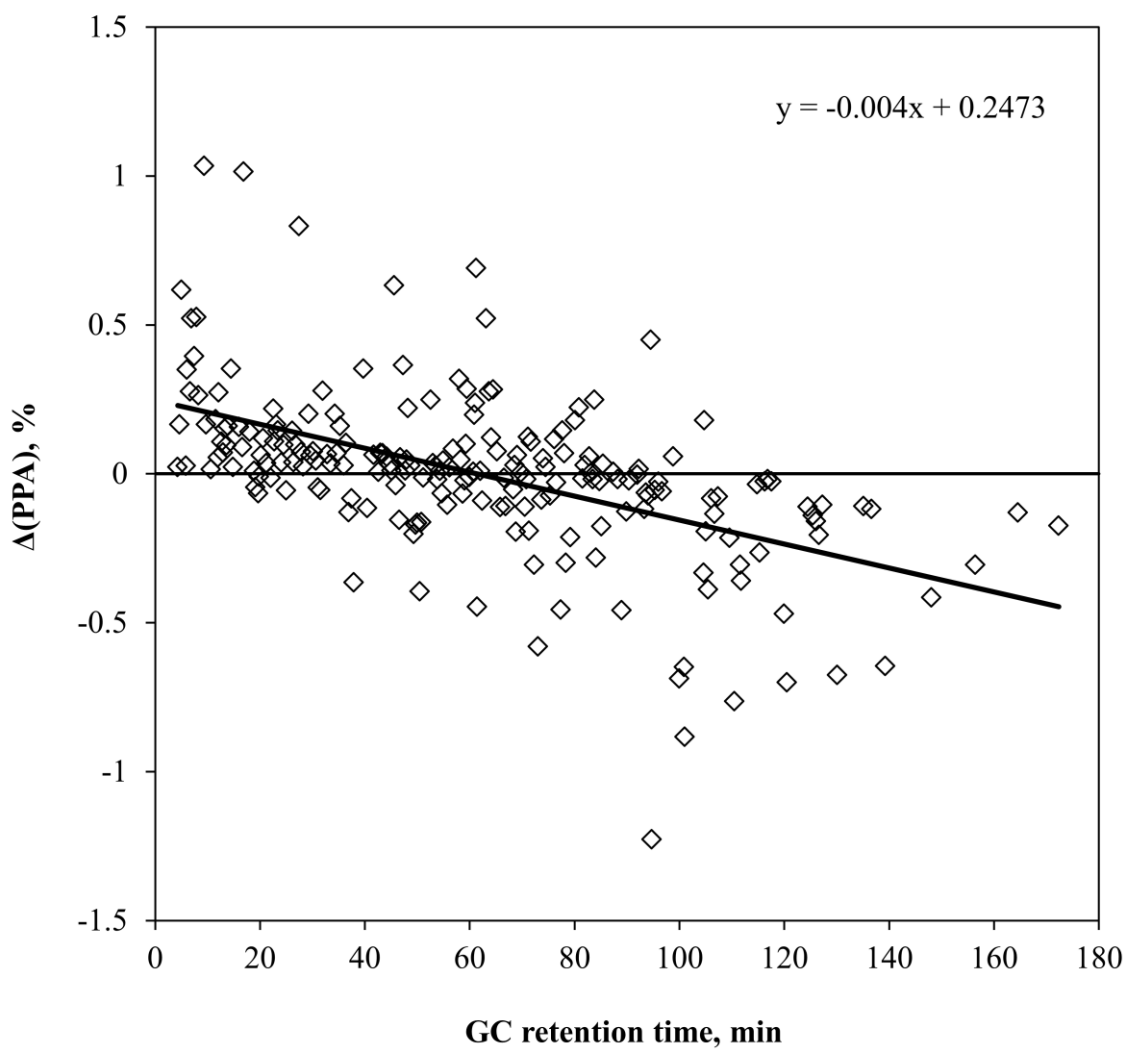


Fig. D-51 $\Delta(\text{PPA})$ for thermally stressed DF (Continuous, DF, #4, S4).

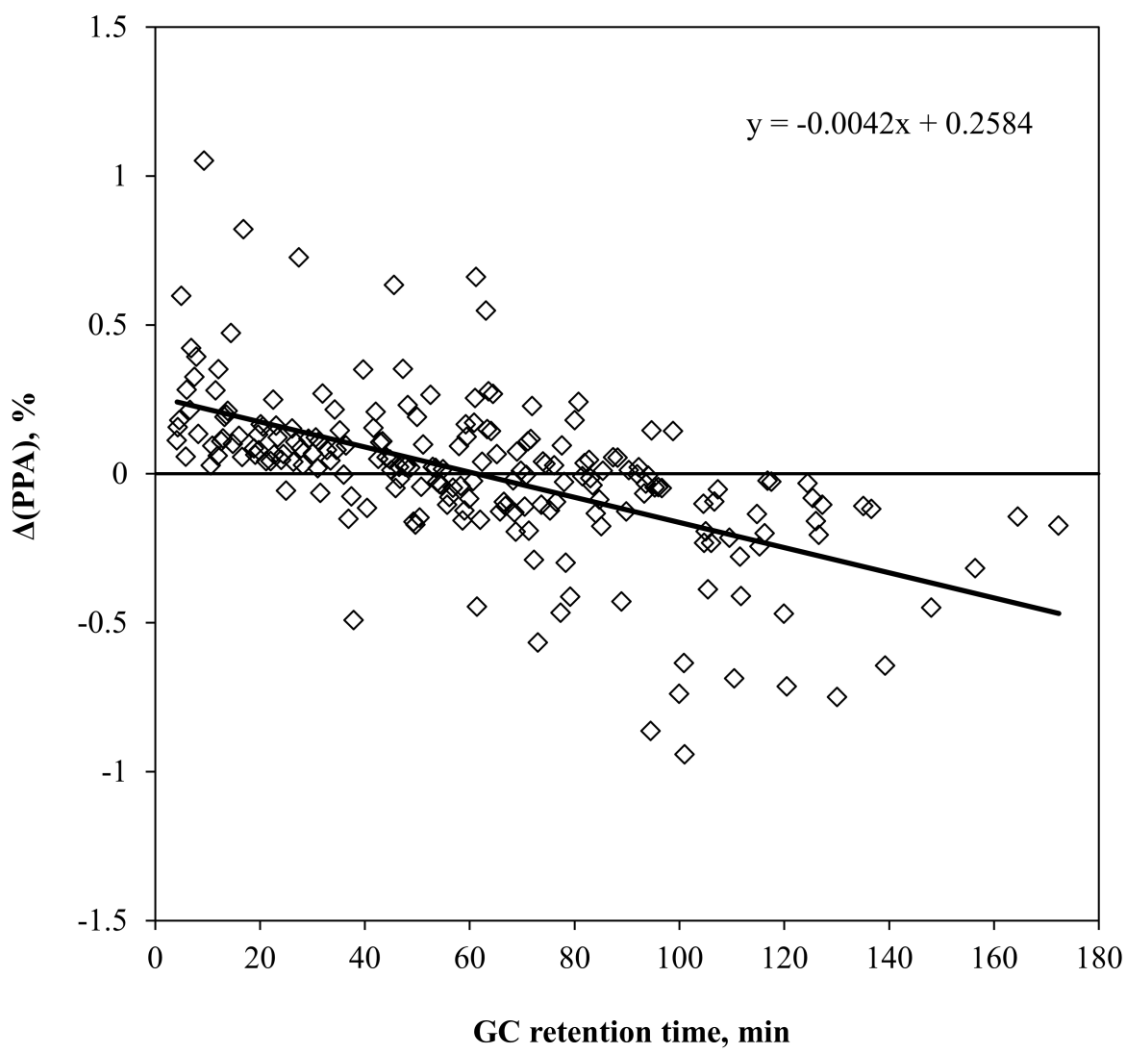


Fig. D-52 $\Delta(\text{PPA})$ for thermally stressed DF (Continuous, DF, #5, S4).

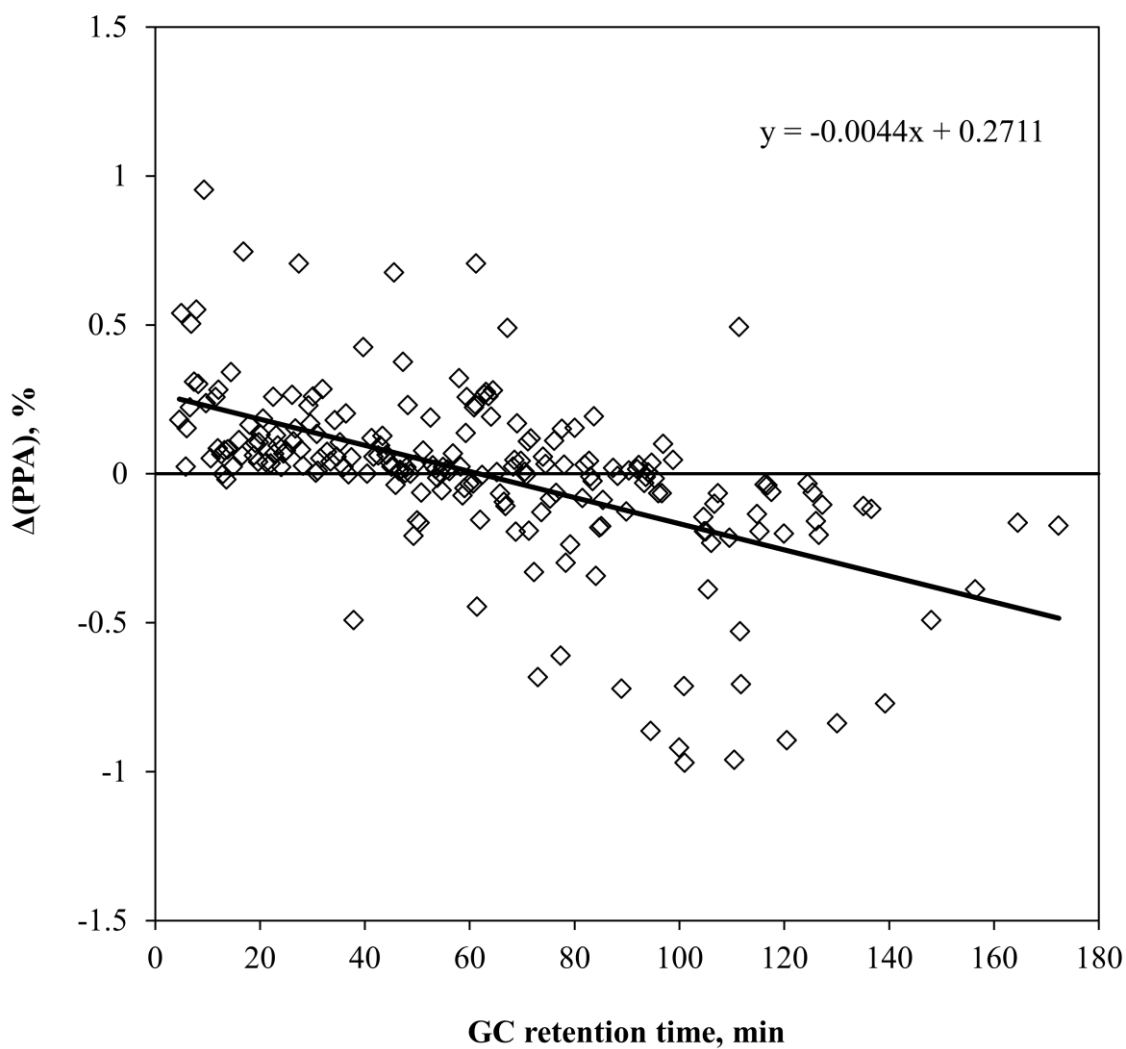


Fig. D-53 $\Delta(\text{PPA})$ for thermally stressed DF (Continuous, DF, #6, S4).

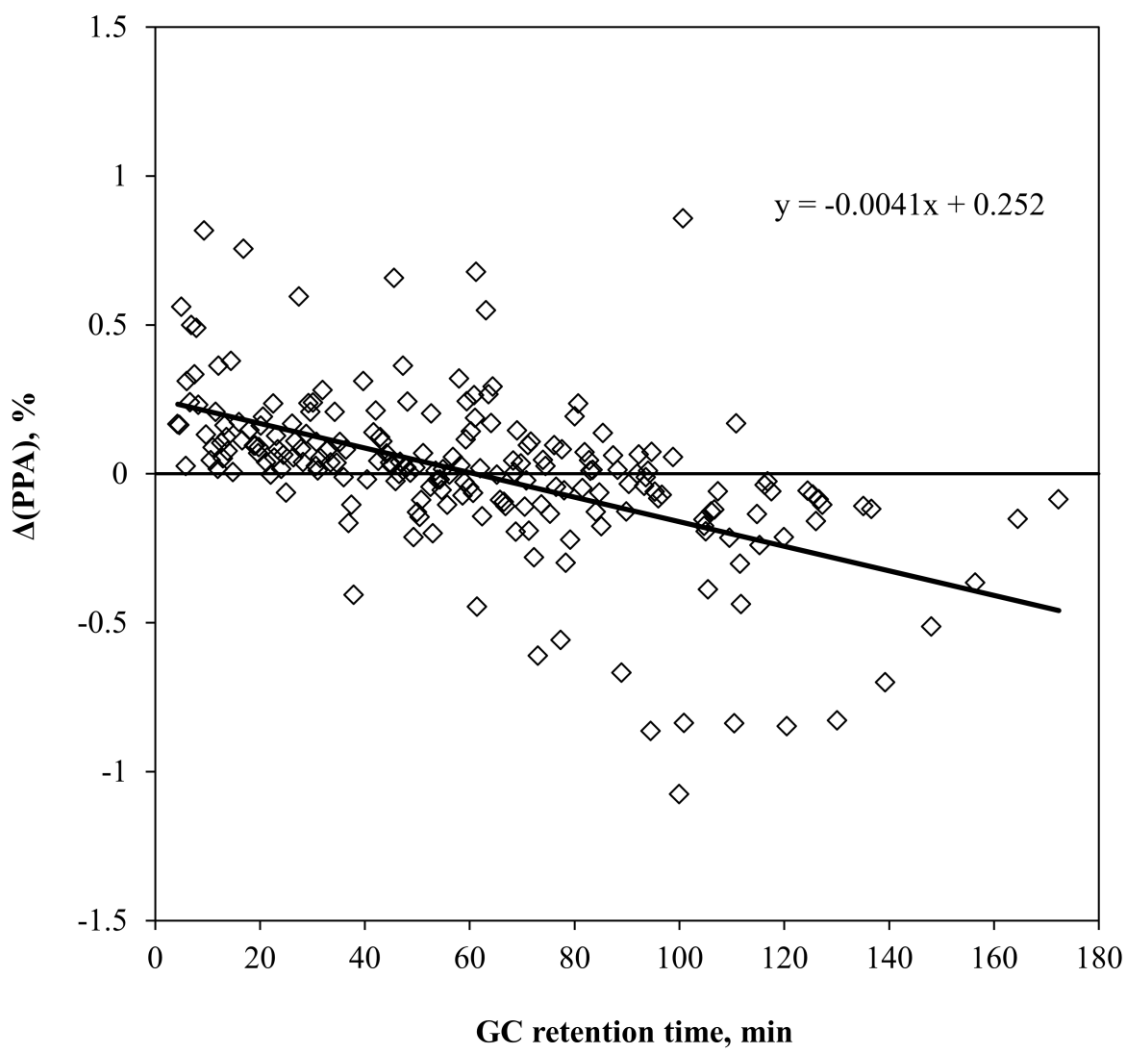


Fig. D-54 $\Delta(\text{PPA})$ for thermally stressed DF (Continuous, DF, #7, S4).

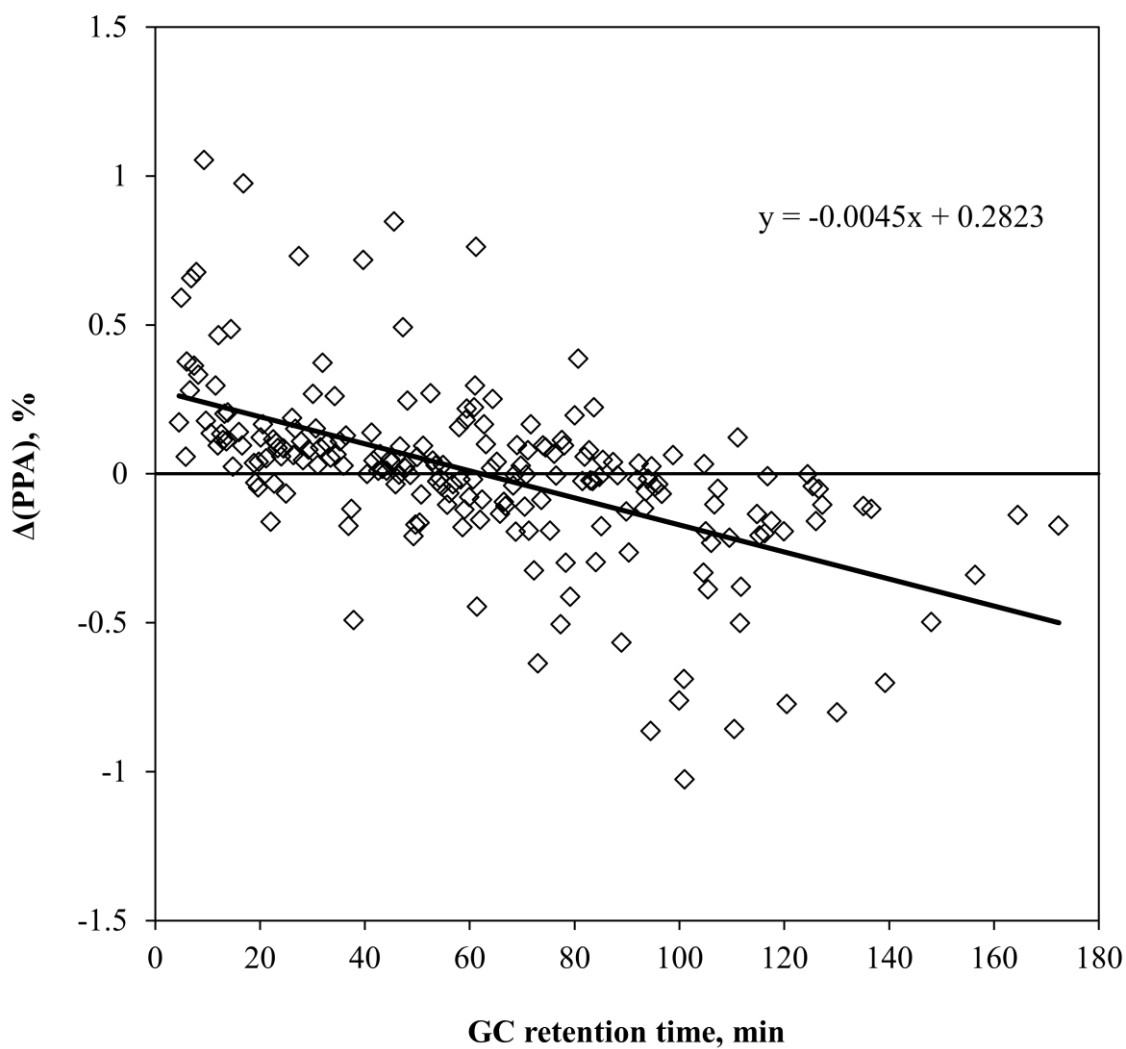


Fig. D-55 $\Delta(\text{PPA})$ for thermally stressed DF (Continuous, DF, #8, S4).

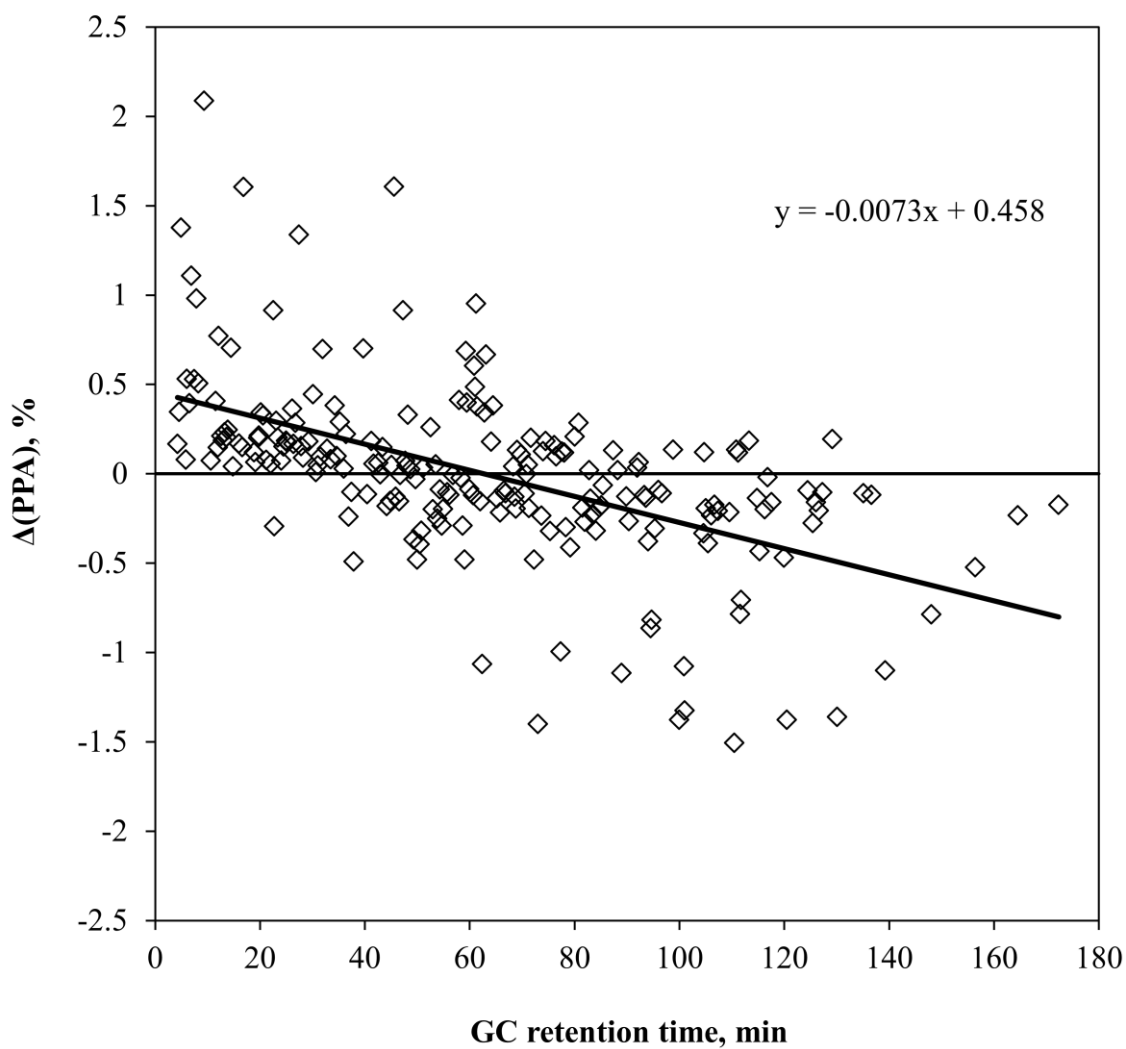


Fig. D-56 $\Delta(\text{PPA})$ for thermally stressed DF (Continuous, DF, #9, S4).

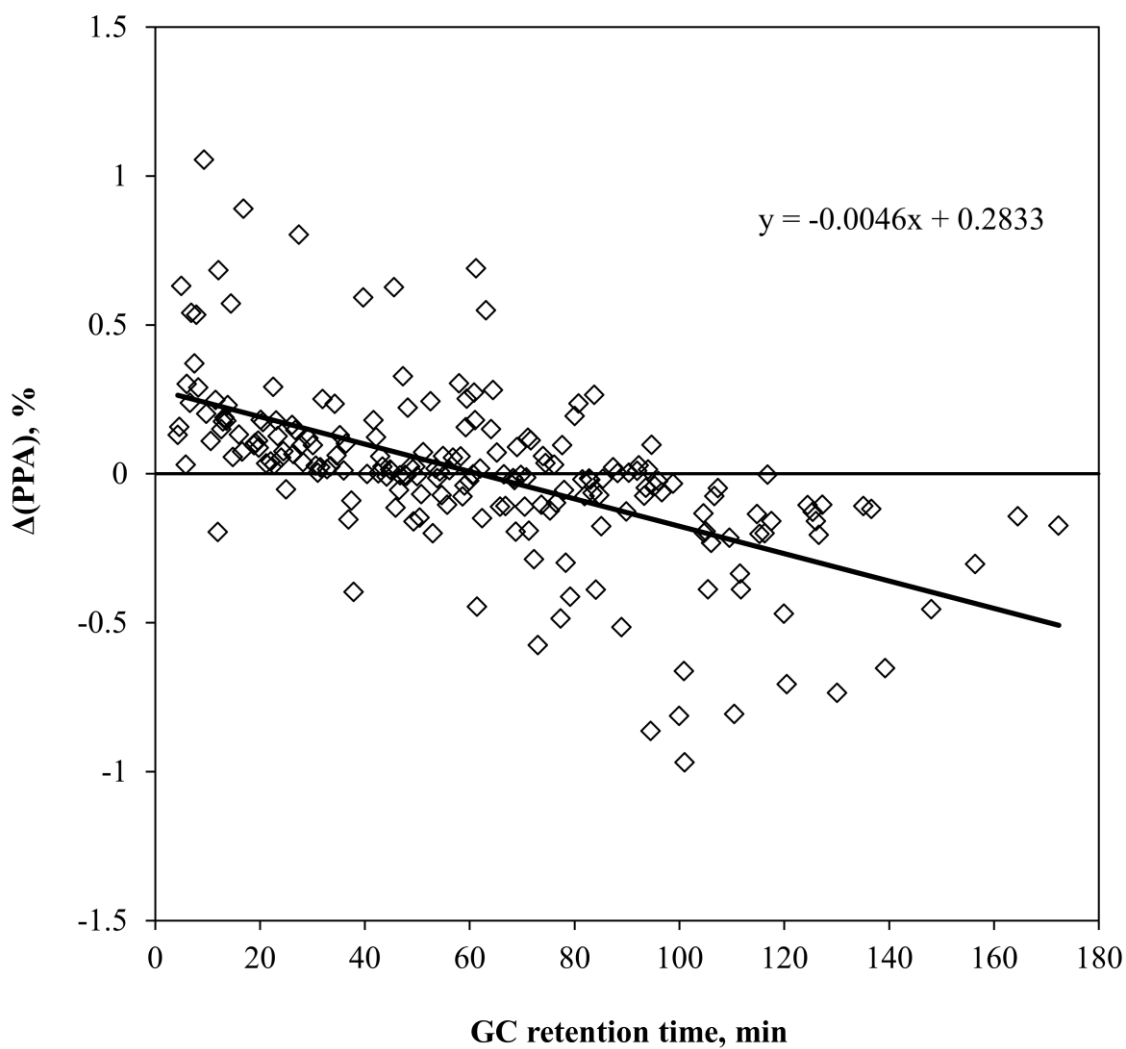


Fig. D-57 $\Delta(\text{PPA})$ for thermally stressed DF (Continuous, DF, #10, S4).

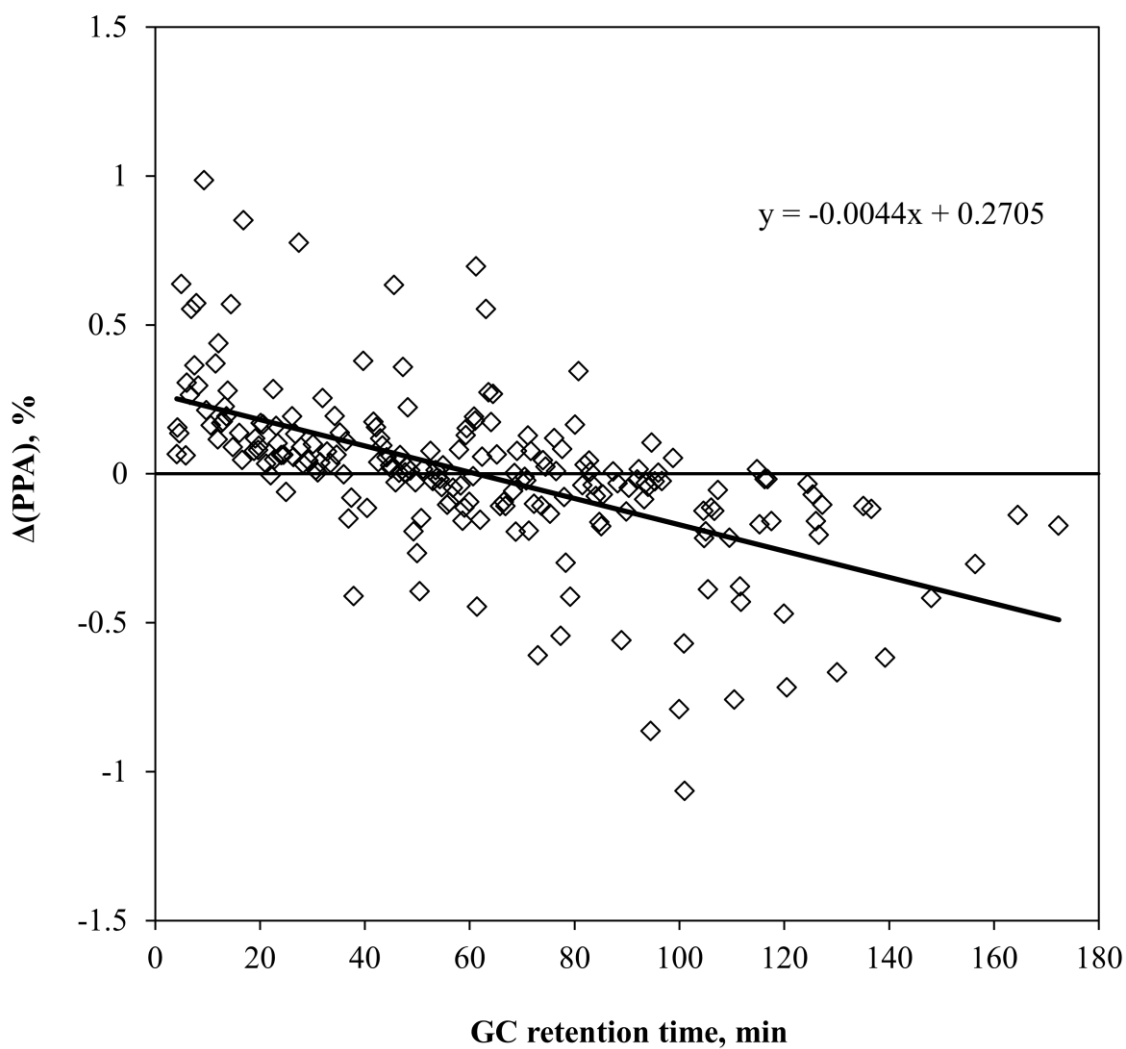


Fig. D-58 $\Delta(\text{PPA})$ for thermally stressed DF (Continuous, DF, #11, S4).

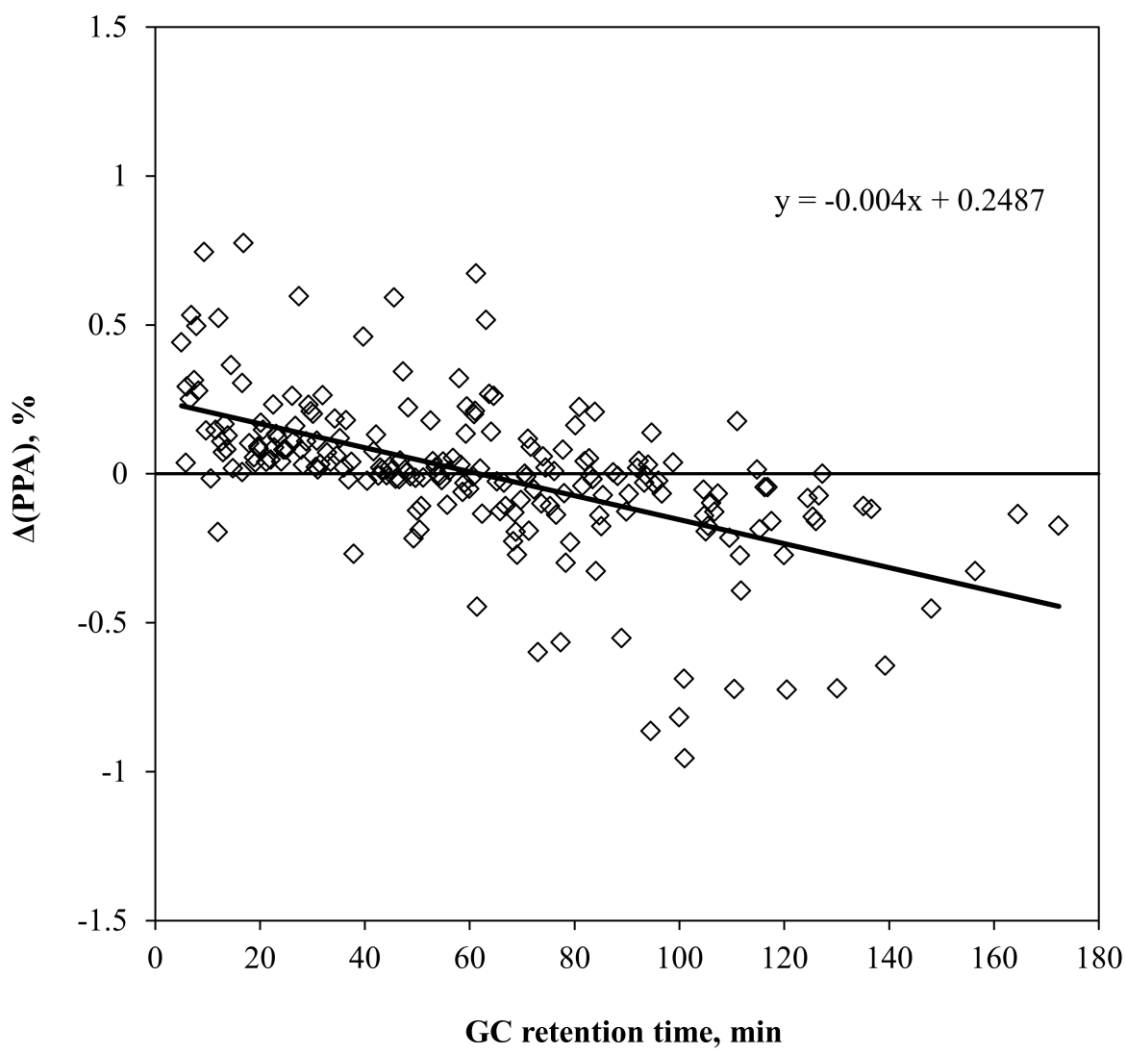


Fig. D-59 $\Delta(\text{PPA})$ for thermally stressed DF (Continuous, DF, #12, S4).

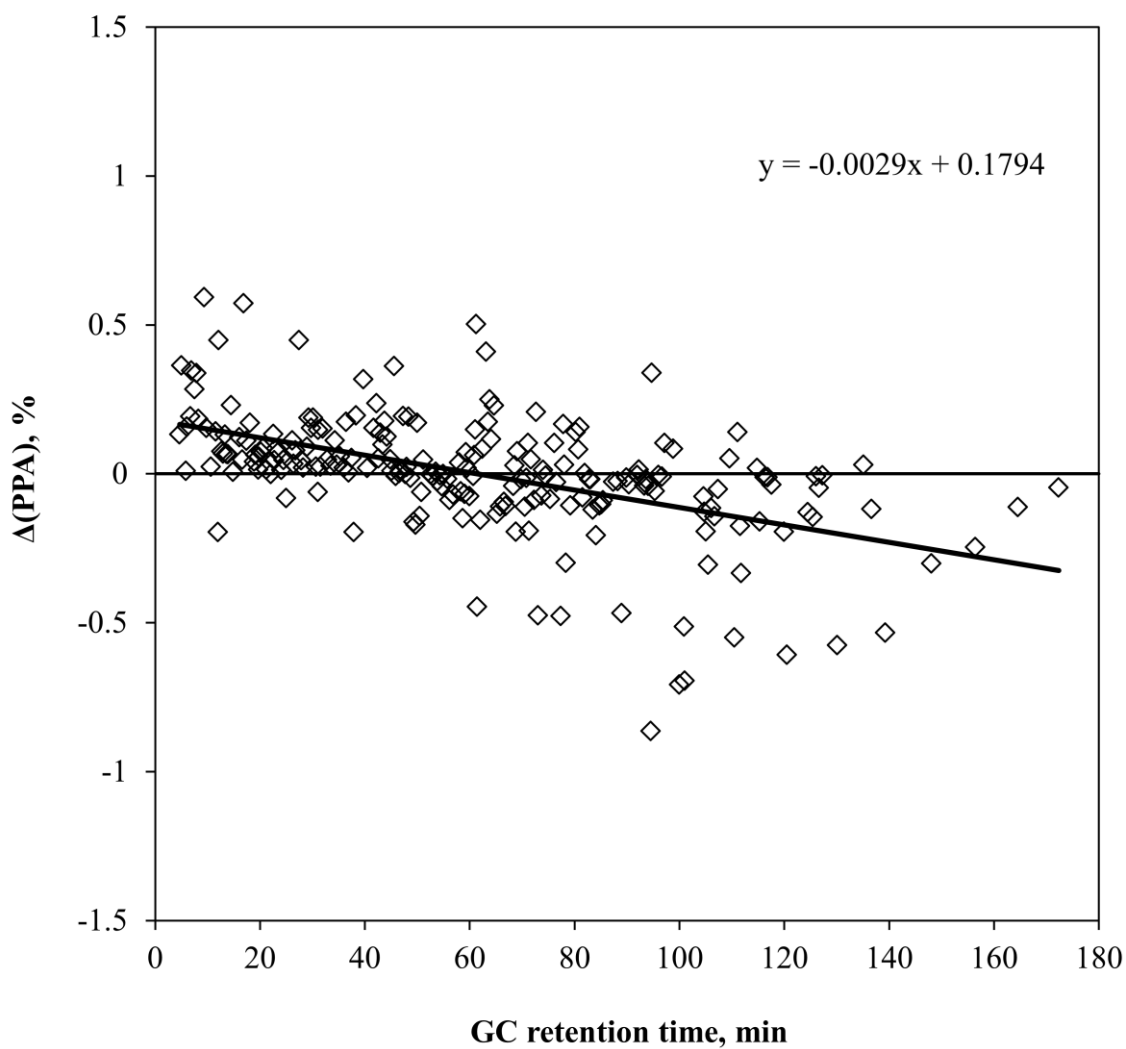


Fig. D-60 $\Delta(\text{PPA})$ for thermally stressed DF (Continuous, DF/CO₂, #1, S4).

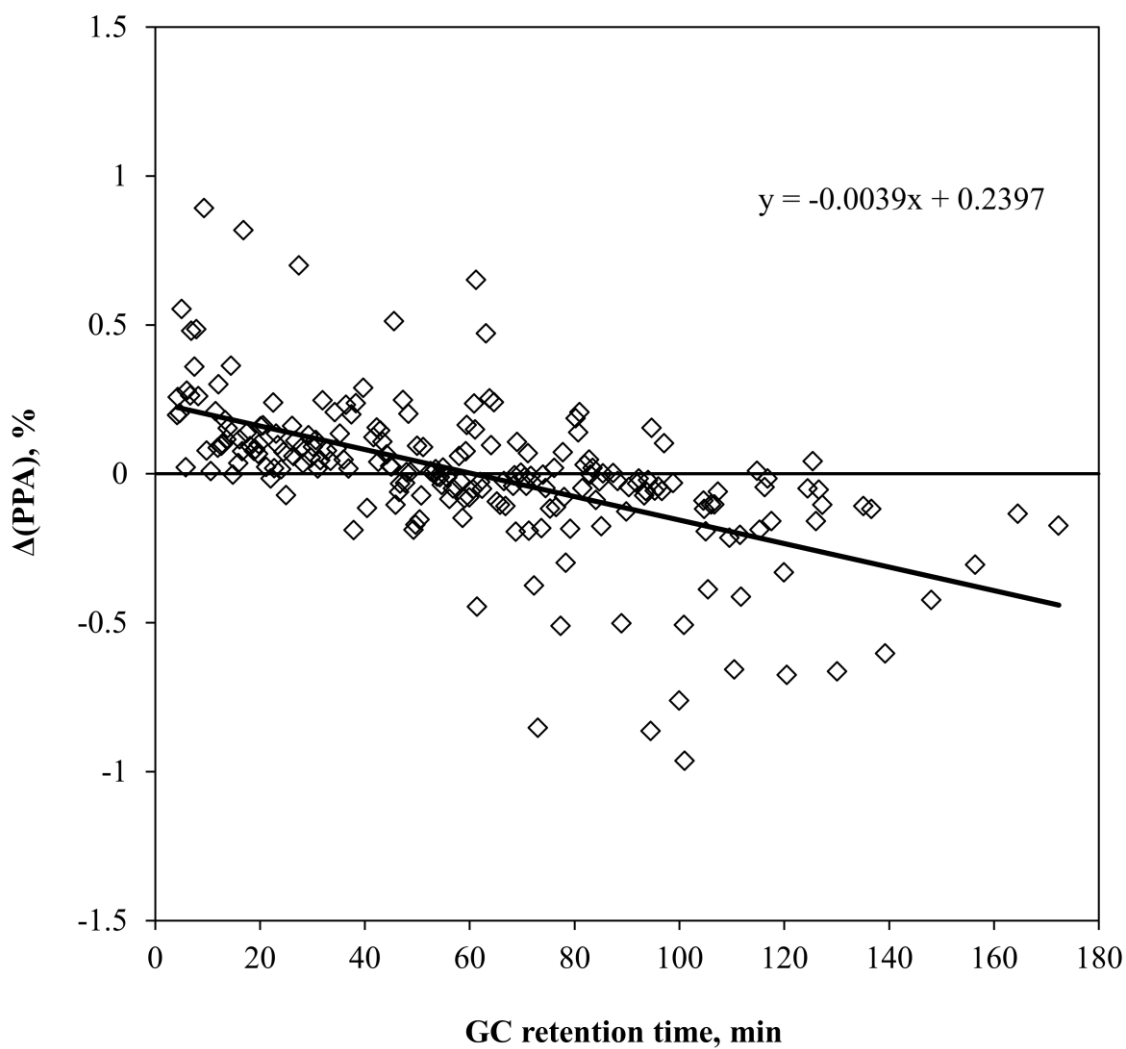


Fig. D-61 $\Delta(\text{PPA})$ for thermally stressed DF (Continuous, DF/CO₂, #2, S4).

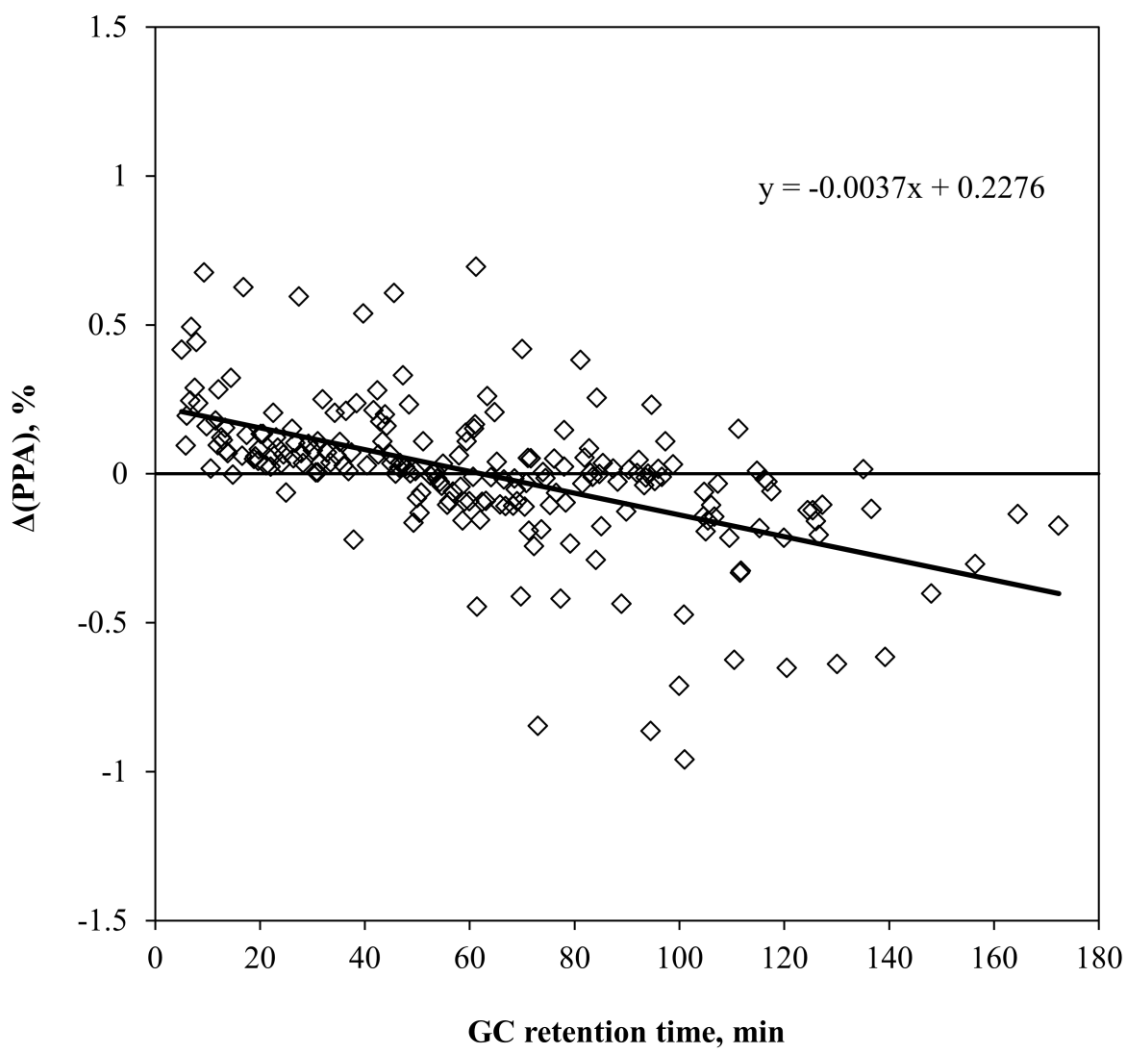


Fig. D-62 $\Delta(\text{PPA})$ for thermally stressed DF (Continuous, DF/CO₂, #3, S4).

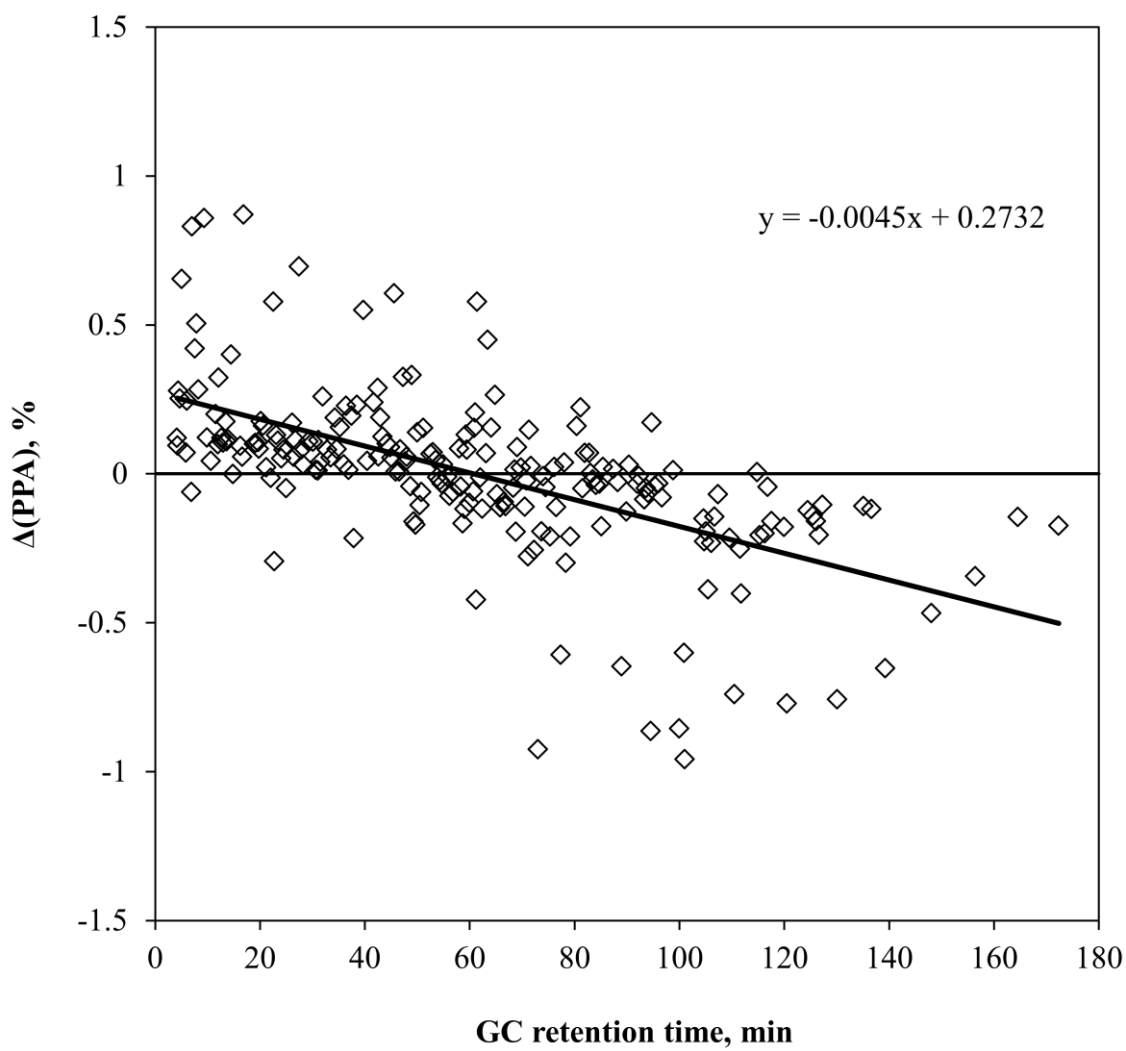


Fig. D-63 $\Delta(\text{PPA})$ for thermally stressed DF (Continuous, DF/CO₂, #4, S4).

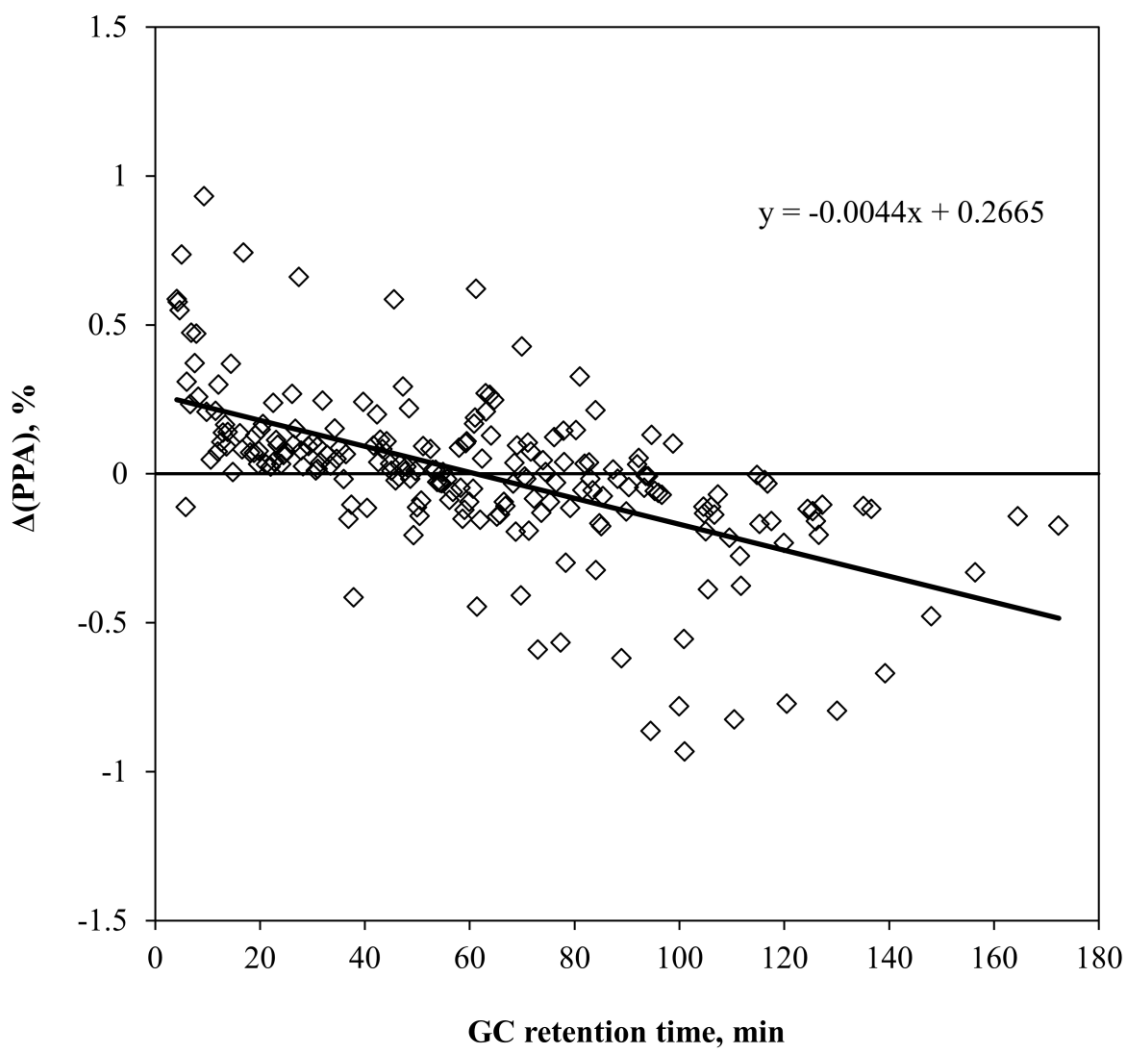


Fig. D-64 $\Delta(\text{PPA})$ for thermally stressed DF (Continuous, DF/CO₂, #5, S4).

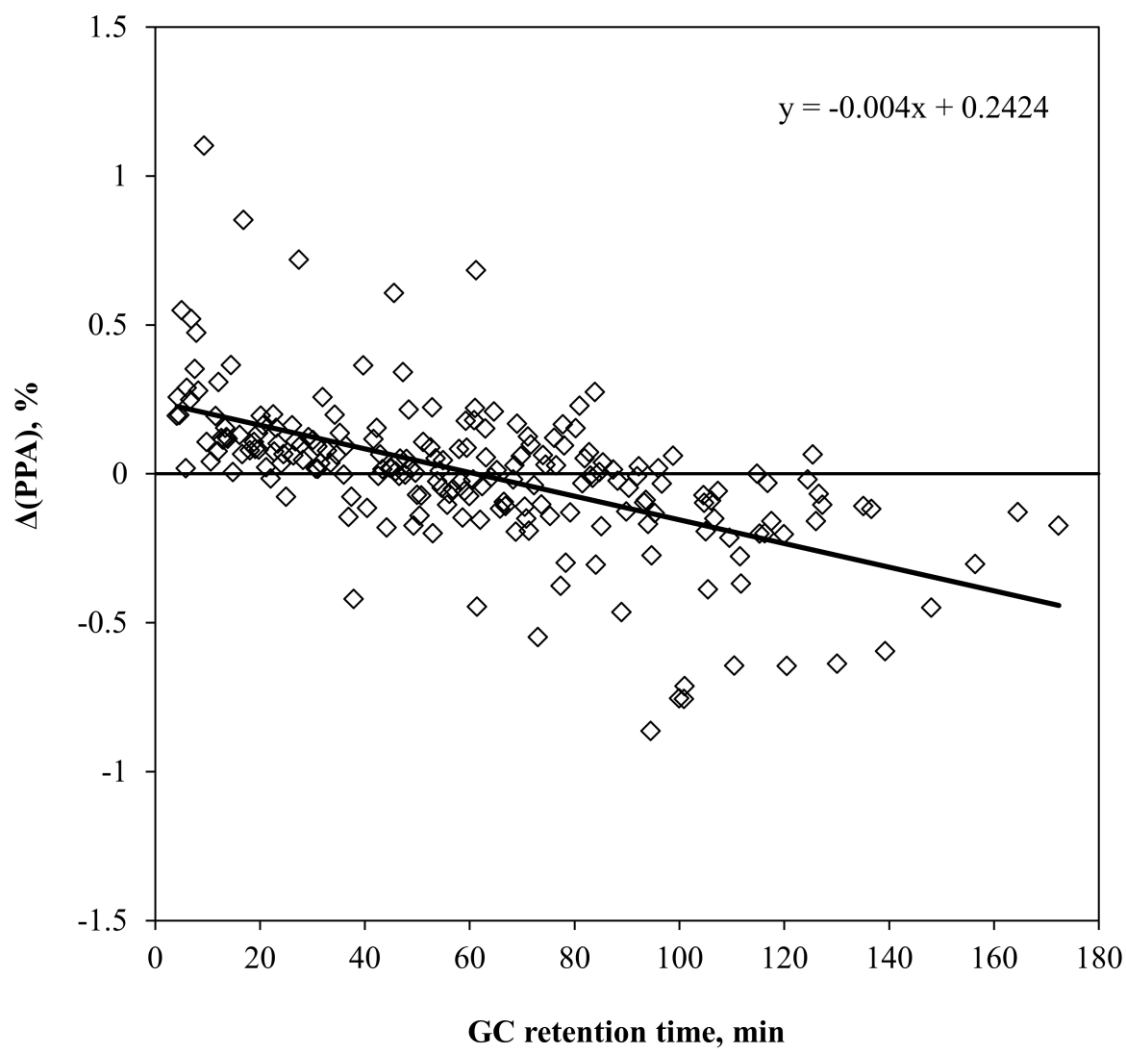


Fig. D-65 $\Delta(\text{PPA})$ for thermally stressed DF (Continuous, DF/CO₂, #6, S4).

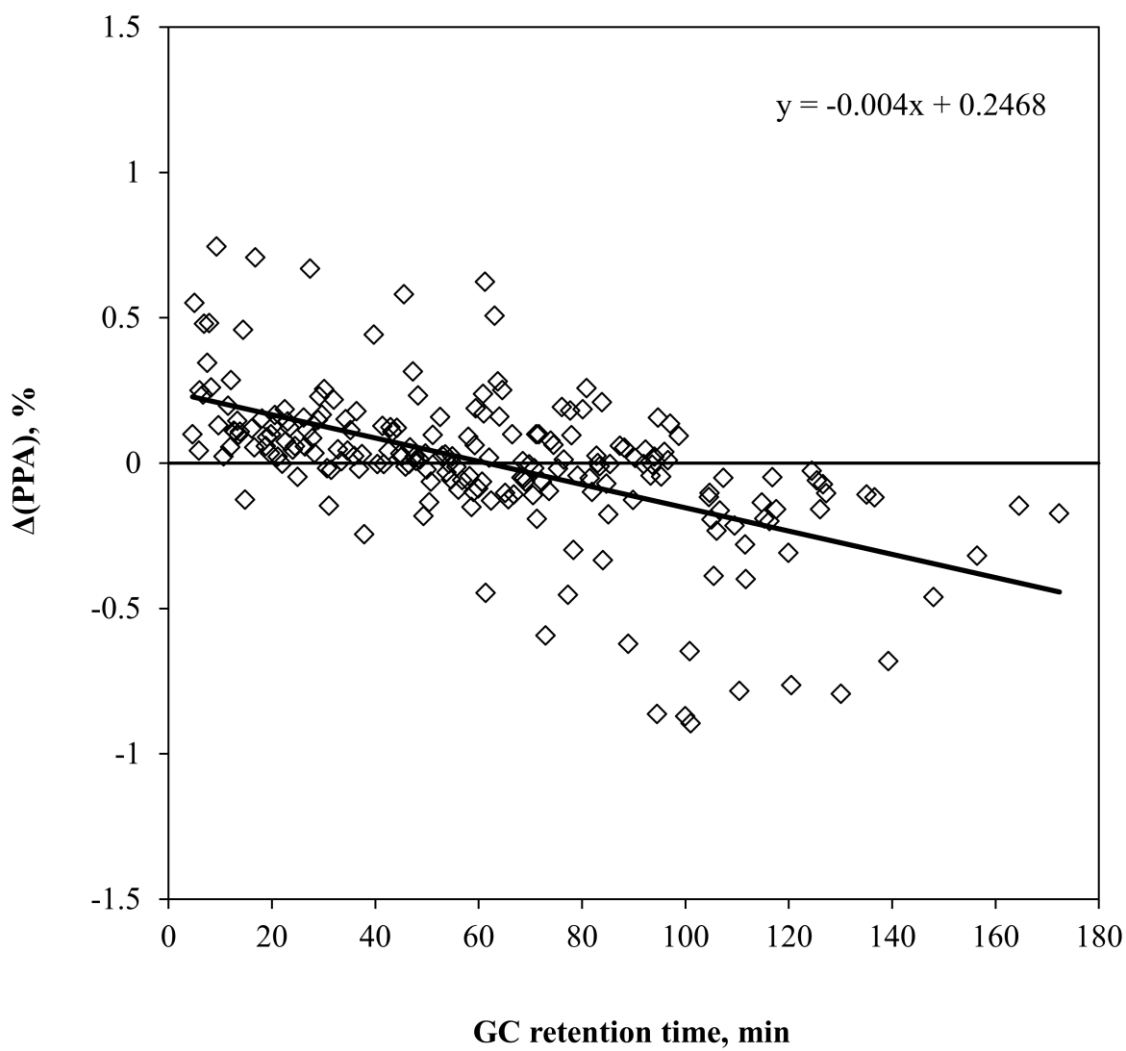


Fig. D-66 $\Delta(\text{PPA})$ for thermally stressed DF (Continuous, DF/CO₂, #7, S4).

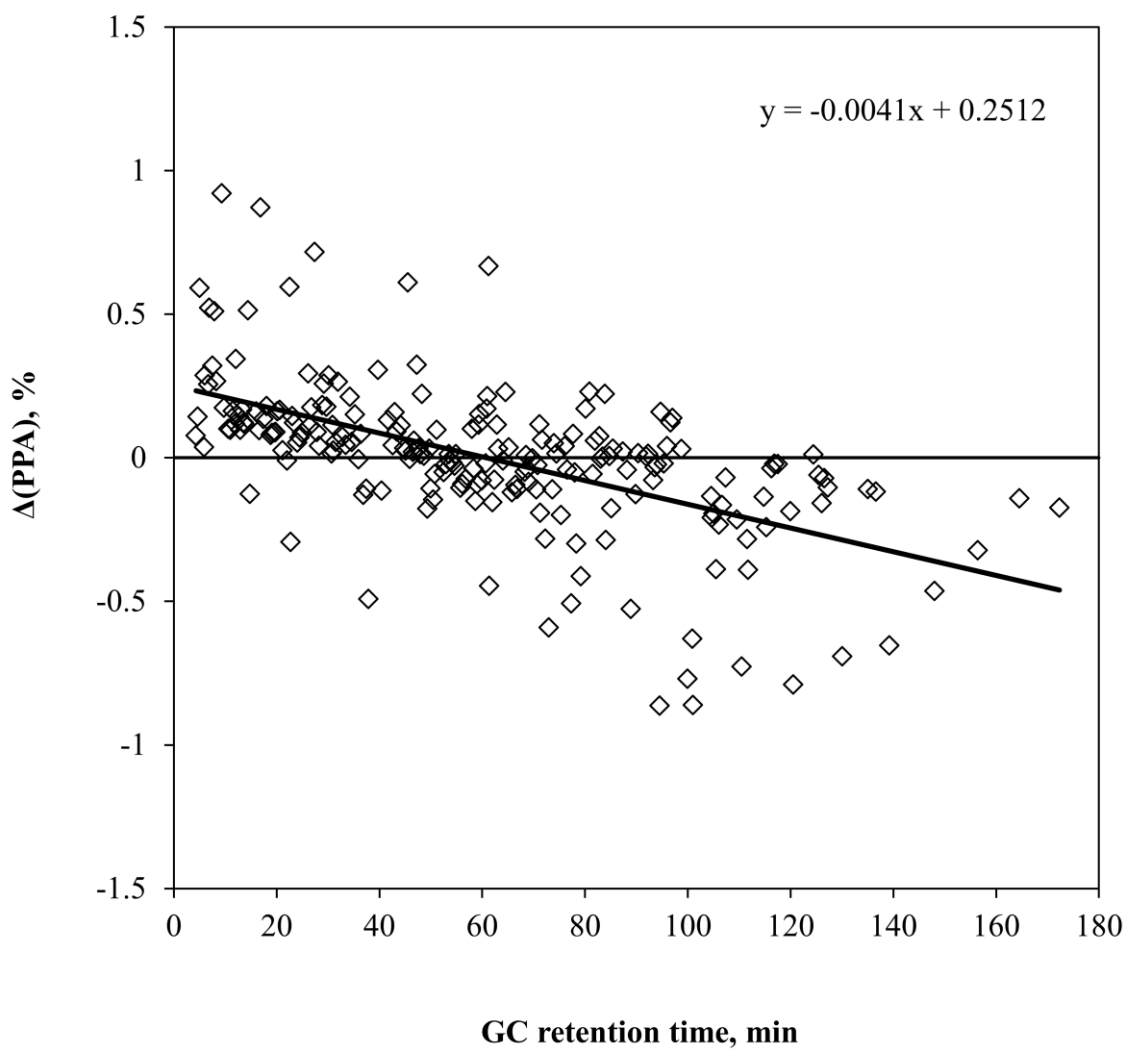


Fig. D-67 $\Delta(\text{PPA})$ for thermally stressed DF (Continuous, DF/CO₂, #8, S4).

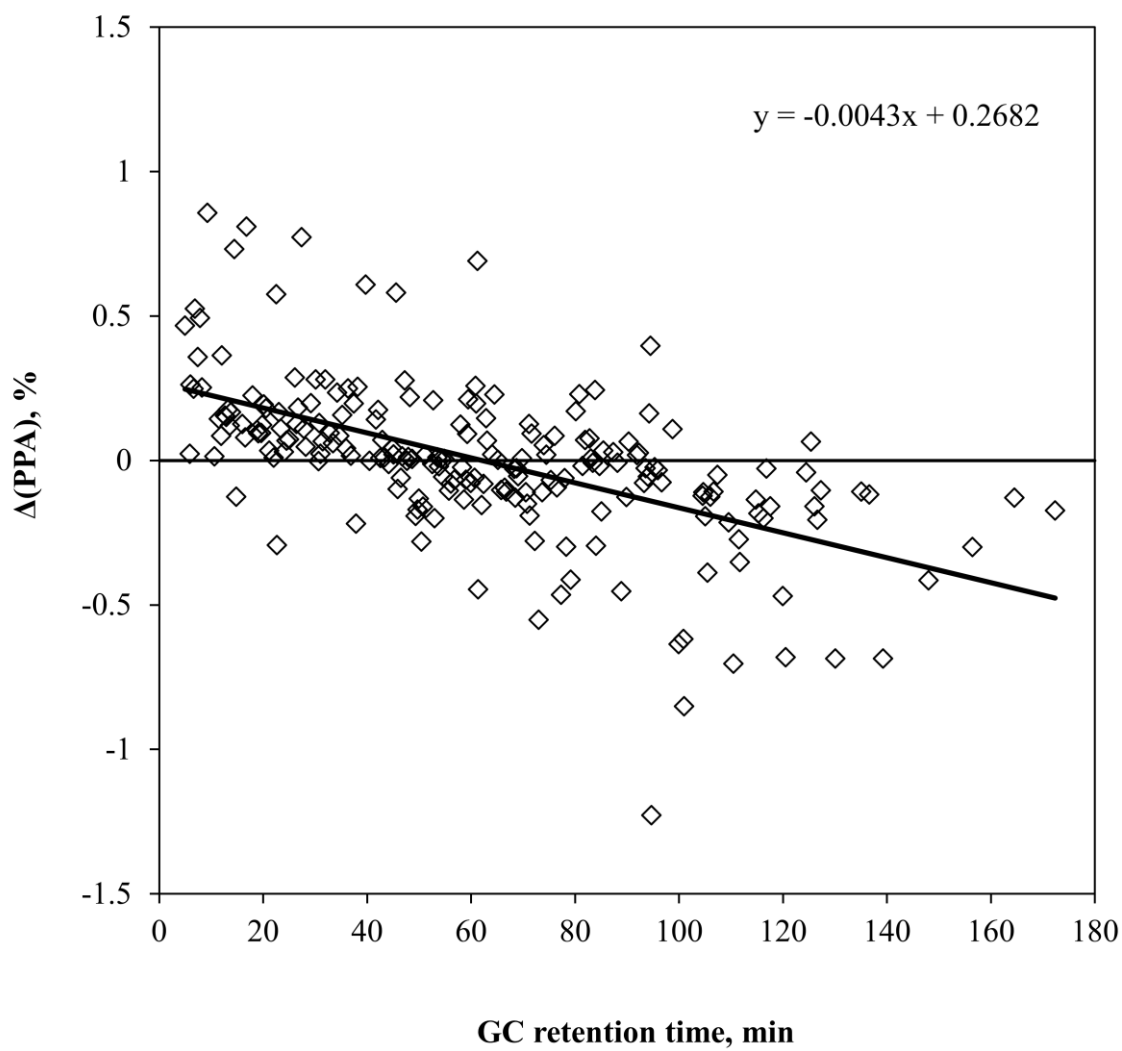


Fig. D-68 $\Delta(\text{PPA})$ for thermally stressed DF (Continuous, DF/CO₂, #9, S4).

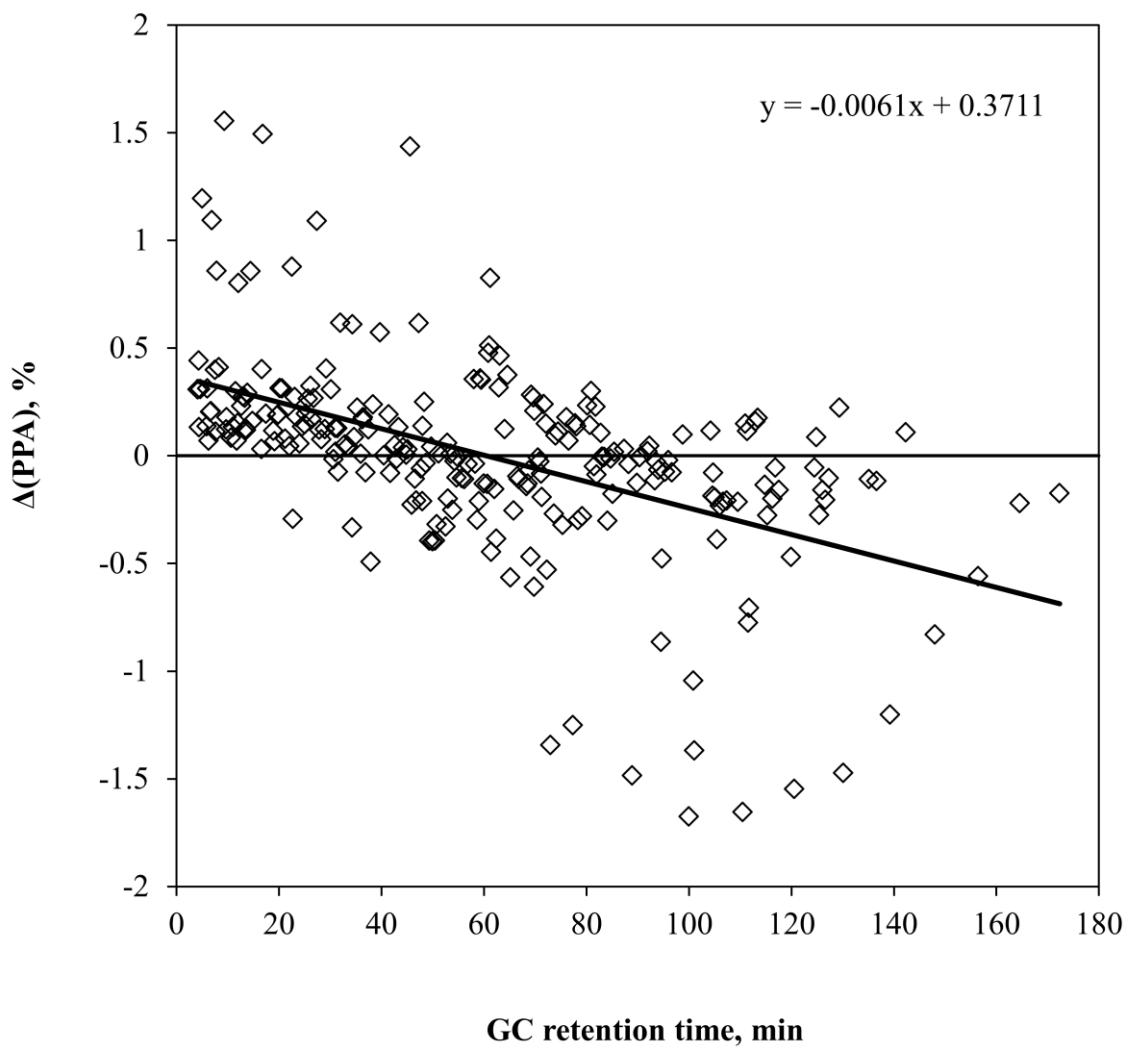


Fig. D-69 $\Delta(\text{PPA})$ for thermally stressed DF (Continuous, DF/CO₂, #10, S4).

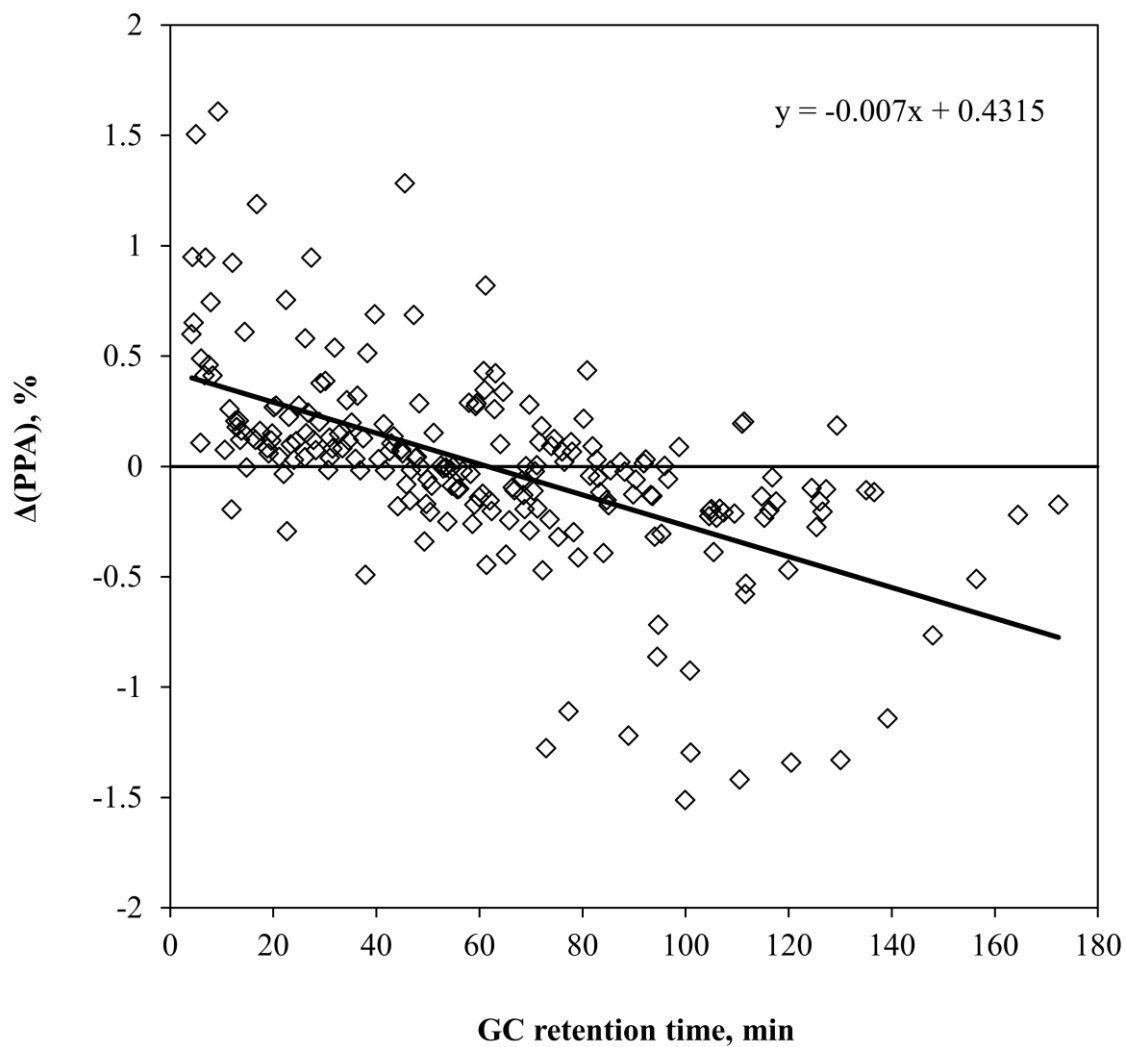


Fig. D-70 $\Delta(\text{PPA})$ for thermally stressed DF (Continuous, DF/CO₂, #11, S4).

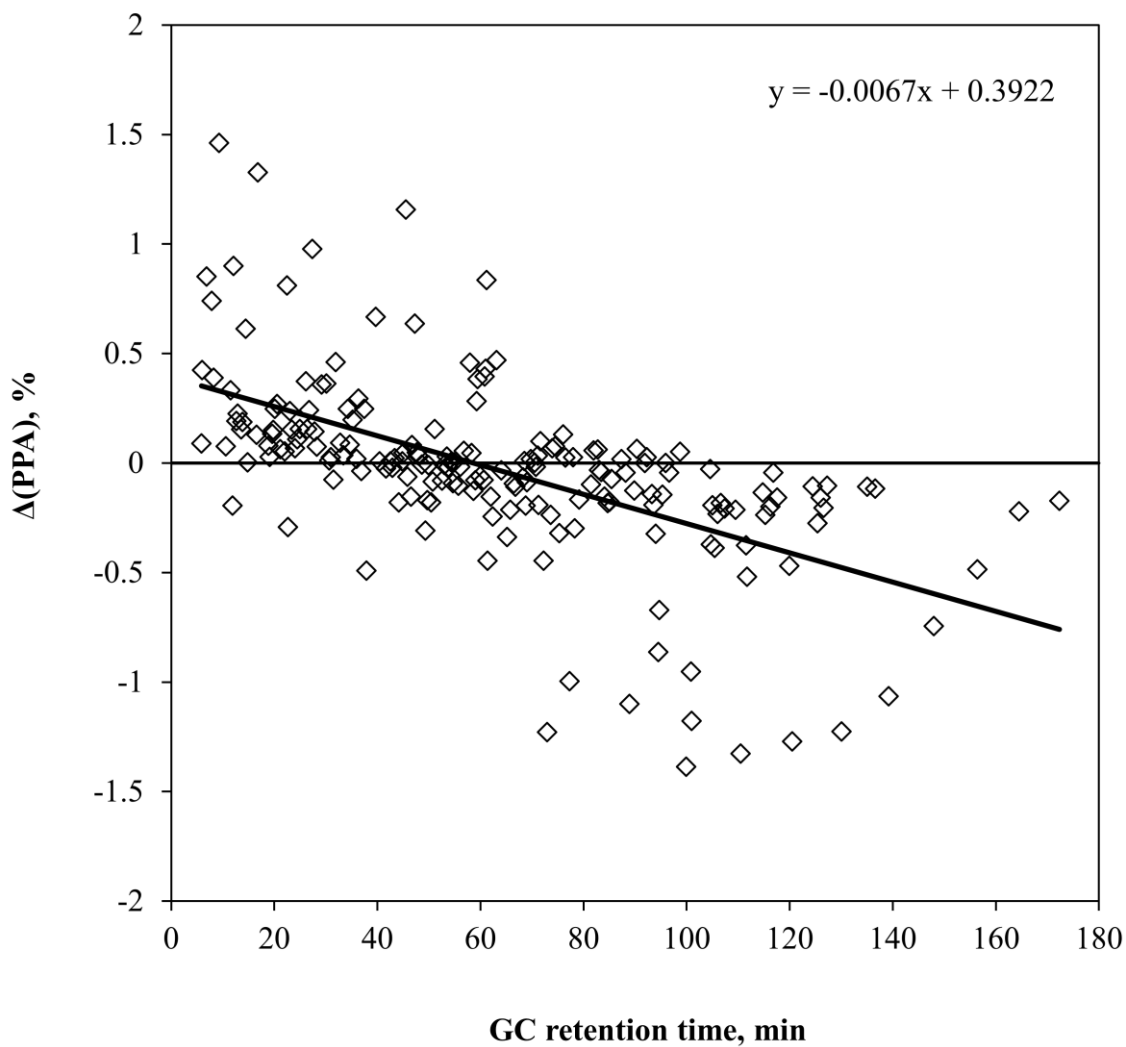


Fig. D-71 $\Delta(\text{PPA})$ for thermally stressed DF (Continuous, DF/CO₂, #12, S4).

APPENDIX E

PERMISSIONS TO QUOTE/REPRODUCE

COPYRIGHT MATERIAL

ELSEVIER LICENSE 1

Feb 01, 2011

This is a License Agreement between Ronghong Lin ("You") and Elsevier ("Elsevier") provided by Copyright Clearance Center ("CCC"). The license consists of your order details, the terms and conditions provided by Elsevier, and the payment terms and conditions.

All payments must be made in full to CCC. For payment instructions, please see information listed at the bottom of this form.

| | |
|---|--|
| Supplier | Elsevier Limited The Boulevard, Langford Lane Kidlington, Oxford, OX5 1GB, UK |
| Registered Company Number | 1982084 |
| Customer name | Ronghong Lin |
| Customer address | 132 Remington Ave Syracuse, NY 13210 |
| License number | 2600400148039 |
| License date | Feb 01, 2011 |
| Licensed content publisher | Elsevier |
| Licensed content publication | Journal of Chromatography A |
| Licensed content title | Determination of diffusion coefficients by supercritical fluid chromatography: Effects of mobile phase mean velocity and column orientation |
| Licensed content author | Ronghong Lin, Lawrence L. Tavlarides |
| Licensed content date | 25 June 2010 |
| Licensed content volume number | 1217 |
| Licensed content issue number | 26 |
| Number of pages | 9 |
| Start Page | 4454 |
| End Page | 4462 |
| Type of Use | reuse in a thesis/dissertation |
| Portion | full article |
| Format | both print and electronic |
| Are you the author of this Elsevier article? | Yes |
| Will you be translating? | No |
| Order reference number | |
| Title of your thesis/dissertation | ISSUES ON CLEAN DIESEL COMBUSTION |

| | |
|---|---|
| | TECHNOLOGY USING SUPERCRITICAL FLUIDS: THERMOPHYSICAL PROPERTIES AND THERMAL STABILITY OF DIESEL FUEL |
| Expected completion date | Apr 2011 |
| Estimated size (number of pages) | 250 |
| Elsevier VAT number | GB 494 6272 12 |
| Permissions price | 0.00 USD |
| VAT/Local Sales Tax | 0.0 USD / 0.0 GBP |
| Total | 0.00 USD |
| Terms and Conditions | Not attached |

ELSEVIER LICENSE 2

Feb 01, 2011

This is a License Agreement between Ronghong Lin ("You") and Elsevier ("Elsevier") provided by Copyright Clearance Center ("CCC"). The license consists of your order details, the terms and conditions provided by Elsevier, and the payment terms and conditions.

All payments must be made in full to CCC. For payment instructions, please see information listed at the bottom of this form.

| | |
|-------------------------------------|---|
| Supplier | Elsevier Limited The Boulevard, Langford Lane Kidlington, Oxford, OX5 1GB, UK |
| Registered Company Number | 1982084 |
| Customer name | Ronghong Lin |
| Customer address | 132 Remington Ave Syracuse, NY 13210 |
| License number | 2600411073742 |
| License date | Feb 01, 2011 |
| Licensed content publisher | Elsevier |
| Licensed content publication | The Journal of Supercritical Fluids |
| Licensed content title | Diffusion coefficients of diesel fuel and surrogate compounds in supercritical carbon dioxide |
| Licensed content author | Ronghong Lin, Lawrence L. Tavlarides |
| Licensed content date | February 2010 |

| | |
|---|---|
| Licensed content volume number | 52 |
| Licensed content issue number | 1 |
| Number of pages | 9 |
| Start Page | 47 |
| End Page | 55 |
| Type of Use | reuse in a thesis/dissertation |
| Intended publisher of new work | other |
| Portion | full article |
| Format | both print and electronic |
| Are you the author of this Elsevier article? | Yes |
| Will you be translating? | No |
| Order reference number | |
| Title of your thesis/dissertation | ISSUES ON CLEAN DIESEL COMBUSTION TECHNOLOGY USING SUPERCRITICAL FLUIDS: THERMOPHYSICAL PROPERTIES AND THERMAL STABILITY OF DIESEL FUEL |
| Expected completion date | Apr 2011 |
| Estimated size (number of pages) | 250 |
| Elsevier VAT number | GB 494 6272 12 |
| Permissions price | 0.00 USD |
| VAT/Local Sales Tax | 0.0 USD / 0.0 GBP |
| Total | 0.00 USD |
| Terms and Conditions | Not attached |

ELSEVIER LICENSE 3

Feb 01, 2011

This is a License Agreement between Ronghong Lin ("You") and Elsevier ("Elsevier") provided by Copyright Clearance Center ("CCC"). The license consists of your order details, the terms and conditions provided by Elsevier, and the payment terms and conditions.

All payments must be made in full to CCC. For payment instructions, please see information listed at the bottom of this form.

| | |
|-----------------|--|
| Supplier | Elsevier Limited The Boulevard, Langford Lane |
|-----------------|--|

| | |
|---|---|
| Registered Company Number | Kidlington,Oxford,OX5 1GB,UK 1982084 |
| Customer name | Ronghong Lin |
| Customer address | 132 Remington Ave Syracuse, NY 13210 |
| License number | 2600420530979 |
| License date | Feb 01, 2011 |
| Licensed content publisher | Elsevier |
| Licensed content publication | Progress in Energy and Combustion Science |
| Licensed content title | Recent progress in the development of diesel surrogate fuels |
| Licensed content author | William J. Pitz, Charles J. Mueller |
| Licensed content date | 3 August 2010 |
| Licensed content volume number | n/a |
| Licensed content issue number | n/a |
| Number of pages | 1 |
| Start Page | 0 |
| End Page | 0 |
| Type of Use | reuse in a thesis/dissertation |
| Intended publisher of new work | other |
| Portion | figures/tables/illustrations |
| Number of figures/tables/illustrations | 1 |
| Format | both print and electronic |
| Are you the author of this Elsevier article? | No |
| Will you be translating? | No |
| Order reference number | |
| Title of your thesis/dissertation | ISSUES ON CLEAN DIESEL COMBUSTION TECHNOLOGY USING SUPERCRITICAL FLUIDS: THERMOPHYSICAL PROPERTIES AND THERMAL STABILITY OF DIESEL FUEL |
| Expected completion date | Apr 2011 |
| Estimated size (number of pages) | 250 |
| Elsevier VAT number | GB 494 6272 12 |
| Permissions price | 0.00 USD |
| VAT/Local Sales Tax | 0.0 USD / 0.0 GBP |
| Total | 0.00 USD |
| Terms and Conditions | Not attached |

BIBLIOGRAPHY

- Abu-Eishah, S. I., 1999. Modification of the predictive capability of the PRSV-2 equation of state for critical volumes of binary mixtures, *Fluid Phase Equilibria* 157(1), 1-16.
- Ago, K., Nishiumi, H., 1999. Mutual diffusion coefficients of benzene in supercritical carbon dioxide, *Journal of Chemical Engineering of Japan* 32(5), 563-568.
- Ahern, B., Djutrisno, I., Donahue, K., Haldeman, C., Hynek, S., Johnson, K., Valbert, J., Woods, M., Taylor, J., Tester, J., 2001. Dramatic emissions reductions with a direct injection diesel engine burning supercritical fuel/water mixtures. Society of Automotive Engineers, [Special Publication] SP SP-1645(SI and Diesel Engine Performance and Fuel Effects), 113-118.
- Alizadeh, A., Nieto de Castro, C. A., Wakeham, W. A., 1980. The theory of the Taylor dispersion technique for liquid diffusivity measurements, *International Journal of Thermophysics* 1(3), 243-284.
- Alriksson, M., Denbratt, I., 2006. Low temperature combustion in a heavy duty diesel engine using high levels of EGR, SAE Paper 2006-01-0075.
- Altin, O., Eser, S., 2004. Carbon deposit formation from thermal stressing of petroleum fuels, *Prepr. Pap.-Am. Chem. Soc., Div. Fuel Chem.* 49(2), 764-766.
- Anitescu, G., Tavlarides, L. L., Geana, D., 2009. Phase transitions and thermal behavior of fuel/diluent mixtures, *Energy & Fuels* 23(6), 3068-3077.
- API, 2006. API Technical Data Book. Washington, DC: The American Petroleum Institute and EPCON International.
- Aris, R., 1956. On the dispersion of a solute in a fluid flowing through a tube,

Proceedings of the Royal Society of London. Series A. Mathematical and Physical Sciences 235(1200), 67-77.

Bacha, J. D., Lesnini, D. G., 1997. Diesel fuel thermal stability at 300 °F, 6th International Conference on Stability and Handling of Liquid Fuels, 671-684.

Balster, L. M., Balster, W. J., Jones, E. G., 1996. Thermal stability of jet-fuel/paraffin blends, Energy & Fuels 10(6), 1176-1180.

Banavali, R., Chheda, B., 2000. Improvement of thermal stability of diesel fuel using tertiary alkyl primary amines, IASH 2000, the 7th International Conference on Stability and Handling of Liquid Fuels, 85-109.

Barths, H., Hasse, C., Bikas, G., Peters, N., 2000. Simulation of combustion in direct injection diesel engines using a eulerian particle flamelet model, Proceedings of the Combustion Institute 28(1), 1161-1168.

Barths, H., Pitsch, H., Peters, N., 1999. 3D simulation of DI diesel combustion and pollutant formation using a two-component reference fuel, Oil & Gas Science and Technology - Rev. IFP 54(2), 233-244.

Batts, B. D., Fathoni, A. Z., 1991. A literature review on fuel stability studies with particular emphasis on diesel oil, Energy & Fuels 5(1), 2-21.

Beal, E. J., Hardy, D. R., 1994. Thermal stability of diesel fuels by quantitative gravimetric JFTOT, ACS Preprints 39(3), 958-961.

Beaver, B., Gao, L., Burgess-Clifford, C., Sobkowiak, M., 2005. On the mechanisms of formation of thermal oxidative deposits in jet fuels. Are unified mechanisms possible for both storage and thermal oxidative deposit formation for middle distillate fuels? Energy & Fuels 19(4), 1574-1579.

Belardini, P., Bertoli, C., Beatrice, C., D'Anna, A., Del Giacomo, N., 1996. Application of a

reduced kinetic model for soot formation and burnout in three-dimensional diesel combustion computations, Symposium (International) on Combustion 26(2), 2517-2524.

Bellan, J., 2004. Subcritical/supercritical droplet cluster behavior in dense and dilute regions of sprays, Progress in Astronautics and Aeronautics 200(Liquid Rocket Thrust Chambers), 323-338.

Blank, D. A., Shih, T.-M., 1990. Hypergolic combustion model for four-stroke heat-barrier piston engines, Numerical Heat Transfer, Part A: Applications: An International Journal of Computation and Methodology 17(1), 1-28.

Brule, M. R., Lin, C. T., Lee, L. L., Starling, K. E., 1982. Multiparameter corresponding-states correlation of coal-fluid thermodynamic properties, AIChE Journal 28(4), 616-625.

Bruno, T. J., 1994. Measurement of diffusion in fluid systems: applications to the supercritical fluid region, Journal of Thermophysics and Heat Transfer 8(2), 329-333.

Bueno, J. L., Suarez, J. J., Dizey, J., Medina, I., 1993. Infinite dilution diffusion coefficients: benzene derivatives as solutes in supercritical carbon dioxide, Journal of Chemical & Engineering Data 38(3), 344-349.

Canaan, R. E., Dec, J. E., Green, R. M., Daly, D. T., 1998. The influence of fuel volatility on the liquid-phase fuel penetration in a heavy-duty D.I. diesel engine, SAE Paper 980510.

Cathonnet, M., 1994. Chemical kinetic modeling of combustion from 1969 to 2019, Combustion Science and Technology 98(4), 265-279.

Cavett, R. H., 1962. Physical data for distillation calculations: vapor-liquid equilibria, API

Proceeding, Div.Ref. 43(III), 351-366.

Cheiky, M. C., Grottenthaler, D. L., 2010. Dual solenoid fuel injector with catalytic activator section, U.S. Pat. Appl. Publ. 2009-612440; 2008-117897P(20100126471), 14.

Chen, L. D., 1994. Heat transfer, fouling, and combustion of supercritical fuels, Report (AFOSR-TR-94-0321; Order No. AD-A279 906), 67.

Chin, J., Lefebvre, A., 1992. Experimental study on hydrocarbon fuel thermal stability, Journal of Thermal Science 1(1), 70-74.

ConocoPhillips, 2007. No.2 diesel fuel material safety data sheet,2011(4/4), 7.

Constantinou, L., Gani, R., 1994. New group contribution method for estimating properties of pure compounds, AIChE Journal 40(10), 1697-1710.

Cormier, T. A., 2001. PHATCAT Power-Head and Thrust Chamber Analysis Tool, Master thesis, Georgia Institute of Technology.

Curran, H. J., Fisher, E. M., Glaude, P. -A., Marinov, N. M., Pitz, W. J., Westbrook, C. K., Layton, D. W., Flynn, P. F., Durrett, R. P., Zur Loye, A. O., Akinyemi, O. C., Dryer, F. L., 2001. Detailed chemical kinetic modeling of diesel combustion with oxygenated fuels, SAE Paper 2001-01-0653.

Curran, H. J., Gaffuri, P., Pitz, W. J., Westbrook, C. K., 2002. A comprehensive modeling study of iso-octane oxidation, Combustion and Flame 129(3), 253-280.

Curran, H. J., Gaffuri, P., Pitz, W. J., Westbrook, C. K., 1998. A comprehensive modeling study of n-heptane oxidation, Combustion and Flame 114(1-2), 149-177.

Cussler, E. L., 2009. Diffusion: Mass Transfer in Fluid Systems. New York: Cambridge University Press.

- Dagaut, P., 2002. On the kinetics of hydrocarbons oxidation from natural gas to kerosene and diesel fuel, *Physical Chemistry Chemical Physics* 4(11), 2079-2094.
- Dean, W. R., 1928. The stream-line motion of fluid in a curved pipe, *Philosophical Magazine Series 7* 5(30), 673-695.
- Dean, W. R., 1927. Note on the motion of fluid in a curved pipe, *Philosophical Magazine Series 7* 4(20), 208-223.
- Dec, J. E., 1997. A conceptual model of DI diesel combustion based on laser sheet imaging, *SAE Paper 970873*.
- Doungthip, T., Ervin, J. S., Williams, T. F., Bento, J., 2002. Studies of injection of jet fuel at supercritical conditions, *Industrial & Engineering Chemistry Research* 41(23), 5856-5866.
- Edwards, T., 2006. Cracking and deposition behavior of supercritical hydrocarbon aviation fuels, *Combustion Science and Technology* 178(1-3), 307-334.
- Edwards, T., Atria, J. V., 1995. Deposition from high temperature jet fuels, *Preprints - American Chemical Society. Division of Petroleum Chemistry* 40(4), 649-654.
- Edwards, T., Liberio, P. D., 1994. The relationship between oxidation and pyrolysis in fuels heated to $\sim 590^{\circ}\text{C}$ (1100°F), *Preprints - American Chemical Society. Division of Petroleum Chemistry* 39(1), 92-96.
- Edwards, J., 2008. Numerical simulation of aerated-liquid and supercritical injection of hydrocarbon fuels, *Abstracts of Papers, 235th ACS National Meeting, New Orleans, LA, United States, April 6-10, 2008*, IEC-054.
- Edwards, T., Zabarnick, S., 1993. Supercritical fuel deposition mechanisms, *Industrial & Engineering Chemistry Research* 32(12), 3117-3122.

- Ely, J. F., Huber, M. L., 2007. NIST thermophysical properties of hydrocarbon mixtures database (SUPERTRAPP). NIST Standard Reference Database 4. Version 3.2.
- Erdogan, M. E., Chatwin, P. C., 1967. The effects of curvature and buoyancy on the laminar dispersion of solute in a horizontal tube, *Journal of Fluid Mechanics Digital Archive* 29(03), 465-484.
- Ervin, J. S., Williams, T. F., Bento, J., Dounghip, T., 2000. Studies of jet fuel thermal stability and flow characteristics within a nozzle under supercritical conditions, *Preprints - American Chemical Society. Division of Petroleum Chemistry* 45(3), 526-530.
- Ervin, J. S., Williams, T. F., Hartman, G., 1998. Effect of test period on the rate of fouling in a complex flowing system : Structure of jet fuels V, *Preprints - American Chemical Society. Division of Petroleum Chemistry* 43(3), 373-377.
- Ervin, J. S., Ward, T. A., Williams, T. F., Bento, J., 2003. Surface deposition within treated and untreated stainless steel tubes resulting from thermal-oxidative and pyrolytic degradation of jet fuel, *Energy & Fuels* 17(3), 577-586.
- Eser, S., Venkataraman, R., Altin, O., 2006. Deposition of carbonaceous solids on different substrates from thermal stressing of JP-8 and jet A fuels, *Industrial & Engineering Chemistry Research* 45(26), 8946-8955.
- Etter, D. O., Kay, W. B., 1961. Critical properties of mixtures of normal paraffin hydrocarbons, *Journal of Chemical & Engineering Data* 6(3), 409-414.
- Fan, X., Yu, G., Li, J., Zhang, X., Sung, C.-J., 2006. Investigation of vaporized kerosene injection and combustion in a supersonic model combustor, *Journal of Propulsion and Power* 22(1), 103-110.
- Fan, X., Yu, G., 2006. Experiments on supersonic combustion of supercritical kerosene,

Tuijin Jishu 27(1), 79-82.

- Farrell, J. T., Cernansky, N. P., Dryer, F. L., Friend, D. G., Hergart, C. A., Law, C. K., DcDavid, R. M., Mueller, C. J., Patel, A. K., Pitsch, H., 2007. Development of an experimental database and kinetic models for surrogate diesel fuels, SAE Paper 2007-01-0201.
- Fournet, R., Battin-Leclerc, F., Glaude, P. A., Judenherc, B., Warth, V., Côme, G. M., Scacchi, G., Ristori, A., Pengloan, G., Dagaut, P., Cathonnet, M., 2001. The gas-phase oxidation of n-hexadecane, *International Journal of Chemical Kinetics* 33(10), 574-586.
- Friend, D. G., Huber, M. L., 1994. Thermophysical property standard reference data from NIST, *International Journal of Thermophysics* 15(6), 1279-1288.
- Fu, H., Coelho, L. A. F., Matthews, M. A., 2000. Diffusion coefficients of model contaminants in dense CO₂, *The Journal of Supercritical Fluids* 18(2), 141-155.
- Fujimoto, H., Senda, J., Shibata, I., Matsui, K., 1995. New concept on lower exhaust emission of diesel engine, SAE Paper 952062.
- Funazukuri, T., Hachisu, S., Wakao, N., 1991. Measurements of binary diffusion coefficients of C16-C24 unsaturated fatty acid methyl esters in supercritical carbon dioxide, *Industrial & Engineering Chemistry Research* 30(6), 1323-1329.
- Funazukuri, T., Kong, C. Y., Kagei, S., 2001. Infinite dilution binary diffusion coefficients of benzene in carbon dioxide by the Taylor dispersion technique at temperatures from 308.15 to 328.15 K and pressures from 6 to 30 MPa, *International Journal of Thermophysics* 22(6), 1643-1660.
- Funazukuri, T., Kong, C. Y., Kagei, S., 2000a. Binary diffusion coefficients of acetone in carbon dioxide at 308.2 and 313.2 K in the pressure range from 7.9 to 40 MPa,

International Journal of Thermophysics 21(3), 651-669.

Funazukuri, T., Kong, C. Y., Kagei, S., 2000b. Infinite-dilution binary diffusion coefficients of 2-propanone, 2-butanone, 2-pentanone, and 3-pentanone in CO₂ by the Taylor dispersion technique from 308.15 to 328.15 K in the pressure range from 8 to 35 MPa, International Journal of Thermophysics 21(6), 1279-1290.

Funazukuri, T., Nishimoto, N., 1996. Tracer diffusion coefficients of benzene in dense CO₂ at 313.2 K and 8.5–30 MPa, Fluid Phase Equilibria 125(1-2), 235-243.

Funazukuri, T., Hachisu, S., Wakao, N., 1989. Measurement of diffusion coefficients of C18 unsaturated fatty acid methyl esters, naphthalene, and benzene in supercritical carbon dioxide by a tracer response technique, Analytical Chemistry 61(2), 118-122.

Funazukuri, T., Kong, C. Y., Kagei, S., 2006. Binary diffusion coefficients in supercritical fluids: Recent progress in measurements and correlations for binary diffusion coefficients, The Journal of Supercritical Fluids 38(2), 201-210.

Funazukuri, T., Kong, C. Y., Kagei, S., 2004. Impulse response techniques to measure binary diffusion coefficients under supercritical conditions, Journal of Chromatography A 1037(1-2), 411-429.

Funazukuri, T., Kong, C. Y., Kagei, S., 2000. On the measurement of anomalous binary diffusion coefficients in the near-critical region, Industrial & Engineering Chemistry Research 39(3), 835-837.

Gemci, T., Yakut, K., Chigier, N., Ho, T. C., 2004. Experimental study of flash atomization of binary hydrocarbon liquids, International Journal of Multiphase Flow 30(4), 395-417.

Gerrish, H. C., Ayer, B. E., 1936. Influence of fuel-oil temperature on the combustion in a

prechamber compression ignition engine, NACA TN565.

Giarratano, P. J., Jones, M. C., 1975. Deterioration of heat transfer to supercritical helium at 2.5 atmospheres, *International Journal of Heat and Mass Transfer* 18(5), 649-653.

Goodrum, J. W., 2002. Volatility and boiling points of biodiesel from vegetable oils and tallow, *Biomass and Bioenergy* 22(3), 205-211.

Griffiths, A., 1910. On the movement of a coloured Index along a capillary tube, and its application to the measurement of the circulation of water in a closed circuit, *Proceedings of the Physical Society of London* 23(1), 190-197.

Gül, Ö., Rudnick, L. R., Schobert, H. H., 2006. The effect of chemical composition of coal-based jet fuels on the deposit tendency and morphology, *Energy & Fuels* 20(6), 2478-2485.

Gül, Ö., Rudnick, L. R., Schobert, H. H., 2005. The effect of reaction temperature and fuel treatment on deposit formation of jet fuels, *Prepr. Pap.-Am. Chem. Soc., Div. Fuel Chem.* 50(2), 744-746.

Gupta, A., 2003. Physical and chemical properties, in: Chohey, N. P. (Ed), *Handbook of Chemical Engineering Calculations*, 3rd Ed. Edition, McGraw-Hill Professional, pp. 1.1-1.80.

Gurin, V., Novak, P., Wilson, B., Prakhin, M., 2006. Method and apparatus for liquid fuel preparation to improve combustion, *US Pat.* (7011048 B2).

Gustavsson, J., Golovitchev, V. I., 2003. Spray combustion simulation based on detailed chemistry approach for diesel fuel surrogate model, *SAE paper* 2003-01-1848.

Haldeman, C. W., III, 2002. Subcritical, near-critical, and near-supercritical mixtures of water and liquid hydrocarbon fuels, *PCT Int. Appl.* 2002-US11419; 2001-

829016(2002081602).

Haldeman, C. W., Ahern, B. S., Johnson, K. H., 1999. Supercritical water fuel composition and combustion system, PCT Int. Appl. 1998-US27012; 1997-992983(9931204).

Hamosfakidis, V., Reitz, R. D., 2003. Optimization of a hydrocarbon fuel ignition model for two single component surrogates of diesel fuel, Combustion and Flame 132(3), 433-450.

Harstad, K., Bellan, J., 2004. High-pressure binary mass diffusion coefficients for combustion applications, Industrial & Engineering Chemistry Research 43(2), 645-654.

Hazlett, R. N., 1992. Physicochemical aspects of aviation fuel thermal stability, in: Kirklin, P. W., David, P. (Eds), Aviation Fuel: Thermal Stability Requirements. Philadelphia, PA, ASTM, pp. 18-33.

Hazlett, R. N., 1991. Thermal Oxidation Stability of Aviation Turbine Fuels. Philadelphia, PA: ASTM.

He, C., Yu, Y., 1998. New equation for infinite-dilution diffusion coefficients in supercritical and high-temperature liquid solvents, Industrial & Engineering Chemistry Research 37(9), 3793-3798.

Heidemann, R. A., 1994. The classical theory of critical points, in: Kiran, J., Levelt Sengers, J. M. H. (Eds), Supercritical Fluids: Fundamentals for Applications, NATO ASI Series E: 273 Edition. Dordrecht, Holland, Kluwer Academic Publishers, pp. 39-64.

Heidemann, R. A., Khalil, A. M., 1980. The calculation of critical points, AIChE Journal 26(5), 769-779.

Helfrish, T. M., 2006. Cycle Performance of A Pulse Detonation Engine with Supercritical Fuel Injection, Master Thesis, Air Force Institute of Technology.

- Hernandez, J. J., Sanz-Argent, J., Benajes, J., Molina, S., 2008. Selection of a diesel fuel surrogate for the prediction of auto-ignition under HCCI engine conditions, *Fuel* 87(6), 655-665.
- Hicks, C. P., Young, C. L., 1975. Gas-liquid critical properties of binary mixtures, *Chemical reviews* 75(2), 119-175.
- Hirasaki, G. J., Mohanty, K. K., 2001. Fluid-rock characterization and interactions in NMR well logging, DOE/BC/15201-1.
- Holmes, V. V., Pahnke, A. J., Uyehara, O. A., Myers, P. S., 1953. Combustion of a low-volatility fuel in a turbojet combustion chamber – effects of fuel vaporization, *Trans. ASME* 75, 1303-1310.
- Hoppie, L. O., 1987. Method and apparatus for achieving hypergolic combustion by partial catalytic combustion, US Pat. 4,651,703.
- Hoppie, L. O., 1984. Method for reducing ignition delay of fuel, US Pat 4,448,176.
- Hoppie, L. O., 1982. The influence of initial fuel temperature on ignition delay, SAE Paper 820,356.
- Hoppie, L. O., Chute, R., Scharnweber, D. H., Waichunas, K. P., 1987a. Apparatus and method for compressive heating of fuel to achieve hypergolic combustion, US Pat. 4,644,925.
- Hoppie, L. O., Chute, R., Scharnweber, D. H., Waichunas, K. P., 1987b. Apparatus and method for multiphasic pretreatment of fuel to achieve hypergolic combustion, US Pat. 4,672,938.
- Hoppie, L. O., Chute, R., Scharnweber, D. H., Waichunas, K. P., 1987c. Regenerative fuel heating apparatus and method for hypergolic combustion, US Pat. 4,669,433.

- Hourri, A., Okambawa, R., Benard, P., Bose, T. K., 1982. Compressibility factor for mixtures of natural gas and hydrogen: comparison between experimental and calculated values using SUPERTRAPP, *Hydrogen Energy Progress* 2, 1679-1688.
- Huang, H., Sobel, D., Spadaccini, L., 2002. Endothermic heat-sink of hydrocarbon fuels for scramjet cooling, 38th AIAA/AMSE/SAE/ASEE Joint Propulsion Conference and Exhibit (AIAA 2002-3871).
- Huang, H., Su, W., 2005. A new reduced chemical kinetic model for autoignition and oxidation of lean n-heptane/air mixtures in HCCI engines, SAE Paper 2005-01-0118.
- Huang, Z., Shao, Y., Shiga, S., Nakamura, H., Karasawa, T., 1994a. The orifice flow pattern, pressure characteristics, and their effects on the atomization of fuel containing dissolved gas, *Atomization and Sprays* 4(2), 123-133.
- Huang, Z., Shao, Y., Shiga, S., Nakamura, H., Karasawa, T., Nagasaka, T., 1994b. Atomization behavior of fuel containing dissolved gas, *Atomization and Sprays* 4(3), 253-262.
- Huang, Z., Zhang, S., Zhang, L., 1996. Evaluation of the effect of injection of fuel containing dissolved gas (IFCDG) on diesel combustion and emissions, *Journal of Combustion Science and Technology* 2(4), 299-306.
- Huang, H., Spadaccini, L. J., Sobel, D. R., 2004. Fuel-cooled thermal management for advanced aeroengines, *Journal of Engineering for Gas Turbines and Power* 126(2), 284-293.
- Huang, Z., Shao, Y., Shiga, S., Nakamura, H., 1994. Controlling mechanism and resulting spray characteristics of injection of fuel containing dissolved gas, *Journal of Thermal Science* 3(3), 191-199.

- Huber, M. L., Hanley, H. J. M., 1996. The Corresponding-States Principle: Dense Fluids, in: Millat, J., Dymond, J. H., Nieto de Castro, C. A. (Eds), Transport Properties of Fluids: Their Correlation, Prediction and Estimation, Cambridge University Press, pp. 283-295.
- Jacobsen, R. T., Stewart, R. B., 1973. Thermodynamic properties of nitrogen including liquid and vapor phases from 63K to 2000K with pressures to 10,000 bar, Journal of Physical and Chemical Reference Data 2(4), 757-922.
- Janssen, L. A. M., 1976. Axial dispersion in laminar flow through coiled tubes, Chemical Engineering Science 31(3), 215-218.
- Jensen, G. E., Woodward, R. D., Pal, S., Santoro, R. J., 2004. Study of supercritical hydrocarbon fuels injected into a subsonic cross-flow with combustion, Preprints - American Chemical Society, Division of Petroleum Chemistry 49(4), 517-520.
- Joback, K. G., Reid, R. C., 1987. Estimation of pure-component properties from group-contributions, Chemical Engineering Communications 57(1-6), 233-243.
- Kalitchin, Z. D., Ivanov, S. K., Boneva, M. I., Ivanov, A., Kanariev, K., Georgiev, P. T., Tanielyan, S. K., 1997. Thermo-chemical and thermo-oxidative stability of diesel fuels containing components of light catalytic gas oil, 6th International Conference on Stability and Handling of Liquid Fuels , 685-697.
- Kao, M., Lee, M., Ferng, Y., Chieng, C., 2010. Heat transfer deterioration in a supercritical water channel, Nuclear Engineering and Design 240(10), 3321-3328.
- Kawano, D., Goto, Y., Odaka, M., Senda, J., 2004. Modeling atomization and vaporization processes of flash-boiling spray, SAE Paper 2004-01-0534.
- Kawano, D., Ishii, H., Suzuki, H., Goto, Y., Odaka, M., Senda, J., 2006. Numerical study on flash-boiling spray of multicomponent fuel, Heat Transfer - Asian Research 35(5),

369-385.

Kelbaliev, R. F., 2001. Deterioration of heat transfer at supercritical pressures of a substance, *Journal of Engineering Physics and Thermophysics (Translation of Inzhenerno-Fizicheskii Zhurnal)* 74(2), 416-420.

Kesler, M. G., Lee, B. I., 1976. Improve prediction of enthalpy of fractions, *Hydrocarbon Processing* 55(3), 153-158.

Kim, H., Pae, S., Min, K., 2002. Reduced chemical kinetic model for the ignition delay of hydrocarbon fuels and DME, *Combustion Science and Technology* 174(8), 221-238.

Klincewicz, K. M., Reid, R. C., 1984. Estimation of critical properties with group contribution methods, *AIChE Journal* 30(1), 137-142.

Kolev, N. I., 2007. *Multiphase Flow Dynamics 3: Turbulence, Gas Absorption and Release, Diesel Fuel Properties*. New York: Springer.

Kong, C. Y., Funazukuri, T., Kagei, S., 2008. Reliability of binary diffusion coefficients determined from tailing response curves measured by the Taylor dispersion method in the near critical region, *The Journal of Supercritical Fluids* 44(3), 294-300.

Korsten, H., 1998. *Critical Properties of Hydrocarbon Systems*, *Chemical Engineering & Technology* 21(3), 229-244.

Koshizuka, S., Takano, N., Oka, Y., 1995. Numerical analysis of deterioration phenomena in heat transfer to supercritical water, *International Journal of Heat and Mass Transfer* 38(16), 3077-3084.

Kreglewski, A., Kay, W. B., 1969. Critical constants of conformed mixtures, *The Journal of physical chemistry* 73(10), 3359-3366.

- Krishnan, A., 1992. Influence of supercritical conditions on pre-combustion chemistry and transport behavior of jet fuels, Report (CFDRC-4240/2, AFOSR-TR-93-0137; Order No. AD-A261813), 60.
- Kulkarni, A. K., Neches, S. J., 1994. Simulation of liquid spray atomization in supercritical environment using various surface tension models, ICLASS 94, Proceedings of the 6th International Conference on Liquid Atomization and Spray Systems, Rouen, July 18-22, 1994 , 190-197.
- Laesecke, A., Lüddecke, T. O. D., Hafer, R. F., Morris, D. J., 1999. Viscosity measurements of ammonia, R32, and R134a. Vapor buoyancy and radial acceleration in capillary viscometers, International Journal of Thermophysics 20(2), 401-434.
- Lai, C., Tan, C., 1995. Measurement of molecular diffusion coefficients in supercritical carbon dioxide using a coated capillary column, Industrial & Engineering Chemistry Research 34(2), 674-680.
- Lang, X., Dalai, A. K., Bakhshi, N. N., Reaney, M. J., Hertz, P. B., 2001. Preparation and characterization of bio-diesels from various bio-oils, Bioresource technology 80(1), 53-62.
- Lee, S., 2006. Investigation of two low emissions strategies for diesel engines: Premixed charge compression ignition (PCCI) and stoichiometric combustion, 229.
- Lemmon, E. W., Huber, M. L., McLinden, M. O., 2010. NIST Standard Reference Database 23: Reference Fluid Thermodynamic and Transport Properties-REFPROP, Version 9.0.
- Lemmon, E. W., McLinden, M. O., Huber, M. L., 2002. NIST Standard Reference Database 23: Reference Fluid Thermodynamic and Transport Properties-REFPROP, Version 7.0.

- Levelt Sengers, J. M. H., Deiters, U. K., Klask, U., Swidersky, P., Schneider, G. M., 1993. Application of the Taylor dispersion method in supercritical fluids, *International Journal of Thermophysics* 14(4), 893-922.
- Li, L., Kiran, E., 1990. Estimation of critical properties of binary mixtures using group contribution methods, *Chemical Engineering Communications* 94, 131-141.
- Li, C. C., 1971. Critical temperature estimation for simple mixtures, *The Canadian Journal of Chemical Engineering* 49(5), 709-710.
- Li, H., Hsu, S. M., Wang, J. C., 1996. Thermal-oxidative characteristics of some high-temperature diesel lubricants, *Journal of Synthetic Lubrication* 13(2), 129-148.
- Lin, R., Tavlarides, L.L., 2010. Diffusion coefficients of diesel fuel and surrogate compounds in supercritical carbon dioxide, *The Journal of Supercritical Fluids* 52(1), 47-55.
- Lin, R., Tavlarides, L.L., 2010. Determination of diffusion coefficients by supercritical fluid chromatography: Effects of mobile phase mean velocity and column orientation, *Journal of Chromatography A* 1217 (26), 4454-4462.
- Linne, D. L., Meyer, M. L., Edwards, T., Eitman, D. A., 1997. Evaluation of heat transfer and thermal stability of supercritical JP-7 fuel, NASA Technical Memorandum 107485 AIAA-97-3041.
- Linstrom, P. J., Mallard, W. G. (Eds), 2009. NIST Chemistry WebBook, NIST Standard Reference Database Number 69. Gaithersburg MD, 20899: National Institute of Standards and Technology.
- Liong, K. K., Wells, P. A., Foster, N. R., 1991. Diffusion in supercritical fluids, *The Journal of Supercritical Fluids* 4(2), 91-108.
- Lydersen, A., 1955. Estimation of critical properties of organic compounds by the

method of group contributions, University of Wisconsin-Madison.

Magnussen, B. F., Hjertager, B. H., 1976. On mathematical modeling of turbulent combustion with special emphasis on soot formation and combustion, Proceeding of 16th International Symposium on Combustion, 719-729.

Majt, P. M., Foster, D. E., 1983. Compression-ignited homogeneous charge combustion, SAE paper 830,264.

Mantell, C., Rodríguez, M., Martínez de la Ossa, E., 2003. Measurement of the diffusion coefficient of a model food dye (malvidin 3,5-diglucoside) in a high pressure CO₂+methanol system by the chromatographic peak-broadening technique, The Journal of Supercritical Fluids 25(1), 57-68.

Marrero-Morejón, J., Pardillo-Fontdevila, E., 1999. Estimation of pure compound properties using group-interaction contributions, AIChE Journal 45(3), 615-621.

Matthews, M. A., 1986. Diffusion Coefficients at Infinite Dilution in N-Alkane Solvents at Temperatures to 573 K and Pressures to 3.5 Mpa, Dissertation, Texas A&M University.

Maurice, L. Q., Lander, H., Edwards, T., Harrison, W. E., 2001. Advanced aviation fuels: a look ahead via a historical perspective, Fuel 80(5), 747-756.

Merkisz, J., Kozak, W., Bajerlein, M., Markowski, J., 2007. The influence of exhaust gases dissolved in diesel oil on fuel spray particulary parameters, SAE Paper 2007-01-0488.

Micci, M. M., Long, L. N., 2000. Molecular Dynamics Investigation of Supercritical Fuels, Final Report, A161973, Pennsylvania State University.

Michelsen, M. L., 1982. The isothermal flash problem. Part II. Phase-split calculation, Fluid Phase Equilibria 9(1), 21-40.

- Michelsen, M. L., 1980. Calculation of phase envelopes and critical points for multicomponent mixtures, *Fluid Phase Equilibria* 4(1-2), 1-10.
- Miller, J. A., Kee, R. J., Westbrook, C. K., 1990. Chemical kinetics and combustion modeling, *Annual Review of Physical Chemistry* 41(1), 345-387.
- Min, Y. -K., 1986. Optimal Hypergolic Combustion in an Internal Combustion Engine, Dissertation, Marquette University.
- Mokry, S. J., Kirillov, P. L., Pioro, I. L., Gospodinov, Y. K., 2010. Supercritical water heat transfer in a vertical bare tube: normal, improved, and deteriorated regimes, *Nuclear Technology* 172(1), 60-70.
- Nannoolal, Y., Rarey, J., Ramjugernath, D., 2007. Estimation of pure component properties: Part 2. Estimation of critical property data by group contribution, *Fluid Phase Equilibria* 252(1-2), 1-27.
- Nickolaus, D., Lefebvre, A. H., 1987. Fuel thermal stability effects on spray characteristics, *J. Propul. Pow.* 3(6), 502-507.
- Nielsen, K. A., 1992. Supercritical fluids as diluents in combustion of liquid fuels and water materials, US Pat. 5,170,727.
- Nishiumi, H., Fujita, M., Agou, K., 1996. Diffusion of acetone in supercritical carbon dioxide, *Fluid Phase Equilibria* 117(1-2), 356-363.
- Nishiumi, H., Kubota, T., 2007. Fundamental behavior of benzene–CO₂ mutual diffusion coefficients in the critical region of CO₂, *Fluid Phase Equilibria* 261(1-2), 146-151.
- NIST, 2003. Workshop on Combustion Simulation Databases for Real Transportation Fuels, National Institute of Standards and Technology, NIST IR 7155.
- Noel, L., Maroteaux, F., Ahmed, A., 2004. Numerical study of HCCI combustion in diesel

engines using reduced chemical kinetics of n-heptane with multidimensional CFD code, SAE Paper 2004-01-1909.

Nunge, R. J., Lin, T. -S., Gill, W. N., 1972. Laminar dispersion in curved tubes and channels, *Journal of Fluid Mechanics Digital Archive* 51(02), 363-383.

O'Brien, J., Ahern, B., Djutrisno, I., Donahue, K., Haldeman, C. W., Hynek, S., Johnson, K., Woods, M., Tester, J. W., 2001. Dramatic emissions reductions with a direct injection diesel engine burning supercritical fuel/water mixtures, SAE paper 2001-01-3526.

Office of Science, US DOE, 2008. Energy Frontier Research Centers: Tackling Our Energy Challenges in a New Era of Science.

Office of Science, US DOE, 2007. Basic Research Needs for Clean and Efficient Combustion of 21st Century Transportation Fuels.

Oschwald, M., Smith, J. J., Branam, R., Hussong, J., Schik, A., Chehroudi, B., Talley, D., 2006. Injection of fluids into supercritical environments. *Combustion Science and Technology* 178(1-3), 49-100.

Pande, S. G., Hardy, D. R., Kamin, R. A., Nowack, C. J., Colbert, J. E., Morris, R. E., Salvucci, L., 2001. Quest for a reliable method for determining aviation fuel thermal stability: comparison of turbulent and laminar flow test devices, *Energy & Fuels* 15(1), 224-235.

Pioro, I. L., Khartabil, H. F., Duffey, R. B., 2004. Heat transfer to supercritical fluids flowing in channels—empirical correlations (survey), *Nuclear Engineering and Design* 230(1-3), 69-91.

Pitz, W. J., Mueller, C. J., 2010. Recent progress in the development of diesel surrogate fuels, *Progress in Energy and Combustion Science* 37(3), 330-350.

- Pizarro, C., Suárez-Iglesias, O., Medina, I., Bueno, J. L., 2009a. Binary diffusion coefficients of 2-ethyltoluene, 3-ethyltoluene, and 4-ethyltoluene in supercritical carbon dioxide, *Journal of Chemical & Engineering Data* 54(5), 1467-1471.
- Pizarro, C., Suárez-Iglesias, O., Medina, I., Bueno, J. L., 2009b. Binary diffusion coefficients for 2,3-dimethylaniline, 2,6-dimethylaniline, 2-methylanisole, 4-methylanisole and 3-nitrotoluene in supercritical carbon dioxide, *The Journal of Supercritical Fluids* 48(1), 1-8.
- Poling, B. E., Prausnitz, J. M., O'Connell, J. P. (Eds), 2001. *The Properties of Gases and Liquids*. New York, NY: McGraw-Hill.
- Pratt, K. C., Wakeham, W. A., 1975. The mutual diffusion coefficient for binary mixtures of water and the isomers of propanol, *Proceedings of the Royal Society B: Biological Sciences* 342(1630), 401-419.
- Rashkovan, A., Kholmer, V., Sher, E., 2004a. Effervescent atomization of gasoline containing dissolved CO₂, *Atomization and Sprays* 14(4), 341-354.
- Rashkovan, A., Rivin, B., Sher, E., 2004b. Optimization of gasoline-dissolved CO₂ injectors, *SAE Paper* 2004-01-0543.
- Rashkovan, A., Sher, E., 2006. Flow pattern observations of gasoline dissolved CO₂ inside an injector, *Atomization and Sprays* 16(6), 615-626.
- Reejhsinghani, N. S., Gill, W. N., Barduhn, A. J., 1966. Laminar dispersion in capillaries: Part III. Experiments in horizontal tubes including observations on natural convection effects, *AIChE Journal* 12(5), 916-921.
- Reimuller, C. J., 1976. Fuel vaporization and injection system for internal combustion engine, *US Pat.* 3,945,352.
- Riazi, M. R., Daubert, T. E., 1980. Simplify property predictions, *Hydrocarbon Processing*

59(3), 115-116.

- Ristori, A., Dagaut, P., Cathonnet, M., 2001. The oxidation of n-Hexadecane: experimental and detailed kinetic modeling, *Combustion and Flame* 125(3), 1128-1137.
- Roth, M., 1991. Diffusion and thermodynamic measurements by supercritical fluid chromatography, *Journal of Microcolumn Separations* 3(3), 173-184.
- Rudnick, L. R., Buchanan, R. P., Medina, F., 2006. Evaluation of oxidation-mediated volatility of hydrocarbon lubricant base fluids, *Journal of Synthetic Lubrication* 23(1), 11-26.
- Sadus, R. J., 1994. Calculating critical transitions of fluid mixtures: Theory vs. experiment, *AIChE Journal* 40(8), 1376-1403.
- Sahetchian, K., Champoussin, J. C., Brun, M., Levy, N., Blin-Simiand, N., Aligrot, C., Jorand, F., Socoliuc, M., Heiss, A., Guerassi, N., 1995. Experimental study and modeling of dodecane ignition in a diesel engine, *Combustion and Flame* 103(3), 207-220.
- Sassiat, P. R., Mourier, P., Caude, M. H., Rosset, R. H., 1987. Measurement of diffusion coefficients in supercritical carbon dioxide and correlation with the equation of Wilke and Chang, *Analytical Chemistry* 59(8), 1164-1170.
- Scharnweber, D. H., 1984. Hypergolic combustion demonstration in a reciprocating internal combustion engine, U.S. Army TACOM R&D Center, Warren, MI 13042.
- Scharnweber, D. H., Hoppie, L. O., 1985. Hypergolic combustion in an internal combustion engine, SAE paper 850,089.
- Scharnweber, D. H., Hoppie, L. O., Haefner, D. R., 1989. Method and apparatus for activating fuel prior to combustion, US Pat. 4,865,003.

- Schefer, R. W., Keller, J. O., 2007. Method for control of NO_x emission from combustors using fuel dilution, US Pat. 7,162,864.
- Scheibel, E. G., 1954. Correspondence. Liquid Diffusivities. Viscosity of Gases, Industrial & Engineering Chemistry 46(9), 2007-2008.
- Schwab, S. D., Henly, T. J., Moxley, J. F., Miller, K. T., 2000. Thermal stability of diesel fuel, IASH 2000, Proceeding of the 7th International Conference on Stability and Handling of Liquid Fuels, 13-32.
- Senda, J., Asai, T., Kawaguchi, B., Fujimoto, H., 2000. Characteristics of gas-dissolved diesel fuel spray (spray characteristics and simulating flash boiling process), JSME International Journal 43(3), 503-510.
- Senda, J., Hashimoto, K., Ifuku, Y., Fujimoto, H., 1997. CO₂ mixed fuel combustion system for reduction of NO and soot emission in diesel engine, SAE Paper 970,319.
- Senda, J., Hojyo, Y., Fujimoto, H., 1994. Modelling of atomization process in flash boiling spray, SAE Paper 941,925.
- Senda, J., Ikeda, M., Yamamoto, M., Kawaguchi, B., Fujimoto, H., 1999. Low emission diesel combustion system by use of reformed fuel with liquefied CO₂ and n-tridecane, SAE Paper 1999-01-1136.
- Senda, J., Kawano, D., Hotta, I., Kawakami, K., Fujimoto, H., 2000. Fuel design concept for low emission in engine system, SAE Paper 2000-01-1258.
- Senda, J., Kawano, D., Kawakami, K., Shimada, A., Fujimoto, H., 2001. Fuel design concept research for low exhaust emissions by use of mixing fuels, The fifth international symposium on diagnostics and modeling of combustion in internal combustion engines (COMODIA 2001), 396-401.

- Senda, J., Shibata, I., Asai, T., Fujimoto, H., 1997. Improvement of spray characteristics in N₂ gas and liquefied CO₂ dissolved diesel fuel, Proceedings of ICLASS-97(Seoul) 1, 141-148.
- Senda, J., Wada, Y., Kawano, D., Fujimoto, H., 2008. Improvement of combustion and emissions in diesel engines by means of enhanced mixture formation based on flash boiling of mixed fuel, International Journal of Engine Research 9(1), 15-27.
- Seshadri, K., 2003. Chemical Kinetic Characterization of Autoignition and Combustion of Diesel and JP-8, Final Report # A992924.
- Sharma, N. Y., Som, S. K., 2004. Influence of fuel volatility and spray parameters on combustion characteristics and NO_x emission in a gas turbine combustor, Applied Thermal Engineering 24(5-6), 885-903.
- Shiga, S., Huang, Z., Shao, Y., Karasawa, T., Nakamura, H., Makita, S., 1994. Investigation of gas-dissolving effect on the spray-formation of a steady-jet, Proceedings of ICLASS-94 VI-2, 601-608.
- Shiga, S., Makita, S., Karasawa, T., Nakamura, H., 1997. A parametric study on the utilization of gas dissolution effect in steady sprays, Proceedings of ICLASS-97 1, 369-376.
- Shiralkar, B. S., Griffith, P., 1969. Deterioration in heat transfer to fluid at supercritical pressure and high heat fluxes, Journal of Heat Transfer 91(1), 27-36.
- Silva, C. M., Filho, C. A., Quadri, M. B., Macedo, E. A., 2004. Binary diffusion coefficients of α -pinene and β -pinene in supercritical carbon dioxide, The Journal of Supercritical Fluids 32(1-3), 167-175.
- Sim, W. J., Daubert, T. E., 1980. Prediction of Vapor-Liquid Equilibria of Undefined Mixtures, Industrial & Engineering Chemistry Process Design and Development

19(3), 386-393.

- Simmie, J. M., 2003. Detailed chemical kinetic models for the combustion of hydrocarbon fuels, *Progress in Energy and Combustion Science* 29(6), 599-634.
- Smith, B. L., Ott, L. S., Bruno, T. J., 2008. Composition-explicit distillation curves of diesel fuel with glycol ether and glycol ester oxygenates: fuel analysis metrology to enable decreased particulate emissions, *Environmental science & technology* 42(20), 7682-7689.
- Smith, R. L., Teja, A. S., Kay, W. B., 1987. Measurement of critical temperatures of thermally unstable n-Alkanes, *AIChE Journal* 33(2), 232-238.
- Smith, R. L., Watson, K. M., 1937. Boiling points and critical properties of hydrocarbons, *Industrial & Engineering Chemistry* 29(12), 1408-1414.
- Solomon, A. S. P., Chen, L. -D., Farth, G. M., 1982. Investigation of spray characteristics for flashing injection of fuels containing dissolved air and superheated fuels, *NASA Contractor Report* 3563.
- Somers, M. L., McClaine, J. W., Wornat, M. J., 2007. The formation of polycyclic aromatic hydrocarbons from the supercritical pyrolysis of 1-methylnaphthalene, *Proceedings of the Combustion Institute* 31(1), 501-509.
- Song, C., Eser, S., Schobert, H. H., Hatcher, P. G., 1993. Pyrolytic degradation studies of a coal-derived and a petroleum-derived aviation jet fuel, *Energy & Fuels* 7(2), 234-243.
- Spadaccini, L. J., 1976. Autoignition characteristics of hydrocarbon fuels at elevated temperatures and pressures, *ASME Paper* 76-GT-3.
- Spencer, C. F., Daubert, T. E., 1973. A critical evaluation of methods for the prediction of critical properties of hydrocarbons, *AIChE Journal* 19(3), 482-486.

- Stavinoha, L. L., Barbee, J. G., Yost, D. M., 1986. Thermal Oxidation Stability of Diesel Fuels, Interim report, AD-A173 850, Southwest Research Institute.
- Stewart, J. F., 1999. Supercritical pyrolysis of the endothermic fuels methylcyclohexane, decalin, and tetralin, Dissertation, Princeton University.
- Stiegemeier, B., Meyer, M. L., Taghavi, R., 2002. A thermal stability and heat transfer investigation of five hydrocarbon fuels: JP-7, JP-8, JP-8+100, JP-10, and RP-1, 38th AIAA/ASME/SAE/ASEE Joint Propulsion Conference & Exhibit, AIAA-2002-3873.
- Stradi, B. A., Brennecke, J. F., Kohn, J. P., Stadtherr, M. A., 2001. Reliable computation of mixture critical points, *AIChE Journal* 47(1), 212-221.
- Strauss, K. H., 1992. Thermal stability testing of aviation turbine fuel - a history, in: Kirklin, P. W., David, P. (Eds), *Aviation Fuel: Thermal Stability Requirements*. Philadelphia, PA, ASTM, pp. 8-17.
- Suárez, J. J., Bueno, J. L., Medina, I., 1993. Determination of binary diffusion coefficients of benzene and derivatives in supercritical carbon dioxide, *Chemical Engineering Science* 48(13), 2419-2427.
- Suárez, J. J., Medina, I., Bueno, J. L., 1998. Diffusion coefficients in supercritical fluids: available data and graphical correlations, *Fluid Phase Equilibria* 153(1), 167-212.
- Swaid, I., Schneider, G. M., 1979. Determination of binary diffusion coefficients of benzene and some alkylbenzenes in supercritical CO₂ between 308 and 328 K in the pressure range 80 to 160 bar with supercritical fluid chromatography (SFC), *Berichte der Bunsengesellschaft für physikalische Chemie* 83(10), 969-974.
- Tavlarides, L. L., Anitescu, G., 2009. Supercritical diesel fuel composition, combustion process, and fuel system, US Pat. 7,488,357.

- Taylor, G., 1954. Conditions under which dispersion of a solute in a stream of solvent can be used to measure molecular diffusion, *Proceedings of the Royal Society of London. Series A. Mathematical and Physical Sciences* 225(1163), 473-477.
- Taylor, G., 1953. Dispersion of soluble matter in solvent flowing slowly through a tube, *Proceedings of the Royal Society of London. Series A. Mathematical and Physical Sciences* 219(1137), 186-203.
- Taylor, W. F., 1974. Deposit formation from deoxygenated hydrocarbons. I. general features, *Product R&D* 13(2), 133-138.
- Thring, R. H., 1989. Homogeneous charge compression ignition (HCCI) engines, *SAE paper* 892068.
- Topakoglu, H., 1967. Steady laminar flows of an incompressible viscous fluid in curved pipes, *Indiana University Mathematics Journal* 16(12), 1321-1337.
- Twu, C. H., 1984. An internally consistent correlation for predicting the critical properties and molecular weights of petroleum and coal-tar liquids, *Fluid Phase Equilibria* 16(2), 137-150.
- Umezawa, S., Nagashima, A., 1992. Measurement of the diffusion coefficients of acetone, benzene, and alkane in supercritical CO₂ by the Taylor dispersion method, *The Journal of Supercritical Fluids* 5(4), 242-250.
- van de Ven-Lucassen, I. M. J. J., Kemmere, M. F., Kerkhof, P. J. A. M., 1997. Complications in the use of the Taylor dispersion method for ternary diffusion measurements: methanol + acetone + water mixtures, *Journal of Solution Chemistry* 26(12), 1145-1167.
- Venkataraman, R., Eser, S., 2008. Characterization of deposits formed on diesel injectors in field test and from thermal oxidative degradation of n-hexadecane in a

- laboratory reactor, *Chemistry Central Journal* 2(1), 25-35.
- Vesovic, V., 2001. Predicting the viscosity of natural gas, *International Journal of Thermophysics* 22(2), 415-426.
- Vijayaraghavan, S., 2003. *Thermodynamic Studies on Alternate Binary Working Fluid Combinations and Configurations for a Combined Power and Cooling Cycle*, Dissertation, University of Florida.
- Wakeham, W. A., Cholakov, G. S., Stateva, R. P., 2002. Liquid density and critical properties of hydrocarbons estimated from molecular structure, *Journal of Chemical & Engineering Data* 47(3), 559-570.
- Westbrook, C. K., 2000. Chemical kinetics of hydrocarbon ignition in practical combustion systems, *Proceedings of the Combustion Institute* 28(2), 1563-1577.
- Westbrook, C. K., Dryer, F. L., 1984. Chemical kinetic modeling of hydrocarbon combustion, *Progress in Energy and Combustion Science* 10(1), 1-57.
- Xi, J., Zhong, B. J., 2006. Reduced kinetic mechanism of n-heptane oxidation in modeling polycyclic aromatic hydrocarbon formation in diesel combustion, *Chemical Engineering & Technology* 29(12), 1461-1468.
- Xiao, J., Huang, Z., Qiao, X., Hou, Y., 2008. The effect of CO₂ dissolved in a diesel fuel on the jet flame characteristics, *Fuel* 87(3), 395-404.
- Xiao, J., Qiao, X., Huang, Z., Fang, J., 2004. Study of droplet size and velocity of fuel containing CO₂ spray by means of PDA, *Chinese Science Bulletin* 49(11), 1195-1199.
- Yang, V., 2000. Modeling of supercritical vaporization, mixing, and combustion processes in liquid-fueled propulsion systems, *Proceedings of the Combustion Institute* 28(Pt. 1), 925-942.

- Yang, V., Hsiao, G. C., Shuen, J., Hsieh, K., 1996. Droplet behavior at supercritical conditions, *Progress in Astronautics and Aeronautics 166*(Recent Advances in Spray Combustion: Spray Atomization and Drop Burning Phenomena, Vol. 1), 413-437.
- Yang, X., Coelho, L. A. F., Matthews, M. A., 2000. Near-critical behavior of mutual diffusion coefficients for five solutes in supercritical carbon dioxide, *Industrial & Engineering Chemistry Research* 39(8), 3059-3068.
- Yu, J., Eser, S., 1997a. Kinetics of supercritical-phase thermal decomposition of C10-C14 normal alkanes and their mixtures, *Industrial & Engineering Chemistry Research* 36(3), 585-591.
- Yu, J., Eser, S., 1997b. Thermal decomposition of C10-C14 normal alkanes in near-critical and supercritical regions: product distributions and reaction mechanisms, *Industrial & Engineering Chemistry Research* 36(3), 574-584.
- Yu, J., Eser, S., 1995. Determination of Critical Properties (T_c , P_c) of Some Jet Fuels, *Industrial & Engineering Chemistry Research* 34(1), 404-409.
- Zeng, Y., Lee, C. F., 2001. An atomization model for flash boiling sprays, *Combustion Science and Technology* 169(1), 45-67.
- Zhang, J., Jiang, D., Huang, Z., Obokata, T., Shiga, S., Araki, M., 2005. Experimental study on flashing atomization of methane/liquid fuel binary mixtures, *Energy & Fuels* 19(5), 2050-2055.
- Zhou, P., 1984. Correlation of the average boiling points of petroleum fractions with pseudocritical constants, *International Chemical Engineering* 24, 731-741.

BIOGRAPHICAL DATA

NAME OF AUTHOR: Ronghong Lin

PLACE OF BIRTH: Wenling, Zhejiang, China

DATE OF BIRTH: June 26, 1979

GRADUATE AND UNDERGRADUATE SCHOOLS ATTENDED:

Syracuse University, Syracuse, New York.

Beijing University of Chemical Technology, Beijing, China.

DEGREES AWARDED:

M.Sc. in Chemical Engineering, 2008, Syracuse University, Syracuse, New York.

B. Eng. in Chemical Engineering, 2001, Beijing University of Chemical Technology, Beijing, China.

AWARDS AND HONORS:

Graduate Fellow, Syracuse University, 2004-2005, 2006-2007, 2009-2010.

Nunan Travel Grant, 2010.

Nunan Research Day Poster Competition Department Winner, 2010.

Phi Beta Delta International Honor Society, 2009.

LCS School of Engineering Summer Fellowship, 2008.

Golden Key International Honor Society, 2007.

PROFESSIONAL EXPERIENCE:

Graduate Research Assistant, Department of Biomedical and Chemical Engineering, Syracuse University, 6/2005-3/2011.

Teaching Assistant, Department of Biomedical and Chemical Engineering, Syracuse University, 8/2005-5/2006, 8/2007-12/2007.

Assistant Project Manager, China National Chemical Construction Corporation, Beijing, China, 8/2001-6/2004.

Undergraduate Research Assistant, Department of Biochemical Engineering, Beijing University of Chemical Technology, Beijing, China, 2/2001-6/2001.